Diffusion of nanoparticles nearby elastic cell membranes: A theoretical study

Von der Universität Bayreuth
zur Erlangung des Grades eines
Doktors der Naturwissenschaften (Dr. rer. nat.)
genehmigte Abhandlung

von

Abdallah Daddi Moussa Ider

geboren in Beni-Isguen, Algerien

Vorsitzender	Prof. Dr. Holger Kress
Erstgutachter	Prof. Dr. Stephan Gekle
Zweitgutachter	Prof. Dr. Walter Zimmermann
Drittprüfer	Prof. Dr. Arthur Peeters

Tag der Einreichung	11.05.2017
Tag des Kolloquiums	26.07.2017

To my parents

Abstract

Elastic confinements are an important component of many soft matter systems and dictate the transport properties of suspended particles under flow. In this thesis, we present a fully analytical theory of the hydrodynamic interactions and Brownian motion of nanoparticles immersed in a Newtonian fluid, moving in close vicinity to a realistically modeled elastic cell membrane. The membrane is attached to a cross-linked cytoskeleton network providing a resistance towards shearing and consists of a lipid bilayer to enable resistance towards bending. We assume that the fluid surrounding the particles is governed by the linear Stokes equations where the viscous forces dominate over the inertial forces. Our analytical calculations start with the computation of the Green's functions representing the flow field due to a concentrated point force singularity acting nearby the elastic membrane. We then compute the frequency-dependent mobility functions connecting the force and torque with the translational and rotational velocities of the suspended particles. Thereupon, we derive analytical expressions of the diffusion tensor which can directly be obtained from the particle mobility functions via the fluctuation-dissipation theorem. Our most important finding is that the elastic nature of the confining membrane induces a memory effect in the system, leading to a long-lived anomalous subdiffusive behavior of nearby particles.

The determination of the Green's functions in the presence of an elastic boundary consists of writing the general solution of the Stokes equations as a sum of a bulk contribution and a correction term that is required to satisfy the regularity and boundary conditions imposed at the membrane. Depending on the membrane geometry we use three vastly different analytical approaches: (a) two dimensional Fourier transform technique for planar membranes, (b) a Fourier-Bessel integral for cylindrical membranes and (c) spherical harmonics for membranes with spherical geometry. Accordingly, the Green's functions can conveniently be expressed in terms of infinite integrals over the wavenumber or as convergent infinite sums of spherical harmonics. By considering a vanishing actuation frequency, the Green's functions are found to be identical to that predicted nearby a hard boundary with stick boundary conditions.

The exactly known Green's functions allow then for the analysis of the effect of the membrane on the motion of particles, notably for the calculation of self- and pair-mobility functions relevant to fluid

transport nearby elastic membranes. Analytical expressions of the mobility functions can be obtained by considering a distribution of point force singularities over the surface of the particles. Nonetheless, we restrict ourselves in most cases to the commonly employed point-particle approximation. The latter represents the leading-order term in an expansion of the mobility function in a power series with respect to the ratio between the particle radius and the distance from the membrane for the self-mobilities, or between the particle radius and the interparticle distance for the pair-mobilities. We show that this approximation despite its simplicity can surprisingly lead to a good estimate of the mobility functions when comparing with fully resolved numerical simulations performed using truly finite-sized particles.

The computation of the frequency-dependent mobility functions provides the memory kernel of the particle-membrane system and thus allows for the investigation of the diffusional motion of Brownian particles nearby elastic cell membranes via a generalized Langevin formalism. A complete characterization of particle diffusion can be performed by computing the mean-square displacement (MSD) which is known to be a linear function of time in bulk fluid. Nearby an elastic membrane however, the MSD exhibits a transient anomalous subdiffusion at intermediate time scales of motion with a scaling exponent that depends strongly on the distance separating the particles from the confining membrane. The steady MSD is found to follow a standard linear behavior and the diffusion coefficient approaches the one predicted close to a hard boundary. Using physical parameters corresponding to a typical red blood cell membrane, we find that the subdiffusive regime may enhance residence times and binding rates of nearby nanoparticles by up to 50 % and therefore might be of possible physiological significance for the uptake of targeted nanocarriers or viral particles by cell membranes via endocytosis.

Key words Stokes flow • anomalous diffusion • Brownian motion • Green's functions • singularity methods • boundary integral methods • membrane mechanics • elasticity theory • biological fluid dynamics • hydrodynamic mobility.

Zusammenfassung

Elastische Wände sind wichtige Komponenten im Kontext weicher Materie und bestimmen die Transporteigenschaften von Partikeln in Suspension unter Einfluss von Strömung. In dieser Arbeit präsentieren wir eine vollständig analytische Theorie der hydrodynamischen Wechselwirkungen und der Brownschen Bewegung von Nanopartikeln, die in eine Newtonsche Flüssigkeit eingebettet sind und sich in unmittelbarer Nähe zu einer realistisch modellierten elastischen Zellmembran bewegen. Die Membran ist verbunden mit dem vernetzten Zytoskelett der Zelle, das einen Widerstand gegen Scherdeformationenen bietet, und baut sich aus einer Lipiddoppelschicht auf, die einen Widerstand gegen Biegdeformationen bietet. Wir nehmen an, dass die die Partikel umgebende Flüssigkeit durch die linearen Stokes-Gleichungen beschrieben werden kann, wobei die viskosen Kräfte über die Trägheitskräfte dominieren. Diese Näherung ist angebracht aufgrund kleiner Geschwindigkeiten auf Skalen einzelner Zellen. Unsere analytischen Berechnungen basieren auf der Berechnung der Greenschen Funktionen, die das Strömungsfeld aufgrund einer Punktkraft-Singularität widerspiegeln, die in der Nähe der elastischen Membran wirkt. Wir berechnen dann die frequenzabhängigen Mobilitätsfunktionen, die die Kraft und das Drehmoment mit den Translations- und Rotationsgeschwindigkeiten der suspendierten Teilchen in Verbindung setzen. Daraufhin leiten wir analytische Ausdrücke des Diffusionstensors ab, die direkt aus den Mobilitätsfunktionen über das Fluktuationsdissipationstheorem erhalten werden können. Unser wichtigstes Ergebnis ist, dass die elastischen Eigenschaften der Membran einen Gedächtniseffekt im System induzieren, was zu einem langlebigen anomalen subdiffusiven Verhalten der nahe gelegenen Partikel führt.

Die Bestimmung der Greenschen Funktionen in Gegenwart einer elastischen Membran besteht darin, die allgemeine Lösung der Stokes-Gleichungen als Summe eines Bulk-Terms und eines Korrekturterms zu schreiben, der erforderlich ist, um die an der Membran auferlegten Regelmäßigkeits- und Randbedingungen zu erfüllen. Je nach Membrangeometrie verwenden wir drei sehr unterschiedliche analytische Ansätze: (a) zweidimensionale Fourier-Transformation für planare Membranen, (b) Fourier-Bessel-Integral für zylindrische Membranen und (c) Kugelflächenfunktionen für Membranen mit sphärischer Geometrie. Dementsprechend können die Greenschen Funktionen in Form von unendlichen Integralen über die Wellenzahl oder als konvergente unendliche Summen von Kugelflächenfunktionen

ausgedrückt werden. In Grenzfall einer verschwindenden Frequenz werden die Greenschen Funktionen identisch mit denen, die in der Nähe einer harten Wand mit Haftbedingung vorhergesagt werden.

Die exakt berechneten Greenschen Funktionen erlauben die Untersuchung des Einfluss der Membran auf die Bewegung von Partikeln, insbesondere wird die Berechnung von Eigen- und Paar-Mobilitätsfunktionen möglich. Diese sind für den Transport von Suspensionen in elastischen Gefäßen relevant. Analytische Ausdrücke für die Mobilitätsfunktionen können durch Berücksichtigung einer Verteilung von Punktkräften über die Teilchenoberfläche erhalten werden. Dennoch beschränken wir uns in den meisten Fällen auf die allgemein verwendete Punktpartikel-Näherung. Letztere repräsentiert die führende Ordnung der Entwicklung der Mobilitätsfunktion als Potenzreihe des Verhältnisses zwischen Partikelradius und Abstand von der Membran für die Eigen-Mobilitäten oder zwischen Partikelradius und Partikelabstand für die Paar-Mobilitäten. Wir zeigen, dass die Punktpartikel-Näherung, trotz ihrer Einfachheit überraschenderweise zu guter Übereinstimmung in den Mobilitätsfunktionen führt verglichen mit numerischen Simulationen von Partikeln mit endlichem Radius.

Die Berechnung der frequenzabhängigen Mobilitätsfunktionen liefert den Gedächtnisterm des Partikel-Membran-Systems und ermöglicht so die Untersuchung der Diffusionsbewegung von Brownschen Partikeln in der Nähe der elastischen Zellmembran über einen generalisierten Langevin-Formalismus. Eine vollständige Charakterisierung der Partikeldiffusion kann durchgeführt werden, indem die mittlere quadratische Verschiebung (MSD) berechnet wird, von der bekannt ist, dass sie im Bulk eine lineare Funktion der Zeit ist. In der Nähe einer elastischen Membran jedoch weist das MSD eine transiente anomale Subdiffusion auf, die auf intermediären Zeitskalen stattfindet und einen Skalierungsexponenten besitzt, der stark von der Distanz zur Membran abhängt. Das MSD im Grenzfall langer Zeiten zeigt ein normales lineares Verhalten und der Diffusionskoeffizient nimmt den nahe an einer harten Wand vorhergesagten Wert an. Unter Verwendung von physikalischen Parametern, die einer Membran eines roten Blutkörperchens entsprechen, finden wir, dass das Subdiffusionsregime die Verweilzeiten und Bindungsraten von nahe gelegenen Nanopartikeln bis zu 50 % erhöhen kann und daher eine mögliche physiologische Bedeutung für die Aufnahme von medizinisch verwendeten Nanopartikeln oder Viren durch Endozytose aufweist.

Schlüsselwörter Stokes-Strömung • anomale Diffusion • Brownsche Bewegung • Greensche Funktionen • Singularitätsmethoden • Randintegralmethoden • Membranmechanik • Elastizitätstheorie • biologische Fluiddynamik • hydrodynamische Mobilität.

Contents

Part I

Extended abstract

Chapter 1

Introduction

> We are here and now. Further than that, all knowledge is moonshine.
>
> Henry Louis Mencken

1.1 Motivation

Diffusion and hydrodynamic interactions between nanosized particles in soft matter systems is a long standing and established research topic. Over the last few decades, considerable effort has been devoted to the study of nanoparticle dynamics in blood flow [1–5] due to their importance and relevance in basic scientific research and potential biological and technological applications. Notable examples include drug delivery and chemotherapy via nanocarriers [6–9] which release the active agent in disease sites such as tumors or inflammation areas. During uptake by a living cell via endocytosis [10–12], nanoparticles often come into close vicinity of cell membranes which alter their motion in a complex fashion. Furthermore, nanoparticles play a key role in a variety of biological functions including cell division [13–16] and metabolism [17–19]. Due to their small size, the dynamics of nanoparticles is strongly affected by Brownian motion.

At small length and time scales of motion, an accurate description of fluid flows is achieved by the linear Stokes equations [20], where viscous forces are more important than inertial forces. In these conditions, a complete representation of the motion of a suspended particle is possible via the hydrodynamic mobility function, which bridges between the velocity moments of the particle and the moments of the force density on its surface. Particle motion in an unbounded medium is well understood and has been studied since a long time ago since the pioneering work of Stokes [21] who computed analytically the friction of fluids on the motion of pendulums. Nonetheless, particle motion in real situations often occurs in geometric confinements. When a small particle moves in close vicinity of an interface, the mobility is remarkably changed relative to its values in a bulk fluid. The effect of confining boundaries on nearby particles in a viscous fluid plays an important role in a variety of processes ranging from the rheology of colloidal suspensions [22–26] to the transport of nanoparticles and various molecules through nanochannels [27, 28].

1.2 State of the art

The first attempt to address the near-wall hindered mobility dates back to Lorentz [29] who used the image solution technique to compute the fluid motion resulting from a point-force acting nearby

an infinitely extended planar hard-wall. His solution method permits the determination of the particle mobility functions provided that the particle is at moderate distance from the wall. Analytical solutions that account for truly finite-sized particles have been later derived using bispherical coordinates [30–32]. The latter method has successfully been employed by Jeffery and coworkers to address the steady rotation of a solid of revolution [33] or the motion of two spheres in a viscous fluid [34]. The slow viscous translational motion of a sphere parallel to a planar wall has further been investigated using matched asymptotic expansions [35, 36], finding that the wall introduces a coupling between rotation and translation. Both the translational and rotational motions have later been reconsidered by Perkins & Jones who expressed the particle mobility in terms of a set of scalar functions that depend on the sphere radius and distance to a free [37] or rigid interface [38, 39]. Lorentz calculations have been extended to account for finite frequency of motion by Wakiya for the motion parallel to a hard-wall [40].

Under a uniform shear flow, near-wall particle dynamics has first been investigated using bipolar coordinates by Goldman [41] to derive exact solutions of the Stokes equations for the translational and rotational motions of a neutrally buoyant sphere. His solution is supplemented by a lubrication-theory-like approximation valid when the gap between the sphere and the wall is small, and by a method of reflection valid in the opposite case. Particle motion in shear flow past a plane wall has been later revisited using bipolar coordinates [42–44] and the image representation technique [45]. More recently, the hard-wall effect on the velocity autocorrelation function and long-time tails of Brownian motion has been studied by Felderhof [46, 47] and has recently been confirmed experimentally using optical traps [48]. The predicted long-time tails have been verified by direct inverse Fourier transform [49] and by a computational study using large-scale molecular dynamics simulations [50].

The influence of a second boundary on particle hydrodynamic mobility has also received researchers' attention since a long time ago. The most simple and intuitive approach is due to Oseen [51] who suggested that the particle mobility of a sphere confined between two rigid walls could conveniently be approximated by superposition of the leading-order terms from each single wall. A more rigorous approach has been adopted by Faxén [52, 53], who computed in his dissertation the particle mobility parallel to the walls for the special cases when the particle is in the mid-plane or the quarter-plane between the two hard-walls [20]. For an arbitrary position between the two walls, exact solutions for a point particle are obtained and expressed in terms of convergent series using the image technique for both incompressible [54, 55] and compressible flows [56–58]. For a truly extended particle, multipole expansions [59, 60] as well as joint analytical-numerical solutions have been presented for the motion perpendicular [61] and parallel [62] between two plane rigid boundaries. It has been found that the first-order reflexion theory proposed by Ho & Leal [63] provides reasonable agreement with their exact results only when the sphere is sufficiently far away from both walls. Further theoretical investigations have been carried out nearby two perpendicular walls [64] and for a sphere confined on the centerline of a rectangular channel [65].

During the past few decades, the field remarkably regained greater interest after the advent of experimental techniques which allow an accurate and reliable measurement of particle mobility nearby complex interfaces. Among the most efficient techniques that have been utilized are laser [66, 67] and optical tweezers [68–73], fluorescence [74, 75] and digital video microscopy [76–82], evanescent wave dynamic light scattering [83–96] and the three-dimensional total internal reflection velocimetry technique [97]. Calculations of the mobility functions have been extended to include particles nearby interfaces with partial slip [98–100], an interface separating two mutually immiscible liquids [101] or inside a liquid film between two incompressible fluids [102]. Explicit analytical expressions for the flow field induced by a point-force acting close to a fluid-fluid interface have been further obtained using the image solution technique [103]. For a truly extended particle, analytical solutions have been later proposed by Lee and coworkers using a generalization of the method of Lorentz [104] and bipolar coordinates [105]. The effect of small deformations of an initially flat fluid interface on the force and

torque experienced by a nearby translating and rotating sphere has also been considered [106, 107]. Additional works have been carried out nearby a viscous interface [108–110] or an interface covered with surfactant [111–113].

A great deal of attention has been also given to particle motion nearby curved boundaries such as cylindrical channels, due to their relevance as model systems for particle transport in tubular confinements and microfluidic devices [114–116]. In particular, the axial motion along the cylinder axis has been studied using the method of reflections by Wakiya [117], Bohlin [118] and Faxén [119], to name a few, expressing the mobility in power series of the ratio of particle to cylinder diameter. More recently, Zimmerman [120] presented a computer extended series approach for the determination of the drag force up the 21st order, thus complementing the singular perturbation solution known in the literature. These works have been extended to finite-sized spheres [121, 122] and non-spherical particles [123, 124]. For an arbitrarily positioned particle, the procedure has been generalized to yield expressions in terms of the particle and channel radius, and the eccentricity of the position of the particle, as derived *e.g.* in the works of Happel and collaborators [125–128] and Liron & Shahar [129]. The slow motion of two spherical particles symmetrically placed about the axis of a cylinder in the direction perpendicular to their line of centers has later been studied by Greenstein & Happel [130]. Experimental verification of these theoretical results has been performed *e.g.* by the use of laser interferometry by Lecoq *et al.* [131] where an excellent agreement has been found with the point-particle approximation. Digital video microscopy measurements by Cui *et al.* [76, 132] of the hydrodynamic coupling between Brownian colloidal particles diffusing along a linear channel revealed a sharply screened hydrodynamic interaction, resulting in a significant interaction only when the interparticle distance is relatively small. Theoretical developments have been supplemented by computer simulations of the resistance functions for spheres, bubbles and drops in cylindrical tubes [133–138]. Other works include the asymmetric motion perpendicular to the axis [139], finite length of the tube [140] and the flow around a line of equispaced spheres moving at a prescribed velocity along the axis of a circular tube [141]. Transient effects have also be taken into account in recent works by Felderhof, both in the case of an incompressible [142] and compressible fluid [143–145].

The rotational motion of a sphere inside a cylinder is of enormous importance in the theory of rotational viscometers [146–148] and in determining the power required for the agitation of viscous fluids [149, 150]. The symmetric slow rotation of a sphere inside an infinitely long hard cylinder has been first investigated by Haberman [151] and independently by Brenner & Sonshine [152], giving the hydrodynamic torque acting on the rotating sphere up to the 14th order in the ratio of particle to cylinder diameter. The rotation of an axially symmetric body of otherwise arbitrary shape within a circular cylinder of finite length has been theoretically investigated by Brenner [153] using the point couple approximation technique. The frictional force [154] and torque [155] exerted on a slowly rotating eccentrically positioned sphere within an infinitely long circular cylinder has been studied by Greenstein and coworkers, and later by Zheng *et al.* [156] who reviewed and corrected previous calculations. Complementary theoretical works have been conducted by Hirschfeld and coworkers [157, 158] to determine the first- and second-order wall effects upon the viscous asymmetric motion of an arbitrarily-shaped particle, arbitrarily positioned and oriented within a circular hard cylinder. Additionally, perturbative solutions for the rotation of eccentric spheres flowing in a cylindrical tube have been derived by Tözeren [159–161], finding a good agreement with the previous calculations. Further, modeling of hydrodynamic interactions involving a torus and circular cylinder using point singularities has been presented [162].

Considerable advances have been made into understanding the slow motion of particles of non-spherical shape, such as spheroids or rod-like particles due to their importance in the modeling of viruses or parasitic particles [163]. The first attempt to investigate the Brownian motion of an anisotropic particle dates back to Perrin [164, 165] who computed analytically the drag coefficients for a spheroid diffusing in a bulk fluid. A few decades later, Batchelor [166] pioneered the idea that

the flow field surrounding an elongated particle (often termed as a slender body), may appropriately be represented by a line distribution of point-force singularities along the line connecting the foci. The method has successfully been applied to a wide range of free-stream profiles and body shapes [167] and near boundaries such as a planar hard-wall [168–170] or a fluid-fluid interface [171]. Using the multipole expansion of the near-wall flow field, Lisicki *et al.* [172] have recently shown that to leading-order, the mobility of an arbitrary axisymmetric particle near a hard-wall can be expressed in closed form by combining the relevant Green's functions with the particle bulk mobility functions. They have shown that the mobility corrections scale as powers of inverse wall-particle distance and their angular structure can be expressed as simple polynomials in sines and cosines of the particle inclination angle to the wall. Direct numerical simulations of axisymmetric colloidal particles near a wall have been carried out using boundary integral methods [173], stochastic rotation dynamics [174, 175] and recently finite element methods [176]. Diffusion of micrometer-sized ellipsoidal particles has been experimentally investigated using digital video microscopy [177–179], elucidating the effects of coupling between rotational and translational motion. Experiments on actin filaments have been conducted using fluorescence imaging and particle tracking [180] finding that the measured diffusion coefficients can conveniently be accounted for by a correction resting on the hydrodynamic theory of a long cylinder confined between two walls. The confined Brownian rotational diffusion coefficients of carbon nanotubes have been measured using fluorescence video microscopy [181] and optical microscopy [182], where a reasonable agreement has been reported with theoretical predictions. Using light scattering measurements, the translational and rotational diffusion constants of TMV, a simple rod-shaped helical virus, have been determined [183] based on previous theoretical treatment by Pecora [184]. Additionally, the three-dimensional rotational diffusion of nanorods [185] and rod-like colloids have been measured using video [186] and confocal microscopy [187].

Despite enormous and extensive studies on particle motion nearby solid or fluid boundaries, only little is known about the influence of elastic interfaces on the dynamics of nearby particles. Hitherto, particle motion nearby a planar membrane endowed with surface tension [188, 189], bending resistance [190] or membrane elasticity [191, 192] has been theoretically studied. Further theoretical investigations near elastic interfaces have been carried out via thin-film soft lubrication theory [193–195]. Experimentally, particle motion nearby elastic cell membranes has been investigated using optical traps [196–199], magnetic particle actuation [200] and quasi-elastic light scattering [201–203], where a significant decrease in the mobility normal to the cell membrane has been observed in line with theoretical predictions. Setting a particle nearby a cell membrane has been further used in interfacial microrheological experiments as an efficient and often accurate way to extract membrane unknown moduli [198, 204].

1.3 Thesis contribution

The present thesis is a further contribution to the works that have been carried out in this field and is devoted to the theoretical and numerical modeling of particle motion nearby a realistically modeled elastic membrane simultaneously endowed with both shearing and bending rigidities [205–209], such as a red blood cell (RBC) membrane. Unlike fluid-solid or fluid-fluid interfaces, elastic membranes stand apart as they endow the system with memory. Accordingly, particle motion depends strongly on its prior history and diffusional dynamics is treated within a generalized Langevin formalism non-local in time. This behavior implies the emergence of a transient anomalous subdiffusive regime induced by the elastic nature of the membrane. Moreover, the membrane undergoes deformation in both in-plane and out-of-plane directions in response to the imbalance of the stress tensor at the interface between the fluids on both sides. As a result, a reflected backflow is created as the membrane relaxes back to its undeformed state, altering the motion of the particle in a complex fashion. Our calculations have been extended nearby cylindrical [210, 211] and spherical membranes [212, 213]

and inside a spherical elastic cavity [214], finding that the shearing effect plays a more significant role than bending. Our analytical predictions have favorably been compared with fully resolved boundary integral simulations where a very good agreement is obtained.

1.4 Thesis outline

The reminder of the first part of this cumulative thesis is composed of six chapters and is meant to be an introduction for the publications appended in the second part. In chapter 2, we introduce a physical model system for biological cell membranes and discuss their mechanical behavior, in particular their resistance towards shearing and bending. Additionally, we outline the main derivation steps of the traction jump equations across an elastic membrane undergoing elastic deformation due to an external load. In chapter 3, we provide the reader with a broad overview on the computation of the Green's functions, which represent the solution of the governing equations of fluid motion due to a point force acting nearby an elastic membrane of various geometries. For that, we first introduce the two-dimensional (2D) Fourier transform technique we employe to find analytical expressions of the Green's functions nearby an infinitely extended planar elastic membrane. We then present the Fourier-Bessel integral technique which is well suited for membranes with cylindrical geometry and the spherical harmonics technique which is found to be appropriate for spherical membranes. We then define in chapter 4 the particle hydrodynamic mobility functions and present an analytical method for their determination from the Green's functions by combining the multipole expansion and Faxén's theorem. In chapter 5, we introduce the multipole method and show how the leading-order mobility of an axisymmetric particle nearby an interface can be determined from the knowledge of the system Green's functions and particle bulk mobilities. We then investigate in chapter 6 the diffusional motion of a Brownian particle nearby a cell membrane and examine the mean-square displacement for diffusion parallel or perpendicular to a planar membrane. Finally, we present in chapter 7 the boundary integral method (BIM) we use to assess the accuracy and appropriateness of our theoretical predictions. The appendix includes further technical details regarding the 2D Fourier transform, relevant for the computation of the Green's functions nearby planar membranes. The second part includes the publications related to this thesis.

Chapter 2

Membrane model

> If the facts don't fit the theory, change the facts.
>
> Albert Einstein

2.1 Overview

The basic biological function of membranes is to protect the cell from its surroundings and regulate diffusion of proteins, ions and other molecules across the cell. The red blood cell membranes consist of a lipid bilayer with embedded proteins providing the membrane a resistance towards bending. The lipid bilayer is made of two layers of lipid molecules and are usually composed of a hydrophilic phosphate head and a hydrohobic tail (see Fig. 2.1 for a cartoon representation of a lipid bilyer.) The packing of lipid molecules within the bilayer affects the cell mechanical properties including its resistance towards shearing and bending. The resistance against bending is described following the celebrated Helfrich model [224] and is characterized by the bending modulus κ_{B} and the Gaussian curvature modulus κ_{K} [225].

Additionally, RBC membranes are endowed with cross-linked cytoskeleton networks that provide the mechanical flexibility required to cope with the shear stresses encountered during cell motion in the microcirculation. The networks can exhibit highly nonlinear elasticity and their physical treatment goes beyond linear elasticity theory. The membrane elasticity is commonly described by the well-established Skalak model [216] which incorporates into a single strain energy functional both the resistance towards shearing and area conservation. Accordingly, the Skalak model is characterized by a shear modulus κ_{S} and an area dilatation (extension) modulus κ_{A} [217–221]. The latter is typically very large compared to κ_{S} to mimic membrane area incompressibility. Other elastic models have been further proposed in the literature including the neo-Hookean model [222] and the zero-thickness shell model [223], both of which are characterized by a unique shear modulus κ_{S}.

In the following, we shall introduce a parametrization for the membrane and determine analytical expressions of the traction jump equations across a membrane possessing shearing and bending rigidities.

2.2 Membrane parametrization

Here we show how to derive analytically the traction jump equations across an elastic membrane endowed with shearing and bending resistances. For this, we shall recall and employ some basic

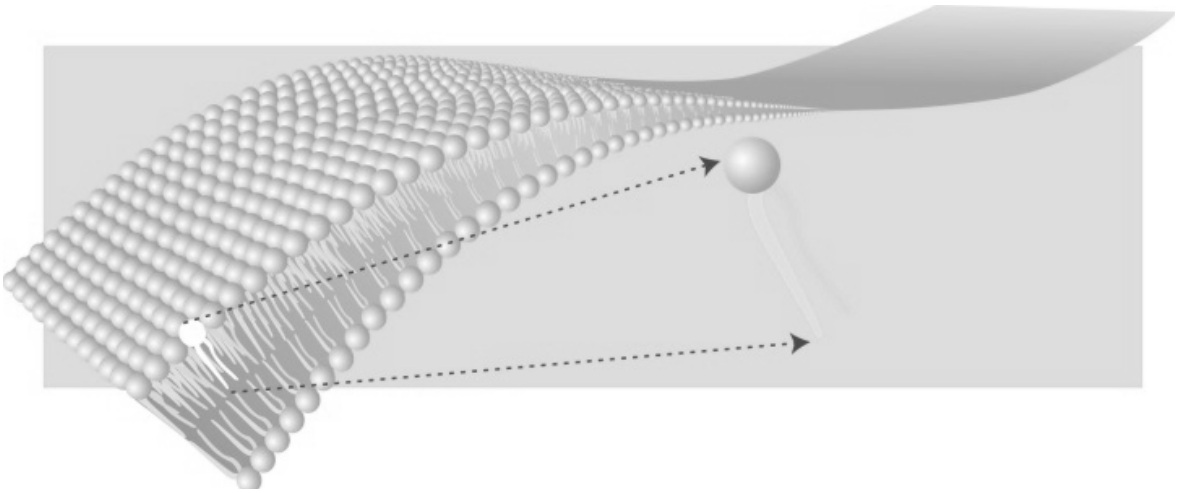

Figure 2.1: An elastic membrane consisting of the lipid bilayer. Illustration taken from the paper by Peletier and Röger [215].

concepts of differential geometry [226] in order to describe the surface of a membrane undergoing small deformation. We adopt a local coordinate system $\{\theta^1, \theta^2\}$ for the undeformed membrane surface and describe a mapping that assigns each pair (θ^1, θ^2) to the position vector $\boldsymbol{A}$ defined in the Cartesian coordinate system as [227]

$$\boldsymbol{A}(\theta^1, \theta^2) = A_x \boldsymbol{e}_x + A_y \boldsymbol{e}_y + A_z \boldsymbol{e}_z \,, \tag{2.1}$$

where A_x, A_y and A_z are functions of θ^1 and θ^2.

After deformation, the position vector reads

$$\boldsymbol{a}(\theta^1, \theta^2) = (A_x + u_x)\boldsymbol{e}_x + (A_y + u_y)\boldsymbol{e}_y + (A_z + u_z)\boldsymbol{e}_z \,, \tag{2.2}$$

where u_x, u_y and u_z are the Cartesian components of the displacement vector which are all functions of θ^1 and θ^2. Hereafter, we shall use capital roman letters for the undeformed state and small roman letters for the deformed. The membrane can be defined by the covariant base vectors

$$\boldsymbol{g}_\alpha := \frac{\partial \boldsymbol{a}}{\partial \theta^\alpha} \,, \qquad \alpha \in \{1, 2\} \,, \tag{2.3}$$

which are tangent to the membrane surface but not generally perpendicular to each other. We now complete the basis by defining the unit normal vector $\boldsymbol{n}$ as

$$\boldsymbol{n} = \frac{\boldsymbol{g}_1 \times \boldsymbol{g}_2}{|\boldsymbol{g}_1 \times \boldsymbol{g}_2|} \,. \tag{2.4}$$

The covariant components of the metric tensor are defined in the usual way by the scalar product $g_{\alpha\beta} = \boldsymbol{g}_\alpha \cdot \boldsymbol{g}_\beta$. The contravariant tensor $g^{\alpha\beta}$ is the inverse of the metric tensor and satisfies the identity

$$g_{\alpha\beta} g^{\beta\gamma} = \delta_\alpha^\gamma \,, \tag{2.5}$$

where δ_α^γ is the delta Kronecker tensor. Here Einstein's summation convention over repeated indices is used. Clearly, both the covariant and contravariant tensors are symmetric by construction. The corresponding tensors in the undeformed state $G_{\alpha\beta}$ and $G^{\alpha\beta}$ can immediately be obtained by considering vanishing displacements in $g_{\alpha\beta}$ and $g^{\alpha\beta}$, respectively. In what follows, we shall derive a

linearized form of the underlying equilibrium equations for a membrane under load conditions.

2.3 Shearing and bending

Depending on the biological composition of the cell, the membrane may exhibit a resistance towards shearing and/or bending. In this section, we shall consider first an idealized membrane with pure shearing resistance such as that of an artificial elastic capsule designed for drug delivery. We then consider the situation where the membrane resists only towards bending as it is the case for a fluid vesicle. Finally, we show how to derive the traction jump equations when the membrane is endowed simultaneously with both shearing and bending rigidities.

2.3.1 Shearing

Here we derive the traction jump equations across a membrane endowed with an in-plane shearing resistance. We introduce the transformation gradient as [228]

$$\mathrm{d}a_\alpha = F_{\alpha\beta}\,\mathrm{d}A_\beta\,, \tag{2.6}$$

bridging between the infinitesimal displacements in the deformed and undeformed spaces. From Eq. (2.3), it can clearly be seen that $\mathrm{d}\boldsymbol{a} = \boldsymbol{g}_\alpha\,\mathrm{d}\theta^\alpha$ and that $\mathrm{d}\boldsymbol{A} = \boldsymbol{G}_\alpha\,\mathrm{d}\theta^\alpha$, leading to an expression of the transformation gradient tensor as a dyadic product such that $\boldsymbol{F} = \boldsymbol{g}_\alpha \otimes \boldsymbol{G}^\alpha$.

We now define the right Cauchy-Green deformation tensor $C_{\alpha\beta} = F_{\gamma\alpha}F_{\gamma\beta}$ whose invariants are given by Green and Adkins as [229, 230]

$$I_1 = G^{\alpha\beta}g_{\alpha\beta} - 2\,, \tag{2.7a}$$

$$I_2 = \det G^{\alpha\beta}\det g_{\alpha\beta} - 1\,. \tag{2.7b}$$

Provided knowledge of the membrane constitutive law, the contravariant components of the stress tensor $\tau^{\alpha\beta}$ can readily be obtained from [218]

$$\tau^{\alpha\beta} = \frac{2}{J_\mathrm{S}}\frac{\partial W}{\partial I_1}\,G^{\alpha\beta} + 2J_\mathrm{S}\,\frac{\partial W}{\partial I_2}\,g^{\alpha\beta}\,, \tag{2.8}$$

wherein W is the areal strain energy functional and $J_\mathrm{S} := \sqrt{1+I_2}$ is the Jacobian determinant, representing the ratio between the deformed and undeformed local surface areas. As already pointed out, various models have been proposed in the literature to describe the elastic properties of cell membranes. The most simple and popular one is the neo-Hookean (NH) model whose areal strain energy reads [218]

$$W^\mathrm{NH}(I_1, I_2) = \frac{\kappa_\mathrm{S}}{6}\left(I_1 - 1 + \frac{1}{1+I_2}\right)\,. \tag{2.9}$$

There exists another formulation which is equivalent to the neo-Hookean model in the small deformation limit, known as the zero-thickness shell formulation, employed by Ramanujan and Pozrikidis (RP), in which the areal strain energy is given by [223]

$$W^\mathrm{RP} = \frac{\kappa_\mathrm{S}}{6}\left(I_1 - \ln(I_2+1) + \frac{1}{2}\ln^2(I_2+1)\right)\,. \tag{2.10}$$

The Skalak model [216] is more commonly used for RBC membranes because it explicitly includes the local area-incompressibility constraint into the model. The corresponding areal strain energy

reads [219]

$$W^{\mathrm{SK}} = \frac{\kappa_{\mathrm{S}}}{12}\left((I_1^2 + 2I_1 - 2I_2) + CI_2^2\right)\,, \tag{2.11}$$

where $C := \kappa_{\mathrm{A}}/\kappa_{\mathrm{S}}$ is the Skalak parameter. For $C = 1$, the Skalak model predicts for small deformations the same behavior as the Neo-Hookean or the thin-shell formulation [218].

Having introduced the stress tensor resulting from membrane deformation, we now write the equilibrium equations balancing between the membrane elastic forces and external load as

$$\nabla_\alpha \tau^{\alpha\beta} + \Delta f^\beta = 0\,, \tag{2.12a}$$

$$\tau^{\alpha\beta} b_{\alpha\beta} + \Delta f^n = 0\,, \tag{2.12b}$$

where $\Delta \boldsymbol{f} = \Delta f^\beta \boldsymbol{g}_\beta + \Delta f^n \boldsymbol{n}$ is the traction jump vector across the membrane. Here ∇_α stands for the covariant derivative, which for a second-rank tensor is defined as

$$\nabla_\alpha \tau^{\alpha\beta} = \tau^{\alpha\beta}_{,\alpha} + \Gamma^\alpha_{\alpha\eta}\tau^{\eta\beta} + \Gamma^\beta_{\alpha\eta}\tau^{\alpha\eta}\,, \tag{2.13}$$

where $\Gamma^\lambda_{\alpha\beta}$ are the Christoffel symbols of the second kind which read [231]

$$\Gamma^\lambda_{\alpha\beta} = \frac{1}{2} g^{\lambda\eta}\left(g_{\alpha\eta,\beta} + g_{\eta\beta,\alpha} - g_{\alpha\beta,\eta}\right)\,. \tag{2.14}$$

Moreover, $b_{\alpha\beta}$ is the curvature (second fundamental form) tensor defined by

$$b_{\alpha\beta} = \frac{\partial \boldsymbol{g}_\alpha}{\partial \theta^\beta} \cdot \boldsymbol{n} = -\boldsymbol{g}_\alpha \cdot \frac{\partial \boldsymbol{n}}{\partial \theta^\beta}\,. \tag{2.15}$$

In the following, we shall derive the equilibrium equations for a membrane that exhibits a pure resistance towards bending.

2.3.2 Bending

According to the Helfrich model, the bending energy is described by a quadratic curvature-elastic continuum model as

$$E_{\mathrm{B}} = \int_S 2\kappa_{\mathrm{B}}\left(H - H_0\right)^2 \,\mathrm{d}S + \int_S \kappa_{\mathrm{K}} K \,\mathrm{d}S\,, \tag{2.16}$$

where H is the mean curvature defined as the average of the principal curvatures κ_1 and κ_2, and K is the Gaussian curvature, defined as the product of κ_1 and κ_2. Here H_0 is the spontaneous curvature for which we consistently take the initial undisturbed shape throughout this thesis. For an excellent overview of the Helfrich model and its actual numerical implementation, we refer the acknowledgeable reader to a recent review article by Guckenberger and Gekle [232].

The traction jump equations across a membrane endowed with a resistance towards bending can readily be obtained via a variational approach by minimizing the sum of the bending and external potential energy to obtain

$$\Delta \boldsymbol{f} = -2\kappa_{\mathrm{B}}\left(2(H^2 - K + H_0 H) + \Delta_{\parallel}\right)\left(H - H_0\right)\boldsymbol{n}\,, \tag{2.17}$$

and it is commonly denominated the Euler-Lagrange equation [233–236]. The mean and Gaussian curvatures are respectively expressed by

$$H = \frac{1}{2}\, b^\alpha_\alpha\,, \qquad K = \det\, b^\beta_\alpha\,, \tag{2.18}$$

with b_α^β being the mixed version of the curvature tensor related to the covariant representation of the curvature tensor by $b_\alpha^\beta = b_{\alpha\delta} g^{\delta\beta}$. Continuing, $\Delta_\parallel$ denotes the Laplace-Beltrami operator defined for a given scalar function $\phi(\theta^1, \theta^2)$ as [227]

$$\Delta_\parallel \phi = \frac{1}{\sqrt{g}} \frac{\partial}{\partial \theta^\alpha} \left(\sqrt{g} g^{\alpha\beta} \frac{\partial \phi}{\partial \theta^\beta} \right) , \tag{2.19}$$

wherein g is the determinant of the metric tensor. Interestingly, bending as derived from the Helfrich model does not introduce a jump in the tangential traction [237].

It is worth mentioning that bending stresses are sometimes computed by assuming a linear isotropic model for the bending moments. Accordingly, the membrane bending moment is related to the curvature tensor via the linear relation [238, 239]

$$M_\alpha^\beta = -\kappa_\mathrm{B} \left(b_\alpha^\beta - B_\alpha^\beta \right) . \tag{2.20}$$

The contravariant components of the transverse shearing vector $\boldsymbol{Q}$ can then be obtained from a local torque balance with the applied moment as $Q^\beta = \nabla_\alpha M^{\alpha\beta}$. We note that the raising and lowering indices operations imply that $M^{\alpha\beta} = M_{\gamma\alpha} g^{\gamma\beta}$. In this way, the equilibrium equations read

$$\nabla_\alpha N^{\alpha\beta} - b_\alpha^\beta Q^\alpha + \Delta f^\beta = 0 , \tag{2.21a}$$

$$N^{\alpha\beta} b_{\alpha\beta} + \nabla_\alpha Q^\alpha + \Delta f^n = 0 , \tag{2.21b}$$

where for a first-rank tensor the covariant derivative is defined as $\nabla_\beta Q^\alpha = \partial_\beta Q^\alpha + \Gamma^\alpha_{\beta\delta} Q^\delta$. Moreover, $N^{\alpha\beta}$ is the in-plane tension tensor determined from a local torque balance and expressed by [232]

$$N^{\alpha\beta} = \frac{1}{2} \kappa_\mathrm{B} B_\gamma^\mu b_{\lambda\mu} \left(g^{\alpha\lambda} g^{\gamma\beta} - g^{\alpha\gamma} g^{\lambda\beta} \right) . \tag{2.22}$$

For a membrane endowed simultaneously with both shearing and bending rigidities, the resulting traction jump equations are obtained by linear superposition of the traction jump due to pure shearing and pure bending as stated by Eqs. (2.12) and (2.21), respectively. Under flow conditions, the elastic stresses are balanced by a jump in the fluid stress tensor across the membrane and the underlying equilibrium equations serve as boundary conditions for the computation of the Green's functions as explained in more details in the next chapter.

Chapter 3

Green's functions

> Science may set limits to knowledge, but should not set limits to imagination.
>
> Bertrand Russell

In the context of linear hydrodynamics, the Green's functions are the solutions of the Stokes equations subject to a point-force acting on the fluid. The solution for an arbitrarily force distribution can readily be determined through the superposition principle thanks to the linearity of the equations governing the fluid motion. We define the flow Reynolds number Re, representing the ratio of inertial forces to viscous forces as

$$\mathrm{Re} = \frac{UL}{\nu}\,, \tag{3.1}$$

where L and U are respectively characteristic length and velocity of the flow, and ν is the fluid kinematic viscosity, defined as the ratio between dynamic viscosity η and density ρ. Throughout this thesis, our theoretical developments are valid in the limit of small Reynolds number where viscous effects dominate. Accordingly, the distance traveled by suspended particles is assumed to be very short on the characteristic time scale associated with vorticity diffusion.

In this chapter, we shall be interested in finding analytical solutions of the steady Stokes equations governing the dynamics of an incompressible viscous flow [240],

$$\eta\boldsymbol{\nabla}^2\boldsymbol{v}(\boldsymbol{r}) - \boldsymbol{\nabla}p(\boldsymbol{r}) + \boldsymbol{f}(\boldsymbol{r}) = 0\,, \tag{3.2}$$

$$\boldsymbol{\nabla}\cdot\boldsymbol{v}(\boldsymbol{r}) = 0\,, \tag{3.3}$$

in the presence of nearby elastic confinements. Here $\boldsymbol{v}$ denotes the fluid velocity, p is the pressure field and $\boldsymbol{f}$ is an arbitrary time-dependent force density exerted on the fluid by an immersed particle. We first consider the point-particle approximation in which we only take the monopole force moment into account such that $\boldsymbol{f}(\boldsymbol{r}) = \boldsymbol{F}\,\delta(\boldsymbol{r}-\boldsymbol{r}_0)$, where $\boldsymbol{r}_0$ is the particle position. For an infinite medium, the solution for the velocity field is known as the Oseen tensor [51].

Depending on the membrane geometry, we shall employ three very different analytical approaches. First, we begin with the simplistic situation where the membrane is planar and infinitely extended along the horizontal plane. In this case, the Green's functions can readily be found using a 2D Fourier transform technique. Second, we describe the Fourier-Bessel Integral technique which is found to be convenient for solving the fluid motion equations in domains bounded by a cylindrical geometry. Third, we present the spherical harmonics technique based on the idea of expanding the velocity field and pressure in terms of spherical harmonics centered at the origin. The latter method is perfectly suited for searching for solutions of the Stokes equations in the presence of a spherical boundary.

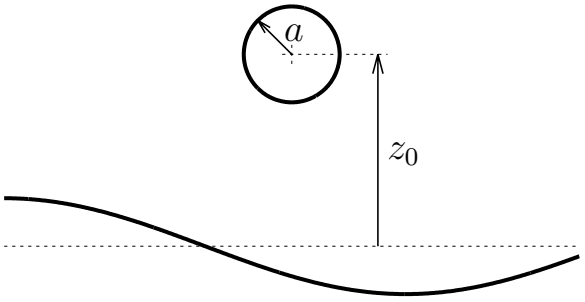

Figure 3.1: Illustration of particle motion nearby an elastic membrane. The membrane is extended in the xy plane and the solid particle of radius a is located at $z = z_0$.

3.1 Fourier transform technique

As already pointed out, the equations governing the fluid motion nearby planar interfaces are more conveniently solved using a 2D Fourier transform technique. The latter consists of transforming the partial differential equations (3.2) and (3.3) governing the fluid motion into ordinary differential equations for the out-of-plane coordinate z, whereas the dependence on the in-plane coordinates x and y are Fourier transformed into wavevector components q_x and q_y.

The Fourier transform technique can also be applied for the determination of the Green's functions in systems composed with two or more parallel interfaces. Nevertheless, although the method is perfectly suited for planar geometries, it can unfortunately not be applied for general shapes. In what follows, we shall provide some technical details regarding this analytical method.

3.1.1 Formulation

The fluid motion is described by the steady Stokes equations stated by Eqs. (3.2) and (3.3). We assume that the point-force $\boldsymbol{F}$ is acting at the position $\boldsymbol{r}_0 = (0, 0, z_0)$ with $z_0 > 0$, above an elastic membrane infinitely extended in the xy plane (see Fig. 3.1 for an illustration of the system setup.) Without loss of generality, we assume that the fluid has the same and constant properties everywhere.

We define the spacial 2D (forward) Fourier transform

$$\mathscr{F}\{f(\boldsymbol{\rho})\} = \tilde{f}(\boldsymbol{q}) = \int_{\mathbb{R}^2} f(\boldsymbol{\rho}) e^{-i\boldsymbol{q}\cdot\boldsymbol{\rho}} \,\mathrm{d}^2\boldsymbol{\rho}\,, \tag{3.4}$$

together with its inverse transform

$$\mathscr{F}^{-1}\{\tilde{f}(\boldsymbol{q})\} = f(\boldsymbol{\rho}) = \frac{1}{(2\pi)^2} \int_{\mathbb{R}^2} \tilde{f}(\boldsymbol{q}) e^{i\boldsymbol{q}\cdot\boldsymbol{\rho}} \,\mathrm{d}^2\boldsymbol{q}\,, \tag{3.5}$$

where $\boldsymbol{\rho} = (x, y)$ is the projection of the position vector $\boldsymbol{r}$ onto the horizontal plane, and $\boldsymbol{q} = (q_x, q_y)$ is the Fourier transform variable. It turns out to be convenient to use the orthogonal coordinate system previously introduced by Bickel [188, 190] in which all the vector fields are decomposed into longitudinal, transverse and normal components. For a given Fourier transformed quantity $\tilde{\boldsymbol{A}}$, whose

horizontal components in the Cartesian coordinate basis are $(\tilde{A}_x, \tilde{A}_y)$, its components in the new orthogonal base are given by the following orthogonal transformation

$$\begin{pmatrix} \tilde{A}_x \\ \tilde{A}_y \end{pmatrix} = \frac{1}{q} \begin{pmatrix} q_x & q_y \\ q_y & -q_x \end{pmatrix} \begin{pmatrix} \tilde{A}_l \\ \tilde{A}_t \end{pmatrix}, \tag{3.6}$$

where $\tilde{A}_l$ and $\tilde{A}_t$ refer to the longitudinal and transverse components, respectively, and $q := |\boldsymbol{q}|$ is the wavenumber. Clearly, the normal component $\tilde{A}_z$ is left unchanged by this transformation. Note that the inverse transformation is also given by the same transformation matrix in Eq. (3.6).

As the membrane shape depends on the history of particle motion, we shall perform additionally a Fourier analysis in time. For a function $f(t)$ living in the real space, its (forward) Fourier transform to the frequency domain is defined as

$$f(\omega) = \int_{\mathbb{R}} f(t) e^{-i\omega t} \, \mathrm{d}t \,, \tag{3.7}$$

and the inverse Fourier transform back to the real space reads

$$f(t) = \frac{1}{2\pi} \int_{\mathbb{R}} f(\omega) e^{i\omega t} \, \mathrm{d}\omega \,. \tag{3.8}$$

Since both the spatial and temporal Fourier transforms are performed here, we shall use the convention where the two functions $f(t)$ and $f(\omega)$ are distinguished only by their argument. The tilde will therefore be reserved for the spatial 2D Fourier transform.

The steady Stokes equations (3.2) and (3.3) upon 2D Fourier transform result in the following ordinary differential equations with the variable z,

$$\eta(-q^2 \tilde{v}_l + \tilde{v}_{l,zz}) - iq\tilde{p} + F_l \, \delta(z - z_0) = 0 \,, \tag{3.9}$$

$$\eta(-q^2 \tilde{v}_t + \tilde{v}_{t,zz}) + F_t \, \delta(z - z_0) = 0 \,, \tag{3.10}$$

$$\eta(-q^2 \tilde{v}_z + \tilde{v}_{z,zz}) - \tilde{p}_{,z} + F_z \, \delta(z - z_0) = 0 \,, \tag{3.11}$$

$$iq\tilde{v}_l + \tilde{v}_{z,z} = 0 \,, \tag{3.12}$$

obtained after making use of the transformation equations (3.6). The transverse component $\tilde{v}_t$ is therefore separated out and can directly be obtained by solving Eq. (3.10). Moreover, the pressure in Eq. (3.9) can readily be eliminated using Eq. (3.11). Since the continuity equation (3.12) gives a direct relation between the components $\tilde{v}_l$ and $\tilde{v_z}$, a fourth-order differential equation for the normal velocity $\tilde{v}_z$ is obtained as

$$\tilde{v}_{z,zzzz} - 2q^2 \tilde{v}_{z,zz} + q^4 \tilde{v}_z = \frac{q^2}{\eta} F_z \, \delta(z - z_0) + \frac{iq}{\eta} F_l \, \delta'(z - z_0) \,, \tag{3.13}$$

where δ' is the derivative of the delta Dirac function, satisfying the property $x\delta'(x) = -\delta(x)$, for $x \in \mathbb{R}$. The components of the Green tensor in Fourier space are defined as

$$\begin{pmatrix} \tilde{v}_z \\ \tilde{v}_l \\ \tilde{v}_t \end{pmatrix} = \begin{pmatrix} \tilde{\mathcal{G}}_{zz} & \tilde{\mathcal{G}}_{zl} & 0 \\ \tilde{\mathcal{G}}_{lz} & \tilde{\mathcal{G}}_{ll} & 0 \\ 0 & 0 & \tilde{\mathcal{G}}_{tt} \end{pmatrix} \begin{pmatrix} F_z \\ F_l \\ F_t \end{pmatrix} . \tag{3.14}$$

Having introduced the governing equations of fluid motion, the Green's functions in the presence of a planar elastic membrane can therefore be determined by applying the relevant boundary conditions. At the undisplaced membrane, we require the natural continuity of the velocity components and the

discontinuity of the fluid stress tensor due to membrane shearing and bending, previously derived in chapter 2. The Green's functions serve then as a direct input for the computation of the particle hydrodynamic mobilities as it will be detailed in chapter 4.

We further define the characteristic frequency for shearing and bending as

$$\beta := \frac{6z_0\eta B\omega}{\kappa_{\mathrm{S}}}\,, \qquad \beta_{\mathrm{B}} := 2z_0\left(\frac{4\eta\omega}{\kappa_{\mathrm{B}}}\right)^{1/3}\,, \tag{3.15}$$

with $B := 2/(1+C)$ for the Skalak model and $B = 1$ otherwise[1]. Moreover, we define the reduced bending modulus, quantifying the coupling between shearing and bending as $E_{\mathrm{B}} := \kappa_{\mathrm{B}}/(\kappa_{\mathrm{S}} z_0^2)$.

In the vanishing frequency limit, or equivalently for infinite membrane shearing and bending rigidities, the Green tensor nearby a hard-wall is recovered [241]

$$\boldsymbol{\mathcal{G}}^{\mathrm{B}}(\boldsymbol{r}) = \boldsymbol{\mathcal{G}}^{(0)}(\boldsymbol{r}_{\mathrm{rel}}) - \boldsymbol{\mathcal{G}}^{(0)}(\boldsymbol{R}) + \boldsymbol{\mathcal{G}}^{\mathrm{D}}(\boldsymbol{R}) - \boldsymbol{\mathcal{G}}^{\mathrm{SD}}(\boldsymbol{R})\,, \tag{3.16}$$

and it is commonly denominated the Blake tensor [242]. Here $\boldsymbol{r}_{\mathrm{rel}} := \boldsymbol{r} - \boldsymbol{r}_0$ and $\boldsymbol{R} := \boldsymbol{r} - \overline{\boldsymbol{r}_0}$ with $\overline{\boldsymbol{r}_0} = (0,0,-z_0)$ being the position of the Stokeslet image. Furthermore, $r := |\boldsymbol{r}|$ and $R := |\boldsymbol{R}|$. The infinite space Green's function (Oseen tensor) $\boldsymbol{\mathcal{G}}^{(0)}$, the Stokes doublet $\boldsymbol{\mathcal{G}}^{\mathrm{D}}$ and the source doublet $\boldsymbol{\mathcal{G}}^{\mathrm{SD}}$ are given by

$$\mathcal{G}^{(0)}_{\alpha\beta}(\boldsymbol{r}) = \frac{1}{8\pi\eta}\left(\frac{\delta_{\alpha\beta}}{r} + \frac{r_\alpha r_\beta}{r^3}\right)\,, \tag{3.17}$$

$$\mathcal{G}^{\mathrm{D}}_{\alpha\beta}(\boldsymbol{R}) = \frac{2z_0^2(1-2\delta_{\beta z})}{8\pi\eta}\left(\frac{\delta_{\alpha\beta}}{R^3} - \frac{3R_\alpha R_\beta}{R^5}\right)\,, \tag{3.18}$$

$$\mathcal{G}^{\mathrm{SD}}_{\alpha\beta}(\boldsymbol{R}) = \frac{2z_0(1-2\delta_{\beta z})}{8\pi\eta}\left(\frac{\delta_{\alpha\beta}R_z}{R^3} - \frac{\delta_{\alpha z}R_\beta}{R^3} + \frac{\delta_{\beta z}R_\alpha}{R^3} - \frac{3R_\alpha R_\beta R_z}{R^5}\right)\,. \tag{3.19}$$

It is worth noting that nearby a single membrane, shearing and bending present a decoupled nature. Therefore, the Green's functions nearby a membrane endowed simultaneously with both shearing and bending rigidities can appropriately be determined by linear superposition of the Green's functions associated with membranes with pure shearing and pure bending as obtained independently. This interesting feature is however not observed nearby two parallel elastic membranes [Pub2] where shearing and bending present a coupling behavior. Further details have been discussed in our publications for the Green's functions nearby a single [Pub1] or two [Pub2] planar elastic membranes.

In the following, we shall introduce the Fourier-Bessel integral technique which we have employed for the determination of the Green's functions associated with a point-force acting at the centerline of an elastic cylinder whose membrane exhibits a resistance towards shearing and bending.

3.2 Fourier-Bessel integral technique

Many biological and industrial processes occur in cylindrical confinements where they play a key role in determining the diffusional dynamics of suspended particles. In this section, we compute the Green's functions associated with a point-force acting at the centerline of a cylindrical elastic tube of initial (undeformed) radius R. The tube membrane exhibits resistance against shearing and bending. We choose the cylindrical coordinate system (r, ϕ, z) where the z coordinate is directed along the cylinder axis with the origin located at the center of a particle whose radius is $a \ll R$. We label the flow properties inside and outside the cylinder 1 and 2, respectively.

[1] As already pointed out in chapter 2, the neo-Hookean model and the zero-thickness shell formulation model are equivalent to the Skalak model when $C = 1$ for small deformation.

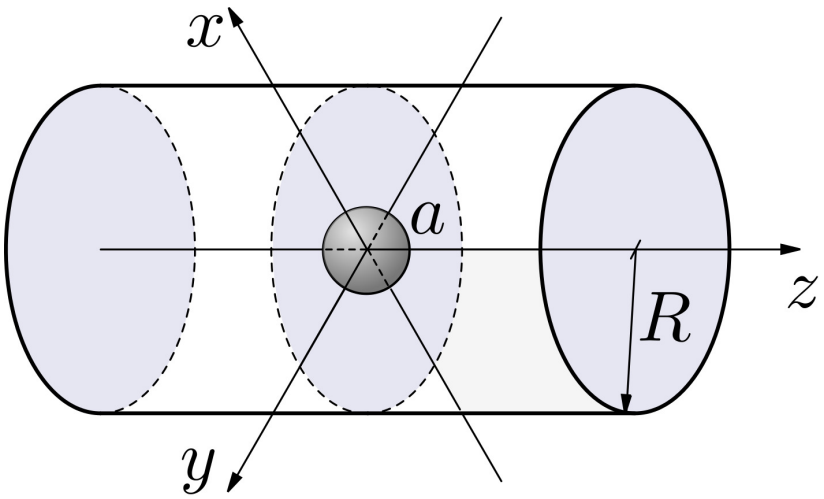

Figure 3.2: Illustration of the system setup. A small spherical solid particle of radius a located at the origin moving on the centerline of a deformable elastic tube of radius R.

We proceed by computing the Green's functions which are solutions of the forced Stokes equations (3.2) and (3.3) inside the tube (for $r < R$) and the homogeneous (force free) Stokes equations outside (for $r > R$). We therefore need to solve the governing equations for a point-force $\boldsymbol{F}$ acting at the origin and subject to the regularity conditions

$$|\boldsymbol{v}_1| < \infty \ \text{ for } |\boldsymbol{r}| = 0\,, \tag{3.20}$$

$$\boldsymbol{v}_1 \to \boldsymbol{0} \ \text{ for } z \to \infty\,, \tag{3.21}$$

$$\boldsymbol{v}_2 \to \boldsymbol{0} \ \text{ for } |\boldsymbol{r}| \to \infty\,, \tag{3.22}$$

together with the boundary conditions stemming from shearing and bending which are imposed at the membrane.

We begin by expressing the solution of Eqs. (3.2) inside the cylinder as a sum of a point-force flow field and the flow reflected from the interface,

$$\boldsymbol{v}_1 = \boldsymbol{v}^{\mathrm{S}} + \boldsymbol{v}^*\,,$$
$$p_1 = p^{\mathrm{S}} + p^*\,,$$

where $\boldsymbol{v}^{\mathrm{S}}$ and p^{S} are the Stokeslet solution in an infinite (unbounded) medium, and $\boldsymbol{v}^*$ and p^* are the solutions of the force free Stokes equations, required to satisfy the regularity and boundary conditions.

The resolution methodology consists of expanding the velocity and pressure fields in the form of Fourier integrals in two distinct regions, inside and outside the cylindrical membrane. The solution is then written in terms of integrals of harmonic functions with unknown coefficients, which we then determine from the usual boundary conditions of continuity of fluid velocities and traction jumps deriving from the elastic properties of the membrane. The cases of axial (axisymmetric) and radial (asymmetric) motion are treated separately.

The detailed solution has been reported in our publication [Pub6]. Therein, we have shown that the image solution for the axisymmetric motion due to an axial point-force acting along the cylinder

axis $\boldsymbol{F} = F_z \boldsymbol{e}_z$ can be written as an infinite integral over the wavenumber q as

$$v_r^* = \frac{F_z}{4\pi^2\eta} \int_0^\infty q\Big(\big(rqI_0 - I_1\big)\phi_\parallel^* + I_1\psi_\parallel^* \Big) \sin qz \,\mathrm{d}q \,, \tag{3.23}$$

$$v_z^* = \frac{F_z}{4\pi^2\eta} \int_0^\infty q\Big(\big(rqI_1(qr) + I_0\big)\phi_\parallel^* + I_0\psi_\parallel^* \Big) \cos qz \,\mathrm{d}q \,, \tag{3.24}$$

$$p^* = \frac{F_z}{2\pi^2} \int_0^\infty q^2 \phi_\parallel^* I_0 \sin qz \,\mathrm{d}q \,, \tag{3.25}$$

and $v_\phi^* = 0$ due to axisymmetry. Moreover, I_k denotes the kth order modified Bessel function of the first kind [243] having the argument qr which is dropped for brevity. Here $\phi_\parallel^*$ and $\psi_\parallel^*$ are two unknown functions which depend on the wavenumber q only, to be determined from the boundary conditions.

For a force directed perpendicular to the cylinder axis, the image solution has a more complex form due to asymmetry and can be expressed in a similar fashion as an infinite integral over q as

$$v_r^* = \frac{F_r}{4\pi^2\eta r} \int_0^\infty \left(\left(\big(2 + (qr)^2\big) I_1 - qrI_0 \right) \phi_\perp^* + (qrI_0 - I_1)\, \psi_\perp^* + I_1\, \gamma_\perp^* \right) \cos qz \,\mathrm{d}q \,, \tag{3.26}$$

$$v_\phi^* = \frac{F_\phi}{4\pi^2\eta r} \int_0^\infty \left((qrI_0 - 2I_1)\, \phi_\perp^* + I_1\psi_\perp^* + (qrI_0 - I_1)\, \gamma_\perp^* \right) \cos qz \,\mathrm{d}q \,, \tag{3.27}$$

$$v_z^* = -\frac{F_r}{4\pi^2\eta} \int_0^\infty q\big(qrI_0\phi_\perp^* + I_1\psi_\perp^* \big) \sin qz \,\mathrm{d}q \,, \tag{3.28}$$

$$p^* = \frac{F_r}{2\pi^2} \int_0^\infty q^2 I_1 \phi_\perp^* \cos qz \,\mathrm{d}q \,, \tag{3.29}$$

where F_r and F_ϕ are the radial and polar components of the force, respectively, and $\phi_\perp^*$, $\psi_\perp^*$ and $\gamma_\perp^*$ are three wavenumber-dependent unknown functions.

The solutions outside the cylinder can also be determined and expressed in an analogous way but they are rather not relevant for the calculations of the particle mobility functions and are thus omitted here.

In the vanishing frequency limit, we recover the solutions nearby a hard-cylinder as first obtained by Liron & Shahar [129]. For the axial motion we obtain

$$\frac{\psi_\parallel^*}{R} = \frac{(I_0K_1 + I_1K_0)s^2 - (I_0K_0 + I_1K_1)s + 2I_1K_0}{s\big(sI_0^2 - sI_1^2 - 2I_0I_1\big)} \,, \tag{3.30}$$

$$\frac{\phi_\parallel^*}{R} = \frac{2I_1K_0 - (I_0K_0 + I_1K_1)s}{s\big(sI_0^2 - sI_1^2 - 2I_0I_1\big)} \,, \tag{3.31}$$

where K_k denotes the kth order modified Bessel function of the second kind and $s := qR$ is the argument of the modified Bessel functions. For the asymmetric motion perpendicular to the cylinder axis, the unknown functions read in this limit

$$\frac{\phi_\perp^*}{R} = \frac{s(sI_0 - I_1)(I_0K_0 + I_1K_1) - 2I_1^2K_0}{s\left(s(sI_0 - I_1)(I_0^2 - I_1^2) - 2I_0I_1^2\right)} \,, \tag{3.32}$$

$$\frac{\psi_\perp^*}{R} = \frac{s(I_1 - sI_0)(I_0K_1 + I_1K_0)}{s(sI_0 - I_1)(I_0^2 - I_1^2) - 2I_0I_1^2} \,, \tag{3.33}$$

$$\frac{\gamma_\perp^*}{R} = 2\,\frac{sI_1(I_0K_0 + I_1K_1) + 2I_1^2K_0 - s^2K_0(I_0^2 - I_1^2)}{s\left(s(sI_0 - I_1)(I_0^2 - I_1^2) - 2I_0I_1^2\right)} \,. \tag{3.34}$$

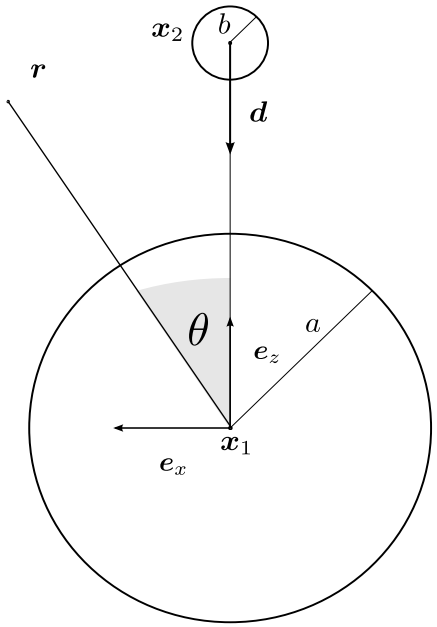

Figure 3.3: Illustration of a small solid spherical particle of radius b positioned at $\boldsymbol{x}_2 = R\boldsymbol{e}_z$ nearby a large spherical capsule of radius a centered at the origin. In an axisymmetric configuration, the force is directed parallel the unit vector $\boldsymbol{d} \equiv -\boldsymbol{e}_z$ while in a asymmetric configuration the force is perpendicular to $\boldsymbol{d}$.

Interestingly, the latter hard limits are recovered even when the membrane is endowed with a pure shearing resistance. We further mention that for elastic cylindrical membranes, shearing and bending present a coupled nature. As a result, the contributions to the Green's functions from shearing and bending cannot be added independently on top of each other as it is the case for a single planar membrane.

A similar resolution methodology can be adopted for the determination of the flow field due to a point-torque (point-couple) exerted along or perpendicular to the cylinder axis. In this case, the solution of fluid motion can readily be used for the determination of the rotational mobilities of particles located on the centerline of a an elastic tube. These calculations have been considered in details in our publication [Pub7].

In the following, we shall briefly outline the main derivation steps for the computation of the Green's functions for a point-force acting outside a spherical elastic membrane.

3.3 Spherical harmonics technique

Membranes in soft matter systems often assume spherical shapes such as that of vesicles [244–246] or elastic capsules [247]. In this section, we shall outline the main derivation steps for the determination of the Green's functions associated with a point-force acting at the center of a solid particle of radius b nearby a large spherical membrane of radius a. Here we shall use the term "capsule" to denote a spherical particle containing some fluid inside and enclosed by an elastic membrane possessing both shearing and bending resistances.

It is most natural to solve the fluid equations of motion in the spherical coordinate system. We consider that the origin of coordinates is located at $\boldsymbol{x}_1$, the center of the large capsule. The mathematical problem is equivalent to solving the forced Stokes equations (3.2) and (3.3) for a point-force $\boldsymbol{F}$ acting at $\boldsymbol{x}_2 = R\boldsymbol{e}_z$, with $R > a$. We define the unit vector $\boldsymbol{d} := (\boldsymbol{x}_1 - \boldsymbol{x}_2)/|\boldsymbol{x}_1 - \boldsymbol{x}_2|$ connecting

between the center of the capsule and the point-force position (see Fig. 3.3 for an illustration.) Inside the capsule, the fluid motion is governed by the homogeneous (force free) Stokes equation. We shall consider the cases that the force is acting either parallel or perpendicular to the vector $\boldsymbol{d}$.

The resolution approach is based on the image solution method proposed by Fuentes *et al.* [248, 249] who computed about three decades ago the motion of two unequal size viscous drops in Stokes flow. Accordingly, the exterior fluid velocity can be written in the usual way as a sum of two distinct contributions,

$$\boldsymbol{v} = \boldsymbol{v}^{\mathrm{S}} + \boldsymbol{v}^{*}\,, \tag{3.35}$$

where $\boldsymbol{v}^{\mathrm{S}}$ is the velocity field induced by a point-force acting at $\boldsymbol{x}_2$ in an infinite medium, *i.e.* in the absence of the capsule and $\boldsymbol{v}^{*}$ is the image system required to satisfy the boundary conditions at the capsule membrane.

The determination of the Green's functions proceeds through the three following main steps. First, the velocity $\boldsymbol{v}^{\mathrm{S}}$ due to the Stokeslet acting at $\boldsymbol{x}_2$ is written in terms of spherical harmonics which are transformed afterward into harmonics based at $\boldsymbol{x}_1$ via the Legendre expansion [250]. Second, the image system solution $\boldsymbol{v}^{*}$ is expressed as multipole series at $\boldsymbol{x}_2$ which subsequently is rewritten in terms of spherical harmonics centered at $\boldsymbol{x}_1$. Third, the solution inside the capsule $\boldsymbol{v}^{(i)}$ is expressed using Lamb's solution [251] also written in terms of spherical harmonics centered at $\boldsymbol{x}_1$. The last step consists of determining the series expansion coefficients by satisfying the boundary conditions at the membrane surface. It appeared convenient to scale all the lengths by the capsule radius a. Analytical expressions for the Green's functions in the axisymmetric and asymmetric cases have been reported in our two part series publications [Pub8, Pub9].

Outside the capsule, the image solution for the axisymmetric motion, *i.e.* for $\boldsymbol{F} \parallel \boldsymbol{d}$ can conveniently be written in the form of an infinite sum as

$$\boldsymbol{v}^{*} = -\frac{F}{8\pi\eta}\sum_{n=0}^{\infty}\left[A_n^{\parallel}\Big((n-1)\boldsymbol{d}\,\varphi_n + (n+1)\boldsymbol{r}\varphi_{n+1}\Big) + 2(n+1)B_n^{\parallel}\boldsymbol{\nabla}\varphi_{n+1}\right], \tag{3.36}$$

where $A_n^{\parallel}$ and $B_n^{\parallel}$ are series coefficients to be determined from the boundary conditions. Moreover, φ_n are the harmonics of degree n, related to the Legendre polynomials of degree n via the relation

$$\varphi_n(r,\theta) := \frac{(\boldsymbol{d}\cdot\boldsymbol{\nabla})^n}{n!}\frac{1}{r} = \frac{1}{r^{n+1}}\,P_n(\cos\theta)\,. \tag{3.37}$$

Similar, for the asymmetric motion, *i.e.* for $\boldsymbol{F} \perp \boldsymbol{d}$, the image solution can be written in terms of an infinite series as

$$\boldsymbol{v}^{*} = \frac{1}{8\pi\eta}\sum_{n=0}^{\infty}\left[A_n^{\perp}\Big((1-n)\boldsymbol{F}\varphi_n - \boldsymbol{r}\psi_n\Big) - 2B_n^{\perp}\boldsymbol{\nabla}\psi_n\right] + \sum_{n=1}^{\infty}\Big[C_n^{\perp} - A_{n+1}^{\perp}\Big]\boldsymbol{\gamma}_n\,, \tag{3.38}$$

where the coefficients $A_n^{\perp}$, $B_n^{\perp}$ and $C_n^{\perp}$ are to be determined from the boundary conditions. We have further defined the harmonics

$$\psi_n = (\boldsymbol{F}\cdot\boldsymbol{\nabla})\varphi_n\,, \qquad \boldsymbol{\gamma}_n = (\boldsymbol{t}\times\boldsymbol{\nabla})\varphi_n\,, \tag{3.39}$$

with $\boldsymbol{t} = \boldsymbol{F}\times\boldsymbol{d}$.

In the vanishing frequency limit, we recover the solutions nearby a rigid sphere, namely [240]

$$A_n^{\parallel} = -\left(n+\frac{3}{2}\right)\frac{1}{R^{n+1}} + \left(n+\frac{1}{2}\right)\frac{1}{R^{n+3}}\,, \tag{3.40}$$

$$B_n^{\parallel} = -\frac{1}{4}(1-R^2)^2\frac{1}{R^{n+5}}\,, \tag{3.41}$$

for the axisymmetric motion and

$$A_n^{\perp} = \frac{1}{2(n+2)}\left(\frac{(2n+3)(n-1)}{R^{n+1}} - \frac{(2n+1)(n+1)}{R^{n+3}}\right), \tag{3.42}$$

$$B_n^{\perp} = \frac{n-1}{4(n+2)}\frac{1}{R^{n+1}} + \frac{n+1}{4(n+4)}\frac{1}{R^{n+5}} - \frac{n^2+3n-1}{2(n+2)(n+4)}\frac{1}{R^{n+3}}\,, \tag{3.43}$$

$$C_n^{\perp} = \frac{2n+3}{n+3}\left(\frac{1}{R^{n+2}} - \frac{1}{R^{n+4}}\right), \tag{3.44}$$

for the asymmetric motion. Similar, the hard-sphere limit is recovered as well for a spherical membrane with pure shearing, *i.e.* in the same way as observed for cylindrical membranes.

Analogous theoretical calculations can be carried out to compute the flow field due to a point-force acting *inside* a spherical elastic cavity. In particular, an exact analytical solution of the hydrodynamic mobility is possible using the stream function technique when the particle center coincides with the center of the cavity. Further details and discussions can be found in a publication that is in preparation [Pub10].

The Green's functions obtained from the outlined derivations and given in details in our publications will serve as a basis for the computation of the particle mobilities in the presence of planar, cylindrical or spherical confinements. This will be the subject of the next chapter.

Chapter 4

Particle mobility

> Know how to solve every problem that has ever been solved.
>
> Richard Feynman

Having outlined in the previous chapter the derivation of the Green's functions nearby an elastic boundary, we now probe the effect of nearby membranes on the motion of suspended particles. Particularly, we shall be interested in the determination of the particle self- and pair-mobility functions. In this section, we present analytical calculations of the particle mobilities in the presence of arbitrary shaped membrane and outline the approach we use for their computation using a combination of the multipole expansion and Faxén's theorem.

We consider the situation of particles moving in a viscous fluid governed by the steady Stokes equations stated by Eqs. (3.2) and (3.3). The grand mobility is a tensorial quantity that couples the velocity moments of the particles relative to an imposed flow to the moments of the force density on the particles' surfaces,

$$\begin{pmatrix} \boldsymbol{V} - \boldsymbol{v}_0 \\ \boldsymbol{\Omega} - \boldsymbol{\omega}_0 \\ -\boldsymbol{S} \end{pmatrix} = \begin{pmatrix} \boldsymbol{\mu}^{tt} & \boldsymbol{\mu}^{tr} & \boldsymbol{\mu}^{td} \\ \boldsymbol{\mu}^{rt} & \boldsymbol{\mu}^{rr} & \boldsymbol{\mu}^{rd} \\ \boldsymbol{\mu}^{dt} & \boldsymbol{\mu}^{dr} & \boldsymbol{\mu}^{dd} \end{pmatrix} \begin{pmatrix} \boldsymbol{F} \\ \boldsymbol{L} \\ \boldsymbol{E}_0 \end{pmatrix} , \tag{4.1}$$

wherein $\boldsymbol{v}_0, \boldsymbol{\omega}_0$ and $\boldsymbol{E}_0$ are the velocity, vorticity and the rate of strain of the imposed flow, respectively, and $\boldsymbol{F}$, $\boldsymbol{L}$ and $\boldsymbol{S}$ are the hydrodynamic force, torque and stresslet (symmetric force dipole) exerted on the particles. Moreover, t, r and d are the lowest-order multipole matrix elements corresponding to translational, rotational and dipolar motion types.

We now consider a representative configuration of a pair of particles denoted γ and λ located nearby an elastic membrane, as schematically sketched in Fig. 4.1. We shall restrict ourselves throughout this thesis to the case of quiescent fluid where the background fluid is at rest. Accordingly, the disturbance velocity field caused at any point $\boldsymbol{r}$ by the particle labeled λ located at $\boldsymbol{r}_\lambda$ can be written as

$$\boldsymbol{v}(\boldsymbol{r}, \boldsymbol{r}_\lambda, \omega) = \boldsymbol{v}^{(0)}(\boldsymbol{r}, \boldsymbol{r}_\lambda) + \boldsymbol{v}^*(\boldsymbol{r}, \boldsymbol{r}_\lambda, \omega) \, , \tag{4.2}$$

where a Fourier transformation has been applied to the temporal dependence of all fields. Here $\boldsymbol{v}^{(0)}$ denotes the induced fluid flow in an unbounded (infinite) fluid and $\boldsymbol{v}^*$ is the flow field required to satisfy the boundary conditions at the membrane. The disturbance field can be written as an integral over the surface of the sphere λ as

$$\boldsymbol{v}(\boldsymbol{r}, \boldsymbol{r}_\lambda, \omega) = \oint_{S_\lambda} \boldsymbol{\mathcal{G}}(\boldsymbol{r}, \boldsymbol{r}', \omega) \cdot \boldsymbol{f}_\lambda(\boldsymbol{r}', \omega) \, \mathrm{d}^2\boldsymbol{r}' \, , \tag{4.3}$$

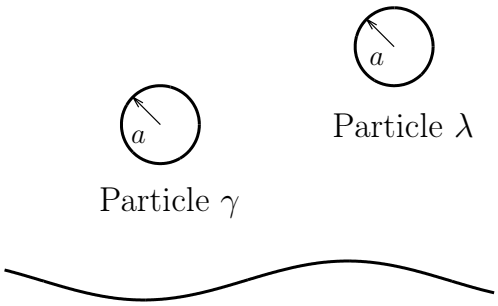

Figure 4.1: Illustration of particle motion nearby an elastic membrane of arbitrary shape. The particles labeled γ and λ have a radius a and are located at $\boldsymbol{r}_\gamma$ and $\boldsymbol{r}_\lambda$, respectively.

where $\boldsymbol{\mathcal{G}}$ is the Green's function associated with a point-force acting at $\boldsymbol{r}_\lambda$. Similar, the Green's functions can be split up into two distinct contributions,

$$\boldsymbol{\mathcal{G}}(\boldsymbol{r},\boldsymbol{r}',\omega) = \boldsymbol{\mathcal{G}}^{(0)}(\boldsymbol{r},\boldsymbol{r}') + \boldsymbol{\mathcal{G}}_{\mathrm{M}}(\boldsymbol{r},\boldsymbol{r}',\omega)\,, \tag{4.4}$$

where $\boldsymbol{\mathcal{G}}^{(0)}$ is the infinite-space Green's function (Oseen tensor) given by Eq. (3.17). The second term $\boldsymbol{\mathcal{G}}_{\mathrm{M}}$ represents the frequency-dependent correction to the Green's function due to the presence of the membrane.

Far away from the particle λ, the integration vector variable $\boldsymbol{r}'$ in Eq. (4.3) can conveniently be expanded around the particle center $\boldsymbol{r}_\lambda$ following a multipole (Taylor) expansion approach. Up to the second order, and assuming a constant force density over the particle surface, the disturbance velocity can be approximated by [252, 253]

$$\boldsymbol{v}(\boldsymbol{r},\boldsymbol{r}_\lambda,\omega) \approx \left(1+\frac{a^2}{6}\boldsymbol{\nabla}^2_{\boldsymbol{r}_\lambda}\right)\boldsymbol{\mathcal{G}}(\boldsymbol{r},\boldsymbol{r}_\lambda,\omega)\cdot\boldsymbol{F}(\omega) + \frac{1}{2}\,\boldsymbol{\nabla}_{\boldsymbol{r}_\lambda}\times\boldsymbol{\mathcal{G}}(\boldsymbol{r},\boldsymbol{r}_\lambda,\omega)\cdot\boldsymbol{L}(\omega)\,, \tag{4.5}$$

where $\boldsymbol{\nabla}_{\boldsymbol{r}_\lambda}$ stands for the gradient operator taken with respect to the singularity position $\boldsymbol{r}_\lambda$ and the curl of a given tensor $\boldsymbol{\mathcal{T}}$ is defined as [254]

$$(\boldsymbol{\nabla}\times\boldsymbol{\mathcal{T}})_{\alpha\beta} = \epsilon_{\alpha\mu\nu}\partial_\mu\mathcal{T}_{\nu\beta}\,, \tag{4.6}$$

with $\epsilon_{\alpha\mu\nu}$ being the Levi-Civita tensor. Note that for a single sphere in bulk, the flow field given by Eq. (4.5) satisfies exactly the no-slip boundary conditions at the surface of the sphere [255].

Using Faxén's theorem [256], the translational and rotational velocities of the adjacent particle γ in this flow read [252, 253]

$$\boldsymbol{V}_\gamma(\omega) = \mu_0^{tt}\boldsymbol{F}_\gamma(\omega) + \left(1+\frac{a^2}{6}\boldsymbol{\nabla}^2_{\boldsymbol{r}_\gamma}\right)\boldsymbol{v}(\boldsymbol{r}_\gamma,\boldsymbol{r}_\lambda,\omega)\,, \tag{4.7}$$

$$\boldsymbol{\Omega}_\gamma(\omega) = \mu_0^{rr}\boldsymbol{L}_\gamma(\omega) + \frac{1}{2}\,\boldsymbol{\nabla}_{\boldsymbol{r}_\gamma}\times\boldsymbol{v}(\boldsymbol{r}_\gamma,\boldsymbol{r}_\lambda,\omega)\,, \tag{4.8}$$

where $\mu_0^{tt} := 1/(6\pi\eta a)$ and $\mu_0^{rr} := 1/(8\pi\eta a^3)$ denote the translational and rotational bulk mobilities, respectively. We further emphasize that the disturbance flow $\boldsymbol{v}$ incorporates both the disturbance from

the particle λ and the disturbance caused by the presence of the membrane. By inserting Eq. (4.5) into the Faxén's formulas stated by Eqs. (4.7) and (4.8), the frequency-dependent translational, coupling and rotational pair-mobility tensors can be obtained from the *total* Green's functions as

$$\boldsymbol{\mu}^{tt,\gamma\lambda}(\omega) = \left(1 + \frac{a^2}{6}\boldsymbol{\nabla}^2_{\boldsymbol{r}_\gamma}\right)\left(1 + \frac{a^2}{6}\boldsymbol{\nabla}^2_{\boldsymbol{r}_\lambda}\right)\boldsymbol{\mathcal{G}}(\boldsymbol{r}_\gamma, \boldsymbol{r}_\lambda, \omega)\,, \tag{4.9}$$

$$\boldsymbol{\mu}^{tr,\gamma\lambda}(\omega) = \frac{1}{2}\left(1 + \frac{a^2}{6}\boldsymbol{\nabla}^2_{\boldsymbol{r}_\gamma}\right)\boldsymbol{\nabla}_{\boldsymbol{r}_\lambda} \times \boldsymbol{\mathcal{G}}(\boldsymbol{r}_\gamma, \boldsymbol{r}_\lambda, \omega)\,, \tag{4.10}$$

$$\boldsymbol{\mu}^{rr,\gamma\lambda}(\omega) = \frac{1}{4}\boldsymbol{\nabla}_{\boldsymbol{r}_\gamma} \times \boldsymbol{\nabla}_{\boldsymbol{r}_\lambda} \times \boldsymbol{\mathcal{G}}(\boldsymbol{r}_\gamma, \boldsymbol{r}_\lambda, \omega)\,. \tag{4.11}$$

Special care should be undertaken when taking the gradient operators with respect to the position of either γ or λ. The components of the rt pair-mobility tensor can be determined in an analogous way. This however, is not necessary thanks to the symmetry property of the mobility tensor. For the self-mobilities, only the correction to the flow field $\boldsymbol{v}^*$ due to the presence of the membrane in Eq. (4.2) should be considered in the Faxén's formulas. Therefore, the frequency-dependent self-mobility tensors are directly determined from the *correction* to the Green's functions to obtain

$$\boldsymbol{\mu}^{tt,\gamma\gamma}(\omega) = \mu_0^{tt}\,\mathbf{1} + \lim_{\boldsymbol{r}\to\boldsymbol{r}_\gamma}\left(1 + \frac{a^2}{6}\boldsymbol{\nabla}^2_{\boldsymbol{r}}\right)\left(1 + \frac{a^2}{6}\boldsymbol{\nabla}^2_{\boldsymbol{r}_\gamma}\right)\boldsymbol{\mathcal{G}}_{\mathrm{M}}(\boldsymbol{r}, \boldsymbol{r}_\gamma, \omega)\,, \tag{4.12}$$

$$\boldsymbol{\mu}^{tr,\gamma\gamma}(\omega) = \frac{1}{2}\lim_{\boldsymbol{r}\to\boldsymbol{r}_\gamma}\left(1 + \frac{a^2}{6}\boldsymbol{\nabla}^2_{\boldsymbol{r}_\gamma}\right)\boldsymbol{\nabla}_{\boldsymbol{r}} \times \boldsymbol{\mathcal{G}}_{\mathrm{M}}(\boldsymbol{r}, \boldsymbol{r}_\gamma, \omega)\,, \tag{4.13}$$

$$\boldsymbol{\mu}^{rr,\gamma\gamma}(\omega) = \mu_0^{rr}\,\mathbf{1} + \frac{1}{4}\lim_{\boldsymbol{r}\to\boldsymbol{r}_\gamma}\boldsymbol{\nabla}_{\boldsymbol{r}_\gamma} \times \boldsymbol{\nabla}_{\boldsymbol{r}} \times \boldsymbol{\mathcal{G}}_{\mathrm{M}}(\boldsymbol{r}, \boldsymbol{r}_\gamma, \omega)\,, \tag{4.14}$$

where $\mathbf{1}$ denotes the unit tensor. We note that the particle self- and pair-mobility functions in the point-particle approximation are obtained by setting $a = 0$ in the above equations. Based on the solution of the Green's functions obtained in the previous chapter, we shall present in the following illustrative calculations of the mobility functions nearby membranes of various shapes.

4.1 Planar membrane

Here we consider a pair of particles positioned a distance h apart and a distance z_0 above a planar elastic membrane, such that $\boldsymbol{x}_\gamma = (0, 0, z_0)$ and $\boldsymbol{x}_\lambda = (h, 0, z_0)$. As previously pointed out, the corrections to the particle self- and pair-mobilities nearby a planar membrane can conveniently be split up into a contribution due to shearing together with a contribution due to bending. We shall denote by $\boldsymbol{\mu}^{ab,\gamma\gamma} = \boldsymbol{\mu}^{ab,\mathrm{S}}$ with $a, b \in \{t, r\}$ the self-mobility tensor and by $\boldsymbol{\mu}^{ab,\gamma\lambda} = \boldsymbol{\mu}^{ab,\mathrm{P}}$ the pair-mobility tensor. The self-mobility corrections can conveniently be expressed as a power series of $\epsilon := a/z_0$ while the pair-mobilities as a power series of $\sigma := a/h$. The self- and pair-mobility tensors nearby a planar membrane for this typical configuration have the form

$$\boldsymbol{\mu}^{\mathrm{S}} = \begin{pmatrix} \mu^{\mathrm{S}}_{xx} & 0 & 0 \\ 0 & \mu^{\mathrm{S}}_{yy} & 0 \\ 0 & 0 & \mu^{\mathrm{S}}_{zz} \end{pmatrix}, \qquad \boldsymbol{\mu}^{\mathrm{P}} = \begin{pmatrix} \mu^{\mathrm{P}}_{xx} & 0 & \mu^{\mathrm{P}}_{xz} \\ 0 & \mu^{\mathrm{P}}_{yy} & 0 \\ \mu^{\mathrm{P}}_{zx} & 0 & \mu^{\mathrm{P}}_{zz} \end{pmatrix}. \tag{4.15}$$

Intuitively, the xx and yy components of the self mobility are equal since they are both associated with motion parallel to the membrane, while the zz component is associated with the perpendicular motion. Moreover, the off-diagonal components xz and zx of the pair-mobility in the current configuration have same absolute value and differ only in sign. We further note that $\mu^{tr}_{xz} = \mu^{rt}_{zx}$ as required by the symmetry of the mobility tensors.

Analytical predictions of the translational self- and pair-mobilities have been reported in our publication [Pub3] while the coupling and rotational mobilities have been considered in a publication that is in preparation [Pub4]. In the vanishing frequency limit, we recover the well-known self-mobility corrections nearby a no-slip planar wall [252]

$$\frac{\Delta\mu_{\parallel}^{\mathrm{S}}}{\mu_0} = -\frac{9}{16}\,\epsilon + \frac{1}{8}\,\epsilon^3 - \frac{1}{16}\,\epsilon^5\,, \qquad \frac{\Delta\mu_{\perp}^{\mathrm{S}}}{\mu_0} = -\frac{9}{8}\,\epsilon + \frac{1}{2}\,\epsilon^3 - \frac{1}{8}\,\epsilon^5\,, \tag{4.16}$$

for the parallel and perpendicular motion, respectively. Note that the leading order terms in ϵ represent the self-mobility correction in the point-particle framework. Clearly, the motion perpendicular to the wall is significantly slowed down compared to the parallel motion.

In attempt to investigate the effect of membrane finite curvature on the mobility functions, we shall further investigate the particle mobility functions nearby cylindrical and spherical membranes.

4.2 Cylindrical membrane

Having computed in chapter 3 the Green's functions nearby a cylindrical membrane, we now turn our attention to the computation of the mobility functions. Here we restrict ourselves to the point-particle approximation but higher order corrections terms can readily be obtained, although this is technically demanding for non-planar geometries. The leading-order self-mobility correction is calculated by evaluating the reflected flow field at the particle position as given by Eqs. (3.24) and (3.26), for axial and radial motion, respectively. We obtain

$$\frac{\Delta\mu_{\parallel}^{\mathrm{S}}}{\mu_0} = \frac{3}{2\pi}\frac{a}{R}\int_0^{\infty}\frac{s}{R}\left(\psi_{\parallel}^{*} + \phi_{\parallel}^{*}\right)\,\mathrm{d}s\,, \tag{4.17}$$

$$\frac{\Delta\mu_{\perp}^{\mathrm{S}}}{\mu_0} = \frac{3}{4\pi}\frac{a}{R}\int_0^{\infty}\frac{s}{R}\left(\psi_{\perp}^{*} + \gamma_{\perp}^{*}\right)\mathrm{d}s\,. \tag{4.18}$$

Clearly, the correction vanishes for a very wide channel as $R \to \infty$. The corrections nearby a no-slip cylinder are obtained in the vanishing frequency limit provided that the membrane possesses a resistance towards shearing, and can be approximated by

$$\frac{\Delta\mu_{\parallel}^{\mathrm{S}}}{\mu_0} \approx -2.10444\,\frac{a}{R}\,, \qquad \frac{\Delta\mu_{\perp}^{\mathrm{S}}}{\mu_0} \approx -1.80436\,\frac{a}{R}\,, \tag{4.19}$$

for the axial and radial motion, respectively. Note that the axial motion along the cylinder axis is more slowed down compared to the radial motion.

Due to the strong confinement induced by the presence of the cylindrical membrane, considering higher order correction terms becomes necessary for an accurate determination of the mobility when the particle is of comparable size to that of the cylinder. In the next section, we shall perform analogous investigations for particle motion nearby a spherical elastic membrane.

4.3 Spherical membrane

The exact Green's functions evaluated in the previous chapter allow for the calculations of the particle mobilities nearby a spherical membrane. Similar, we restrict ourselves here for simplicity to the point-particle approximation but going beyond that is feasible although somewhat tedious. The leading-order correction can directly be obtained by evaluating the reflected flow field at the

particle position, as given by Eqs. (3.36) and (3.38), for the axisymmetric and asymmetric motion, respectively.

After computation, we find that the correction to the self-mobilities can conveniently be expressed in terms of an infinite series as

$$\frac{\Delta\mu_{\parallel}}{\mu_0} = \frac{3b}{4}\sum_{n=0}^{\infty} 2\left(A_n^{\parallel} - (n+1)(n+2)\xi^2 B_n^{\parallel}\right)\xi^{n+1}\,, \tag{4.20}$$

$$\frac{\Delta\mu_{\perp}}{\mu_0} = \frac{3b}{4}\sum_{n=0}^{\infty} \left(A_n^{\perp} + (n+1)(n+2)\xi^2 B_n^{\perp} - (n+1)\xi C_n^{\perp}\right)\xi^{n+1}\,, \tag{4.21}$$

where $\xi := 1/R \in [0,1)$, bearing in mind that all the lengths have been scaled by the capsule radius a. In the vanishing frequency limit, we recover the corrections nearby a no-slip sphere, namely [257]

$$\frac{\Delta\mu_{\parallel}}{\mu_0} = -\frac{\xi^3(15-7\xi^2+\xi^4)}{4(1-\xi^2)}\frac{b}{R}\,, \qquad \frac{\Delta\mu_{\perp}}{\mu_0} = -\frac{\xi^5(17+\xi^2)}{16(1-\xi^2)}\frac{b}{R}\,. \tag{4.22}$$

It is worth mentioning that the hard limits are recovered only if the membrane possesses a non-vanishing resistance towards shearing, *i.e.* in the same way as previously observed for cylindrical membranes.

Chapter 5

Multipole method

Ars Conjectandi, (The Art of Conjecturing)

Jacobi Bernoulli

The calculations presented in the previous section are applied for the determination of the mobility functions of spherically shaped particles. Here we extend our results by evaluating the leading-order corrections to the mobility functions of axisymmetric particles nearby an elastic membrane. For this goal, we shall first present some analytical tools based on the multipole method that will be necessary for our further calculations.

5.1 Preliminaries

The multipole method is a well-established analytic-numerical method intended for solving problems related to particle motion in the Stokes regime. It has been developed during the last few decades by Felderhof and collaborators [258–264]. The method is based on an expansion in spherical basis functions and is meant to provide the friction and mobility tensors to arbitrary accuracy. In this chapter, we show how the Green tensor is expanded in terms of complete sets of solutions to the steady Stokes equations and introduce the multipole description. We then use these results to compute the leading-order correction to the mobility function of an axisymmetric particle nearby a planar elastic membrane.

We now consider a suspension of N hard spherical particles of radius a moving in an infinite incompressible Newtonian fluid. Here we use the concept of "induced forces" introduced by Bedeaux and Mazur [265] in which the validity of the Stokes equations can formally be extended inside the particles. At the surface of each particle, we impose the usual stick boundary condition

$$\boldsymbol{v}(\boldsymbol{r}) = \boldsymbol{v}_i(\boldsymbol{r}) = \boldsymbol{V}_i + \boldsymbol{\Omega_i} \times (\boldsymbol{r} - \boldsymbol{R}_i)\,, \tag{5.1}$$

for $|\boldsymbol{r} - \boldsymbol{R}_i| \leq a$, where $\boldsymbol{V}_i$ and $\boldsymbol{\Omega}_i$ are respectively the translational and angular velocities of a sphere labeled i whose center is located at $\boldsymbol{R}_i$. By decomposing the total force density in terms of separate contributions coming from each of the force densities $\boldsymbol{f}_j(\boldsymbol{r})$ on sphere j, a formal solution of the Stokes equations can be written as [263]

$$\boldsymbol{v}_i(\boldsymbol{r}) - \boldsymbol{v}_0(\boldsymbol{r}) = \sum_{j=1}^{N} \int \boldsymbol{\mathcal{G}}(\boldsymbol{r}, \boldsymbol{r}') \cdot \boldsymbol{f}_j(\boldsymbol{r}')\, \mathrm{d}\boldsymbol{r}'\,, \quad \boldsymbol{r} \in S_i\,, \tag{5.2}$$

where $\boldsymbol{v}_0$ is a regular solution to the Stokes equations, representing an incident flow which may be imposed in the absence of the particles. The latter equation can further be rewritten by separating out the contributions from distinct particles and the particle i itself. Defining the Green integral operator or simply propagator as

$$[\boldsymbol{\mathcal{P}}(ij)\boldsymbol{f}_j](\boldsymbol{r}) := \int \boldsymbol{\mathcal{G}}(\boldsymbol{r},\boldsymbol{r}')\cdot\boldsymbol{f}_j(\boldsymbol{r}')\,\mathrm{d}\boldsymbol{r}'\,, \tag{5.3}$$

Eq. (5.2) can therefore be written as

$$\boldsymbol{v}_i(\boldsymbol{r}) - \boldsymbol{v}_0(\boldsymbol{r}) = \boldsymbol{\mathcal{Z}}_0^{-1}\boldsymbol{f}_i(\boldsymbol{r}) + \sum_{j\neq i}^{N}[\boldsymbol{\mathcal{P}}(ij)\boldsymbol{f}_j](\boldsymbol{r})\,,\quad i=1,\ldots,N\,, \tag{5.4}$$

where $\boldsymbol{\mathcal{Z}}_0$ is the friction kernel, also known as the particle resistance operator.

5.2 Spherical basis set of solutions

The basic idea behind the multipole expansion is to expand the velocities and force densities in a basis set of functions with suitable spherical symmetry. We define two sets of spherical solutions to the homogeneous (force free) Stokes equations denoted $\{\boldsymbol{v}^+_{lm\sigma}(\boldsymbol{r})\}$ and $\{\boldsymbol{v}^-_{lm\sigma}(\boldsymbol{r})\}$ [261, 263]. The set $\boldsymbol{v}^+_{lm\sigma}$ is regular at $\boldsymbol{r}=0$ and diverges at infinity whereas the set $\boldsymbol{v}^-_{lm\sigma}$ is singular at $\boldsymbol{r}=0$ and vanishes at infinity. The angular momentum l takes the values $l=1,2,3,\ldots$, the azimuthal number $m=-l,-l+1,\ldots,l-1,l$ and the superscript $\sigma=0,1,2$. Accordingly, the Oseen tensor $\boldsymbol{\mathcal{G}}^{(0)}$ can be expanded about some arbitrary origin $\boldsymbol{r}_0$ as [37]

$$\boldsymbol{\mathcal{G}}^{(0)}(\boldsymbol{r}-\boldsymbol{r}') = \frac{1}{\eta}\sum_{lm\sigma}\frac{1}{n_{lm}^2}\,\boldsymbol{v}^-_{lm\sigma}(\boldsymbol{r}_>)\overline{\boldsymbol{v}^+_{lm\sigma}(\boldsymbol{r}_<)}\,, \tag{5.5}$$

wherein the bar denotes the complex conjugate and $\boldsymbol{r}_>$ and $\boldsymbol{r}_<$ are are the longer and shorter vectors of the difference $\boldsymbol{r}-\boldsymbol{r}_0$ and $\boldsymbol{r}'-\boldsymbol{r}_0$, respectively. Furthermore, n_{lm} is a normalization

$$n_{lm} = \left(\frac{4\pi}{2l+1}\frac{(l+m)!}{(l-m)!}\right)^{1/2}\,. \tag{5.6}$$

Moreover, we define the complementary set of solutions $\{\boldsymbol{w}^\pm_{lm\sigma}(\boldsymbol{r})\}$ satisfying the following orthogonality property on a sphere of radius a [263]

$$\langle \boldsymbol{w}^\pm_{lm\sigma}(\boldsymbol{r})\delta_a|\boldsymbol{v}^\pm_{l'm'\sigma'}(\boldsymbol{r})\rangle = \delta_{ll'}\delta_{mm'}\delta_{\sigma\sigma'}\,, \tag{5.7}$$

where the scalar product of two vectors $\boldsymbol{v}_1$ and $\boldsymbol{v}_2$ is defined by

$$\langle \boldsymbol{v}_1|\boldsymbol{v}_2\rangle := \int \overline{\boldsymbol{v}_1(\boldsymbol{r})}\cdot\boldsymbol{v}_2(\boldsymbol{r})\,\mathrm{d}\boldsymbol{r}\,, \tag{5.8}$$

and $\delta_a(\boldsymbol{r}) = a^{-1}\,\delta\left(|\boldsymbol{r}|-a\right)$. Expanding the field $\boldsymbol{v}_i-\boldsymbol{v}_0$ on the surface of the particle i in terms of the set of solutions $\{\boldsymbol{v}^+_{lm\sigma}\}$ centered on $\boldsymbol{R}_i$ we obtain

$$\boldsymbol{v}_i(\boldsymbol{r}) - \boldsymbol{v}_0(\boldsymbol{r}) = \sum_{lm\sigma} c(ilm\sigma)\boldsymbol{v}^+_{lm\sigma}(\boldsymbol{r}-\boldsymbol{R}_i)\,. \tag{5.9}$$

By making use of the orthogonality property Eq. (5.7), the expansion coefficients $c(ilm\sigma)$ are calcu-

lated as

$$c(ilm\sigma) = \langle \boldsymbol{w}^{+}_{lm\sigma}(i)\delta_a(i)|\boldsymbol{v}_i - \boldsymbol{v}_0\rangle\,, \tag{5.10}$$

wherein $\boldsymbol{w}^{+}_{lm\sigma}(i)$ and $\delta_a(i)$ are shorthands for $\boldsymbol{w}^{+}_{lm\sigma}(\boldsymbol{r}-\boldsymbol{R}_i)$ and $\delta_a(\boldsymbol{r}-\boldsymbol{R}_i)$, respectively. Similar, we define the force multipole moments on the sphere labeled j by

$$f(jlm\sigma) = \int \overline{\boldsymbol{v}^{+}_{lm\sigma}(\boldsymbol{r}'-\boldsymbol{R}_j)}\cdot\boldsymbol{f}_j(\boldsymbol{r}')\,\mathrm{d}\boldsymbol{r}' = \langle \boldsymbol{v}^{+}_{lm\sigma}|\boldsymbol{f}_j\rangle\,. \tag{5.11}$$

Continuing, the Green tensor associated with the present geometry can be decomposed in the usual way into two contributions,

$$\boldsymbol{\mathcal{G}} = \boldsymbol{\mathcal{G}}^{(0)} + \boldsymbol{\mathcal{G}}_{\mathrm{M}}\,, \tag{5.12}$$

where $\boldsymbol{\mathcal{G}}_{\mathrm{M}}$ is the (known) correction arising from the boundary, which can be a rigid or free interface or an elastic membrane. An analogous expansion in a basis set of functions can be made for the correction $\boldsymbol{\mathcal{G}}_{\mathrm{M}}$ as well. Accordingly, the associated propagator can be split up into a bulk contribution $\boldsymbol{\mathcal{P}}^{(0)}$ together with a correction stemming from the presence of the boundary $\boldsymbol{\mathcal{P}}_{\mathrm{M}}$ such that

$$\boldsymbol{\mathcal{P}} = \boldsymbol{\mathcal{P}}^{(0)} + \boldsymbol{\mathcal{P}}_{\mathrm{M}}\,. \tag{5.13}$$

Inserting Eqs. (5.9) and (5.11) into Eq. (5.4), the following infinite system of equations is obtained

$$c(ilm\sigma) = \sum_{jl'm'\sigma'} (lm\sigma|\boldsymbol{\mathcal{M}}(ij)|l'm'\sigma')f(jl'm'\sigma')\,, \tag{5.14}$$

where $(lm\sigma|\boldsymbol{\mathcal{M}}(ij)|l'm'\sigma')$ stands for the multipole matrix elements of the operator $\boldsymbol{\mathcal{M}}$ defined as

$$\boldsymbol{\mathcal{M}}(ij) = \boldsymbol{\mathcal{Z}}_0^{-1}(i)\delta_{ij} + \boldsymbol{\mathcal{P}}(ij)(1-\delta_{ij})\,. \tag{5.15}$$

By collecting the expansion coefficients of the velocities $\boldsymbol{v}_i - \boldsymbol{v}_0$ and force density $\boldsymbol{f}$ in infinite-dimensional vectors $\boldsymbol{c}$ and $\boldsymbol{f}$, Eq. (5.14) can be written in a compact and often more transparent form as [172]

$$\boldsymbol{c} = \left(\boldsymbol{\mathcal{Z}}_0^{-1} + \boldsymbol{\mathcal{P}}\right)\cdot\boldsymbol{f}\,, \tag{5.16}$$

which upon inversion gives the grand resistance matrix $\boldsymbol{\mathcal{Z}}$

$$\boldsymbol{f} = \boldsymbol{\mathcal{Z}}\cdot\boldsymbol{c}\,, \qquad \boldsymbol{\mathcal{Z}} = \left(\boldsymbol{\mathcal{Z}}_0^{-1} + \boldsymbol{\mathcal{P}}\right)^{-1}\,. \tag{5.17}$$

The lowest-order multipole matrix elements are commonly denoted as t (translational), r (rotational) and d (dipolar), corresponding to $(lm\sigma)$ equal to $(1m0)$, $1m1$ and $2m0$. These have already been presented in chapter 4. Projecting the matrix $\boldsymbol{\mathcal{Z}}$ on the subset t, r, d, the generalized friction matrix reads

$$\begin{pmatrix}\boldsymbol{F}\\ \boldsymbol{T}\\ \boldsymbol{S}\end{pmatrix} = \begin{pmatrix}\boldsymbol{\zeta}^{tt} & \boldsymbol{\zeta}^{tr} & \boldsymbol{\zeta}^{td}\\ \boldsymbol{\zeta}^{rt} & \boldsymbol{\zeta}^{rr} & \boldsymbol{\zeta}^{rd}\\ \boldsymbol{\zeta}^{dt} & \boldsymbol{\zeta}^{dr} & \boldsymbol{\zeta}^{dd}\end{pmatrix}\begin{pmatrix}\boldsymbol{v}_0 - \boldsymbol{V}\\ \boldsymbol{\omega}_0 - \boldsymbol{\Omega}\\ \boldsymbol{E}_0\end{pmatrix}\,. \tag{5.18}$$

Numerically, the infinite matrices $\boldsymbol{\mathcal{Z}}_0$ and $\boldsymbol{\mathcal{P}}$ are truncated at the multipole order ℓ in such a way that only the multipole elements $l \leq \ell$ are considered. Afterward, the matrix $(\boldsymbol{\mathcal{Z}}_0^{-1} + \boldsymbol{\mathcal{P}})$ is inverted, leading directly to the determination of the force multipoles.

Asymptotic expressions for the correction to the bulk friction matrix can be obtained using the scattering expansion technique [266]. Accordingly, the grand resistance matrix

$$\boldsymbol{\mathcal{Z}} = \left(\boldsymbol{\mathcal{Z}}_0^{-1} + \boldsymbol{\mathcal{P}}^{(0)} + \boldsymbol{\mathcal{P}}_{\mathrm{M}}\right)^{-1}\,, \tag{5.19}$$

can be expanded by assuming that the contribution from the boundary is small compared to the bulk contribution to obtain [172]

$$\boldsymbol{\mathcal{Z}} = \boldsymbol{\mathcal{Z}}_{\mathrm{B}} - \boldsymbol{\mathcal{Z}}_{\mathrm{B}}\boldsymbol{\mathcal{P}}_{\mathrm{M}}\boldsymbol{\mathcal{Z}}_{\mathrm{B}} + \boldsymbol{\mathcal{Z}}_{\mathrm{B}}\boldsymbol{\mathcal{P}}_{\mathrm{M}}\boldsymbol{\mathcal{Z}}_{\mathrm{B}}\boldsymbol{\mathcal{P}}_{\mathrm{M}}\boldsymbol{\mathcal{Z}}_{\mathrm{B}} - \cdots , \tag{5.20}$$

wherein $\boldsymbol{\mathcal{Z}}_{\mathrm{B}} := \left(\boldsymbol{\mathcal{Z}}_0^{-1} + \boldsymbol{\mathcal{P}}^{(0)}\right)^{-1}$ is the particle bulk resistance matrix.

It is worth mentioning that the multipole method briefly described above has been implemented in the HYDROMULTIPOLE code [262] developed by Wajnryb and collaborators in Warschau back in the nineties. Hereafter, we shall introduce the bulk mobility tensor of an axisymmetric particle and the strategy we follow for the computation of its hydrodynamic mobility nearby an elastic interface.

5.3 Mobility of an axisymmetric particle

We now consider an axially symmetric particle immersed in an incompressible Newtonian fluid, moving close to an elastic membrane, as illustrated for a prolate spheroid [1] in Fig. 5.1. The position of the center of the particle is $\boldsymbol{r}_0 = (0, 0, z_0)$, while its orientation is described by the unit vector $\boldsymbol{u}_1$ pointing along the symmetry axis. The laboratory frame is spanned by the basis vectors $\{\boldsymbol{e}_x, \boldsymbol{e}_y, \boldsymbol{e}_z\}$.

The undisplaced membrane is located at the plane $z = 0$ and extended infinitely in the horizontal plane xy. It is convenient to introduce the body-fixed frame of reference, formed by the three basis vectors $\{\boldsymbol{u}_1, \boldsymbol{u}_2, \boldsymbol{u}_3\}$. The unit vector $\boldsymbol{u}_2$ is parallel to the undisplaced membrane and perpendicular to the particle axis, and $\boldsymbol{u}_3$ completes the orthonormal basis. We define θ as the angle between $\boldsymbol{u}_1$ and the unit vector $\boldsymbol{e}_z$ normal to the undisplaced membrane such that $\cos\theta = \boldsymbol{e}_z \cdot \boldsymbol{u}_1$. The basis vectors in the particle frame are then given by $\boldsymbol{u}_2 = (\boldsymbol{e}_z \times \boldsymbol{u}_1)/\left|\boldsymbol{e}_z \times \boldsymbol{u}_1\right|$ and $\boldsymbol{u}_3 = \boldsymbol{u}_1 \times \boldsymbol{u}_2$.

For an axisymmetric particle with inversional symmetry, such as a rod-like particle of a spheroid, the particle mobility *in bulk* has the form [267]

$$\boldsymbol{\mu}_0 = \begin{pmatrix} \boldsymbol{\mu}_0^{tt} & 0 & 0 \\ 0 & \boldsymbol{\mu}_0^{rr} & \boldsymbol{\mu}_0^{rd} \\ 0 & \boldsymbol{\mu}_0^{dr} & \boldsymbol{\mu}_0^{dd} \end{pmatrix} . \tag{5.21}$$

The bulk translational and rotational mobility tensors of a general axisymmetric particle can be written as a function of the orientation vector $\boldsymbol{u}_1$ as

$$\boldsymbol{\mu}_0^{tt,rr} = \mu_{\parallel}^{t,r}\boldsymbol{u}_1\boldsymbol{u}_1 + \mu_{\perp}^{t,r}(\mathbf{1} - \boldsymbol{u}_1\boldsymbol{u}_1) , \tag{5.22}$$

where $\mu_{\parallel}^{t,r}$ and $\mu_{\perp}^{t,r}$ are the (known) bulk mobilities for the translational/rotational motion along or perpendicular to the spheroid axis of revolution. The third-order tensors $\boldsymbol{\mu}_0^{rd}$ and $\boldsymbol{\mu}_0^{dr}$ have the Cartesian components

$$(\mu_0^{rd})_{\alpha\beta\gamma} = \mu^{rd} u_\sigma \overline{\epsilon_{\sigma\alpha\beta} u_\gamma}^{(\beta\gamma)} , \tag{5.23}$$

$$(\mu_0^{dr})_{\alpha\beta\gamma} = \mu^{dr} \overline{u_\alpha \epsilon_{\beta\gamma\sigma}}^{(\alpha\beta)} u_\sigma , \tag{5.24}$$

where the symbol $\overline{\square}^{(\alpha\beta)}$ denotes the symmetric and traceless part with respect to indices α, β [172]. Moreover, it follows from the Lorentz reciprocal theorem that [240]

$$\mu^{dr} = \mu^{rd} . \tag{5.25}$$

[1] Spheroid is an ellipsoid of revolution and prolate refers to an elongated spheroid obtained by rotating an ellipse about its major axis.

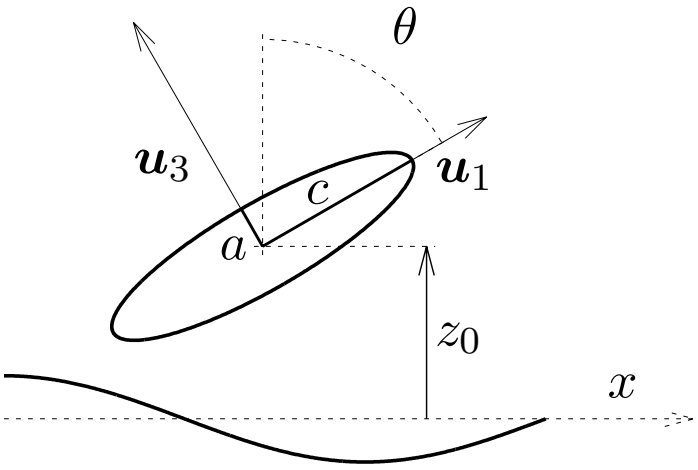

Figure 5.1: Illustration of a spheroidal particle located at $z = z_0$ above an elastic cell membrane. The short and long axes are denoted by a and c, respectively. The unit vector $\boldsymbol{u}_1$ is pointing along the spheroid symmetry axis and $\boldsymbol{u}_2$ is the unit vector perpendicular to the plane of the figure. The unit vector $\boldsymbol{u}_3$ is defined to be orthogonal to both $\boldsymbol{u}_1$ and $\boldsymbol{u}_2$.

In the following, asymptotic corrections to the bulk mobility nearby an elastic membrane shall be provided. As recently shown by Lisicki *et al.* [172], by building up the axisymmetric particle with a conglomerate of interacting solid particles, the leading-order correction to the propagator nearby a boundary takes the simple form $\boldsymbol{\mathcal{P}}_{\mathrm{M}}(\boldsymbol{R} = 2z_0\boldsymbol{n})$, where $\boldsymbol{n}$ is the vector normal to the wall. That is to say that, for a particle sufficiently far away from the wall, the dominant correction to the friction matrix can be viewed as an interaction between the particle center and its hydrodynamic image with respect to the wall. In this way, the form of the matrix elements of $\boldsymbol{\mathcal{P}}_{\mathrm{M}}$ is identical to that of the bulk mobility tensor, with the orientation vector $\boldsymbol{u}$ replaced by the normal vector $\boldsymbol{n}$. Therefore, the matrix elements of $\boldsymbol{\mathcal{P}}_{\mathrm{M}}$ can be expressed as

$$\boldsymbol{\mathcal{P}}_{\mathrm{M}}^{\alpha\beta}(\boldsymbol{R} = 2z_0\boldsymbol{n}) = \frac{1}{8\pi\eta}\frac{1}{(2z_0)^a}\,\boldsymbol{g}^{\alpha\beta}(\boldsymbol{n})\,, \tag{5.26}$$

where $\boldsymbol{g}^{\alpha\beta}$ are the directional tensors where $\alpha, \beta \in \{t, r, d\}$. Moreover, $a = l + l' + \sigma + \sigma' - 1$ with the indices l, σ refer to the superscript α while l', σ' refer to β, so that $a = 1$ for tt, $a = 2$ for (tr, rt, td, dt) and $a = 2$ for (dr, rd, rr, dd).

Knowing the expression of the propagator, the friction matrix can readily be obtained from Eq. (5.20). The friction matrix can be split up into the bulk and the correction term as

$$\boldsymbol{\zeta} = \boldsymbol{\zeta}_0 + \Delta\boldsymbol{\zeta}\,. \tag{5.27}$$

The corrections to the particle mobility can be obtained by an inversion procedure from the equation $\boldsymbol{\mu}\,\boldsymbol{\zeta} = \mathbf{1}$, defining the relations between elements of the friction and mobility tensors, to finally

obtain [208]

$$\boldsymbol{\Delta\mu}^{tt} = \frac{1}{8\pi\eta}\frac{1}{2z_0}\boldsymbol{g}^{tt} + \mathcal{O}(z_0^{-3})\,, \tag{5.28}$$

$$\boldsymbol{\Delta\mu}^{tr} = -\frac{1}{8\pi\eta}\frac{1}{(2z_0)^2}\boldsymbol{g}^{td}\boldsymbol{\mu}_0^{dr} + \mathcal{O}(z_0^{-3})\,, \tag{5.29}$$

$$\boldsymbol{\Delta\mu}^{rt} = \frac{1}{8\pi\eta}\frac{1}{(2z_0)^2}\boldsymbol{\mu}_0^{rd}\boldsymbol{g}^{dt} + \mathcal{O}(z_0^{-3})\,, \tag{5.30}$$

$$\boldsymbol{\Delta\mu}^{rr} = \frac{1}{8\pi\eta}\frac{1}{(2z_0)^3}\left[\boldsymbol{g}^{rr} - \boldsymbol{\mu}_0^{rd}\boldsymbol{g}^{dr} + \boldsymbol{g}^{rd}\boldsymbol{\mu}_0^{dr} - \boldsymbol{\mu}_0^{rd}\boldsymbol{g}^{dd}\boldsymbol{\mu}_0^{dr}\right] + \mathcal{O}(z_0^{-4})\,. \tag{5.31}$$

Interestingly, the leading-order correction to the translational mobility decays with distance from the membrane as z_0^{-1} whereas the coupling and rotational mobility exhibit a faster decay as z_0^{-2} and z_0^{-3}, respectively. In the reference frame of the particle spanned by the unit basis vectors $\{\boldsymbol{u}_1, \boldsymbol{u}_2, \boldsymbol{u}_3\}$, the mobility correction tensors of an axisymmetric particle have the form

$$\Delta\boldsymbol{\mu}^{tt,rr} = \begin{pmatrix} \Delta\mu_{11}^{tt,rr} & 0 & \Delta\mu_{13}^{tt,rr} \\ 0 & \Delta\mu_{22}^{tt,rr} & 0 \\ \Delta\mu_{13}^{tt,rr} & 0 & \Delta\mu_{33}^{tt,rr} \end{pmatrix}, \qquad \Delta\boldsymbol{\mu}^{tr} = \begin{pmatrix} 0 & \Delta\mu_{12}^{tr} & 0 \\ 0 & 0 & \Delta\mu_{23}^{tr} \\ 0 & \Delta\mu_{32}^{tr} & 0 \end{pmatrix}, \tag{5.32}$$

for the translational/rotational and the translation-rotation coupling tensor, respectively. The rotation-translation coupling tensor is obtained by simply taking the transpose of the translation-rotation coupling tensor given above.

As we have shown in our publication [Pub5], the dominant term in the mobility corrections for an axisymmetric particle possesses a simple angular structure stemming from the contraction of the particle friction tensors with the vertical multipole components of the Green tensor in the present geometry. Polynomials in sine and cosine functions of the inclination angle result from the transformation of the corresponding tensors into the common frame of reference. Further derivation details and results have been reported in [Pub5].

The frequency-dependent mobilities calculated in chapters 4 and 5 serve as an input for the computation of the particle diffusion tensor, via the fluctuation-dissipation theorem. In the next chapter, we shall investigate theoretically the Brownian motion nearby elastic cell membranes and show that the aforementioned memory effect induces a long-lived subdiffusive behavior on the nearby suspended particles.

Chapter 6

Brownian motion

> Not everything that can be counted counts, and not everything that counts can be counted.
>
> Albert Einstein

Brownian motion is the apparently random movement of particles suspended in a fluid resulting from their collision with the surrounding atoms or molecules. Brownian motion is named after the British botanist Robert Brown in 1827, who observed through a microscope the random trajectories of pollen grains immersed in water. A physical explanation of the mechanisms by which particles undergo such random movements has been provided in 1905 by Einstein in his seminal work [268]. A few years later, Einstein's result was confirmed experimentally by Perrin [269, 270] providing direct evidence that atoms and molecules exist. In 1926, Perrin was awarded a Nobel Prize in physics "for his work on the discontinuous structure of matter, and especially for his discovery of sedimentation equilibrium." [271].

6.1 Langevin equation

The dynamics of an isolated Brownian particle in a bulk fluid is governed by the celebrated Langevin equation. The latter is a stochastic differential equation [272] for one dimensional motion in a viscous fluid and reads [273]

$$m\,\frac{\mathrm{d}V(t)}{\mathrm{d}t} = -\gamma_0 V(t) + F(t)\,, \tag{6.1}$$

where m is the particle mass, $V(t)$ is the particle translational velocity, $\gamma_0 = \mu_0^{-1} = 6\pi\eta a$ is the bulk friction coefficient and $F(t)$ is the stochastic random force modeling the effect of the background noise caused by the fluid on the Brownian particle. The random force is Gaussian distributed and satisfies the statistical properties

$$\langle F(t)\rangle = 0\,, \qquad \langle F(t)F(t')\rangle = 2\gamma_0 k_\mathrm{B} T\delta(t-t')\,, \tag{6.2}$$

where brackets mean ensemble average, k_B is the Boltzmann constant and T is the absolute temperature of the system. Here we assume that there are no other external forces acting on the particle.

In a suspension of particles, there are three vastly different timescales, denoted τ_S, τ_B and τ_P. The time τ_S is the short atomic timescale, which is of the order of picoseconds. The second timescale τ_B is the Brownian timescale, required for the particle to relax towards that of the fluid. It is of the order of the ratio between the particle mass and the bulk friction coefficient, that is $\tau_\mathrm{B} \simeq m/\gamma_0$. In

typical colloidal systems, this time is of the order of microseconds. Lastly, τ_{P} is the time required for the particle to diffuse across its own radius a, such that $\tau_{\mathrm{P}} \simeq a^2/D_0$, where D_0 is the molecular diffusion coefficient. The latter can be calculated from Einstein's relation [268]

$$D_0 = \frac{k_{\mathrm{B}}T}{\gamma_0}\,. \tag{6.3}$$

The time τ_{P} is of the order of hours or even days and strongly depends on the particle size. Hereinafter, we shall be focusing on diffusion in the *overdamped regime*, *i.e.* for timescales in the range $\tau_{\mathrm{B}} \ll \tau \ll \tau_{\mathrm{P}}$.

The presence of an elastic membrane introduces a memory in the system [274] and the particle dynamics should therefore be treated within a generalized Langevin formalism [275, 276]

$$m\,\frac{\mathrm{d}V(t)}{\mathrm{d}t} = -\int_{-\infty}^{t} \gamma(t-t')V(t')\,\mathrm{d}t' + F(t)\,, \tag{6.4}$$

where $\gamma(t)$ is the time dependent friction retardation function (expressed in $\mathrm{kg/s^2}$). In the particular case when $\gamma(t) = 2\gamma_0\,\delta(t)$, Eq. (6.4) is reduced to the classical non-retarded Langevin equation given by Eq. (6.1), in which the random force has been assumed to be a purely Gaussian process delta correlated in time.

The computation of the particle mean-square displacement (MSD) requires as an intermediate step the determination of the velocity autocorrelation function via the fluctuation-dissipation theorem. This will be the subject of the next section.

6.2 Fluctuation-dissipation theorem

By evaluating the Fourier transform of both members in Eq. (6.4) as previously defined by Eq. (3.7), we obtain

$$im\omega V(\omega) = -\int_{t=-\infty}^{\infty} e^{-i\omega t}\,\mathrm{d}t \int_{t'=-\infty}^{t'=t} \gamma(t-t')V(t')\,\mathrm{d}t' + F(\omega)\,. \tag{6.5}$$

Using the change of variables $u = t - t'$, together with the shift property in time domain of Fourier transforms[1], the particle velocity is related to the fluctuating force via the equation

$$V(\omega) = \frac{F(\omega)}{im\omega + \gamma[\omega]}\,, \tag{6.6}$$

where $\gamma[\omega]$ is the Fourier-Laplace (also called one-sided Fourier) transform of the retardation function, defined by

$$\gamma[\omega] = \int_0^{\infty} \gamma(t)e^{i\omega t}\,\mathrm{d}t\,. \tag{6.7}$$

In virtue of the fluctuation-dissipation theorem (FDT) [275], the frictional forces and the random forces are not independent quantities, but they are rather related to each other via the correlation

$$\langle F(\omega)\overline{F(\omega')}\rangle = \phi_{\mathrm{F}}(\omega)\,\delta(\omega+\omega')\,, \tag{6.8}$$

where $\phi_{\mathrm{F}}(\omega)$ is the Fourier transform of the velocity autocorrelation function $\phi_{\mathrm{F}}(t)$, known also in the literature as the power spectrum of $F(\omega)$. In term of the friction kernel, the power spectrum is

[1] The shift in time domain is the property $\mathscr{F}\{F(t-x)\} = e^{-ix\omega}F(\omega)$ for $x \in \mathbb{R}$.

given by

$$\phi_{\mathrm{F}}(\omega) = k_{\mathrm{B}}T\left(\gamma[\omega] + \gamma[-\omega]\right) = 2k_{\mathrm{B}}T\,\mathrm{Re}\left(\gamma[\omega]\right)\,, \tag{6.9}$$

noting that $\overline{\gamma[\omega]} = \gamma[-\omega]$, as can be inferred from Eq. (6.7). The power spectra of $V(\omega)$ and $F(\omega)$ are thus related to each other via the relation

$$\phi_{\mathrm{V}}(\omega) = \frac{\phi_{\mathrm{F}}(\omega)}{|im\omega + \gamma[\omega]|^2}\,. \tag{6.10}$$

By making use of Eq. (6.9), we obtain

$$\phi_{\mathrm{V}}(\omega) = \frac{k_{\mathrm{B}}T}{im\omega + \gamma[\omega]} + c.c.\,, \tag{6.11}$$

where *c.c.* stands for complex conjugate. Provided that $\gamma[\omega]$ is known, it is therefore possible to transform $\phi_{\mathrm{V}}(\omega)$ back to the time domain, leading directly to the velocity autocorrelation function

$$\phi_{\mathrm{V}}(t) := \langle V(0)V(t)\rangle = \frac{k_{\mathrm{B}}T}{2\pi}\int_{-\infty}^{\infty}\left(\frac{1}{im\omega + \gamma[\omega]} + c.c.\right)e^{i\omega t}\,\mathrm{d}\omega\,. \tag{6.12}$$

It can be shown that the contribution from the second term in Eq. (6.12) vanishes for $t > 0$ since the integrand is analytic in the upper half plane in which $\mathrm{Im}\,\omega > 0$ [277]. As a result, the velocity autocorrelation function can be written for $t > 0$ as

$$\phi_{\mathrm{V}}(t) = \frac{k_{\mathrm{B}}T}{2\pi}\int_{-\infty-i\epsilon}^{\infty-i\epsilon}\frac{e^{i\omega t}}{im\omega + \gamma[\omega]}\,\mathrm{d}\omega\,, \tag{6.13}$$

where $\epsilon > 0$ is a contour integration parameter. In the overdamped regime, *i.e.* in the massless limit, Eq. (6.13) is drastically simplified to finally obtain [277]

$$\phi_{\mathrm{V}}(t) = \frac{k_{\mathrm{B}}T}{2\pi}\int_{-\infty}^{\infty}\mu(\omega)e^{i\omega t}\,\mathrm{d}\omega\,. \tag{6.14}$$

for $t > 0$.

6.3 Diffusion near cell membranes

Having computed the velocity autocorrelation function ϕ_{V}, the mean-squared displacement (MSD) can thus be obtained. The distance traveled by the Brownian particle in a time interval $[0, t]$ is the integral of its velocity, such that

$$x(t) = \int_0^t V(t_1)\,\mathrm{d}t_1\,, \tag{6.15}$$

whose square reads

$$x(t)^2 = \int_0^t\int_0^t V(t_1)V(t_2)\,\mathrm{d}t_1\,\mathrm{d}t_2\,. \tag{6.16}$$

Using the change of variables $t_2 = t_1 + s$, and integrating with respect to the variable t_1, the mean-squared displacement reads

$$\langle x(t)^2\rangle = 2\int_0^t (t-s)\phi_{\mathrm{V}}(s)\,\mathrm{d}s\,, \tag{6.17}$$

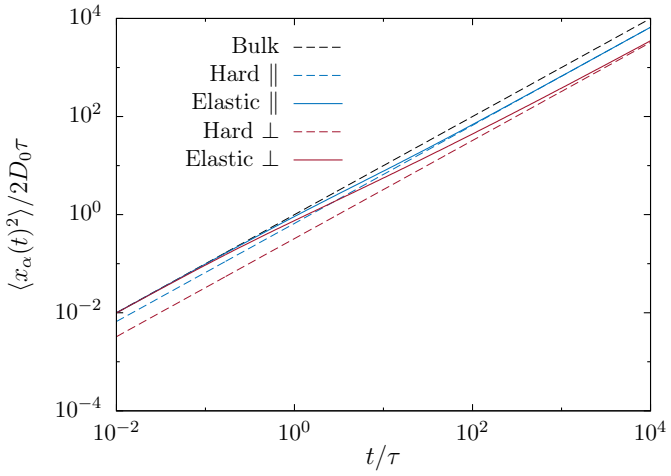

Figure 6.1: Scaled mean-squared displacement versus the scaled time for a particle diffusion parallel (blue) or perpendicular (red) to an elastic membrane for $a/z_0 = 3/5$. Here we take $\tau = T_S = T_B$ as a characteristic time scale for the particle-membrane system.

noting that the autocorrelation is a stationary process that depends only on the time difference $t_1 - t_2$ [277]. The particle long-time diffusion coefficient is computed as

$$D_\infty := \lim_{t\to\infty} \frac{\langle x(t)^2\rangle}{2t} = \int_0^\infty \phi_V(s)\,\mathrm{d}s\,. \tag{6.18}$$

In the following, we shall be interested in the MSD of a solid particle initially located at $z = z_0$, moving parallel or perpendicular to a planar elastic membrane possessing both shearing and bending rigidities. Analogous predictions can be performed nearby a membrane of an arbitrary shape provided that the frequency-dependent mobility functions associated with the geometry of interest are known.

The resulting MSD is the sum of the MSDs for parallel diffusion along the x and y directions and the MSD for perpendicular diffusion along the z direction such that

$$\langle r(t)^2\rangle = 2\langle x_\parallel(t)^2\rangle + \langle x_\perp(t)^2\rangle\,. \tag{6.19}$$

We further emphasize that we neglect here the z-dependence of the mobility functions in our MSD calculations for diffusion normal to the membrane. Indeed, it would be of interest to investigate the more complex scenario in which $\langle x_\perp(t)^2\rangle$ is of the same order of magnitude as z_0^2, and thus accounting for the z-dependence of the mobility becomes crucial for an accurate computation of the particle diffusion normal to the membrane.

Another way to quantify the slowing down of the particle is to investigate the time-dependent scaling exponent of the MSD, which is defined as the logarithmic derivative of the MSD such that

$$\gamma_\alpha(t) := \frac{\mathrm{d}\ln\langle x_\alpha(t)^2\rangle}{\mathrm{d}\ln t}\,, \qquad \alpha \in \{\parallel, \perp\}\,. \tag{6.20}$$

If diffusion is normal (standard), then the scaling exponent is one. Anomalous subdiffusion is characterized by a scaling exponent that is less than one and is often encountered in biological media with obstacles [278] or binding sites [279]. In the following, we shall present some illustrative results to get an idea about the mechanism of diffusion nearby cell membranes. Further results have been reported in our publications [Pub1, Pub2, Pub3, Pub9].

In Fig. 6.1, we show the particle time-dependent MSD for the diffusional motion parallel (blue) and perpendicular (red) to a planar elastic membrane. The ratio of the particle radius to the distance from the membrane is taken $a/z_0 = 3/5$. We define the characteristic time scale for shearing as $T_S := 6z_0\eta/\kappa_S$, and for bending as $T_B := 4\eta z_0^3/\kappa_B$. We then scale the time by $\tau := T_S = T_B$ for which membrane shearing and bending moduli are related via the relation $z_0^2 = 3\kappa_B/(2\kappa_S)$.

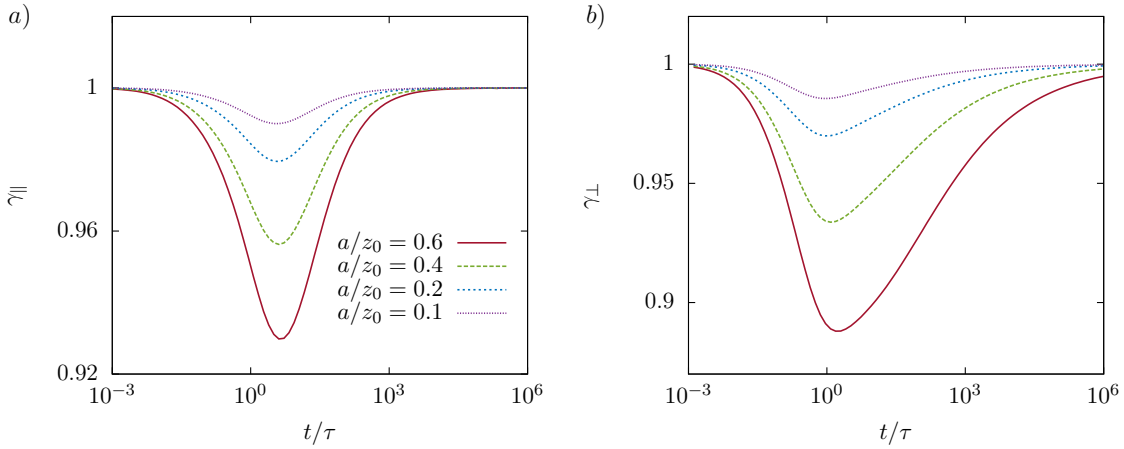

Figure 6.2: Variations of the scaling exponent for the motion parallel (a) and perpendicular (b) to the membranes as given by Eq. (6.20) versus the scaled time.

At short time scales for which $t \ll \tau$, we observe that the MSDs follow faithfully the linear behavior in a bulk fluid, with the normal diffusion coefficient D_0 predicted from Einstein's theory. This is justified by the fact that the particle does not yet feel the presence of the membrane at these short time scales. As the time increases, the MSDs substantially bend down to asymmetrically approach the linear behavior predicted nearby a non-slip hard-wall.

Fig. 6.2 shows the temporal evolution of the scaling exponent as defined by Eq. (6.20) which is found to be strongly dependent on the distance separating the particle from the membrane. We first remark that the scaling exponent amounts to a value of 1 as $t \to 0$ and as $t \to \infty$, at which the particle experiences normal diffusion. For $t \sim \tau$, we observe a bending down of the scaling exponent, resulting in a long-lasting subdiffusive regime that extends up to $10^3\tau$ in the parallel direction and even further in the perpendicular direction. As the ratio a/z_0 gets larger, the hydrodynamic coupling between the particle and the membrane becomes more important and thus the subdiffusive behavior is enhanced. For $a/z_0 = 3/5$, we find that the exponent can go as low as 0.93 for the parallel motion and as low as 0.88 for the perpendicular motion.

In the next chapter, we present the boundary integral method we use to verify and validate our analytical theory together with some technical implementation details.

Chapter 7

Numerical method

docendo disco, scribendo cogito

Seneca the Younger

For the simulations we use the boundary integral method (BIM) [280] whose foundation is the steady Stokes equations (3.2) and (3.3). The core idea of the method is to expresses the solution of the Stokes equations in terms of singularity distributions over the domain boundary [238]. The method permits a complete description of the fluid flow inside a control volume while requiring only the knowledge of velocity or traction on boundaries. A special advantage of BIM is the fact that only a single 2D grid is needed which can be used for the surface deformation as well as for the 3D flow computation.

7.1 Boundary integral equation

We consider a suspension of N particles moving under the influence of an imposed external flow $\boldsymbol{v}^\infty$. The velocity of a point $\boldsymbol{x}$ in the fluid domain is given by the integral representation [280]

$$v_j(\boldsymbol{x}) = v_j^\infty(\boldsymbol{x}) - \sum_{m=1}^{N} (N_m \Delta \boldsymbol{f})_j(\boldsymbol{x}) + \sum_{m=1}^{N} (1-\lambda_m)\,(K_m \boldsymbol{v})_j(\boldsymbol{x})\,, \tag{7.1}$$

where $\Delta \boldsymbol{f}$ denotes the jump of the traction across the particles. We define the single layer integral for a given vectorial function $\boldsymbol{g}$ as

$$(N_m\,\boldsymbol{g})_j(\boldsymbol{x}) := \int_{S_m} g_i(\boldsymbol{y})\,\mathcal{G}_{ij}^{(0)}(\boldsymbol{y},\boldsymbol{x})\,\mathrm{d}S(\boldsymbol{y})\,, \tag{7.2}$$

where integration over the surface of the particle S_m needs to be performed. The double layer integral is defined as

$$(K_m\,\boldsymbol{g})_j(\boldsymbol{x}) := \int_{S_m} g_i(\boldsymbol{y})\,\mathcal{T}_{ijk}^{(0)}(\boldsymbol{y},\boldsymbol{x})\,n_k(\boldsymbol{y})\,\mathrm{d}S(\boldsymbol{y})\,. \tag{7.3}$$

The remaining quantities are the viscosity contrast $\lambda_m := \eta_m/\eta$ representing the ratio of inner to outer viscosity, the outer normal vector $\boldsymbol{n}$ pointing into the ambient fluid, the free-space Stokeslet defined by Eq. (3.17), and the corresponding Stresslet

$$\mathcal{T}_{ijk}^{(0)}(\boldsymbol{y},\boldsymbol{x}) := -\frac{3}{4\pi}\frac{s_i s_j s_k}{s^5}\,, \tag{7.4}$$

with $\boldsymbol{s} := \boldsymbol{y} - \boldsymbol{x}$ and $s := |\boldsymbol{s}|$.

Taking the limit when $\boldsymbol{x}$ approaches the surface of the pth particle, we derive the boundary integral equation, which is a Fredholm integral of the second kind for the velocity,

$$v_j(\boldsymbol{x}) = \frac{2}{1+\lambda_p}\left(v_j^{\infty}(\boldsymbol{x}) - \sum_{m=1}^{N}(N_m\Delta\boldsymbol{f})_j(\boldsymbol{x}) + \sum_{m=1}^{N}(1-\lambda_m)\,(K_m^{\mathrm{PV}}\boldsymbol{v})_j(\boldsymbol{x})\right), \tag{7.5}$$

where PV denotes the principal value of the double-layer integral [238]. Taking $\lambda_p = 1$ with $1 \le p \le N$, the last equation is drastically simplified and reduced to a Fredholm equation of the first kind.

7.2 Completed double layer BIM

We now consider N deformable particles (referred to as BIM objects which in our case have an elastic nature) and $\overline{N}$ rigid particles (referred to as CDL objects) flowing under the influence of an imposed flow field. Treating rigid objects in the direct formulation is difficult and inefficient since it would lead to a Fredholm equation of the first kind. Instead, it is worthwhile to employ an extension called the completed double layer boundary integral method (CDLBIM) [281–283]. Restricting to a unit viscosity contrast for the BIM objects, the CDLBIM equations read

$$v_j(\boldsymbol{x}) = H_j(\boldsymbol{x}), \quad \boldsymbol{x} \in S_p, \tag{7.6a}$$

$$\frac{1}{2}\,\phi_j(\boldsymbol{x}) + \sum_{i=1}^{6}\varphi_j^{(i)}(\boldsymbol{x})\,\langle\boldsymbol{\varphi}^{(i)},\boldsymbol{\phi}\rangle = H_j(\boldsymbol{x}), \quad \boldsymbol{x} \in \overline{S}_q. \tag{7.6b}$$

where S_p is the surface of the pth deformable BIM object, and $\overline{S}_q$ is the surface of the qth rigid CDL object, where $1 \le p \le N$ and $1 \le q \le \overline{N}$. Moreover, $\boldsymbol{v}$ represents the velocity on the BIM objects while $\boldsymbol{\phi}$ denotes the so-called double layer density function on $\overline{S}$. The latter is an unphysical auxiliary field. However, the corresponding physical translational and rotational velocities can be retrieved via

$$\boldsymbol{V}(\boldsymbol{x}) = \sum_{i=1}^{3}\boldsymbol{\varphi}^{(i)}(\boldsymbol{x})\langle\boldsymbol{\varphi}^{(i)},\boldsymbol{\phi}\rangle, \quad \boldsymbol{x} \in \overline{S}_q, \tag{7.7a}$$

$$\boldsymbol{\Omega}(\boldsymbol{x}) \times (\boldsymbol{x} - \boldsymbol{X}_q) = \sum_{i=1}^{3}\boldsymbol{\varphi}^{(i+3)}(\boldsymbol{x})\langle\boldsymbol{\varphi}^{(i+3)},\boldsymbol{\phi}\rangle, \quad \boldsymbol{x} \in \overline{S}_q, \tag{7.7b}$$

where $\boldsymbol{X}_q$ being the centroid of the particle q and $\boldsymbol{\varphi}^{(i)}$ are known functions representing the six possible rigid body movements of the solid particles [281]. The brackets denote the inner product in the vector space of real functions whose domain is $\overline{S}_q$. Continuing, the function H_j is given by

$$\begin{aligned} H_j(\boldsymbol{x}) := v_j^{\infty}(\boldsymbol{x}) &- \sum_{m=1}^{N}(N_m\Delta\boldsymbol{f})_j(\boldsymbol{x}) - \sum_{m=1}^{\overline{N}}(K_m\boldsymbol{\phi})_j(\boldsymbol{x}) \\ &+ \sum_{m=1}^{\overline{N}}\left(\mathcal{G}_{jk}^{(0)}(\boldsymbol{x},\boldsymbol{X}_k)F_k + \mathcal{R}_{jk}^{(0)}(\boldsymbol{x},\boldsymbol{X}_k)L_k\right), \end{aligned} \tag{7.8}$$

where $\boldsymbol{F}_k$ and $\boldsymbol{L}_k$ are the known force and torque acting on the particle surface, respectively. Moreover, the rotlet solution reads

$$\mathcal{R}_{ij}^{(0)}(\boldsymbol{y},\boldsymbol{x}) := \frac{1}{8\pi}\frac{\epsilon_{ijk}s_k}{s^3}. \tag{7.9}$$

Clearly, in the absence of CDL objects, Eq. (7.6a) reduces to the standard boundary integral equation given by Eq. (7.5) in the general case for arbitrary viscosity contrast.

Given the traction jumps $\Delta \boldsymbol{f}$ computed from the current deformation, and the forces and torques as inputs, equations (7.6) constitute a set of Fredholm integral equations of the second kind for the unknown velocity $\boldsymbol{v}$ on the BIM objects and the density $\boldsymbol{\phi}$ on the rigid particles. To solve this equation numerically, we discretize all surfaces with flat triangles. For a rigid spherical particle, this is done by consecutively refining an icosahedron [219, 284]. We perform the integration numerically by a Gaussian quadrature with seven points per triangle [285] together with linear interpolation of nodal values across each triangle [280]. The singularities appearing in the single layer integral are treated via the polar integration rule [286], while the singularities of the double layer integral are eliminated by the standard singularity subtraction scheme [280]. With this the integral equation can be evaluated at all nodes, forming a dense and asymmetric linear system of equations which is then subsequently solved by GMRES [287]. The residuum of the solver is consistently fixed to 10^{-4}. This provides us with the velocity $\boldsymbol{v}$ at each node of the BIM objects and, after application of equation (7.7), also of the rigid particle. The dynamical evolution of the system is hence obtained by solving the kinematic condition [238]

$$\frac{\mathrm{d}\boldsymbol{x}}{\mathrm{d}t} = \boldsymbol{v}(\boldsymbol{x})\,, \tag{7.10}$$

with the explicit Euler scheme. Throughout this thesis, we chose a step size that is dependent on the wiggling frequency of the force (see the last section of this chapter for more details.)

7.3 Computation of the traction jumps

Here we provide some technical details regarding the computation of the traction jump $\Delta \boldsymbol{f}$ across the membranes, as required for Eq. (7.8). The membranes are endowed with shear and area elasticity together with bending rigidity.

7.3.1 Shear elasticity

We employ either the neo-Hookean or the Skalak model whose areal energy densities W are given by Eq. (2.9) and (2.11), respectively. The strain invariants I_1 and I_2 are related to the principal in-plane stretch ratios via $I_1 = \lambda_1^2 + \lambda_2^2 - 2$ and $I_2 = \lambda_1^2\lambda_2^2 - 1$. Hence, the total energy of a membrane S_p is given by

$$E_\mathrm{S} = \int_{S_p^{(0)}} W \,\mathrm{d}S_0\,, \tag{7.11}$$

where the integration is performed over the surface in the reference state $S_p^{(0)}$. To obtain the force at each node, we assume that the deformation is a linear function of position in each triangle. After discretization of the integral, the energy E_S depends explicitly on the node positions $\boldsymbol{x}_i$. Therefore, according to the principle of virtual work, the total force is then given by the gradient

$$\boldsymbol{F}(\boldsymbol{x}_i) = \frac{\partial E_\mathrm{S}}{\partial \boldsymbol{x}_i}\,. \tag{7.12}$$

This derivative can be computed analytically as detailed in references [219, 288]. The traction jump is thus obtained by

$$\Delta \boldsymbol{f}(\boldsymbol{x}_i) = \frac{\boldsymbol{F}(\boldsymbol{x}_i)}{A_i}\,, \tag{7.13}$$

whereas A_i is the area associated with node $\boldsymbol{x}_i$ and is taken as one third of the total area of the triangles containing the node [283].

7.3.2 Bending rigidity

The bending forces are modeled according to the constitutive law proposed Helfrich [224] leading to the traction jump stated by Eq. (2.17). The mean curvature H is calculated according to the relation $H(\boldsymbol{x}) = -\frac{1}{2}\left(\Delta_{\parallel} x_i\right) n_i(\boldsymbol{x})$. We use the algorithms presented by Meyer *et al.* [289] for the computation of the Laplace-Beltrami operator $\Delta_{\parallel}$ and the Gaussian curvature K. The normal vector $\boldsymbol{n}$ is computed according to the "mean weighted by angle" method. This provides reasonable results in the application of viscous flows [237]. We note that we set $\Delta \boldsymbol{f}$ to zero for nodes located at the border of open meshes.

7.4 Determination of particle mobilities

Now we consider two particles labeled γ and λ moving nearby an elastic membrane as schematically illustrated in Fig. 4.1. For the numerical determination of the particle mobility functions, a harmonic force $\boldsymbol{F}_\lambda(t) = \boldsymbol{A}_\lambda e^{i\omega_0 t}$ or torque $\boldsymbol{L}_\lambda(t) = \boldsymbol{B}_\lambda e^{i\omega_0 t}$ is exerted at the surface of the particle λ. After a brief transient evolution, the translational and rotational velocities of the particle γ evolve as $\boldsymbol{V}_\gamma(t) = \boldsymbol{C}_\gamma e^{i(\omega_0 t + \delta_\gamma)}$ and $\boldsymbol{\Omega}_\gamma(t) = \boldsymbol{D}_\gamma e^{i(\omega_0 t + \varphi_\gamma)}$, respectively, and analogously for the particle λ. The amplitudes and phase shifts can accurately be determined by a fitting procedure of the numerically recorded velocities using the trust region method [290]. In this way, the tt and rt components can be computed for a torque-free particle as

$$\mu_{\alpha\beta}^{tt,\lambda\lambda} = \frac{C_{\lambda\alpha}}{A_{\lambda\beta}}\, e^{i\delta_\lambda}\,, \qquad \mu_{\alpha\beta}^{rt,\lambda\lambda} = \frac{D_{\lambda\alpha}}{A_{\lambda\beta}}\, e^{i\varphi_\lambda}\,, \tag{7.14}$$

for the self-mobilities and

$$\mu_{\alpha\beta}^{tt,\gamma\lambda} = \frac{C_{\gamma\alpha}}{A_{\lambda\beta}}\, e^{i\delta_\lambda}\,, \qquad \mu_{\alpha\beta}^{rt,\gamma\lambda} = \frac{D_{\gamma\alpha}}{A_{\lambda\beta}}\, e^{i\varphi_\lambda}\,, \tag{7.15}$$

for the pair-mobilities. For a force-free particle, the components tr and rr are computed from

$$\mu_{\alpha\beta}^{tr,\lambda\lambda} = \frac{C_{\lambda\alpha}}{B_{\lambda\beta}}\, e^{i\delta_\lambda}\,, \quad \mu_{\alpha\beta}^{rr,\lambda\lambda} = \frac{D_{\lambda\alpha}}{B_{\lambda\beta}}\, e^{i\varphi_\lambda}\,, \tag{7.16}$$

for the self-mobilities and

$$\mu_{\alpha\beta}^{tr,\gamma\lambda} = \frac{C_{\gamma\alpha}}{B_{\lambda\beta}}\, e^{i\delta_\gamma}\,, \quad \mu_{\alpha\beta}^{rr,\gamma\lambda} = \frac{D_{\gamma\alpha}}{B_{\lambda\beta}}\, e^{i\varphi_\gamma}\,. \tag{7.17}$$

for the pair-mobilities.

Appendix

> In mathematics you don't understand things. You just get used to them.
>
> Johann von Neumann

In this appendix, we shall provide some technical details with regard to the computation of the 2D forward and inverse Fourier transform relevant for the calculation of the Green's functions nearby planar elastic membranes.

The spatial 2D Fourier transform as defined by Eq. (3.4) can also be expressed using polar coordinates. By introducing the coordinate transformations $x = \rho\cos\phi$ and $y = \rho\sin\phi$, and similarly for the wavevector components $q_x = q\cos\theta$ and $q_y = q\sin\theta$, we obtain

$$\tilde{f}(q,\theta) = \int_0^\infty \int_{-\pi}^{\pi} f(\rho,\phi) e^{-i\rho q\cos(\theta-\phi)} \rho \,\mathrm{d}\rho \,\mathrm{d}\phi \,. \tag{7.18}$$

Depending on the symmetry properties of $f(\rho,\phi)$ we shall consider two different cases separately.

Radially symmetric functions

For radially symmetric functions, *i.e.* when f depends only on the radial distance ρ, the integral given by Eq. (7.18) can be expressed as

$$\tilde{f}(q,\theta) = \int_0^\infty \rho f(\rho) \int_{-\pi}^{\pi} e^{-i\rho q\cos(\theta-\phi)} \,\mathrm{d}\phi \,\mathrm{d}\rho \,. \tag{7.19}$$

Introducing the zero-order Bessel function [291]

$$J_0(\rho q) := \frac{1}{2\pi}\int_{-\pi}^{\pi} e^{-i\rho q\cos\phi} \,\mathrm{d}\phi = \frac{1}{2\pi}\int_{-\pi}^{\pi} e^{-i\rho q\cos(\theta-\phi)} \,\mathrm{d}\phi \,. \tag{7.20}$$

Eq. (7.19) can then be written as

$$\tilde{f}(q) = 2\pi \int_0^\infty \rho f(\rho) J_0(q\rho) \,\mathrm{d}\rho \,, \tag{7.21}$$

which is in fact nothing but the zeroth order Hankel transform of $f(\rho)$ apart from a factor of 2π. Similarly, it can be shown that the inverse 2D Fourier transform stated by Eq. (3.5) can be written for radially symmetric functions as

$$\mathscr{F}^{-1}\{\tilde{f}(q)\} = \frac{1}{2\pi}\int_0^\infty q\tilde{f}(q) J_0(\rho q) \,\mathrm{d}q \,. \tag{7.22}$$

Non-radially symmetric functions

In order to perform the inverse 2D Fourier transform for a non-radially symmetric function, we shall use a generalization of the method previously applied for radially symmetric functions. When f is a function of both ρ and ϕ, and periodic in ϕ, it can then be expanded into a Fourier series as

$$f(\rho,\phi) = \sum_{n=-\infty}^{\infty} f_n(\rho) e^{in\phi}\,, \tag{7.23}$$

where the Fourier coefficients are given by

$$f_n(\rho) = \frac{1}{2\pi}\int_0^{2\pi} f(\rho,\phi) e^{-in\phi}\,\mathrm{d}\phi\,. \tag{7.24}$$

In the same way, the Fourier transform $\tilde{f}(q,\theta)$ can also be expanded into a Fourier series such that

$$\tilde{f}(q,\theta) = \sum_{n=-\infty}^{\infty} \tilde{f}_n(q) e^{in\theta}\,, \tag{7.25}$$

where

$$\tilde{f}_n(q) = \frac{1}{2\pi}\int_0^{2\pi} \tilde{f}(q,\theta) e^{-in\theta}\,\mathrm{d}\theta\,. \tag{7.26}$$

By making use of the following remarkable identity [292, 293]

$$e^{-i\mathbf{q}.\boldsymbol{\rho}} = \sum_{m=-\infty}^{\infty} i^{-m} J_m(q\rho) e^{-im\phi} e^{im\theta}\,, \tag{7.27}$$

together with the Fourier series given in Eq. (7.23), the forward 2D Fourier transform is then obtained as

$$\tilde{f}(q,\theta) = \int_0^{\infty}\int_0^{2\pi} \left(\sum_{n=-\infty}^{\infty} f_n(\rho) e^{in\phi}\right)\left(\sum_{m=-\infty}^{\infty} i^{-m} J_m(q\rho) e^{-im\phi} e^{im\theta}\right)\mathrm{d}\phi\rho\,\mathrm{d}\rho\,. \tag{7.28}$$

Since

$$\int_0^{2\pi} e^{in\phi}\mathrm{d}\phi = 2\pi\delta_{n0}\,, \tag{7.29}$$

only the terms with $m = n$ remain, leading to

$$\tilde{f}(q,\theta) = \sum_{n=-\infty}^{\infty} 2\pi i^{-n} e^{in\theta}\int_0^{\infty} f_n(\rho) J_n(q\rho)\rho\,\mathrm{d}\rho\,. \tag{7.30}$$

By identification with the Fourier series of $\tilde{f}$ as written in (7.25), we immediately recover the Fourier coefficients,

$$\tilde{f}_n(q) = 2\pi i^{-n}\int_0^{\infty} f_n(\rho) J_n(q\rho)\rho\,\mathrm{d}\rho\,, \tag{7.31}$$

which is the nth order Hankel transform of $f_n(\rho)$ multiplied by $2\pi i^{-n}$. In a similar way, it is easy to obtain the inverse Fourier transform of $\tilde{f}$ by using this time the identity

$$e^{i\mathbf{q}.\boldsymbol{\rho}} = \sum_{m=-\infty}^{\infty} i^{m} J_m(q\rho) e^{im\phi} e^{-im\theta}\,, \tag{7.32}$$

to find the Fourier series coefficients $f_n(\rho)$ as

$$f_n(\rho) = \frac{i^n}{2\pi} \int_0^\infty \tilde{f}_n(q) J_n(\rho q) q \, \mathrm{d}q \, . \tag{7.33}$$

In summary, in order to find the inverse Fourier transform for a given non-radially symmetric function $\tilde{f}(\rho, \phi)$, two steps are required:

1. Evaluate the function series $\tilde{f}_n(q)$ from Eq. (7.26).
2. Find $f_n(\rho)$ using the formula (7.33).

The solution $f(\rho, \phi)$ is written as infinite series as presented in Eq. (7.23).

Summary and outlooks

> There are no such things as applied sciences, only applications of science.
>
> Louis Pasteur

We present an analytical theory supplemented by fully resolved boundary integral simulations of the hydrodynamic interactions and diffusion of particles nearby a realistically modeled red blood cell membrane endowed with resistance towards shearing and bending. In the first step, the theory provides the Green's functions which are solutions of the linear hydrodynamic equations for the fluid flow field induced by a concentrated point-force singularity acting close to the membrane. Depending on the membrane geometry, we adopt three different approaches for the computation of the Green's functions. Firstly, we present the 2D Fourier transform technique which is based on transforming the Stokes equations governing the fluid motion into a linear system of ordinary differential equations written in the spatial and temporal frequency domains. The method is known to be appropriate for the determination of the solutions of the Stokes equations in systems composed by parallel planar interfaces. Upon inverse Fourier transformation, the resulting Green's functions can conveniently be expressed as convergent infinite integrals over the wavenumber. Secondly, we present the Fourier-Bessel integral technique which consists of expanding the solution in the form of Fourier integrals which involve unknown coefficients that can be determined from the boundary conditions. The method is perfectly suited for domains bounded by interfaces of cylindrical geometry. Thirdly, we present the spherical harmonics technique which is based on the idea of expressing the solution of the fluid flow nearby spherical boundaries in terms of infinite sums of independent harmonics with unknown coefficients. The sum can then be truncated at some finite integer depending on the desired precision. In the limits of vanishing forcing frequencies, all three approaches yield the correct hard-wall limits with stick boundary conditions.

In the next step, we characterize the fluid mediated hydrodynamic interactions between particles by analytically computing the hydrodynamic mobility functions which couple the particles' translational and rotational velocities to the torques and forces applied on their surfaces. For that, we employ a combination of the multipole expansion and Faxén theorem to yield analytical expressions of the particle self- and pair-mobilities obtained directly from the Green's functions associated with the geometry of interest. For a planar elastic membrane, the corrections to the mobility function are expressed as a power series up to the 5th order of the ratio between particle radius and distance from the membrane for the self-mobilities, and between particle radius and interparticle distance for the pair-mobilities. The mobilities are found to be complex valued frequency-dependent functions whose real parts are generally logistic-like functions, whereas the imaginary parts exhibit at intermediate frequencies typical peak structures. The latter are a clear signature of the memory effect induced by the elastic nature of the membrane. In the high frequency limit, the corrections to the mobilities vanish and thus we recover the behavior in a bulk fluid.

We further show that the particle mobilities nearby a single membrane can appropriately be

expressed as a linear superposition of the contributions due to shearing and bending as obtained independently. Additionally, we demonstrate that the shearing and bending related parts may have additive or suppressive contribution to the total mobility. This interesting behavior is elucidated by considering the steady motion of two particles towards a membrane. The interaction nearby a membrane with pure bending resistance is found to be always repulsive, *i.e.* as in the case of a hard wall, while nearby a membrane of pure shearing, the interaction may be attractive. Moreover, we show that there exists a frequency range in which some of the pair-mobility components may interestingly exceed their bulk values. This leads to a short-lived superdiffusive behavior when considering the joint mean-square displacement.

Considering curved membranes, we find that membrane shearing manifests itself in a more pronounced way compared to bending and thus strongly determines the qualitative behavior of elastically confined particles near red blood cell membranes. Moreover, we recover the Green's functions and particle mobilities in the hard boundary limits only if the membrane possesses some finite resistance towards shearing. For curved membranes, our theoretical calculations are restricted to the point-particle approximation representing the leading order term in the mobility corrections but going beyond that is feasible although laborious. We further show that for spherical membranes, curvature leads to the appearance of a prominent additional low-frequency peak in the mobility functions. The peak is attributed to the fact that the traction jumps due to shearing involve a contribution from the normal displacement in contrast to planar membranes where these traction jumps depend solely on the in-plane tangential displacements. Furthermore, we examine the motion of a spherical capsule due to a nearby point force, finding that the pair-mobility function is uniquely dependent on shearing resistance and can well be describe by a Debye-like model with a single relaxation time.

In the last step, the analytical calculations of the frequency-dependent mobilities provide the friction kernel of the system and thus enable the study of particle diffusional dynamics nearby elastic cell membranes. For that purpose, we apply a generalized Langevin equation governing the time evolution of the particle velocity in systems with memory effect. Using the fluctuation-dissipation theorem relating the friction forces to the stochastic random forces, we compute the particle mean-square displacement which fully characterizes the diffusion process. We show that in the presence of the membrane the particle undergoes a long-lasting anomalous subdiffusion at intermediate time scales of motion. The steady diffusion coefficient is found to be universal and identical to that predicted nearby a hard wall with stick boundary conditions. This subdiffusive behavior can significantly enhance residence time and binding rates nearby membranes and thus may increase the probability to trigger the uptake of particles via endocytosis.

Outlooks

As a future perspective, it would be of interest to supplement and complement the present work by considering further related aspects of particle motion nearby elastic confinement. Possible research topics include

- computing the Green's functions and mobility functions nearby a planar membrane with finite size by solving non-trivial dual integral equations that arise from this mixed boundary problem.
- elucidating the role of inertia by carrying out analogous calculations at finite Reynolds number using matched asymptotic solutions. The analytical predictions can then be compared with numerical simulations performed using a full Navier Stokes solver that accounts for fluid inertia, *e.g.* the lattice Boltzmann method.
- investigating the motion of an axisymmetric particle such as a spheroid or a rod-like particle nearby curved membranes and find out how the coupling and rotational mobilities scale with

distance from the membrane.

- exploring the asymmetric motions of spherical particles inside a spherical elastic cavity.
- carrying out analytical calculations of the self and pair-mobility functions of particles moving inside an elastic cylinder for arbitrary eccentricity. The solution can be formulated as an infinite sum of Fourier-Bessel integrals over the wavenumber. The obtained results can then be compared with those obtained earlier for an infinitely extended planar elastic membrane by considering a very wide channel. A low frequency peak in the imaginary part is expected to occur in the imaginary part together with a dispersion step in the real part, *i.e.* in the same way as observed previously nearby a spherical membrane.
- performing "exact" analytical calculations of the Green's functions and particle frequency-dependent mobilities nearby elastic confinements using the bipolar coordinate technique.
- carrying out analogous theoretical investigations by computing the remaining components of the grand mobility tensor. This allows to address particle motion relative to an arbitrary external flow, *e.g.* an oscillatory shear flow.
- computing the lift force induced by the elastic membrane on a nearby particle by accounting for the second order term in the kinematic condition at the membrane surface. The lift force is expected to be quadratic in the particle parallel translational velocity.
- investigating the motion of swimming microorganisms and self-propelled active particles nearby and through cell membranes, where the aforementioned memory effect or mobility sign reversal may lead to interesting and novel behaviors.

Bibliography

[1] E. C. Eckstein, A. W. Tilles, and F. J. Millero. *Microvasc. Res.*, 36(1):31–39, 1988.

[2] C. Yeh and E. C. Eckstein. *Biophys. J.*, 66(5):1706–1716, 1994.

[3] A. J. Thompson, E. M. Mastria, and O. Eniola-Adefeso. *Biomaterials*, 34(23):5863–5871, 2013.

[4] K. Müller, D. A. Fedosov, and Gompper G. *Sci. Rep.*, 4:1–8, 2014.

[5] G. Gompper and D. A. Fedosov. *Wiley Interdiscip. Rev. Syst. Biol. Med.*, 8(2):157–168, 2016.

[6] R. Langer. *Nature*, 392(6679):5–10, 1998.

[7] S. Naahidi, M. Jafari, F. Edalat, K. Raymond, A. Khademhosseini, and P. Chen. *J. Control. Release*, 166(2):182–194, 2013.

[8] H. Al-Obaidi and A. T. Florence. *J. Drug Deliv. Sci. Technol.*, 30:266–277, 2015.

[9] J. Liu, T. Wei, J. Zhao, Y. Huang, H. Deng, A. Kumar, C. Wang, Z. Liang, X. Ma, *Biomaterials*, 91:44–56, 2016.

[10] G. J. Doherty and H. T. McMahon. *Annu. Rev. Biochem.*, 78(1):857–902, 2009.

[11] A. Meinel, B. Tränkle, W. Römer, and A. Rohrbach. *Soft Matter*, 10(20):3667–3678, 2014.

[12] J. Agudo-Canalejo and R. Lipowsky. *ACS Nano*, 9(4):3704–3720, 2015.

[13] A. Wodarz. *Nat. Cell Biol.*, 4(2):E39–E44, 2002.

[14] J. C. Crocker and B. D. Hoffman. *Methods Cell Biol.*, 83:141–178, 2007.

[15] C. P. Brangwynne, G. H. Koenderink, F. C. MacKintosh, and D. A. Weitz. *Trends Cell Biol.*, 19(9):423–427, 2009.

[16] J. A. Kim, C. Åberg, A. Salvati, and K. A. Dawson. *Nat. Nanotechnol.*, 7(1):62–68, 2012.

[17] A. M. Koch, F. Reynolds, M. F. Kircher, H. P. Merkle, R. Weissleder, and *Bioconjugate Chem.*, 14(6):1115–1121, 2003.

[18] A. S. Arbab, L. A. Bashaw, B. R. Miller, E. K. Jordan, B. K. Lewis, H. Kalish, *Radiology*, 229(3):838–846, 2003.

[19] J.-S. Chang, K. L. B. Chang, D.-F. Hwang, and Z.-L. Kong. *Environ. Sci. Technol.*, 41(6):2064–2068, 2007.

[20] J. Happel and H. Brenner. *Low Reynolds number hydrodynamics: with special applications to particulate media*, volume 1. Springer, 2012.

[21] G. G. Stokes. *On the effect of the internal friction of fluids on the motion of pendulums*, volume 9. Pitt Press, 1851.

[22] H. Löwen. *Phys. Rep.*, 237(5):249–324, 1994.

[23] C Allain, M Cloitre, and M Wafra. *Phys. Rev. Lett.*, 74(8):1478, 1995.

[24] H. Tanaka and T. Araki. *Phys. Rev. Lett.*, 85(6):1338, 2000.

[25] L. Isa, R. Besseling, A. N. Morozov, and W. C. K. Poon. *Phys. Rev. Lett.*, 102(5):058302, 2009.

[26] M. Glässl, M. Hilt, and W. Zimmermann. *Eur. Phys. J. E*, 32(3):265–272, 2010.

[27] S. M. Stavis, J. B. Edel, K. T. Samiee, and H. G. Craighead. *Lab Chip*, 5(3):337–343, 2005.

[28] D. Huh, K. L. Mills, X. Zhu, M. A. Burns, M. D. Thouless, and S. Takayama. *Nat. Mater.*, 6(6):424–428, 2007.

[29] H. A. Lorentz. *Abh. Theor. Phys.*, 1:23, 1907.

[30] H. Brenner. *Chem. Eng. Sci.*, 16:242–251, 1961.

[31] W. R. Dean and M. E. O'Neill. *Mathematika*, 10(01):13–24, 1963.

[32] M. E. O'Neill. *Mathematika*, 11(01):67–74, 1964.

[33] G. B. Jeffery. *Proc. London Math. Soc.*, 2(1):327–338, 1915.

[34] M. Stimson and G. B. Jeffery. *Proc. Roy. Soc. London. Series A*, 111(757):110–116, 1926.

[35] M. E. O'Neill and K. Stewartson. *J. Fluid Mech.*, 27(04):705–724, 1967.

[36] A. J. Goldman, R. G. Cox, and H Brenner. *Chem. Eng. Sci.*, 22:637–651, 1967.

[37] G. S. Perkins and R. B. Jones. *Physica A*, 171(3):575–604, 1991.

[38] G. S. Perkins and R. B. Jones. *Physica A*, 189(3-4):447–477, 1992.

[39] G. S. Perkins. *Image methods for a spherical particle near a planar interface in electrostatics and hydrodynamics*. PhD thesis, Queen Mary, University of London, 1992.

[40] S. Wakiya. *J. Phys. Soc. Japan*, 19(8):1401–1408, 1964.

[41] A. J. Goldman, R. G. Cox, and H Brenner. *Chem. Eng. Sci.*, 22:653–660, 1967.

[42] A. Tözeren and R. Skalak. *J. Fluid Mech.*, 82(02):289–307, 1977.

[43] M. Chaoui and F. Feuillebois. *Quart. J. Mech. Appl. Math.*, 56(3):381–410, 2003.

[44] M. Chaoui. *Migration d'une particule proche d'une paroi en écoulement de cisaillement*. PhD thesis, 1995.

[45] B. Cichocki and R. B. Jones. *Physica A*, 258(3):273–302, 1998.

[46] B. U. Felderhof. *J. Phys. Chem. B*, 109:21406–21412, 2005.

[47] B. U. Felderhof. *J. Chem. Phys.*, 123(18):184903, 2005.

[48] S. Jeney, B. Lukić, J. A. Kraus, T. Franosch, and L. Forró. *Phys. Rev. Lett.*, 100(24):240604, 2008.

[49] T. Franosch and S. Jeney. *Phys. Rev. E*, 79(3):031402, 2009.

[50] K. Huang and I. Szlufarska. *Nat. Commun.*, 6, 2015.

[51] C. W. Oseen. *Neuere Methoden und Ergebnisse in der Hydrodynamik*. 1928.

[52] H. Faxén. *Einwirkung der Gefässwände auf den Widerstand gegen die Bewegung einer kleinen Kugel in einer zähen Flüssigkeit.* PhD thesis, Uppsala University, Uppsala, Sweden, 1921.

[53] H. Faxén. *Ann. Phys.*, 373(10):89–119, 1922.

[54] N. Liron and S. Mochon. *J. Eng. Math.*, 10(4):287–303, 1976.

[55] S. Bhattacharya and J. Bławzdziewicz. *J. Math. Phys.*, 43(11):5720–5731, 2002.

[56] B. U. Felderhof. *J. Chem. Phys.*, 124(5):054111, 2006.

[57] B. U. Felderhof. *J. Chem. Phys.*, 133(7):074707, 2010.

[58] B. U. Felderhof. *J. Fluid Mech.*, 656:223–230, 2010.

[59] S. Bhattacharya, J. Bławzdziewicz, and E. Wajnryb. *J. Comput. Phys.*, 212(2):718–738, 2006.

[60] J. W. Swan and J. F. Brady. *Phys. Fluids*, 22(10):103301, 2010.

[61] P. Ganatos, S. Weinbaum, and R. Pfeffer. *J. Fluid Mech.*, 99:739–753, 8 1980.

[62] P. Ganatos, R. Pfeffer, and S. Weinbaum. *J. Fluid Mech.*, 99:755–783, 8 1980.

[63] B. P. Ho and L. G. Leal. *J. Fluid Mech.*, 65(02):365–400, 1974.

[64] O. Sano and H. Hasimoto. *J. Phys. Soc. Japan*, 40(3):884–890, 1976.

[65] R. G. M. van Der Sman. *J. Colloid Interface Sci*, 351(1):43–49, 2010.

[66] A. Meyer, A. Marshall, B. G. Bush, and E. M. Furst. *J. Rheol.*, 50(1):77–92, 2006.

[67] N. Khatibzadeh, A. B. Stilgoe, A. A. M. Bui, Y. Rocha, G. M. Cruz, V. Loke, *Sci. Rep.*, 4, 2014.

[68] B. Lin, J. Yu, and S. A. Rice. *Phys. Rev. E*, 62:3909–3919, Sep 2000.

[69] E. R. Dufresne, D. Altman, and D. G. Grier. *Europhys. Lett.*, 53(2):264, 2001.

[70] E. Schäffer, S. F. Nørrelykke, and J. Howard. *Langmuir*, 23(7):3654–3665, 2007.

[71] P. P. Lele, J. W. Swan, J. F. Brady, N. J. Wagner, and E. M. Furst. *Soft Matter*, 7(15):6844–6852, 2011.

[72] J. Mo, A. Simha, and M. G. Raizen. *Phys. Rev. E*, 92(6):062106, 2015.

[73] J. Mo. *Short timescale Brownian motion and applications.* PhD thesis, The University of Texas at Austin, 2015.

[74] K. D. Kihm, A. Banerjee, C. K. Choi, and T. Takagi. *Exp. Fluids*, 37(6):811–824, 2004.

[75] R. Sadr, H. Li, and M. Yoda. *Experiments in fluids*, 38(1):90–98, 2005.

[76] B. Cui, H. Diamant, and B. Lin. *Phys. Rev. Lett.*, 89:188302, Oct 2002.

[77] H. B. Eral, J. M. Oh, D. van den Ende, F. Mugele, and M. H. G. Duits. *Langmuir*, 26(22):16722–16729, 2010.

[78] P. Sharma, S. Ghosh, and S. Bhattacharya. *Appl. Phys. Lett.*, 97(10):104101, 2010.

[79] J. C. Benavides-Parra, M. D. Carbajal-Tinoco, A. Conde-Gallardo, E. Ayón-Beato, J. J. Godina-Nava, M. Hernández-Contreras, and L. Velasco-Sevilla. Brownian motion of a colloidal particle near a soft interface. In *AIP Conf. Proc.*, volume 1420, pp. 128–132. AIP, 2012.

[80] S. L. Dettmer, S. Pagliara, K. Misiunas, and U. F. Keyser. *Phys. Rev. E*, 89(6):062305, 2014.

[81] B. Tränkle, D. Ruh, and A. Rohrbach. *Soft Matter*, 12(10):2729–2736, 2016.

[82] J. C. Benavides-Parra, D. Jacinto-Méndez, G. Brotons, and M. D. *J. Chem. Phys.*, 145(11):114902, 2016.

[83] T. G. Mason and D. A. Weitz. *Phys. Rev. Lett.*, 75(14):2770, 1995.

[84] L. Lobry and N. Ostrowsky. *Phys. Rev. B*, 53:12050–12056, May 1996.

[85] M. A. Bevan and D. C. Prieve. *J. Chem. Phys.*, 113(3):1228–1236, 2000.

[86] A. R. Clapp and R. B. Dickinson. *Langmuir*, 17(7):2182–2191, 2001.

[87] A. Banerjee and K. D. Kihm. *Phys. Rev. E*, 72(4):042101, 2005.

[88] V. N. Michailidou, G. Petekidis, J. W. Swan, and J. F. Brady. *Phys. Rev. Lett.*, 102:068302, Feb 2009.

[89] B. Cichocki, E. Wajnryb, J. Bławzdziewicz, J. K. G. Dhont, and P. R. Lang. *J. Chem. Phys.*, 132(7):074704, 2010.

[90] M. Lisicki, B. Cichocki, J. K. G. Dhont, and P. R. Lang. *J. Chem. Phys.*, 136(20):204704, 2012.

[91] S. A. Rogers, M. Lisicki, B. Cichocki, J. K. G. Dhont, and P. R. Lang. *Phys. Rev. Lett.*, 109(9):098305, 2012.

[92] V. N. Michailidou, J. W. Swan, J. F. Brady, and G. Petekidis. *J. Chem. Phys.*, 139(16):164905, 2013.

[93] W. Wang and P. Huang. *Phys. Fluids*, 26(9):092003, 2014.

[94] M. Lisicki, B. Cichocki, S. A. Rogers, J. K. G. Dhont, and P. R. Lang. *Soft Matter*, 10(24):4312–4323, 2014.

[95] M. Lisicki. *Evanescent wave dynamic light scattering by optically anisotropic Brownian particles.* PhD thesis, University of Warsaw, 2015.

[96] Y. Liu. *Near–wall dynamics of colloidal particles studied by evanescent wave dynamic light scattering.* PhD thesis, Heinrich Heine University Düsseldorf, 2017.

[97] P. Huang and K. S. Breuer. *Phys. Rev. E*, 76(4):046307, 2007.

[98] E. Lauga and T. M. Squires. *Phys. Fluids*, 17(10):103102, 2005.

[99] E. Lauga, M. Brenner, and H. Stone. Microfluidics: the no-slip boundary condition. In *Springer handbook of experimental fluid mechanics*, pp. 1219–1240. Springer, 2007.

[100] B. U. Felderhof. *Phys. Rev. E*, 85:046303, Apr 2012.

[101] E. Bart. *Chem. Eng. Sci.*, 23(3):193–210, 1968.

[102] B. U. Felderhof. *J. Chem. Phys.*, 124(12):124705, 2006.

[103] K. Aderogba and J. R. Blake. *Bull. Austral. Math. Soc.*, 18(03):345–356, 1978.

[104] S. H. Lee, R. S. Chadwick, and L. G. Leal. *J. Fluid Mech.*, 93:705–726, 8 1979.

[105] S. H. Lee and L. G. Leal. *J. Fluid Mech.*, 98:193–224, 1980.

[106] C. Berdan II and L. G. Leal. *J. Colloid Interface Sci.*, 87(1):62 – 80, 1982.

[107] J. Urzay, S. G. Llewellyn Smith, and B. J. Glover. *Phys. Fluids*, 19(10):103106, 2007.

[108] K. D. Danov, R. Aust, F. Durst, and U. Lange. *J. Colloid Interface Sci.*, 175(1):36–45, 1995.

[109] K. D. Danov, R. Aust, F. Durst, and U. Lange. *Int. J. Multiph. Flow*, 21(6):1169–1189, 1995.

[110] K. D. Danov, T. D. Gurkov, H. Raszillier, and F. Durst. *Chem. Eng. Sci.*, 53(19):3413–3434, 1998.

[111] R. Shail. *J. Eng. Math.*, 17(3):239–256, 1983.

[112] J. Bławzdziewicz, V. Cristini, and M. Loewenberg. *Phys. Fluids*, 11(2):251–258, 1999.

[113] J. Bławzdziewicz, ML Ekiel-Jeżewska, and E Wajnryb. *J. Chem. Phys.*, 133(11):114703, 2010.

[114] P. Gravesen, J. Branebjerg, and O. S. Jensen. *J. Micromech. Microeng.*, 3(4):168, 1993.

[115] Q.-H. Wei, C. Bechinger, and P. Leiderer. *Science*, 287(5453):625–627, 2000.

[116] C. Lutz, M. Kollmann, and C. Bechinger. *Phys. Rev. Lett.*, 93(2):026001, 2004.

[117] S. Wakiya. *J. Phys. Soc. Japan*, 8(2):254–256, 1953.

[118] T. Bohlin. *Trans. Roy. Inst. Technol. Stockholm*, 155:64, 1960.

[119] H. Faxén. *Colloid Polym. Sci.*, 167(2):146–146, 1959.

[120] W. B. Zimmerman. *Int. J. Eng. Sci.*, 42(17):1753–1778, 2004.

[121] S. Leichtberg, R. Pfeffer, and S. Weinbaum. *Int. J. Multiphase Flow*, 3:147, 1976.

[122] M. Kedzierski and E. Wajnryb. *J. Chem. Phys.*, 133(15):154105, 2010.

[123] S. Wakiya. *J. Phys. Soc. Japan*, 12(10):1130–1141, 1957.

[124] H. Y. Yeh and H. J. Keh. *Eur. J. Mech. B Fluid*, 39:52–58, 2013.

[125] J. Happel and B. J. Bryne. *Ind. Eng. Chem.*, 46(6):1181–1186, 1954.

[126] H. Brenner and J. Happel. *J. Fluid Mech.*, 4(02):195–213, 1958.

[127] T. Greenstein and J. Happel. *J. Fluid Mech.*, 34(04):705–710, 1968.

[128] P. M. Bungay and H. Brenner. *Int. J. Multiphase Flow*, 1(1):25–56, 1973.

[129] N. Liron and R. Shahar. *J. Fluid Mech.*, 86(04):727–744, 1978.

[130] T. Greenstein and J. Happel. *Appl. Sci. Res.*, 22(1):345–359, 1970.

[131] N. Lecoq, F. Feuillebois, N. Anthore, R. Anthore, F. Bostel, and C. Petipas. *Phys. Fluids A*, 5(1):3–12, 1993.

[132] B. Cui, B. Lin, S. Sharma, and S. A. Rice. *J. Chem. Phys.*, 116(7):3119–3127, 2002.

[133] J. J. L. Higdon and G. P. Muldowney. *J. Fluid Mech.*, 298:193–210, 9 1995.

[134] C. Pozrikidis. *J. Eng. Math.*, 53(1):1–20, 2005.

[135] H. J. Keh and T. H. Hsieh. *Langmuir*, 23(15):7928–7935, 2007.

[136] S. Bhattacharya, C. Mishra, and S. Bhattacharya. *J. Fluid Mech.*, 642:295, 2010.

[137] A. Imperio, J. T. Padding, and W. J. Briels. *J. Chem. Phys.*, 134(15):154904, 2011.

[138] S. Navardi, S. Bhattacharya, and H. Wu. *Comput. Fluids*, 121:145, 2015.

[139] H. Hasimoto. *J. Phys. Soc. Japan*, 41(6):2143–2144, 1976.

[140] O. Sano. *J. Phys. Soc. Japan*, 56(8):2713–2720, 1987.

[141] G. J. Sheard and K. Ryan. *J. Fluid Mech.*, 592:233–262, 2007.

[142] B. U. Felderhof. *J. Fluid Mech.*, 637:285–303, 2009.

[143] B. U. Felderhof. *J. Fluid Mech.*, 644:97–106, 2010.

[144] B. U. Felderhof. *J. Fluid Mech.*, 649:329–340, 2010.

[145] B. U. Felderhof and G. Ooms. *J. Fluid Mech.*, 668:100–112, 2011.

[146] J. R. Van Wazer. *Viscosity and flow measurement: a laboratory handbook of rheology.* Interscience Publishers, 1963.

[147] R. L. Whitmore. *Rheology of the Circulation.* Pergamon, 1968.

[148] H. A. Barnes. *J. Nonnewton Fluid Mech.*, 94(2):213–217, 2000.

[149] A. B. Metzner, R. H. Feehs, H. L. Ramos, R. E. Otto, and J. D. Tuthill. *AlChE J.*, 7(1):3–9, 1961.

[150] R. Shinnar. *J. Fluid Mech.*, 10(02):259–275, 1961.

[151] W. L. Haberman. Flow about a sphere rotating in a viscous liquid inside a coaxially rotating cylinder. David taylor model basin report no. 1578., US Navy Dept., Washington DC, 1961.

[152] H. Brenner and R. M. Sonshine. *Quart. J. Mech. Appl. Math.*, 17(1):55–63, 1964.

[153] H. Brenner. *Appl. Sci. Res., Section A*, 13(1):81–120, 1964.

[154] T. Greenstein and T. J. Som. *Phys. Fluids*, 19(1):161–162, 1976.

[155] T. Greenstein and G. L. Schiavina. *Int. J. Multiph. Flow*, 2(3):353–355, 1975.

[156] G. H. Zheng, R. L. Powell, and P. Stroeve. *Ind. Eng. Chem. Res.*, 31(4):1190–1194, 1992.

[157] B. R. Hirschfeld. *A Theoretical Study of the slow asymmetric settling of an arbitrarily-positioned particle in a circular cylinder.* PhD thesis, New York University, 1972.

[158] B. R. Hirschfeld, H. Brenner, and A. Falade. *PhysicoChem. Hydrodyn*, 5:99–133, 1984.

[159] H. Tözeren. *J. Appl. Mech.*, 49(2):279–283, 1982.

[160] H. Tözeren. *Int. J. Num. Meth. Fluids*, 4(2):159–170, 1984.

[161] H. Tözeren. *J. Fluid Mech.*, 129:77–90, 1983.

[162] M. E. O'Neill. *Chem. Eng. Comm.*, 148(1):161–182, 1996.

[163] E. M. Plummer and M. Manchester. *Wiley Interdiscip Rev Nanomed Nanobiotechnol*, 3(2):174–196,

[164] F. Perrin. *J. Phys. Radium*, 5:497–511, 1934.

[165] F. Perrin. *J. Phys. Radium*, 7:1–11, 1936.

[166] G. K. Batchelor. *J. Fluid Mech.*, 44(03):419–440, 1970.

[167] A. T. Chwang and T. Y.-T. Wu. *J. Fluid Mech.*, 67(04):787–815, 1975.

[168] N. J. De Mestre and W. B. Russel. *J. Eng. Math.*, 9(2):81–91, 1975.

[169] D. Schiby and I. Gallily. *J. Colloid Interface Sci.*, 77(2):328–352, 1980.

[170] W. H. Mitchell and S. E. Spagnolie. *J. Fluid Mech.*, 772:600, 2015.

[171] J. R. Blake and G. R. Fulford. *Bull. Aust. Math. Soc.*, 24(01):27–36, 1981.

[172] M. Lisicki, B. Cichocki, and E. Wajnryb. *J. Chem. Phys.*, 145:034904, 2016.

[173] R. Hsu and P. Ganatos. *J. Fluid Mech.*, 207:29–72, 1989.

[174] J. T. Padding and W. J. Briels. *J. Chem. Phys.*, 132:054511, 2010.

[175] A. Neild, J. T. Padding, L. Yu, B. Bhaduri, W. J. Briels, and T. W. Ng. *Phys. Rev. E*, 82(4):041126, 2010.

[176] M. De Corato, F. Greco, G. Davino, and P. L. Maffettone. *J. Chem. Phys.*, 142(19):194901, 2015.

[177] Y. Han, A. M. Alsayed, M. Nobili, J. Zhang, T. C. Lubensky, and A. G. Yodh. *Science*, 314(5799):626–630, 2006.

[178] Y. Han, A. Alsayed, M. Nobili, and A. G. Yodh. *Phys. Rev. E*, 80:011403, 2009.

[179] Z. Zheng and Y. Han. *J. Chem. Phys.*, 133(12):124509, 2010.

[180] G. Li and J. X. Tang. *Phys. Rev. E*, 69(6):061921, 2004.

[181] R. Duggal and M. Pasquali. *Phys. Rev. Lett.*, 96(24):246104, 2006.

[182] B. Bhaduri, A. Neild, and T. W. Ng. *Appl. Phys. Lett.*, 92(8):084105, 2008.

[183] H. Z. Cummins, F. D. Carlson, T. J. Herbert, and G. Woods. *Biophys. J.*, 9(4):518–546, 1969.

[184] R. Pecora. *J. Chem. Phys.*, 48(9):4126–4128, 1968.

[185] F. C. Cheong and D. G. Grier. *Optics express*, 18(7):6555–6562, 2010.

[186] R. Colin, M. Yan, L. Chevry, J.-F. Berret, and B Abou. *Europhys. Lett.*, 97(3):30008, 2012.

[187] D. Mukhija and M. J. Solomon. *J. Colloid Interface Sci.*, 314(1):98 – 106, 2007.

[188] T. Bickel. *Phys. Rev. E*, 75:041403, 2007.

[189] T. Bickel. *Europhys. Lett.*, 106(1):16004, 2014.

[190] T. Bickel. *Eur. Phys. J. E*, 20:379–385, 2006.

[191] B. U. Felderhof. *J. Chem. Phys.*, 125(14):144718, 2006.

[192] B. U. Felderhof. *J. Chem. Phys.*, 125(12):124904, 2006.

[193] T. Salez and L. Mahadevan. *J. Fluid Mech.*, 779:181–196, 9 2015.

[194] B. Saintyves, T. Jules, T. Salez, and L. Mahadevan. *Proc. Nat. Acad. Sci.*, 113(21):5847–5849, 2016.

[195] B. Rallabandi, B. Saintyves, T. Jules, T. Salez, C. Schönecker, *Phys. Rev. Fluids*, 2, 074102, 2017

[196] H. Kress, E. H. K. Stelzer, G. Griffiths, and A. Rohrbach. *Phys. Rev. E*, 71(6):061927, 2005.

[197] R. Shlomovitz, A. Evans, T. Boatwright, M. Dennin, and A. Levine. *Phys. Rev. Lett.*, 110(13):137802, 2013.

[198] T. Boatwright, M. Dennin, R. Shlomovitz, A. A. Evans, and A. J. Levine. *Phys. Fluids*, 26(7):071904, 2014.

[199] F. Jünger, F. Kohler, A. Meinel, T. Meyer, R. Nitschke, B. Erhard, and *Biophys. J.*, 109(5):869–882, 2015.

[200] M. Irmscher, A. M de Jong, H. Kress, and M. W. J. Prins. *Biophys. J.*, 102(3):698–708, 2012.

[201] D. Mizuno, Y. Kimura, and R. Hayakawa. *Langmuir*, 16(24):9547–9554, 2000.

[202] D. Mizuno, Y. Kimura, and R. Hayakawa. *Phys. Rev. E*, 70:011509, 2004.

[203] Y. Kimura, T. Mori, A. Yamamoto, and D. Mizuno. *J. Phys. Condens. Matter*, 17(31):S2937, 2005.

[204] T. A. Waigh. *Rep. Prog. Phys.*, 79(7):074601, 2016.

[205] A. Daddi-Moussa-Ider, A. Guckenberger, and S. Gekle. *Phys. Rev. E*, 93:012612, 2016.

[206] A. Daddi-Moussa-Ider, A. Guckenberger, and S. Gekle. *Phys. Fluids*, 28(7):071903, 2016.

[207] A. Daddi-Moussa-Ider and S. Gekle. *J. Chem. Phys.*, 145(1):014905, 2016.

[208] A. Daddi-Moussa-Ider, M. Lisicki, and S. Gekle. *J. Fluid Mech.*, 811:210–233, 2017.

[209] A. Daddi-Moussa-Ider and S. Gekle. *in preparation*, 2017.

[210] A. Daddi-Moussa-Ider, M. Lisicki, and S. Gekle. *submitted*, 2017.

[211] A. Daddi-Moussa-Ider, M. Lisicki, and S. Gekle. *submitted*, 2017.

[212] A. Daddi-Moussa-Ider and S. Gekle. *Phys. Rev. E*, 95:013108, 2017.

[213] A. Daddi-Moussa-Ider, M. Lisicki, and S. Gekle. *submitted*, 2017.

[214] A. Daddi-Moussa-Ider and S. Gekle. *in preparation*, 2017.

[215] M. A. Peletier and M. Röger. *Arch. Rational Mech. Anal.*, 193(3):475–537, 2009.

[216] R. Skalak, A. Tozeren, R. P. Zarda, and S. Chien. *Biophys. J.*, 13(3):245–264, 1973.

[217] Y. Lefebvre and D. Barthès-Biesel. *J. Fluid Mech.*, 589:157–181, Oct 2007.

[218] E. Lac, D. Barthès-Biesel, N. A. Pelekasis, and J. Tsamopoulos. *J. Fluid Mech.*, 516:303–334, 10 2004.

[219] T. Krüger, F. Varnik, and D. Raabe. *Comp. Math. Appl.*, 61:3485–3505, 2011.

[220] S. Gekle. *Biophys. J.*, 110(2):514–520, 2016.

[221] C. Bächer, L. Schrack, and S. Gekle. *Phys. Rev. Fluids*, 2:013102, 2017.

[222] D. Barthès-Biesel. *Ann. Rev. Fluid Mech.*, 48:25–52, 2016.

[223] S. Ramanujan and C. Pozrikidis. *J. Fluid Mech.*, 361:117–143, 1998.

[224] W. Helfrich. *Z. Naturf. C.*, 28:693, 1973.

[225] M. Hu, J. J. Briguglio, and M. Deserno. *Biophys. J.*, 102(6):1403–1410, 2012.

[226] S. Kobayashi and K. Nomizu. *Foundations of differential geometry*, volume 2.

[227] M. Deserno. *Chem. Phys. Lipids*, 185:11–45, 2015.

[228] R. W. Ogden. *Non-linear elastic deformations.*

[229] A. E. Green and J. C. Adkins. *Large Elastic Deformations and Non-linear Continuum Mechanics.*

[230] L. Zhu. *Simulation of individual cells in flow.* PhD thesis, KTH Royal Institute of Technology in Stockholm, 2014.

[231] J. L. Synge and A. Schild. *Tensor calculus*, volume 5.

[232] A. Guckenberger and S. Gekle. *J. Phys. Cond. Mat.*, 29:203001, 2017.

[233] J. T. Jenkins. *J. Math. Biol.*, 4(2):149–169, 1977.

[234] T. R. Powers. *Rev. Mod. Phys.*, 82(2):1607, 2010.

[235] A. Laadhari, C. Misbah, and P. Saramito. *Physica D: Nonlinear Phenom.*, 239(16):1567 – 1572, 2010.

[236] K. Sinha and M. D. Graham. *Phys. Rev. E*, 92:042710, Oct 2015.

[237] A. Guckenberger, M. P. Schraml, P. G. Chen, M. Leonetti, and S. Gekle. *Comp. Phys. Comm.*, 207:1–23, 2016.

[238] C. Pozrikidis. *J. Comput. Phys.*, 169:250, 2001.

[239] H. Zhao, A. H. G. Isfahani, L. N. Olson, and J. B. Freund. *J. Comput. Phys.*, 229:3726, 2010.

[240] S. Kim and S. J. Karrila. *Microhydrodynamics: principles and selected applications.* Courier Corporation, 2013.

[241] Y. von Hansen, M. Hinczewski, and R. R. Netz. *J. Chem. Phys.*, 134(23):235102, 2011.

[242] J. R. Blake. *Math. Proc. Camb. Phil. Soc.*, 70(02):303–310, 1971.

[243] M. Abramowitz, I. A Stegun, et al. *Handbook of mathematical functions*, volume 1.

[244] B. Kaoui, G. H. Ristow, I. Cantat, C. Misbah, and W. Zimmermann. *Phys. Rev. E*, 77(2):021903, 2008.

[245] B. Kaoui and J. Harting. *Rheol. Acta*, 55(6):465–475, 2016.

[246] B. Kaoui. *Phys. Rev. E*, 95, 063310, 2017.

[247] M. Rachik, D. Barthès-Biesel, M. Carin, and F. Edwards-Levy. *J. Colloid Interface Sci.*, 301(1):217–226, 2006.

[248] Y. O. Fuentes, S. Kim, and D. J. Jeffrey. *Phys. Fluids*, 31(9):2445–2455, 1988.

[249] Y. O. Fuentes, S. Kim, and D. J. Jeffrey. *Phys. Fluids A*, 1(1):61–76, 1989.

[250] H. Bateman, A. Erdélyi, W. Magnus, F. Oberhettinger, and F. G. Tricomi. *Higher transcendental functions*, volume 2.

[251] H. Lamb. *Hydrodynamics.* Cambridge university press, 1932.

[252] J. W. Swan and J. F. Brady. *Phys. Fluids*, 19(11):113306, 2007.

[253] C. Aponte-Rivera and R. N. Zia. *Phys. Rev. Fluids*, 1:023301, 2016.

[254] E. Wajnryb, K. A. Mizerski, P. J. Zuk, and P. Szymczak. *J. Fluid Mech.*, 731:R3, 2013.

[255] Y. W. Kim and R. R. Netz. *J. Chem. Phys.*, 124(11):114709, 2006.

[256] L. Durlofsky, J. F. Brady, and G. Bossis. *J. Fluid Mech.*, 180:21–49, 1987.

[257] M. L. Ekiel-Jeżewska and B. U. Felderhof. *J. Chem. Phys.*, 142(1):014904, 2015.

[258] R. Schmitz and B. U. Felderhof. *Physica A*, 92(3):423–437, 1978.

[259] R. Schmitz and B. U. Felderhof. *Physica A*, 113(1-2):103–116, 1982.

[260] R. Schmitz and B. U. Felderhof. *Physica A*, 116(1-2):163–177, 1982.

[261] B. Cichocki, B. U. Felderhof, and R. Schmitz. *PhysicoChem. Hyd*, 10:383–403, 1988.

[262] B. Cichocki, B. U. Felderhof, K. Hinsen, E. Wajnryb, and J. Bławzdziewicz *J. Chem. Phys.*, 100(5):3780–3790, 1994.

[263] B. Cichocki, R. B. Jones, R. Kutteh, and E. Wajnryb. *J. Chem. Phys.*, 112(5):2548–2561, 2000.

[264] M. L. Ekiel-Jeżewska and E. Wajnryb. Precise multipole method for calculating hydrodynamic interactions between spherical particles in the stokes flow. *Theoretical Methods for Micro Scale Viscous Flows*, pp. 127–172, 2009.

[265] D. Bedeaux and P. Mazur. *Physica*, 78(3):505–515, 1974.

[266] B. U. Felderhof. *Physica A*, 151(1):1–16, 1988.

[267] E. Wajnryb and J. S. Dahler. *Adv. Chem. Phys.*, 102:193–314, 1997.

[268] A. Einstein. *Ann. Phys.*, 17:549–560, 1905.

[269] J. Perrin. *Ann. Chim. Phys.*, 18:5114, 1909.

[270] J. Perrin. *J. Phys. Theor. Appl.*, 9(1):5–39, 1910.

[271] A. Agarwal. *Nobel Prize Winners in Physics.*

[272] P. Protter. *Stochastic Differential Equations.*

[273] P. Langevin. *C. R. Acad. Sci. (Paris)*, 146:530–533, 1908.

[274] G. Ciccotti and J. P. Ryckaert. *J. Stat. Phys.*, 26(1):73–82, 1981.

[275] R. Kubo. *Rep. Prog. Phys.*, 29(1):255, 1966.

[276] R. Morgado, F. A. Oliveira, G. G. Batrouni, and A. Hansen. *Phys. Rev. Lett.*, 89(10):100601, 2002.

[277] R. Kubo, M. Toda, and N. Hashitsume. Statistical physics II, 1985.

[278] M. J. Saxton. *Biophys. J.*, 66(2):394–401, 1994.

[279] Michael J Saxton. *Biophys. J.*, 70(3):1250–1262, 1996.

[280] C. Pozrikidis. *Boundary Integral and Singularity Methods for Linearized Viscous Flow.* Number 8 in Cambridge Texts in Applied Mathematics. Cambridge University Press, New York, 1992.

[281] M. Kohr and I. I. Pop. *Viscous incompressible flow for low Reynolds numbers*, volume 16. Wit Pr/Comp. Mech., 2004.

[282] E. E. Keaveny and M. J. Shelley. *J. Comput. Phys.*, 230(5):2141–2159, 2011.

[283] H. Zhao, E. S. G. Shaqfeh, and V. Narsimhan. *Phys. Fluids*, 24(1):011902, 2012.

[284] T. Krüger, H. Kusumaatmaja, A. Kuzmin, O. Shardt, G. Silva, and E. M. Viggen. *The Lattice Boltzmann Method.* Springer, 2017

[285] G. R. Cowper. *International J. for Num. Meth. in Engineering*, 7(3):405–408, 1973.

[286] C. Pozrikidis. *J. Fluid Mech.*, 297:123–152, 1995.

[287] Y. Saad and M. H. Schultz. *SIAM J. Sci. Comput.*, 7(3):856–869, 1986.

[288] T. Krüger. *Computer simulation study of collective phenomena in dense suspensions of red blood cells under shear.* Springer, 2012.

[289] M. Meyer, M. Desbrun, P. Schröder, and A. H. Barr. Discrete differential-geometry operators for triangulated 2-manifolds. In H. C. Hege and K. Polthier, editors, *Visualization and Mathematics III*, pp. 35–57. Springer, 2003.

[290] A. R. Conn, N. I. M. Gould, and Ph. L. Toint. *Trust region methods*, volume 1.

[291] G. N. Watson. *A treatise on the theory of Bessel functions.*

[292] G. Chirikjian and A. Kyatkin. *Engineering Applications of Noncommutative Harmonic Analysis: With Emphasis on Rotation and Motion Groups.* CRC Press, 2001.

[293] N. Baddour. *J. Opt. Soc. Am. A*, 26(8), 2009.

Part II

Publications

List of publications as part of this thesis

[Pub1] A. Daddi-Moussa-Ider, A. Guckenberger and S. Gekle,
Long-lived anomalous thermal diffusion induced by elastic cell membranes on nearby particles, *Phys. Rev. E* **93**, 012612 (2016)

[Pub2] A. Daddi-Moussa-Ider, A. Guckenberger and S. Gekle,
Particle mobility between two planar elastic membranes: Brownian motion and membrane deformation, *Phys. Fluids* **28**, 071903 (2016)

[Pub3] A. Daddi-Moussa-Ider, and S. Gekle,
Hydrodynamic interaction between particles near elastic interfaces, *J. Chem. Phys.*, **145**, 014905 (2016)

[Pub4] A. Daddi-Moussa-Ider and S. Gekle,
Hydrodynamic coupling and rotational mobilities nearby planar elastic membranes, *in preparation* (2017)

[Pub5] A. Daddi-Moussa-Ider, M. Lisicki and S. Gekle,
Mobility of an axisymmetric particle near an elastic interface, *J. Fluid Mech.* **811**, 210-233 (2017)

[Pub6] A. Daddi-Moussa-Ider, M. Lisicki and S. Gekle,
Hydrodynamic mobility of a sphere moving on the centerline of an elastic tube, *under review* (2017)

[Pub7] A. Daddi-Moussa-Ider, M. Lisicki and S. Gekle,
Slow rotation of a spherical particle inside an elastic tube, *under review* (2017)

[Pub8] A. Daddi-Moussa-Ider, and S. Gekle,
Hydrodynamic mobility of a solid particle near a spherical elastic membrane: Axisymmetric motion, *Phys. Rev. E* **95**, 013108 (2017)

[Pub9] A. Daddi-Moussa-Ider, M. Lisicki and S. Gekle,
Hydrodynamic mobility of a solid particle near a spherical elastic membrane. II. Asymmetric motion, *Phys. Rev. E* **95**, 053117 (2017)

[Pub10] A. Daddi-Moussa-Ider and S. Gekle,
Creeping motion of a solid particle inside an elastic spherical cavity, *in preparation* (2017)

Contributions to conferences and seminars

Oral Presentations

- 81. Jahrestagung der DPG / DPG-Frühjahrstagung. Dresden, Germany. 19–24 March 2017.
- Flowing Matter Conference. Porto, Portugal. 23–27 January 2017.
- Seminar at Heinrich-Heine-Universität Düsseldorf, Germany, invited by Prof. Dr. Hartmut Löwen. 15 December 2016.
- DFD APS Meeting. Porland, Oregon, USA. 20–22 Nov 2016.
- Seminar at University of Nevada, Reno. Nevada, USA, invited by Prof. Dr. Miles Greiner. 17 November 2016.
- Seminar at DAMTP, University of Cambridge, United Kingdom, invited by Dr. Maciej Lisicki. 7 June 2016.
- 80. Jahrestagung der DPG / DPG-Frühjahrstagung. Regensburg, Germany. 6–11 March 2016.
- Flowing Matter Conference. Porto, Portugal. 11–15 January 2016.

Poster Presentations

- Northeast Complex Fluids and Soft Matter Workshop. Princeton, New Jersey, USA. 26 Mai 2017.
- 630th WE-Heraeus Seminar. Bayreuth, Germany. 9–12 October 2016.
- 4th International Soft Matter Conference (ISMC). Grenoble, France. 12–16 September 2016.
- Active Complex Matter Summer School. Cargèse, Corsica, France. 12-23 July 2016.
- Workshop / Summer School on Hydrodynamic Fluctuations in Soft-Matter Simulations. Prato, Italy. 9–12 February 2016.
- Espresso Sommer School. Stuttgart, Germany. 5–9 October 2015.
- Summer School of the DFG Priority Programme 1726 – Microswimmers. Jülich, Germany. 21–25 September 2015.
- 79. Jahrestagung der DPG / DPG-Frühjahrstagung. Berlin, Germany. 15–20 March 2015.

Publication 1

Long-lived anomalous thermal diffusion induced by elastic cell membranes on nearby particles

A. Daddi-Moussa-Ider, A. Guckenberger and S. Gekle

Phys. Rev. E **93**, 012612 (2016)

DOI: 10.1103/PhysRevE.93.012612

Abstract

The physical approach of a small particle (virus, medical drug) to the cell membrane represents the crucial first step before active internalization and is governed by thermal diffusion. Using a fully analytical theory we show that the stretching and bending of the elastic membrane by the approaching particle induces a memory in the system which leads to anomalous diffusion, even though the particle is immersed in a purely Newtonian liquid. For typical cell membranes the transient subdiffusive regime extends beyond 10ms and can enhance residence times and binding rates up to 50%. Our analytical predictions are validated by numerical simulations.

1 Introduction

Endocytosis, the uptake of a small particle by a living cell is one of the most important processes in biology [1–3]. Current research is focused mainly on the biophysical and biochemical mechanisms which govern endocytosis when particle and cell are in direct physical contact. Much less investigated, yet equally important, is the approach of the particle to the cell membrane before physical contact is established [4]. In many physiologically relevant situations, e.g., inside the blood stream, the cell and the particle are both suspended in a surrounding liquid and the approach is governed by thermal diffusion of the small particle. The thermal diffusion of small particles (fibrinogen) naturally occurring in human blood has furthermore been suggested as the root cause of red blood cell aggregation [5–7].

Thermal diffusion of a spherical particle in a bulk fluid is well understood and governed by the celebrated Stokes-Einstein relation. This relation builds a bridge between the particle mobility when an external force is applied to it and the random trajectories observed when only thermal fluctuations are present. Particle mobilities and thermal diffusion near solid walls have been thoroughly investigated both theoretically [8–13] and experimentally [14–25] finding a reduction of the particle mobility due to the proximity of the wall. Some theoretical works have investigated particle mobilities and diffusion close to fluid-fluid interfaces endowed with surface tension [26–29] or surface elasticity [30–32] with corresponding experiments [33–39]. For the case of a membrane with bending resistance transient subdiffusive behavior has been observed in the perpendicular direction [40]. Regarding biological cells, recent experiments have measured particle mobilities near different types of cells as well as giant unilamellar vesicles (GUVs), both of which possess an elastic membrane separating two fluids, and found that the mobility near the cell walls does decrease but not as strongly as near a hard wall [4].

Here we derive a fully analytical theory for the diffusion of a small particle in the vicinity of a realistic cell membrane possessing shear and bending resistance with fluid on both sides. As the typical sizes and velocities are small, the theory is derived in the small Reynolds number regime neglecting the non-linear term, but including the unsteady contribution in the Navier-Stokes equations. Our most important finding is that there exists a long-lasting subdiffusive regime with local exponents as low as 0.87 extending over time scales beyond 10ms. Such behavior is qualitatively different from diffusion near hard walls where the diffusion, albeit being slowed down, still remains normal (i.e. the mean-square-displacement increases linearly with time). Remarkably, our system exhibits subdiffusion in a purely Newtonian liquid whereas most commonly subdiffusion is observed for particles in viscoelastic media. The subdiffusive regime increases the residence time of the particle in the vicinity of the membrane by up to 50% and is thus expected to be of important physiological significance. Our analytical particle mobilities are quantitatively verified by detailed boundary-integral simulations. Power-spectral densities which are amenable to direct experimental validation using optical traps are provided.

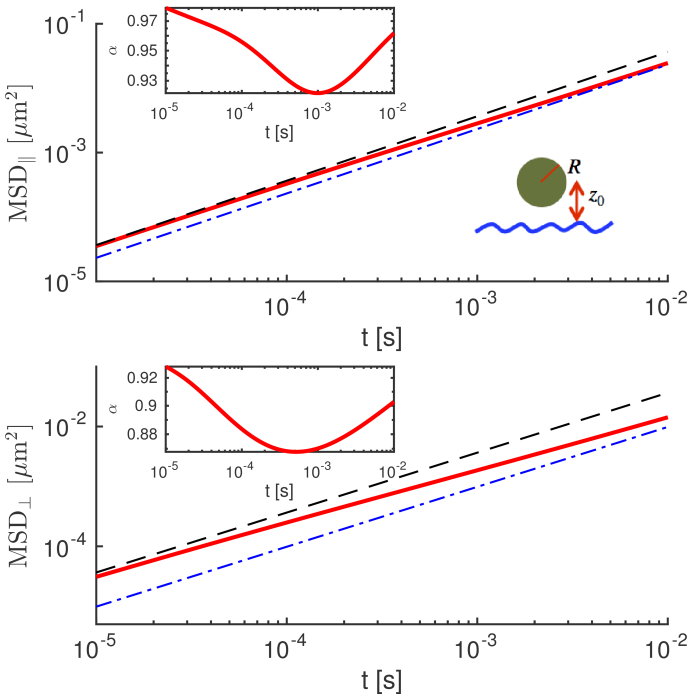

Figure 1: Mean-square displacement (red line) of a particle with radius R=100nm diffusing z_0=153nm above a red-blood cell membrane in lateral (top) and perpendicular (bottom) direction as predicted by our theory at $T = 300$K. For short times $t \lesssim 50\mu$s the MSD follows bulk behavior (black dashed line) while for long times the MSD follows hard-wall behavior (blue dash-dotted line). In between, a subdiffusive regime is evident extending up to 10ms and beyond. Insets show the local exponent which goes down until 0.87 for perpendicular diffusion.

2 Results

A spherical particle with radius $R = 100$nm is located at a distance $z_0 = 153$nm above an elastic membrane and exhibits diffusive motion as illustrated in the inset of Fig. 1. The membrane has a shear resistance $\kappa_S = 5 \cdot 10^{-6}$N/m and bending modulus $\kappa_B = 2 \cdot 10^{-19}$Nm which are typical values of red blood cells [41]. The area dilatation modulus is $\kappa_A = 100\kappa_S$. The fluid properties correspond to blood plasma with viscosity $\eta = 1.2$mPas. Figure 1 shows the mean-square-displacement (MSD) for parallel as well as perpendicular motion as obtained from our fully analytical theory to be described below. For short times ($t < 50\mu$s) the MSD follows a linear behavior with the normal bulk diffusion coefficient D_0 since the membrane does not have sufficient time to react on these short scales. This is in agreement with a simple balance between viscosity and elasticity for shear, $\tau_S = \eta R/\kappa_S \approx 37\mu$s, and bending, $\tau_B = \eta R^3/\kappa_B \approx 22\mu$s. For $t > 50\mu$s we observe a downward bending of the MSD which is a clear signature of subdiffusive behavior. Indeed, as shown in the insets of Fig. 1, the local exponent $\alpha = \frac{\partial \log\langle x^2\rangle}{\partial \log t}$ diminishes from 1 down to 0.92 in the parallel and 0.87 in the perpendicular direction. The subdiffusive regime extends up to 10ms in the parallel and even further in the perpendicular direction, which is long enough to be of possible physiological significance. Finally, for long times, the behavior turns back to normal diffusion with $\alpha \approx 1$. Compared to the short-time regime, however, the diffusion coefficient is now significantly lower and approaches the well-known behavior near a solid hard wall with $D_{\text{wall},\parallel} = D_0(1 - 9/16R/z_0)$ in the parallel and $D_{\text{wall},\perp} = D_0(1 - 9/8R/z_0)$ in the perpendicular case, respectively. Diffusion for long times therefore turns out to depend only on the particle distance and to be independent of the membrane properties.

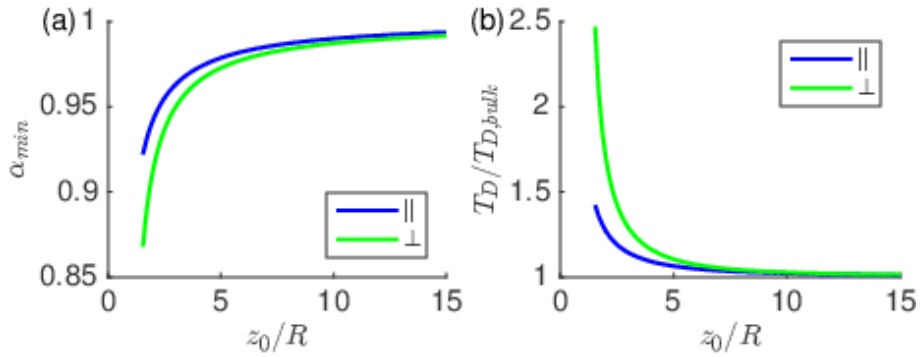

Figure 2: (a) Minimum of the local exponent plotted against particle-membrane separation. Significant subdiffusion is observed up to distances roughly ten times the particle radius. (b) The time required to diffuse one particle radius increases due to the presence of the membrane thus leading to an enhanced residence time of the particle in the vicinity of the membrane which may increase the probability of triggering endocytosis.

In Fig. 2 (a) we show the minimum of the local exponent for different particle-membrane separations. Even for distances ten times the particle radius, a significant deviation of the local exponent from 1 is still observable. From the MSDs it is straightforward to estimate the time T_D required by the particle to diffuse a distance equal to its own radius which gives an approximate measure of the "diffusion speed". As expected based on the data from Fig. 1, diffusion in the perpendicular direction is slowed down significantly more than for lateral motion, see Fig. 2 (b), in agreement with recent experimental observations [4].

Experimentally, long MSDs can be difficult to measure as the particle may move out of the focal plane during the recording time. A commonly used technique is therefore to confine the particle to its position using optical traps. One then records the power spectral density (PSD) of particle fluctuations around its equilibrium position. The PSDs predicted by our theory for a typical optical trap with spring constant $K = 10^{-5}\mathrm{N/m}$ [4] as a function of frequency $f = \omega/2\pi$ are shown in Fig. 3. The general behavior of the unconstrained system is not qualitatively altered by the optical confinement: for high frequencies the behavior is bulk-like (mirroring the bulk-like MSD at short times) while for low frequencies the PSD approaches that expected near a solid wall (mirroring the hard-wall like MSD at long times). The frequency range of the transition lies mainly below 1 kHz and should thus be experimentally accessible.

3 Theory

Our theoretical development leading to figures 1 through 3 proceeds via the calculation of particle mobilities and the fluctuation-dissipation theorem and can be sketched as follows (a detailed derivation is given in Appendices A-C). We consider a spherical particle of radius R driven by an oscillating force $\boldsymbol{F}_\omega(t) = \boldsymbol{F}_0 e^{i\omega t}$ in a fluid with density ρ and dynamic viscosity η whose complex mobility $\mu(\omega)$ for a fixed ω is defined as

$$\boldsymbol{V}_\omega(t) = \mu(\omega)\,\boldsymbol{F}_\omega(t)\ , \tag{3.34}$$

and can be separated into the three contributions

$$\mu(\omega) = \mu_0 + \mu_0^u(\omega) + \Delta\mu(\omega, z_0)\ . \tag{3.35}$$

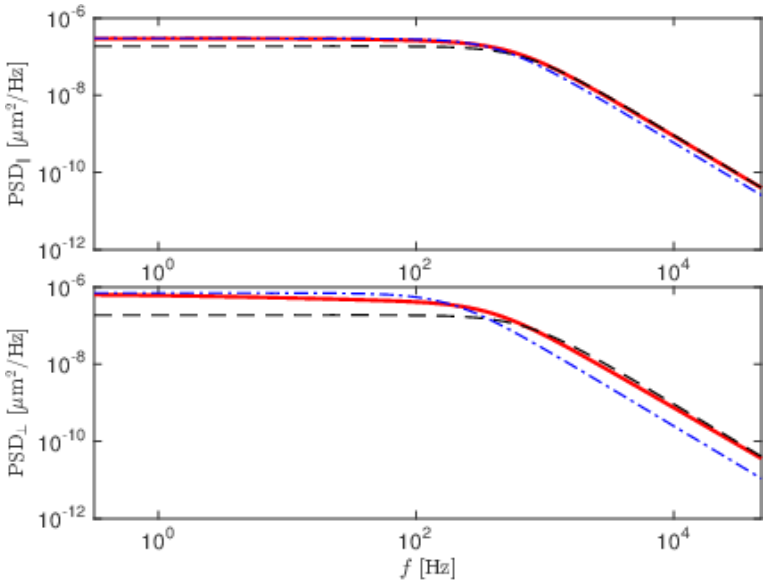

Figure 3: Predicted power-spectral density of position fluctuations if the same bead as in Fig. 1 is confined by a typical optical trap of strength $K = 10^{-5}$N/m [4]. Similar as in the MSD of Fig. 1 a transition from hard-wall-like behavior (blue dash-dotted line) for low frequencies to bulk-like behavior (black dashed line) at high frequencies is seen.

Here, $\mu_0 = 1/(6\pi\eta R)$ is the usual steady-state bulk mobility,

$$\mu_0^u(\omega) = \mu_0 \left(e^{-R\lambda\sqrt{-i}} - 1 \right) \tag{3.36}$$

with $\lambda^2 = \rho\omega/\eta$ is the correction due to fluid inertia [42] and $\Delta\mu\,(\omega, z_0)$ is the correction due to the elastic membrane at distance z_0. In order to derive the mobility corrections, we employ the commonly used approximation of a small particle ($R/z_0 \ll 1$). Using numerical simulations of a truly extended particle, we will show below that this approximation is surprisingly good even for $R/z_0 = 0.65$. The problem is thus equivalent to solving the unsteady Stokes equations with an arbitrary time dependent point force $\boldsymbol{F}$ located at $\boldsymbol{r}_0$

$$\begin{aligned} -\rho\frac{\partial \boldsymbol{v}}{\partial t} + \eta\boldsymbol{\nabla}^2\boldsymbol{v} - \boldsymbol{\nabla}p + \boldsymbol{F}\delta(\boldsymbol{r} - \boldsymbol{r}_0) = 0\,, \\ \boldsymbol{\nabla}\cdot\boldsymbol{v} = 0\,, \end{aligned} \tag{3.37}$$

with the fluid velocity $\boldsymbol{v}$, the pressure p and the point force position $\boldsymbol{r}_0$. The elastic membrane is located at $z = 0$, has infinite extent in x and y directions and is surrounded by fluid on both sides. Following the usual approximation of small deformations, we impose the traction jump at $z = 0$ which follows from the Skalak [43] and Helfrich [44] laws for the shear and bending resistance as detailed in Appendix A

$$\begin{aligned} \Delta f^x &= -\frac{\kappa_\mathrm{S}}{3}\left(2\,(1+C)\,u_{x,xx} + u_{x,yy} + (1+2C)\,u_{y,xy}\right)\,, \\ \Delta f^y &= -\frac{\kappa_\mathrm{S}}{3}\left(u_{y,xx} + 2\,(1+C)\,u_{y,yy} + (1+2C)\,u_{x,xy}\right)\,, \\ \Delta f^z &= \kappa_\mathrm{B}\left(u_{z,xxxx} + 2u_{z,xxyy} + u_{z,yyyy}\right)\,, \end{aligned} \tag{3.38}$$

where the membrane deformation is $\boldsymbol{u}$ and the notation $u_{,\cdot}$ denotes partial spatial derivatives. The moduli are κ_S for shear resistance and κ_B for bending resistance while the ratio between shear and area dilatation modulus is $C = \kappa_\mathrm{A}/\kappa_\mathrm{S}$. The no-slip condition at the membrane surface relates the surface deformation to the local fluid velocity

$$\frac{\mathrm{d}\boldsymbol{u}}{\mathrm{d}t} = \boldsymbol{v}|_{z=0} \,, \tag{3.39}$$

Together with equations (3.37), (3.38) and (3.39) this represents a closed mathematical problem for the velocity field $\boldsymbol{v}$. For its solution, the Stokes equations (3.37) are first Fourier-transformed into frequency space. The dependency on the x and y coordinates is Fourier-transformed into wave vectors q_x and q_y which subsequently allows us to consider the contributions of the longitudinal and transversal velocity components separately [27]. After eliminating the pressure, this leads to three differential equations for the three velocity components for which an analytical solution can be found. From the velocity field the mobility correction of the particle is directly obtained. The details are given in Appendix B.

The mobility correction is a tensorial quantity which in the present case has two components for the mobility parallel $\Delta\mu_\parallel(\omega, z_0)$ and perpendicular $\Delta\mu_\perp(\omega, z_0)$ to the membrane. Furthermore, the mobility correction in each direction can be split into a contribution $\Delta\mu_\mathrm{B}$ due to bending resistance and a contribution $\Delta\mu_\mathrm{S}$ due to shear resistance and area dilatation. The final results are conveniently expressed in terms of the dimensionless numbers:

$$\begin{aligned} \beta &= \frac{12 z_0 \eta \omega}{\kappa_\mathrm{S} + \kappa_\mathrm{A}} \,, \\ \beta_\mathrm{B} &= 2 z_0 \left(\frac{4\eta\omega}{\kappa_\mathrm{B}}\right)^{1/3} \,, \\ \sigma &= z_0 \left(\frac{\rho\omega}{\eta}\right)^{1/2} \,, \end{aligned} \tag{3.40}$$

where β captures the effect of shear resistance and area dilatation, β_B the effect of bending resistance and σ the effect of fluid inertia on the mobility corrections.

The mobility corrections are

$$\frac{\Delta\mu_{\parallel,\mathrm{S}}}{\mu_0} = \frac{3i}{\sigma^2}\frac{R}{z_0}\int_0^\infty \frac{s^3(re^{-r} - se^{-s})^2}{4(r-s)s^2 - \beta\sigma^2}\,\mathrm{d}s \,, + \frac{3i}{4}\frac{R}{z_0}\int_0^\infty \frac{s^3 e^{-2r}}{r\left(\frac{1+C}{2}\beta r - is^2\right)}\,\mathrm{d}s \,, \tag{3.41}$$

$$\frac{\Delta\mu_{\parallel,\mathrm{B}}}{\mu_0} = \frac{3i}{\sigma^2}\frac{R}{z_0}\int_0^\infty \frac{4rs^7(e^{-r} - e^{-s})^2}{16s^5(r-s) - r\beta_\mathrm{B}^3\sigma^2}\,\mathrm{d}s \,, \tag{3.42}$$

$$\frac{\Delta\mu_{\perp,\mathrm{S}}}{\mu_0} = \frac{6i}{\sigma^2}\frac{R}{z_0}\int_0^\infty \frac{s^5\left(e^{-s} - e^{-r}\right)^2}{4(r-s)s^2 - \sigma^2\beta}\,\mathrm{d}s \,, \tag{3.43}$$

$$\frac{\Delta\mu_{\perp,\mathrm{B}}}{\mu_0} = \frac{6i}{\sigma^2}\frac{R}{z_0}\int_0^\infty \frac{4s^7(se^{-r} - re^{-s})^2}{r(16s^5(r-s) - r\beta_\mathrm{B}^3\sigma^2)}\,\mathrm{d}s \,, \tag{3.44}$$

with $r = \sqrt{s^2 + i\sigma^2}$. The integrals are well-behaved and thus amenable to straightforward numerical integration. The effect of inertia on the diffusion has recently been investigated in bulk systems [45–49]. However, as shown in the Supporting Information [50] for the realistic situation treated in figure 1, the contribution of fluid inertia is completely negligible in the frequency range that is affected by membrane elasticity which is the focus of this work.

In the following, we will thus consider the case $\sigma = 0$, for which an analytical solution is possible:

$$\frac{\Delta\mu_{\parallel,\mathrm{S}}}{\mu_0} = \frac{3}{8}\frac{R}{z_0}\Bigg(-\frac{5}{4} + \frac{\beta^2}{8} - \frac{3i\beta}{8} + i\beta(1+C)e^{i\beta(1+C)}\mathrm{E}_1(i\beta(1+C)) + \left(-\frac{\beta^2}{2} + \frac{i\beta}{2}\left(1-\frac{\beta^2}{4}\right)\right)e^{i\beta}\mathrm{E}_1(i\beta)\Bigg), \tag{3.45}$$

$$\frac{\Delta\mu_{\parallel,\mathrm{B}}}{\mu_0} = \frac{3}{64}\frac{R}{z_0}\left(-2 + \frac{i\beta_\mathrm{B}^3}{3}\left(\phi_+ + e^{-i\beta_\mathrm{B}}\mathrm{E}_1(-i\beta_\mathrm{B})\right)\right), \tag{3.46}$$

$$\frac{\Delta\mu_{\perp,\mathrm{S}}}{\mu_0} = \frac{9i}{16}\frac{R}{z_0}\frac{1}{\beta}\left(1 - 4e^{i\beta}\mathrm{E}_5(i\beta)\right), \tag{3.47}$$

$$\frac{\Delta\mu_{\perp,\mathrm{B}}}{\mu_0} = \frac{3i\beta_\mathrm{B}}{8}\frac{R}{z_0}\Bigg(\left(\frac{\beta_\mathrm{B}^2}{12} + \frac{i\beta_\mathrm{B}}{6} + \frac{1}{6}\right)\phi_+ + \frac{\sqrt{3}}{6}(\beta_\mathrm{B}+i)\phi_- + \frac{5i}{2\beta_\mathrm{B}} + e^{-i\beta_\mathrm{B}}\mathrm{E}_1(-i\beta_\mathrm{B})\left(\frac{\beta_\mathrm{B}^2}{12} - \frac{i\beta_\mathrm{B}}{3} - \frac{1}{3}\right)\Bigg), \tag{3.48}$$

with

$$\phi_\pm = e^{-i\overline{z_\mathrm{B}}}\mathrm{E}_1\left(-i\overline{z_\mathrm{B}}\right) \pm e^{-iz_\mathrm{B}}\mathrm{E}_1\left(-iz_\mathrm{B}\right), \tag{3.49}$$

where $z_\mathrm{B} = j\beta_\mathrm{B}$ and $j = e^{2i\pi/3}$. Bar denotes complex conjugate. E_n denotes the exponential integral $\mathrm{E}_n(x) = \int_1^\infty e^{-xt}/t^n dt$ [51].

From the frequency-dependent mobilities the mean-square displacement in a thermally fluctuating system can be computed using the fluctuation-dissipation theorem with the velocity autocorrelation function $\phi_v(t)$ as an intermediate step [52] as detailed in Appendix C

$$\phi_v(t) = \frac{k_\mathrm{B}T}{2\pi}\int_{-\infty}^{\infty}\mu(\omega)e^{i\omega t}\,\mathrm{d}\omega\,, \tag{3.50}$$

$$\left\langle x(t)^2\right\rangle = 2\int_0^t (t-s)\phi_v(s)\,\mathrm{d}s\,. \tag{3.51}$$

Using the mobilities from Eqs. (3.45) - (3.48), the MSD can be analytically computed and the resulting equations are given in Appendix C. In order to compute the MSDs shown in figure 1 mobilities are calculated using the initial particle-membrane distance z_0, which is equivalent to assuming a not too large deviation of the particle from its initial position.

Similarly, the power spectral densities of the position fluctuations as shown in figure 3 can be calculated as [12]

$$S(\omega) = \frac{2k_\mathrm{B}T\mathrm{Re}\left[\mu(\omega)^{-1}\right]}{\left(\omega\mathrm{Re}\left[\mu(\omega)^{-1}\right]\right)^2 + \left(\omega\mathrm{Im}\left[\mu(\omega)^{-1}\right] + K\right)^2}\,. \tag{3.52}$$

4 Mobility Simulations

We use boundary-integral (BIM) simulations to obtain a direct validation of the frequency-dependent mobilities and to assess the accuracy of the point-particle approximation for finite-radius particles. BIMs are a standard method for solving the steady Stokes equations [53] including elastic surfaces [54]. Some details on our implementation are given in the SI. Compared with most other flow solvers, BIMs have the advantage that they are able to treat a truly inifinite fluid domain thus excluding artifacts due to periodic replications of the system.

We simulate a spherical particle driven by an oscillating force with frequency ω. By recording the

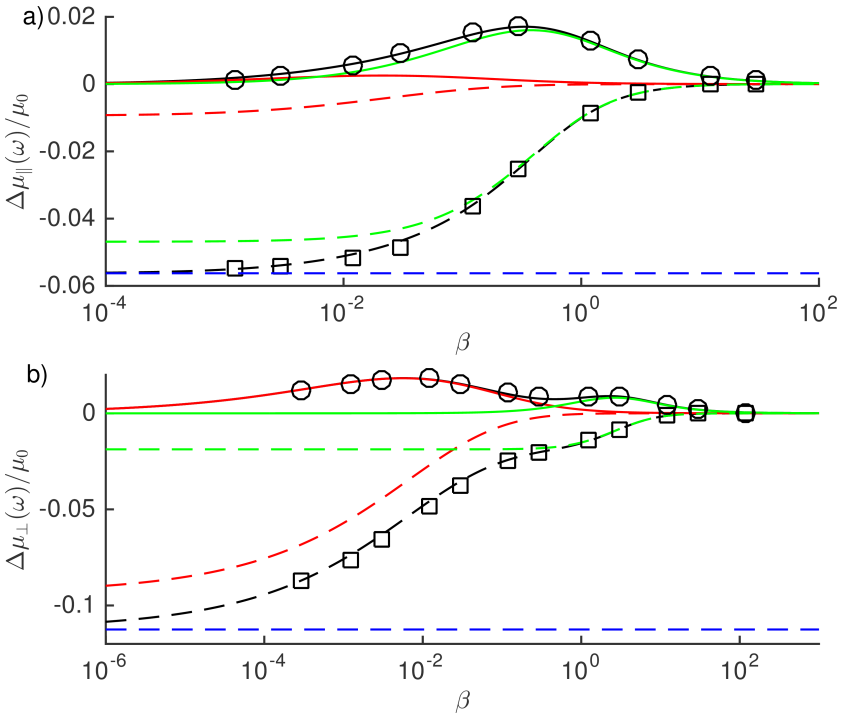

Figure 4: The complex mobility of a spherical particle driven by a sinusoidal force with frequency ω situated a distance z_0 above the membrane. Theoretical predictions from Eqs. (3.45)-(3.48) are shown as black dashed lines (real part) and black solid lines (imaginary part) and compared to BIM simulations shown as circles (real part) and squares (imaginary part). The green and red lines show the contributions due to shear and bending resistance, respectively. For $R/z_0 = 0.1$ (with $C = 1$, $\kappa_S R^2/\kappa_B = 2$) the agreement between theory and simulations is excellent. For very low frequencies the hard wall behavior is obtained (blue dashed line).

instantaneous particle velocity, the mobility correction $\Delta\mu(\omega)$ can be obtained from the amplitude ratio and the phase shift between force and velocity as illustrated in the SI.

In Fig. 4 we compare our theoretical prediction to the result of BIM simulations with $R/z_0 = 0.1$ and find excellent agreement. Splitting the mobility correction into the contributions due to shear/area resistance (green line in Fig. 4) on the one hand and bending resistance (red line) on the other, we find that bending resistance manifests itself at significantly lower frequencies than shear resistance. As might intuitively be expected, the parallel mobility is mainly determined by shear resistance, while for the perpendicular mobility bending resistance dominates. Yet, we note that for both directions, shear/area resistance and bending resistance are important. This becomes apparent especially at low frequencies: neither shear/area resistance nor bending resistance alone are able to recover the hard-wall limit. As shown in the SI, a similar effect appears in the limit of infinitely stiff membranes: only if shear and bending stiffness both tend to infinity does one recover the hard-wall limit.

Finally, we investigate the validity of the point-particle approximation for particles close to the interface. For this, we use the parameters as in Fig. 1. Even for $R/z_0 = 0.65$ the agreement is still surprisingly good as shown in Fig. 5.

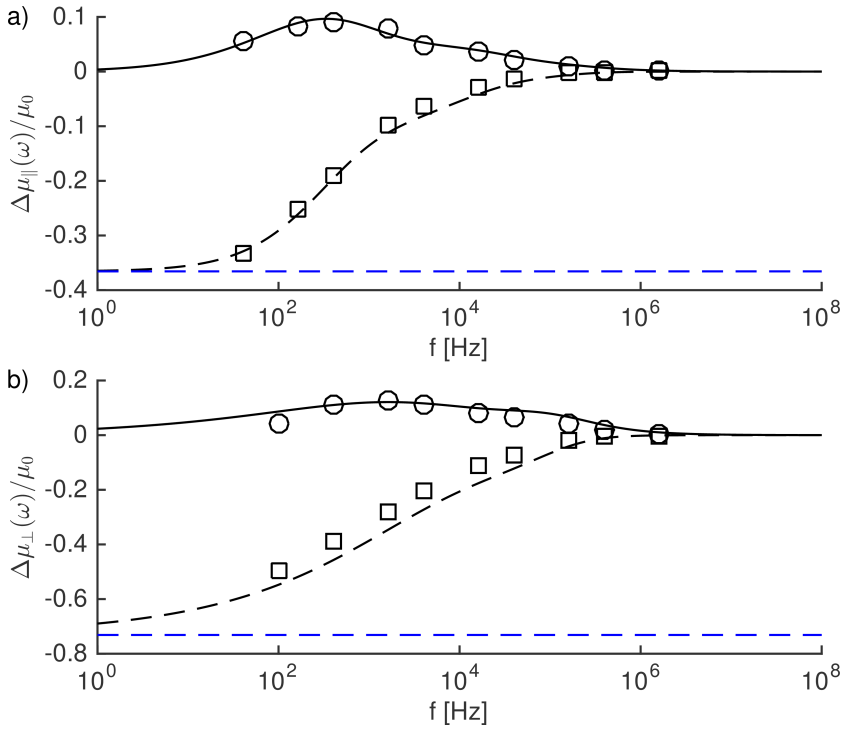

Figure 5: The real part (dashed lines) and the imaginary part (solid lines) of the complex mobility for a particle moving parallel (a) or perpendicular (b) to a realistically modeled red blood cell membrane with parameters corresponding to Fig. 1. Even for $R/z_0 = 0.65$ as used here the agreement is still good.

5 Conclusion

We have presented a fully analytical theory for the thermal diffusion of a small spherical particle in close vicinity to an elastic cell membrane. The frequency-dependent particle mobilities predicted by the theory are in excellent agreement with boundary-integral simulations, even for surprisingly large particles where the point-force approximation made in the theory is no longer strictly valid. Independent of the membrane properties, the mean-square displacement is shown to be bulk-like at short and hard-wall-like at very long times. In between, however, there exists a significant time span during which the particle shows subdiffusion with exponents as low as 0.87. For membrane parameters corresponding to a typical red blood cell the subdiffusive regime extends up to and beyond 10ms and may thus be of possible physiological significance, e.g., for the uptake of drug carriers or viruses by a living cell. Our results can be directly verified experimentally by comparing the power-spectral densities of the position fluctuations in Fig. 3.

In living cells the membrane elastic properties depend on the local cholesterol level [55] which can lead to localized patches of varying stiffness. According to our calculations, adjusting the shear/bending rigidity would allow the cell to specifically influence the endocytosis probability: An enhanced bending stiffness combined with reduced shear elasticity would reduce perpendicular diffusion – keeping the approaching particle close to the membrane for a longer time – and at the same time enhance parallel diffusion – allowing the particle to survey more quickly the cell surface for favorable biochemical binding sites.

Acknowledgments

The authors gratefully acknowledge funding from the Volkswagen Foundation and computing time granted by the Leibniz-Rechenzentrum on SuperMUC.

Appendices

A Membrane mechanics

In this appendix, we give the derivation of the linearized tangential and normal traction jumps as stated in Eq. (3.38) of the main text. Initially, the interface is described by the infinite plane $z = 0$. Let the position vector of a material point before deformation be $\boldsymbol{A}$, and $\boldsymbol{a}$ after deformation. In the undeformed state, we have $\boldsymbol{A}(x, y) = x\boldsymbol{e}_x + y\boldsymbol{e}_y$, where $\boldsymbol{e}_i$, with $i \in \{x, y, z\}$ are the Cartesian base vectors. Hereafter, we shall reserve the capital roman letters for the undeformed state. The membrane can be defined using two covariant base vectors $\boldsymbol{a}_1$ and $\boldsymbol{a}_2$, together with the normal vector $\boldsymbol{n}$. $\boldsymbol{a}_1$ and $\boldsymbol{a}_2$ are the local non-unit tangent vectors to coordinate lines. In the Cartesian coordinate system, $\boldsymbol{a}_1 = \boldsymbol{a}_{,x}$ and $\boldsymbol{a}_2 = \boldsymbol{a}_{,y}$, where the comma denotes a spatial derivative. The unit normal vector to the interface reads

$$\boldsymbol{n} = \frac{\boldsymbol{a}_1 \times \boldsymbol{a}_2}{|\boldsymbol{a}_1 \times \boldsymbol{a}_2|} \,. \tag{A.1}$$

It can be seen that the covariant base vectors in the undeformed state are identical to those of the Cartesian base. The displacement vector of a point on the membrane can be written as

$$\boldsymbol{u} = \boldsymbol{a} - \boldsymbol{A} = u_x\boldsymbol{e}_x + u_y\boldsymbol{e}_y + u_z\boldsymbol{e}_z \,. \tag{A.2}$$

The covariant base vectors are therefore

$$\boldsymbol{a}_1 = (1 + u_{x,x})\,\boldsymbol{e}_x + u_{y,x}\boldsymbol{e}_y + u_{z,x}\boldsymbol{e}_z \,, \tag{A.3}$$

$$\boldsymbol{a}_2 = u_{x,y}\boldsymbol{e}_x + (1 + u_{y,y})\,\boldsymbol{e}_y + u_{z,y}\boldsymbol{e}_z \,, \tag{A.4}$$

and the linearized normal vector reads

$$\boldsymbol{n} \approx -u_{z,x}\boldsymbol{e}_x - u_{z,y}\boldsymbol{e}_y + \boldsymbol{e}_z \,. \tag{A.5}$$

The components of the metric tensor in the deformed state are defined by the inner product $a_{\alpha\beta} = \boldsymbol{a}_\alpha \cdot \boldsymbol{a}_\beta$. Note that $A_{\alpha\beta}$ is then nothing but the second order identity tensor $\delta_{\alpha\beta}$. Form Eqs. (A.3) and (A.4), $a_{\alpha\beta}$ can straightforwardly be computed. The contravariant tensor (conjugate metric) is the inverse of the covariant tensor. We directly have to the first order

$$a^{\alpha\beta} \approx \begin{pmatrix} 1 - 2u_{x,x} & -2\epsilon \\ -2\epsilon & 1 - 2u_{y,y} \end{pmatrix} , \tag{A.6}$$

where $2\epsilon = u_{x,y} + u_{y,x}$ is the engineering shear strain. In the following, we will first derive the in-plane stress tensor. A resistance to bending will be added independently by assuming a linear isotropic model equivalent to the Helfrich model for small deformations [56].

In-plane stress tensor

Here we use the Einstein summation convention, in which a covariant index followed by the identical contravariant index (or vice versa) is implicitly summed over the index. The two invariants of the

transformation are given by Green and Adkins [57]

$$I_1 = A^{\alpha\beta} a_{\alpha\beta} - 2\,, \tag{A.7}$$

$$I_2 = \det A^{\alpha\beta} \det a_{\alpha\beta} - 1\,, \tag{A.8}$$

where $A^{\alpha\beta} = \delta_{\alpha\beta}$, is the contravariant metric tensor of the undeformed state. The two invariants are found to be equal and they are given by $I_1 = I_2 = 2e = 2\,(u_{x,x} + u_{y,y})$, where e denotes the dilatation. The contravariant components of the stress tensor $\tau^{\alpha\beta}$ are related to the strain energy $W(I_1, I_2)$ via a constitutive law. We have [58]

$$\tau^{\alpha\beta} = \frac{2}{J_s}\frac{\partial W}{\partial I_1} A^{\alpha\beta} + 2J_s \frac{\partial W}{\partial I_2} a^{\alpha\beta}, \tag{A.9}$$

where $J_s \coloneqq \sqrt{1 + I_2} \approx 1 + e$ is the Jacobian determinant, representing the ratio between the deformed and undeformed local surface area.

Several models have been proposed in order to describe the mechanics of elastic membranes. The neo-Hookean model is characterized by a single parameter containing the membrane elastic shear and area dilatation modulus, while the Skalak model [43] uses two separate parameters for shear and area dilatation resistance, respectively. The strain energy in the Skalak model reads [59]

$$W^{\mathrm{SK}} = \frac{\kappa_{\mathrm{S}}}{12}\left((I_1^2 + 2I_1 - 2I_2) + CI_2^2\right)\,, \tag{A.10}$$

where $C = \kappa_{\mathrm{A}}/\kappa_{\mathrm{S}}$ is the ratio between the area dilatation and the shear modulus. By taking $C = 1$, the Skalak model predicts the same behavior as the neo-Hookean for small deformations [58]. The calculations yield to the first order a stress tensor in the form of

$$\tau^{\alpha\beta} \approx \frac{2\kappa_{\mathrm{S}}}{3}\begin{pmatrix} u_{x,x} + Ce & \epsilon \\ \epsilon & u_{y,y} + Ce \end{pmatrix}. \tag{A.11}$$

Bending resistance

Under the action of an external load, the initially plane membrane bends. For small membrane curvatures, the bending moment M can be related to the curvature tensor via the linear isotropic model [56, 60]

$$M_\alpha^\beta = -\kappa_{\mathrm{B}}(b_\alpha^\beta - B_\alpha^\beta)\,, \tag{A.12}$$

where κ_{B} is the bending modulus, having the dimension of energy. Here b_α^β is the mixed version of the second fundamental form which follows from the curvature tensor (second fundamental form)

$$b_{\alpha\beta} = \boldsymbol{n} \cdot \boldsymbol{a}_{\alpha,\beta} \quad \text{for} \quad \alpha, \beta \in \{1, 2\}\,, \tag{A.13}$$

via $b_\alpha^\beta = b_{\alpha\delta} a^{\delta\beta} \approx u_{z,\alpha\beta}$. As the surface reference is a flat membrane, B_α^β therefore vanishes. The bending moment reads

$$M_\alpha^\beta \approx -\kappa_{\mathrm{B}} u_{z,\alpha\beta}\,. \tag{A.14}$$

The surface transverse shear vector $\boldsymbol{Q}$ is obtained from a local torque balance with the exerted moment by [60]

$$\nabla_\alpha M^{\alpha\beta} - Q^\beta = 0\,, \tag{A.15}$$

where ∇_α is the covariant derivative defined for a contravariant tensor $M^{\alpha\beta}$ by

$$\nabla_\lambda M^{\alpha\beta} = \partial_\lambda M^{\alpha\beta} + \Gamma^\alpha_{\lambda\eta} M^{\eta\beta} + \Gamma^\beta_{\lambda\eta} M^{\alpha\eta}\,, \tag{A.16}$$

where $\Gamma^{\lambda}_{\alpha\beta}$ are the Christoffel symbols of the second kind, defined by $\Gamma^{\lambda}_{\alpha\beta} = \boldsymbol{a}_{\alpha,\beta} \cdot \boldsymbol{a}^{\lambda}$, and $\boldsymbol{a}^{\lambda}$ are the contravariant basis vectors, which are related to those of the covariant basis via the contravariant metric tensor by $\boldsymbol{a}^{\alpha} = a^{\alpha\beta}\boldsymbol{a}_{\beta}$. To first order, only the partial derivative in Eq. (A.16) remains.

The raising and lowering indices operation on the second order tensor M implies that $M^{\alpha\beta} = a^{\alpha\gamma}a^{\beta\delta}M_{\gamma\delta}$, which, to the first order, is the same as M^{β}_{α} given by Eq. (A.14). The contravariant component of the transverse shear vector is therefore

$$Q^{\beta} \approx -\kappa_{\mathrm{B}} u_{z,\alpha\beta\alpha} \,. \tag{A.17}$$

Equilibrium Equation

The membrane equilibrium condition including both the shear and the bending forces reads [60]

$$\nabla_{\alpha}\tau^{\alpha\beta} - b^{\beta}_{\alpha}Q^{\alpha} = -\Delta f^{\beta} \,, \tag{A.18}$$

$$\tau^{\alpha\beta}b_{\alpha\beta} + \nabla_{\alpha}Q^{\alpha} = -\Delta f^{z} \,, \tag{A.19}$$

where Δf^{β}, with $\beta \in \{x, y\}$ is the tangential traction jump at the elastic wall, and Δf^{z} is the normal traction jump. The second term on the left-hand side (LHS) of Eq. (A.18) is irrelevant in the first order approximation. The same is true for the first term on the LHS of Eq. (A.19).

Finally, the linearized traction jump across the membrane is

$$\begin{aligned} \frac{\kappa_{\mathrm{S}}}{3}\big(\Delta_{\parallel}u_{\beta} + (1+2C)e_{,\beta}\big) &= -\Delta f^{\beta} \,, \\ \kappa_{\mathrm{B}}\Delta^{2}_{\parallel}u_{z} &= +\Delta f^{z} \,, \end{aligned} \tag{A.20}$$

where $\Delta_{\parallel} f = f_{,xx} + f_{,yy}$ is the horizontal Laplace-Beltrami of a given function f. Eqs. (A.20) are equivalent to Eqs. (3.38) of the main text.

B Derivation of particle mobilities

B.1 Hydrodynamic equations in Fourier space

We start by transforming Eqs. (3.37) of the main text to Fourier space. The spatial 2D Fourier transform for a given function f is defined as

$$\mathscr{F}\{f(\boldsymbol{\rho})\} = \tilde{f}(\boldsymbol{q}) = \int_{\mathbb{R}^2} f(\boldsymbol{\rho}) e^{-i\boldsymbol{q}\cdot\boldsymbol{\rho}} d^2\boldsymbol{\rho} \,, \tag{B.1}$$

where $\boldsymbol{\rho} = (x, y)$ is the projection of the position vector $\boldsymbol{r}$ onto the horizontal plane, and $\boldsymbol{q} = (q_x, q_y)$ is the Fourier transform variable. Similarly as in Bickel [27], all the vector fields are subsequently decomposed into longitudinal, transversal and normal components. For a given quantity $\tilde{\boldsymbol{Q}}$, whose components are $(\tilde{Q}_x, \tilde{Q}_y)$ in the Cartesian coordinate base, its components in the new orthogonal base $(\tilde{Q}_l, \tilde{Q}_t)$ are given by the following transformation

$$\begin{pmatrix} \tilde{Q}_x \\ \tilde{Q}_y \end{pmatrix} = \frac{1}{q}\begin{pmatrix} q_x & q_y \\ q_y & -q_x \end{pmatrix}\begin{pmatrix} \tilde{Q}_l \\ \tilde{Q}_t \end{pmatrix} , \tag{B.2}$$

where $q \coloneqq |\boldsymbol{q}|$. Note that the inverse transformation is given also by Eq. (B.2). Since the membrane shape depends on the history of the particle motion we also perform a Fourier analysis in time which

for a function $f(t)$ is

$$\mathscr{F}\{f(t)\} = f(\omega) = \int_{\mathbb{R}} f(t)e^{-i\omega t}dt\,. \tag{B.3}$$

In the following, the Fourier-transformed function pair $f(t)$ and $f(\omega)$ are distinguished only by their argument while the tilde is reserved to denote the spatial 2D Fourier transforms. The unsteady Stokes equations (3.37) thus become

$$-(i\rho\omega + \eta q^2)\tilde{v}_l + \eta\tilde{v}_{l,zz} - iq\tilde{p} + F_l\delta(z - z_0) = 0\,, \tag{B.4}$$

$$-(i\rho\omega + \eta q^2)\tilde{v}_t + \eta\tilde{v}_{t,zz} + F_t\delta(z - z_0) = 0\,, \tag{B.5}$$

$$-(i\rho\omega + \eta q^2)\tilde{v}_z + \eta\tilde{v}_{z,zz} - \tilde{p}_{,z} + F_z\delta(z - z_0) = 0\,, \tag{B.6}$$

$$iq\tilde{v}_l + \tilde{v}_{z,z} = 0\,. \tag{B.7}$$

The pressure in Eq. (B.4) can be eliminated using Eq. (B.6). Since the continuity equation (B.7) gives a direct relation between the components $\tilde{v}_l$ and $\tilde{v_z}$, the following fourth-order differential equation for v_z is obtained

$$\tilde{v}_{z,zzzz} - (2q^2 + i\lambda^2)\tilde{v}_{z,zz} + q^2(q^2 + i\lambda^2)\tilde{v}_z = \frac{q^2}{\eta}F_z\delta(z - z_0) + \frac{iqF_l}{\eta}\delta'(z - z_0)\,, \tag{B.8}$$

where δ' is the derivative of the delta Dirac function, satisfying the property $x\delta'(x) = -\delta(x)$ for a real x, and $\lambda^2 = \rho\omega/\eta$.

B.2 Boundary conditions

Velocity boundary conditions

At the interface $z = 0$, the velocity components are continuous

$$[\tilde{v}_\alpha] = 0\,, \tag{B.9}$$

where $\alpha \in \{l, t, z\}$ and $[f] = f(z = 0^+) - f(z = 0^-)$ denotes the jump of quantity f across the interface. In addition, the no-slip condition Eq. (3.39) gives

$$\tilde{v}_\alpha(q, z = 0, \omega) = i\omega\tilde{u}_\alpha(q, \omega)\,. \tag{B.10}$$

Tangential stress jump

The presence of the membrane leads to elastic stresses which, in equilibrium, are balanced by a jump in the fluid stress across the membrane:

$$[\sigma_{z\alpha}] = [\eta(v_{z,\alpha} + v_{\alpha,z})] = \Delta f^\alpha\,, \tag{B.11}$$

where $\alpha \in \{x, y\}$. The tangential traction jump Δf^α for an elastic membrane experiencing a small deformation is given by Eq. (3.38). We mention that only the resistance to shear and area dilatation is relevant to the first order approximation for the tangential traction jump.

Using the transformations given by (B.2) together with the no-slip condition Eq. (B.10), we straightforwardly express the first and second derivatives of u_x and u_y in our new orthogonal basis.

After some algebra, the two tangential conditions are

$$[\tilde{v}_{t,z}] = -i\alpha_{\mathrm{S}} q^2 \tilde{v}_t|_{z=0}\,, \tag{B.12}$$

$$[iq\tilde{v}_z + \tilde{v}_{l,z}] = -4i\alpha q^2 \tilde{v}_l|_{z=0}\,, \tag{B.13}$$

where

$$\alpha_{\mathrm{S}} = \kappa_{\mathrm{S}}/3\eta\omega \tag{B.14}$$

is a characteristic length for shear and

$$\alpha = \alpha_{\mathrm{S}}/B = (\kappa_{\mathrm{S}} + \kappa_{\mathrm{A}})/6\eta\omega\,, \tag{B.15}$$

with $B = 2/(1+C)$.

Eq. (B.12) gives the jump condition at the interface for the transverse velocity component $\tilde{v_t}$. Note that the latter is independent of area-dilatation, whereas both κ_{S} and κ_{A} are involved in the longitudinal and the normal velocities. Eq. (B.13) can be written by employing the incompressibility equation (B.7) together with the continuity of the normal velocity across the interface as

$$[\tilde{v}_{z,zz}] = -4i\alpha q^2 \tilde{v}_{z,z}|_{z=0}\,. \tag{B.16}$$

Normal stress jump

The normal-normal component of the jump in the stress tensor reads

$$[\sigma_{zz}] = [-p + 2\eta v_{z,z}] = \Delta f^z\,. \tag{B.17}$$

Only the bending effect is present in Δf^z to the first order, as it can be seen from Eq. (3.38). Using the incompressibility equation (B.7) and the continuity of the longitudinal velocity component across the interface, the normal stress jump in Fourier space reads

$$[\tilde{v}_{z,zzz}] = 4i\alpha_{\mathrm{B}}^3 q^6 \tilde{v}_z|_{z=0}\,, \tag{B.18}$$

where

$$\alpha_{\mathrm{B}} = \sqrt[3]{\frac{\kappa_{\mathrm{B}}}{4\eta\omega}}\,, \tag{B.19}$$

is a characteristic length for bending.

B.3 Green functions

The Green's functions are tensorial quantities which describe the fluid velocity in direction α

$$\tilde{v}_\alpha = \tilde{\mathcal{G}}_{\alpha\beta}\tilde{F}_\beta\,, \tag{B.20}$$

for $\alpha, \beta \in \{l, t, z\}$. For computing the particle mobilities the relevant quantities are the diagonal components $\tilde{\mathcal{G}}_{tt}$, $\tilde{\mathcal{G}}_{zz}$, and $\tilde{\mathcal{G}}_{ll}$ which can be derived by solving first the independent Eq. (B.5) for $\tilde{\mathcal{G}}_{tt}$, then Eq. (B.8) for $\tilde{\mathcal{G}}_{zz}$ and finally obtaining $\tilde{\mathcal{G}}_{ll}$ from solving Eq. (B.8) and employing the incompressibility condition (B.7) as detailed in the following.

Transverse-transverse component

Let us denote by K the principal square root of $q^2 + i\lambda^2$, i.e.

$$K = \sqrt{\frac{q^2 + \sqrt{q^4 + \lambda^4}}{2}} + i\sqrt{\frac{-q^2 + \sqrt{q^4 + \lambda^4}}{2}}\,. \tag{B.21}$$

Note that for the steady Stokes equations, $\lambda = 0$ and therefore $K = q$. The general solution of Eq. (B.5) for the transverse velocity component is

$$\tilde{v}_t = \begin{cases} Ae^{-Kz} & \text{for } z > z_0\,, \\ Be^{Kz} + Ce^{-Kz} & \text{for } 0 < z < z_0\,, \\ De^{Kz} & \text{for } z < 0\,. \end{cases} \tag{B.22}$$

The integration constants A–D are determined by the boundary conditions. $\tilde{v}_t$ is continuous at $z = z_0$, whereas the first derivative is discontinuous due to the delta Dirac function,

$$\tilde{v}_{t,z}|_{z=z_0^+} - \tilde{v}_{t,z}|_{z=z_0^-} = -\frac{F_t}{\eta}\,. \tag{B.23}$$

In order to evaluate the four constants, two additional equations must be provided. By applying the continuity of the transverse velocity component at the interface together with the tangential traction jump given by Eq. (B.12), we find that the transverse-transverse component of the Green function is given by

$$\tilde{\mathcal{G}}_{tt} = \frac{1}{2\eta K}\left(e^{-K|z-z_0|} + \frac{i\alpha_S q^2}{2K - i\alpha_S q^2}e^{-K(z+z_0)}\right)\,, \tag{B.24}$$

for $z \geq 0$ and by

$$\tilde{\mathcal{G}}_{tt} = \frac{1}{\eta}\frac{1}{2K - i\alpha_S q^2}e^{-K(z_0-z)}\,, \tag{B.25}$$

for $z \leq 0$. For the steady Stokes equations, the solution reads

$$\tilde{\mathcal{G}}_{tt} = \frac{1}{2\eta q}\left(e^{-q|z-z_0|} + \frac{i\alpha_S q}{2 - i\alpha_S q}e^{-q(z+z_0)}\right)\,, \tag{B.26}$$

for $z \geq 0$ and

$$\tilde{\mathcal{G}}_{tt} = \frac{1}{\eta q}\frac{1}{2 - i\alpha_S q}e^{-q(z_0-z)}\,, \tag{B.27}$$

for $z \leq 0$.

Normal-normal component

As we are interested here in $\tilde{\mathcal{G}}_{zz}$ we set $\tilde{F}_l = 0$ in Eq. (B.8). The general solution of this fourth order differential equation is

$$\tilde{v}_z = \begin{cases} Ae^{-qz} + Be^{-Kz} & \text{for } z > z_0\,, \\ Ce^{qz} + De^{-qz} + Ee^{Kz} + Fe^{-Kz} & \text{for } 0 < z < z_0\,, \\ Ge^{qz} + He^{Kz} & \text{for } z < 0\,. \end{cases} \tag{B.28}$$

At the singularity position, i.e. at $z = z_0$, the velocity $\tilde{v}_z$ and its first two derivatives are continuous. However, the delta Dirac function imposes the discontinuity of the third derivative

$$\tilde{v}_{z,zzz}|_{z=z_0^+} - \tilde{v}_{z,zzz}|_{z=z_0^-} = \frac{q^2 F_z}{\eta}\,. \tag{B.29}$$

At the membrane, $\tilde{v}_z$ and its first derivative are continuous. However, shear and bending impose a discontinuity in the second and third derivatives respectively (Eqs. (B.16) and (B.18)). The system can readily be solved in order to determine the constants. The calculations are straightforward but lengthy and thus omitted here. We find that the normal-normal component of the Green function is given in a compact form by

$$\begin{aligned}\tilde{\mathcal{G}}_{zz} = \frac{q}{2\mu KZS}\Bigg(&Ke^{-q|z-z_0|} - qe^{-K|z-z_0|} + \operatorname{sgn}(z)\frac{2i\alpha q^3 K(P-Q)}{ZPQ(2i\alpha q^2 - S)}\left(e^{-q|z|} - e^{-K|z|}\right)\\ &+ \frac{2i\alpha_{\mathrm{B}}^3 q^5 (qP - KQ)}{ZPQ(2i\alpha_{\mathrm{B}}^3 q^5 - KS)}\left(Ke^{-q|z|} - qe^{-K|z|}\right)\Bigg)\,.\end{aligned} \tag{B.30}$$

Here $P = e^{qz_0}$, $Q = e^{Kz_0}$, $S = K + q$ and $Z = K - q$.

For the steady Stokes equations, i.e. by taking the limits when $K \to q$ and $Q \to P$, one gets

$$\tilde{\mathcal{G}}_{zz} = \frac{1}{4\eta q}\left(\left(1 + q|z - z_0|\right)e^{-q|z-z_0|} + \left(\frac{i\alpha z z_0 q^3}{1 - i\alpha q} + \frac{i\alpha_{\mathrm{B}}^3 q^3 (1 + qz_0)(1 + qz)}{1 - i\alpha_{\mathrm{B}}^3 q^3}\right)e^{-q(z+z_0)}\right), \tag{B.31}$$

for $z \geq 0$ and

$$\tilde{\mathcal{G}}_{zz} = \frac{1}{4\eta q}\left(1 + q(z_0 - z) + \frac{i\alpha z z_0 q^3}{1 - i\alpha q} + \frac{i\alpha_{\mathrm{B}}^3 q^3 (1 + qz_0)(1 - qz)}{1 - i\alpha_{\mathrm{B}}^3 q^3}\right)e^{-q(z_0 - z)}\,, \tag{B.32}$$

for $z \leq 0$. Note that both the shear and the bending moduli are involved in the normal-normal component of the Green functions.

Longitudinal-longitudinal component

When the normal force F_z is set to zero in Eq. (B.8), and only a tangential force F_l is applied, the derivative of the Dirac function imposes the discontinuity of the second derivative at $z = z_0$, whereas the third derivative is continuous. We have

$$\tilde{v}_{z,zz}|_{z=z_0^+} - \tilde{v}_{z,zz}|_{z=z_0^-} = \frac{iqF_l}{\eta}\,. \tag{B.33}$$

After solving Eq. (B.8) for the normal velocity $\tilde{v}_z$, the longitudinal velocity $\tilde{v}_l$ can directly be obtained thanks to the incompressibility equation (B.7). We find that the longitudinal-longitudinal component $\tilde{\mathcal{G}}_{ll}$ is

$$\begin{aligned}\tilde{\mathcal{G}}_{ll} = \frac{1}{2\eta ZS}\Bigg(&Ke^{-K|z-z_0|} - qe^{-q|z-z_0|} + \frac{2i\alpha q^2 (KP - qQ)}{ZPQ(2i\alpha q^2 - S)}\left(qe^{-q|z|} - Ke^{-K|z|}\right)\\ &+ \operatorname{sgn}(z)\frac{2i\alpha_{\mathrm{B}}^3 q^6 K(P-Q)}{ZPQ(2i\alpha_{\mathrm{B}}^3 q^5 - KS)}\left(e^{-q|z|} - e^{-K|z|}\right)\Bigg)\,.\end{aligned} \tag{B.34}$$

When the steady Stokes equations are considered, one simply gets

$$\tilde{\mathcal{G}}_{ll} = \frac{1}{4\eta q}\left((1-q|z-z_0|)e^{-q|z-z_0|} + \left(\frac{i\alpha q(1-qz_0)(1-qz)}{1-i\alpha q} + \frac{izz_0\alpha_{\mathrm{B}}^3 q^5}{1-i\alpha_{\mathrm{B}}^3 q^3}\right)e^{-q(z+z_0)}\right), \tag{B.35}$$

for $z \geq 0$ and

$$\tilde{\mathcal{G}}_{ll} = \frac{1}{4\eta q}\left(1-q(z_0-z) + \frac{i\alpha q(1+qz)(1-qz_0)}{1-i\alpha q} + \frac{izz_0\alpha_{\mathrm{B}}^3 q^5}{1-i\alpha_{\mathrm{B}}^3 q^3}\right)e^{-q(z_0-z)}, \tag{B.36}$$

for $z \leq 0$.

B.4 Particle mobilities

We now obtain the mobility corrections defined in Eq. (3.34) and given specifically in Eqs. (3.41)–(3.44) (including the inertial term) and Eqs. (3.45)-(3.48) (without fluid inertia) of the main text. For this, using Eq. (B.2) on Eq. (B.20), one derives the transformation of the tensorial Green's functions back to Cartesian directions:

$$\tilde{\mathcal{G}}_{xx}(\boldsymbol{q},z,\omega) = \frac{q_y^2}{q^2}\,\tilde{\mathcal{G}}_{tt}(\boldsymbol{q},z,\omega) + \frac{q_x^2}{q^2}\,\tilde{\mathcal{G}}_{ll}(\boldsymbol{q},z,\omega), \tag{B.37}$$

$$\tilde{\mathcal{G}}_{yy}(\boldsymbol{q},z,\omega) = \frac{q_x^2}{q^2}\,\tilde{\mathcal{G}}_{tt}(\boldsymbol{q},z,\omega) + \frac{q_y^2}{q^2}\,\tilde{\mathcal{G}}_{ll}(\boldsymbol{q},z,\omega). \tag{B.38}$$

We then subtract the infinite space Green's functions in the Fourier domain which can be obtained via the above derivation with the membrane moduli set to zero, i.e.

$$\Delta\tilde{\mathcal{G}}^{(0)}_{\gamma\gamma}(\boldsymbol{q},z,\omega) = \tilde{\mathcal{G}}_{\gamma\gamma}(\boldsymbol{q},z,\omega) - \tilde{\mathcal{G}}_{\gamma\gamma}(\boldsymbol{q},z,\omega)|_{\alpha,\alpha_{\mathrm{B}}=0}, \tag{B.39}$$

where $\gamma \in \{x,y,z\}$. This defines the wave-vector dependent corrections

$$\begin{aligned}\Delta\tilde{\mathcal{G}}_{\parallel}(\boldsymbol{q},z,\omega) &= \tilde{\mathcal{G}}_{xx}(\boldsymbol{q},z,\omega) - \tilde{\mathcal{G}}^{(0)}_{xx}(\boldsymbol{q},z,\omega),\\ &= \tilde{\mathcal{G}}_{yy}(\boldsymbol{q},z,\omega) - \tilde{\mathcal{G}}^{(0)}_{yy}(\boldsymbol{q},z,\omega),\\ \Delta\tilde{\mathcal{G}}_{\perp}(q,z,\omega) &= \tilde{\mathcal{G}}_{zz}(q,z,\omega) - \tilde{\mathcal{G}}^{(0)}_{zz}(q,z,\omega).\end{aligned} \tag{B.40}$$

Due to the point-particle approximation it is sufficient to obtain the fluid velocity at the particle position which is equal to the velocity of the particle itself. Instead of the full inverse Fourier transform of the Green's functions to real space coordinates ($\boldsymbol{\rho}$, z), we can thus limit ourselves to evaluate the inverse Fourier transform of Eqs. (B.40) at ($\boldsymbol{\rho}=0$, $z=z_0$). By passage to polar coordinates $q_x = q\cos\phi$ and $q_y = q\sin\phi$, the correction in the particle mobility to the first order of R/z_0 can be obtained

$$\begin{aligned}\Delta\mu_{\parallel}(\omega) &= \frac{1}{(2\pi)^2}\int_0^{2\pi}\int_0^{\infty}\Delta\tilde{\mathcal{G}}_{\parallel}(q,\phi,z=z_0,\omega)\,q\,\mathrm{d}q\,\mathrm{d}\phi\\ \Delta\mu_{\perp}(\omega) &= \frac{1}{2\pi}\int_0^{\infty}\Delta\tilde{\mathcal{G}}_{\perp}(q,z=z_0,\omega)\,q\,\mathrm{d}q,\end{aligned} \tag{B.41}$$

which directly lead to Eqs. (3.41)–(3.44) of the main text. A similar procedure can be followed for the steady case where the fluid inertia is neglected leading to Eqs. (3.45)-(3.48).

C Computing mean square displacements from particle mobilities

C.1 Time dependent mobility corrections

A crucial step in order to compute the mean-square-displacements as described in the following section is to transform the frequency-dependent particle mobilities back to the time domain. As shown in the Supporting Information, the inertial contribution to the mobilitiy correction is negligible for realistic scenarios and we therefore restrict ourselves from now on to the case $\sigma = 0$. For the sake of simplicity, we do not start from the real-space particle mobilities given in Eqs. (3.45)–(3.48), but instead depart from the wave-vector-dependent Green's functions in Eq. (B.40) to perform first an inverse Fourier transform in time followed by an inverse Fourier transform in space. Note that the inverse order is possible for the shear-related part, but the calculations are much more complicated.

Parallel mobility

Shear effect. Considering only the part due to shear resistance in Eqs. (B.35) and (B.26) and using Eq. (B.40) with (B.39), we find after passing to polar coordinates:

$$\Delta\tilde{\mathcal{G}}_{\parallel,\mathrm{S}}(q,\phi,\omega)|_{z=z_0} = \frac{iz_0e^{-2qz_0}}{2\eta}\left(\frac{\sin^2\phi}{T_\mathrm{S}\omega - iqz_0} + \frac{(1-qz_0)^2\cos^2\phi}{BT_\mathrm{S}\omega - 2iqz_0}\right), \tag{C.1}$$

where $T_\mathrm{S} = 6z_0\eta/\kappa_\mathrm{S}$ is a characteristic time for shear. The temporal inverse Fourier transform reads

$$\Delta\tilde{\mathcal{G}}_{\parallel,\mathrm{S}}(q,\phi,t)|_{z=z_0} = -\frac{z_0e^{-2qz_0}\theta(t)}{2\eta T_\mathrm{S}}\left(e^{-\frac{qz_0t}{T_\mathrm{S}}}\sin^2\phi + \frac{(1-qz_0)^2}{B}\,e^{\frac{-2qz_0t}{BT_\mathrm{S}}}\cos^2\phi\right). \tag{C.2}$$

An exact expression of the time dependent mobility correction due to shear in the parallel case can then be obtained by spatial inverse Fourier transform

$$\frac{\Delta\mu_{\parallel,\mathrm{S}}(\tau)}{\mu_0} = -\frac{3}{32}\frac{R}{z_0}\frac{\theta(\tau)}{T_\mathrm{S}}\frac{N_B(\tau)}{(2+\tau)^2(\tau+B)^4}, \tag{C.3}$$

where $\tau = t/T_\mathrm{S}$, and again $B = 2/(1+C)$. $\theta(t)$ denotes the Heaviside step function, with $\theta(0) = 1/2$ and

$$N_B(\tau) = 4B^3(1+2B) + 36B^3\tau + B(B^2+48B+8)\tau^2 + 40B\tau^3 + 2(B+4)\tau^4. \tag{C.4}$$

Bending effect. Considering the part due to bending resistance we obtain

$$\Delta\tilde{\mathcal{G}}_{\parallel,\mathrm{B}}(q,\phi,\omega)|_{z=z_0} = \frac{\cos^2\phi}{4\eta}\frac{iq^4z_0^5}{T_\mathrm{B}\omega - iq^3z_0^3}\,e^{-2qz_0}, \tag{C.5}$$

to give after applying the temporal inverse Fourier transform

$$\Delta\tilde{\mathcal{G}}_{\parallel,\mathrm{B}}(q,\phi,t)|_{z=z_0} = -\frac{q^4z_0^5\theta(t)\cos^2\phi}{4\eta T_\mathrm{B}}\,e^{-2qz_0-\frac{tq^3z_0^3}{T_\mathrm{B}}}. \tag{C.6}$$

The time dependent mobility can immediately be obtained after applying the inverse Fourier transform

$$\frac{\Delta\mu_{\parallel,\mathrm{B}}(t)}{\mu_0} = -\frac{3}{8}\frac{a}{z_0}\frac{\theta(t)}{T_\mathrm{B}}\int_0^\infty u^5e^{-2u-\frac{t}{T_\mathrm{B}}u^3}\,\mathrm{d}u, \tag{C.7}$$

where $T_\mathrm{B} = 4\eta z_0^3/\kappa_\mathrm{B}$. The presence of u^3 in the exponential argument makes the analytical evaluation

of this integral impossible. To overcome this difficulty, we evaluate the integral numerically and fit the result (as a function of t) with an analytical empirical form which is necessary to proceed further. This procedure is known as the Batchelor parametrization [61]. It can be shown that the integral decays following a t^{-2} law for larger times. Therefore, we can write

$$\frac{\Delta\mu_{\parallel,\mathrm{B}}(\tau_{\parallel,\mathrm{B}})}{\mu_0} = -\frac{45}{64}\frac{R}{z_0}\frac{\theta(\tau_{\parallel,\mathrm{B}})}{T_\mathrm{B}}\frac{1}{\left(\tau_{\parallel,\mathrm{B}}^p+1\right)^{\frac{2}{p}}}\,, \tag{C.8}$$

where $p = 1/2$ is the fitting parameter and $\tau_{\parallel,\mathrm{B}} = 2/5t/T_\mathrm{B}$. A comparison between the numerically obtained value of the integral and the fitting formula in presented in the SI, where a good agreement is obtained.

Perpendicular motion

Shear effect. Considering only the part due to shear resistance in Eq. (B.31) and using Eq. (B.40) with Eq. (B.39) we find after passing to polar coordinates:

$$\Delta\tilde{\mathcal{G}}_{\perp,\mathrm{S}}(q,\omega)|_{z=z_0} = \frac{iq^2z_0^3}{2\eta}\frac{e^{-2qz_0}}{BT_\mathrm{S}\omega - 2iqz_0}\,. \tag{C.9}$$

The computation of the temporal inverse Fourier transform leads to

$$\Delta\tilde{\mathcal{G}}_{\perp,\mathrm{S}}(q,t)|_{z=z_0} = -\frac{q^2z_0^3\theta(t)}{2\eta BT_\mathrm{S}}\,e^{-2qz_0\left(1+\frac{t}{BT_\mathrm{S}}\right)}\,. \tag{C.10}$$

After applying the spatial inverse Fourier transform to this equation, we find that the time dependent mobility correction due to shear reads

$$\frac{\Delta\mu_{\perp,\mathrm{S}}(\tau)}{\mu_0} = -\frac{9}{16}\frac{R}{z_0}\frac{\theta(\tau)}{T_\mathrm{S}}\frac{B^3}{(\tau+B)^4}\,. \tag{C.11}$$

Bending effect. Considering only the part due to bending resistance we obtain

$$\Delta\tilde{\mathcal{G}}_{\perp,\mathrm{B}}(q,\omega)|_{z=z_0} = \frac{iq^2z_0^3(1+qz_0)^2}{4\eta}\frac{e^{-2qz_0}}{T_\mathrm{B}\omega - iq^3z_0^3}\,. \tag{C.12}$$

The temporal inverse Fourier transform is

$$\Delta\tilde{\mathcal{G}}_{\perp,\mathrm{B}}(q,t)|_{z=z_0} = -\frac{q^2z_0^3(1+qz_0)^2\theta(t)}{4\eta T_\mathrm{B}}e^{-2qz_0-\frac{tq^3z_0^3}{T_\mathrm{B}}}\,. \tag{C.13}$$

After Fourier-transform in space, the time dependent mobility correction due to bending is expressed by the following improper integral

$$\frac{\Delta\mu_{\perp,\mathrm{B}}(t)}{\mu_0} = -\frac{3}{4}\frac{a}{z_0}\frac{\theta(t)}{T_\mathrm{B}}\int_0^\infty u^3(1+u)^2e^{-2u-\frac{tu^3}{T_\mathrm{B}}}\,\mathrm{d}u\,. \tag{C.14}$$

As above, we use the Batchelor parametrization [61] to represent the integral. At $t = 0$, the integral above can be solved analytically, and it is equal to 15/4. At larger times, the integral decays

monotonically following a $t^{-4/3}$ law. We set

$$\frac{\Delta\mu_{\perp,\mathrm{B}}(\tau_{\perp,\mathrm{B}})}{\mu_0} = -\frac{45}{16}\frac{R}{z_0}\frac{\theta(\tau_\mathrm{B})}{T_\mathrm{B}}\frac{1}{\left(\tau_{\perp,\mathrm{B}}^p + 1\right)^{\frac{4}{3p}}}\,, \tag{C.15}$$

where $\tau_{\perp,\mathrm{B}} = 9\pi/4t/T_\mathrm{B}$ and $p = 2/3$ is a fitting parameter, governing the evolution of the mobility correction at short times. Again, the fitting formula and the numerical solution are in excellent agreement as seen in the Supporting Information.

C.2 Mean-square-displacements

The dynamics of a Brownian particle are governed by the generalized Langevin equation [62]

$$m\frac{\mathrm{d}v_\alpha}{\mathrm{d}t} = -\int_{-\infty}^{t}\gamma_\alpha(t-t')v_\alpha(t')\,\mathrm{d}t' + F(t)\,, \tag{C.16}$$

where m is the particle mass and v_α is its velocity in direction $\alpha = \parallel, \perp$. $\gamma_\alpha(t)$ denotes the time dependent friction retardation function (expressed in $\mathrm{kg}\,/\,\mathrm{s}^2$), and F is the random force which is zero on average. The random force results from the impacts with the fluid molecules due to the thermal fluctuation. The relation between the mobility and the friction function is given by [52, Eq. (1.6.4) p. 32] [63]

$$\mu_\alpha(\omega) = \frac{1}{im\omega + \gamma_\alpha[\omega]}\,, \tag{C.17}$$

where $\gamma_\alpha[\omega]$ is the one-sided Fourier transform of the retardation function defined by

$$\gamma_\alpha[\omega] = \int_0^\infty \gamma_\alpha(t)e^{-i\omega t}\,\mathrm{d}t\,. \tag{C.18}$$

The frictional forces and the random forces are not independent quantities, but are related to each other via the fluctuation-dissipation theorem (FDT) [62]. According to the FDT, the velocity autocorrelation function (VACF) has the following expression [52, Eq. (1.6.14) p. 34]

$$\phi_{v,\alpha}(t) \coloneqq \langle v_\alpha(0)v_\alpha(t)\rangle = \frac{k_\mathrm{B}T}{2\pi}\int_{-\infty}^{\infty}\mu_\alpha(\omega)e^{i\omega t}\,\mathrm{d}\omega\,. \tag{C.19}$$

In the overdamped regime, i.e. for a massless particle, Eq. (C.19) is reduced to

$$\phi_{v,\alpha}(t) = D_0\left(2\delta(t) + \frac{\Delta\mu_\alpha(t)}{\mu_0}\right)\,, \tag{C.20}$$

where $D_0 = k_\mathrm{B}T\mu_0$, is the bulk diffusion coefficient given by the Einstein relation [64].

Next, the particle MSDs can be computed knowing the VACF as [62]

$$\begin{aligned}\langle x(t)^2\rangle &= 2\int_0^t (t-s)\phi_{v,\parallel}(s)\,\mathrm{d}s\\ \langle z(t)^2\rangle &= 2\int_0^t (t-s)\phi_{v,\perp}(s)\,\mathrm{d}s\,,\end{aligned} \tag{C.21}$$

which can be conveniently split up into a bulk contribution and a correction defined by:

$$\Delta_{\parallel}(t) = 1 - \frac{\langle x(t)^2 \rangle}{2D_0 t} \quad \text{and} \quad \Delta_{\perp}(t) = 1 - \frac{\langle z(t)^2 \rangle}{2D_0 t}\,. \tag{C.22}$$

By inserting the time-dependent mobility corrections derived in Eqs. (C.3), (C.8), (C.11), (C.15) in Eq. (C.20) and using Eqs. (C.21) we obtain analytical expressions for the excess mean-square-displacement as follows:

$$\Delta_{\perp,\mathrm{S}}(\tau) = \frac{3}{16}\frac{R}{z_0}\frac{\tau(3B+2\tau)}{2(B+\tau)^2}\,, \tag{C.23}$$

$$\Delta_{\perp,\mathrm{B}}(\tau_{\perp,\mathrm{B}}) = \frac{15}{16}\frac{R}{z_0}\frac{2}{\pi}\left(\arctan\tau_{\perp,\mathrm{B}}^{\frac{1}{3}} - \frac{2}{\tau_{\perp,\mathrm{B}}^{\frac{1}{3}}} + \frac{2}{\tau_{\perp,\mathrm{B}}}\ln\left(1+\tau_{\perp,\mathrm{B}}^{\frac{2}{3}}\right)\right)\,, \tag{C.24}$$

$$\Delta_{\parallel,\mathrm{S}}(\tau) = \frac{15}{32}\frac{R}{z_0}\frac{1}{10}\left(\frac{(2\tau+3B)(5\tau+4B)}{(B+\tau)^2} - \frac{4B}{\tau}\ln\left(1+\frac{\tau}{B}\right) - \frac{16}{\tau}\ln\left(1+\frac{\tau}{2}\right)\right)\,, \tag{C.25}$$

$$\Delta_{\parallel,\mathrm{B}}(\tau_{\parallel,\mathrm{B}}) = \frac{3}{32}\frac{R}{z_0}\left(\frac{\tau_{\parallel,\mathrm{B}}^{3/2} + 2\tau_{\parallel,\mathrm{B}} + 9\sqrt{\tau_{\parallel,\mathrm{B}}} + 6}{\sqrt{\tau_{\parallel,\mathrm{B}}}(1+\sqrt{\tau_{\parallel,\mathrm{B}}})^2} - \frac{6}{\tau_{\parallel,\mathrm{B}}}\ln\left(1+\sqrt{\tau_{\parallel,\mathrm{B}}}\right)\right)\,. \tag{C.26}$$

Bibliography

[1] G. J. Doherty and H. T. McMahon, Annu. Rev. Biochem. **78**, 857 (2009).

[2] D. M. Richards and R. G. Endres, Biophys. J **107**, 1542 (2014).

[3] A. Meinel, B. Tränkle, W. Römer, and A. Rohrbach, Soft Matter **10**, 3667 (2014).

[4] F. Jünger, F. Kohler, A. Meinel, T. Meyer, R. Nitschke, B. Erhard, and A. Rohrbach, Biophys. J **109**, 869 (2015).

[5] B. Neu and H. J. Meiselman, Biophys. J **83**, 2482 (2002).

[6] P. Steffen, C. Verdier, and C. Wagner, Phys. Rev. Lett. **110**, 018102 (2013).

[7] M. Brust, O. Aouane, M. Thiébaud, D. Flormann, C. Verdier, L. Kaestner, M. W. Laschke, H. Selmi, A. Benyoussef, T. Podgorski, G. Coupier, C. Misbah, and C. Wagner, Sci. Rep. **4** (2014).

[8] A. J. Goldman, R. G. Cox, and H. Brenner, Chem. Eng. Sci. **22**, 637 (1967).

[9] G. S. Perkins and R. B. Jones, Physica A , 1 (1992).

[10] E. Lauga and T. M. Squires, Phys. Fluids **17**, 103102 (2005).

[11] B. U. Felderhof, J. Phys. Chem. B **109**, 21406 (2005).

[12] T. Franosch and S. Jeney, Phys. Rev. E **79**, 031402 (2009).

[13] H.-Y. Yu, D. M. Eckmann, P. S. Ayyaswamy, and R. Radhakrishnan, Phys. Rev. E **91**, 052303 (2015).

[14] A. Banerjee and K. Kihm, Phys. Rev. E **72**, 042101 (2005).

[15] P. Holmqvist, J. Dhont, and P. Lang, Phys. Rev. E **74**, 021402 (2006).

[16] C. K. Choi, C. H. Margraves, and K. D. Kihm, Phys. Fluids **19**, 103305 (2007).

[17] M. D. Carbajal-Tinoco, R. Lopez-Fernandez, and J. L. Arauz-Lara, Phys. Rev. Lett. **99**, 138303 (2007).

[18] E. Schäffer, S. F. Nørrelykke, and J. Howard, Langmuir **23**, 3654 (2007).

[19] P. Huang and K. Breuer, Phys. Rev. E **76**, 046307 (2007).

[20] M. Kyoung and E. D. Sheets, Biophys. J **95**, 5789 (2008).

[21] Y. Kazoe and M. Yoda, Appl. Phys. Lett. **99**, 124104 (2011).

[22] P. P. Lele, J. W. Swan, J. F. Brady, N. J. Wagner, and E. M. Furst, Soft Matter **7**, 6844 (2011).

[23] S. A. Rogers, M. Lisicki, B. Cichocki, J. K. G. Dhont, and P. R. Lang, Phys. Rev. Lett. **109**, 098305 (2012).

[24] S. L. Dettmer, S. Pagliara, K. Misiunas, and U. F. Keyser, Phys. Rev. E **89**, 062305 (2014).

[25] M. Lisicki, B. Cichocki, S. A. Rogers, J. K. G. Dhont, and P. R. Lang, Soft Matter **10**, 4312 (2014).

[26] S. H. Lee and L. G. Leal, J. Fluid Mech. **98**, 193 (1980).

[27] T. Bickel, Phys. Rev. E **75**, 041403 (2007).

[28] J. Bławzdziewicz, M. L. Ekiel-Jeżewska, and E. Wajnryb, J. Chem. Phys. **133**, 114703 (2010).

[29] T. Bickel, Europhys. Lett. **106**, 16004 (2014).

[30] B. U. Felderhof, J. Chem. Phys. **125**, 144718 (2006).

[31] R. Shlomovitz, A. A. Evans, T. Boatwright, M. Dennin, and A. J. Levine, Phys. Fluids **26**, 071903 (2014).

[32] T. Salez and L. Mahadevan, J. Fluid Mech. **779**, 181 (2015).

[33] S. Jeney, B. Lukić, J. A. Kraus, T. Franosch, and L. Forró, Phys. Rev. Lett. **100**, 240604 (2008).

[34] G. M. Wang, R. Prabhakar, and E. M. Sevick, Phys. Rev. Lett. **103**, 248303 (2009).

[35] R. Shlomovitz, A. Evans, T. Boatwright, M. Dennin, and A. Levine, Phys. Rev. Lett. **110**, 137802 (2013).

[36] W. Zhang, S. Chen, N. Li, J. Zhang, and W. Chen, Appl. Phys. Lett. **103**, 154102 (2013).

[37] W. Wang and P. Huang, Phys. Fluids **26**, 092003 (2014).

[38] W. Zhang, S. Chen, N. Li, J. Z. Zhang, and W. Chen, PLoS ONE **9**, e85173 (2014).

[39] T. Boatwright, M. Dennin, R. Shlomovitz, A. A. Evans, and A. J. Levine, Phys. Fluids **26**, 071904 (2014).

[40] T. Bickel, Eur. Phys. J. E **20**, 379 (2006).

[41] J. B. Freund, Phys. Fluids **25**, 110807 (2013).

[42] C. Pozrikidis, *Introduction to theoretical and computational fluid dynamics* (Oxford University Press, 2011).

[43] R. Skalak, A. Tozeren, R. P. Zarda, and S. Chien, Biophys. J. **13(3)**, 245–264 (1973).

[44] W. Helfrich, Z. Naturforsch. C **28**, 693 (1973).

[45] T. Franosch, M. Grimm, M. Belushkin, F. M. Mor, G. Foffi, L. Forró, and S. Jeney, Nature **478**, 85 (2011).

[46] T. Li and M. G. Raizen, Ann. Phys. **525**, 281 (2013).

[47] J. Duplat, S. Kheifets, T. Li, M. Raizen, and E. Villermaux, Phys. Rev. E **87**, 020105 (2013).

[48] S. Kheifets, A. Simha, K. Melin, T. Li, and M. G. Raizen, Science **343**, 1493 (2014).

[49] G. Pesce, G. Volpe, G. Volpe, and A. Sasso, Phys. Rev. E **90**, 042309 (2014).

[50] See Supplemental Material at http://link.aps.org/supplemental/10.1103/PhysRevE.93.012612 for a comparison between the steady and the unsteady mobility corrections for the physical parameters corresponding to Fig. 1 with a fluid density $\rho = 10^3$ kg/m^3.

[51] M. Abramowitz and I. A. Stegun, *Handbook of mathematical functions* (Dover, 1972).

[52] R. Kubo, M. Toda, and N. Hashitsume, "Statistical physics II" (1985).

[53] C. Pozrikidis, *Boundary integral and singularity methods for linearized viscous flow* (Cambridge University Press, 1992).

[54] C. Pozrikidis, J. Comput. Phys. **169**, 250 (2001).

[55] F. J. Byfield, H. Aranda-Espinoza, V. G. Romanenko, G. H. Rothblat, and I. Levitan, Biophys. J **87**, 3336 (2004).

[56] C. Pozrikidis, J. Fluid Mech. **440**, 269 (2001).

[57] A. E. Green and J. C. Adkins, *Large Elastic Deformations and Non-linear Continuum Mechanics* (Oxford University Press, 1960).

[58] E. Lac, D. Barthès-Biesel, N. A. Pelekasis, and J. Tsamopoulos, J. Fluid Mech. **516**, 303 (2004).

[59] T. Krüger, F. Varnik, and D. Raabe, Comput. Math. Appl. **61**, 3485 (2011).

[60] H. Zhao, A. H. G. Isfahani, L. N. Olson, and J. B. Freund, J. Comput. Phys. **229**, 3726 (2010).

[61] G. K. Batchelor, Q. J. Roy. Meteor. Soc. **76**, 133 (1950).

[62] R. Kubo, Rep. Prog. Phys. **29**, 255 (1966).

[63] Note that the retardation function as defined by Kubo in [52] does not incorporate the particle mass m. I.e. $\gamma(t)$ as it appears in the generalized Langevin equation is expressed in s^{-2} while ours in kg / s^2. That is the reason why m appears as a factor in Eq. (1.6.14) p. 34.

[64] A. Einstein, Ann. Phys. **8**, 549 (1905).

Publication 2

Particle mobility between two planar elastic membranes: Brownian motion and membrane deformation

A. Daddi-Moussa-Ider, A. Guckenberger and S. Gekle

Phys. Fluids **28**, 071903 (2016)

DOI: 10.1063/1.4955013

Abstract

We study the motion of a solid particle immersed in a Newtonian fluid and confined between two parallel elastic membranes possessing shear and bending rigidity. The hydrodynamic mobility depends on the frequency of the particle motion due to the elastic energy stored in the membrane. Unlike the single-membrane case, a coupling between shearing and bending exists. The commonly used approximation of superposing two single-membrane contributions is found to give reasonable results only for motions in the parallel, but not in the perpendicular direction. We also compute analytically the membrane deformation resulting from the motion of the particle, showing that the presence of the second membrane reduces deformation. Using the fluctuation-dissipation theorem we compute the Brownian motion of the particle, finding a long-lasting subdiffusive regime at intermediate time scales. We finally assess the accuracy of the employed point-particle approximation via boundary-integral simulations for a truly extended particle. They are found to be in excellent agreement with the analytical predictions.

1 Introduction

The hydrodynamic motion of nanoparticles near elastic membranes plays an essential role in a variety of biological processes and medical applications. Examples include the potential use of nanoparticles as drug delivery agents [1–3] or possible adverse health effects due to nanoparticles generated, e.g., from combustion processes and chemical industries [4]. One of the strongest biological side effects is expected when nanoparticles are taken up by living cells through endocytosis [5–8] for which the hydrodynamically governed approach towards the cell membrane is the essential first step.

Several theoretical and experimental studies have investigated particle dynamics near a single boundary such as a rigid wall [9–32] or cylinder [33], a fluid-fluid interface [34–41], a partial-slip interface [42, 43] and an elastic membrane [44–52]. The latter stands apart from both rigid and fluid interfaces as the stretching of the elastic membrane by the moving particle introduces a memory effect in the system.

The influence of a second boundary on particle dynamics has so far been studied only for hard walls. The most simple approach is due to Oseen [53] who suggested that the hydrodynamic mobility of a sphere confined between two rigid walls could be approximated by superposition of the leading-order terms from each single wall. A more rigorous attempt goes back to Faxén [54] who computed in his dissertation the particle mobility parallel to the walls for the special cases when the particle is in the mid-plane or the quarter-plane between the two hard walls [55]. For an arbitrary location between the two walls, exact solutions for a point particle can be obtained in terms of convergent series using the image technique [56–59]. For a truly extended particle, multipole expansions [60] as well as joint analytical-numerical solutions have been presented [61, 62]. Experimentally, the Brownian dynamics of a spherical particle confined between two parallel rigid walls has been studied using direct imaging measurements in the parallel direction [63] who found good agreement with Oseen's superposition approximation. Dynamic-light-scattering [57] and video microscopy combined with optical traps [64, 65] also found good agreement with theoretical predictions. Despite the significant progress in this field, the particle motion between two confining elastic interfaces has not been studied so far. An understanding of how the particle motion is affected by two adjacent elastic walls can be useful to model the diffusion of medical drugs across the extracellular space between neighboring cells [66] or the transport of macromolecules across endothelial cells that line the surface of blood vessels [67].

In this paper, we derive an analytical theory for the translational motion of a small solid particle confined between two parallel elastic membranes with both shear and bending resistance. The theoretical predictions are confirmed by boundary integral simulations. We find that shearing and

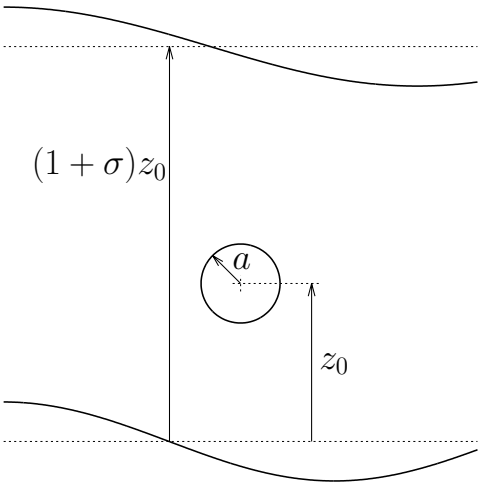

Figure 1: Illustration of the problem setup: A spherical particle of radius a at vertical position z_0 moves between two membranes located at $z = 0$ and $z = (1 + \sigma)z_0$. The membranes have infinite extent in the x and y directions.

bending contributions are intrinsically coupled which is in strong contrast to the single-membrane case where shearing and bending parts are independent and add up linearly to produce the full particle mobility [51]. We show that Oseen's often used superposition approximation leads to a reasonably good prediction of the particle mobility only for the parallel, but not for the perpendicular motion, with errors in the mobility correction as high as 55 %. Furthermore, we investigate the membrane deformation induced by the moving particle and show that the presence of the second membrane significantly reduces deformation compared to the single membrane case. Finally, the subdiffusive nature of the Brownian motion, which has recently been observed near a single membrane [44, 51] is shown to be further enhanced by the presence of the second membrane.

The paper is organized as follows. In Sec. 2, we detail the mathematical derivation of the particle mobility for the motion perpendicular and parallel to the membranes. In Sec. 3, we present the boundary integral method (BIM) and its implementation together with the procedure that we use to extract the particle mobility. Particle mobilities, membrane deformations and mean-square displacements are provided in dimensionless form in Sec. 4. Concluding remarks are offered in Sec. 5.

2 Mathematical formulation

2.1 Problem setup

We consider a small spherical solid particle of radius a located at $z = z_0 > 0$, moving between two parallel elastic membranes having infinite extent in the xy plane. The first undisplaced membrane is located at $z = 0$ and the second one at $z = (1 + \sigma)z_0$, where $\sigma \geq 1$ is a parameter (see Fig. 1 for an illustration.) For $\sigma = 1$, the particle is at equal distance from the two membranes. The one-membrane limit may be recovered by taking the limit when σ tends to infinity. Furthermore, the fluid in the whole domain is considered as incompressible and with constant dynamic viscosity η.

2.2 Particle mobility

We aim at computing the particle mobility $\mu_{\alpha\beta}$, a geometry and frequency dependent tensorial quantity that relates the velocity $\boldsymbol{V}$ of a solid particle located at $\boldsymbol{r}_0$ to a force $\boldsymbol{F}$ applied on its

surface. Transforming to temporal Fourier space, we have

$$V_\alpha(\omega) = \mu_{\alpha\beta}(\boldsymbol{r}_0, \omega) F_\beta(\omega)\,. \tag{2.1}$$

Summation over repeated indices is assumed. The particle mobility can be split up into two contributions:

$$\mu_{\alpha\beta}(\boldsymbol{r}_0, \omega) = \mu_0\, \delta_{\alpha\beta} + \Delta\mu_{\alpha\beta}(\boldsymbol{r}_0, \omega)\,, \tag{2.2}$$

where $\mu_0 = 1/(6\pi\eta a)$ is the common bulk mobility and $\delta_{\alpha\beta}$ is the Kronecker tensor. The mobility correction $\Delta\mu_{\alpha\beta}$ in the point particle approximation $a \ll z_0$ is expressed as

$$\Delta\mu_{\alpha\beta}(\boldsymbol{r}_0, \omega) = \lim_{\boldsymbol{r}\to\boldsymbol{r}_0} \left(\mathcal{G}_{\alpha\beta}(\boldsymbol{r}, \boldsymbol{r}_0, \omega) - \mathcal{G}^{(0)}_{\alpha\beta}(\boldsymbol{r}, \boldsymbol{r}_0) \right)\,, \tag{2.3}$$

where $\mathcal{G}_{\alpha\beta}$ is the Green's function of the fluid velocity $\boldsymbol{v}$ in the presence of the membranes, defined as

$$v_\alpha(\boldsymbol{r}, \omega) = \mathcal{G}_{\alpha\beta}(\boldsymbol{r}, \boldsymbol{r}_0, \omega) F_\beta(\omega)\,, \tag{2.4}$$

and $\mathcal{G}^{(0)}_{\alpha\beta}$ is the infinite space Green's function, given by

$$\mathcal{G}^{(0)}_{\alpha\beta}(\boldsymbol{r}, \boldsymbol{r}_0) = \frac{1}{8\pi\eta} \left(\frac{\delta_{\alpha\beta}}{s} + \frac{s_\alpha s_\beta}{s^3} \right)\,, \tag{2.5}$$

where $\boldsymbol{s} := \boldsymbol{r} - \boldsymbol{r}_0$ and $s := |\boldsymbol{s}|$.

The particle mobility can be obtained after solving the forced equations of fluid motion for the present boundary conditions. We solve them by Fourier-transforming the coordinates parallel to the membranes x and y. Afterward, the mobility corrections are obtained from Eq. (2.3). The particle mobility provides the memory kernel of our system and serves as an input for the generalized Langevin equation that governs the diffusional dynamics of the Brownian particle, as will be described in details in Sec. 4.

2.3 Stokes equations

For a small Reynolds number, the fluid velocity $\boldsymbol{v}(\boldsymbol{r}, t)$ and pressure $p(\boldsymbol{r}, t)$ are governed by the steady Stokes equations

$$\eta \boldsymbol{\nabla}^2 \boldsymbol{v} - \boldsymbol{\nabla} p + \boldsymbol{F}\delta(\boldsymbol{r} - \boldsymbol{r}_0) = 0\,, \tag{2.6}$$

$$\boldsymbol{\nabla} \cdot \boldsymbol{v} = 0\,, \tag{2.7}$$

where $\boldsymbol{F}(t)$ denotes a time-dependent point force (expressed in Newton) acting on the particle position $\boldsymbol{r}_0 = (0, 0, z_0)$. Furthermore, δ signifies the three-dimensional Dirac delta function. In a previous work [51], we have shown that the unsteady term in the momentum equation leads to negligible contribution in the mobility correction and is thus not considered here. The no-slip boundary condition at the membranes provides a direct link between the fluid velocity and the membrane displacement field $\boldsymbol{u}(x, y)$, which at leading order in deformation reads

$$\boldsymbol{v} = \left.\frac{\mathrm{d}\boldsymbol{u}}{\mathrm{d}t}\right|_{z=0} \quad \text{and} \quad \boldsymbol{v} = \left.\frac{\mathrm{d}\boldsymbol{u}}{\mathrm{d}t}\right|_{z=(1+\sigma)z_0}\,. \tag{2.8}$$

Hereafter, we shall denote by z_m the vertical position of each undisplaced membrane, i.e. $z_\mathrm{m} \in \{0, (1+\sigma)z_0\}$. The velocity is continuous at z_m whereas the stretching and bending forces impose a discontinuity in the fluid stress tensor. Deformation properties of the RBC membrane are modeled by

the Skalak model [68] involving as parameters the shear modulus κ_S and the area expansion modulus κ_A [51]. The membrane resists toward bending according to the Helfrich model [69]. Membrane viscosity can in principle be included into our model by adding an imaginary part to the shear modulus κ_S. Yet, since membrane viscosity is a damping term akin to the already included fluid viscosity, we do not expect our results to change significantly if it were to be included. As we shall see below, the anomalous diffusion on which we focus in the present paper comes from the membrane elasticity providing a memory to the system.

With the Skalak and Helfrich models it follows that the linearized tangential and normal fluid stress jumps across the interface are related to the membrane displacement field at z_m by [51]

$$[\sigma_{z\alpha}] = -\frac{\kappa_\mathrm{S}}{3}\left(\Delta_\parallel u_\alpha + (1+2C)e_{,\alpha}\right), \quad \alpha \in \{x,y\}, \tag{2.9a}$$

$$[\sigma_{zz}] = \kappa_\mathrm{B}\Delta_\parallel^2 u_z, \tag{2.9b}$$

where $[g] = g(z_\mathrm{m}^+) - g(z_\mathrm{m}^-)$ denotes the jump of a quantity g across the membrane located at z_m. Furthermore, $C := \kappa_\mathrm{A}/\kappa_\mathrm{S}$ is the ratio of the area expansion to shear modulus, $\Delta_\parallel = \partial_{,xx} + \partial_{,yy}$ is the Laplace-Beltrami operator along the membrane and $e = u_{x,x} + u_{y,y}$ is the dilatation. A comma in indices denotes derivatives. The components $\sigma_{z\alpha}$ of the stress tensor are expressed by

$$\sigma_{z\alpha} = -p\,\delta_{z\alpha} + \eta(v_{z,\alpha} + v_{\alpha,z}), \quad \alpha \in \{x,y,z\}. \tag{2.10}$$

The Stokes equations can conveniently be solved using a two-dimensional Fourier transform technique [36, 45, 51]. Moreover, the dependence of the membrane shape on the motion history suggests a temporal Fourier mode analysis. Here we use the common convention of a negative exponent in the forward Fourier transforms. As both spacial as well as temporal transformations will be performed, we shall reserve the tilde for the spatially transformed functions while the function and its temporal Fourier transform will be distinguished uniquely by their arguments.

Continuing, it is convenient to adopt the orthogonal coordinate system in which the Fourier transformed vectors are decomposed into longitudinal, transverse and normal components [36, 51, 70], denoted by $\tilde{v}_l$, $\tilde{v}_t$ and $\tilde{v}_z$, respectively. For some given vectorial quantity $\tilde{\boldsymbol{Q}}$, the passage from the new orthogonal basis to the usual Cartesian basis can be performed via the orthogonal transformation

$$\begin{pmatrix} \tilde{Q}_x \\ \tilde{Q}_y \end{pmatrix} = \frac{1}{q}\begin{pmatrix} q_x & q_y \\ q_y & -q_x \end{pmatrix}\begin{pmatrix} \tilde{Q}_l \\ \tilde{Q}_t \end{pmatrix}, \tag{2.11}$$

where q_x and the q_y are the components of the wavevector $\boldsymbol{q}$ and $q := |\boldsymbol{q}|$. Note that the component $\tilde{Q}_z$ along the direction normal to the membranes is left unchanged.

After applying these transformations to Eqs. (2.6) and (2.7), we can eliminate the pressure and obtain two decoupled ordinary differential equations for $\tilde{v}_t$ and $\tilde{v}_z$, such that [36, 51]

$$q^2\tilde{v}_t - \tilde{v}_{t,zz} = \frac{F_t}{\eta}\,\delta(z-z_0), \tag{2.12a}$$

$$\tilde{v}_{z,zzzz} - 2q^2\tilde{v}_{z,zz} + q^4\tilde{v}_z = \frac{q^2F_z}{\eta}\,\delta(z-z_0) + \frac{iqF_l}{\eta}\,\delta'(z-z_0), \tag{2.12b}$$

where δ' stands for the derivative of the Dirac delta function. The incompressibility equation (2.7) allows for the determination of $\tilde{v}_l$ from $\tilde{v}_z$ such that

$$\tilde{v}_l = \frac{i\tilde{v}_{z,z}}{q}. \tag{2.13}$$

For the sake of amenable mathematical equations, we will only consider the case that the two membranes have the same elastic and bending properties. Indeed, this is usually encountered in blood vessels where the RBCs posses similar physical properties. After some algebra it can be shown that the stress jump due to shear and area expansion from Eq. (2.9a) imposes the following discontinuities at z_m [51]:

$$[\tilde{v}_{t,z}] = -iB\alpha q^2 \tilde{v}_t\big|_{z=z_\mathrm{m}} , \tag{2.14a}$$

$$[\tilde{v}_{z,zz}] = -4i\alpha q^2 \tilde{v}_{z,z}\big|_{z=z_\mathrm{m}} , \tag{2.14b}$$

where $\alpha := \kappa_\mathrm{S}/(3B\eta\omega)$ with $B := 2/(1+C)$ is a characteristic length for shear and area expansion. The normal stress jump given by Eq. (2.9b) leads to

$$[\tilde{v}_{z,zzz}] = 4i\alpha_\mathrm{B}^3 q^6 \tilde{v}_z\big|_{z=z_\mathrm{m}} , \tag{2.15}$$

where $\alpha_\mathrm{B} := (\kappa_\mathrm{B}/(4\eta\omega))^{1/3}$ is a characteristic length for bending.

2.4 Solutions

The basic approach for solving such a system of equations (2.12) and (2.13) to obtain the particle mobility was detailed in an earlier work [51]. Here we only outline the major differences and steps.

Since the system is isotropic with respect to the x and y directions the mobility tensor only contains diagonal components. The normal-normal component $\tilde{\mathcal{G}}_{zz}$ can be obtained from solving Eq. (2.12b) in which only the normal force F_z is considered, i.e. $F_l = 0$. By applying the appropriate boundary conditions at z_m and z_0, the integration constants are readily determined. At $z = z_\mathrm{m}$, the normal velocity $\tilde{v}_z$ and its first derivative are continuous whereas the second and third derivatives are discontinuous because of shearing and bending, as prescribed in Eqs. (2.14b) and (2.15) respectively. At the point force position, i.e. at $z = z_0$, the normal velocity and its first and second derivatives are continuous while the Dirac delta function imposes the discontinuity of the third derivative (see Eq. (2.12b)).

For the motion parallel to the membranes, it is sufficient to consider a force F_x and solve for the Green's function component $\tilde{\mathcal{G}}_{xx}$. The latter can be expressed by employing Eq. (2.11) via

$$\tilde{\mathcal{G}}_{xx}(q,\phi,\omega) = \tilde{\mathcal{G}}_{tt}(q,\omega)\sin^2\phi + \tilde{\mathcal{G}}_{ll}(q,\omega)\cos^2\phi\,, \tag{2.16}$$

where $\phi := \arctan(q_y/q_x)$. Accordingly, the determination of $\tilde{\mathcal{G}}_{xx}$ requires two steps. First, the transverse-transverse component $\tilde{\mathcal{G}}_{tt}$ is determined from solving Eq. (2.12a). The transverse velocity $\tilde{v}_t$ is continuous at the membranes whereas shearing imposes the discontinuity of the first derivative as prescribed by Eq. (2.14a). At $z = z_0$, the transverse velocity is continuous while its first derivative is discontinuous because of the Dirac delta function (see Eq. (2.12a)). Second, the normal velocity component $\tilde{v}_z$ is determined as an intermediate step from solving first Eq. (2.12b) by only considering the longitudinal force F_l, i.e. $F_z = 0$. In this situation, the Dirac delta function imposes the discontinuity of the second derivative at z_0 whereas the third derivative is continuous. Afterward, the velocity component $\tilde{v}_l$ is immediately recovered thanks to the incompressibility equation (2.13), giving access to the longitudinal-longitudinal component $\tilde{\mathcal{G}}_{ll}$.

What remains for the determination of the particle mobility is to apply the spatial inverse Fourier transform by integrating over ϕ and the wavenumber q. In the point particle approximation, the mobility correction can readily be calculated by subtracting the bulk term and taking the limit when $\boldsymbol{r}$ tends to $\boldsymbol{r}_0$, as described by Eq. (2.3).

For convenience, we define the subscripts $\perp$ and $\parallel$ to denote the tensorial components zz and xx, respectively. The yy component of the mobility tensor is identical to the xx component. Moreover,

we define $k_\perp^\sigma(\beta,\beta_\mathrm{B})$ and $k_\parallel^\sigma(\beta,\beta_\mathrm{B})$, two frequency dependent complex quantities which are related to the first order correction in the mobility via

$$\frac{\Delta\mu_\alpha(z_0,\omega)}{\mu_0} = -k_\alpha^\sigma(\beta,\beta_\mathrm{B})\frac{a}{z_0}\,, \quad \alpha\in\{\perp,\parallel\}\,, \tag{2.17}$$

where $\beta := 2z_0/\alpha \sim \omega$ and $\beta_\mathrm{B} := 2z_0/\alpha_\mathrm{B} \sim \omega^{1/3}$ are two dimensionless frequencies related to the shear and bending effects, respectively. Analytical expressions for $k_\alpha^\sigma(\beta,\beta_\mathrm{B})$ can be obtained with computer algebra software, but they are not listed here due to their complexity and lengthiness [71]. These expressions are the basis for the computation of the Brownian motion and therefore constitute one of the central results of our work.

We proceed to investigate the limiting case of Eq. (2.17) in which both shearing and bending modulus tend to infinity and therefore β and β_B both tend to zero. In this case, which physically represents a hard wall, the general expression for k_α^σ as it appears in Eq. (2.17) reduces to

$$k_\perp^\sigma(0,0) = \int_0^\infty \frac{3}{4\Gamma}\left(\phi_+^1 e^{2\sigma u} - \phi_-^1 e^{-2\sigma u} + \phi_+^\sigma e^{2u} - \phi_-^\sigma e^{-2u} + e^{-2(1+\sigma)u} - \psi_+\right)\mathrm{d}u\,, \tag{2.18a}$$

$$k_\parallel^\sigma(0,0) = \int_0^\infty \left(\frac{3}{8\Gamma}\left(\phi_-^1 e^{2\sigma u} - \phi_+^1 e^{-2\sigma u} + \phi_-^\sigma e^{2u} - \phi_+^\sigma e^{-2u} + e^{-2(1+\sigma)u} - \psi_-\right) - \frac{3}{4}\frac{e^{2u}+e^{2\sigma u}-2}{e^{2(1+\sigma)u}-1}\right)\mathrm{d}u\,, \tag{2.18b}$$

where we defined

$$\phi_\pm^\sigma := \sigma u(\sigma u \pm 1) + \frac{1}{2}\,, \tag{2.19a}$$

$$\psi_\pm := 1 + 2(1+\sigma)^2u^2 \pm 2(1+\sigma)(1+2\sigma u^2)u\,, \tag{2.19b}$$

$$\Gamma := 1 + 2(1+\sigma)^2u^2 - \cosh\left(2(1+\sigma)u\right)\,. \tag{2.19c}$$

Expressions (2.18) are valid for arbitrary positions of the upper wall given by $(1+\sigma)z_0$. For specific values of σ we recover three results obtained earlier: First, the single hard wall limits $k_\perp^\infty(0,0) = 9/8$ and $k_\parallel^\infty(0,0) = 9/16$ [9, 34] are obtained for $\sigma\to\infty$. Second, the two wall case for $\sigma = 1$ and $\sigma = 3$ lead to the first order correction terms for the parallel motion as computed by Faxén [55], namely $k_\parallel^1(0,0)\approx 1.0041$ and $k_\parallel^3(0,0)\approx 0.6526$. Third, we find the result by Felderhof [59] for the perpendicular motion, $k_\perp^1(0,0)\approx 1.4516$.

2.5 Coupling of shear and bending contributions

In this subsection we address one particular aspect of the boundary conditions for the two membranes. In our recent work [51] we found that the particle mobility near a single elastic membrane could be expressed as the linear combination of the two independent shear and bending contributions. For the two membrane case as discussed in the present work, however, the solution of Eq. (2.12b) requires to simultaneously consider the boundary conditions stated by Eqs. (2.14b) and (2.15). This is a qualitative difference compared to the one membrane case.

To see this, consider two different setups, one with only bending resistance ($\alpha = 0$) and one with only shear resistance ($\alpha_\mathrm{B} = 0$). Furthermore, let the corresponding perpendicular velocities be denoted by $\tilde{v}_z^\mathrm{B}$ and $\tilde{v}_z^\mathrm{S}$, respectively. If the expression $\tilde{v}_z^\mathrm{S} + \tilde{v}_z^\mathrm{B} - \tilde{v}_z^\mathrm{bulk}$ should be the solution of two membranes with shear and bending resistance, it would have to fulfill the boundary conditions (2.14b)

and (2.15). This is true if and only if

$$\tilde{v}^{\mathrm{B}}_{z,z}\big|_{z=z_{\mathrm{m}}} = 0 \quad \text{and} \quad \tilde{v}^{\mathrm{S}}_{z}\big|_{z=z_{\mathrm{m}}} = 0\,, \tag{2.20}$$

which is in general satisfied only in the one membrane limit. As a result, the contributions from shearing and bending cannot be added independently on top of each other in the resulting mobility corrections, defined by Eq. (2.17).

2.6 Computation of membrane deformations

A force acting on a particle will induce a motion in the fluid. As a result, the imbalance in the stress tensor across the membranes leads to their deformation. In this subsection we compute the deformation resulting from a time dependent point force located at z_0, whereas the force is oriented perpendicularly or parallel to the membranes. Once the fluid velocity field is computed in the whole domain, the displacement field for each membrane can be obtained via Eq. (2.8). For each membrane we define a frequency and wavevector dependent reaction tensor $\tilde{\psi}_{\alpha\beta}$ as

$$\tilde{u}_\alpha(\boldsymbol{q},\omega) = \tilde{\psi}_{\alpha\beta}(\boldsymbol{q},\omega)F_\beta(\omega)\,. \tag{2.21}$$

For the perpendicular motion, the radial symmetry suggests that the displacement vector will have a normal component u_z and a radial component u_r. By performing the spatial inverse Fourier transform for a radially symmetric function [72], we immediately get the normal-normal component of the reaction tensor in real-space:

$$\psi_{zz}(\rho,\omega) = \frac{1}{2\pi}\int_0^\infty \tilde{\psi}_{zz}(q,\omega)\, J_0(\rho q)\, q\,\mathrm{d}q\,, \tag{2.22}$$

where $\rho := \sqrt{x^2+y^2}$ and J_0 is the zeroth-order Bessel function.

To compute the radial-normal component, we first note that from the transformation equations (2.11) $\tilde{\psi}_{xz} = \tilde{\psi}_{lz}\cos\phi$ since $\tilde{\psi}_{tz} = 0$ in virtue of the decoupled nature of Eqs. (2.12a) and (2.12b). Thus, the spatial inverse Fourier transform applied to the non-radially symmetric function $\tilde{\psi}_{xz}(q,\phi,\omega)$ leads to

$$\psi_{rz}(\rho,\omega) = \frac{i}{2\pi}\int_0^\infty \tilde{\psi}_{lz}(q,\omega)\, J_1(\rho q)\, q\,\mathrm{d}q\,, \tag{2.23}$$

using the fact that $\psi_{xz} = \psi_{rz}\cos\theta$ and $\psi_{yz} = \psi_{rz}\sin\theta$ where $\theta := \arctan(y/x)$.

Let us consider next the deformation due to a time dependent point force parallel to the membranes. Due to the symmetry it suffices to consider a force applied along the x-direction. Furthermore, this force can be decomposed into a longitudinal component $F_l = F_x\cos\phi$ and a transverse component $F_t = F_x\sin\phi$. For the normal-tangential component ψ_{zx}, it follows from the transformation equations (2.11) that $\tilde{\psi}_{zx} = \tilde{\psi}_{zl}\cos\phi$ since $\tilde{\psi}_{zt} = 0$ for the same reason as $\tilde{\psi}_{tz}$. Therefore, the inverse Fourier transform back into real space gives

$$\psi_{zx}(\rho,\theta,\omega) = \frac{i\cos\theta}{2\pi}\int_0^\infty \tilde{\psi}_{zl}(q,\omega)\, J_1(\rho q)\, q\,\mathrm{d}q\,, \tag{2.24}$$

meaning that the vertical deformation is maximal in the plane $y = 0$ containing the support of the vector force, and vanishes in the plane $x = 0$ perpendicular to it.

To compute the lateral stretching of the membrane due to a parallel force on the particle, we require the components ψ_{xx} and ψ_{yx} giving access to the two in-plane displacements u_x and u_y, respectively. It follows immediately from applying the transformation equations (2.11) together with

the definition of the reaction tensor Eq. (2.21) that

$$\tilde{\psi}_{xx}(q,\phi,\omega) = \tilde{\psi}_{ll}(q,\omega)\cos^2\phi + \tilde{\psi}_{tt}(q,\omega)\sin^2\phi\,, \tag{2.25}$$

leading after spatial inverse Fourier transform to

$$\psi_{xx}(\rho,\theta,\omega) = \frac{1}{4\pi}\int_0^\infty \left(\left(\tilde{\psi}_{ll}(q,\omega) + \tilde{\psi}_{tt}(q,\omega)\right) J_0(\rho q) + \left(\tilde{\psi}_{tt}(q,\omega) - \tilde{\psi}_{ll}(q,\omega)\right) J_2(\rho q)\cos 2\theta \right) q\,\mathrm{d}q\,. \tag{2.26}$$

Similar, for ψ_{yx} we have

$$\tilde{\psi}_{yx}(q,\phi,\omega) = \left(\tilde{\psi}_{ll}(q,\omega) - \tilde{\psi}_{tt}(q,\omega)\right)\cos\phi\sin\phi\,, \tag{2.27}$$

whose inverse Fourier transform is

$$\psi_{yx}(\rho,\theta,\omega) = \frac{\sin 2\theta}{4\pi}\int_0^\infty \left(\tilde{\psi}_{tt}(q,\omega) - \tilde{\psi}_{ll}(q,\omega)\right) J_2(\rho q)\, q\,\mathrm{d}q\,. \tag{2.28}$$

Although not transparent from Eq. (2.26), the deformation in the x-direction is maximal in the plane $y = 0$ and minimal in the plane $x = 0$. On the other hand, deformation is maximal for the y-direction in the bisector planes $y = \pm x$, and vanishes in the planes $x = 0$ and $y = 0$. Under the action of an arbitrary time dependent point force $\boldsymbol{F}(t)$, the membrane deformation can subsequently be obtained by applying the temporal inverse Fourier transform.

3 Simulations

3.1 Boundary Integral Method

For the simulations we use the boundary integral method (BIM) [73] whose foundation is the steady Stokes equations. The core idea is to write them as an integral equation, made possible by the fact that we deal with a linear equation. However, treating rigid objects in the direct formulation is difficult and inefficient since it would lead to a Fredholm equation of the first kind. Instead, we employ an extension called the completed double layer boundary integral equation method (CDLBIEM) [74, 75]. For the system with the two membranes the equations read

$$v_j(\boldsymbol{x}) = H_j(\boldsymbol{x})\,, \quad \boldsymbol{x} \in S_\mathrm{m}\,, \tag{3.1a}$$

$$\frac{1}{2}\phi_j(\boldsymbol{x}) + \sum_{i=1}^{6} \varphi_j^{(i)}(\boldsymbol{x})\,\langle \boldsymbol{\varphi}^{(i)}, \boldsymbol{\phi}\rangle = H_j(\boldsymbol{x})\,, \quad \boldsymbol{x} \in S_\mathrm{p}\,. \tag{3.1b}$$

Here, $S_\mathrm{m} := S_{\mathrm{m}_1} \cup S_{\mathrm{m}_2}$ where $S_{\mathrm{m}1}$ and $S_{\mathrm{m}2}$ are the surfaces of the two elastic membranes, and S_p is the surface of the rigid particle of radius a. The two membranes have a square shape with a length of $300a$. $\boldsymbol{v}$ represents the velocity on the membranes while $\boldsymbol{\phi}$ denotes the so-called double layer density function on S_p. The latter is an unphysical auxiliary field. However, the corresponding physical velocity can be retrieved via

$$V_j(\boldsymbol{x}) = \sum_{i=1}^{6} \varphi_j^{(i)}(\boldsymbol{x})\,\langle \boldsymbol{\varphi}^{(i)}, \boldsymbol{\phi}\rangle\,, \quad \boldsymbol{x} \in S_\mathrm{p}\,. \tag{3.2}$$

where the $\boldsymbol{\varphi}^{(i)}$ are known functions representing the six possible rigid body movements of the solid particle [74]. The brackets denote the inner product in the vector space of real functions whose

domain is S_p. Continuing, the function H_j with $j = 1, 2, 3$ is given by

$$H_j(\boldsymbol{x}) := -(N_\mathrm{m}\Delta\boldsymbol{f})_j(\boldsymbol{x}) - (K_\mathrm{p}\boldsymbol{\phi})_j(\boldsymbol{x}) + \mathcal{G}^{(0)}_{jk}(\boldsymbol{x}, \boldsymbol{x}_\mathrm{c})F_k\,, \tag{3.3}$$

with $\boldsymbol{x}_\mathrm{c}$ being the particle centroid. We defined the single layer integral via

$$(N_\mathrm{m}\Delta\boldsymbol{f})_j(\boldsymbol{x}) := \int_{S_\mathrm{m}} \Delta f_i(\boldsymbol{y})\mathcal{G}^{(0)}_{ij}(\boldsymbol{y}, \boldsymbol{x})\,\mathrm{d}S(\boldsymbol{y}) \tag{3.4}$$

where integration over both membrane surfaces $S_\mathrm{m} := S_{\mathrm{m}_1} \cup S_{\mathrm{m}_2}$ needs to be performed. The double layer integral is

$$(K_\mathrm{p}\boldsymbol{\phi})_j(\boldsymbol{x}) := \oint_{S_\mathrm{p}} \phi_i(\boldsymbol{y})\mathcal{T}^{(0)}_{ijk}(\boldsymbol{y}, \boldsymbol{x})n_k(\boldsymbol{y})\,\mathrm{d}S(\boldsymbol{y})\,. \tag{3.5}$$

The remaining quantities are the jump of the traction $\Delta\boldsymbol{f}$ across the membranes, the known force $\boldsymbol{F}$ acting on the rigid particle, the outer normal vector $\boldsymbol{n}$, the free-space Stokeslet as defined in Eq. (2.5), and the corresponding Stresslet

$$\mathcal{T}^{(0)}_{ijk}(\boldsymbol{y}, \boldsymbol{x}) := -\frac{3}{4\pi}\frac{s_i s_j s_k}{s^5}\,, \tag{3.6}$$

with $\boldsymbol{s} := \boldsymbol{y} - \boldsymbol{x}$ and $s := |\boldsymbol{s}|$.

Given the traction jump $\Delta\boldsymbol{f}$ (computed from the current deformation as explained in the appendix) and the force $\boldsymbol{F}$ as input, equations (3.1) constitute a set of Fredholm integral equations of the second kind for the unknown velocity $\boldsymbol{v}$ on the membranes and the density $\boldsymbol{\phi}$ on the rigid particle. To solve this equation numerically, we discretize all surfaces with flat triangles. For the rigid particle, this is done by consecutively refining an icosahedron [87] while gmsh [76] was used for the membranes: The quadratic planes were meshed with triangles, with increasing resolution towards their center. We perform the integration numerically by a Gaussian quadrature with seven points per triangle [77] together with linear interpolation of nodal values across each triangle [73]. The singularities appearing in the single layer integral are treated via the polar integration rule [78], while the singularities of the double layer integral are eliminated by the standard singularity subtraction scheme [73]. With this the integral equation can be evaluated at all nodes, forming a dense and asymmetric linear system of equations which is then subsequently solved by GMRES [79]. The residuum of the solver was fixed to 10^{-4}. This provides us with the velocity $\boldsymbol{v}$ at each node of the two membranes and, after application of equation (3.2), also of the rigid particle. The dynamical evolution of the system is hence obtained by solving the kinematic condition [80]

$$\frac{\mathrm{d}\boldsymbol{x}}{\mathrm{d}t} = \boldsymbol{v}(\boldsymbol{x}) \tag{3.7}$$

with the explicit Euler scheme. We chose a step size that is dependent on the wiggling frequency of the force (cf. the next section).

3.2 Obtaining the mobility from BIM simulations

In order to obtain the frequency dependent particle mobility from the BIM simulations, an oscillating force $\boldsymbol{F}(t) = \boldsymbol{A}e^{i\omega_0 t}$ of amplitude $\boldsymbol{A}$ and frequency ω_0 is exerted on the particle, in the direction perpendicular or parallel to the membranes. After an initial transitory evolution, the particle begins to oscillate with the same frequency as $\boldsymbol{V}e^{i(\omega_0 t+\delta)}$. The velocity amplitude $\boldsymbol{V}$ and the phase shift δ can be accurately obtained by fitting the numerically recorded velocity. For that, we use a nonlinear least-squares solver based on the trust region method [81]. The complex frequency dependent particle mobility can then be evaluated from

$$\mu_\alpha(\omega_0) = \frac{V_\alpha}{A_\alpha}e^{i\delta}\,. \tag{3.8}$$

For each applied frequency, the force is exerted during three periods in order to ensure that the steady state has been reached properly. Therefore, lower frequencies require larger computation times. For instance, for $\beta = 10^{-3}$, which is the lowest scaled frequency that we use in our simulations, each period requires around 30 hours using 40 CPUs.

4 Results and discussion

4.1 Particle mobility

We consider a spherical particle equally distant from both membranes ($\sigma = 1$) and located at $z_0 = 10a$. The membrane reduced bending modulus, defined as $E_\mathrm{B} := \kappa_\mathrm{B}/(a^2\kappa_\mathrm{S})$, is taken to be $E_\mathrm{B} = 1/2$. We examine the case where $C = 1$, for which the Skalak model is equivalent to the common neo-Hookean model [82] for small deformations [83]. As shown in Fig. 2, the analytical and numerical results are in very good agreement for the whole range of the applied frequencies, similar as in earlier work for a single membrane [51].

For a frequency of zero, the imaginary part vanishes. On the other hand, the real part reaches its minimal value which corresponds to the two-hard-walls limit, namely $-1.4516a/z_0$ and $-1.0041a/z_0$ for the perpendicular and parallel motions, respectively. This is in agreement with earlier works [55, 59].

By taking the frequency to infinity, both the real and imaginary parts of the particle mobility correction vanish and one recovers the bulk behavior in which the particle motion is no longer affected by the presence of the membranes. In between, the imaginary part peaks around $\beta \approx 1$ and $\beta_\mathrm{B} \approx 1$ for the perpendicular motion, and around $\beta \approx 1$ for the parallel motion. The peak around $\beta \approx 1$, which is observed in both directions, is a shearing signature in the mobility correction, whereas the frequency peak around $\beta_\mathrm{B} \approx 1$ is a signature of bending. The latter is found to be insignificant in the parallel motion. Physically, the peak frequencies correspond to the situation where the particle-membranes system naturally vibrates to absorb more energy.

As already remarked, a commonly used approximation to compute mobilities between two walls is Oseen's approach [53] which assumes that the mobility corrections can be approximated by superposing the contributions from each membrane independently as

$$\frac{\Delta\mu_\alpha(z_0,\omega)}{\mu_0} = -\left(k_\alpha^\infty(\beta,\beta_\mathrm{B}) + \frac{k_\alpha^\infty(\sigma\beta,\sigma\beta_\mathrm{B})}{\sigma}\right)\frac{a}{z_0}\,, \tag{4.1}$$

which reduces in the two-hard-wall limit to

$$\frac{\Delta\mu_\alpha(z_0,0)}{\mu_0} = -k_\alpha^\infty(0,0)\left(1+\frac{1}{\sigma}\right)\frac{a}{z_0}\,. \tag{4.2}$$

The superposition approximation as given by Eq. (4.1) for the elastic membranes is compared in Fig. 2 against our analytical predictions from Eq. (2.17) (see also the Supporting Material) and numerical simulations in order to assess its accuracy. For the perpendicular motion, we observe that it only agrees well with the analytical predictions and the BIM simulations for frequencies $\beta_\mathrm{B} > 1$. At lower frequencies substantial disagreement is observed which, in the limit of a vanishing frequency (hard-walls), amounts to 55 %. This deviation is due to the fact that the superposition approximation allows the fluid to drain away, as the no-slip boundary condition is no longer satisfied at both membranes simultaneously. As expected, it is therefore more pronounced the more the membrane deforms, i.e. for smaller frequencies. On the other hand, for the motion parallel to the membranes, the agreement is reasonable down to a dimensionless frequency β of order unity. Below that, however, a significant mismatch between the two curves is observed. In the limit for a vanishing frequency, a

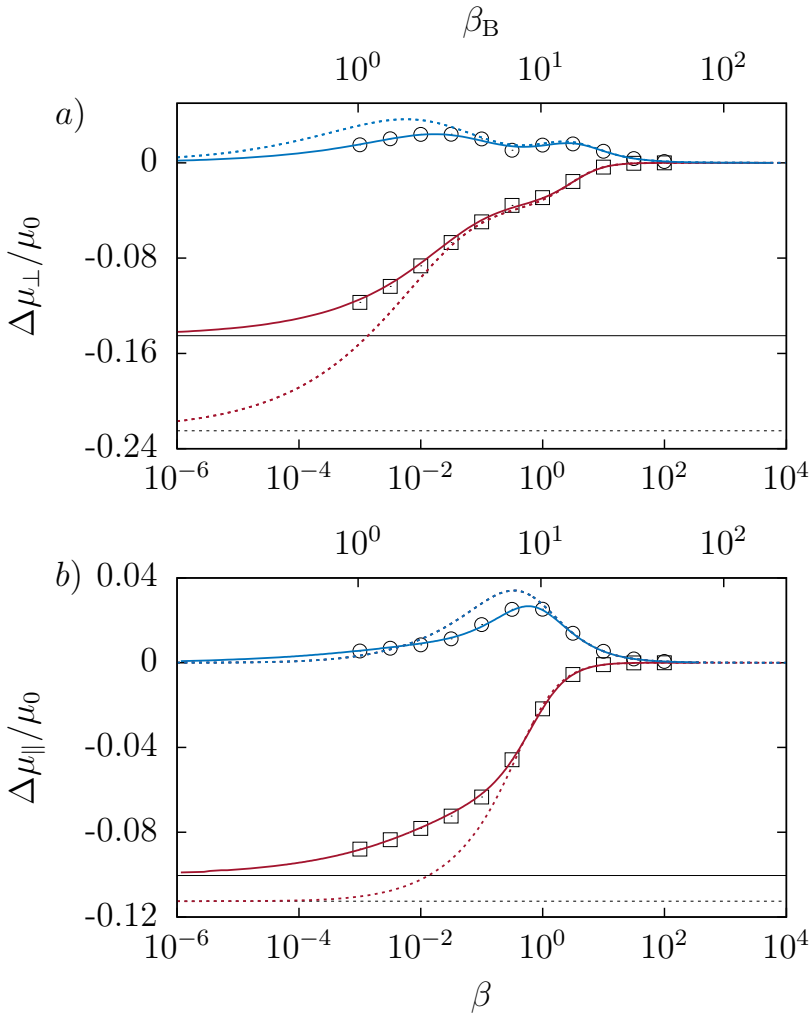

Figure 2: (Color online) The scaled frequency dependent correction to the particle mobility versus the dimensionless frequencies β (lower axis) and β_B (upper axis) for the perpendicular (a) and parallel (b) motions. Here, the particle is equidistant from both membranes ($\sigma = 1$) and located at $z_0 = 10a$. The theoretical predictions from Eq. (2.17) are shown as red lines (real part) and blue lines (imaginary part) whereas the BIM simulation results are marked as rectangles (real part) and circles (imaginary part). Dashed lines represent the superposition approximation by summing up the contributions of each membrane independently as given by Eq. (4.1). The solid horizontal lines indicate the two-hard-wall limits ($-1.4516a/z_0$ and $-1.0041a/z_0$ for the perpendicular and parallel motions, respectively) and the dotted horizontal lines result from the superposition approximation of the hard wall as stated in Eq. (4.2). For the other simulation parameters, see main text.

relative deviation of 12 % from Faxén's value is obtained. All in all, the superposition approximation consistently underestimates the particle mobility.

4.2 Membrane deformation

We now consider the membrane deformation induced by the moving particle. For this, we set the complex driving force to be harmonic with components $F_\alpha(t) = A_\alpha e^{i\omega_0 t}$, whose temporal Fourier

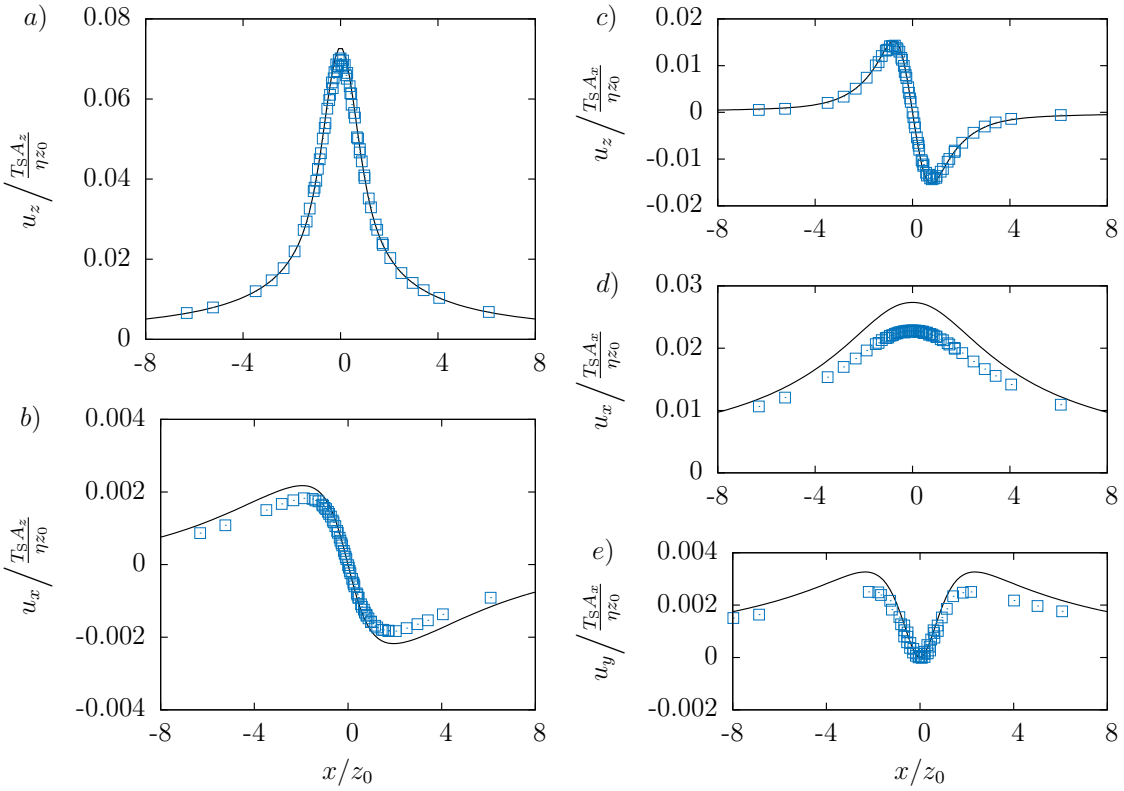

Figure 3: (Color online) Comparison between analytical predictions (solid lines) and numerical simulations (symbols) of the scaled membrane displacement as given by Eq. (4.3) for the motion perpendicular (a and b) and parallel (c, d and e) to the membranes, for the parameters given in Fig. 2 ($\sigma = 1$). In this example, we take $\omega_0 T_S = 1$ and $t\omega_0 = \pi/2$.

transform is $F_\alpha(\omega) = 2\pi A_\alpha \delta(\omega - \omega_0)$. In this case, the membrane displacement is expressed as

$$u_\alpha(\rho, \theta, t) = \psi_{\alpha\beta}(\rho, \theta, \omega_0) A_\beta e^{i\omega_0 t}\,. \tag{4.3}$$

The physical displacement of the membrane is obtained by simply taking the real part of the right hand side in Eq. (4.3).

Fig. 3 depicts a comparison of the membrane displacements between analytical predictions and BIM simulations. Here we use the same set of parameters as in Fig. 2. As the particle is equally distant from both membranes, the displacement fields of each membrane are equal in magnitude, but may differ in sign. For instance, for a particle moving perpendicularly to the membranes, the normal displacements of each membrane have the same sign whereas the radial displacements have opposite signs. However, the vertical displacements in the parallel motion have different signs from each other whereas the in-plane displacements have similar signs. Hereafter, all the components are evaluated in their plane of maximal displacement: u_z and u_x in the plane $y = 0$ and u_y in the plane $y = x$. The theoretical predictions are found to be in good agreement with the numerical simulations for both the perpendicular and parallel motions. The reason behind the small discrepancy between theory and simulation is most likely the fact that the analytical theory treats truly infinite membranes whereas the corresponding BIM simulations necessarily only account for finite sized membranes.

In the perpendicular motion, the deformation is more pronounced in the normal than in the x-direction. The maximum displacement for the first occurs at the center. Far away, the membrane

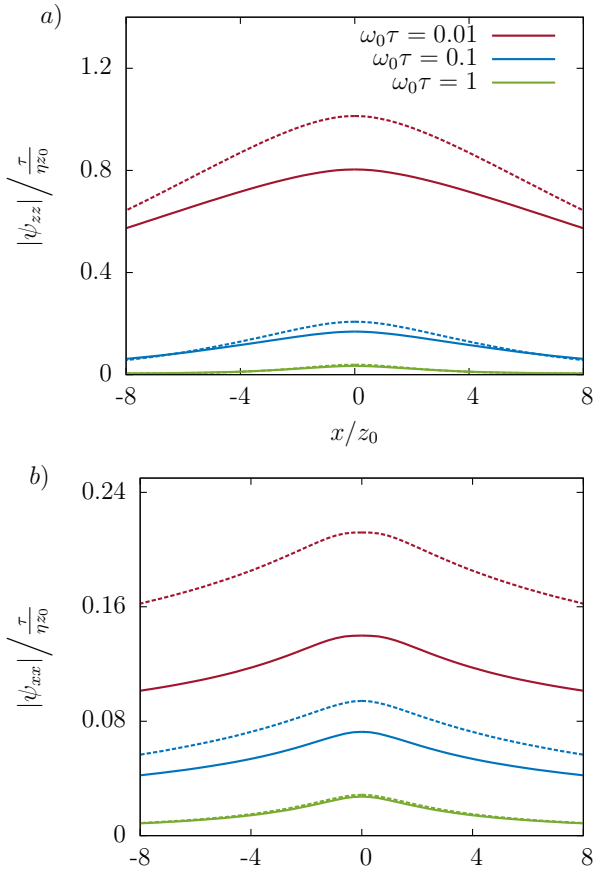

Figure 4: (Color online) Effect of the oscillation frequency on the amplitude of the reaction tensor's z-z component (a) and x-x component (b) for $\sigma = 1$ (solid line) and $\sigma = \infty$ (dashed line).

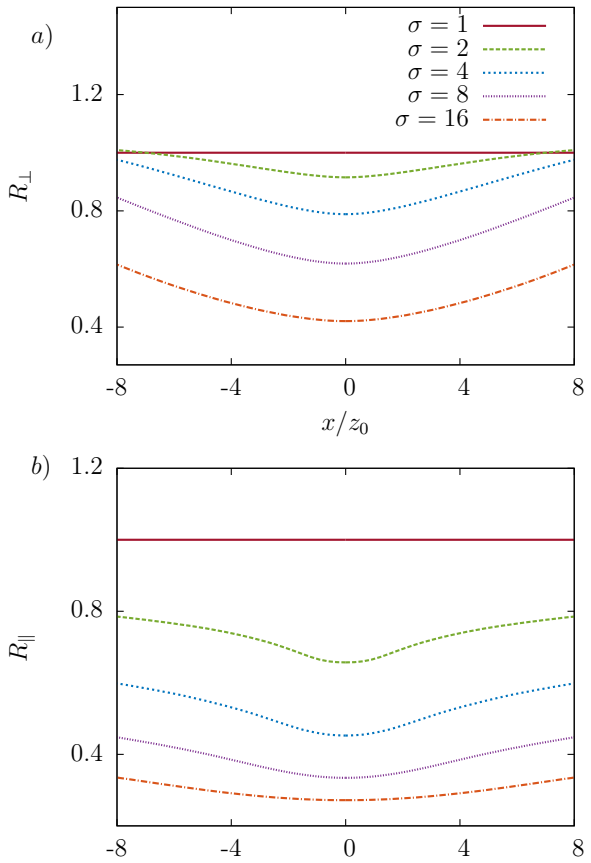

Figure 5: (Color online) (a) $R_\perp$ and (b) $R_\parallel$ for different values of σ for $\omega_0\tau = 0.01$ with $z_0 = (3\kappa_B/(2\kappa_S))^{1/2}$.

deformation decays rapidly with distance and vanishes as x tends to infinity. On the other hand, radial symmetry implies that the displacement u_r should vanish at the origin, suggesting the existence of an extremum at some intermediate radial position. The latter is found to be in magnitude around 40 times smaller than that obtained for the normal displacement. Accordingly, the in-plane deformation does not play a significant role for the motion perpendicular to the membranes.

Considering the translational motion parallel to the membranes, we observe that the displaced membranes exhibit a fundamentally different shape. Not surprisingly, it turns out that the in-plane deformation u_x along the direction parallel to the applied force is the most significant. The maximum displacements reached in u_z and u_y are respectively found to be about twice and 10 times smaller in comparison with that reached in u_x.

Membrane deformability is largely determined by shearing and bending properties. Henceforth, we shall consider a typical case for which both effects have the same relevance. Thus, before we can continue, we define the characteristic time scale for shearing as $T_S := 6\eta z_0/\kappa_S$ and the characteristic time scale for bending as $T_B := 4\eta z_0^3/\kappa_B$ [51]. Both time scales are equal for a distance $z_0 = (3\kappa_B/(2\kappa_S))^{1/2}$. We adapt this value for the remainder of this section. Furthermore, let $\tau := T_S = T_B$.

It is also of interest to compute the maximum displacement (amplitude) of the membrane during the particle oscillation. The maximum is not necessarily reached for $t\omega_0 = \pi/2$, as taken in Fig. 3. In Fig. 4, we show the effect of frequency on the oscillation amplitude. Higher frequencies induce smaller deformation, because the membrane does not have enough time to respond to the fast particle

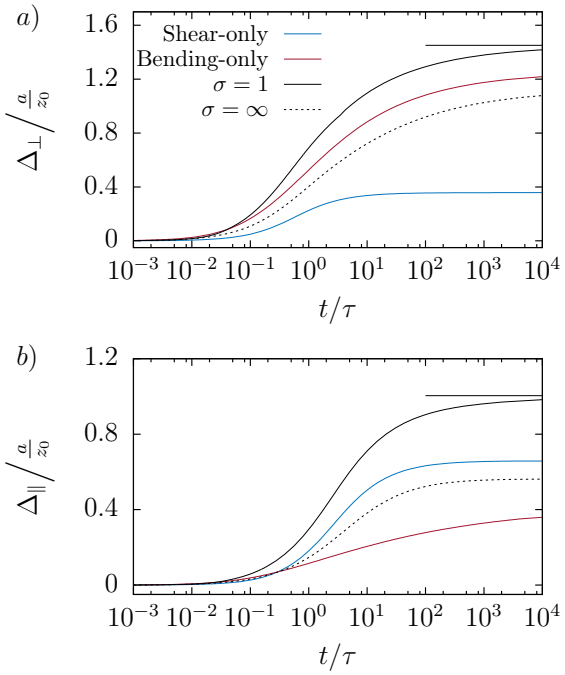

Figure 6: (Color online) Scaled excess MSD versus the scaled time for the perpendicular (a) and parallel (b) motions with $\sigma = 1$ (black solid line) and $\sigma = \infty$ (black dotted line). A shear-only and a bending-only membrane are shown in blue and red, respectively. The horizontal solid line corresponds to the two-hard-walls limits. For the other parameters, see the main text.

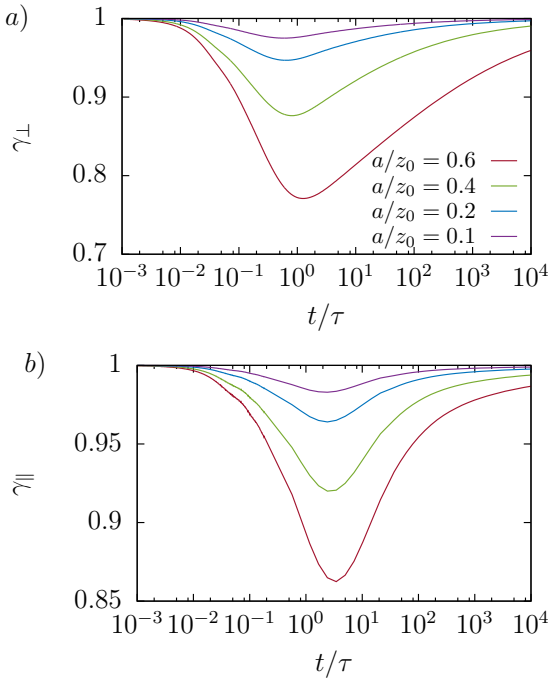

Figure 7: (Color online) Variations of the scaling exponent for the motion perpendicular (a) and parallel (b) to the membranes as given by Eq. (4.8) versus the scaled time for $\sigma = 1$.

wiggling. By comparing the reaction tensor amplitudes with and without a second membrane, we see that the presence of a second membrane reduces $|\psi_{zz}|$ less strongly than $|\psi_{xx}|$. This is similar to the observations for the MSD in the next section (see Fig. 6).

In order to examine the effect of the disposition of the upper membrane relative to the lower one, we define the following ratios of the reaction tensor amplitudes between the upper and lower membranes:

$$R_\perp := \frac{|\psi_{zz}|_{\text{upper}}}{|\psi_{zz}|_{\text{lower}}} \quad \text{and} \quad R_\parallel := \frac{|\psi_{xx}|_{\text{upper}}}{|\psi_{xx}|_{\text{lower}}}\,. \tag{4.4}$$

These are two quantities that vanish for $\sigma \to \infty$ and are equal to one for $\sigma = 1$. In Fig. 5, we plot the variations of $R_\perp$ and $R_\parallel$ as functions of the scaled distance from the membrane center for different values of σ. Here the calculations are carried out in the plane of maximal displacement $y = 0$, for a scaled frequency of $\omega_0\tau = 0.01$. We remark that the upper membrane shows significantly less vertical displacement as σ increases (ratio less than unity.) Further apart from the center, where less deformation occurs, the two membranes have an essentially comparable deformation behavior, and both ratios approach the upper limit one as x increases.

4.3 Brownian motion

The computation of the particle mean-square displacement (MSD) requires as an intermediate step the determination of the velocity autocorrelation function $\phi_{v,\alpha}(t) := \langle V_\alpha(0)V_\alpha(t)\rangle$. The latter is related

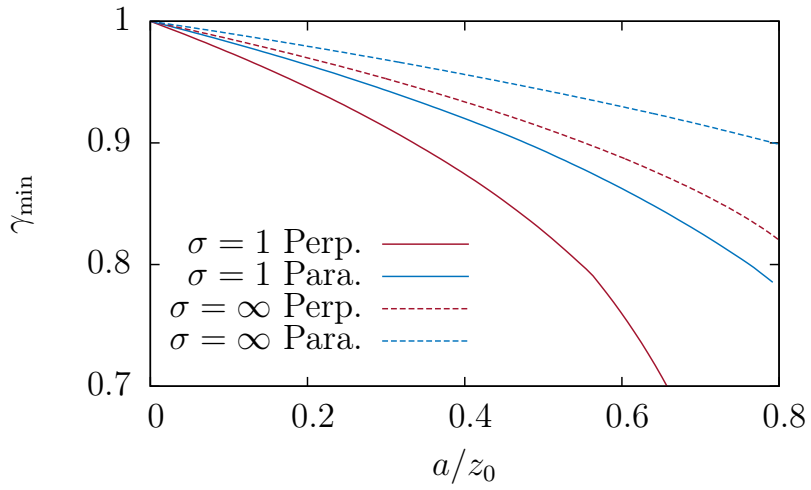

Figure 8: (Color online) Minimum of the scaling exponent versus a/z_0 for the perpendicular and parallel motions, for $\sigma = 1$ and $\sigma = \infty$.

to the temporal inverse Fourier transform of the particle mobility via Kubo's fluctuation-dissipation theorem (FDT) such that [84]

$$\phi_{v,\alpha}(t) = \frac{k_\mathrm{B}T}{2\pi} \int_{-\infty}^{\infty} \left(\mu_{\alpha\alpha}(\omega) + \overline{\mu_{\alpha\alpha}(\omega)} \right) e^{i\omega t} \mathrm{d}\omega \,, \tag{4.5}$$

where k_B is the Boltzmann constant and T the absolute temperature of the system. The bar denotes complex conjugate.

The particle MSD is computed as

$$\langle \Delta r_\alpha(t)^2 \rangle = 2 \int_0^t (t-s) \phi_{v,\alpha}(s) \, \mathrm{d}s \,. \tag{4.6}$$

For convenience, we define the excess MSD as

$$\Delta_\alpha(t) := 1 - \frac{\langle \Delta r_\alpha(t)^2 \rangle}{2 D_0 t} \,, \tag{4.7}$$

where $D_0 = \mu_0 k_\mathrm{B} T$ is the bulk diffusion coefficient given by the Einstein relation [85].

We show in Fig. 6 the variations of the perpendicular and parallel excess MSDs as computed from Eq. (4.7) versus the scaled time. For short times, the particle does not yet perceive the membranes and thus experiences a bulk diffusion. By increasing the time up to $t \approx \tau$, the effect of the confining membranes becomes noticeable. By comparing the total excess MSDs for $\sigma = \infty$ and $\sigma = 1$ we find that diffusion in the long-time limit is slowed down by a factor 1.78 for the parallel direction, but only a factor 1.29 in the perpendicular direction, due to the introduction of the second membrane.

As explained in Sec. 2.5, the particle mobility and, consequently, also the MSD cannot be split up directly into a shear and bending contribution for the two membrane case. We therefore consider the two cases separately, taking one membrane with $\alpha = 0$ and one with $\alpha_\mathrm{B} = 0$. We find that for the shear-only membrane ($\alpha_\mathrm{B} = 0$, blue curve in Fig. 6) the time needed to reach the steady state is about 10τ for the perpendicular motion, and about 100τ for the parallel motion. On the other hand, the bending-only membrane ($\alpha = 0$, red curve in Fig. 6) takes for both directions a significantly longer time of about $10^4\tau$ before the steady state is attained.

Another way to quantify the slowing down of the particle is to investigate the time-dependent scaling exponent of the MSD, which can be defined as

$$\gamma_\alpha(t) := \frac{\mathrm{d}\ln\langle\Delta r_\alpha(t)^2\rangle}{\mathrm{d}\ln t} = 1 - \frac{t}{1-\Delta_\alpha(t)}\frac{\mathrm{d}\Delta_\alpha(t)}{\mathrm{d}t}\,. \tag{4.8}$$

Fig. 7 shows the temporal evolution of the scaling exponent which strongly depends on the distance separating the particle from the membranes. We first remark that the scaling exponent is $\gamma(t) = 1$ at $t = 0$ and for $t \to \infty$. The particle thus experiences normal diffusion in these cases. This is similar to the single-membrane case [51]. For $t \approx \tau$, we observe a bending down of the scaling exponent, resulting in a subdiffusive regime that extends up to $10^3\tau$ in the parallel and even further in the perpendicular direction. In Fig. 8 we present the variation of the minimal scaling exponent for $\sigma = 1$ and $\sigma = \infty$ upon varying the particle-membrane distance. For $a/z_0 = 0.6$, the exponent is found to be as low as 0.75 for the perpendicular motion, and 0.86 for the parallel motion. These values are significantly smaller than the ones previously found in the one-membrane limit ($\sigma = \infty$) [51], where the scaling exponent is around 0.89 and 0.92 for the perpendicular and parallel motions, respectively. We therefore conclude that the second membrane leads to a notable slow-down of the dynamics.

5 Conclusions

We have investigated the translational motion of a spherical particle confined between two parallel elastic membranes and determined the frequency dependent mobility for the motion perpendicular and parallel to the membranes in the point particle limit. Contrary to the single wall, shear and bending are intrinsically coupled and their contributions cannot be added linearly. Our analytical predictions have been compared to boundary integral simulations for a finite-sized particle and very good agreement has been observed. The frequently used superposition approximation, originally suggested by Oseen [53] for two hard walls, has been tested for elastic membranes. Reasonably good agreement with the analytically exact predictions is observed for the parallel, but not for the perpendicular motion, especially in the low frequency regime.

Subsequently, we have provided analytical predictions validated by numerical simulations of the membrane deformation due to a particle upon which an oscillating force is exerted perpendicular or parallel to the membranes. We have observed that the deformation is most pronounced in the direction along which the force acts, and that the presence of the second membrane significantly reduces the membrane deformations.

Finally, we have shown that the elastic membranes induce a memory effect in the system, leading to a subdiffusive Brownian motion at intermediate time scales. This is qualitatively similar, yet more pronounced, as in the single membrane situation [51]. To provide typical physical values, consider a red blood cell with a shear modulus of $\kappa_\mathrm{S} = 5\times10^{-6}\,\mathrm{N/m}$ and a bending modulus of $\kappa_\mathrm{B} = 2\times10^{-19}\,\mathrm{Nm}$ that flows in a fluid with dynamic viscosity $\eta = 1.2\times10^{-3}\,\mathrm{Pa\,s}$ [86]. A typical nanoparticle of radius $a = 150\,\mathrm{nm}$ that is located at a distance of $z_0 = 250\,\mathrm{nm}$ from both red blood cells will undergo a long-lived subdiffusive motion that can last up to 100 ms. The corresponding scaling exponent of the MSD can go as low as 0.77 in the perpendicular and as low as 0.87 in the parallel direction.

In the future, it will be interesting to carry out similar calculations in more severe confinements such as cylindrical elastic channels where even stronger effects are expected.

Acknowledgments

The authors gratefully acknowledge funding from the Volkswagen Foundation and the KONWIHR network as well as computing time granted by the Leibniz-Rechenzentrum on SuperMUC.

Appendix

A Computation of the traction jump for the membranes

In this appendix, we provide some technical details regarding the computation of the traction jump $\Delta \boldsymbol{f}$ across the membranes, as required for Eq. (3.3). The membranes are endowed with shear and area elasticity together with some bending rigidity.

A.1 Shear and area elasticity

We employ the Skalak model [68] which is often used to model the membranes of red blood cells. Its areal energy density is given by [87]

$$\epsilon_{\mathrm{S}} = \frac{\kappa_{\mathrm{S}}}{12}(I_1^2 + 2I_1 - 2I_2 + CI_2^2)\,. \tag{A.1}$$

The strain invariants I_1 and I_2 are related to the principal in-plane stretch ratios via $I_1 = \lambda_1^2+\lambda_2^2-2$ and $I_2 = \lambda_1^2\lambda_2^2 - 1$. Hence, the total energy of a membrane S_{m_i} is given by

$$E_{\mathrm{S}} = \int_{S_{\mathrm{m}_i}^{(0)}} \epsilon_{\mathrm{S}}\,\mathrm{d}S_0\,, \tag{A.2}$$

where the integration is performed over the surface in the reference state $S_{\mathrm{m}_i}^{(0)}$. In our case this is a simple flat sheet. To obtain the force at each node, we assume that the deformation is a linear function of position in each triangle. After discretization of the integral the energy E_{S} depends explicitly on the node positions $\boldsymbol{x}_i$. Therefore, according to the principle of virtual work, the total force is then given by the gradient

$$\boldsymbol{F}(\boldsymbol{x}_i) = \frac{\partial E_{\mathrm{S}}}{\partial \boldsymbol{x}_i}\,. \tag{A.3}$$

This derivative can be computed analytically as detailed in references [88, 89]. The traction jump is thus obtained by

$$\Delta \boldsymbol{f}(\boldsymbol{x}_i) = \frac{\boldsymbol{F}(\boldsymbol{x}_i)}{A_i}\,, \tag{A.4}$$

whereas A_i is the area associated with node $\boldsymbol{x}_i$ and is taken as one third of the total area of the triangles containing the node [75].

A.2 Bending rigidity

The bending forces are modeled according to the constitutive law proposed by Canham [90] and Helfrich [69], which for a flat reference state becomes

$$E_{\mathrm{B}} = 2\kappa_{\mathrm{B}} \int_{S_{\mathrm{m}_i}} H^2\,\mathrm{d}S\,. \tag{A.5}$$

H denotes the mean curvature and κ_{B} the bending modulus. Applying the principle of virtual work is possible *before* the discretization, leading to the following contribution to the traction jump [91, 92]:

$$\Delta \boldsymbol{f}(\boldsymbol{x}) = -2\kappa_{\mathrm{B}}\left(2H(H^2 - K) + \Delta_{\mathrm{S}} H\right)\boldsymbol{n}\,. \tag{A.6}$$

The mean curvature H is calculated according to the relation $H(\boldsymbol{x}) = -\frac{1}{2}\left(\Delta_{\mathrm{S}} x_i\right) n_i(\boldsymbol{x})$. We use the algorithms presented by Meyer *et al.* [93] for the computation of the Laplace-Beltrami operator Δ_{S}

and the Gaussian curvature K. The normal vector $\boldsymbol{n}$ is computed according to the "mean weighted by angle" method [94]. This provides reasonable results in the application of viscous flows [95]. Note that we set $\Delta \boldsymbol{f}$ to zero for nodes located at the border of the meshes.

Bibliography

[1] H. Hillaireau and P. Couvreur, Cell. Mol. Life Sci. **66**, 2873 (2009).

[2] J. M. Rosenholm, C. Sahlgren, and M. Linden, Nanoscale **2**, 1870 (2010).

[3] V. P. Chauhan, T. Stylianopoulos, Y. Boucher, and R. K. Jain, Annu. Rev. Chem. Biomol. Eng. **2**, 281 (2011).

[4] B. M. Rothen-Rutishauser, S. Schürch, B. Haenni, N. Kapp, and P. Gehr, Environ. Sci. Technol. **40**, 4353 (2006).

[5] C. Muhlfeld, P. Gehr, and B. Rothen-Rutishauser, Swiss Med. Wkly. **138**, 387 (2008).

[6] G. J. Doherty and H. T. McMahon, Annu. Rev. Biochem. **78**, 857 (2009).

[7] D. M. Richards and R. G. Endres, Biophys. J. **107**, 1542 (2014).

[8] A. Meinel, B. Tränkle, W. Römer, and A. Rohrbach, Soft Matter **10**, 3667 (2014).

[9] H. A. Lorentz, Abh. Theor. Phys. **1**, 23 (1907).

[10] J. R. Blake, in *Math. Proc. Cambridge Philos. Soc.*, Vol. 70 (Cambridge Univ Press, 1971) pp. 303–310.

[11] B. Cichocki and R. Jones, Physica A **258**, 273 (1998).

[12] A. Banerjee and K. Kihm, Phys. Rev. E **72**, 042101 (2005).

[13] P. Holmqvist, J. Dhont, and P. Lang, Phys. Rev. E **74**, 021402 (2006).

[14] C. K. Choi, C. H. Margraves, and K. D. Kihm, Phys. Fluids **19**, 103305 (2007).

[15] E. Schäffer, S. F. Nørrelykke, and J. Howard, Langmuir **23**, 3654 (2007).

[16] M. D. Carbajal-Tinoco, R. Lopez-Fernandez, and J. L. Arauz-Lara, Phys. Rev. Lett. **99**, 138303 (2007).

[17] P. Huang and K. Breuer, Phys. Rev. E **76**, 046307 (2007).

[18] M. Kyoung and E. D. Sheets, Biophys. J. **95**, 5789 (2008).

[19] P. Sharma, S. Ghosh, and S. Bhattacharya, Appl. Phys. Lett. **97**, 104101 (2010).

[20] Y. Kazoe and M. Yoda, Appl. Phys. Lett. **99**, 124104 (2011).

[21] P. P. Lele, J. W. Swan, J. F. Brady, N. J. Wagner, and E. M. Furst, Soft Matter **7**, 6844 (2011).

[22] S. L. Dettmer, S. Pagliara, K. Misiunas, and U. F. Keyser, Phys. Rev. E **89**, 062305 (2014).

[23] J. W. Swan and J. F. Brady, Phys. Fluids **19**, 113306 (2007).

[24] S. Jeney, B. Lukić, J. A. Kraus, T. Franosch, and L. Forró, Phys. Rev. Lett. **100**, 240604 (2008).

[25] T. Franosch and S. Jeney, Phys. Rev. E **79**, 031402 (2009).

[26] V. N. Michailidou, G. Petekidis, J. W. Swan, and J. F. Brady, Phys. Rev. Lett. **102**, 068302 (2009).

[27] V. N. Michailidou, J. W. Swan, J. F. Brady, and G. Petekidis, J. Chem. Phys. **139**, 164905 (2013).

[28] M. Lisicki, B. Cichocki, J. K. G. Dhont, and P. R. Lang, J. Chem. Phys. **136**, 204704 (2012).

[29] S. A. Rogers, M. Lisicki, B. Cichocki, J. K. G. Dhont, and P. R. Lang, Phys. Rev. Lett. **109**, 098305 (2012).

[30] M. Lisicki, B. Cichocki, S. A. Rogers, J. K. G. Dhont, and P. R. Lang, Soft Matter **10**, 4312 (2014).

[31] T. Watarai and T. Iwai, Appl. Phys. Express **7**, 032502 (2014).

[32] H.-Y. Yu, D. M. Eckmann, P. S. Ayyaswamy, and R. Radhakrishnan, Phys. Rev. E **91**, 052303 (2015).

[33] H. B. Eral, J. M. Oh, D. van den Ende, F. Mugele, and M. H. G. Duits, Langmuir **26**, 16722 (2010).

[34] S. H. Lee, R. S. Chadwick, and L. G. Leal, J. Fluid Mech. **93**, 705 (1979).

[35] C. Berdan II and L. G. Leal, J. Colloid Interface Sci. **87**, 62 (1982).

[36] T. Bickel, Phys. Rev. E **75**, 041403 (2007).

[37] G. M. Wang, R. Prabhakar, and E. M. Sevick, Phys. Rev. Lett. **103**, 248303 (2009).

[38] J. Bławzdziewicz, M. L. Ekiel-Jeżewska, and E. Wajnryb, J. Chem. Phys. **133**, 114702 (2010).

[39] W. Zhang, S. Chen, N. Li, J. Zhang, and W. Chen, Appl. Phys. Lett. **103**, 154102 (2013).

[40] T. Bickel, Europhys. Lett. **106**, 16004 (2014).

[41] W. Wang and P. Huang, Phys. Fluids **26**, 092003 (2014).

[42] E. Lauga and T. M. Squires, Phys. Fluids **17** (2005).

[43] B. U. Felderhof, Phys. Rev. E **85**, 046303 (2012).

[44] T. Bickel, Eur. Phys. J. E **20**, 379 (2006).

[45] B. U. Felderhof, J. Chem. Phys. **125**, 144718 (2006).

[46] R. Shlomovitz, A. Evans, T. Boatwright, M. Dennin, and A. Levine, Phys. Rev. Lett. **110**, 137802 (2013).

[47] R. Shlomovitz, A. A. Evans, T. Boatwright, M. Dennin, and A. J. Levine, Phys. Fluids **26**, 071903 (2014).

[48] T. Boatwright, M. Dennin, R. Shlomovitz, A. A. Evans, and A. J. Levine, Phys. Fluids **26**, 071904 (2014).

[49] T. Salez and L. Mahadevan, J. Fluid Mech. **779**, 181 (2015).

[50] F. Jünger, F. Kohler, A. Meinel, T. Meyer, R. Nitschke, B. Erhard, and A. Rohrbach, Biophys. J. **109**, 869 (2015).

[51] A. Daddi-Moussa-Ider, A. Guckenberger, and S. Gekle, Phys. Rev. E **93**, 012612 (2016).

[52] B. Saintyves, T. Jules, T. Salez, and L. Mahadevan, Proc. Nat. Acad. Sci. **113**, 5847 (2016).

[53] C. W. Oseen, "Neuere Methoden und Ergebnisse in der Hydrodynamik," (1928).

[54] H. Faxén, *Einwirkung der Gefässwände auf den Widerstand gegen die Bewegung einer kleinen Kugel in einer zähen Flüssigkeit*, Ph.D. thesis, Uppsala University, Uppsala, Sweden (1921).

[55] J. Happel and H. Brenner, *Low Reynolds number hydrodynamics: with special applications to particulate media*, Vol. 1 (Springer Science & Business Media, 2012).

[56] N. Liron and S. Mochon, J. Eng. Math. **10**, 287 (1976).

[57] L. Lobry and N. Ostrowsky, Phys. Rev. B **53**, 12050 (1996).

[58] S. Bhattacharya and J. Bławzdziewicz, J. Math. Phys. **43**, 5720 (2002).

[59] B. Felderhof, J. Chem. Phys. **124**, 054111 (2006).

[60] J. W. Swan and J. F. Brady, Phys. Fluids **22**, 103301 (2010).

[61] P. Ganatos, S. Weinbaum, and R. Pfeffer, J. Fluid Mech. **99**, 739 (1980).

[62] P. Ganatos, R. Pfeffer, and S. Weinbaum, J. Fluid Mech. **99**, 755 (1980).

[63] E. R. Dufresne, D. Altman, and D. G. Grier, Europhys. Lett. **53**, 264 (2001).

[64] B. Lin, J. Yu, and S. A. Rice, Phys. Rev. E **62**, 3909 (2000).

[65] B. Tränkle, D. Ruh, and A. Rohrbach, Soft Matter **12**, 2729 (2016).

[66] C. Nicholson and E. Syková, Trends Neurosci. **21**, 207 (1998).

[67] H. Maeda, H. Nakamura, and J. Fang, Adv. Drug Deliv. Rev. **65**, 71 (2013).

[68] R. Skalak, A. Tozeren, R. P. Zarda, and S. Chien, Biophys. J. **13(3)**, 245 (1973).

[69] W. Helfrich, Z. Naturef. C. **28:693** (1973).

[70] M. Thiébaud and T. Bickel, Phys. Rev. E **81**, 031602 (2010).

[71] See Supplemental Material at http://dx.doi.org/10.1063/1.4955013 for a Maple script (Maple 17 or later) providing the particle mobility corrections in both directions of motion..

[72] N. Baddour, J. Opt. Soc. Am. A **26** (2009).

[73] C. Pozrikidis, *Boundary Integral and Singularity Methods for Linearized Viscous Flow*, Cambridge Texts in Applied Mathematics No. 8 (Cambridge University Press, New York, 1992).

[74] M. Kohr and I. Pop, AMC **10**, 12 (2004).

[75] H. Zhao, E. S. G. Shaqfeh, and V. Narsimhan, Phys. Fluids **24**, 011902 (2012).

[76] C. Geuzaine and J.-F. Remacle, Int. J. Numer. Meth. Eng. **79**, 1309 (2009).

[77] G. R. Cowper, Int. J. Numer. Meth. Eng. **7**, 405 (1973).

[78] C. Pozrikidis, J. Fluid Mech. **297**, 123 (1995).

[79] Y. Saad and M. Schultz, SIAM J. Sci. Comput. **7**, 856 (1986).

[80] C. Pozrikidis, J. Comput. Phys. **169**, 250 (2001).

[81] A. R. Conn, N. I. M. Gould, and P. L. Toint, *Trust region methods*, Vol. 1 (SIAM, 2000).

[82] S. Ramanujan and C. Pozrikidis, J. Fluid Mech. **361**, 117 (1998).

[83] E. Lac, D. Barthès-Biesel, N. A. Pelekasis, and J. Tsamopoulos, J. Fluid Mech. **516**, 303 (2004).

[84] R. Kubo, M. Toda, and N. Hashitsume, "Statistical physics II," (1985).

[85] A. Einstein, Ann. Phys. **8**, 549 (1905).

[86] J. B. Freund, Phys. Fluids **25**, 110807 (2013).

[87] T. Krüger, F. Varnik, and D. Raabe, Comput. Math. Appl. **61**, 3485 (2011).

[88] M. Kraus, W. Wintz, U. Seifert, and R. Lipowsky, Phys. Rev. Lett. **77**, 3685 (1996).

[89] T. Krüger, *Computer simulation study of collective phenomena in dense suspensions of red blood cells under shear*, Ph.D. thesis, Ruhr-Universität Bochum (2011).

[90] P. B. Canham, J. Theo. Biol. **26**, 61 (1970).

[91] O.-Y. Zhong-Can and W. Helfrich, Phys. Rev. A **39**, 5280 (1989).

[92] A. Laadhari, C. Misbah, and P. Saramito, Physica D **239**, 1567 (2010).

[93] M. Meyer, M. Desbrun, P. Schröder, and A. H. Barr, in *Visualization and Mathematics III*, Mathematics and Visualization No. III, edited by H.-C. Hege and K. Polthier (Springer, Berlin, Heidelberg, 2003) pp. 35–57.

[94] S. Jin, R. R. Lewis, and D. West, Vis. Comput. **21**, 71 (2005).

[95] A. Guckenberger, M. P. Schraml, P. G. Chen, M. Leonetti, and S. Gekle, Comp. Phys. Comm. **207**, 1 (2016).

Publication 3

Hydrodynamic interaction between particles near elastic interfaces

A. Daddi-Moussa-Ider and S. Gekle

J. Chem. Phys., **145**, 014905 (2016)

DOI: 10.1063/1.4955099

Abstract

We present an analytical calculation of the hydrodynamic interaction between two spherical particles near an elastic interface such as a cell membrane. The theory predicts the frequency dependent self- and pair-mobilities accounting for the finite particle size up to the 5th order in the ratio between particle diameter and wall distance as well as between diameter and interparticle distance. We find that particle motion towards a membrane with pure bending resistance always leads to mutual repulsion similar as in the well-known case of a hard-wall. In the vicinity of a membrane with shearing resistance, however, we observe an attractive interaction in a certain parameter range which is in contrast to the behavior near a hard wall. This attraction might facilitate surface chemical reactions. Furthermore, we show that there exists a frequency range in which the pair-mobility for perpendicular motion exceeds its bulk value, leading to short-lived superdiffusive behavior. Using the analytical particle mobilities we compute collective and relative diffusion coefficients. The appropriateness of the approximations in our analytical results is demonstrated by corresponding boundary integral simulations which are in excellent agreement with the theoretical predictions.

1 Introduction

The hydrodynamic interaction between particles moving through a liquid is essential to determine the behavior of colloidal suspensions [1], polymer solutions [2, 3], chemical reaction kinetics [4, 5], bilayer assembly [6] or cellular flows [7, 8]. As an example, hydrodynamic interactions result in a notable alteration of the collective motion behavior of catalytically powered self-propelled particles [9] or bacterial suspensions [10–14]. Many of the occurring phenomena can be explained on the basis of two-particle interactions [15] which in bulk are well understood. Some of the most intriguing observations, however, are made when particles interact hydrodynamically in the close vicinity of interfaces – a prominent example being the attraction of like-charged colloid particles during their motion away from a hard wall [16–18].

In the low Reynolds number regime hydrodynamic interactions between two particles are fully described by the mobility tensor which provides a linear relation between the force applied on one particle and the resulting velocity of either the same or the neighboring particle. In an unbounded flow, algebraic expressions for the hydrodynamic interactions between two [15, 19–23] and several [24–29] spherical particles are well established. Experimentally, the predicted hydrodynamic coupling has been confirmed using optical tweezers [30–33] and atomic force microscopy [34].

The presence of an interface is known to drastically alter the hydrodynamic mobility. For a single particle, this wall-induced drag effect has been studied extensively over recent decades theoretically and numerically near a rigid [35–44], a fluid-fluid [45–50] or an elastic interface [51–57]. While rigid interfaces in general simply lead to a reduction of particle mobility, the memory effect caused by elastic interfaces leads to a frequency dependence of the particle mobility and can cause novel phenomena such as transient subdiffusion [55]. On the experimental side, the single particle mobility has been investigated using optical tweezers [58–60], evanescent wave dynamic light scattering [61–70] or video microscopy [71–73]. The influence of a nearby elastic cell membrane has recently been investigated using magnetic particle actuation [74] and optical traps [52, 75, 76].

Hydrodynamic interactions between two particles near a planar rigid wall have been studied theoretically [17, 77] and experimentally using optical tweezers [78, 79] and digital video microscopy [80]. Narrow channels [81, 82], 2D confinement [83] or liquid-liquid interfaces have also been investigated [84, 85]. Near elastic interfaces, however, no work regarding hydrodynamic interactions has so far been reported. Given the complex behavior of a single particle near an elastic interface (caused by the above-mentioned memory effect) such hydrodynamic interactions can be expected to present a very rich phenomenology.

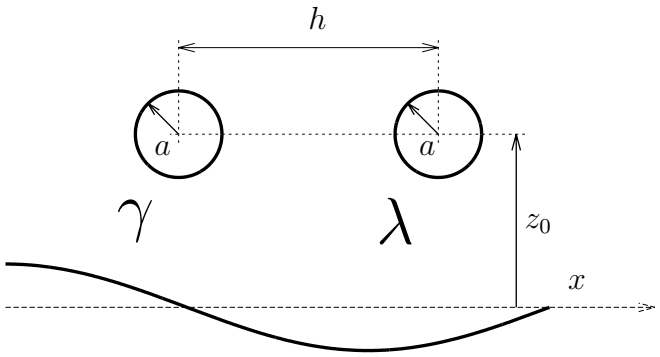

Figure 1: Illustration of the problem setup. Two small particles labeled γ and λ of radius a are located a distance $h := x_\lambda - x_\gamma$ apart and a distance z_0 above an elastic membrane. The dimensionless length scales of the problem are $\epsilon := a/z_0$ and $\sigma := a/h$.

In this paper, we calculate the motion of two spherical particles positioned above an elastic membrane both analytically and numerically. We find that the shearing and bending related parts in the pair-mobility can in some situations have opposite contributions to the total mobility. Most prominently, we find that two particles approaching an idealized membrane exhibiting only shear resistance will be attracted to each other which is just opposite to the well-known hydrodynamic repulsion for motion towards a hard wall [17]. Additionally, we show that the pair-mobility at intermediate frequencies may even exceed its bulk value, a feature which is not observed in bulk or near a rigid wall. This increase in pair-mobility results in a short-lived superdiffusion in the joint mean-square displacement.

The remainder of the paper is organized as follows. In Sec. 2, we introduce the theoretical approach to computing the frequency-dependent self- and pair-mobilities from the multipole expansion and Faxén's theorem, up to the 5th order in the ratio between particle radius and particle-wall or particle-particle distance. In Sec. 3, we present the boundary integral method which we have used to numerically confirm our theoretical predictions. In Sec. 4, we provide analytical expressions of the particle self- and pair-mobilities in terms of power series, finding excellent agreement with our numerical simulations. Expressions of the self- and pair-diffusion coefficients are derived in Sec. 5. Concluding remarks are made in Sec. 6.

2 Theory

We consider a pair of particles of radius a suspended in a Newtonian fluid of viscosity η above a planar elastic membrane extending in the xy plane. The two particles are placed at $\boldsymbol{r}_\gamma = (x_\gamma, 0, z_0)$ and $\boldsymbol{r}_\lambda = (x_\lambda, 0, z_0)$, i.e. the line connecting the two particles is parallel to the undisplaced membrane. We denote by $h := x_\lambda - x_\gamma$ the center-to-center separation measured from the left (γ) to the right (λ) particle (see Fig. 1 for an illustration).

The particle mobility is a tensorial quantity that linearly couples the velocity V_{γ_α} of particle γ in direction α to an external force in the direction β applied on the same ($F_{\gamma\beta}$) or the other ($F_{\lambda\beta}$) particle. Transforming to the frequency domain we thus have [86, ch. 7]

$$V_{\gamma_\alpha}(\omega) = \mu^{\gamma\gamma}_{\alpha\beta}(\boldsymbol{r}_\gamma, \boldsymbol{r}_\gamma, \omega) F_{\gamma\beta}(\omega) + \mu^{\gamma\lambda}_{\alpha\beta}(\boldsymbol{r}_\gamma, \boldsymbol{r}_\lambda, \omega) F_{\lambda\beta}(\omega)\,,$$

where Einstein's convention for summation over repeated indices is assumed. The particle mobility

tensor in the present geometry can be written as an algebraic sum of two distinct contributions

$$\mu^{\gamma\lambda}_{\alpha\beta}(\boldsymbol{r}_\gamma, \boldsymbol{r}_\lambda, \omega) = b^{\gamma\lambda}_{\alpha\beta}(\boldsymbol{r}_\gamma, \boldsymbol{r}_\lambda) + \Delta\mu^{\gamma\lambda}_{\alpha\beta}(\boldsymbol{r}_\gamma, \boldsymbol{r}_\lambda, \omega)\,, \tag{2.1}$$

where $b^{\gamma\lambda}_{\alpha\beta}$ is the pair-mobility in an unbounded geometry (bulk flow), and $\Delta\mu^{\gamma\lambda}_{\alpha\beta}$ is the frequency-dependent correction due to the presence of the elastic membrane. An analogous relation holds for $\mu^{\gamma\gamma}_{\alpha\beta}$.

For the determination of the particle mobility, we consider a force density $\boldsymbol{f}$ acting on the surface S_λ of the particle λ, related to the total force by

$$F_{\lambda\beta}(\omega) = \oint_{S_\lambda} f_\beta(\boldsymbol{r}', \omega)\,\mathrm{d}^2\boldsymbol{r}'\,,$$

which induces the disturbance flow velocity at point $\boldsymbol{r}$

$$v_\alpha(\boldsymbol{r}, \boldsymbol{r}_\lambda, \omega) = \oint_{S_\lambda} \mathcal{G}_{\alpha\beta}(\boldsymbol{r}, \boldsymbol{r}', \omega) f_\beta(\boldsymbol{r}', \omega)\,\mathrm{d}^2\boldsymbol{r}'\,, \tag{2.2}$$

where $\mathcal{G}_{\alpha\beta}$ denotes the velocity Green's function (Stokeslet), i.e. the flow velocity field resulting from a point-force acting on $\boldsymbol{r}_\lambda$. The disturbance velocity at any point $\boldsymbol{r}$ can be split up into two parts,

$$v_\alpha(\boldsymbol{r}, \boldsymbol{r}_\lambda, \omega) = v^{(0)}_\alpha(\boldsymbol{r}, \boldsymbol{r}_\lambda) + \Delta v_\alpha(\boldsymbol{r}, \boldsymbol{r}_\lambda, \omega)\,, \tag{2.3}$$

where $v^{(0)}_\alpha$ is the flow field induced by the particle λ in an unbounded geometry, and Δv_α is the flow satisfying the no-slip boundary condition at the membrane. In this way, the Green's function can be written as

$$\mathcal{G}_{\alpha\beta}(\boldsymbol{r}, \boldsymbol{r}', \omega) = \mathcal{G}^{(0)}_{\alpha\beta}(\boldsymbol{r}, \boldsymbol{r}') + \Delta\mathcal{G}_{\alpha\beta}(\boldsymbol{r}, \boldsymbol{r}', \omega)\,, \tag{2.4}$$

where $\mathcal{G}^{(0)}_{\alpha\beta}$ is the infinite-space Green's function (Oseen's tensor) given by

$$\mathcal{G}^{(0)}_{\alpha\beta}(\boldsymbol{r}, \boldsymbol{r}') = \frac{1}{8\pi\eta}\left(\frac{\delta_{\alpha\beta}}{s} + \frac{s_\alpha s_\beta}{s^3}\right)\,, \tag{2.5}$$

with $\boldsymbol{s} := \boldsymbol{r} - \boldsymbol{r}'$ and $s := |\boldsymbol{s}|$. The term $\Delta\mathcal{G}_{\alpha\beta}$ represents the frequency-dependent correction due to the presence of the membrane. Far away from the particle λ, the vector $\boldsymbol{r}'$ in Eq. (2.2) can be expanded around the particle center $\boldsymbol{r}_\lambda$ following a multipole expansion approach. Up to the second order, and assuming a constant force density, the disturbance velocity can be approximated by [77, 87–89]

$$v_\alpha(\boldsymbol{r}, \boldsymbol{r}_\lambda, \omega) \approx \left(1 + \frac{a^2}{6}\boldsymbol{\nabla}^2_{\boldsymbol{r}_\lambda}\right)\mathcal{G}_{\alpha\beta}(\boldsymbol{r}, \boldsymbol{r}_\lambda, \omega) F_{\lambda\beta}(\omega)\,, \tag{2.6}$$

where $\boldsymbol{\nabla}_{\boldsymbol{r}_\lambda}$ stands for the gradient operator taken with respect to the singularity position $\boldsymbol{r}_\lambda$. Note that for a single sphere in bulk, the flow field given by Eq. (2.6) satisfies exactly the no-slip boundary conditions at the surface of the sphere, i.e. in the frame moving with the particle, both the normal and tangential velocities vanish. Using Faxén's theorem, the velocity of the second particle γ in this flow reads [77, 87–89]

$$V_{\gamma\alpha}(\omega) = \mu_0 F_{\gamma\alpha}(\omega) + \left(1 + \frac{a^2}{6}\boldsymbol{\nabla}^2_{\boldsymbol{r}_\gamma}\right) v_\alpha(\boldsymbol{r}_\gamma, \boldsymbol{r}_\lambda, \omega)\,, \tag{2.7}$$

where $\mu_0 := 1/(6\pi\eta a)$ denotes the usual bulk mobility, given by the Stokes' law. The disturbance flow v_α incorporates both the disturbance from the particle λ and the disturbance caused by the

presence of the membrane. By plugging Eq. (2.6) into Faxén's formula given by Eq. (2.7), the $\alpha\beta$ component of the frequency-dependent pair-mobilities can be obtained from

$$\mu^{\gamma\lambda}_{\alpha\beta}(\omega) = \left(1 + \frac{a^2}{6}\boldsymbol{\nabla}^2_{\boldsymbol{r}_\gamma}\right)\left(1 + \frac{a^2}{6}\boldsymbol{\nabla}^2_{\boldsymbol{r}_\lambda}\right)\mathcal{G}_{\alpha\beta}(\boldsymbol{r}_\gamma, \boldsymbol{r}_\lambda, \omega)\,. \tag{2.8}$$

For the self-mobilities, only the correction in the flow field Δv_α due to the presence of the membrane in Eq. (2.3) is considered in Faxén's formula (the influence of the second particle on the self-mobility is neglected here for simplicity [77, 88]). Therefore, the frequency-dependent self-mobilities read

$$\mu^{\gamma\gamma}_{\alpha\beta}(\omega) = \mu_0 + \lim_{\boldsymbol{r}\to\boldsymbol{r}_\gamma}\left(1 + \frac{a^2}{6}\boldsymbol{\nabla}^2_{\boldsymbol{r}}\right)\left(1 + \frac{a^2}{6}\boldsymbol{\nabla}^2_{\boldsymbol{r}_\gamma}\right)\Delta\mathcal{G}_{\alpha\beta}(\boldsymbol{r}, \boldsymbol{r}_\gamma, \omega)\,, \tag{2.9}$$

and analogously for $\mu^{\lambda\lambda}_{\alpha\beta}$.

In order to use the particle pair- and self-mobilities from Eqs. (2.8) and (2.9), the velocity Green's functions in the presence of the membrane are required. These have been calculated in our earlier work [55] and their derivation is only briefly sketched here with more details in Appendix A.

We proceed by solving the steady Stokes equations with an arbitrary time-dependent point-force $\boldsymbol{F}$ acting at $\boldsymbol{r}_0 = (0, 0, z_0)$,

$$\eta\boldsymbol{\nabla}^2\boldsymbol{v} - \boldsymbol{\nabla}p + \boldsymbol{F}\delta(\boldsymbol{r} - \boldsymbol{r}_0) = 0\,, \tag{2.10}$$

$$\boldsymbol{\nabla}\cdot\boldsymbol{v} = 0\,, \tag{2.11}$$

where p is the pressure field. The determination of the Green's functions at $\boldsymbol{r}_\lambda$ is straightforward thanks to the system translational symmetry along the xy plane. After solving the above equations and appropriately applying the boundary conditions at the membrane, we find that the Green's functions are conveniently expressed by

$$\mathcal{G}_{zz}(\boldsymbol{r}, \boldsymbol{r}_\lambda, \omega) = \frac{1}{2\pi}\int_0^\infty \tilde{\mathcal{G}}_{zz}(q, z, z_0, \omega)J_0(\rho q)\, q\,\mathrm{d}q\,, \tag{2.12a}$$

$$\mathcal{G}_{xx}(\boldsymbol{r}, \boldsymbol{r}_\lambda, \omega) = \frac{1}{4\pi}\int_0^\infty \left(\tilde{\mathcal{G}}_{+}(q, z, z_0, \omega)J_0(\rho q) + \tilde{\mathcal{G}}_{-}(q, z, z_0, \omega)J_2(\rho q)\cos 2\theta\right) q\,\mathrm{d}q\,, \tag{2.12b}$$

$$\mathcal{G}_{yy}(\boldsymbol{r}, \boldsymbol{r}_\lambda, \omega) = \frac{1}{4\pi}\int_0^\infty \left(\tilde{\mathcal{G}}_{+}(q, z, z_0, \omega)J_0(\rho q) - \tilde{\mathcal{G}}_{-}(q, z, z_0, \omega)J_2(\rho q)\cos 2\theta\right) q\,\mathrm{d}q\,, \tag{2.12c}$$

$$\mathcal{G}_{xz}(\boldsymbol{r}, \boldsymbol{r}_\lambda, \omega) = \frac{i\cos\theta}{2\pi}\int_0^\infty \tilde{\mathcal{G}}_{lz}(q, z, z_0, \omega)J_1(\rho q)\,\mathrm{d}q\,, \tag{2.12d}$$

where $\rho := \sqrt{(x - x_\lambda)^2 + y^2}$, $\theta := \arctan(y/(x - x_\lambda))$ with $\boldsymbol{r} = (x, y, z)$. Here J_n denotes the Bessel function of the first kind of order n. The functions $\tilde{\mathcal{G}}_{\pm}$, $\tilde{\mathcal{G}}_{lz}$ and $\tilde{\mathcal{G}}_{zz}$ are provided in Appendix A. It is worth to mention here that the unsteady term in the Stokes equations leads to negligible contribution in the correction to the Green's functions [55], and it is therefore not considered in the present work.

The membrane elasticity is described by the well-established Skalak model [90], commonly used to describe deformation properties of red blood cell (RBC) membranes [91–93]. The elastic model has as parameters the shearing modulus κ_S and the area-expansion modulus κ_A. The two moduli are related via the dimensionless number $C := \kappa_\mathrm{A}/\kappa_\mathrm{S}$. Moreover, the membrane resists towards bending according to Helfrich's model [94], with the corresponding bending rigidity κ_B.

3 Boundary integral methods

In this section, we introduce the numerical method used to compute the particle self- and pair-mobilities. The numerical results will subsequently be compared with the analytical predictions presented in Sec. 2.

For solving the fluid motion equations in the inertia-free Stokes regime, we use a boundary integral method (BIM). The method is well suited for problems with deforming boundaries such as RBC membranes [95, 96]. In order to solve for the particle velocity given an exerted force, a completed double layer boundary integral method (CDLBIM) [97, 98] has been combined with the classical BIM [99]. The integral equations for the two-particle membrane systems read

$$\begin{aligned} v_\beta(\boldsymbol{x}) &= H_\beta(\boldsymbol{x})\,, \quad \boldsymbol{x} \in S_\mathrm{m}\,, \\ \frac{1}{2}\phi_\beta(\boldsymbol{x}) + \sum_{\alpha=1}^{6} \varphi_\beta^{(\alpha)}(\boldsymbol{x})\,\langle \boldsymbol{\varphi}^{(\alpha)}, \boldsymbol{\phi}\rangle &= H_\beta(\boldsymbol{x})\,, \quad \boldsymbol{x} \in S_\mathrm{p}\,. \end{aligned} \tag{3.1}$$

where S_m is the surface of the elastic membrane and $S_\mathrm{p} := S_{\mathrm{p}_\gamma} \cup S_{\mathrm{p}_\lambda}$ is the surface of the two spheres. Here $\boldsymbol{v}$ denotes the velocity on the membrane whereas $\boldsymbol{\phi}$ represents the double layer density function on S_p, related to the velocity of the particle γ via

$$V_{\gamma\beta}(\boldsymbol{x}) = \sum_{\alpha=1}^{6} \varphi_\beta^{(\alpha)}(\boldsymbol{x})\,\langle \boldsymbol{\varphi}^{(\alpha)}, \boldsymbol{\phi}\rangle\,, \quad \boldsymbol{x} \in S_{\mathrm{p}_\gamma}\,. \tag{3.2}$$

where $\boldsymbol{\varphi}^{(\alpha)}$ are known functions [98]. The brackets stand for the inner product in the space of real functions whose domain is S_{p_γ}, and the function H_β is defined by

$$H_\beta(\boldsymbol{x}) := -(N_\mathrm{m}\Delta\boldsymbol{f})_\beta(\boldsymbol{x}) - (K_\mathrm{p}\boldsymbol{\phi})_\beta(\boldsymbol{x}) + \mathcal{G}^{(0)}_{\beta\mu}(\boldsymbol{x}, \boldsymbol{x}_{\lambda_\mathrm{c}})F_\mu\,,$$

with $\boldsymbol{x}_{\lambda_\mathrm{c}}$ being the centroid of the sphere labeled λ upon which the force is applied. The single layer integral is defined as

$$(N_\mathrm{m}\Delta\boldsymbol{f})_\beta(\boldsymbol{x}) := \int_{S_\mathrm{m}} \Delta f_\alpha(\boldsymbol{y})\mathcal{G}^{(0)}_{\alpha\beta}(\boldsymbol{y}, \boldsymbol{x})\,\mathrm{d}S(\boldsymbol{y})$$

and the double layer integral as

$$(K_\mathrm{p}\boldsymbol{\phi})_\beta(\boldsymbol{x}) := \oint_{S_\mathrm{p}} \phi_\alpha(\boldsymbol{y})\mathcal{T}^{(0)}_{\alpha\beta\mu}(\boldsymbol{y}, \boldsymbol{x})n_\mu(\boldsymbol{y})\,\mathrm{d}S(\boldsymbol{y})\,.$$

Here, $\Delta\boldsymbol{f}$ is the traction jump, $\boldsymbol{n}$ denotes the outer normal vector at the particle surfaces and $\boldsymbol{F}$ is the force acting on the rigid particle. The infinite-space Green's function is given by Eq. (2.5) and the corresponding Stresslet, defined as the symmetric part of the first moment of the force density, reads [86]

$$\mathcal{T}^{(0)}_{\alpha\beta\mu}(\boldsymbol{y}, \boldsymbol{x}) = -\frac{3}{4\pi}\frac{s_\alpha s_\beta s_\mu}{s^5}\,,$$

with $\boldsymbol{s} := \boldsymbol{y} - \boldsymbol{x}$ and $s := |\boldsymbol{s}|$. The traction jump across the membrane $\Delta\boldsymbol{f}$ is an input for the equations, determined from the instantaneous deformation of the membrane. In order to solve Eqs. (3.1) numerically, the membrane and particles' surfaces are discretized with flat triangles. The resulting linear system of equations for the velocity $\boldsymbol{v}$ on the membrane and the density $\boldsymbol{\phi}$ on the rigid particles is solved iteratively by GMRES [100]. The velocity of each particle is determined from (3.2). For further details concerning the algorithm and its implementation, we refer the reader to Ref. [55]. Bending forces are computed using Method C from [101].

In order to compute the particle self- and pair-mobilities numerically, a harmonic oscillating force $\boldsymbol{F}_\lambda(t) = \boldsymbol{A}_\lambda e^{i\omega_0 t}$ of amplitude $\boldsymbol{A}_\lambda$ and frequency ω_0 is applied at the surface of the particle λ. After a brief transient time, both particles begin to oscillate at the same frequency as $\boldsymbol{V}_\lambda(t) = \boldsymbol{B}_\lambda e^{i(\omega_0 t+\delta_\lambda)}$ and as $\boldsymbol{V}_\gamma(t) = \boldsymbol{B}_\gamma e^{i(\omega_0 t+\delta_\gamma)}$. The velocity amplitudes and phase shifts can accurately be obtained by a fitting procedure of the numerically recorded particle velocities. For that, we use a nonlinear least-squares algorithm based on the trust region method [102]. Afterward, the $\alpha\beta$ component of the frequency-dependent complex self- and pair-mobilities can be calculated as

$$\mu^{\lambda\lambda}_{\alpha\beta} = \frac{B_{\lambda\alpha}}{A_{\lambda\beta}}\, e^{i\delta_\lambda}\,, \quad \mu^{\gamma\lambda}_{\alpha\beta} = \frac{B_{\gamma\alpha}}{A_{\lambda\beta}}\, e^{i\delta_\gamma}\,.$$

4 Results

For a single membrane, the corrections to the particle mobility can conveniently be split up into a correction due to shearing and area expansion together with a correction due to bending [55]. In the following, we denote by $\mu^{\gamma\gamma}_{\alpha\beta} = \mu^{\lambda\lambda}_{\alpha\beta} = \mu^{\mathrm{S}}_{\alpha\beta}$ ("self") the components of the self-mobility tensor, and by $\mu^{\gamma\lambda}_{\alpha\beta} = \mu^{\lambda\gamma}_{\beta\alpha} = \mu^{\mathrm{P}}_{\alpha\beta}$ ("pair") the components of the pair-mobility tensor. Note that for $\alpha \neq \beta$, $\mu^{\mathrm{S}}_{\alpha\beta} = 0$ and that $\mu^{\mathrm{P}}_{\alpha\beta} = -\mu^{\mathrm{P}}_{\beta\alpha}$.

4.1 Self-mobilities for finite-sized particles

Mathematical expressions for the translational particle self-mobility corrections will be derived in terms of $\epsilon = a/z_0$. The point-particle approximation presented in earlier work [55] represents the first order in the perturbation series, valid when the particle is far away from the membrane.

Perpendicular to membrane

The particle mobility perpendicular to the membrane is readily obtained after plugging the correction $\Delta\mathcal{G}_{zz}$ as defined by Eq. (2.4) to the normal-normal component of the Green's function from Eq. (2.12a) into Eq. (2.9). After computation, we find that the contribution due to shearing and bending can be expressed as

$$\frac{\Delta\mu^{\mathrm{S}}_{zz,\mathrm{S}}}{\mu_0} = e^{i\beta}\left(-\frac{9}{16}\,\mathrm{E}_4(i\beta)\epsilon + \frac{3}{4}\,\mathrm{E}_5(i\beta)\epsilon^3 - \frac{5}{16}\,\mathrm{E}_6(i\beta)\epsilon^5 \right), \tag{4.1a}$$

$$\frac{\Delta\mu^{\mathrm{S}}_{zz,\mathrm{B}}}{\mu_0} = \epsilon f_1 + \epsilon^3 f_3 + \epsilon^5 f_5\,, \tag{4.1b}$$

where the subscripts S and B stand for shearing and bending, respectively. The function E_n is the generalized exponential integral defined as $\mathrm{E}_n(x) := \int_1^\infty t^{-n} e^{-xt}\mathrm{d}t$ [103]. Furthermore, $\beta := 6Bz_0\eta\omega/\kappa_{\mathrm{S}}$ is a dimensionless frequency associated with the shearing resistance, whereas $B := 2/(1+C)$. Moreover, $\beta_{\mathrm{B}} := 2z_0(4\eta\omega/\kappa_{\mathrm{B}})^{1/3}$ is a dimensionless number associated with bending. The

functions f_i, with $i \in \{1,3,5\}$ are defined by

$$f_1 = -\frac{15}{16} + \frac{3i\beta_\mathrm{B}}{8}\left(\left(\frac{\beta_\mathrm{B}^2}{12} + \frac{i\beta_\mathrm{B}}{6} + \frac{1}{6}\right)\phi_+ + \frac{\sqrt{3}}{6}(\beta_\mathrm{B}+i)\phi_- + \left(\frac{\beta_\mathrm{B}^2}{12} - \frac{i\beta_\mathrm{B}}{3} - \frac{1}{3}\right)\psi\right),$$
$$f_3 = \frac{5}{16} - \frac{\beta_\mathrm{B}^3}{48}\left(\left(\frac{\beta_\mathrm{B}}{4}+i\right)\phi_+ + \frac{i\sqrt{3}\beta_\mathrm{B}}{4}\phi_- - \left(\frac{\beta_\mathrm{B}}{2}-i\right)\psi + \frac{3i}{2}\right),$$
$$f_5 = -\frac{1}{16} + \frac{\beta_\mathrm{B}^3}{384}\left(\frac{\beta_\mathrm{B}^2}{3}\left(\frac{\sqrt{3}}{2}\phi_- + \frac{i}{2}\phi_+ - i\psi\right) + i\right),$$

with

$$\phi_\pm := e^{-i\overline{z_\mathrm{B}}}\,\mathrm{E}_1\left(-i\overline{z_\mathrm{B}}\right) \pm e^{-iz_\mathrm{B}}\,\mathrm{E}_1\left(-iz_\mathrm{B}\right),$$
$$\psi := e^{-i\beta_\mathrm{B}}\,\mathrm{E}_1(-i\beta_\mathrm{B}),$$

where $z_\mathrm{B} := j\beta_\mathrm{B}$ and $j := e^{2i\pi/3}$ being the principal cubic-root of unity. The bar designates complex conjugate.

The total mobility correction is obtained by adding the individual contributions due to shearing and bending, as given by Eqs. (4.1a) and (4.1b). In the vanishing frequency limit, the known result for a hard-wall [89] is obtained:

$$\lim_{\beta,\beta_\mathrm{B}\to 0} \frac{\Delta\mu_{zz}^\mathrm{S}}{\mu_0} = -\frac{9}{8}\epsilon + \frac{1}{2}\epsilon^3 - \frac{1}{8}\epsilon^5. \tag{4.2}$$

The particle mobility near an elastic membrane is determined by membrane shearing and bending properties. We therefore consider a typical case for which both effect manifests themselves equally. For that purpose, we define a characteristic time scale for shearing as $T_\mathrm{S} := 6z_0\eta/\kappa_\mathrm{S}$ together with a characteristic time scale for bending as $T_\mathrm{B} := 4\eta z_0^3/\kappa_\mathrm{B}$ [55]. Then we take $z_0^2\kappa_\mathrm{S}/\kappa_\mathrm{B} = 3/2$ such that the two time scales are equal and can be denoted by $T_\mathrm{S} = T_\mathrm{B} =: T$. In this case, the two dimensionless numbers β and β_B are related by $\beta_\mathrm{B} = 2(\beta/B)^{1/3}$. The situation for a membrane with the typical parameters of a red blood cell is qualitatively similar as shown in the Supporting Information [104].

In Fig. 2 *a*), we show the particle scaled self-mobility corrections versus the scaled frequency β, as stated by Eqs. (4.1a) and (4.1b). The particle is set a distance $z_0 = 2a$ above the membrane. We observe that the real part is a monotonically increasing function with respect to frequency while the imaginary part exhibits a bell-shaped dependence on frequency centered around $\beta \sim 1$. In the limit of infinite frequencies, both the real and imaginary parts of the self-mobility corrections vanish, and thus one recovers the bulk behavior. For the perpendicular motion we observe that the particle mobility correction is primarily determined by the bending part.

A very good agreement is obtained between the analytical predictions and the numerical simulations over the whole range of frequencies. Additionally, we assess the accuracy of the point-particle approximation employed in earlier work [55], in which only the first order correction term in the perturbation parameter ϵ was considered. While this approximation slightly underestimates particle mobilities, it nevertheless leads to a surprisingly good prediction, even though the particle is set only one diameter above the membrane.

Parallel to membrane

We proceed in a similar way for the motion parallel to the membrane. By plugging the correction $\Delta\mathcal{G}_{xx}$ from the Green's function in Eq. (2.12b) into Eq. (2.9) we find

$$\frac{\Delta\mu^{\mathrm{S}}_{xx,\mathrm{S}}}{\mu_0} = e^{i\beta}\bigg(-\frac{3}{32}\Big(3\,\mathrm{E}_4(i\beta) - 4\,\mathrm{E}_3(i\beta) + 2\,\mathrm{E}_2(i\beta) + 4e^{iC\beta}\,\mathrm{E}_2(i(1+C)\beta)\Big)\epsilon \tag{4.3a}$$
$$+ \frac{3}{16}\left(2\,\mathrm{E}_5(i\beta) - \mathrm{E}_4(i\beta)\right)\epsilon^3 - \frac{5}{32}\,\mathrm{E}_6(i\beta)\epsilon^5\bigg)\,,$$
$$\frac{\Delta\mu^{\mathrm{S}}_{xx,\mathrm{B}}}{\mu_0} = \epsilon g_1 + \epsilon^3 g_3 + \epsilon^5 g_5\,, \tag{4.3b}$$

where we defined

$$g_1 = -\frac{3}{32} + \frac{i\beta_{\mathrm{B}}^3}{64}(\phi_+ + \psi)\,,$$
$$g_3 = \frac{3}{32} + \frac{\beta_{\mathrm{B}}^3}{64}\left(-i + \frac{\beta_{\mathrm{B}}}{3}\left(\psi - \frac{1}{2}\phi_+ - \frac{i\sqrt{3}}{2}\phi_-\right)\right)\,,$$
$$g_5 = -\frac{1}{32} + \frac{\beta_{\mathrm{B}}^3}{768}\left(i + \frac{\beta_{\mathrm{B}}^2}{3}\left(\frac{i}{2}\phi_+ + \frac{\sqrt{3}}{2}\phi_- - i\psi\right)\right)\,.$$

The well-known hard-wall limit, as first calculated by Faxén [89, 105], is recovered by considering the vanishing frequency limit:

$$\lim_{\beta,\beta_{\mathrm{B}}\to 0}\frac{\Delta\mu^{\mathrm{S}}_{xx}}{\mu_0} = -\frac{9}{16}\epsilon + \frac{1}{8}\epsilon^3 - \frac{1}{16}\epsilon^5\,. \tag{4.4}$$

The mobility corrections in the parallel direction are shown in Fig. 2 *b*). We observe that the total correction is mainly determined by the shearing part in contrast to the perpendicular case where bending dominates.

4.2 Pair-mobilities for finite-sized particles

In the following, expressions for the pair-mobility corrections in terms of a power series in $\sigma = a/h$ will be provided. To start, let us first recall the particle pair-mobilities in an unbounded geometry. By applying Eq. (2.8) to the infinite space Green's function Eq. (2.5), the bulk pair-mobilities for the motion perpendicular to and along the line of centers read [86, p. 190]

$$\frac{\mu^{\mathrm{P}}_{zz}}{\mu_0} = \frac{3}{4}\sigma + \frac{1}{2}\sigma^3\,, \quad \frac{\mu^{\mathrm{P}}_{xx}}{\mu_0} = \frac{3}{2}\sigma - \sigma^3\,, \tag{4.5}$$

and are commonly denominated the Rotne-Prager tensor [26, 106]. Note that the terms with σ^5 vanish for the bulk mobilities when considering only the first reflection as is done here. The axial symmetry along the line connecting the two spheres in bulk requires that $\mu^{\mathrm{P}}_{yy} = \mu^{\mathrm{P}}_{zz}$ and that the off-diagonal components of the mobility tensor are zero. Physically, the parameter σ only takes values between 0 and 1/2 as overlap between the two particles is not allowed. In this interval, the pair-mobility perpendicular to the line of centers μ^{P}_{zz} is always lower than the pair-mobility μ^{P}_{xx}, since it is easier to move the fluid aside than to push it into or to squeeze it out of the gap between the two particles.

Consider next the pair-mobilities near an elastic membrane. By applying Eq. (2.8) to Eqs. (2.12a) through (2.12d), we find that the corrections to the pair-mobilities can conveniently be expressed in

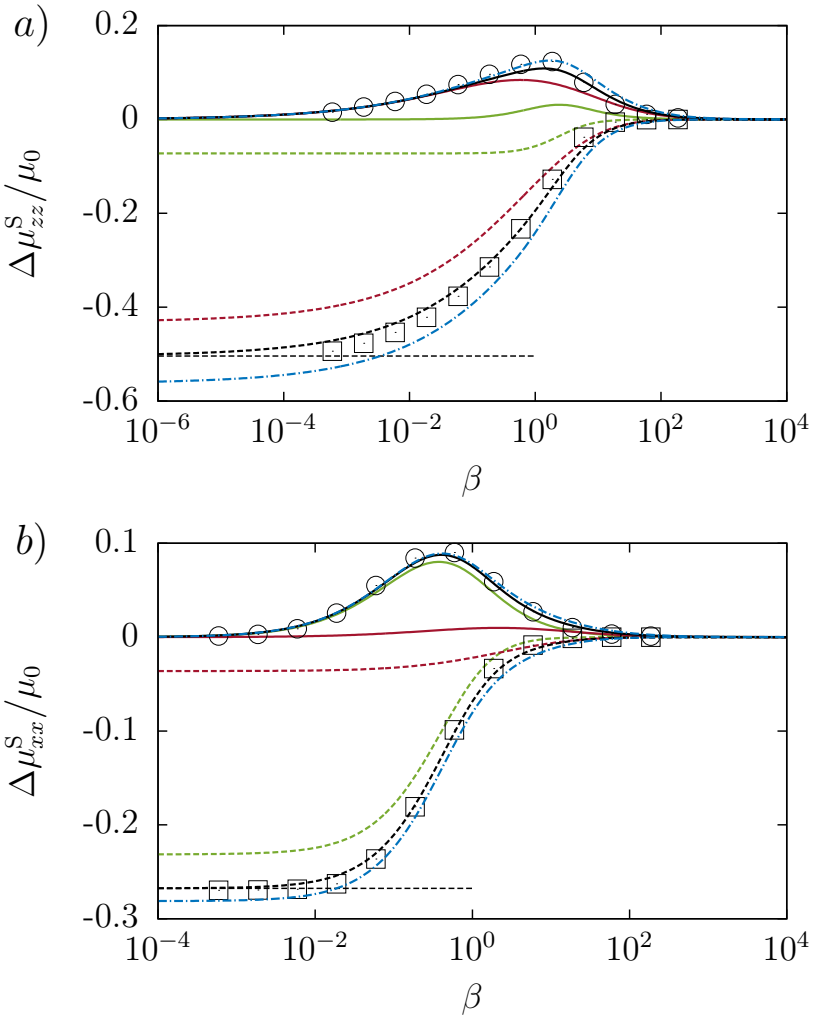

Figure 2: (Color online) The scaled frequency-dependent self-mobility correction versus the scaled frequency for the motion perpendicular (a) and parallel (b) to the membrane. The particle is located at $z_0 = 2a$. We take $z_0^2\kappa_S/\kappa_B = 3/2$ and $C = 1$ in the Skalak model. The analytical predictions are shown as dashed lines for the real part, and as solid lines for the imaginary part. Symbols refer to BIM simulations. The shearing and bending contributions are shown in green and red respectively. The dotted-dashed line in blue corresponds to the first order correction in the particle self-mobility, as previously determined in Ref. [55]. Horizontal dashed lines represent the mobility corrections near a hard-wall as given by Eqs. (4.2) and (4.4).

terms of the following convergent integrals,

$$\frac{\Delta\mu^{P}_{zz}}{\mu_0} = \int_0^\infty -\frac{i\sigma u^3}{3\xi^{5/2}}\left(\frac{\Lambda^2}{2iu-\beta}+\frac{4\Gamma_-^2}{8iu^3-\beta_B^3}\right)\chi_0 e^{-2u}\mathrm{d}u\,, \tag{4.6a}$$

$$\frac{\Delta\mu^{P}_{xx}}{\mu_0} = \int_0^\infty \left(\frac{i\sigma}{6\xi^{5/2}}\left(\frac{\Gamma_+^2}{2iu-\beta}+\frac{4u^4\Lambda^2}{8iu^3-\beta_B^3}\right)\left(\xi^{1/2}\chi_1-2u\chi_0\right)-\frac{3\sigma B}{2}\frac{\chi_1}{Bu+i\beta}\right)e^{-2u}\mathrm{d}u\,, \tag{4.6b}$$

$$\frac{\Delta\mu^{P}_{yy}}{\mu_0} = \int_0^\infty \left(-\frac{i\sigma}{6\xi^{2}}\left(\frac{\Gamma_+^2}{2iu-\beta}+\frac{4u^4\Lambda^2}{8iu^3-\beta_B^3}\right)\chi_1+\frac{3\sigma B}{2\xi^{1/2}}\frac{\xi^{1/2}\chi_1-2u\chi_0}{Bu+i\beta}\right)e^{-2u}\mathrm{d}u\,, \tag{4.6c}$$

$$\frac{\Delta\mu^{P}_{xz}}{\mu_0} = \int_0^\infty \frac{i\sigma u^2}{3\xi^{5/2}}\Lambda\left(\frac{\Gamma_+}{2iu-\beta}+\frac{4u^2\Gamma_-}{8iu^3-\beta_B^3}\right)\chi_1 e^{-2u}\mathrm{d}u\,, \tag{4.6d}$$

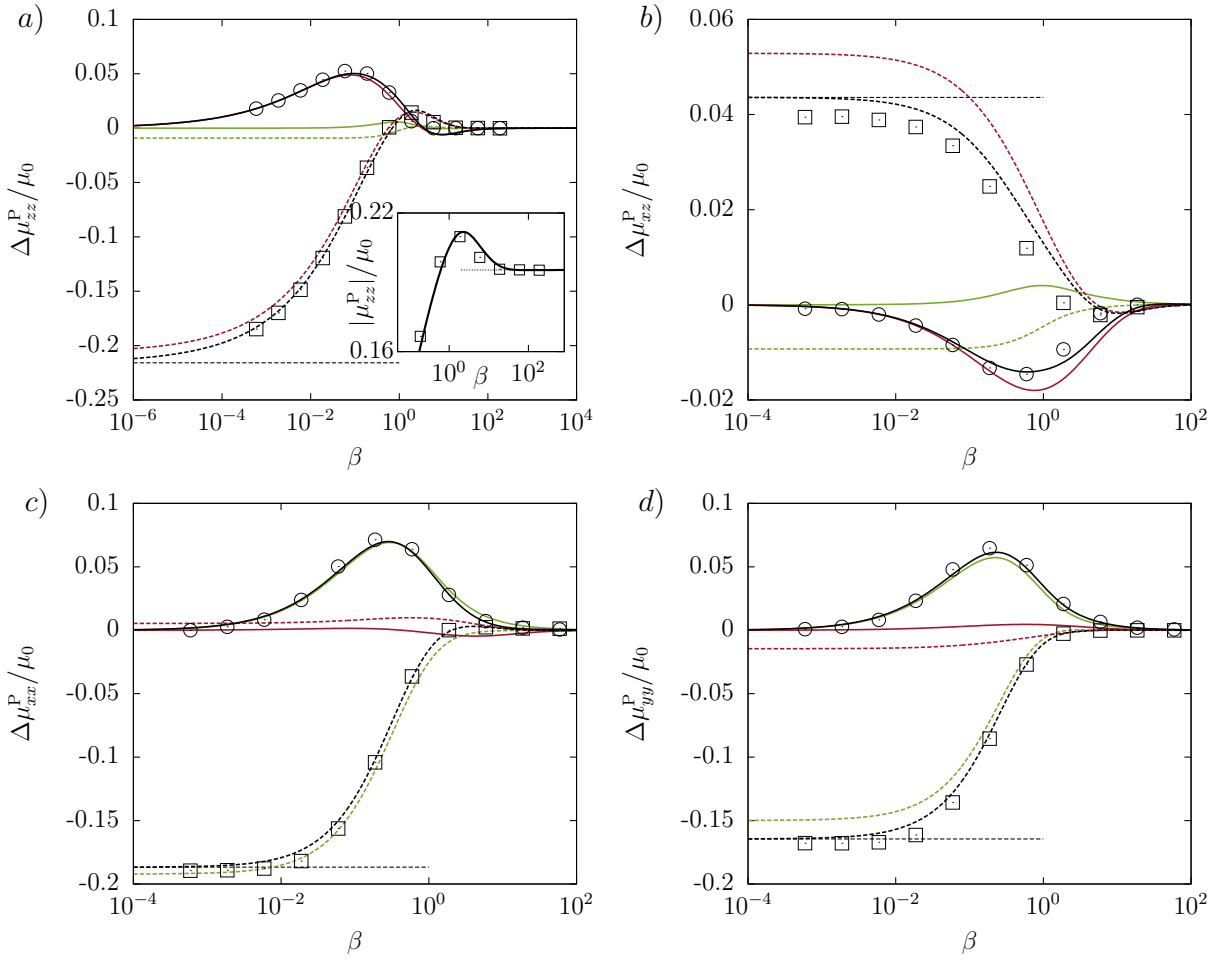

Figure 3: (Color online) The scaled pair-mobility corrections versus the scaled frequency β. The two particles are located above the membrane at $z_0 = 2a$ with a distance $h = 4a$. The real and imaginary parts of the mobility correction are shown as dashed and solid lines, respectively. The shearing and bending related parts are shown in green and red, respectively. The hard-wall limits are shown as horizontal dashed lines. The inset in a) shows that the amplitude of the total pair-mobility component zz exceeds its bulk value (dotted line) in a small frequency range around $\beta \sim 1$.

where $\xi := 4z_0^2/h^2 = 4\sigma^2/\epsilon^2$ and

$$\begin{aligned} \Lambda &:= 4\sigma^2 u - 3\xi\,, \\ \Gamma_\pm &:= 4\sigma^2 u^2 - 3u\xi \pm 3\xi\,, \\ \chi_n &:= J_n\left(\frac{2u}{\xi^{1/2}}\right)\,. \end{aligned}$$

The terms involving β and β_{B} in Eqs. (4.6a) through (4.6d) are the contributions coming from shearing and bending, respectively. Due to symmetry, $\mu^{\mathrm{P}}_{\alpha y} = 0$ for $\alpha \in \{x, z\}$.

For future reference, we note that each component of the frequency-dependent particle self- and pair-mobility tensor can conveniently be cast in the form

$$\frac{\mu(\omega)}{\mu_0} = b + \int_0^\infty \frac{\varphi_1(u)}{\varphi_2(u) + i\omega T}\,\mathrm{d}u\,, \tag{4.7}$$

where indices and superscripts have been omitted. Here b denotes the scaled bulk mobility (cf. Eq. (2.1)), and the integral term represents either shearing or bending related parts in the mobility correction. Note that φ_1 and φ_2 are real functions which do not depend on frequency. Moreover, $\varphi_2(u) = 2u/B$ or $\varphi_2(u) = u$ for the shearing related parts and $\varphi_2(u) = u^3$ for bending such that $\varphi_2(u) \geq 0, \forall u \in [0, \infty)$.

In the vanishing frequency limit, i.e. for β, β_B both taken to zero we recover the pair-mobilities near a hard-wall with stick boundary conditions, namely

$$\frac{\Delta\mu^\mathrm{P}_{zz}}{\mu_0} = -\frac{3}{4}\frac{3\xi^2 + \frac{5}{2}\xi + 1}{(1+\xi)^{5/2}}\sigma + \frac{4\xi^2 - 4\xi - \frac{1}{2}}{(1+\xi)^{7/2}}\sigma^3 - \frac{4\xi^2 - 12\xi + \frac{3}{2}}{(1+\xi)^{9/2}}\sigma^5\,, \tag{4.8a}$$

$$\frac{\Delta\mu^\mathrm{P}_{xx}}{\mu_0} = -\frac{3}{2}\frac{1 + \xi + \frac{3}{4}\xi^2}{(1+\xi)^{5/2}}\sigma + \frac{\xi^2 - \frac{11}{2}\xi + 1}{(1+\xi)^{7/2}}\sigma^3 - \frac{2\xi^2 - \frac{27}{2}\xi + 2}{(1+\xi)^{9/2}}\sigma^5\,, \tag{4.8b}$$

$$\frac{\Delta\mu^\mathrm{P}_{yy}}{\mu_0} = -\frac{3}{4}\frac{1 + \frac{3}{2}\xi}{(1+\xi)^{3/2}}\sigma + \frac{\xi - \frac{1}{2}}{(1+\xi)^{5/2}}\sigma^3 - \frac{2\xi - \frac{1}{2}}{(1+\xi)^{7/2}}\sigma^5\,, \tag{4.8c}$$

$$\frac{\Delta\mu^\mathrm{P}_{xz}}{\mu_0} = \frac{9}{8}\frac{\xi^{3/2}}{(1+\xi)^{5/2}}\sigma - \frac{3}{2}\frac{(4\xi - 1)\xi^{1/2}}{(1+\xi)^{7/2}}\sigma^3 + \frac{5}{2}\frac{(4\xi - 3)\xi^{1/2}}{(1+\xi)^{9/2}}\sigma^5\,, \tag{4.8d}$$

in agreement with the results by Swan and Brady [77].

In Fig. 3 we plot the particle pair-mobilities as given by Eqs. (4.6a) through (4.6d) as functions of the dimensionless frequency β for $h = 4a$. We observe that the real and imaginary parts have basically the same evolution as the self-mobilities. Nevertheless, two qualitatively different effects are apparent from Fig. 3: First, the amplitude of the normal-normal pair-mobility $\left|\mu^\mathrm{P}_{zz}\right|$ in a small frequency range even exceeds its bulk value. This enhanced mobility results in a short-lasting superdiffusive behavior as will be described in Sec. 5.

Secondly, for the components xx and xz in Fig. 3 we find that, unlike the self-mobilities, shearing and bending may have opposite contributions to the total pair-mobilities. For the xz component this implies the interesting behavior that hydrodynamic interactions can be either attractive or repulsive depending on the membrane properties. This will be investigated in more detail in the next subsection.

4.3 Perpendicular steady motion

A situation in which hydrodynamic interactions are particularly relevant is the steady approach of two particles towards an interface, such as e.g. drug molecules approaching a cell membrane, reactant species approaching a catalyst interface, charged colloids being attracted by an oppositely charged membrane, etc. For hard walls, it is known that hydrodynamic interactions in this case are repulsive [17, 77, 80] leading to the dispersion of particles on the surface. Near elastic membranes, the different signs of the bending and shear contributions to the pair-mobility in Fig. 3 *b*) point to a much more complex scenario including the possibility of particle attraction.

The physical situation of two particles being initially located at $z = z_0$ and suddenly set into motion towards the interface is described by a Heaviside step function force $\boldsymbol{F}(t) = \boldsymbol{A}\theta(t)$. Its Fourier transform to the frequency domain reads [107]

$$\boldsymbol{F}(\omega) = \left(\pi\delta(\omega) - \frac{i}{\omega}\right)\boldsymbol{A}\,.$$

Using the general form of Eq. (4.7), the scaled particle velocity in the temporal domain is then given by

$$\frac{V(\tau)}{\mu_0 A} = \left(b + \int_0^\infty \frac{\varphi_1(u)}{\varphi_2(u)}\left(1 - e^{-\varphi_2(u)\tau}\right)\mathrm{d}u\right)\theta(\tau)\,, \tag{4.9}$$

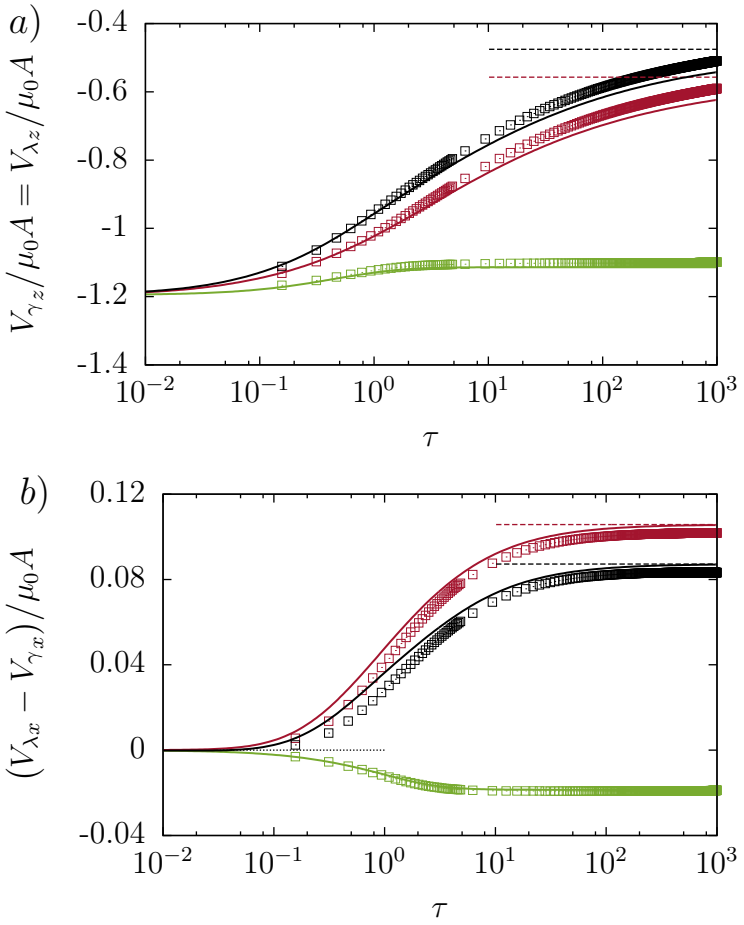

Figure 4: (Color online) The scaled particle velocities perpendicular to the membrane (a) and relative to each other (b) versus the scaled time for a constant force acting downward on both particles near a membrane endowed with only shearing (green), only bending (red) or both rigidities (black). Solid lines are the analytical predictions as given by Eq. (4.9), symbols are obtained by boundary-integral simulations. Horizontal dotted and dashed lines stand for the bulk and vanishing frequency limits respectively.

where $\tau := t/T$ is a dimensionless time. At larger times, the exponential in Eq. (4.9) can be neglected compared to one. In this way, we recover the steady velocity near a hard-wall.

In corresponding BIM simulations, a constant force of small amplitude towards the wall is applied on both particles in order to retain the system symmetry. At the end of the simulations, the vertical position of the particles changes by about 8 % compared to their initial positions z_0.

In Fig. 4 a) we show the time dependence of the vertical velocity which at first increases and then approaches its steady-state value. Figure 4 b) shows the relative velocity between the two particles: clearly, the motion is attractive for a membrane with negligible bending resistance (such as a typical artificial capsule) which is the opposite of the behavior near a membrane with only bending resistance (such as a vesicle) or a hard wall.

In order to illustrate more clearly for which wall and particle distances a repulsion/attraction is expected we show in Fig. 5 the pair-mobility correction for the shear $\Delta\mu^{\mathrm{P}}_{xz,\mathrm{S}}$ and bending $\Delta\mu^{\mathrm{P}}_{xz,\mathrm{B}}$ contributions in the (ϵ, σ) plane. To reduce the parameter space and to bring out the considered effects most clearly, we consider the idealized limit $\omega \to 0$. In this limit, the contributions become

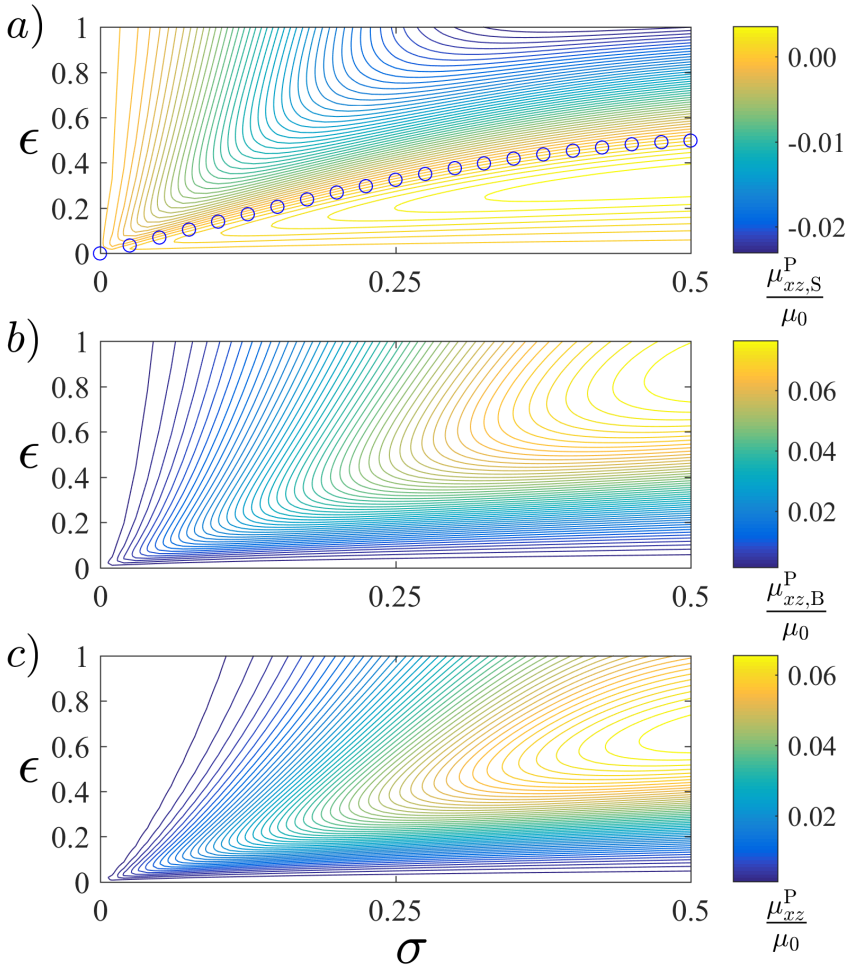

Figure 5: (Color online) Contour diagram (ϵ, σ) of the shearing (a) and bending (b) contribution in the vanishing frequency limit in the xz pair-mobility as stated by Eq. (B.1d) for shearing and by Eq. (B.2d) for bending. $c)$ is the same contour near a hard-wall as given by Eq. (4.8d). The perturbation solution given by Eq. (4.10) is presented as circles in (a). Contrary to a membrane with bending resistance and to a hard wall, the mobility changes sign near a membrane with shearing resistance. This sign change directly reflects the physically observable situation as the bulk contribution for the xz pair-mobility is zero.

independent of the elastic moduli since $\omega \to 0$ directly implies that $\beta, \beta_B \to 0$ meaning that even infinitesimally small shearing and bending resistances would make the membrane behave identical to the hard wall. This unphysical behavior is remedied in a realistic situation where a small bending resistance will lead to a correspondingly large time scale T_{B} and thus to a long-lived transient regime as given by Eq. (4.9) and shown in the Supporting Information. Therefore, the contours shown in Fig. 5 faithfully represent the behavior of membranes with small bending (Fig. 5 a)) or small shear (Fig. 5 b)) resistance. The corresponding equations can be found in Appendix B.

By equating Eq. (B.1d) to zero and solving the resulting equation perturbatively, the threshold

lines where the shearing contribution changes sign are given up to fifth order in σ by

$$\epsilon_{\mathrm{th}} = \sqrt{2}\left(\sigma - \frac{4}{3}\sigma^3 + \frac{17}{27}\sigma^5\right) + \mathcal{O}(\sigma^7)\,. \tag{4.10}$$

Eq. (4.10) is shown as circles in Fig. 5. The bending contribution in Fig. 5 *b*) always has a positive sign corresponding to a repulsive interaction similar as the hard wall.

Similar changes in sign are observed for $\Delta\mu^{\mathrm{P}}_{zz,\mathrm{S}}$ for shear and $\Delta\mu^{\mathrm{P}}_{xx,\mathrm{B}}$ for bending. The corresponding contours are given in the Supporting Information. Their physical relevance, however, is less important than for $\Delta\mu^{\mathrm{P}}_{xz}$ shown in Fig. 5 as the effects may be overshadowed by the bulk values of the mobilities (which is zero only for μ^{P}_{xz}).

5 Diffusion

The diffusive dynamics of a pair of Brownian particles is governed by the generalized Langevin equation written for each velocity component of particle γ as [108]

$$m\frac{\mathrm{d}V_{\gamma_\alpha}}{\mathrm{d}t} = -\int_{-\infty}^{t}\zeta^{\gamma\gamma}_{\alpha\beta}(t-t')V_{\gamma_\beta}(t')\mathrm{d}t' - \int_{-\infty}^{t}\zeta^{\gamma\lambda}_{\alpha\beta}(t-t')V_{\lambda_\beta}(t')\mathrm{d}t' + F_{\gamma_\alpha}(t)\,. \tag{5.1}$$

A similar equation can be written for the velocity components of the other particle λ. Here, m denotes the particles' mass, $\zeta^{\gamma\lambda}_{\alpha\beta}(t)$ stands for the time-dependent two-particle friction retardation tensor (expressed in kg/s^2) and F_{γ_α} is a random force which is zero on average. By evaluating the Fourier transform of both members in Eq. (5.1) and using the change of variables $w = t - t'$ together with the shift property in the time domain of Fourier transforms we get

$$im\omega V_{\gamma_\alpha}(\omega) + \zeta^{\gamma\gamma}_{\alpha\beta}[\omega]V_{\gamma_\beta}(\omega) + \zeta^{\gamma\lambda}_{\alpha\beta}[\omega]V_{\lambda_\beta}(\omega) = F_{\gamma_\alpha}(\omega)\,, \tag{5.2}$$

where $\zeta^{\gamma\lambda}_{\alpha\beta}[\omega]$ and $\zeta^{\gamma\gamma}_{\alpha\beta}[\omega]$ are the Fourier-Laplace transforms of the retardation function defined as

$$\zeta^{\gamma\lambda}_{\alpha\beta}[\omega] := \int_0^\infty \zeta^{\gamma\lambda}_{\alpha\beta}(t)e^{-i\omega t}\mathrm{d}t\,, \tag{5.3}$$

and analogously for $\zeta^{\gamma\gamma}_{\alpha\beta}[\omega]$.

In the following, we shall consider the overdamped regime for which the particles are massless ($m = 0$). Solving Eq. (5.2) for the particle velocities and equating with the definition of the mobilities,

$$V_{\gamma_\alpha}(\omega) = \mu^{\gamma\gamma}_{\alpha\beta}(\omega)F_{\gamma_\beta}(\omega) + \mu^{\gamma\lambda}_{\alpha\beta}(\omega)F_{\lambda_\beta}(\omega)\,, \tag{5.4a}$$

$$V_{\lambda_\alpha}(\omega) = \mu^{\lambda\lambda}_{\alpha\beta}(\omega)F_{\lambda_\beta}(\omega) + \mu^{\lambda\gamma}_{\alpha\beta}(\omega)F_{\gamma_\beta}(\omega)\,, \tag{5.4b}$$

leads to expressions of the mobilities in terms of the friction coefficients:

$$\begin{aligned}
\mu^{\mathrm{S}}_{xx}(\omega) &= \frac{\zeta^{\mathrm{S}}_{xx}\zeta^{\mathrm{P}}_{zz}}{(\zeta^{\mathrm{S}\,2}_{xx} - \zeta^{\mathrm{P}\,2}_{xx})\zeta^{\mathrm{P}}_{zz} - \zeta^{\mathrm{P}}_{xx}\zeta^{\mathrm{P}\,2}_{xz}}\,,\\
\mu^{\mathrm{P}}_{xx}(\omega) &= -\frac{\zeta^{\mathrm{P}}_{xx}\zeta^{\mathrm{P}}_{zz}}{(\zeta^{\mathrm{S}\,2}_{xx} - \zeta^{\mathrm{P}\,2}_{xx})\zeta^{\mathrm{P}}_{zz} - \zeta^{\mathrm{P}}_{xx}\zeta^{\mathrm{P}\,2}_{xz}}\,,\\
\mu^{\mathrm{S}}_{yy}(\omega) &= \frac{\zeta^{\mathrm{S}}_{yy}}{\zeta^{\mathrm{S}\,2}_{yy} - \zeta^{\mathrm{P}\,2}_{yy}}\,,\\
\mu^{\mathrm{P}}_{yy}(\omega) &= -\frac{\zeta^{\mathrm{P}}_{yy}}{\zeta^{\mathrm{S}\,2}_{yy} - \zeta^{\mathrm{P}\,2}_{yy}}\,.\\
\mu^{\mathrm{S}}_{zz}(\omega) &= \frac{\zeta^{\mathrm{S}}_{xx}\zeta^{\mathrm{S}}_{zz}}{(\zeta^{\mathrm{S}\,2}_{zz} - \zeta^{\mathrm{P}\,2}_{zz})\zeta^{\mathrm{S}}_{xx} - \zeta^{\mathrm{S}}_{zz}\zeta^{\mathrm{P}\,2}_{xz}}\,,\\
\mu^{\mathrm{P}}_{zz}(\omega) &= -\frac{\zeta^{\mathrm{S}}_{xx}\zeta^{\mathrm{P}}_{zz}}{(\zeta^{\mathrm{S}\,2}_{zz} - \zeta^{\mathrm{P}\,2}_{zz})\zeta^{\mathrm{S}}_{xx} - \zeta^{\mathrm{S}}_{zz}\zeta^{\mathrm{P}\,2}_{xz}}\,,\\
\mu^{\mathrm{P}}_{xz}(\omega) &= -\frac{\zeta^{\mathrm{S}}_{zz}\zeta^{\mathrm{P}}_{xz}}{(\zeta^{\mathrm{S}\,2}_{zz} - \zeta^{\mathrm{P}\,2}_{zz})\zeta^{\mathrm{S}}_{xx} - \zeta^{\mathrm{S}}_{zz}\zeta^{\mathrm{P}\,2}_{xz}}\,,
\end{aligned}$$

where the brackets [ ] are dropped out for the sake of clarity. Similar as for the mobilities, the self- and pair components of the retardation function are denoted by $\zeta^{\gamma\gamma}_{\alpha\beta} = \zeta^{\lambda\lambda}_{\alpha\beta} = \zeta^{\mathrm{S}}_{\alpha\beta}$ and $\zeta^{\gamma\lambda}_{\alpha\beta} = \zeta^{\lambda\gamma}_{\beta\alpha} = \zeta^{\mathrm{P}}_{\alpha\beta}$, respectively. Note that $\zeta^{\mathrm{P}}_{xx}\zeta^{\mathrm{S}}_{zz} = \zeta^{\mathrm{S}}_{xx}\zeta^{\mathrm{P}}_{zz}$ so that $\mu^{\mathrm{S}}_{xz} = 0$ as required by symmetry.

According to the fluctuation-dissipation theorem, the frictional and random forces are related via [109][p. 33][110]

$$\langle F_\gamma(\omega)\overline{F_\lambda(\omega')}\rangle = k_{\mathrm{B}}T\left(\zeta^{\gamma\lambda}_{\alpha\beta}[\omega] + \overline{\zeta^{\gamma\lambda}_{\alpha\beta}[\omega]}\right)\delta(\omega-\omega')\,, \tag{5.6}$$

and analogously for the $\gamma\gamma$ component, where k_{B} is the Boltzmann constant and T is the absolute temperature of the system [111].

Multiplying Eq. (5.4a) by its complex conjugate, taking the ensemble average and using Eq. (5.6), it can be shown that the velocity power spectrum obeys the relation

$$\mathcal{P}_{\mathrm{V}}{}^{\mathrm{S}}_{\alpha\beta}(\omega) = k_{\mathrm{B}}T\left(\mu^{\mathrm{S}}_{\alpha\beta}(\omega) + \overline{\mu^{\mathrm{S}}_{\alpha\beta}(\omega)}\right)\,. \tag{5.7}$$

Next, by considering both Eqs. (5.4a) and (5.4b) together with Eq. (5.6) we find in a similar fashion

$$\mathcal{P}_{\mathrm{V}}{}^{\mathrm{P}}_{\alpha\beta}(\omega) = k_{\mathrm{B}}T\left(\mu^{\mathrm{P}}_{\alpha\beta}(\omega) + \overline{\mu^{\mathrm{P}}_{\alpha\beta}(\omega)}\right)\,. \tag{5.8}$$

According to the Wiener-Khinchin-Einstein theorem, the velocity auto/cross-correlation functions can directly be obtained from the temporal inverse Fourier transform as [109]

$$\phi^{\gamma\lambda}_{\alpha\beta}(t) = \frac{k_{\mathrm{B}}T}{2\pi}\int_{-\infty}^{\infty}\left(\mu^{\gamma\lambda}_{\alpha\beta}(\omega) + \overline{\mu^{\gamma\lambda}_{\alpha\beta}(\omega)}\right)e^{i\omega t}\mathrm{d}\omega\,. \tag{5.9}$$

It can be shown using the residue theorem [109, p. 34] that the integral over the second term in Eq. (5.9) vanishes if the mobility is an analytic function for $\mathrm{Im}(\omega) < 0$. The present mobilities all fulfill this condition as can be seen by their general form in Eq. (4.7).

Most commonly, diffusion is studied in terms of the mean-square displacement (MSD) which can

be calculated from the correlation function as [109, p. 37]

$$\langle \Delta r_{\gamma_\alpha}(t) \Delta r_{\lambda\beta}(t) \rangle = 2 \int_0^t (t-s) \phi_{\alpha\beta}^{\gamma\lambda}(s) \mathrm{d}s \,, \tag{5.10}$$

where Δr_{γ_α} denotes the displacement of the particle γ in the direction α. Furthermore, we define the time-dependent pair-diffusion tensor as

$$D_{\alpha\beta}^{\gamma\lambda}(t) := \frac{\langle \Delta r_{\gamma_\alpha}(t) \Delta r_{\lambda\beta}(t) \rangle}{2t} \,. \tag{5.11}$$

Analogous relations to Eqs. (5.9)-(5.11) hold for the $\gamma\gamma$ component. We now consider the collective motions of the center of mass $\boldsymbol{\rho} := \boldsymbol{r}_\lambda + \boldsymbol{r}_\gamma$ as well as the relative motion $\boldsymbol{h} := \boldsymbol{r}_\lambda - \boldsymbol{r}_\gamma$ with the corresponding diagonal pair-diffusion tensor

$$D_{\alpha\alpha}^{C,R} = 2 \left(D_{\alpha\alpha}^{\mathrm{S}} \pm D_{\alpha\alpha}^{\mathrm{P}} \right) \,, \tag{5.12}$$

where the positive sign applies for the collective mode of motion and the negative sign to the relative mode. In the absence of the membrane, Eqs. (5.12) reduces to the generalization of the Einstein relation as calculated by Batchelor [25] for the relative mode, namely

$$\frac{D_{zz}^{\mathrm{R}}}{2D_0} = 1 - \frac{3}{4}\sigma - \frac{\sigma^3}{2} \,, \quad \frac{D_{xx}^{\mathrm{R}}}{2D_0} = 1 - \frac{3}{2}\sigma + \sigma^3 \,, \tag{5.13}$$

where $D_0 := \mu_0 k_{\mathrm{B}} T$ is the diffusion coefficient. The collective diffusion coefficients read

$$\frac{D_{zz}^{\mathrm{C}}}{2D_0} = 1 + \frac{3}{4}\sigma + \frac{\sigma^3}{2} \,, \quad \frac{D_{xx}^{\mathrm{C}}}{2D_0} = 1 + \frac{3}{2}\sigma - \sigma^3 \,, \tag{5.14}$$

5.1 Self-diffusion for finite-sized particles

From Eqs. (5.9)-(5.11) we first obtain the scaled self-diffusion coefficient for the motion of a single particle perpendicular to the membrane,

$$\begin{aligned} \frac{D_{zz}^{\mathrm{S}}}{D_0} = 1 &- \frac{3}{32} \frac{\tau_{\mathrm{S}}(3B + 2\tau_{\mathrm{S}})}{(B+\tau_{\mathrm{S}})^2} \epsilon + \frac{\tau_{\mathrm{S}}}{16} \frac{3\tau_{\mathrm{S}}^2 + 8B\tau_{\mathrm{S}} + 6B^2}{(B+\tau_{\mathrm{S}})^3} \epsilon^3 - \frac{\tau_{\mathrm{S}}}{64} \frac{4\tau_{\mathrm{S}}^3 + 15B\tau_{\mathrm{S}}^2 + 20B^2\tau_{\mathrm{S}} + 10B^3}{(B+\tau_{\mathrm{S}})^4} \epsilon^5 \\ &- \frac{\epsilon}{12} \int_0^\infty \left(3 + 3u - \epsilon^2 u^2\right)^2 \left(1 - \frac{1 - e^{-\tau_{\mathrm{B}} u^3}}{\tau_{\mathrm{B}} u^3} \right) e^{-2u} \mathrm{d}u \,, \end{aligned} \tag{5.15}$$

where $\tau_{\mathrm{S}} := t/T_{\mathrm{S}}$ and $\tau_{\mathrm{B}} := t/T_{\mathrm{B}}$ are dimensionless times for shearing and bending, respectively.

For motion parallel to the membrane the scaled self-diffusion coefficient reads

$$\begin{aligned} \frac{D_{xx}^{\mathrm{S}}}{D_0} = 1 &- \frac{3}{64} \left(\frac{(2\tau_{\mathrm{S}} + 3B)(5\tau_{\mathrm{S}} + 4B)}{(\tau_{\mathrm{S}} + B)^2} - \frac{4B}{\tau_{\mathrm{S}}} \ln\left(1 + \frac{\tau_{\mathrm{S}}}{B}\right) - \frac{16}{\tau_{\mathrm{S}}} \ln\left(1 + \frac{\tau_{\mathrm{S}}}{2}\right) \right) \epsilon \\ &+ \frac{\tau_{\mathrm{S}}}{32} \frac{\tau_{\mathrm{S}}^2 + 3B\tau_{\mathrm{S}} + 3B^2}{(\tau_{\mathrm{S}} + B)^3} \epsilon^3 - \frac{\tau_{\mathrm{S}}}{128} \frac{4\tau_{\mathrm{S}}^3 + 15B\tau_{\mathrm{S}}^2 + 20B^2\tau_{\mathrm{S}} + 10B^3}{(\tau_{\mathrm{S}} + B)^4} \epsilon^5 \\ &- \frac{\epsilon}{12} \int_0^\infty \left(3 - \epsilon^2 u\right)^2 \left(u^2 - \frac{1 - e^{-\tau_{\mathrm{B}} u^3}}{\tau_{\mathrm{B}} u} \right) e^{-2u} \mathrm{d}u \,. \end{aligned} \tag{5.16}$$

We mention that Eqs. (5.15) and (5.16) correspond to leading order in ϵ to the ones reported in our

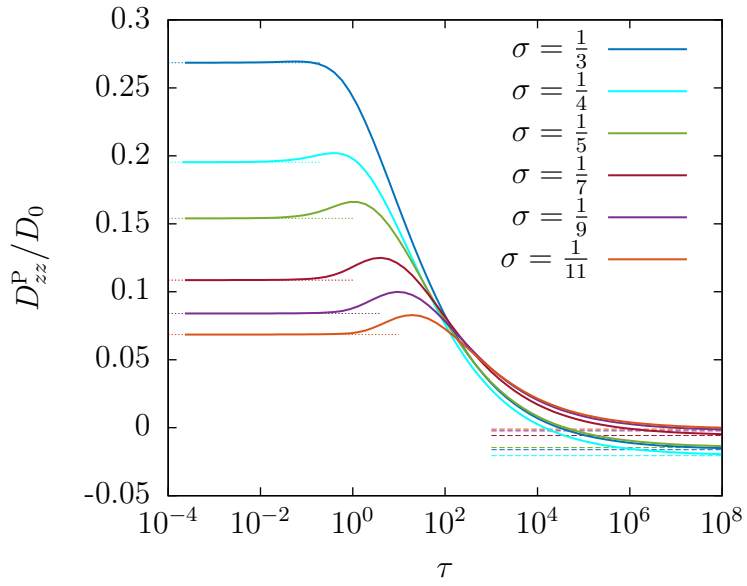

Figure 6: (Color online) The zz component of the scaled pair-diffusion tensor versus the scaled time as given by Eq. (5.16a) for different values of σ with the parameters of Fig. 3. Horizontal dotted and dashed lines represent the bulk and hard-wall limits, respectively. For large inter-particle distances (small σ) a short superdiffusive regime is observed.

earlier work [55]. For long times, the perpendicular velocity auto-correlation function $\phi^{\mathrm{S}}_{zz,\mathrm{S}}$ decays as t^{-4} whereas the bending part $\phi^{\mathrm{S}}_{zz,\mathrm{B}}$ as $t^{-4/3}$. For parallel motion, both the shearing and bending parts in the velocity auto-correlation function have a long-time tail of t^{-2}.

5.2 Pair-diffusion for finite-sized particles

The pair-diffusion coefficients are readily obtained by plugging Eqs. (4.6a) through (4.6d) into Eqs. (5.9)-(5.11):

$$\frac{D^{\mathrm{P}}_{zz}}{D_0} = \frac{3\sigma}{4} + \frac{\sigma^3}{2} - \frac{\sigma}{12\xi^{5/2}} \int_0^\infty \left(u\Lambda^2 \Pi_{\mathrm{S}} + \frac{2\Gamma_-^2}{u^3} \Pi_{\mathrm{B}} \right) \chi_0 e^{-2u} \mathrm{d}u \,, \tag{5.16a}$$

$$\frac{D^{\mathrm{P}}_{xx}}{D_0} = \frac{3\sigma}{2} - \sigma^3 - \sigma \int_0^\infty \left(\frac{1}{24\xi^{5/2}} \left(-\xi^{1/2}\chi_1 + 2u\chi_0 \right) \left(\Gamma_+^2 \Pi_{\mathrm{S}} + 2\Lambda^2 \Pi_{\mathrm{B}} \right) + \frac{3\chi_1}{2} \Pi'_{\mathrm{S}} \right) \frac{e^{-2u}}{u^2} \mathrm{d}u \,, \tag{5.16b}$$

$$\frac{D^{\mathrm{P}}_{yy}}{D_0} = \frac{3\sigma}{4} + \frac{\sigma^3}{2} - \sigma \int_0^\infty \left(\frac{\chi_1}{24\xi^2} \left(\Gamma_+^2 \Pi_{\mathrm{S}} + 2\Lambda^2 \Pi_{\mathrm{B}} \right) + \frac{3\Pi'_{\mathrm{S}}}{2\xi^{1/2}} \left(-\xi^{1/2}\chi_1 + 2u\chi_0 \right) \right) \frac{e^{-2u}}{u^2} \mathrm{d}u \,, \tag{5.16c}$$

$$\frac{D^{\mathrm{P}}_{xz}}{D_0} = \frac{\sigma}{12\xi^{5/2}} \int_0^\infty \left(\Gamma_+ \Pi_{\mathrm{S}} + \frac{2\Gamma_- \Pi_{\mathrm{B}}}{u^2} \right) \chi_1 \Lambda e^{-2u} \mathrm{d}u \,, \tag{5.16d}$$

where we define

$$\Pi_{\mathrm{S}} := \frac{B e^{-\frac{2u\tau_{\mathrm{S}}}{B}} + 2u\tau_{\mathrm{S}} - B}{\tau_{\mathrm{S}}} \,, \quad \Pi'_{\mathrm{S}} := \frac{e^{-\tau_{\mathrm{S}} u} + \tau_{\mathrm{S}} u - 1}{\tau_{\mathrm{S}}} \,, \quad \Pi_{\mathrm{B}} := \frac{e^{-\tau_{\mathrm{B}} u^3} + \tau_{\mathrm{B}} u^3 - 1}{\tau_{\mathrm{B}}} \,.$$

We observe that the xx, yy and zz cross-correlation functions have the same large time behavior as their corresponding auto-correlation functions. For the component ϕ^{P}_{xz}, the shearing and bending

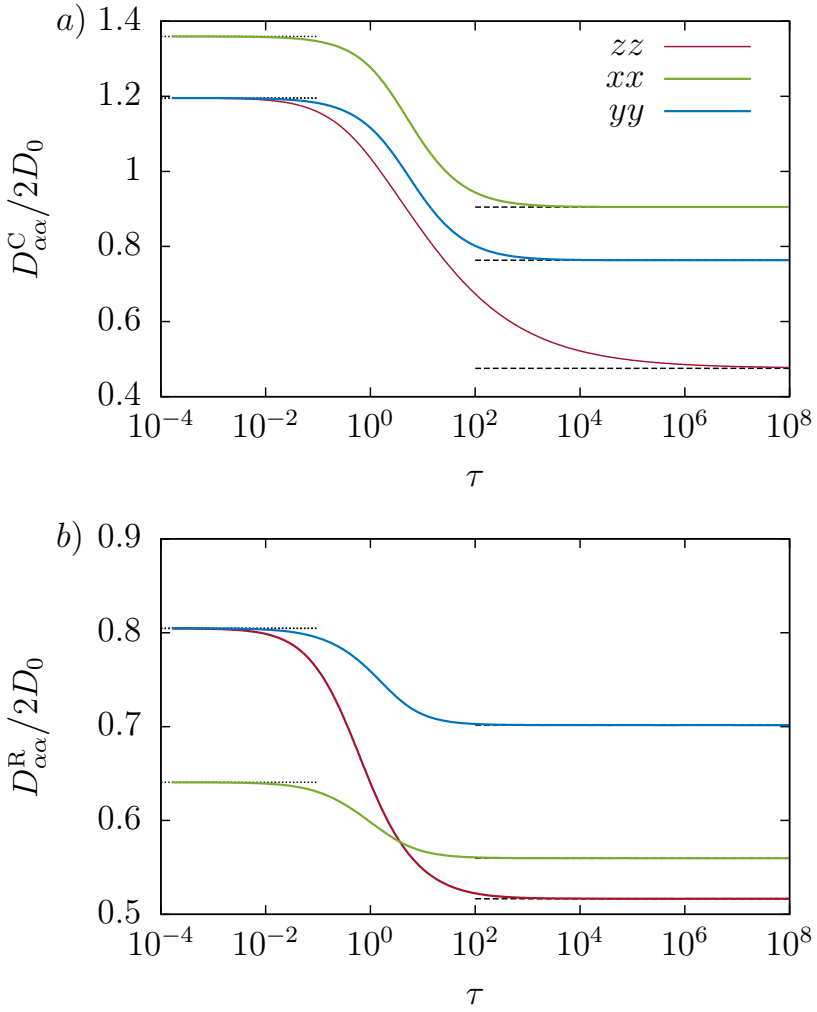

Figure 7: (Color online) The scaled collective (a) and relative (b) diffusion coefficients as defined by Eq. (5.12) versus the scaled time. The horizontal dotted and dashed lines correspond to the bulk and hard-wall limits, respectively.

related parts have large-time tails of t^{-4} and t^{-2}, respectively.

Fig. 6 shows the variations of the zz component of the scaled pair-diffusion coefficient as stated by Eq. (5.16a) upon varying σ. We observe that as σ decreases, i.e. when the two particles stand further apart, the pair-diffusion coefficient can rise and exceed the bulk value for intermediate time scales as hinted on already by the pair-mobility around $\beta \sim 1$ (cf. inset of Fig. 3 a). Such behavior is a clear signature of a short-lived superdiffusive regime.

In Fig. 7 we show the variations of the scaled collective and relative diffusion coefficients as defined by Eq. (5.12), versus the scaled time τ, using the parameters of Fig. 3. At shorter time scales, the particle pair exhibits a normal bulk diffusion, since the motion is hardly affected by the presence of the membrane. As a result, the diffusion coefficients are the same as calculated by Batchelor and given by Eq. (5.13). As the time increases, both diffusion coefficients' curves bend down substantially to asymptotically approach the diffusion coefficients near a hard-wall.

6 Conclusions

We have investigated the hydrodynamic interaction of a finite-size particle pair nearby an elastic membrane endowed with shear and bending rigidity. Using multipole expansions together with Faxén's law, we have provided analytical expressions for the frequency-dependent self- and pair-mobilities. We have demonstrated that shearing and bending contributions may give positive or negative contributions to particle pair-mobilities depending on the inter-particle distance and the pair location above the membrane. Most prominently, we have found that two particles approaching a membrane with only shearing resistance (as is typically assumed for elastic capsules) may experience hydrodynamic attraction in contrast to the well-known case of a hard wall where the interaction is repulsive. This unexpected effect will facilitate chemical reactions near the surface and may possibly even lead to the formation of particle clusters near elastic membranes. On the other hand, membranes with bending resistance (such as vesicles) induce repulsive interactions similar to the hard wall. All our theoretical mobilities are validated by detailed boundary integral simulations.

Using the frequency-dependent particle mobilities, we have computed self- and pair-diffusion coefficients. Most commonly, relative and collective pair-diffusion is subdiffusive on intermediate time scales similar to earlier observations on the diffusion of a single particle [55]. A notable exception is the zz-component of the pair-mobility tensor which for certain parameters and frequencies surpasses its corresponding bulk value. This induces a short-lasting superdiffusive regime in the corresponding mean-square-displacement.

Acknowledgments

The authors gratefully acknowledge funding from the Volkswagen Foundation as well as computing time granted by the Leibniz-Rechenzentrum on SuperMUC.

Appendices

A Derivation of Green's functions

In this appendix, we briefly sketch the derivation of the Green's functions in the presence of an elastic membrane, as stated by Eqs. (2.12a) through (2.12d) of the main text. For the solution of the steady Stokes equations Eqs. (2.10) and (2.11), we use a two-dimensional Fourier transform technique. The variables x and y are transformed into the wavevector components q_x and q_y. Here we use the convention with a negative exponent for the forward Fourier transforms. The transformed equations read

$$\begin{aligned} -q^2\tilde{v}_x + \tilde{v}_{x,zz} + iq_x\tilde{p} + \tilde{F}_x\delta(z-z_0) &= 0\,, \\ -q^2\tilde{v}_y + \tilde{v}_{y,zz} + iq_y\tilde{p} + \tilde{F}_y\delta(z-z_0) &= 0\,, \\ -q^2\tilde{v}_z + \tilde{v}_{z,zz} - \tilde{p}_{,z} + \tilde{F}_z\delta(z-z_0) &= 0\,, \\ -iq_x\tilde{v}_x - iq_y\tilde{v}_y + \tilde{v}_{z,z} &= 0\,, \end{aligned}$$

where a comma in indices denotes the spatial derivative with respect to the following coordinate.

We introduce a new orthonormal system in which the Fourier transformed vectorial quantities are decomposed into longitudinal, transverse and normal components, denoted by $\tilde{v}_l$, $\tilde{v}_t$ and $\tilde{v}_z$ respectively. The corresponding orthonormal in-plane unit vector basis are

$$\boldsymbol{q}_l := \frac{q_x}{q}\boldsymbol{e}_x + \frac{q_y}{q}\boldsymbol{e}_y\,, \quad \boldsymbol{q}_t := \frac{q_y}{q}\boldsymbol{e}_x - \frac{q_x}{q}\boldsymbol{e}_y\,, \tag{A.1}$$

where $q := \sqrt{q_x^2 + q_y^2}$ is the wavenumber. After transformation, the momentum equations become [48]

$$q^2\tilde{v}_t - \tilde{v}_{t,zz} = \frac{\tilde{F}_t}{\eta}\delta(z - z_0)\,, \tag{A.2a}$$

$$\tilde{v}_{z,zzzz} - 2q^2\tilde{v}_{z,zz} + q^4\tilde{v}_z = \frac{q^2\tilde{F}_z}{\eta}\delta(z - z_0) + \frac{iq\tilde{F}_l}{\eta}\delta'(z - z_0)\,, \tag{A.2b}$$

where δ' is the derivative of the Dirac delta function. The longitudinal component $\tilde{v}_l$ is readily determined from $\tilde{v}_z$ via the incompressibility equation (2.11) such that

$$\tilde{v}_l = \frac{i\tilde{v}_{z,z}}{q}\,. \tag{A.3}$$

According to the Skalak [90] and Helfrich [94] models, the linearized tangential and normal traction jumps across the membrane are related to the membrane displacement field $\boldsymbol{u}$ at $z = 0$ by [55]

$$[\sigma_{z\alpha}] = -\frac{\kappa_\mathrm{S}}{3}\left(\Delta_\parallel u_\alpha + (1 + 2C)e_{,\alpha}\right)\,, \quad \alpha \in \{x, y\}\,, \tag{A.4a}$$

$$[\sigma_{zz}] = \kappa_\mathrm{B}\Delta_\parallel^2 u_z\,, \tag{A.4b}$$

where the notation $[w] := w(0^+) - w(0^-)$ designates the jump of the quantity w across the membrane. Here $C := \kappa_\mathrm{A}/\kappa_\mathrm{S}$ is a dimensionless number representing the ratio of the area expansion modulus to shear modulus, and κ_B is the membrane bending modulus. $\Delta_\parallel := \partial_{,xx} + \partial_{,yy}$ denotes the Laplace-Beltrami operator along the membrane and $e := u_{x,x} + u_{y,y}$ is the dilatation function, mathematically defined as the trace of the in-plane strain tensor.

The membrane displacement $\boldsymbol{u}$ as appearing in Eqs. (A.4a) and (A.4b) is related to the fluid velocity by the no-slip boundary condition at the undisplaced membrane which reads

$$\tilde{v}_\alpha = i\omega\tilde{u}_\alpha|_{z=0}\,. \tag{A.5}$$

After solving the transformed equations (A.2a), (A.2b) and (A.3) and properly applying the boundary conditions at the membrane, we find that the diagonal components of the Green's function for $z \geq 0$ read

$$\tilde{\mathcal{G}}_{zz} = \frac{1}{4\eta q}\left((1 + q|z - z_0|)\,e^{-q|z-z_0|} + \left(\frac{i\alpha z z_0 q^3}{1 - i\alpha q} + \frac{i\alpha_\mathrm{B}^3 q^3(1 + qz)(1 + qz_0)}{1 - i\alpha_\mathrm{B}^3 q^3}\right)e^{-q(z+z_0)}\right),$$

$$\tilde{\mathcal{G}}_{ll} = \frac{1}{4\eta q}\left((1 - q|z - z_0|)e^{-q|z-z_0|} + \left(\frac{i\alpha q(1 - qz_0)(1 - qz)}{1 - i\alpha q} + \frac{izz_0\alpha_\mathrm{B}^3 q^5}{1 - i\alpha_\mathrm{B}^3 q^3}\right)e^{-q(z+z_0)}\right),$$

$$\tilde{\mathcal{G}}_{tt} = \frac{1}{2\eta q}\left(e^{-q|z-z_0|} + \frac{iB\alpha q}{2 - iB\alpha q}e^{-q(z+z_0)}\right),$$

and the off-diagonal component $\tilde{\mathcal{G}}_{lz}$ reads

$$\tilde{\mathcal{G}}_{lz} = \frac{i}{4\eta q}\left(-q(z - z_0)e^{-q|z-z_0|} + \left(\frac{i\alpha z_0 q^2(1 - qz)}{1 - i\alpha q} - \frac{i\alpha_\mathrm{B}^3 z q^4(1 + qz_0)}{1 - i\alpha_\mathrm{B}^3 q^3}\right)e^{-q(z+z_0)}\right),$$

where $\alpha := \kappa_\mathrm{S}/(3B\eta\omega)$ is a characteristic length scale for shearing and area expansion with $B := 2/(1 + C)$, and $\alpha_\mathrm{B} := (\kappa_\mathrm{B}/(4\eta\omega))^{1/3}$ is a characteristic length scale for bending. Furthermore, $\tilde{\mathcal{G}}_{tz} = \tilde{\mathcal{G}}_{zt} = 0$ because of the decoupled nature of Eqs. (A.2a) and (A.2b). Employing the transformation equations

(A.1) back to the usual Cartesian basis, we obtain

$$\begin{aligned}\tilde{\mathcal{G}}_{xx}(\boldsymbol{q},z,\omega) &= \tilde{\mathcal{G}}_{ll}(q,z,\omega)\cos^2\phi + \tilde{\mathcal{G}}_{tt}(q,z,\omega)\sin^2\phi\,,\\ \tilde{\mathcal{G}}_{yy}(\boldsymbol{q},z,\omega) &= \tilde{\mathcal{G}}_{ll}(q,z,\omega)\sin^2\phi + \tilde{\mathcal{G}}_{tt}(q,z,\omega)\cos^2\phi\,,\\ \tilde{\mathcal{G}}_{xz}(\boldsymbol{q},z,\omega) &= \tilde{\mathcal{G}}_{lz}(q,z,\omega)\cos\phi\,,\end{aligned}$$

where $\phi := \arctan(q_y/q_x)$.

The components $\tilde{\mathcal{G}}_{yz}$ and $\tilde{\mathcal{G}}_{zy}$ are irrelevant for our discussion because the resulting mobilities vanish, thus they are omitted here. In addition, the component $\tilde{\mathcal{G}}_{zx}$ leads to the same mobility as $\tilde{\mathcal{G}}_{xz}$ because of the symmetry of the mobility tensor. Furthermore, we define

$$\tilde{\mathcal{G}}_{\pm}(q,z,\omega) := \tilde{\mathcal{G}}_{tt}(q,z,\omega) \pm \tilde{\mathcal{G}}_{ll}(q,z,\omega)\,.$$

Eqs. (2.12a)-(2.12d) of the main text follow immediately after performing the two dimensional inverse spatial Fourier transform of the Green's function [107].

B Vanishing frequency behavior

In the following, analytical expressions of the shearing and bending related parts in the particle self- and pair-mobilities are provided in the vanishing frequency limit.

B.1 Self mobilities

By taking the vanishing frequencies limit in Eqs. (4.1a) and (4.1b), the shearing and bending related corrections for the perpendicular motion read

$$\begin{aligned}\lim_{\beta\to 0}\frac{\Delta\mu^{\mathrm{S}}_{zz,\mathrm{S}}}{\mu_0} &= -\frac{3}{16}\epsilon + \frac{3}{16}\epsilon^3 - \frac{1}{16}\epsilon^5\,,\\ \lim_{\beta_{\mathrm{B}}\to 0}\frac{\Delta\mu^{\mathrm{S}}_{zz,\mathrm{B}}}{\mu_0} &= -\frac{15}{16}\epsilon + \frac{5}{16}\epsilon^3 - \frac{1}{16}\epsilon^5\,,\end{aligned}$$

leading to the hard-wall limit Eq. (4.2) after summing up both contributions term by term. Similarly, for the parallel motion, by taking the vanishing frequency limit in Eqs. (4.3a) and (4.3b) we get

$$\begin{aligned}\lim_{\beta\to 0}\frac{\Delta\mu^{\mathrm{S}}_{xx,\mathrm{S}}}{\mu_0} &= -\frac{15}{32}\epsilon + \frac{1}{32}\epsilon^3 - \frac{1}{32}\epsilon^5\,,\\ \lim_{\beta_{\mathrm{B}}\to 0}\frac{\Delta\mu^{\mathrm{S}}_{xx,\mathrm{B}}}{\mu_0} &= -\frac{3}{32}\epsilon + \frac{3}{32}\epsilon^3 - \frac{1}{32}\epsilon^5\,,\end{aligned}$$

which also give the hard-wall limit Eq. (4.4) when summing up both parts.

B.2 Pair mobilities

By considering independently the shearing and bending related parts in the pair-mobility corrections as given by Eqs. (4.6a) through (4.6d), and taking the vanishing frequency limit, we obtain for the

shearing part

$$\lim_{\beta\to 0}\frac{\Delta\mu^{\mathrm{P}}_{zz,\mathrm{S}}}{\mu_0} = -\frac{3}{16}\frac{\xi(2\xi-1)}{(1+\xi)^{5/2}}\sigma + \frac{3}{4}\frac{\xi(2\xi-3)}{(1+\xi)^{7/2}}\sigma^3 - \frac{2\xi^2-6\xi+\frac{3}{4}}{(1+\xi)^{9/2}}\sigma^5\,, \tag{B.1a}$$

$$\lim_{\beta\to 0}\frac{\Delta\mu^{\mathrm{P}}_{xx,\mathrm{S}}}{\mu_0} = -\frac{3}{16}\frac{5\xi^2+10\xi+8}{(1+\xi)^{5/2}}\sigma + \frac{1}{4}\frac{\xi^2-10\xi+4}{(1+\xi)^{7/2}}\sigma^3 - \frac{\xi^2-\frac{27}{4}\xi+1}{(1+\xi)^{9/2}}\sigma^5\,, \tag{B.1b}$$

$$\lim_{\beta\to 0}\frac{\Delta\mu^{\mathrm{P}}_{yy,\mathrm{S}}}{\mu_0} = -\frac{3}{16}\frac{5\xi+4}{(1+\xi)^{3/2}}\sigma + \frac{1}{4}\frac{\xi-2}{(1+\xi)^{5/2}}\sigma^3 - \frac{\xi-\frac{1}{4}}{(1+\xi)^{7/2}}\sigma^5\,, \tag{B.1c}$$

$$\lim_{\beta\to 0}\frac{\Delta\mu^{\mathrm{P}}_{xz,\mathrm{S}}}{\mu_0} = \frac{3}{16}\frac{(\xi-2)\xi^{1/2}}{(1+\xi)^{5/2}}\sigma - \frac{3}{4}\frac{(3\xi-2)\xi^{1/2}}{(1+\xi)^{7/2}}\sigma^3 + \frac{5}{4}\frac{(4\xi-3)\xi^{1/2}}{(1+\xi)^{9/2}}\sigma^5\,, \tag{B.1d}$$

and for the bending part

$$\lim_{\beta_{\mathrm{B}}\to 0}\frac{\Delta\mu^{\mathrm{P}}_{zz,\mathrm{B}}}{\mu_0} = -\frac{3}{16}\frac{10\xi^2+11\xi+4}{(1+\xi)^{5/2}}\sigma + \frac{1}{4}\frac{10\xi^2-7\xi-2}{(1+\xi)^{7/2}}\sigma^3 - \frac{2\xi^2-6\xi+\frac{3}{4}}{(1+\xi)^{9/2}}\sigma^5\,, \tag{B.2a}$$

$$\lim_{\beta_{\mathrm{B}}\to 0}\frac{\Delta\mu^{\mathrm{P}}_{xx,\mathrm{B}}}{\mu_0} = -\frac{3}{16}\frac{\xi(\xi-2)}{(1+\xi)^{5/2}}\sigma + \frac{3}{4}\frac{\xi(\xi-4)}{(1+\xi)^{7/2}}\sigma^3 - \frac{\xi^2-\frac{27}{4}\xi+1}{(1+\xi)^{9/2}}\sigma^5\,, \tag{B.2b}$$

$$\lim_{\beta_{\mathrm{B}}\to 0}\frac{\Delta\mu^{\mathrm{P}}_{yy,\mathrm{B}}}{\mu_0} = -\frac{3}{16}\frac{\xi}{(1+\xi)^{3/2}}\sigma + \frac{3}{4}\frac{\xi}{(1+\xi)^{5/2}}\sigma^3 - \frac{\xi-\frac{1}{4}}{(1+\xi)^{7/2}}\sigma^5\,, \tag{B.2c}$$

$$\lim_{\beta_{\mathrm{B}}\to 0}\frac{\Delta\mu^{\mathrm{P}}_{xz,\mathrm{B}}}{\mu_0} = \frac{3}{16}\frac{(5\xi+2)\xi^{1/2}}{(1+\xi)^{5/2}}\sigma - \frac{15}{4}\frac{\xi^{3/2}}{(1+\xi)^{7/2}}\sigma^3 + \frac{5}{4}\frac{(4\xi-3)\xi^{1/2}}{(1+\xi)^{9/2}}\sigma^5\,. \tag{B.2d}$$

The total correction as given by Eqs. (4.8a) through (4.8d) is recovered by summing up term by term both contributions.

Bibliography

[1] J. A. Morrone, J. Li, and B. J. Berne, J. Phys. Chem. B **116**, 378 (2012).

[2] O. B. Usta, A. J. C. Ladd, and J. E. Butler, J. Chem. Phys. **122**, 094902 (2005).

[3] M. Wojciechowski, P. Szymczak, and M. Cieplak, Phys. Biol. **7**, 046011 (2010).

[4] Y. von Hansen, R. R. Netz, and M. Hinczewski, J. Chem. Phys. **132**, 135103 (2010).

[5] M. Długosz, J. M. Antosiewicz, P. Zieliński, and J. Trylska, J. Phys. Chem. B **116**, 5437 (2012).

[6] T. Ando and J. Skolnick, Biophys. J. **104**, 96 (2013).

[7] A. S. Popel and P. C. Johnson, Annu. Rev. Fluid Mech. **37**, 43 (2005).

[8] C. Misbah and C. Wagner, C. R. Physique **14**, 447 (2013).

[9] J. J. Molina, Y. Nakayama, and R. Yamamoto, Soft Matter **9**, 4923 (2013).

[10] H. H. Wensink, J. Dunkel, S. Heidenreich, K. Drescher, R. E. Goldstein, H. Löwen, and J. M. Yeomans, Proc. Natl. Acad. Sci. **109**, 14308 (2012).

[11] J. Dunkel, S. Heidenreich, K. Drescher, H. H. Wensink, M. Bär, and R. E. Goldstein, Phys. Rev. Lett. **110**, 228102 (2013).

[12] D. Lopez and E. Lauga, Phys. Fluids **26**, 071902 (2014).

[13] A. Zöttl and H. Stark, Phys. Rev. Lett. **112**, 118101 (2014).

[14] J. Elgeti, R. G. Winkler, and G. Gompper, Rep. Prog. Phys. **78**, 056601 (2015).

[15] É. Guazzelli and J. F. Morris, *A physical introduction to suspension dynamics* (Cambridge University Press, 2012).

[16] A. E. Larsen, D. G. Grier, *et al.*, Nature **385**, 230 (1997).

[17] T. M. Squires and M. P. Brenner, Phys. Rev. Lett. **85**, 4976 (2000).

[18] S. H. Behrens and D. G. Grier, Phys. Rev. E **64**, 050401 (2001).

[19] B. U. Felderhof, Physica A **89**, 373 (1977).

[20] S. Kim and R. T. Mifflin, Phys. Fluids **28**, 2033 (1985).

[21] B. J. Yoon and S. Kim, J. Fluid Mech. **185**, 437 (1987).

[22] B. Cichocki, B. U. Felderhof, and R. Schmitz, PhysicoChem. Hyd **10**, 383 (1988).

[23] J. Happel and H. Brenner, *Low Reynolds number hydrodynamics: with special applications to particulate media*, Vol. 1 (Springer Science & Business Media, 2012).

[24] J. M. Deutch and I. Oppenheim, J. Chem. Phys. **54**, 3547 (1971).

[25] G. K. Batchelor, J. Fluid Mech. **74**, 1 (1976).

[26] D. L. Ermak and J. McCammon, J. Chem. Phys. **69**, 1352 (1978).

[27] A. J. C. Ladd, J. Chem. Phys. **88**, 5051 (1988).

[28] M. L. Ekiel-Jeżewska and B. U. Felderhof, J. Chem. Phys. **142**, 014904 (2015).

[29] R. N. Zia, J. W. Swan, and Y. Su, J. Chem. Phys. **143**, 224901 (2015).

[30] J. C. Crocker, J. Chem. Phys. **106**, 2837 (1997).

[31] J.-C. Meiners and S. R. Quake, Phys. Rev. Lett. **82**, 2211 (1999).

[32] P. Bartlett, S. I. Henderson, and S. J. Mitchell, Phil. Trans. R. Soc. A **359**, 883 (2001).

[33] S. Henderson, S. Mitchell, and P. Bartlett, Phys. Rev. Lett. **88**, 088302 (2002).

[34] M. Radiom, B. Robbins, M. Paul, and W. Ducker, Phys. Fluids **27**, 022002 (2015).

[35] E. Lauga and T. M. Squires, Phys. Fluids **17** (2005).

[36] H. A. Lorentz, Abh. Theor. Phys. **1**, 23 (1907).

[37] G. D. M. MacKay and S. G. Mason, J. Colloid Sci. **16**, 632 (1961).

[38] T. Gotoh and Y. Kaneda, J. Chem. Phys. **76**, 3193 (1982).

[39] B. Cichocki and R. B. Jones, Physica A **258**, 273 (1998).

[40] T. Franosch and S. Jeney, Phys. Rev. E **79**, 031402 (2009).

[41] B. U. Felderhof, Phys. Rev. E **85**, 046303 (2012).

[42] J. T. Padding and W. J. Briels, J. Chem. Phys. **132**, 054511 (2010).

[43] M. De Corato, F. Greco, G. D'Avino, and P. L. Maffettone, J. Chem. Phys. **142** (2015).

[44] K. Huang and I. Szlufarska, Nat. Comm. **6** (2015).

[45] S. H. Lee, R. S. Chadwick, and L. G. Leal, J. Fluid Mech. **93**, 705 (1979).

[46] C. Berdan and L. G. Leal, J. Colloid Interface Sci. **87**, 62 (1982).

[47] T. Bickel, Eur. Phys. J. E **20**, 379 (2006).

[48] T. Bickel, Phys. Rev. E **75**, 041403 (2007).

[49] J. Bławzdziewicz, M. Ekiel-Jeżewska, and E. Wajnryb, J. Chem. Phys. **133**, 114703 (2010).

[50] J. Bławzdziewicz, M. L. Ekiel-Jeżewska, and E. Wajnryb, J. Chem. Phys. **133** (2010).

[51] B. U. Felderhof, J. Chem. Phys. **125**, 144718 (2006).

[52] R. Shlomovitz, A. Evans, T. Boatwright, M. Dennin, and A. Levine, Phys. Rev. Lett. **110**, 137802 (2013).

[53] R. Shlomovitz, A. A. Evans, T. Boatwright, M. Dennin, and A. J. Levine, Phys. Fluids **26**, 071903 (2014).

[54] T. Salez and L. Mahadevan, J. Fluid Mech. **779**, 181 (2015).

[55] A. Daddi-Moussa-Ider, A. Guckenberger, and S. Gekle, Phys. Rev. E **93**, 012612 (2016).

[56] A. Daddi-Moussa-Ider, A. Guckenberger, and S. Gekle, Phys. Fluids **28**, 071903 (2016).

[57] B. Saintyves, T. Jules, T. Salez, and L. Mahadevan, Proc. Nat. Acad. Sci. **113**, 5847 (2016).

[58] L. P. Faucheux and A. J. Libchaber, Phys. Rev. E **49**, 5158 (1994).

[59] E. R. Dufresne, D. Altman, and D. G. Grier, Europhys. Lett. **53**, 264 (2001).

[60] E. Schäffer, S. F. Nørrelykke, and J. Howard, Langmuir **23**, 3654 (2007).

[61] P. Holmqvist, J. K. G. Dhont, and P. R. Lang, J. Chem. Phys. **126**, 044707 (2007).

[62] V. N. Michailidou, G. Petekidis, J. W. Swan, and J. F. Brady, Phys. Rev. Lett. **102**, 068302 (2009).

[63] G. M. Wang, R. Prabhakar, and E. M. Sevick, Phys. Rev. Lett. **103**, 248303 (2009).

[64] Y. Kazoe and M. Yoda, Appl. Phys. Lett. **99**, 124104 (2011).

[65] M. Lisicki, B. Cichocki, J. K. G. Dhont, and P. R. Lang, J. Chem. Phys. **136**, 204704 (2012).

[66] S. A. Rogers, M. Lisicki, B. Cichocki, J. K. G. Dhont, and P. R. Lang, Phys. Rev. Lett. **109**, 098305 (2012).

[67] V. N. Michailidou, J. W. Swan, J. F. Brady, and G. Petekidis, J. Chem. Phys. **139**, 164905 (2013).

[68] W. Wang and P. Huang, Phys. Fluids **26**, 092003 (2014).

[69] T. Watarai and T. Iwai, Appl. Phys. Express **7**, 032502 (2014).

[70] M. Lisicki, B. Cichocki, S. A. Rogers, J. K. G. Dhont, and P. R. Lang, Soft Matter **10**, 4312 (2014).

[71] H. B. Eral, J. M. Oh, D. van den Ende, F. Mugele, and M. H. G. Duits, Langmuir **26**, 16722 (2010).

[72] A. E. Cervantes-Martínez, A. Ramírez-Saito, R. Armenta-Calderón, M. A. Ojeda-López, and J. L. Arauz-Lara, Phys. Rev. E **83**, 030402 (2011).

[73] S. L. Dettmer, S. Pagliara, K. Misiunas, and U. F. Keyser, Phys. Rev. E **89**, 062305 (2014).

[74] M. Irmscher, A. M. de Jong, H. Kress, and M. W. J. Prins, Biophys. J. **102**, 698 (2012).

[75] T. Boatwright, M. Dennin, R. Shlomovitz, A. A. Evans, and A. J. Levine, Phys. Fluids **26**, 071904 (2014).

[76] F. Jünger, F. Kohler, A. Meinel, T. Meyer, R. Nitschke, B. Erhard, and A. Rohrbach, Biophys. J. **109**, 869 (2015).

[77] J. W. Swan and J. F. Brady, Phys. Fluids **19**, 113306 (2007).

[78] P. P. Lele, J. W. Swan, J. F. Brady, N. J. Wagner, and E. M. Furst, Soft Matter **7**, 6844 (2011).

[79] B. Tränkle, D. Ruh, and A. Rohrbach, Soft Matter (2016).

[80] E. R. Dufresne, T. M. Squires, M. P. Brenner, and D. G. Grier, Phys. Rev. Lett. **85**, 3317 (2000).

[81] B. Cui, H. Diamant, and B. Lin, Phys. Rev. Lett. **89**, 188302 (2002).

[82] K. Misiunas, S. Pagliara, E. Lauga, J. R. Lister, and U. F. Keyser, Phys. Rev. Lett. **115**, 038301 (2015).

[83] J. Bleibel, A. Domínguez, F. Günther, J. Harting, and M. Oettel, Soft Matter **10**, 2945 (2014).

[84] W. Zhang, S. Chen, N. Li, J. Zhang, and W. Chen, Appl. Phys. Lett. **103**, 154102 (2013).

[85] W. Zhang, S. Chen, N. Li, J. Zhang, and W. Chen, PloS one **9**, e85173 (2014).

[86] S. Kim and S. J. Karrila, *Microhydrodynamics: principles and selected applications* (Dover Publications, Inc. Mineola, New York, 2005).

[87] Y. W. Kim and R. R. Netz, J. Chem. Phys. **124**, 114709 (2006).

[88] E. Gauger, M. T. Downton, and H. Stark, Eur. Phys. J. E **28**, 231 (2008).

[89] J. W. Swan and J. F. Brady, Phys. Fluids **22**, 103301 (2010).

[90] R. Skalak, A. Tozeren, R. P. Zarda, and S. Chien, Biophys. J. **13(3)**, 245 (1973).

[91] C. D. Eggleton and A. S. Popel, Phys. Fluids **10**, 1834 (1998).

[92] T. Krüger, F. Varnik, and D. Raabe, Computers and Mathematics with Applications **61**, 3485 (2011).

[93] T. Krüger, *Computer simulation study of collective phenomena in dense suspensions of red blood cells under shear* (Springer Science & Business Media, 2012).

[94] W. Helfrich, Z. Naturef. C. **28:693** (1973).

[95] C. Pozrikidis, J. Comput. Phys. **169**, 250 (2001).

[96] H. Zhao and E. S. G. Shaqfeh, Phys. Rev. E **83**, 061924 (2011).

[97] H. Power and G. Miranda, SIAM J. on App. Math. **47**, pp. 689 (1987).

[98] M. Kohr and I. Pop, AMC **10**, 12 (2004).

[99] H. Zhao, E. S. G. Shaqfeh, and V. Narsimhan, Phys. Fluids **24** (2012).

[100] Y. Saad and M. H. Schultz, SIAM J. Sci. Comput. **7**, 856 (1986).

[101] A. Guckenberger, M. P. Schraml, P. G. Chen, M. Leonetti, and S. Gekle, Comp. Phys. Comm. **207**, 1 (2016).

[102] A. R. Conn, N. I. M. Gould, and P. L. Toint, *Trust region methods*, Vol. 1 (Siam, 2000).

[103] M. Abramowitz, I. A. Stegun, *et al.*, *Handbook of mathematical functions*, Vol. 1 (Dover New York, 1972).

[104] See Supplemental Material at http://dx.doi.org/10.1063/1.4955099 for the frequency-dependent mobilities where typical values for the RBC parameters are used.

[105] H. Faxén, Ann. Phys. **373**, 89 (1922).

[106] J. Rotne and S. Prager, J. Chem. Phys. **50**, 4831 (1969).

[107] R. Bracewell, *The Fourier Transform and Its Applications* (McGraw-Hill, 1999).

[108] R. Kubo, Rep. Prog. Phys. **29**, 255 (1966).

[109] R. Kubo, M. Toda, and N. Hashitsume, "Statistical physics II," (1985).

[110] S. Kheifets, A. Simha, K. Melin, T. Li, and M. G. Raizen, Science **343**, 1493 (2014).

[111] In Ref. [109], a factor 2π appears in the denominator of Eq. (5.6) in contrast to the present work, as they consider the factor 2π in the forward Fourier transform (left-hand side) and we consider it in the inverse transform while the Laplace transform (right-hand side) is defined identically.

Publication 4

Hydrodynamic coupling and rotational mobilities nearby planar elastic membranes

A. Daddi-Moussa-Ider and S. Gekle

In preparation (2017)

Abstract

In this paper, we study the coupling and rotational hydrodynamic interactions between spherical particles nearby a planar elastic membrane exhibiting resistance towards shearing and bending. Using a combination of the multipole expansion and Faxén's theorem, we express the frequency-dependent hydrodynamic mobility functions as power series of the ratio between particle radius and distance from the membrane as well as between radius and interparticle distance. We find that the shearing and bending related contributions to the particle mobility may undergo under some circumstances a change of sign. As a model system for bacterial locomotion, we study the rotational motion of a torque-free doublet nearby an elastic membrane, finding that the steady rotation rate around its center of mass may differ in magnitude and direction depending on membrane shearing and bending properties. Nearby a membrane with pure shearing, the doublet undergoes clockwise rotation i.e. in the same way as observed nearby a no-slip wall. Nearby a membrane with pure bending however, we find that the doublet rotates counterclockwise. Our analytical predictions are supplemented and compared with fully resolved boundary integral simulations where a very good agreement is obtained.

1 Introduction

The dynamics of elastic membranes is important for understanding the biological functions and transport properties in living cells [1–4]. The assessment of hydrodynamic interactions between membranes and suspended tracer particles can be used as a monitor for determining the membrane mechanical properties via interfacial microrheology measurements [5–10]. The method has the advantage of being non-destructive and has extensively been employed for the determination of viscous and elastic moduli [11–14] and the characterization of fluctuating forces in complex fluids [15, 16].

At small length and time scales of motion, an accurate description of the fluid flow surrounding the particles is well achieved by the linear Stokes equations [17]. In these conditions, a complete description of particle motion is possible via the hydrodynamic mobility tensor, which bridges between the translational and rotational velocities of the suspended particles and the forces and torques applied on their surfaces. Particle motion in an unbounded medium is well understood and has been studied since a long time ago [18]. However, motion in real situations often occurs in geometric confinements, where the hydrodynamic mobility is notably changed relative to its value in a bulk fluid.

During the past few decades, the field knew greater interest among physicists after the advent of elaborate experimental techniques which allow an accurate and reliable measurement of particle mobility nearby interfaces. Among the most efficient techniques that have been utilized are laser [19, 20] and optical tweezers [21–26], fluorescence [27, 28] and digital video microscopy [29–33], evanescent wave dynamic light scattering [34–47] and three-dimensional total internal reflection velocimetry technique [48]. Calculations of mobility functions have been carried out to include particles nearby hard-walls [49–62], interfaces with partial slip [63–65], an interface separating two mutually immiscible liquids [66–71], inside a liquid film between two fluids [72] or nearby a spherical drop [73, 74]. Further works have examined particle dynamics nearby viscous interfaces [75–77] or an interface covered with surfactant [78–84].

More recently, particle motion close to membranes with surface elasticity has been attracted researchers' attention, due to their relevance as realistic models for cell membranes [85–88]. Unlike fluid-solid or fluid-fluid interfaces, elastic membranes stand apart as they endow the system with memory. Accordingly, the motion of the particles depend strongly on their prior history and their diffusional dynamics is treated within a generalized Langevin formalism. This implies the emergence of a long-lived subdiffusive behavior [89–92] induced by the membrane on nearby particles. Particle motion nearby elastic cell membranes has been experimentally investigated using optical traps [93–96], magnetic particle actuation [97] and quasi-elastic light scattering [98–100], where a significant

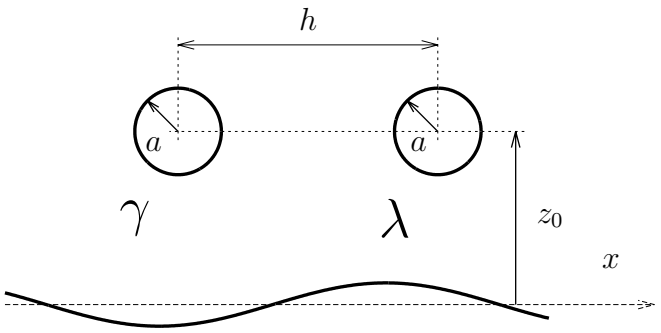

Figure 1: Illustration of the system setup. A sample configuration of a pair of particles labeled γ and λ, located a distance h apart and a distance z_0 above an elastic cell membrane. Here $\boldsymbol{x}_\gamma = (0, 0, z_0)$ and $\boldsymbol{x}_\lambda = (h, 0, z_0)$. We define the dimensionless parameters of the system $\epsilon := a/z_0$ and $\sigma := a/h$.

decrease in the mobility normal to the cell membrane has been observed in line with theoretical predictions.

In our earlier work [101], we have studied analytically and numerically the hydrodynamic interactions between spherical particles undergoing translational motion nearby a planar elastic membrane. We have found that the steady approach of two particles towards an idealized membrane with pure shearing resistance may lead to attractive interactions, in contrast to the behavior know nearby a hard-wall where the interaction is know to be repulsive [102]. In this paper, we complete and supplement our analysis by computing the hydrodynamic coupling and rotational mobilities of a pair of particles moving nearby a realistically modeled red blood cell membrane. We model the membrane using the Skalak model [103] for shearing and area dilatation, and the Helfrich model [104] for bending. We find that the contributions due to shearing and bending of the particle self- and pair-mobilities may have additive or suppressive effects depending on the membrane properties and the relative separation between the interacting particles and the membrane. More importantly, we find that the magnitude and direction of rotation of a torque-free doublet of particles about their center of mass, which can be seen as a model system for bacterial swimming, is strongly dictated by membrane shearing and bending properties.

The remainder of the paper is organized as follows. In Sec. 2 we present the theoretical framework we use to analytically compute the particle mobility functions by combining the multipole expansion and Faxén's theorem. In Sec. 3 we present the completed double layer boundary integral method and the approach we have employed to numerically compute the hydrodynamic mobilities. Sec. 4 provides explicit analytical expressions of the frequency-dependent coupling and rotational self- and pair-mobilities together with a close comparison with numerical simulations where a very good agreement is obtained. Concluding remarks summarizing our findings and results are offered in Sec. 5.

2 Mathematical model

We consider a suspension of N solid spherical particles of radius a immersed in an incompressible Newtonian fluid of viscosity η moving nearby a planar elastic membrane infinitely extended in the xy plane. We assume that the fluid surrounding the particles is at rest. The creeping flow of the

suspending fluid is governed by the forced Stokes equations [18]

$$\eta \boldsymbol{\nabla}^2 \boldsymbol{v} - \boldsymbol{\nabla} p + \sum_{\alpha=1}^{N} \boldsymbol{f}_\alpha = 0\,, \tag{2.1}$$

$$\boldsymbol{\nabla} \cdot \boldsymbol{v} = 0\,, \tag{2.2}$$

where $\boldsymbol{v}$ and p are the velocity and pressure fields, respectively. Here $\boldsymbol{f}_\alpha$ is an arbitrary time dependent force density acting on the fluid due to the presence of the particle α. We denote by $\boldsymbol{\mu}$ the mobility tensor which couples between the velocity moments of the particles to the moments of the force density on the particle surfaces, [17]

$$\begin{pmatrix} \boldsymbol{V} \\ \boldsymbol{\Omega} \end{pmatrix} = \begin{pmatrix} \boldsymbol{\mu}^{tt} & \boldsymbol{\mu}^{tr} \\ \boldsymbol{\mu}^{rt} & \boldsymbol{\mu}^{rr} \end{pmatrix} \begin{pmatrix} \boldsymbol{F} \\ \boldsymbol{L} \end{pmatrix}\,, \tag{2.3}$$

where $\boldsymbol{V}$ and $\boldsymbol{\Omega}$ are the translational and rotational velocities, respectively, and $\boldsymbol{F}$ and $\boldsymbol{L}$ are the hydrodynamic force and torque on the particles. The off-diagonal components are the hydrodynamic coupling mobilities between torque and translation (tr) and between force and rotation (rt) and they are the transpose of each other.

2.1 Multipole expansion and Faxén's theorem

We now consider a representative configuration of a pair of particles denoted γ and λ located a distance h apart and a distance z_0 above an elastic membrane, as schematically sketched in Fig. 1. The fluid on both sides of the membrane is assumed to have the same properties. The disturbance velocity field caused at any observation point $\boldsymbol{r}$ by a particle labeled λ located at $\boldsymbol{r}_\lambda$ can be written as

$$\boldsymbol{v}(\boldsymbol{r}, \boldsymbol{r}_\lambda, \omega) = \boldsymbol{v}^{(0)}(\boldsymbol{r}, \boldsymbol{r}_\lambda) + \boldsymbol{v}^{*}(\boldsymbol{r}, \boldsymbol{r}_\lambda, \omega)\,, \tag{2.4}$$

where $\boldsymbol{v}^{(0)}$ denotes the fluid flow in an unbounded (infinite) fluid and $\boldsymbol{v}^*$ is the flow field required to satisfy the boundary conditions at the membrane. Here all the quantities are Fourier transformed into the frequency space. The disturbance field can be written as an integral over the surface of the sphere λ as

$$\boldsymbol{v}(\boldsymbol{r}, \boldsymbol{r}_\lambda, \omega) = \oint_{S_\lambda} \boldsymbol{\mathcal{G}}(\boldsymbol{r}, \boldsymbol{r}', \omega) \cdot \boldsymbol{f}_\lambda(\boldsymbol{r}', \omega)\, \mathrm{d}^2\boldsymbol{r}'\,, \tag{2.5}$$

where $\boldsymbol{\mathcal{G}}$ denotes the velocity Green's function (Stokeslet), i.e. the flow velocity field resulting from a point-force acting on $\boldsymbol{r}_\lambda$. Similar, the Green's function can be split up into two distinct contributions,

$$\boldsymbol{\mathcal{G}}(\boldsymbol{r}, \boldsymbol{r}', \omega) = \boldsymbol{\mathcal{G}}^{(0)}(\boldsymbol{r}, \boldsymbol{r}') + \boldsymbol{\mathcal{G}}_{\mathrm{M}}(\boldsymbol{r}, \boldsymbol{r}', \omega)\,, \tag{2.6}$$

where $\boldsymbol{\mathcal{G}}^{(0)}$ is the infinite-space Green's function (Oseen's tensor)

$$\mathcal{G}^{(0)}_{\alpha\beta}(\boldsymbol{r}, \boldsymbol{r}') = \frac{1}{8\pi\eta} \left(\frac{\delta_{\alpha\beta}}{s} + \frac{s_\alpha s_\beta}{s^3} \right)\,, \tag{2.7}$$

with $\boldsymbol{s} := \boldsymbol{r} - \boldsymbol{r}'$ and $s := |\boldsymbol{s}|$. The second term $\boldsymbol{\mathcal{G}}_{\mathrm{M}}$ represents the frequency-dependent correction to the Green's function due to the presence of the membrane.

Far away from the particle λ, the integration vector variable $\boldsymbol{r}'$ in Eq. (2.5) can be expanded around the particle center $\boldsymbol{r}_\lambda$ following a multipole expansion approach. Up to the second order, and assuming a constant force density over the particle surface, the disturbance velocity can be

approximated by [60, 61]

$$\boldsymbol{v}(\boldsymbol{r},\boldsymbol{r}_\lambda,\omega) \approx \left(1+\frac{a^2}{6}\boldsymbol{\nabla}^2_{\boldsymbol{r}_\lambda}\right)\boldsymbol{\mathcal{G}}(\boldsymbol{r},\boldsymbol{r}_\lambda,\omega)\cdot\boldsymbol{F}(\omega)+\frac{1}{2}\,\boldsymbol{\nabla}_{\boldsymbol{r}_\lambda}\times\boldsymbol{\mathcal{G}}(\boldsymbol{r},\boldsymbol{r}_\lambda,\omega)\cdot\boldsymbol{L}(\omega)\,, \tag{2.8}$$

where $\boldsymbol{\nabla}_{\boldsymbol{r}_\lambda}$ stands for the gradient operator taken with respect to the singularity position $\boldsymbol{r}_\lambda$ and the curl of a given tensor $\boldsymbol{\mathcal{T}}$ is obtained as [105]

$$(\boldsymbol{\nabla}\times\boldsymbol{\mathcal{T}})_{\alpha\beta}=\epsilon_{\alpha\mu\nu}\partial_\mu\mathcal{T}_{\nu\beta}\,, \tag{2.9}$$

with $\epsilon_{\alpha\mu\nu}$ being the Levi-Civita tensor. Note that for a single sphere in bulk, the flow field given by Eq. (2.8) satisfies exactly the no-slip boundary conditions at the surface of the sphere [106]. Using Faxén's theorem [107], the translational and rotational velocities of the particle γ in this flow reads [60, 61]

$$\boldsymbol{V}_\gamma(\omega)=\mu_0^{tt}\boldsymbol{F}_\gamma(\omega)+\left(1+\frac{a^2}{6}\boldsymbol{\nabla}^2_{\boldsymbol{r}_\gamma}\right)\boldsymbol{v}(\boldsymbol{r}_\gamma,\boldsymbol{r}_\lambda,\omega)\,, \tag{2.10}$$

$$\boldsymbol{\Omega}_\gamma(\omega)=\mu_0^{rr}\boldsymbol{L}_\gamma(\omega)+\frac{1}{2}\,\boldsymbol{\nabla}_{\boldsymbol{r}_\gamma}\times\boldsymbol{v}(\boldsymbol{r}_\gamma,\boldsymbol{r}_\lambda,\omega)\,, \tag{2.11}$$

where $\mu_0^{tt}:=1/(6\pi\eta a)$ and $\mu_0^{rr}:=1/(8\pi\eta a^3)$ denote the translational and rotational bulk mobilities, respectively. We further emphasize that the disturbance flow $\boldsymbol{v}$ incorporates both the disturbance from the particle λ and the disturbance caused by the presence of the membrane. By inserting Eq. (2.8) into Faxén's formula stated by Eqs. (2.10) and (2.11), the frequency-dependent translational, coupling and rotational pair-mobility tensors can be obtained from

$$\boldsymbol{\mu}^{tt,\gamma\lambda}(\omega)=\left(1+\frac{a^2}{6}\boldsymbol{\nabla}^2_{\boldsymbol{r}_\gamma}\right)\left(1+\frac{a^2}{6}\boldsymbol{\nabla}^2_{\boldsymbol{r}_\lambda}\right)\boldsymbol{\mathcal{G}}(\boldsymbol{r}_\gamma,\boldsymbol{r}_\lambda,\omega)\,, \tag{2.12}$$

$$\boldsymbol{\mu}^{tr,\gamma\lambda}(\omega)=\frac{1}{2}\left(1+\frac{a^2}{6}\boldsymbol{\nabla}^2_{\boldsymbol{r}_\gamma}\right)\boldsymbol{\nabla}_{\boldsymbol{r}_\lambda}\times\boldsymbol{\mathcal{G}}(\boldsymbol{r}_\gamma,\boldsymbol{r}_\lambda,\omega)\,, \tag{2.13}$$

$$\boldsymbol{\mu}^{rr,\gamma\lambda}(\omega)=\frac{1}{4}\,\boldsymbol{\nabla}_{\boldsymbol{r}_\gamma}\times\boldsymbol{\nabla}_{\boldsymbol{r}_\lambda}\times\boldsymbol{\mathcal{G}}(\boldsymbol{r}_\gamma,\boldsymbol{r}_\lambda,\omega)\,. \tag{2.14}$$

Special care should be undertaken when taking the gradient operators with respect to the position of either γ or λ. For the self-mobilities, only the correction in the flow field $\boldsymbol{v}^*$ due to the presence of the membrane in Eq. (2.4) should be considered in Faxén's formula. Therefore, the frequency-dependent self-mobility tensors read

$$\boldsymbol{\mu}^{tt,\gamma\gamma}(\omega)=\mu_0^{tt}\,\mathbf{1}+\lim_{\boldsymbol{r}\to\boldsymbol{r}_\gamma}\left(1+\frac{a^2}{6}\boldsymbol{\nabla}^2_{\boldsymbol{r}}\right)\left(1+\frac{a^2}{6}\boldsymbol{\nabla}^2_{\boldsymbol{r}_\gamma}\right)\boldsymbol{\mathcal{G}}_{\mathrm{M}}(\boldsymbol{r},\boldsymbol{r}_\gamma,\omega)\,, \tag{2.15}$$

$$\boldsymbol{\mu}^{tr,\gamma\gamma}(\omega)=\frac{1}{2}\lim_{\boldsymbol{r}\to\boldsymbol{r}_\gamma}\left(1+\frac{a^2}{6}\boldsymbol{\nabla}^2_{\boldsymbol{r}_\gamma}\right)\boldsymbol{\nabla}_{\boldsymbol{r}}\times\boldsymbol{\mathcal{G}}_{\mathrm{M}}(\boldsymbol{r},\boldsymbol{r}_\gamma,\omega)\,, \tag{2.16}$$

$$\boldsymbol{\mu}^{rr,\gamma\gamma}(\omega)=\mu_0^{rr}\,\mathbf{1}+\frac{1}{4}\lim_{\boldsymbol{r}\to\boldsymbol{r}_\gamma}\boldsymbol{\nabla}_{\boldsymbol{r}_\gamma}\times\boldsymbol{\nabla}_{\boldsymbol{r}}\times\boldsymbol{\mathcal{G}}_{\mathrm{M}}(\boldsymbol{r},\boldsymbol{r}_\gamma,\omega)\,, \tag{2.17}$$

where $\mathbf{1}$ denotes the unit tensor.

Having constructed the self- and pair-mobility tensors, the Green's functions associated with the elastic membrane need to be introduced at this point.

2.2 Green's functions

The exact Green's functions for a point-force acting nearby a planar elastic membrane has been determined in our earlier works, see e.g. Refs. [91] and [108]. The membrane is considered as a two dimensional sheet made by an hyperelastic material that exhibits resistance towards shearing and bending. Membrane shearing elasticity is described by the wall-established Skalak model [103] which is often used as a practical model for red-blood cell membranes [109–111]. The model is characterized by the shear modulus κ_{S} and the area dilatation modulus κ_{A}, both related to each other by the Skalak coefficient $C := \kappa_{\mathrm{A}}/\kappa_{\mathrm{S}}$. The resistance towards bending is modeled by the Helfrich model [104, 112], with the corresponding bending modulus κ_{B}. The Green's functions can conveniently be computed using a two-dimensional Fourier transform technique [85–87] and appropriately applying the boundary conditions stemming from shearing and bending of the membrane. For a point-force exerted at $\boldsymbol{x}_\lambda$ above the membrane, the Green's functions can be expressed in terms of infinite integrals over the wavenumber q as

$$\mathcal{G}_{xx}(\boldsymbol{r},\boldsymbol{r}_\lambda,\omega) = \frac{1}{4\pi}\int_0^\infty \Big(\tilde{\mathcal{G}}_+(q,z,z_0,\omega)J_0(\rho_\lambda q) + \tilde{\mathcal{G}}_-(q,z,z_0,\omega)J_2(\rho_\lambda q)\cos 2\theta_\lambda\Big) q\,\mathrm{d}q\,, \tag{2.18a}$$

$$\mathcal{G}_{yy}(\boldsymbol{r},\boldsymbol{r}_\lambda,\omega) = \frac{1}{4\pi}\int_0^\infty \Big(\tilde{\mathcal{G}}_+(q,z,z_0,\omega)J_0(\rho_\lambda q) - \tilde{\mathcal{G}}_-(q,z,z_0,\omega)J_2(\rho_\lambda q)\cos 2\theta_\lambda\Big) q\,\mathrm{d}q\,, \tag{2.18b}$$

$$\mathcal{G}_{zz}(\boldsymbol{r},\boldsymbol{r}_\lambda,\omega) = \frac{1}{2\pi}\int_0^\infty \tilde{\mathcal{G}}_{zz}(q,z,z_0,\omega)J_0(\rho_\lambda q) q\,\mathrm{d}q\,, \tag{2.18c}$$

$$\mathcal{G}_{xy}(\boldsymbol{r},\boldsymbol{r}_\lambda,\omega) = \frac{\sin 2\theta_\lambda}{4\pi}\int_0^\infty \tilde{\mathcal{G}}_-(q,z,z_0,\omega)J_2(\rho_\lambda q) q\,\mathrm{d}q\,, \tag{2.18d}$$

$$\mathcal{G}_{rz}(\boldsymbol{r},\boldsymbol{r}_\lambda,\omega) = \frac{i}{2\pi}\int_0^\infty \tilde{\mathcal{G}}_{lz}(q,z,z_0,\omega)J_1(\rho_\lambda q) q\,\mathrm{d}q\,, \tag{2.18e}$$

$$\mathcal{G}_{zr}(\boldsymbol{r},\boldsymbol{r}_\lambda,\omega) = \frac{i}{2\pi}\int_0^\infty \tilde{\mathcal{G}}_{zl}(q,z,z_0,\omega)J_1(\rho_\lambda q) q\,\mathrm{d}q\,, \tag{2.18f}$$

where $\rho_\lambda^2 := (x-x_\lambda)^2 + y^2$ and $\theta_\lambda := \arctan(y/(x-x_\lambda))$ being the polar angle. Here J_n denotes the Bessel function of the first kind of order n [113]. Moreover,

$$\tilde{\mathcal{G}}_{zz} = \frac{1}{4\eta q}\bigg((1+q|z-z_0|)\,e^{-q|z-z_0|} + \bigg(\frac{i\alpha z z_0 q^3}{1-i\alpha q} + \frac{i\alpha_{\mathrm{B}}^3 q^3(1+qz)(1+qz_0)}{1-i\alpha_{\mathrm{B}}^3 q^3}\bigg) e^{-q(z+z_0)}\bigg)\,,$$

$$\tilde{\mathcal{G}}_{lz} = \frac{i}{4\eta q}\bigg(-q(z-z_0)e^{-q|z-z_0|} + \bigg(\frac{i\alpha z_0 q^2(1-qz)}{1-i\alpha q} - \frac{i\alpha_{\mathrm{B}}^3 z q^4(1+qz_0)}{1-i\alpha_{\mathrm{B}}^3 q^3}\bigg)e^{-q(z+z_0)}\bigg)\,,$$

$$\tilde{\mathcal{G}}_{zl} = \frac{i}{4\eta q}\bigg(-q(z-z_0)e^{-q|z-z_0|} + \bigg(-\frac{i\alpha z q^2(1-qz_0)}{1-i\alpha q} + \frac{i\alpha_{\mathrm{B}}^3 q^4 z_0(1+qz)}{1-i\alpha_{\mathrm{B}}^3 q^3}\bigg)e^{-q(z+z_0)}\bigg)\,.$$

and

$$\tilde{\mathcal{G}}_\pm(q,z,\omega) := \tilde{\mathcal{G}}_{tt}(q,z,\omega) \pm \tilde{\mathcal{G}}_{ll}(q,z,\omega)\,,$$

with

$$\tilde{\mathcal{G}}_{ll} = \frac{1}{4\eta q}\bigg((1-q|z-z_0|)e^{-q|z-z_0|} + \bigg(\frac{i\alpha q(1-qz_0)(1-qz)}{1-i\alpha q} + \frac{izz_0\alpha_{\mathrm{B}}^3 q^5}{1-i\alpha_{\mathrm{B}}^3 q^3}\bigg) e^{-q(z+z_0)}\bigg)\,,$$

$$\tilde{\mathcal{G}}_{tt} = \frac{1}{2\eta q}\left(e^{-q|z-z_0|} + \frac{iB\alpha q}{2-iB\alpha q}e^{-q(z+z_0)}\right)\,,$$

where $\alpha := \kappa_{\mathrm{S}}/(3B\eta\omega)$ is a characteristic length scale for shearing and area expansion with $B := 2/(1+C)$, and $\alpha_{\mathrm{B}}^3 := \kappa_{\mathrm{B}}/(4\eta\omega)$ is a characteristic cubic length scale for bending. Thus, the terms

involving α and α_{B}^3 in the above equations are associated with shearing and bending, respectively. Furthermore, the other components can readily be determined from the usual transformation relations $\mathcal{G}_{xz} = \mathcal{G}_{rz}\cos\theta_\lambda$, $\mathcal{G}_{yz} = \mathcal{G}_{rz}\sin\theta_\lambda$, $\mathcal{G}_{zx} = \mathcal{G}_{zr}\cos\theta_\lambda$, $\mathcal{G}_{zy} = \mathcal{G}_{zr}\sin\theta_\lambda$ and $\mathcal{G}_{yx} = \mathcal{G}_{xy}$. It is worth mentioning that the Green's functions nearby an elastic membrane reduce in the vanishing frequency limit to the celebrated Blake tensor [114] in which the membrane motion is completely restricted.

3 Boundary integral methods

In order to assess the appropriateness and accuracy of the multipole expansion approach employed throughout this work, we shall compare our analytical predictions with fully resolved computer simulations based on the completed double layer boundary integral equation method (CDLBIEM) [115–119]. The method is known to be particularly suited for the simulation of Stokes flows [120] where both solid and deformed boundaries are present. In this way, the translational and rotational velocities of the particles can be determined provided knowledge of the forces and torques exerted on their surfaces. Hereafter, we briefly provide some technical details regarding the numerical method.

The integral equations for the particle-membrane system are expressed as

$$\begin{aligned} v_\beta(\boldsymbol{x}) &= \mathcal{H}_\beta(\boldsymbol{x})\,, \quad \boldsymbol{x}\in S_{\mathrm{m}}\,,\\ \frac{1}{2}\,\phi_\beta(\boldsymbol{x}) + \sum_{\alpha=1}^{6}\varphi_\beta^{(\alpha)}(\boldsymbol{x})\langle\boldsymbol{\varphi}^{(\alpha)},\boldsymbol{\phi}\rangle &= \mathcal{H}_\beta(\boldsymbol{x})\,, \quad \boldsymbol{x}\in S_{\mathrm{p}}\,, \end{aligned}$$

where S_{m} and S_{p} denote the surface of the elastic membrane and the particles respectively. Here $\boldsymbol{v}$ is the velocity of points belonging to the membrane surface and $\boldsymbol{\phi}$ is the so-called double layer density function on the surface of the particles S_{p}, related to the translational and rotational velocities via

$$\begin{aligned} \boldsymbol{V}(\boldsymbol{x}) &= \sum_{\alpha=1}^{3}\boldsymbol{\varphi}^{(\alpha)}(\boldsymbol{x})\langle\boldsymbol{\varphi}^{(\alpha)},\boldsymbol{\phi}\rangle\,, \quad \boldsymbol{x}\in S_{\mathrm{p}}\,,\\ \boldsymbol{\Omega}(\boldsymbol{x})\times(\boldsymbol{x}-\boldsymbol{x}_{\mathrm{c}}) &= \sum_{\alpha=1}^{3}\boldsymbol{\varphi}^{(\alpha+3)}(\boldsymbol{x})\langle\boldsymbol{\varphi}^{(\alpha+3)},\boldsymbol{\phi}\rangle\,, \quad \boldsymbol{x}\in S_{\mathrm{p}}\,, \end{aligned}$$

where $\boldsymbol{x}_{\mathrm{c}}$ is the particle center and $\boldsymbol{\varphi}^{(\alpha)}$ are known vectorial functions that are dependent on particle position, its surface area and the moment of inertia tensor [17][p. 472]. The brackets stand for the inner product which is defined as

$$\langle\boldsymbol{\varphi}^{(\alpha)},\boldsymbol{\phi}\rangle := \oint_{S_{\mathrm{p}}}\boldsymbol{\varphi}^{(\alpha)}(\boldsymbol{y})\cdot\boldsymbol{\phi}(\boldsymbol{y})\,\mathrm{d}S(\boldsymbol{y})\,,$$

and the function $\mathcal{H}_\beta$ is defined by

$$\mathcal{H}_\beta(\boldsymbol{x}) := -(\mathcal{N}_{\mathrm{m}}\Delta\boldsymbol{f})_\beta(\boldsymbol{x}) - (\mathcal{K}_{\mathrm{p}}\boldsymbol{\phi})_\beta(\boldsymbol{x}) + \mathcal{G}^{(0)}_{\beta\mu}(\boldsymbol{x},\boldsymbol{x}_{\mathrm{c}})F_\mu + \mathcal{R}^{(0)}_{\beta\mu}(\boldsymbol{x},\boldsymbol{x}_{\mathrm{c}})L_\mu\,.$$

The single and double layer integrals are given by

$$\begin{aligned} (\mathcal{N}_{\mathrm{m}}\Delta\boldsymbol{f})_\beta(\boldsymbol{x}) &:= \int_{S_{\mathrm{m}}}\Delta f_\alpha(\boldsymbol{y})\mathcal{G}^{(0)}_{\alpha\beta}(\boldsymbol{y},\boldsymbol{x})\,\mathrm{d}S(\boldsymbol{y})\,,\\ (\mathcal{K}_{\mathrm{p}}\boldsymbol{\phi})_\beta(\boldsymbol{x}) &:= \oint_{S_{\mathrm{p}}}\phi_\alpha(\boldsymbol{y})\mathcal{T}^{(0)}_{\alpha\beta\mu}(\boldsymbol{y},\boldsymbol{x})n_\mu(\boldsymbol{y})\,\mathrm{d}S(\boldsymbol{y})\,, \end{aligned}$$

with $\boldsymbol{n}$ being the outer normal vector at the particle surfaces. Moreover, $\Delta\boldsymbol{f}$ is the traction jump, $\mathcal{T}^{(0)}_{\alpha\beta\mu}$ is the Stresslet and $\mathcal{R}^{(0)}_{\beta\mu}$ is the rotlet [17] in an infinite space. From the instantaneous deformation of the membrane, the traction jump across the membrane $\Delta\boldsymbol{f}$ is readily determined from the membrane constitutive models. For further details with regard to the numerical computation of the traction jumps, we refer the reader to Ref. [92, 121].

In our simulations, the planar membrane is a flat quadratic surface with a size of $300a \times 300a$ and is meshed with 1740 triangles created using the open source software gmsh [122]. The spherical particle is discretized by 320 triangular elements obtained by consecutive refinement of an icosahedron [123, 124].

For the determination of the particle mobility functions numerically, a harmonic force $\boldsymbol{F}_\lambda(t) = \boldsymbol{A}_\lambda e^{i\omega_0 t}$ or torque $\boldsymbol{L}_\lambda(t) = \boldsymbol{B}_\lambda e^{i\omega_0 t}$ is exerted at the surface of the particle λ. After a transient evolution, the translational and rotational velocities of the particle γ evolve as $\boldsymbol{V}_\gamma(t) = \boldsymbol{C}_\gamma e^{i(\omega_0 t+\delta_\gamma)}$ and $\boldsymbol{\Omega}_\gamma(t) = \boldsymbol{D}_\gamma e^{i(\omega_0 t+\varphi_\gamma)}$, respectively, and analogously for the particle λ. The amplitudes and phase shifts can accurately be determined by a fitting procedure of the numerically recorded velocities using the trust region method [125]. In this way, the rt components can be computed for a torque-free particle as

$$\mu^{rt,\lambda\lambda}_{\alpha\beta} = \frac{D_{\lambda\alpha}}{A_{\lambda\beta}}\, e^{i\varphi_\lambda}\,, \qquad \mu^{rt,\gamma\lambda}_{\alpha\beta} = \frac{D_{\gamma_\alpha}}{A_{\lambda\beta}}\, e^{i\varphi_\lambda}\,. \tag{3.3}$$

For a force-free particle, the components tr and rr are computed from

$$\mu^{tr,\lambda\lambda}_{\alpha\beta} = \frac{C_{\lambda\alpha}}{B_{\lambda\beta}}\, e^{i\delta_\lambda}\,, \quad \mu^{rr,\lambda\lambda}_{\alpha\beta} = \frac{D_{\lambda\alpha}}{B_{\lambda\beta}}\, e^{i\varphi_\lambda}\,, \tag{3.4}$$

for the self-mobilities and

$$\mu^{tr,\gamma\lambda}_{\alpha\beta} = \frac{C_{\gamma_\alpha}}{B_{\lambda\beta}}\, e^{i\delta_\gamma}\,, \quad \mu^{rr,\gamma\lambda}_{\alpha\beta} = \frac{D_{\gamma_\alpha}}{B_{\lambda\beta}}\, e^{i\varphi_\gamma}\,. \tag{3.5}$$

for the pair-mobilities.

4 Results

In our previous work [101], we have provided analytical expressions of the translational mobility functions for the motion nearby an elastic membrane. We have shown that the frequency-dependent corrections to the particle self- and pair-mobility functions can exactly be written as a linear superposition of the contributions stemming from shearing and bending resistances. In this section, we shall carry out analogous calculations of the coupling and rotational self- and pair-mobilities.

4.1 Self-mobilities

Mathematical expressions for the hydrodynamic coupling and rotational self-mobility corrections will be derived and expressed in terms of power series of the ratio of particle radius to membrane distance $\epsilon := a/z_0$. We have shown that for the translational mobility corrections, the leading order term scales as ϵ. In the course of what follows, we shall show that the coupling and rotational self-mobility corrections scale at leading order as ϵ^2 and ϵ^3, respectively.

Translation-rotation coupling

For isolated particles in an unbounded geometry, no coupling between translation and rotation occurs [126]. The commonly observed Magnus effect [127] resulting in a drift force of a rotating sphere follows from the full non-linear Navier Stokes equations [128]. In the following, the coupling

mobilities will be scaled by $\mu_0^{tr} \equiv \mu_0^{rt} = 1/(6\pi\eta a^2)$. The translation-rotation coupling mobility is readily obtained after inserting the Green's functions as defined by Eq. (2.18) into Eq. (2.16). After computation, we find that the contribution due to shearing and bending can explicitly be expressed as

$$\frac{\mu_{xy,\mathrm{S}}^{tr,\mathrm{S}}}{\mu_0^{tr}} = \frac{3}{64}\left(\beta^2(2+i\beta)\Gamma_1 + i\beta - \beta^2 - 2 + \frac{4i\beta}{B} + \frac{3\beta^2\Gamma_2}{B^2}\right)\epsilon^2 + \left(-\frac{3}{64} + \frac{\beta}{128}\left(2i + \beta - i\beta^2 - \beta^3\Gamma_1\right)\right)\epsilon^4, \tag{4.1}$$

$$\frac{\mu_{xy,\mathrm{B}}^{tr,\mathrm{S}}}{\mu_0^{tr}} = \left(\frac{3}{32} - \frac{i\beta_{\mathrm{B}}^3}{64}\left(\psi + \phi_+\right)\right)\epsilon^2 + \left(-\frac{3}{64} + \frac{\beta_{\mathrm{B}}^3}{384}\left(3i - \beta_{\mathrm{B}}\psi - \psi'\right)\right)\epsilon^4, \tag{4.2}$$

where the subscripts S and B respectively stand for shearing and bending, and the S appearing as a superscript stand for self. The total coupling mobility is obtained by linear superposition. It follows from the symmetry of the mobility tensor that $\mu_{yx}^{tr} = -\mu_{xy}^{tr}$ and that $\mu_{yx}^{tr} = \mu_{xy}^{rt}$. Moreover, the function E_n denotes the generalized exponential integral defined as $\mathrm{E}_n(x) := \int_1^\infty t^{-n}e^{-xt}\mathrm{d}t$ [113]. Here $\beta := 6Bz_0\eta\omega/\kappa_{\mathrm{S}}$ is a dimensionless frequency associated with the shearing resistance and $\beta_{\mathrm{B}} := 2z_0(4\eta\omega/\kappa_{\mathrm{B}})^{1/3}$ is a dimensionless number associated with bending [91]. Furthermore, we define the auxiliary functions

$$\phi_\pm := e^{-i\overline{z_{\mathrm{B}}}}\,\mathrm{E}_1\left(-i\overline{z_{\mathrm{B}}}\right) \pm e^{-iz_{\mathrm{B}}}\,\mathrm{E}_1\left(-iz_{\mathrm{B}}\right),$$
$$\psi := e^{-i\beta_{\mathrm{B}}}\,\mathrm{E}_1(-i\beta_{\mathrm{B}}),$$

where $z_{\mathrm{B}} := j\beta_{\mathrm{B}}$ and $j := e^{2i\pi/3}$ is the principal cubic-root of unity. The bar designates complex conjugate. We further define

$$\Gamma_1 = e^{i\beta}\,\mathrm{E}_1(i\beta), \qquad \Gamma_2 = e^{\frac{2i\beta}{B}}\,\mathrm{E}_1\left(\frac{2i\beta}{B}\right), \tag{4.3}$$

and

$$\psi' = \overline{z_{\mathrm{B}}}e^{-i\overline{z_{\mathrm{B}}}}\,\mathrm{E}_1(-i\overline{z_{\mathrm{B}}}) + z_{\mathrm{B}}e^{-iz_{\mathrm{B}}}\,\mathrm{E}_1(-iz_{\mathrm{B}}). \tag{4.4}$$

We recall that $B = 2/(1+C)$, a parameter associated with the Skalak model. By taking the vanishing frequency limit in Eqs. (4.1) and (4.2), the shearing and bending related corrections for the xy component of coupling mobility read

$$\lim_{\beta\to 0}\frac{\Delta\mu_{xy,\mathrm{S}}^{tr,\mathrm{S}}}{\mu_0^{tr}} = -\frac{3}{32}\epsilon^2 - \frac{3}{64}\epsilon^4, \tag{4.5}$$

$$\lim_{\beta_{\mathrm{B}}\to 0}\frac{\Delta\mu_{xy,\mathrm{B}}^{tr,\mathrm{S}}}{\mu_0^{tr}} = \frac{3}{32}\epsilon^2 - \frac{3}{64}\epsilon^4, \tag{4.6}$$

leading to the hard-wall limit obtained upon summing up both contributions term by term, namely [60]

$$\lim_{\beta,\beta_{\mathrm{B}}\to 0}\frac{\mu_{xy}^{tr,\mathrm{S}}}{\mu_0^{tr}} = -\frac{3}{32}\epsilon^4, \tag{4.7}$$

as first computed by Goldman [129]. Interestingly, the leading order terms with ϵ^2 drop out in the steady limit where the resulting correction to the coupling pair-mobility scales as ϵ^4. We further remark that the shearing and bending related parts have opposite contributions to the total mobility.

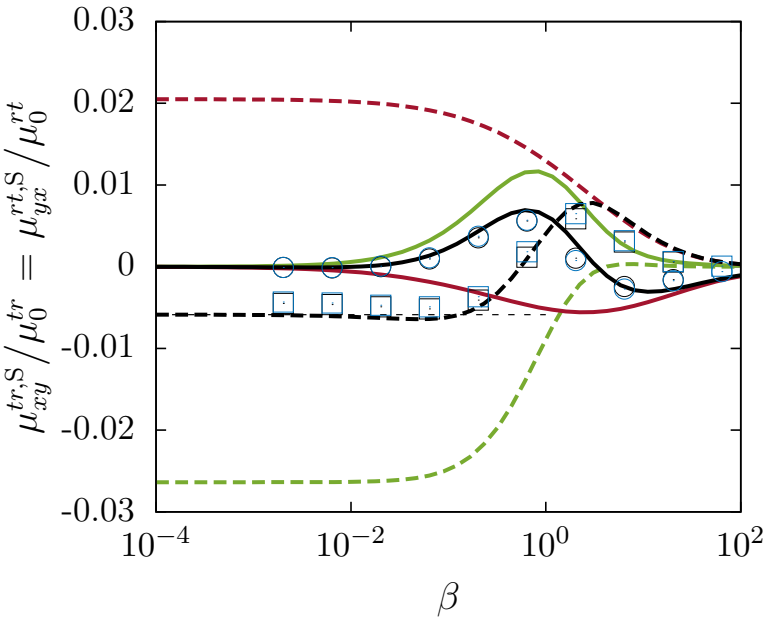

Figure 2: (Color online) The scaled frequency-dependent coupling self-mobility versus the scaled frequency. The solid particle is set a distance $z_0 = 2a$ above a planar elastic membrane whose reduced bending modulus $E_\mathrm{B} = 2/3$. Here we take $C = 1$ in the Skalak parameter. The theoretical predictions are shown as dashed lines for the real (reactive) part, and as solid lines for the imaginary (dissipative) part. Symbols refer to boundary integral simulations results. The shearing/area dilatation and bending related parts as stated by Eqs. (4.1) and (4.2) are shown in green and red, respectively. Blue symbols refer to the rt component as obtained numerically. The horizontal dashed line stands for the coupling self-mobility nearby a no-slip wall given by Eq. (4.7).

This interesting feature will play a significant role in the rotational dynamics of a torque-free doublet of particles nearby an elastic membrane as it is detailed below.

In Fig. 2, we show the scaled coupling self-mobility versus the scaled frequency β of a particle located a distance $z_0 = 2a$ above a planar elastic membrane. Here we consider a reduced bending modulus $E_\mathrm{B} := \kappa_\mathrm{B}/(\kappa_\mathrm{S} z_0^2)$ for which the characteristic time scale for shearing $T_\mathrm{S} := 6z_0\eta/\kappa_\mathrm{S}$ and for bending $T_\mathrm{B} := 4\eta z_0^3/\kappa_\mathrm{B}$ are equal [101]. We further observe that the real and imaginary parts are nonmonotonic functions of frequency that vanish for larger frequencies, thus recovering the behavior in a bulk fluid. In the low frequency regime, the coupling mobility approaches that predicted nearby a hard wall as given by Eq. (4.7). We observe that shearing manifest itself somehow in a more pronounced way compared to bending. The coupling mobilities tr and rt as obtained numerically clearly satisfy the symmetry property required for particles in Stokes flows. A good agreement is obtained between theoretical predictions and boundary integral simulations over the whole range of applied frequencies.

Rotational mobilities

The correction to the rotational-mobility for the rotation around an axis parallel to the membrane is readily obtained by inserting the Green's functions as defined by Eqs. (2.18) into Eq. (2.17) to

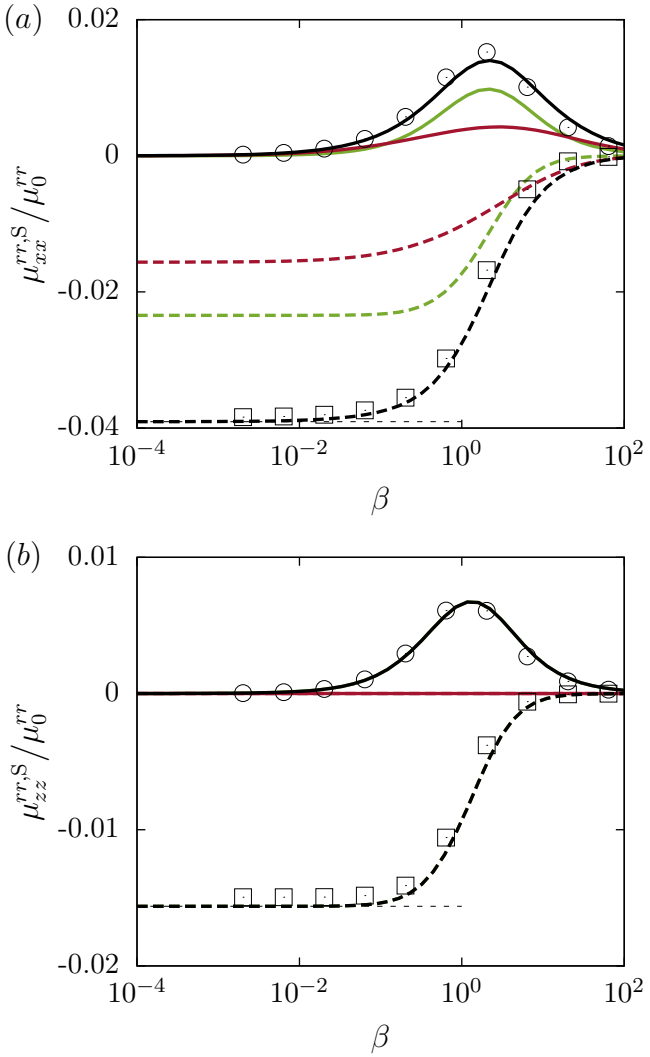

Figure 3: (Color online) The scaled frequency-dependent rotational self-mobility versus the scaled frequency. The analytical predictions are given by Eqs. (4.8) through (4.11). Here we use the same color code as in Fig. 2. Horizontal dashed lines are the hard-wall predictions given by Eqs. (4.14) and (4.15) for the components xx and zz, respectively.

obtain

$$\frac{\Delta\mu_{xx,\mathrm{S}}^{rr,\mathrm{S}}}{\mu_0^{rr}} = -\frac{1}{16}\left(i\beta^3\left(\Gamma_1+\frac{4\Gamma_2}{B^3}\right)-\beta^2\left(1+\frac{2}{B^2}\right)-i\beta\left(1+\frac{1}{B}\right)+3\right)\epsilon^3\,, \tag{4.8}$$

$$\frac{\Delta\mu_{xx,\mathrm{B}}^{rr,\mathrm{S}}}{\mu_0^{rr}} = \frac{1}{48}\left(i\beta_{\mathrm{B}}^3\left(\psi+\phi_+\right)-6\right)\epsilon^3\,, \tag{4.9}$$

for the shearing and bending related parts, respectively. Similar, the total mobility is obtained by superposition of the contributions due to shearing and bending. The component yy has an analogous expression due to the system symmetry along the horizontal plane. Continuing, for the rotation

around an axis perpendicular to the membrane, the shearing and bending related corrections read

$$\frac{\Delta\mu^{rr,\mathrm{S}}_{zz,\mathrm{S}}}{\mu^{rr}_0} = -\frac{3iB}{16\beta}\left(4e^{\frac{2i\beta}{B}}\,\mathrm{E}_5\left(\frac{2i\beta}{B}\right)-1\right)\epsilon^3\,, \tag{4.10}$$

$$\frac{\Delta\mu^{rr,\mathrm{S}}_{zz,\mathrm{B}}}{\mu^{rr}_0} = 0\,. \tag{4.11}$$

Clearly, the rotational self-mobilities have a leading-order term scaling as ϵ^3. Interestingly, the zz component depends only on membrane shearing properties and does not depend on bending. Not surprisingly, the torque exerted on the particle along an axis perpendicular to the planar membrane induces only an in-plane displacement and therefore the resulting stresses do not cause any out-of-plane deformation or bending. By taking the vanishing frequency limit in the xx component of the rotational mobilities in Eqs. (4.8) and (4.9) we obtain

$$\lim_{\beta\to 0}\frac{\Delta\mu^{rr,\mathrm{S}}_{xx,\mathrm{S}}}{\mu^{rr}_0} = -\frac{3}{16}\,\epsilon^3\,, \tag{4.12}$$

$$\lim_{\beta_\mathrm{B}\to 0}\frac{\Delta\mu^{rr,\mathrm{S}}_{xx,\mathrm{B}}}{\mu^{rr}_0} = -\frac{1}{8}\,\epsilon^3\,, \tag{4.13}$$

leading after summing up both contributions term by term to the result near a hard-wall [60]

$$\lim_{\beta,\beta_\mathrm{B}\to 0}\frac{\Delta\mu^{rr,\mathrm{S}}_{xx}}{\mu^{rr}_0} = -\frac{5}{16}\,\epsilon^3\,. \tag{4.14}$$

For the zz component we obtain

$$\lim_{\beta,\beta_\mathrm{B}\to 0}\frac{\Delta\mu^{rr,\mathrm{S}}_{zz}}{\mu^{rr}_0} = \lim_{\beta\to 0}\frac{\Delta\mu^{rr,\mathrm{S}}_{zz,\mathrm{S}}}{\mu^{rr}_0} = -\frac{1}{8}\,\epsilon^3\,. \tag{4.15}$$

In the steady limit, we observe that the correction to the xx component of the rotational self-mobility is 2.5 times larger than that of the zz component. It is therefore much easier to rotate the particle along an axis perpendicular than parallel to a membrane endowed with a finite shearing rigidity.

In Fig. 3, we show the scaled rotational self-mobilities versus the scaled frequency β for the rotation about an axis parallel (a) and perpendicular (b) to the planar elastic membrane. We observe that the real part is a monotonically increasing function of frequency while the imaginary part exhibits the typical peak structure which occurs at $\beta \sim 1$. Considering the xx component, we remark that shearing and bending have additive contribution to the total mobility, in contrast to the behavior observed for the coupling mobilities. Moreover, the contribution due to shearing is found to be to some extent more pronounced than that due to bending. The zz component is solely determined by membrane shearing resistance and that bending does not play any role, in complete agreement with theoretical predictions.

4.2 Pair-mobilities

Having computed the coupling and rotational self-mobilities, we now consider the fluid mediated hydrodynamic interactions between two particles. For a pair of particles in an unbounded geometry, coupling between translation and rotation occurs only when considering higher order reflections, and it is not captured in the Rotne-Prager approximation [130, 131]. Hereafter, expressions for the pair-mobility corrections will be derived and expressed in terms of a power series in $\sigma = a/h$. The

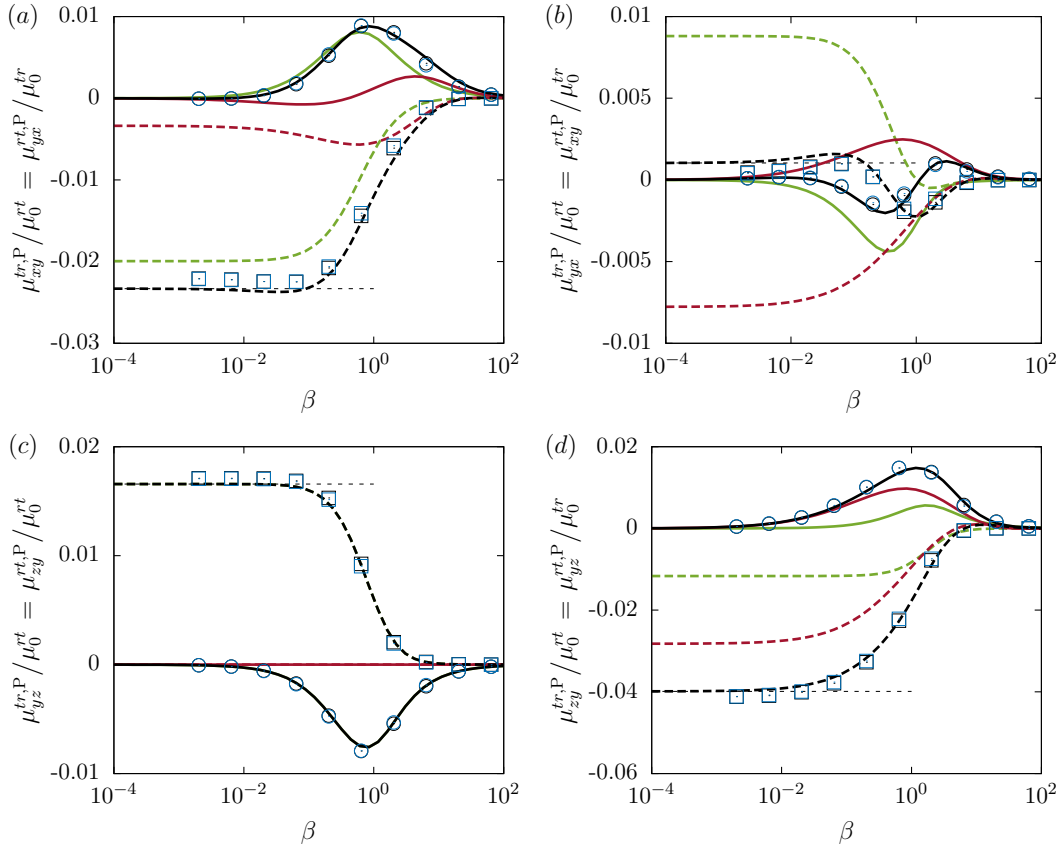

Figure 4: (Color online) The scaled frequency-dependent coupling pair-mobilities versus the scales frequency as predicted theoretically by Eqs. (4.16) through (4.19). The color code is the same as in Fig. (2). Here the pair is located at $z_0 = 2a$ with a distance $h = 4a$. Horizontal dashed lines are the hard-wall predictions given by Eqs. (4.20) through (4.23).

latter takes only physical values strictly between 0 and 1/2 as overlap between the two particles should be avoided. For the translational mobility, we have shown that the leading order corrections scale linearly with respect to σ. We shall show that the leading order corrections terms for the hydrodynamic coupling and rotational pair-mobilities scale as σ^2 and σ^3, respectively.

Translation-rotation coupling

We first consider the translation-rotation coupling components of the pair-mobility tensor nearby an elastic membrane. By inserting the expressions of the Green's functions as stated by Eqs. (2.18) into Eq. (2.13), the coupling pair-mobilities can conveniently be expressed in terms of convergent infinite

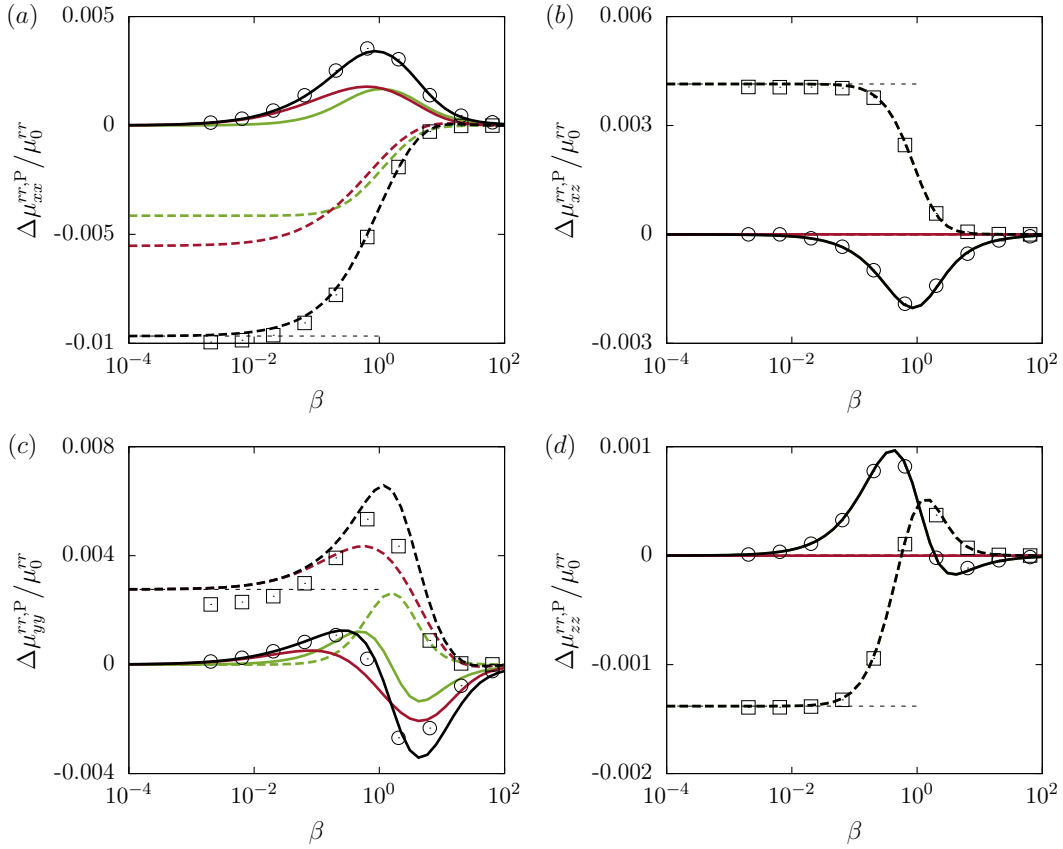

Figure 5: (Color online) The scaled frequency-dependent rotational pair-mobilities versus the scales frequency as predicted theoretically by Eqs. (4.32) through (4.35). Horizontal dashes lines are the corrections predicted nearby a hard wall given by Eqs. (4.36) through (4.39). The color code is the same as in Fig. (2).

integrals as

$$\frac{\mu_{xy}^{tr,\mathrm{P}}}{\mu_0^{tr}} = \int_0^\infty \frac{i\sigma^2 u}{\xi^{1/2}} \left(\frac{1}{\xi^{3/2}} \left(\frac{\xi^{1/2}\chi_1\Gamma_+ - 2u\,(3\xi + u\Lambda)\,\chi_0}{2iu - \beta} + \frac{4u^3\Lambda\varphi}{8iu^3 - \beta_{\mathrm{B}}^3} \right) + \frac{3iB}{2} \frac{\chi_1}{Bu + i\beta} \right) e^{-2u}\,\mathrm{d}u\,, \tag{4.16}$$

$$\frac{\mu_{yx}^{tr,\mathrm{P}}}{\mu_0^{tr}} = \int_0^\infty \frac{\sigma^2 u}{\xi} \left(-\frac{3B}{2} \frac{\varphi}{Bu + i\beta} + \frac{i}{\xi^{1/2}} \left(\frac{\chi_1\Gamma_+}{2iu - \beta} + \frac{4u^3\chi_1\Lambda}{8iu^3 - \beta_{\mathrm{B}}^3} \right) \right) e^{-2u}\,\mathrm{d}u\,, \tag{4.17}$$

$$\frac{\mu_{yz}^{tr,\mathrm{P}}}{\mu_0^{tr}} = \int_0^\infty \frac{3B\sigma^2 u^2 \chi_1}{\xi} \frac{e^{-2u}}{Bu + i\beta}\,\mathrm{d}u\,, \tag{4.18}$$

$$\frac{\mu_{zy}^{tr,\mathrm{P}}}{\mu_0^{tr}} = \int_0^\infty \frac{2i\sigma^2 u^3 \chi_1}{\xi^2} \left(\frac{\Lambda}{2iu - \beta} + \frac{4u\Gamma_-}{8iu^3 - \beta_{\mathrm{B}}^3} \right) e^{-2u}\mathrm{d}u\,, \tag{4.19}$$

where P appearing as a superscript stand for pair, and is a shorthand for the component $\gamma\lambda$. Furthermore, we define the geometric parameter $\xi := 4z_0^2/h^2 = 4\sigma^2/\epsilon^2$ and

$$\begin{aligned}\Lambda &:= 4\sigma^2 u - 3\xi\,,\\ \Gamma_\pm &:= 4\sigma^2 u^2 - 3u\xi \pm 3\xi\,,\\ \chi_n &:= J_n\left(\frac{2u}{\xi^{1/2}}\right),\\ \varphi &:= \xi^{1/2}\chi_1 - 2u\chi_0\,.\end{aligned}$$

The terms involving β and β_{B} in Eqs. (4.16) through (4.19) are the contributions stemming from shearing and bending, respectively.

Interestingly, the component yz (and thus zy of the rt coupling mobility) does not depend on membrane bending properties. In the vanishing frequency limit, or equivalently for infinite membrane shearing and bending moduli, we recover the coupling pair-mobility functions near a hard-wall, with stick boundary conditions namely

$$\lim_{\beta,\beta_{\mathrm{B}}\to 0}\frac{\mu_{xy}^{tr,\mathrm{P}}}{\mu_0^{tr}} = -\frac{9}{4}\frac{\xi^{1/2}}{(1+\xi)^{5/2}}\,\sigma^2 - \frac{3}{2}\frac{\xi^{1/2}(\xi-4)}{(1+\xi)^{7/2}}\,\sigma^4\,, \tag{4.20}$$

$$\lim_{\beta,\beta_{\mathrm{B}}\to 0}\frac{\mu_{yx}^{tr,\mathrm{P}}}{\mu_0^{tr}} = \frac{3}{2}\frac{\xi^{1/2}}{(1+\xi)^{5/2}}\,\sigma^4\,, \tag{4.21}$$

$$\lim_{\beta,\beta_{\mathrm{B}}\to 0}\frac{\mu_{yz}^{tr,\mathrm{P}}}{\mu_0^{tr}} = \frac{3}{4}\frac{\sigma^2}{(1+\xi)^{3/2}}\,, \tag{4.22}$$

$$\lim_{\beta,\beta_{\mathrm{B}}\to 0}\frac{\mu_{zy}^{tr,\mathrm{P}}}{\mu_0^{tr}} = -\frac{3}{4}\frac{1+4\xi}{(1+\xi)^{5/2}}\,\sigma^2 + \frac{3}{2}\frac{4\xi-1}{(1+\xi)^{7/2}}\,\sigma^4\,, \tag{4.23}$$

in full agreement with the results by Swan and Brady [60]. Note that the components xy and zy keep a negative sign and that xy and yz keep a positive sign in the physical range of parameters in which $\epsilon \in [0,1]$ and $\sigma \in [0, \frac{1}{2}]$.

By considering independently the shearing and bending contributions to the pair-mobility corrections from Eqs. (4.16) through (4.19), and taking the limit of vanishing frequency, we obtain for the xy component

$$\lim_{\beta\to 0}\frac{\mu_{xy,\mathrm{S}}^{tr,\mathrm{P}}}{\mu_0^{tr}} = -\frac{3}{8}\frac{\xi^{1/2}(\xi+4)}{(1+\xi)^{5/2}}\,\sigma^2 - \frac{3}{4}\frac{\xi^{1/2}(\xi-4)}{(1+\xi)^{7/2}}\,\sigma^4\,, \tag{4.24}$$

$$\lim_{\beta_{\mathrm{B}}\to 0}\frac{\mu_{xy,\mathrm{B}}^{tr,\mathrm{P}}}{\mu_0^{tr}} = \frac{3}{8}\frac{\xi^{1/2}(\xi-2)}{(1+\xi)^{5/2}}\,\sigma^2 - \frac{3}{4}\frac{\xi^{1/2}(\xi-4)}{(1+\xi)^{7/2}}\,\sigma^4\,, \tag{4.25}$$

leading to Eq. (4.20) after summing up both contributions. It can be shown that the shearing related part is negative whereas the bending related part undergoes a change of sign. By solving Eq. (4.25) perturbatively, the threshold line where the bending contribution changes sign is given in power series of σ by

$$\epsilon_{\mathrm{th}} = \sqrt{2}\sigma\left(1 + \frac{\sigma^2}{3} + \frac{29}{54}\,\sigma^4\right) + \mathcal{O}(\sigma^7)\,. \tag{4.26}$$

Hence, for $\epsilon > \epsilon_{\mathrm{th}}$, the bending related part in the coupling mobility is negative whereas it is positive for $\epsilon < \epsilon_{\mathrm{th}}$.

Considering next the shearing and bending contributions to the component yx, we obtain

$$\lim_{\beta\to 0}\frac{\mu^{tr,\mathrm{P}}_{yx,\mathrm{S}}}{\mu^{tr}_0}=\frac{3}{8}\frac{\xi^{1/2}}{(1+\xi)^{3/2}}\,\sigma^2+\frac{3}{4}\frac{\xi^{1/2}}{(1+\xi)^{5/2}}\,\sigma^4\,, \tag{4.27}$$

$$\lim_{\beta_{\mathrm{B}}\to 0}\frac{\mu^{tr,\mathrm{P}}_{yx,\mathrm{B}}}{\mu^{tr}_0}=-\frac{3}{8}\frac{\xi^{1/2}}{(1+\xi)^{3/2}}\,\sigma^2+\frac{3}{4}\frac{\xi^{1/2}}{(1+\xi)^{5/2}}\,\sigma^4\,, \tag{4.28}$$

which keep positive and negative signs, respectively, leading to Eq. (4.21) by considering both contributions. Continuing, for the yz component we get

$$\lim_{\beta\to 0}\frac{\mu^{tr,\mathrm{P}}_{zy,\mathrm{S}}}{\mu^{tr}_0}=-\frac{9}{8}\frac{\xi}{(1+\xi)^{5/2}}\,\sigma^2+\frac{3}{4}\frac{4\xi-1}{(1+\xi)^{7/2}}\,\sigma^4 \tag{4.29}$$

$$\lim_{\beta_{\mathrm{B}}\to 0}\frac{\mu^{tr,\mathrm{P}}_{zy,\mathrm{B}}}{\mu^{tr}_0}=-\frac{3}{8}\frac{2+5\xi}{(1+\xi)^{5/2}}\,\sigma^2+\frac{3}{4}\frac{4\xi-1}{(1+\xi)^{7/2}}\,\sigma^4\,, \tag{4.30}$$

both of which are negative valued, leading to Eq. (4.23) after summing up both contributions.

Fig. 4 shows the tr and rt coupling pair-mobilities versus the scaled frequency for a pair of particles located above the elastic membrane at $z_0 = 2a$, far apart a distance $h = 4a$. Membrane shearing manifests itself in a more pronounced way for the components xy, yx and yz, whereas bending effect is more significant for the yz component. The simulations results are consistent with the fact that the tr and rt coupling mobility tensors are the transpose of each other, which is indeed ineluctable for Stokes flows. A very good agreement is obtained between theoretical predictions and BIM simulations.

Rotational mobilities

We now turn our attention to the rotational pair-mobility nearby an elastic membrane. In a bulk fluid, the particle rotational mobilities are obtained by inserting the infinite-space Green's function (Oseen tensor) given by Eq. (2.7) into (2.14) to obtain

$$\frac{\mu^{rr,\mathrm{P}}_{xx}}{\mu^{rr}_0}=\sigma^3\,,\qquad \frac{\mu^{rr,\mathrm{P}}_{yy}}{\mu^{rr}_0}=\frac{\mu^{rr,\mathrm{P}}_{zz}}{\mu^{rr}_0}=-\frac{1}{2}\,\sigma^3\,, \tag{4.31}$$

where again $\mu^{rr}_0 = 1/(8\pi\eta a^3)$ is the rotational bulk mobility. Clearly, the two particles undergo rotation in the same direction along their line of centers but in opposite direction for the rotation about a line perpendicular to the line of centers. Moreover, the rotational pair-mobility along the line of centers connecting the two particles is in magnitude twice larger than the rotational pair-mobility perpendicular to it.

Nearby an elastic membrane, the components of the correction to the rotational mobility are

obtained by inserting Eqs. (2.18) into Eq. (2.14) to get

$$\frac{\Delta\mu^{rr}_{xx}}{\mu^{rr}_0} = \int_0^\infty \frac{2\sigma^3u^2}{\xi}\left(\frac{B}{\xi^{1/2}}\frac{\varphi}{Bu+i\beta} - 4i\chi_1\left(\frac{1}{2iu-\beta}+\frac{4u^2}{8iu^3-\beta_{\mathrm{B}}^3}\right)\right)e^{-2u}\,\mathrm{d}u\,, \tag{4.32}$$

$$\frac{\Delta\mu^{rr}_{xz}}{\mu^{rr}_0} = \int_0^\infty \frac{4B\sigma^3u^3\chi_1}{\xi^{3/2}}\frac{e^{-2u}}{Bu+i\beta}\,\mathrm{d}u\,, \tag{4.33}$$

$$\frac{\Delta\mu^{rr}_{yy}}{\mu^{rr}_0} = \int_0^\infty \frac{2\sigma^3u^2}{\xi}\left(\frac{4i\varphi}{\xi^{1/2}}\left(\frac{1}{2iu-\beta}+\frac{4u^2}{8iu^3-\beta_{\mathrm{B}}^3}\right) - \frac{B\chi_1}{Bu+i\beta}\right)e^{-2u}\,\mathrm{d}u\,, \tag{4.34}$$

$$\frac{\Delta\mu^{rr}_{zz}}{\mu^{rr}_0} = \int_0^\infty -\frac{4B\sigma^3u^3\chi_0}{\xi^{3/2}}\frac{e^{-2u}}{Bu+i\beta}\,\mathrm{d}u\,. \tag{4.35}$$

Similar, the terms involving β and β_{B} are related to shearing/area dilatation and bending respectively. It can remarkably be seen that the components xz and zz depends on membrane shearing only. In particular, the correction nearby a no-slip hard-wall is recovered in the zero frequency limit to obtain

$$\frac{\Delta\mu^{rr}_{xx}}{\mu^{rr}_0} = -\frac{1}{2}\frac{2+5\xi}{(1+\xi)^{5/2}}\,\sigma^3\,, \tag{4.36}$$

$$\frac{\Delta\mu^{rr}_{xz}}{\mu^{rr}_0} = \frac{3}{2}\frac{\xi^{1/2}}{(1+\xi)^{5/2}}\,\sigma^3\,, \tag{4.37}$$

$$\frac{\Delta\mu^{rr}_{yy}}{\mu^{rr}_0} = -\frac{1}{2}\frac{5\xi-7}{(1+\xi)^{5/2}}\,\sigma^3\,, \tag{4.38}$$

$$\frac{\Delta\mu^{rr}_{zz}}{\mu^{rr}_0} = -\frac{1}{2}\frac{2\xi-1}{(1+\xi)^{5/2}}\,\sigma^3\,, \tag{4.39}$$

in agreement with the results by Swan and Brady [60]. Interestingly, the components yy and zz undergo a change of sign for $\xi = 7/5$ and $\xi = 1/2$, respectively. By considering the shearing and bending contributions to the pair-mobility corrections independently, from Eqs. (4.32) – (4.35), and taking the vanishing frequency limit, we obtain for the xx component

$$\lim_{\beta\to 0}\frac{\mu^{rr,\mathrm{P}}_{xx,\mathrm{S}}}{\mu^{tr}_0} = -\frac{3}{2}\frac{\xi}{(1+\xi)^{5/2}}\,\sigma^3\,, \tag{4.40}$$

$$\lim_{\beta_{\mathrm{B}}\to 0}\frac{\mu^{rr,\mathrm{P}}_{xx,\mathrm{B}}}{\mu^{tr}_0} = -\frac{\sigma^3}{(1+\xi)^{3/2}}\,, \tag{4.41}$$

leading to Eq. (4.36) after summing up both contributions. For the component xx we obtain

$$\lim_{\beta\to 0}\frac{\mu^{rr,\mathrm{P}}_{yy,\mathrm{S}}}{\mu^{tr}_0} = -\frac{3}{2}\frac{\xi-1}{(1+\xi)^{5/2}}\,\sigma^3\,, \tag{4.42}$$

$$\lim_{\beta_{\mathrm{B}}\to 0}\frac{\mu^{rr,\mathrm{P}}_{yy,\mathrm{B}}}{\mu^{tr}_0} = -\frac{\xi-2}{(1+\xi)^{5/2}}\,\sigma^3\,, \tag{4.43}$$

leading to Eq. (4.38). Accordingly, the shearing and bending related parts in the steady limit vanish for $\xi = 1$ and $\xi = 2$, respectively.

In Fig. 5, we show the particle scaled rotational pair-mobility functions versus the scaled frequency using the same parameters of Fig. 4, i.e. for a distance from the membranes $z_0 = 2a$ and an interparticle distance $h = 4a$. As already pointed out, the components xz and zz depend solely on membrane shearing resistance whereas both shearing and bending manifest themselves for xx

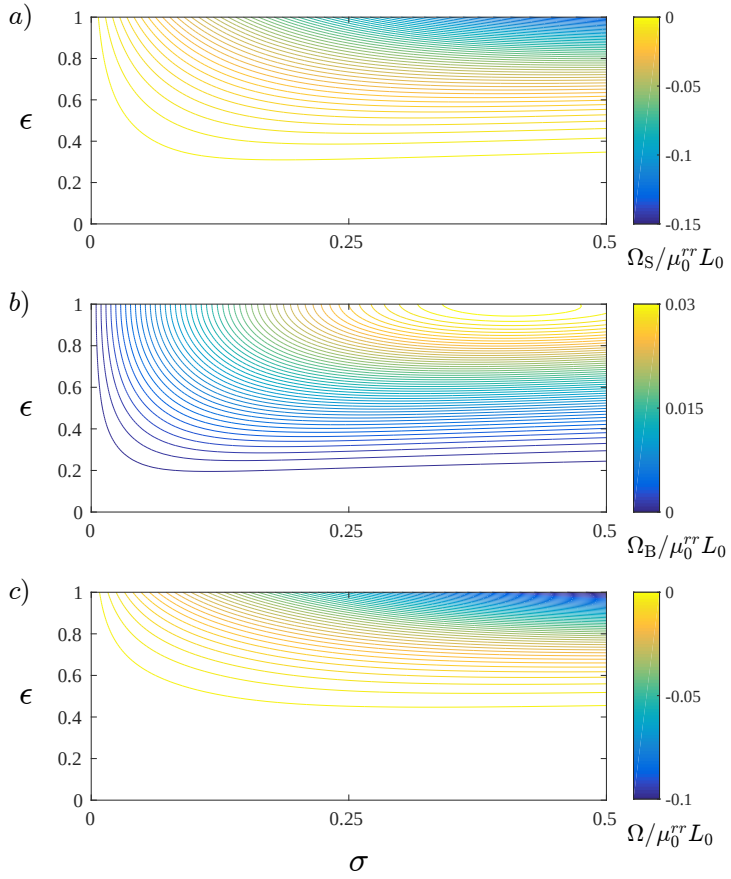

Figure 6: (Color online) Contour diagrams of the scaled steady rotation rate of doublet as stated by Eq. (4.48) for a membrane with pure shearing, Eq. (4.49) for pure bending, and Eq. (4.47) for both shearing and bending.

and yy components. As $\xi = 1$, the shearing related part in the yy mobility vanishes in the zero frequency limit, and the behavior in the low frequency regime is mainly bending dominated. Since the rotational pair-mobilities exhibit a scaling as σ^3, we observe that the corrections are significantly small as compared to the coupling pair-mobilities.

4.3 Doublet co-rotation

In order to elucidate the effect and role of the change of sign observed in the particle self- and pair-mobilities, we shall consider as an example setup the co-rotation of a doublet of particles close to an elastic membrane. We assume equal and opposite external torques applied on the pair of particles along the line of centers, causing the pair to rotate in opposite directions. Due to the aforementioned hydrodynamic coupling between the particles and the membrane, the two particles undergo translational motion along the direction perpendicular to the line of centers. Accordingly, an *induced* rotational motion occurs about the center of mass of the doublet along the z direction with a rotation rate

$$\Omega = -\frac{2L}{h}\left(\mu_{yx}^{tr,\mathrm{S}} - \mu_{yx}^{tr,\mathrm{P}}\right) , \tag{4.44}$$

where the external torques are applied on both particles along the x direction such that $L_{\lambda x} = -L_{\gamma_x} = L(t)$. In the frequency domain, the rotation rate can conveniently be cast in the following

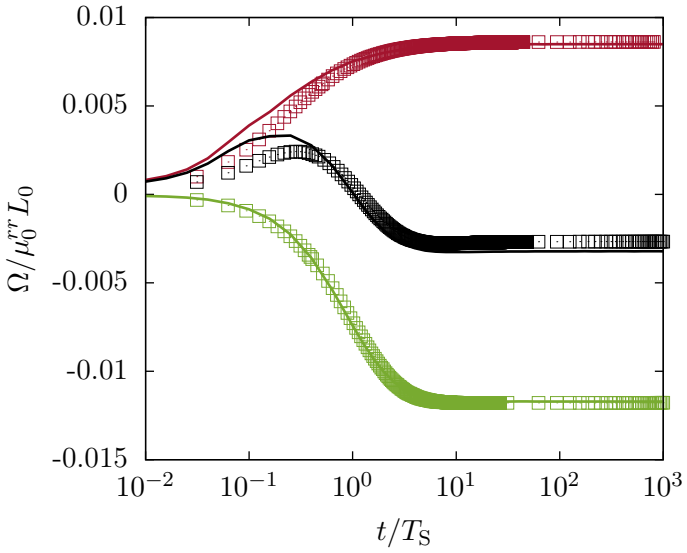

Figure 7: (Color online) Scaled rotation rate of doublet versus the scaled time nearby a membrane with pure shearing (green), pure bending (red) and both rigidities (black). Analytical prediction correspond to Eq. (4.46) and symbols refer to boundary integral simulations. Here we use the same parameters as in Fig. (4) for $z_0 = 2a$ and $h = 4a$.

generic form

$$\Omega(\omega) = L(\omega) \int_0^\infty \frac{\varphi_1(u)}{\varphi_2(u) + i\omega T}\, \mathrm{d}u\,, \tag{4.45}$$

where the integral represents either the shearing or bending related parts. Here $\varphi_2(u) \in \{u, 2u/B\}$ for the shearing contribution and $\varphi_2(u) = u^3$ for bending. Moreover, $\varphi_1(u)$ is a real function that does not depend on frequency. By considering now a Heaviside type function for the torque for which $L(t) = L_0\,\theta(t)$, whose temporal Fourier transform to the frequency domain reads $L(\omega) = (\pi\delta(\omega) - i/\omega)\,L_0$, with $\delta(\omega)$ being the delta Dirac function, the time-dependent rotation rate reads

$$\frac{\Omega(t)}{L_0} = \theta(t) \int_0^\infty \frac{\varphi_1(u)}{\varphi_2(u)} \left(1 - e^{-\varphi_2(u)\tau}\right) \mathrm{d}u\,, \tag{4.46}$$

wherein $\tau := t/T$ is a scaled time. In the steady limit for which $\tau \to \infty$, the rotation rate can be written in a scaled form as

$$\lim_{\tau\to\infty} \frac{\Omega}{\mu_0^{rr} L_0} = \sigma\epsilon^4 \left(\frac{8\sigma^5}{\rho^5} - \frac{1}{4}\right)\,, \tag{4.47}$$

where $\rho^2 = \epsilon^2 + 4\sigma^2$. Now, by considering an idealized membrane with pure shearing or pure bending, we obtain

$$\lim_{\tau\to\infty} \frac{\Omega_\mathrm{S}}{\mu_0^{rr} L_0} = \sigma\epsilon^2 \left(-\frac{1}{4} - \frac{\epsilon^2}{8} + \frac{2\sigma^3}{\rho^3}\left(1 + \frac{2\sigma^2\epsilon^2}{\rho^2}\right)\right)\,, \tag{4.48}$$

$$\lim_{\tau\to\infty} \frac{\Omega_\mathrm{B}}{\mu_0^{rr} L_0} = \sigma\epsilon^2 \left(\frac{1}{4} - \frac{\epsilon^2}{8} - \frac{2\sigma^3}{\rho^3}\left(1 - \frac{2\sigma^2\epsilon^2}{\rho^2}\right)\right)\,, \tag{4.49}$$

leading to Eq. (4.47) after summing up both members term by term. We further note that since the zx components of the tr coupling self- and pair-mobilities vanish, the pair remain at the same height

during its rotational motion above the membrane.

In Fig. 6, we show the contour diagrams of the scaled rotation rate as predicted theoretically by Eqs. (4.47) – (4.49) in the steady limit. Clearly, the steady rotation of a torque-free doublet about its center nearby a membrane with pure shearing is clockwise, i.e. in the same way as nearby a hard-wall. The rotation is however found to be counterclockwise nearby a membrane with pure bending.

In Fig. (7) we present the time-dependent rotation rate of the doublet rotating under a constant external torque exerted along the line of centers, nearby a membrane with shearing-only (green), bending-only (red) or both rigidities (black), as predicted theoretically by Eq. (4.46). We observe that at smaller time scales, for which $t/T_S \ll 1$, the rotation rates amount to small values since the doublet does not yet perceive the presence of the membrane at these short time scales. As the time increases, we observe that the rotation rates asymptotically approach the values predicted in the steady limit. For a membrane with both shearing and bending rigidities, the effect of shearing is noticeably more pronounced, leading to a clockwise rotation as predicted nearby a no-slip wall. For a membrane with pure bending however, the steady rotation rate is positive and therefore the pair undergoes counterclockwise rotation. This interesting behavior can dramatically alter the near membrane dynamics and behavior of force- and torque-free flagellated bacteria and swimming microorganisms that use helical propulsion as a locomotion strategy [132, 133].

5 Conclusions

In this paper, we have studied analytically and numerically the coupling and rotational hydrodynamic mobilities of a pair of particle moving nearby a realistically modeled red blood cell membrane that exhibits resistance towards shearing and bending. We have modeled the elastic membrane by combining the Skalak model for the in-plane shearing resistance and the Helfrich model for the out-of-plane bending resistance. For a vanishing actuation frequency or equivalently for higher membrane shear and bending moduli, our results perfectly coincide with those predicted nearby a hard-wall with stick boundary conditions.

Using the multipole expansion and Faxén's theorem, we have expressed the coupling and rotational self- and pair-mobility functions as power series of the ratio between particle radius and membrane distance and between radius and interparticle distance. We have found that the shearing and bending related contributions may manifest themselves in a additive of suppressive manner depending on the membrane properties and the geometric configuration of the particle-membrane system. As a model system for bacterial locomotion, we have studied the rotational dynamics of torque-free doublet of particles in close vicinity to an elastic membrane, finding that the magnitude and direction of rotation in the steady limit strongly depend on membrane properties: A shearing-only membrane leads to a clockwise rotation whereas rotation is counterclockwise nearby a bending-only membrane.

Finally, we have verified our theoretical predictions via numerical simulations performed using a completed double boundary integral method where a very good agreement is obtained. Our analytically computed mobility functions may find applications as a basis for Brownian simulation studies nearby planar elastic confinements.

Acknowledgments

The authors thank the Volkswagen Foundation for financial support and acknowledge the Gauss Center for Supercomputing e.V. for providing computing time on the GCS Supercomputer SuperMUC at Leibniz Supercomputing Center. We acknowledge partial support from the COST Action MP1305, supported by COST (European Cooperation in Science and Technology).

Bibliography

[1] G. Bao and S. Suresh, Nat. Mater. **2**, 715 (2003).

[2] A. R. Bausch and K. Kroy, Nat. Phys. **2**, 231 (2006).

[3] A. E. Nel, L. Mädler, D. Velegol, T. Xia, E. M. V. Hoek, P. Somasundaran, F. Klaessig, V. Castranova, and M. Thompson, Nat. Mater. **8**, 543 (2009).

[4] Y.-C. Fung, *Biomechanics: mechanical properties of living tissues* (Springer Science & Business Media, 2013).

[5] M. L. Gardel, M. T. Valentine, and D. A. Weitz, in *Microscale diagnostic techniques* (Springer, 2005) pp. 1–49.

[6] P. Cicuta and A. M. Donald, Soft Matter **3**, 1449 (2007).

[7] T. M. Squires and T. G. Mason, Ann. Rev. Fluid Mech. **42**, 413 (2009).

[8] D. Wirtz, Ann. Rev. Biophys. **38**, 301 (2009).

[9] T. M. Squires and T. G. Mason, Rheol. Acta **49**, 1165 (2010).

[10] T. A. Waigh, Rep. Prog. Phys. **79**, 074601 (2016).

[11] T. G. Mason and D. A. Weitz, Phys. Rev. Lett. **74**, 1250 (1995).

[12] B. Schnurr, F. Gittes, F. C. MacKintosh, and C. F. Schmidt, Macromolecules **30**, 7781 (1997).

[13] T. G. Mason, K. Ganesan, J. H. Van Zanten, D. Wirtz, and S. C. Kuo, Phys. Rev. Lett. **79**, 3282 (1997).

[14] D. T. Chen, E. R. Weeks, J. C. Crocker, M. F. Islam, R. Verma, J. Gruber, A. J. Levine, T. C. Lubensky, and A. G. Yodh, Phys. Rev. Lett. **90**, 108301 (2003).

[15] A. W. C. Lau, B. D. Hoffman, A. Davies, J. C. Crocker, and T. C. Lubensky, Phys. Rev. Lett. **91**, 198101 (2003).

[16] C. Wilhelm, Phys. Rev. Lett. **101**, 028101 (2008).

[17] S. Kim and S. J. Karrila, *Microhydrodynamics: principles and selected applications* (Courier Corporation, 2013).

[18] J. Happel and H. Brenner, *Low Reynolds number hydrodynamics: with special applications to particulate media*, Vol. 1 (Springer Science & Business Media, 2012).

[19] A. Meyer, A. Marshall, B. G. Bush, and E. M. Furst, J. Rheol. **50**, 77 (2006).

[20] N. Khatibzadeh, A. B. Stilgoe, A. A. Bui, Y. Rocha, G. M. Cruz, V. Loke, L. Z. Shi, T. A. Nieminen, H. Rubinsztein-Dunlop, and M. W. Berns, Sci. Rep. **4** (2014).

[21] B. Lin, J. Yu, and S. A. Rice, Phys. Rev. E **62**, 3909 (2000).

[22] E. R. Dufresne, D. Altman, and D. G. Grier, EPL (Europhys. Lett.) **53**, 264 (2001).

[23] E. Schäffer, S. F. Nørrelykke, and J. Howard, Langmuir **23**, 3654 (2007).

[24] P. P. Lele, J. W. Swan, J. F. Brady, N. J. Wagner, and E. M. Furst, Soft Matter **7**, 6844 (2011).

[25] J. Mo, A. Simha, and M. G. Raizen, Phys. Rev. E **92**, 062106 (2015).

[26] J. Mo, *Short timescale Brownian motion and applications*, Ph.D. thesis (2015).

[27] K. Kihm, A. Banerjee, C. Choi, and T. Takagi, Exp. Fluids **37**, 811 (2004).

[28] R. Sadr, H. Li, and M. Yoda, Exp. Fluids **38**, 90 (2005).

[29] B. Cui, H. Diamant, and B. Lin, Phys. Rev. Lett. **89**, 188302 (2002).

[30] H. B. Eral, J. M. Oh, D. van den Ende, F. Mugele, and M. H. G. Duits, Langmuir **26**, 16722 (2010).

[31] P. Sharma, S. Ghosh, and S. Bhattacharya, Appl. Phys. Lett. **97**, 104101 (2010).

[32] S. L. Dettmer, S. Pagliara, K. Misiunas, and U. F. Keyser, Phys. Rev. E **89**, 062305 (2014).

[33] B. Tränkle, D. Ruh, and A. Rohrbach, Soft matter **12**, 2729 (2016).

[34] T. G. Mason and D. A. Weitz, Phys. Rev. Lett. **75**, 2770 (1995).

[35] L. Lobry and N. Ostrowsky, Phys. Rev. B **53**, 12050 (1996).

[36] M. A. Bevan and D. C. Prieve, J. Chem. Phys. **113**, 1228 (2000).

[37] A. R. Clapp and R. B. Dickinson, Langmuir **17**, 2182 (2001).

[38] A. Banerjee and K. D. Kihm, Phys. Rev. E **72**, 042101 (2005).

[39] V. N. Michailidou, G. Petekidis, J. W. Swan, and J. F. Brady, Phys. Rev. Lett. **102**, 068302 (2009).

[40] B. Cichocki, E. Wajnryb, J. Bławzdziewicz, J. Dhont, and P. Lang, J. Chem. Phys. **132**, 074704 (2010).

[41] M. Lisicki, B. Cichocki, J. K. G. Dhont, and P. R. Lang, J. Chem. Phys. **136**, 204704 (2012).

[42] S. A. Rogers, M. Lisicki, B. Cichocki, J. K. G. Dhont, and P. R. Lang, Phys. Rev. Lett. **109**, 098305 (2012).

[43] V. N. Michailidou, J. W. Swan, J. F. Brady, and G. Petekidis, J. Chem. Phys. **139**, 164905 (2013).

[44] W. Wang and P. Huang, Phys. Fluids **26**, 092003 (2014).

[45] M. Lisicki, B. Cichocki, S. A. Rogers, J. K. G. Dhont, and P. R. Lang, Soft Matter **10**, 4312 (2014).

[46] M. Lisicki, *Evanescent wave dynamic light scattering by optically anisotropic Brownian particles*, Ph.D. thesis, University of Warsaw (2015).

[47] M. Lisicki, B. Cichocki, and E. Wajnryb, J. Chem. Phys. **145**, 034904 (2016).

[48] P. Huang and K. S. Breuer, Phys. Rev. E **76**, 046307 (2007).

[49] H. A. Lorentz, Abh. Theor. Phys. **1**, 23 (1907).

[50] H. Faxén, Ann. Phys. **373**, 89 (1922).

[51] H. Brenner, Chem. Eng. Sci. **16**, 242 (1961).

[52] W. R. Dean and M. E. O'Neill, Mathematika **10**, 13 (1963).

[53] M. E. O'Neill, Mathematika **11**, 67 (1964).

[54] G. Perkins and R. Jones, Physica A **171**, 575 (1991).

[55] G. Perkins and R. Jones, Physica A **189**, 447 (1992).

[56] S. Wakiya, J. Phys. Soc. Japan **19**, 1401 (1964).

[57] B. U. Felderhof, J. Phys. Chem. B **109**, 21406 (2005).

[58] B. Felderhof, J. Chem. Phys. **123**, 184903 (2005).

[59] B. Cichocki and R. B. Jones, Physica A **258**, 273 (1998).

[60] J. W. Swan and J. F. Brady, Phys. Fluids **19**, 113306 (2007).

[61] J. W. Swan and J. F. Brady, Phys. Fluids **22**, 103301 (2010).

[62] T. Franosch and S. Jeney, Phys. Rev. E **79**, 031402 (2009).

[63] E. Lauga and T. M. Squires, Phys. Fluids **17**, 103102 (2005).

[64] E. Lauga, M. Brenner, and H. Stone, in *Springer handbook of experimental fluid mechanics* (Springer, 2007) pp. 1219–1240.

[65] B. U. Felderhof, Phys. Rev. E **85**, 046303 (2012).

[66] E. Bart, Chem. Eng. Sci. **23**, 193 (1968).

[67] K. Aderogba and J. R. Blake, Bull. Austral. Math. Soc. **18**, 345 (1978).

[68] S. H. Lee, R. S. Chadwick, and L. G. Leal, J. Fluid Mech. **93**, 705 (1979).

[69] S. H. Lee and L. G. Leal, J. Fluid Mech. **98**, 193 (1980).

[70] C. Berdan II and L. G. Leal, J. Colloid Interface Sci. **87**, 62 (1982).

[71] J. Urzay, S. G. Llewellyn Smith, and B. J. Glover, Phys. Fluids **19**, 103106 (2007).

[72] B. Felderhof, J. Chem. Phys. **124**, 124705 (2006).

[73] Y. O. Fuentes, S. Kim, and D. J. Jeffrey, Phys. Fluids **31**, 2445 (1988).

[74] Y. O. Fuentes, S. Kim, and D. J. Jeffrey, Phys. Fluids A **1**, 61 (1989).

[75] K. Danov, R. Aust, F. Durst, and U. Lange, J. Colloid Interface Sci. **175**, 36 (1995).

[76] K. Danov, R. Aust, F. Durst, and U. Lange, Int. J. Multiph. Flow **21**, 1169 (1995).

[77] K. Danov, T. Gurkov, H. Raszillier, and F. Durst, Chem. Eng. Sci. **53**, 3413 (1998).

[78] R. Shail, Int. J. Multiph. Flow **5**, 169 (1979).

[79] R. Shail and D. Gooden, Int. J. Multiph. Flow **7**, 245 (1981).

[80] R. Shail and D. Gooden, Int. J. Multiph. Flow **8**, 627 (1982).

[81] R. Shail and D. Gooden, Int. J. Multiph. Flow **9**, 227 (1983).

[82] R. Shail, J. Eng. Math. **17**, 239 (1983).

[83] J. Bławzdziewicz, V. Cristini, and M. Loewenberg, Phys. Fluids **11**, 251 (1999).

[84] J. Bławzdziewicz, M. Ekiel-Jeżewska, and E. Wajnryb, J. Chem. Phys. **133**, 114703 (2010).

[85] T. Bickel, Eur. Phys. J. E **20**, 379 (2006).

[86] B. U. Felderhof, J. Chem. Phys. **125**, 144718 (2006).

[87] T. Bickel, Phys. Rev. E **75**, 041403 (2007).

[88] A. Daddi-Moussa-Ider and S. Gekle, Phys. Rev. E **95**, 013108 (2017).

[89] M. Weiss, M. Elsner, F. Kartberg, and T. Nilsson, Biophys. J. **87**, 3518 (2004).

[90] I. Golding and E. C. Cox, Phys. Rev. Lett. **96**, 098102 (2006).

[91] A. Daddi-Moussa-Ider, A. Guckenberger, and S. Gekle, Phys. Rev. E **93**, 012612 (2016).

[92] A. Daddi-Moussa-Ider, A. Guckenberger, and S. Gekle, Phys. Fluids **28**, 071903 (2016).

[93] H. Kress, E. H. K. Stelzer, G. Griffiths, and A. Rohrbach, Phys. Rev. E **71**, 061927 (2005).

[94] R. Shlomovitz, A. Evans, T. Boatwright, M. Dennin, and A. Levine, Phys. Rev. Lett. **110**, 137802 (2013).

[95] T. Boatwright, M. Dennin, R. Shlomovitz, A. A. Evans, and A. J. Levine, Phys. Fluids **26**, 071904 (2014).

[96] F. Jünger, F. Kohler, A. Meinel, T. Meyer, R. Nitschke, B. Erhard, and A. Rohrbach, Biophys. J. **109**, 869 (2015).

[97] M. Irmscher, A. M. de Jong, H. Kress, and M. W. J. Prins, Biophys. J. **102**, 698 (2012).

[98] D. Mizuno, Y. Kimura, and R. Hayakawa, Langmuir **16**, 9547 (2000).

[99] D. Mizuno, Y. Kimura, and R. Hayakawa, Phys. Rev. E **70**, 011509 (2004).

[100] Y. Kimura, T. Mori, A. Yamamoto, and D. Mizuno, J. Phys. Condens. Matter **17**, S2937 (2005).

[101] A. Daddi-Moussa-Ider and S. Gekle, J. Chem. Phys. **145**, 014905 (2016).

[102] T. M. Squires and M. P. Brenner, Phys. Rev. Lett. **85**, 4976 (2000).

[103] R. Skalak, A. Tozeren, R. P. Zarda, and S. Chien, Biophys. J. **13(3)**, 245 (1973).

[104] W. Helfrich, Z. Naturf. C. **28**, 693 (1973).

[105] E. Wajnryb, K. A. Mizerski, P. J. Zuk, and P. Szymczak, J. Fluid Mech. **731**, R3 (2013).

[106] Y. W. Kim and R. R. Netz, J. Chem. Phys. **124**, 114709 (2006).

[107] L. Durlofsky, J. F. Brady, and G. Bossis, J. Fluid Mech. **180**, 21 (1987).

[108] A. Daddi-Moussa-Ider, M. Lisicki, and S. Gekle, J. Fluid Mech. **811**, 210 (2017).

[109] E. Foessel, J. Walter, A.-V. Salsac, and D. Barthèse-Biesel, J. Fluid Mech. **672**, 477 (2011).

[110] C. Dupont, A.-V. Salsac, D. Barthès-Biesel, M. Vidrascu, and P. Le Tallec, Phys. Fluids **27**, 051902 (2015).

[111] D. Barthès-Biesel, Ann. Rev. Fluid Mech. **48**, 25 (2016).

[112] A. Guckenberger and S. Gekle, J. Phys. Cond. Mat. (accepted) .

[113] M. Abramowitz, I. A. Stegun, *et al.*, *Handbook of mathematical functions*, Vol. 1 (Dover New York, 1972).

[114] J. R. Blake, Math. Proc. Camb. Phil. Soc. **70**, 303 (1971).

[115] N. Phan-Thien and D. Tullock, J. Mech. Phys. Solids **41**, 1067 (1993).

[116] N. Phan-Thien and D. Tullock, Computational Mechanics **14**, 370 (1994).

[117] M. Kohr and I. I. Pop, *Viscous incompressible flow for low Reynolds numbers*, Vol. 16 (Wit Pr/Comp. Mech., 2004).

[118] H. Zhao and E. S. G. Shaqfeh, Phys. Rev. E **83**, 061924 (2011).

[119] H. Zhao, E. S. G. Shaqfeh, and V. Narsimhan, Phys. Fluids **24**, 011902 (2012).

[120] C. Pozrikidis, J. Comput. Phys. **169**, 250 (2001).

[121] A. Guckenberger, M. P. Schraml, P. G. Chen, M. Leonetti, and S. Gekle, Comp. Phys. Comm. **207**, 1 (2016).

[122] C. Geuzaine and J.-F. Remacle, Int. J. Numer. Meth. Eng. **79**, 1309 (2009).

[123] T. Krüger, F. Varnik, and D. Raabe, Comp. Math. Appl. **61**, 3485 (2011).

[124] S. Gekle, Biophys. J. **110**, 514 (2016).

[125] A. R. Conn, N. I. M. Gould, and P. L. Toint, *Trust region methods*, Vol. 1 (Siam, 2000).

[126] M. Reichert and H. Stark, Phys. Rev. E **69**, 031407 (2004).

[127] G. Magnus, Ann. Phys. **164**, 1 (1853).

[128] S. Hess, Z. Naturforsch. **23**, 1095 (1968).

[129] A. J. Goldman, R. G. Cox, and H. Brenner, Chem. Eng. Sci. **22**, 637 (1967).

[130] J. Rotne and S. Prager, J. Chem. Phys. **50**, 4831 (1969).

[131] D. L. Ermak and J. McCammon, J. Chem. Phys. **69**, 1352 (1978).

[132] E. Lauga, W. R. DiLuzio, G. M. Whitesides, and H. A. Stone, Biophys. J. **90**, 400 (2006).

[133] D. Lopez and E. Lauga, Phys. Fluids **26**, 400 (2014).

Publication 5

Mobility of an axisymmetric particle near an elastic interface

A. Daddi-Moussa-Ider, M. Lisicki and S. Gekle

J. Fluid Mech. **811**, 210-233 (2017)

DOI: 10.1017/jfm.2016.739

1 Abstract

Using a fully analytical theory, we compute the leading order corrections to the translational, rotational and translation-rotation coupling mobilities of an arbitrary axisymmetric particle immersed in a Newtonian fluid moving near an elastic cell membrane that exhibits resistance towards stretching and bending. The frequency-dependent mobility corrections are expressed as general relations involving separately the particle's shape-dependent bulk mobility and the shape-independent parameters such as the membrane-particle distance, the particle orientation and the characteristic frequencies associated with shearing and bending of the membrane. This makes the equations applicable to an arbitrary-shaped axisymmetric particle provided that its bulk mobilities are known, either analytically or numerically. For a spheroidal particle, these general relations reduce to simple expressions in terms of the particle's eccentricity. We find that the corrections to the translation-rotation coupling mobility are primarily determined by bending, whereas shearing manifests itself in a more pronounced way in the rotational mobility. We demonstrate the validity of the analytical approximations by a detailed comparison with boundary integral simulations of a truly extended spheroidal particle. They are found to be in a good agreement over the whole range of applied frequencies.

2 Introduction

Hydrodynamic interactions between nanoparticles and cell membranes play an important role in many medical and biological applications. Prime examples are drug delivery and targeting via nanocarriers which release the active agent in disease sites such as tumours or inflammation areas [1–3]. During navigation through the blood stream, but especially during uptake by a living cell via endocytosis [4–6], nanoparticles frequently come into close contact with cell membranes which alter their hydrodynamic mobilities in a complex fashion.

Over the last few decades, considerable research effort has been devoted to study the motion of particles in the vicinity of interfaces. The particularly simple example of a solid spherical particle has been extensively studied theoretically near a rigid no-slip wall [7–14], an interface separating two immiscible liquids [15–20], an interface with partial-slip [21, 22] and a membrane with surface elasticity [23–31]. Elastic membranes stand apart from both liquid-solid and liquid-liquid interfaces, since the elasticity of the membrane introduces a memory effect in the system causing, e.g., anomalous diffusion [28] or a sign reversal of two-particle hydrodynamic interactions [30]. On the experimental side, the near-wall mobility of a spherical particle has been investigated using optical tweezers [32–35], digital video microscopy [36–39] and evanescent wave dynamic light scattering [40–46], where a significant alteration of particle motion has been observed in line with theoretical predictions. The influence of a nearby elastic cell membrane has been further investigated using optical traps [25, 47–49] and magnetic particle actuation [50].

Particles with a non-spherical shape, such as spheroids or rod-like particles, have also received researchers' attention. The first attempt to investigate the Brownian motion of an anisotropic particle dates back to Perrin [51, 52] who computed analytically the drag coefficients for a spheroid diffusing in a bulk fluid. A few decades later, Batchelor [53] pioneered the idea that the flow field surrounding a slender body, such as an elongated particle, may conveniently be represented by a line distribution of Stokeslets between the foci. The method has successfully been applied to a wide range of external flows [54] and near boundaries such as a plane hard wall [55–57] or a fluid-fluid interface [58]. Using the multipole expansion of the near-wall flow field, Lisicki *et al.* [59] have shown that to leading order the mobility of an arbitrary axisymmetric particle near a hard wall can be expressed in closed form by combining the appropriate Green's function with the particle's bulk mobility. Direct simulation numerical investigations of colloidal axisymmetric particles near a wall have been carried out using boundary integral methods [60], stochastic rotation dynamics [61, 62] and finite element methods [63].

Diffusion of micrometer-sized ellipsoidal particles has been investigated experimentally using digital video microscopy [62, 64–66]. Experiments on actin filaments have been conducted using fluorescence imaging and particle tracking [67] finding that the measured diffusion coefficients can appropriately be accounted for by a correction resting on the hydrodynamic theory of a long cylinder confined between two walls. The confined rotational diffusion coefficients of carbon nanotubes have been measured using fluorescence video microscopy [68] and optical microscopy [69], where a reasonable agreement has been reported with theoretical predictions. More recently, the three-dimensional rotational diffusion of nanorods [70] and rod-like colloids have been measured using video [71] and confocal microscopy [72].

Yet, to the best of our knowledge, motion of a non-spherical particle in the vicinity of deformable elastic interfaces has not been studied so far. In this contribution, we examine the dynamics of an axisymmetric particle near a red blood cell (RBC) membrane using theoretical predictions in close combination with fully resolved boundary integral simulations. The results of the present theory may be used in microrheology experiments in order to characterize the mechanical properties of the membrane [73].

The paper is organised as follows. In Sec. 3, we formulate the theoretical framework for the description of the motion of a colloidal particle in the vicinity of an elastic membrane. We introduce the notion of hydrodynamic friction, mobility, and a model for the membrane. In Sec. 4 we outline the mathematical derivation of the correction to the bulk mobility tensor of the particle due to the presence of an interface and provide explicit expressions for the correction valid for any axially symmetric particle. In Sec. 5, we describe the boundary integral method (BIM) used to numerically compute the components of the mobility tensor. Sec. 6 contains a comparison of analytical predictions and numerical simulations for a spheroidal particle, followed by concluding remarks in Sec. 7. The mathematical details arising in the course of the work are discussed in the Appendices.

3 Hydrodynamics near a membrane

We consider an axially symmetric particle immersed in an incompressible Newtonian fluid, moving close to an elastic membrane. The fluid is assumed to have the same dynamic viscosity η on both sides of the membrane. As an example, we will focus later on a prolate spheroidal particle as shown in figure 1. The position of the centre of the particle is $\boldsymbol{r}_0$, while its orientation is described by the unit vector $\boldsymbol{u}_1$ pointing along the symmetry axis. The laboratory frame is spanned by the basis vectors $\{\boldsymbol{e}_x, \boldsymbol{e}_y, \boldsymbol{e}_z\}$.

We denote by z_0 the vertical distance separating the centre of the particle from the undisplaced membrane located at the plane $z = 0$ and extended infinitely in the horizontal plane xy. It is convenient to introduce the body-fixed frame of reference, formed by the three basis vectors $\{\boldsymbol{u}_1, \boldsymbol{u}_2, \boldsymbol{u}_3\}$. The unit vector $\boldsymbol{u}_2$ is parallel to the undisplaced membrane and perpendicular to the particle axis, and $\boldsymbol{u}_3$ completes the orthonormal basis. We define θ as the angle between $\boldsymbol{u}_1$ and $\boldsymbol{e}_z$ such that $\cos\theta = \boldsymbol{e}_z \cdot \boldsymbol{u}_1$. The basis vectors in the particle frame are then given by $\boldsymbol{u}_2 = (\boldsymbol{e}_z \times \boldsymbol{u}_1)/\left|\boldsymbol{e}_z \times \boldsymbol{u}_1\right|$ and $\boldsymbol{u}_3 = \boldsymbol{u}_1 \times \boldsymbol{u}_2$.

In the inertia-free regime of motion, the fluid dynamics are governed by the stationary incompressible Stokes equations

$$\eta \boldsymbol{\nabla}^2 \boldsymbol{v}(\boldsymbol{r}) - \boldsymbol{\nabla} p(\boldsymbol{r}) + \boldsymbol{f}(\boldsymbol{r}) = 0\,, \tag{3.1}$$

$$\boldsymbol{\nabla} \cdot \boldsymbol{v}(\boldsymbol{r}) = 0\,, \tag{3.2}$$

where $\boldsymbol{v}$ is the fluid velocity, p is the pressure field and $\boldsymbol{f}$ is the force density acting on the fluid due to the presence of the particle. We omit the unsteady term in the Stokes equations, since in realistic situations it leads to a negligible contribution to the mobility corrections [28]. For a discussion

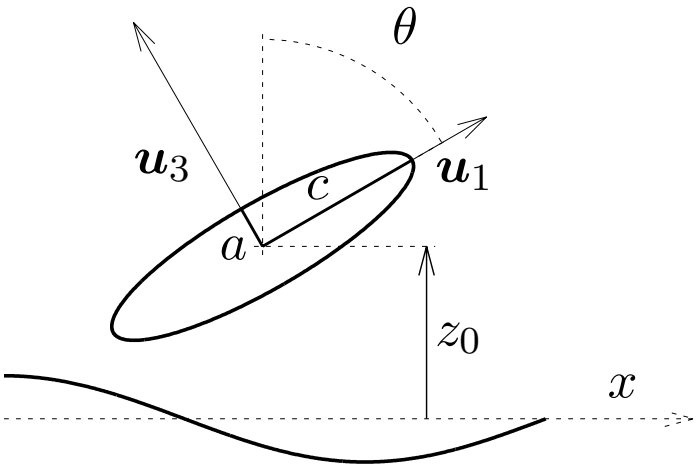

Figure 1: Illustration of a spheroidal particle located at $z = z_0$ above an elastic cell membrane. The short and long axes are denoted by a and c, respectively. The unit vector $\boldsymbol{u}_1$ is pointing along the spheroid symmetry axis and $\boldsymbol{u}_2$ is the unit vector perpendicular to the plane of the figure. The unit vector $\boldsymbol{u}_3$ is defined to be orthogonal to both $\boldsymbol{u}_1$ and $\boldsymbol{u}_2$.

accounting for the unsteady term in bulk flow, see recent work by Felderhof [74]. The flow $\boldsymbol{v}(\boldsymbol{r})$ may be superposed with an arbitrary external flow $\boldsymbol{v}_0(\boldsymbol{r})$ being a solution to the homogeneous Stokes equations in the absence of the particle.

Consider now a colloidal particle near the membrane. The total force $\boldsymbol{F}$, torque $\boldsymbol{T}$ and stresslet (symmetric force dipole) $\boldsymbol{S}$ are linearly related to the velocities (translational $\boldsymbol{V}$ and angular $\boldsymbol{\Omega}$) of the particle relative to an external flow by the generalised friction tensor [75]

$$\begin{pmatrix} \boldsymbol{F} \\ \boldsymbol{T} \\ \boldsymbol{S} \end{pmatrix} = \begin{pmatrix} \boldsymbol{\zeta}^{tt} & \boldsymbol{\zeta}^{tr} & \boldsymbol{\zeta}^{td} \\ \boldsymbol{\zeta}^{rt} & \boldsymbol{\zeta}^{rr} & \boldsymbol{\zeta}^{rd} \\ \boldsymbol{\zeta}^{dt} & \boldsymbol{\zeta}^{dr} & \boldsymbol{\zeta}^{dd} \end{pmatrix} \begin{pmatrix} \boldsymbol{v}_0 - \boldsymbol{V} \\ \boldsymbol{\omega}_0 - \boldsymbol{\Omega} \\ \boldsymbol{E}_0 \end{pmatrix}, \tag{3.3}$$

with $\boldsymbol{v}_0 = \boldsymbol{v}_0(\boldsymbol{r}_0)$, the vorticity $\boldsymbol{\omega}_0 = \frac{1}{2}\boldsymbol{\nabla} \times \boldsymbol{v}_0(\boldsymbol{r}_0)$, and the rate of strain $\boldsymbol{E}_0 = \overline{\boldsymbol{\nabla}\boldsymbol{v}_0}(\boldsymbol{r}_0)$ of the external flow (the bar denotes the symmetric and traceless part of the velocity gradient).

A complimentary relation defines the generalised mobility tensor

$$\begin{pmatrix} \boldsymbol{V} - \boldsymbol{v}_0 \\ \boldsymbol{\Omega} - \boldsymbol{\omega}_0 \\ -\boldsymbol{S} \end{pmatrix} = \begin{pmatrix} \boldsymbol{\mu}^{tt} & \boldsymbol{\mu}^{tr} & \boldsymbol{\mu}^{td} \\ \boldsymbol{\mu}^{rt} & \boldsymbol{\mu}^{rr} & \boldsymbol{\mu}^{rd} \\ \boldsymbol{\mu}^{dt} & \boldsymbol{\mu}^{dr} & \boldsymbol{\mu}^{dd} \end{pmatrix} \begin{pmatrix} \boldsymbol{F} \\ \boldsymbol{T} \\ \boldsymbol{E}_0 \end{pmatrix}. \tag{3.4}$$

Upon examining Eqs. (3.3) and (3.4), we note that the 6×6 mobility tensor $\boldsymbol{\mu}$ is the inverse of the friction tensor $\boldsymbol{\zeta}$

$$\boldsymbol{\zeta}^{-1} = \begin{pmatrix} \boldsymbol{\zeta}^{tt} & \boldsymbol{\zeta}^{tr} \\ \boldsymbol{\zeta}^{rt} & \boldsymbol{\zeta}^{rr} \end{pmatrix}^{-1} = \begin{pmatrix} \boldsymbol{\mu}^{tt} & \boldsymbol{\mu}^{tr} \\ \boldsymbol{\mu}^{rt} & \boldsymbol{\mu}^{rr} \end{pmatrix} = \boldsymbol{\mu}\,. \tag{3.5}$$

Relations between other elements of the generalised mobility and friction tensors may be found directly from Eqs. (3.3) and (3.4). These are general properties of Stokes flows following from the

linearity of the governing equations. Finding an explicit form of these tensors requires the solution of Stokes equations (3.1) and (3.2) with appropriate boundary conditions on the confining interfaces. Since we aim at computing the particle mobility nearby a membrane endowed with surface elasticity and bending resistance, a relevant model for the membrane dynamics needs to be introduced at this point.

The Skalak model [76] is well-established and commonly used to represent RBC membranes [77, 78]. The elastic properties of the interface are characterised by two moduli: elastic shear modulus κ_S and area dilatation modulus κ_A. Resistance towards bending has been further included following the model of Helfrich [79] with the associated bending modulus κ_B. In this approach, the linearized tangential and normal traction jumps across the membrane are related to the membrane displacement field $\boldsymbol{h}$ at $z = 0$ and the dilatation ϵ by [28]

$$[\sigma_{z\alpha}] = -\frac{\kappa_\mathrm{S}}{3}\left(\Delta_\parallel h_\alpha + (1+2C)\partial_\alpha \epsilon\right), \quad \alpha \in \{x, y\}, \tag{3.6}$$

$$[\sigma_{zz}] = \kappa_\mathrm{B}\Delta_\parallel^2 h_z, \tag{3.7}$$

where $[f] := f(z = 0^+) - f(z = 0^-)$ denotes the jump of the quantity f across the membrane. The dilatation $\epsilon := \partial_x h_x + \partial_y h_y$ is the trace of the strain tensor. The Skalak parameter is defined as $C := \kappa_\mathrm{A}/\kappa_\mathrm{S}$. Here $\Delta_\parallel := \partial_x^2 + \partial_y^2$ is the Laplace-Beltrami operator along the membrane. The components $\sigma_{z\alpha}$ of the stress tensor in the fluid are expressed in a standard way by $\sigma_{z\alpha} = -p\delta_{z\alpha} + \eta(\partial_\alpha v_z + \partial_z v_\alpha)$ for $\alpha \in \{x, y, z\}$ [75].

The membrane displacement $\boldsymbol{h}$ and the fluid velocity $\boldsymbol{v}$ are related by the no-slip boundary condition at the undisplaced membrane, which in Fourier space takes the form

$$v_\alpha = i\omega h_\alpha|_{z=0}, \quad \alpha \in \{x, y, z\}, \tag{3.8}$$

with ω being the characteristic frequency of forcing in the system. The frequency-dependent elastic deformation effects are characterised by two dimensionless parameters, as described in Daddi-Moussa-Ider *et al.* [28]

$$\beta = \frac{12 z_0 \eta \omega}{\kappa_\mathrm{S} + \kappa_\mathrm{A}}, \qquad \beta_\mathrm{B} = 2z_0\left(\frac{4\eta\omega}{\kappa_\mathrm{B}}\right)^{1/3}, \tag{3.9}$$

Further details of the derivation of β and β_B can be found in Appendix A. The effect of shear resistance and area dilatation is thus captured by β, while β_B describes the bending resistance of the membrane. In the steady case for which $\beta = \beta_\mathrm{B} = 0$, corresponding to a vanishing frequency or to an infinitely stiff membrane, we expect to recover the results for a hard no-slip wall.

In the case of periodic forcing or time-dependent deformation of the membrane, the quantity of interest is the frequency-dependent mobility tensor. Our aim in this work is to find all the components of $\boldsymbol{\mu}(\omega)$ for an axisymmetric particle close to an elastic membrane. Accordingly, due to the presence of the interface, the near-membrane mobility will then have a correction on top of the bulk mobility $\boldsymbol{\mu}_0$,

$$\boldsymbol{\mu}(\omega) = \boldsymbol{\mu}_0 + \boldsymbol{\Delta\mu}(\omega), \tag{3.10}$$

stemming from the interaction of the flow created by the particle with the boundary. To determine the form of $\boldsymbol{\mu}(\omega)$ in an approximate manner, we use the results by Lisicki *et al.* [59] valid for a hard no-slip wall and generalize them to the case of an elastic membrane. Their idea is based on a multipole expansion [80] of the flow field around an axially symmetric particle close to a boundary, with a corresponding expansion of the force distribution on its surface. If the particle is sufficiently far away from the wall, they have shown that the dominant correction to its friction matrix can be viewed as an interaction between the centre of the particle and its hydrodynamic image. They provide explicit expressions for the elements of the friction tensor for all types of motion (translation,

rotation and coupling terms) which yields the corrected mobility tensor upon inversion. The same route may be followed for a membrane, provided that the form of the Green's tensor for the system is known.

A general Stokes flow can be constructed using the Green's function $\boldsymbol{\mathcal{G}}(\boldsymbol{r}, \boldsymbol{r}')$ being the solution of Eqs. (3.1) and (3.2) subject to a time-dependent point force $\boldsymbol{f}(r) = \boldsymbol{F}(t)\delta(\boldsymbol{r} - \boldsymbol{r}')$ with the appropriate boundary conditions on the membrane. In an unbounded fluid, the Green's tensor is the Oseen tensor [75] $\boldsymbol{\mathcal{G}}_0(\boldsymbol{r}, \boldsymbol{r}') = \boldsymbol{\mathcal{G}}_0(\boldsymbol{r} - \boldsymbol{r}')$, with $\boldsymbol{\mathcal{G}}_0(\boldsymbol{r}) = \left(\mathbf{1} + \boldsymbol{rr}/r^2\right)/(8\pi\eta r)$, with $r := |\boldsymbol{r}|$. In the presence of boundaries, the Green's tensor contains the extra term $\boldsymbol{\Delta\mathcal{G}}$ describing the flow reflected from the membrane, so that $\boldsymbol{\mathcal{G}} = \boldsymbol{\mathcal{G}}_0 + \boldsymbol{\Delta\mathcal{G}}$.

The exact Green's function for a point force close to a membrane has recently been computed by some of us in Ref. [28]. For the resolution of Eqs. (3.1) and (3.2) with a point force acting at $\boldsymbol{r}_0 = (0, 0, z_0)$, the two-dimensional Fourier transform in the xy plane was used to solve the resulting equations with accordingly transformed boundary conditions. The procedure has been previously described in detail and therefore we only list the main steps for the determination of the Green's tensor in Appendix A of this work.

4 Near-membrane mobility tensors

We search for the near-membrane mobility tensor, $\boldsymbol{\mu}(\omega) = \boldsymbol{\mu}_0 + \boldsymbol{\Delta\mu}(\omega)$ by calculating the leading-order correction to the bulk mobility. To this end, we follow the route outlined in a recent contribution by Lisicki *et al.* [59] who derived analytic expressions for the friction tensor of an axially symmetric particle in the presence of a hard no-slip wall. The friction tensor, similarly to the mobility tensor, can be split into the bulk and the correction term

$$\boldsymbol{\zeta} = \boldsymbol{\zeta}_0 + \boldsymbol{\Delta\zeta}. \tag{4.1}$$

The final expressions for the corrected friction tensor involve elements of the bulk friction tensor of the particle, and the distance- and orientation-dependent (derivatives of) the appropriate Green's function. For the hard no-slip wall treated in Lisicki *et al.* [59] the latter is the Blake tensor [81] while in the present case the frequency-dependent Green's functions from Daddi-Moussa-Ider *et al.* [28] are employed. The expressions for the friction tensor with a general Green's function read [59]

$$\boldsymbol{\Delta\zeta}^{tt} = -\frac{1}{8\pi\eta}\frac{1}{2z_0}\boldsymbol{\zeta}_0^{tt}\boldsymbol{g}^{tt}\boldsymbol{\zeta}_0^{tt} + \frac{1}{(8\pi\eta)^2}\frac{1}{(2z_0)^2}\boldsymbol{\zeta}_0^{tt}\boldsymbol{g}^{tt}\boldsymbol{\zeta}_0^{tt}\boldsymbol{g}^{tt}\boldsymbol{\zeta}_0^{tt} + O(z_0^{-3}), \tag{4.2}$$

$$\boldsymbol{\Delta\zeta}^{tr} = -\frac{1}{8\pi\eta}\frac{1}{(2z_0)^2}\boldsymbol{\zeta}_0^{tt}\boldsymbol{g}^{td}\boldsymbol{\zeta}_0^{dr} + O(z_0^{-3}), \tag{4.3}$$

$$\boldsymbol{\Delta\zeta}^{rt} = -\frac{1}{8\pi\eta}\frac{1}{(2z_0)^2}\boldsymbol{\zeta}_0^{rd}\boldsymbol{g}^{dt}\boldsymbol{\zeta}_0^{tt} + O(z_0^{-3}), \tag{4.4}$$

$$\boldsymbol{\Delta\zeta}^{rr} = -\frac{1}{8\pi\eta}\frac{1}{(2z_0)^3}[\boldsymbol{\zeta}_0^{rr}\boldsymbol{g}^{rr}\boldsymbol{\zeta}_0^{rr} + \boldsymbol{\zeta}_0^{rr}\boldsymbol{g}^{rd}\boldsymbol{\zeta}_0^{dr} + \boldsymbol{\zeta}_0^{rd}\boldsymbol{g}^{dr}\boldsymbol{\zeta}_0^{rr} + \boldsymbol{\zeta}_0^{rd}\boldsymbol{g}^{dd}\boldsymbol{\zeta}_0^{dr}] + O(z_0^{-4}). \tag{4.5}$$

where the directional tensors $\boldsymbol{g}$ are defined by

$$\boldsymbol{\Delta\mathcal{G}}^{\gamma\delta} = \frac{1}{8\pi\eta}\frac{1}{(2z_0)^a}\boldsymbol{g}^{\gamma\delta}. \tag{4.6}$$

Here, $\boldsymbol{\Delta\mathcal{G}}^{\gamma\delta}$ are the multipole elements of the Green's integral operator which will be derived below. Further, $\gamma, \delta \in \{t, r, d\}$ and $a = 1$ for tt, $a = 2$ for (tr, rt, td, dt) and $a = 3$ for (dr, rd, rr, dd) parts. In Eqs. (4.2)–(4.5) it should be understood that the tensors are appropriately contracted to yield second-order tensor corrections.

We now apply this result to our system. Our goal is to obtain explicit expressions for the mobility tensors for an axially symmetric particle in the presence of a membrane in terms of its bulk mobilities. This can be done in two steps.

Firstly, we invert the friction relations (4.2)–(4.5), as detailed in Appendix B, to obtain analogous relations for the mobilities:

$$\boldsymbol{\Delta\mu}^{tt} = \frac{1}{8\pi\eta}\frac{1}{2z_0}\boldsymbol{g}^{tt} + O(z_0^{-3})\,, \tag{4.7}$$

$$\boldsymbol{\Delta\mu}^{tr} = -\frac{1}{8\pi\eta}\frac{1}{(2z_0)^2}\boldsymbol{g}^{td}\boldsymbol{\mu}_0^{dr} + O(z_0^{-3})\,, \tag{4.8}$$

$$\boldsymbol{\Delta\mu}^{rt} = \frac{1}{8\pi\eta}\frac{1}{(2z_0)^2}\boldsymbol{\mu}_0^{rd}\boldsymbol{g}^{dt} + O(z_0^{-3})\,, \tag{4.9}$$

$$\boldsymbol{\Delta\mu}^{rr} = \frac{1}{8\pi\eta}\frac{1}{(2z_0)^3}\left[\boldsymbol{g}^{rr} - \boldsymbol{\mu}_0^{rd}\boldsymbol{g}^{dr} + \boldsymbol{g}^{rd}\boldsymbol{\mu}_0^{dr} - \boldsymbol{\mu}_0^{rd}\boldsymbol{g}^{dd}\boldsymbol{\mu}_0^{dr}\right] + O(z_0^{-4})\,. \tag{4.10}$$

These expressions allow straightforward computation of the near-membrane mobilities for arbitrarily-shaped axisymmetric particles if their bulk mobilities are known, either numerically or analytically. Compared to a numerical inversion of the friction tensor, which in principle would be preferable as it avoids the possibility of negative mobilities [59], this approach has the advantage that explicit analytical expressions for the mobility can be obtained.

Remarkably, the final formulae include only one bulk characteristic of the particle, namely the tensors $\boldsymbol{\mu}_0^{rd}$ and $\boldsymbol{\mu}_0^{dr}$ which describe the rotational motion of the particle in response to elongational flow. This form follows from the particular symmetries of an axially symmetric particle with inversional symmetry ($\boldsymbol{u}_1 \leftrightarrow -\boldsymbol{u}_1$).

Secondly, to obtain the directional tensors $\boldsymbol{g}$, we consider a general Green's tensor $\boldsymbol{\mathcal{G}}(\boldsymbol{r},\boldsymbol{r}') = \boldsymbol{\mathcal{G}}_0(\boldsymbol{r}-\boldsymbol{r}') + \boldsymbol{\Delta\mathcal{G}}(\boldsymbol{r},\boldsymbol{r}')$ and a body placed at $\boldsymbol{r}_0$ with a force distribution $\boldsymbol{f}(\boldsymbol{r})$ on its surface. The flow at a point $\boldsymbol{r}$ due to this forcing may be written as the integral equation

$$\boldsymbol{v}(\boldsymbol{r}) = \int \mathrm{d}\boldsymbol{r}'\boldsymbol{\mathcal{G}}(\boldsymbol{r},\boldsymbol{r}')\cdot\boldsymbol{f}(\boldsymbol{r}')\,, \tag{4.11}$$

with the integral performed over the surface of the body. The idea of the derivation of the correction is to find, given the force density, the flow incident on the particle itself due to the presence of an interface. Thus we consider Eq. (4.11) with only the membrane-interaction part $\boldsymbol{\Delta\mathcal{G}}(\boldsymbol{r},\boldsymbol{r}')$ of the Green's tensor and expand it in both arguments around $\boldsymbol{r} = \boldsymbol{r}' = \boldsymbol{r}_0$. The integrals of the subsequent terms on the RHS reproduce the force multipole moments, while the expansion of the LHS yields the multipole expansion of the flow field. By matching the relevant multipoles, we find explicit expressions

for the $\boldsymbol{\Delta\mathcal{G}}^{\gamma\delta}$, with $\gamma, \delta \in \{t, r, d\}$, as described in Lisicki *et al.* [59]. The resulting formulae are

$$\Delta\mathcal{G}^{tt}_{\alpha\beta} = \lim_{\boldsymbol{r},\boldsymbol{r}'\to\boldsymbol{r}_0} \Delta\mathcal{G}_{\alpha\beta}\,, \tag{4.12}$$

$$\Delta\mathcal{G}^{tr}_{\alpha\beta} = \lim_{\boldsymbol{r},\boldsymbol{r}'\to\boldsymbol{r}_0} \frac{1}{2}\epsilon_{\alpha\mu\nu}\partial_\mu\Delta\mathcal{G}_{\nu\beta}\,, \tag{4.13}$$

$$\Delta\mathcal{G}^{rt}_{\alpha\beta} = \lim_{\boldsymbol{r},\boldsymbol{r}'\to\boldsymbol{r}_0} -\frac{1}{2}\epsilon_{\mu\nu\beta}\partial'_\nu\Delta\mathcal{G}_{\alpha\mu}\,, \tag{4.14}$$

$$\Delta\mathcal{G}^{rr}_{\alpha\beta} = \lim_{\boldsymbol{r},\boldsymbol{r}'\to\boldsymbol{r}_0} \frac{1}{4}\epsilon_{\alpha\mu\gamma}\epsilon_{\beta\nu\eta}\partial_\gamma\partial'_\eta\Delta\mathcal{G}_{\mu\nu}\,, \tag{4.15}$$

$$\Delta\mathcal{G}^{td}_{\alpha\beta\gamma} = \lim_{\boldsymbol{r},\boldsymbol{r}'\to\boldsymbol{r}_0} \partial'_\gamma\Delta\mathcal{G}_{\alpha\beta}\,, \tag{4.16}$$

$$\Delta\mathcal{G}^{dt}_{\alpha\beta\gamma} = \lim_{\boldsymbol{r},\boldsymbol{r}'\to\boldsymbol{r}_0} \partial_\alpha\Delta\mathcal{G}_{\beta\gamma}\,, \tag{4.17}$$

$$\Delta\mathcal{G}^{dr}_{\alpha\beta\gamma} = \lim_{\boldsymbol{r},\boldsymbol{r}'\to\boldsymbol{r}_0} -\frac{1}{2}\epsilon_{\gamma\mu\nu}\partial'_\nu\overline{\partial_\alpha\Delta\mathcal{G}_{\beta\mu}}^{(\alpha\beta)}\,, \tag{4.18}$$

$$\Delta\mathcal{G}^{rd}_{\alpha\beta\gamma} = \lim_{\boldsymbol{r},\boldsymbol{r}'\to\boldsymbol{r}_0} \frac{1}{2}\epsilon_{\alpha\mu\nu}\partial'_\mu\overline{\partial_\beta\Delta\mathcal{G}_{\nu\gamma}}^{(\beta\gamma)}\,, \tag{4.19}$$

$$\Delta\mathcal{G}^{dd}_{\alpha\beta\gamma\delta} = \lim_{\boldsymbol{r},\boldsymbol{r}'\to\boldsymbol{r}_0} \overline{\partial_\alpha\partial'_\delta\Delta\mathcal{G}_{\beta\gamma}}^{(\alpha\beta)(\gamma\delta)}\,, \tag{4.20}$$

where $\epsilon_{\alpha\mu\nu}$ is the Levi-Civita tensor and the symbol $\overline{\ }^{(\alpha\beta)}$ denotes the symmetric and traceless part with respect to indices α, β. Explicitly, the reductions for an arbitrary 3rd and 4th order traceless tensor read

$$\begin{aligned}
\overline{M_{\alpha\beta\gamma}}^{(\alpha\beta)} &= \frac{1}{2}\left(M_{\alpha\beta\gamma} + M_{\beta\alpha\gamma}\right), \\
\overline{M_{\alpha\beta\gamma\delta}}^{(\alpha\beta)(\gamma\delta)} &= \frac{1}{4}\left(M_{\alpha\beta\gamma\delta} + M_{\beta\alpha\gamma\delta} + M_{\alpha\beta\delta\gamma} + M_{\beta\alpha\delta\gamma}\right).
\end{aligned}$$

The prime denotes a derivative with respect to the second argument. We note that the tensors $\boldsymbol{\Delta\mathcal{G}}^{dr,rd,dd}$ are traceless due to the incompressibility of the fluid, and therefore the trace needs not be subtracted in the procedure of symmetrization. We further remark that Eqs. (4.12) through (4.20) involve differentiations and elementary operations that are well defined for complex quantities, and hence lead to convergent limits.

It is most natural to consider the correction in the reference frame of the particle, spanned by the three unit basis vectors $\{\boldsymbol{u}_1, \boldsymbol{u}_2, \boldsymbol{u}_3\}$. In this frame, the mobility tensors of an axisymmetric particle have the form

$$\boldsymbol{\Delta\mu}^{tt,rr} = \begin{pmatrix} \Delta\mu^{tt,rr}_{11} & 0 & \Delta\mu^{tt,rr}_{13} \\ 0 & \Delta\mu^{tt,rr}_{22} & 0 \\ \Delta\mu^{tt,rr}_{13} & 0 & \Delta\mu^{tt,rr}_{33} \end{pmatrix} \tag{4.21}$$

for translational and rotational motion, while the translation-rotation coupling tensor reads

$$\boldsymbol{\Delta\mu}^{tr} = \begin{pmatrix} 0 & \Delta\mu^{tr}_{12} & 0 \\ 0 & 0 & \Delta\mu^{tr}_{23} \\ 0 & \Delta\mu^{tr}_{32} & 0 \end{pmatrix}. \tag{4.22}$$

The rotation-translation coupling tensor $\boldsymbol{\Delta\mu}^{rt}$ is obtained by simply taking the transpose of the translation-rotation coupling tensor given above. (See Supplemental Material at https://doi.org/10.1017/jfm.2016.739 for the frequency-dependent mobility corrections expressed in LAB frame).

5 Boundary Integral Method

Here we introduce the boundary-integral method [82] used to numerically compute the mobility tensor of a truly extended spheroidal particle. The method is perfectly suited for treating 3D problems with complex, deforming boundaries such as RBC membranes in the Stokes regime [83, 84]. In order to solve for the particle motion, given an applied force or torque, we combine a completed double layer boundary integral method (CDLBIM) [85] to the classical BIM [86]. The resulting equations are then discretised and transformed into a system of algebraic equations as detailed in [29, 87].

For the numerical determination of the particle mobility components, a harmonic force $\boldsymbol{F}(t) = \boldsymbol{A}e^{i\omega_0 t}$ or torque $\boldsymbol{T}(t) = \boldsymbol{B}e^{i\omega_0 t}$ is applied at the particle surface. After a short transient evolution, the particle linear and angular velocities can be described as $\boldsymbol{V}(t) = \boldsymbol{C}e^{i(\omega_0 t+\delta_t)}$ and $\boldsymbol{\Omega}(t) = \boldsymbol{D}e^{i(\omega_0 t+\delta_r)}$ respectively. The amplitudes and phase shifts can be determined accurately by fitting the numerically recorded velocities using the trust region method [88]. In the LAB frame, the components $\mu^{tt}_{\alpha\beta}$ and $\mu^{rt}_{\alpha\beta}$ of the mobility are determined for a torque-free particle as

$$\mu^{tt}_{\alpha\beta} = \frac{C_\alpha}{A_\beta}e^{i\delta_t}\,, \qquad \mu^{rt}_{\alpha\beta} = \frac{D_\alpha}{A_\beta}e^{i\delta_r}\,. \tag{5.1}$$

For a force-free particle, the components $\mu^{tr}_{\alpha\beta}$ and $\mu^{rr}_{\alpha\beta}$ are obtained from

$$\mu^{tr}_{\alpha\beta} = \frac{C_\alpha}{B_\beta}e^{i\delta_t}\,, \quad \mu^{rr}_{\alpha\beta} = \frac{D_\alpha}{B_\beta}e^{i\delta_r}\,. \tag{5.2}$$

6 Spheroid close to a membrane: theoretical and numerical results

In this Section, we present a comparison of our theoretical results to numerical simulations using the example of a prolate spheroidal particle. To begin with, we discuss the bulk mobility of a spheroid. Further on, we show the explicit form of the correction, and finally compare the components of the corrected mobility matrix to numerical simulations.

The bulk translational and rotational mobility tensors of a general axisymmetric particle have the form

$$\boldsymbol{\mu}_0^{tt,rr} = \mu_\parallel^{t,r}\boldsymbol{u}_1\boldsymbol{u}_1 + \mu_\perp^{t,r}(\mathbf{1} - \boldsymbol{u}_1\boldsymbol{u}_1)\,. \tag{6.1}$$

The third-order tensors $\boldsymbol{\mu}_0^{rd}$ and $\boldsymbol{\mu}_0^{dr}$ have the Cartesian components

$$(\mu_0^{rd})_{\alpha\beta\gamma} = \mu^{rd}u_\sigma\overline{\epsilon_{\sigma\alpha\beta}u_\gamma}^{(\beta\gamma)}\,, \tag{6.2}$$

$$(\mu_0^{dr})_{\alpha\beta\gamma} = \mu^{dr}\overline{u_\alpha\epsilon_{\beta\gamma\sigma}}^{(\alpha\beta)}u_\sigma\,, \tag{6.3}$$

where, following from the Lorentz reciprocal theorem [75]

$$\mu^{dr} = \mu^{rd} =: \lambda\,. \tag{6.4}$$

Note that due to the axial and inversional symmetry in bulk, we have $\boldsymbol{\mu}_0^{tr} = \boldsymbol{\mu}_0^{rt} = 0$ and $\boldsymbol{\mu}_0^{td} = \boldsymbol{\mu}_0^{dt} = 0$.

For a prolate spheroidal particle of eccentricity e, analytical results are available and the bulk

mobility coefficients are given by [75, Tab. 3.4],

$$\mu_{\parallel}^{t} = \frac{1}{6\pi\eta c}\frac{3}{8}\frac{-2e+(1+e^2)L}{e^3}\,, \tag{6.5}$$

$$\mu_{\perp}^{t} = \frac{1}{6\pi\eta c}\frac{3}{16}\frac{2e+(3e^2-1)L}{e^3}\,, \tag{6.6}$$

$$\mu_{\parallel}^{r} = \frac{1}{8\pi\eta c^3}\frac{3}{4}\frac{2e-(1-e^2)L}{e^3(1-e^2)}\,, \tag{6.7}$$

$$\mu_{\perp}^{r} = \frac{1}{8\pi\eta c^3}\frac{3}{4}\frac{-2e+(1+e^2)L}{e^3(2-e^2)}\,, \tag{6.8}$$

where a and c are the short and long axis of the spheroid and

$$e = \sqrt{1-\left(\frac{a}{c}\right)^2}, \quad L = \ln\left(\frac{1+e}{1-e}\right). \tag{6.9}$$

To obtain the final ingredient μ^{rd}, we observe from the definitions in Eqs. (3.3) and (3.4) that $\mu^{rd}_{\alpha\beta\gamma} = \mu^{rr}_{\alpha\delta}\zeta^{rd}_{\delta\beta\gamma}$ and $\mu^{dr}_{\alpha\beta\gamma} = -\zeta^{dr}_{\alpha\beta\delta}\mu^{rr}_{\delta\gamma}$, leading to

$$\mu^{rd} = \mu^{r}_{\perp}\zeta^{rd}. \tag{6.10}$$

The component rd of the friction tensor is [75]

$$\frac{\zeta^{rd}}{8\pi\eta c^3} = \frac{4}{3}\frac{e^5}{-2e+(1+e^2)L}\,. \tag{6.11}$$

Therefore we obtain the rd coefficient of the mobility tensor

$$\lambda = \frac{e^2}{2-e^2}\,. \tag{6.12}$$

Having introduced the bulk hydrodynamic mobilities of a spheroid, we turn our attention to the membrane correction which in the frame of the particle can be written as in Eqs (4.21) and (4.22). We find that the corrections to the translational mobilities as given in general form in Eq. (4.7) can, for a spheroid, be written in closed form as

$$8\pi\eta(2z_0)\Delta\mu^{tt}_{11} = P\sin^2\theta + Q\cos^2\theta, \tag{6.13}$$

$$8\pi\eta(2z_0)\Delta\mu^{tt}_{13} = (P-Q)\sin\theta\cos\theta, \tag{6.14}$$

$$8\pi\eta(2z_0)\Delta\mu^{tt}_{22} = P, \tag{6.15}$$

$$8\pi\eta(2z_0)\Delta\mu^{tt}_{33} = P\cos^2\theta + Q\sin^2\theta, \tag{6.16}$$

and $\Delta\mu^{tt}_{13} = \Delta\mu^{tt}_{31}$. Thus they have the desired symmetry of Eq. (4.21). Expressions for $P(\beta,\beta_{\mathrm{B}}) = P_{\mathrm{S}}(\beta) + P_{\mathrm{B}}(\beta_{\mathrm{B}})$ and $Q(\beta,\beta_{\mathrm{B}}) = Q_{\mathrm{S}}(\beta) + Q_{\mathrm{B}}(\beta_{\mathrm{B}})$ are provided explicitly in Appendix C.

For the translation-rotation coupling, the non-vanishing mobility corrections as given by Eq. (4.8), can be cast in the frame of the particle as

$$8\pi\eta(2z_0)^2\Delta\mu^{tr}_{12} = \lambda\sin\theta\left(M + N\cos^2\theta\right)\,, \tag{6.17}$$

$$8\pi\eta(2z_0)^2\Delta\mu^{tr}_{23} = \lambda M\cos\theta\,, \tag{6.18}$$

$$8\pi\eta(2z_0)^2\Delta\mu^{tr}_{32} = -\lambda\cos\theta\left(M + N\sin^2\theta\right)\,, \tag{6.19}$$

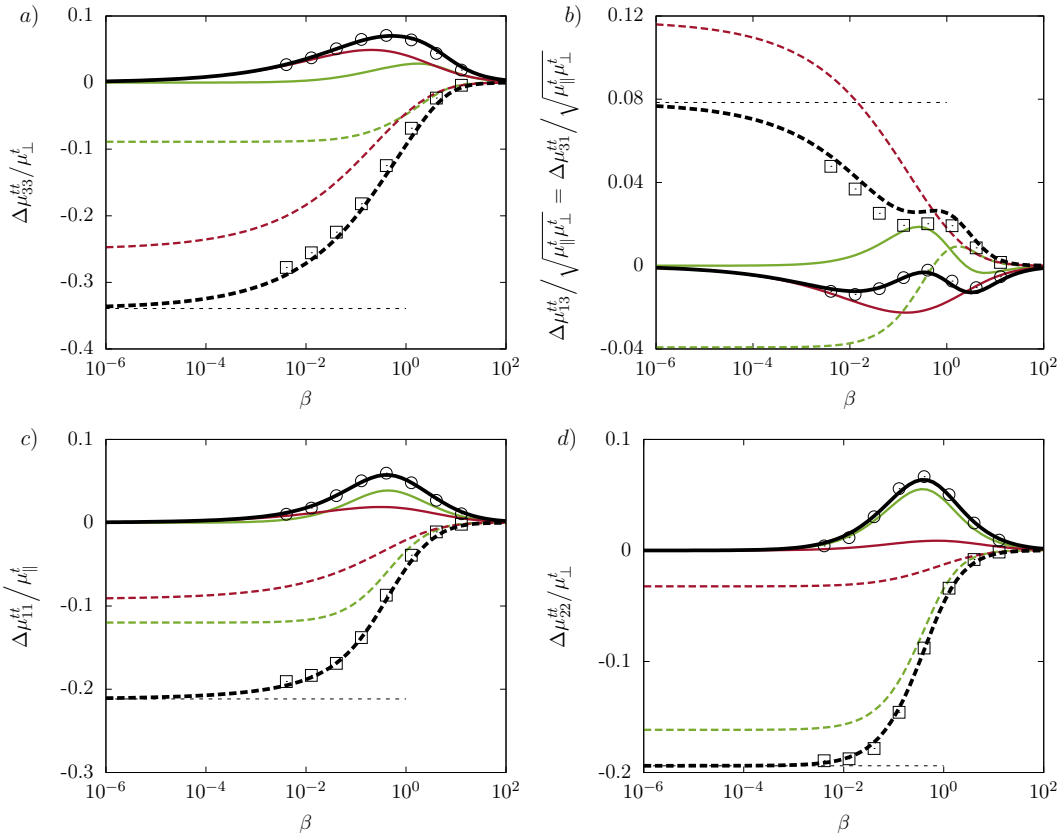

Figure 2: (Color online) The scaled translational mobility correction components versus the scaled frequency. The spheroid is located above the membrane at $z_0 = 2c$ inclined at an angle $\theta = \pi/3$ from the vertical. The analytical predictions of the real and imaginary parts of the translational mobility corrections are shown as dashed and solid lines, respectively. The corrections due to shearing and bending are shown respectively in green (bright grey in a black and white printout) and red (dark grey in a black and white printout). Horizontal dotted lines represent the hard-wall limits from Lisicki *et al.* [59]. BIM simulations are marked as squares and circles for the real and imaginary parts, respectively. For the membrane parameters we take a reduced bending modulus $E_\mathrm{B} := \kappa_\mathrm{B}/(c^2\kappa_\mathrm{S}) = 2/3$ and the Skalak parameter $C = 1$.

where M and N are now functions of the parameters β and β_B, and can likewise be decomposed into shearing and bending contributions. The dependence on the bulk rd mobility λ is explicitly separated out.

Finally, considering the rotational part as stated by Eq. (4.10), the non-vanishing components of the mobility correction in the frame of the particle can conveniently be cast in the following forms

$$8\pi\eta(2z_0)^3\Delta\mu^{rr}_{11} = A_0 + A_2\cos^2\theta\,, \tag{6.20}$$

$$8\pi\eta(2z_0)^3\Delta\mu^{rr}_{13} = D\sin\theta\cos\theta\,, \tag{6.21}$$

$$8\pi\eta(2z_0)^3\Delta\mu^{rr}_{22} = C_0 + \lambda C_2\cos^2\theta + \lambda^2 C_4\cos^4\theta\,, \tag{6.22}$$

$$8\pi\eta(2z_0)^3\Delta\mu^{rr}_{33} = H_0 + H_2\cos^2\theta, \tag{6.23}$$

and with $\Delta\mu^{rr}_{13} = \Delta\mu^{rr}_{31}$. All the functions depend on $(\beta, \beta_\mathrm{B})$ and are decomposed into bending and shearing parts in appendix C. In addition, the functions C, D and H depend on the coefficient λ.

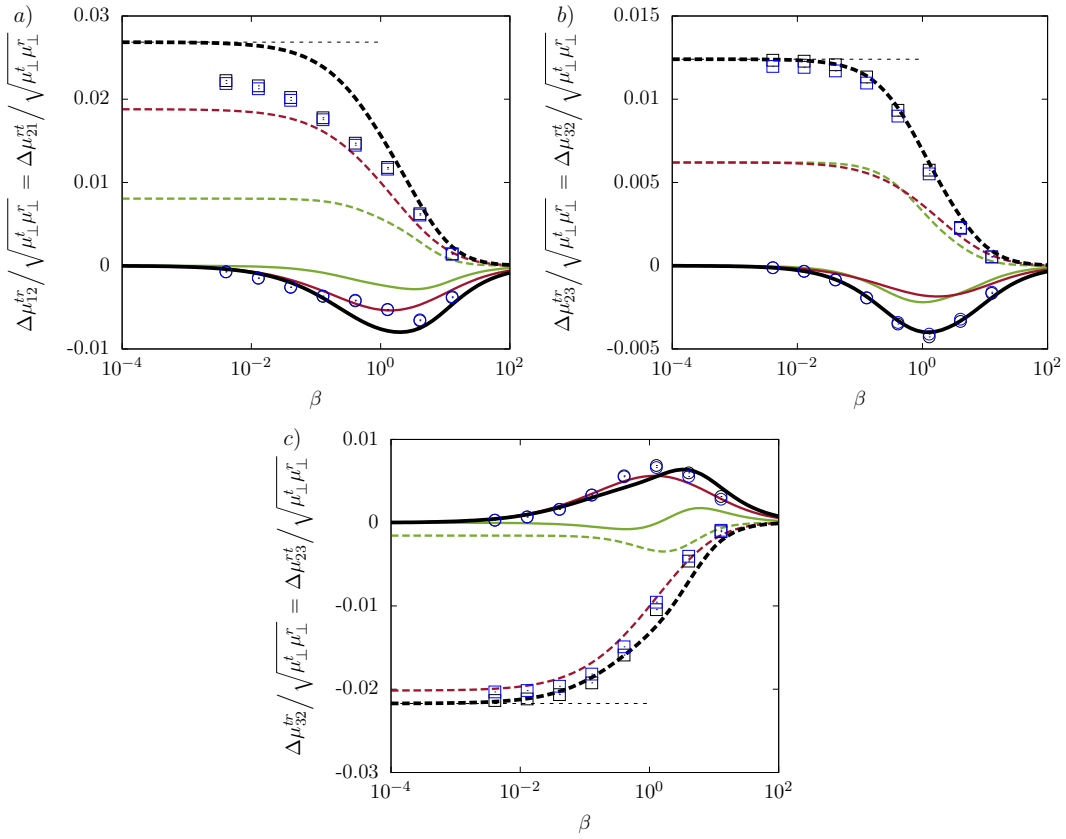

Figure 3: (Color online) The scaled coupling mobility corrections versus the scaled frequency. Black and blue symbols refer to the tr and rt components, respectively, obtained from BIM simulations. The other colors are the same as in figure 2.

It can be seen that the mobility corrections for an axisymmetric particle in their dominant terms possess a simple angular structure. The latter stems from the contraction of the particle friction tensors (which have an axial symmetry, dictated by their shape, with respect to the body axis) with the vertical multipole components of the Blake tensor (which have the same structure but with respect to a different axis, i.e. the vertical direction). This contraction requires transformation of corresponding tensors into the common frame of reference, which generates simple polynomials in sine and cosine functions of the inclination angle as discussed in Lisicki *et al.* [59].

In the following, we shall present a comparison between these analytical predictions and numerical simulations using the Boundary Integral Method, presented in Sec. 5. We consider a prolate spheroid of aspect ratio $p := c/a = 2$, inclined at an angle $\theta = \pi/3$ to the z axis, positioned at $z_0 = 2c$ above a planar elastic membrane. For the membrane, we take a reduced bending modulus $E_\mathrm{B} := c^2\kappa_\mathrm{S}/\kappa_\mathrm{B} = 3/2$ for which the characteristic frequencies β and β_B^3 have the same order of magnitude. The Skalak parameter is $C = 1$. Corresponding data showing the effect of the inclination angle and the reduced bending modulus can be found in the Supporting Information. Our analytical predictions are applicable for large and moderate membrane-particle distances for which $c/z_0 \sim O(1)$ where we find good agreement with numerical simulations.

Henceforth, the mobility corrections will be scaled by the associated bulk values. For diagonal terms, we choose the corresponding diagonal elements, namely $\mu_\parallel^{t,r}$ for $\mu_{11}^{t,r}$ and $\mu_\perp^{t,r}$ for $\mu_{22,33}^{t,r}$. For non-diagonal terms, we use an appropriate combination of bulk mobilities, that is $\sqrt{\mu_\parallel^{t,r}\mu_\perp^{t,r}}$ for

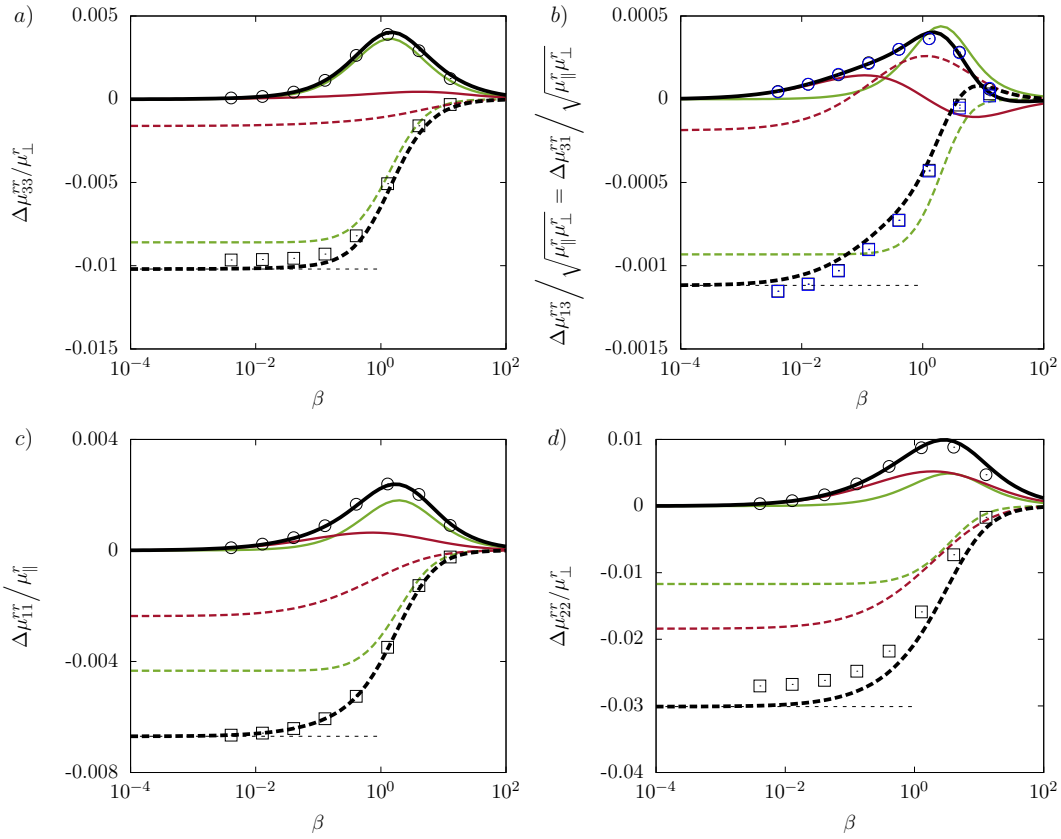

Figure 4: (Color online) The scaled rotational mobility correction component versus the scaled frequency. Black and blue symbols refer to the 13 and 31 components, respectively, obtained from BIM simulations. The color code is the same as in figure 2.

translations and rotations. The translation-rotation coupling tensors are scaled by $\sqrt{\mu^t_\perp \mu^r_\perp}$.

In figure 2 we compare the components of the translational mobility calculated from Eq. (6.13)–(6.16) with those obtained from BIM simulations. For the diagonal components we observe that the real part of the complex mobility corrections is monotonically increasing with frequency. The imaginary part exhibits a non-monotonic bell-shaped dependence on frequency that peaks around $\beta \sim 1$. The off-diagonal components 13 and 31 show a more complex dependence on frequency. In the vanishing frequency limit, we recover the corrections near a hard-wall with stick boundary conditions recently calculated by Lisicki *et al.* [59]. We further remark that for the present inclination of $\theta = \pi/3$ the components 33 and 13 are principally determined by bending resistance whereas shearing effect is more pronounced in the components 11 and 22. A very good agreement is obtained between analytical predictions and numerical simulations for all components over the entire range of frequencies.

By examining the off-diagonal component 31 shown in figure 2 *b*), it is clear that the shearing- and bending-related parts may have opposite contributions to the total translational mobility. This observed trend implies that upon exerting a force along $\boldsymbol{u}_1$, there exists a drift motion along $\boldsymbol{u}_3$, either away or towards the membrane, depending on the shearing and bending properties. In fact, for a membrane with bending-only resistance, such as a fluid vesicle, the spheroid is pushed away from the membrane in the same way as near a hard-wall. On the other hand, for a membrane with shearing-only resistance, such as an artificial capsule, the motion is directed towards the membrane.

Figure 3 shows the corrections to the translation-rotation coupling mobility versus the scaled frequency computed from Eq. (6.17) and (6.19). We observe that bending resistance is essentially the dominant contributor to the coupling mobility. It can be shown that this trend is always the case regardless of spheroid orientation. The BIM simulation results are consistent with the fact that the tr and rt mobility tensors are the transpose of each other and a good agreement is obtained between analytical predictions and simulations. The coupling terms are generally very small compared to the relevant bulk quantities. This makes them somewhat more difficult to obtain precisely from the simulations which explains the small discrepancy notable in figure 3 a).

In figure 4 we present the corrections to the components of the rotational mobility tensor as calculated by Eq. (6.20)–(6.23) compared to the BIM simulations. We remark that the shearing contribution manifests itself in a more pronounced way for the rotational mobilities. Moreover, the correction to the rotational motion is less noticeable compared to the translational motion especially for the off-diagonal component. This observation can be explained by the fact that the rotational mobility corrections exhibit a faster decay with the distance from the membrane, scaling as z_0^{-3} compared to z_0^{-1} for translational motion. Again, a good agreement is obtained for the rotational mobility corrections between analytical predictions and numerical simulations.

7 Conclusions

In this paper we have computed the leading-order translational, rotational and translation-rotation coupling hydrodynamic mobilities of an arbitrary shaped axisymmetric particle immersed in a Newtonian fluid in the vicinity of an elastic cell membrane. The resulting equations contain (i) the particle-independent mulitpole elements of the near-membrane Green's integral operator which have been calculated in analytical form in the present work and (ii) the mobility tensor of the particle *in bulk*. The mobility corrections are frequency-dependent complex quantities due to the memory induced by the membrane. They are expressed in terms of the particle orientation and two dimensionless parameters β and β_{B} that account for the shearing and bending related contributions, respectively. In the zero-frequency limit, or equivalently for infinite elastic and bending moduli, we recover the mobilities near a hard no-slip wall. We apply our general formalism to a prolate spheroid and find very good agreement with numerical simulations performed for a truly extended spheroidal particle over the whole frequency spectrum.

Acknowledgments

ADMI and SG thank the Volkswagen Foundation for financial support and acknowledge the Gauss Center for Supercomputing e.V. for providing computing time on the GCS Supercomputer SuperMUC at Leibniz Supercomputing Center. This work has been supported by the Ministry of Science and Higher Education of Poland via the Mobility Plus Fellowship awarded to ML. This article is based upon work from COST Action MP1305, supported by COST (European Cooperation in Science and Technology).

Appendices

A The Green's function for an elastic membrane

The Green's functions for an elastic membrane have been derived and discussed in detail in earlier papers [28, 30]. Here, we only sketch the derivation which starts with a 2D Fourier transform of the Stokes equations and boundary conditions. It is convenient to introduce an orthogonal basis in

the xy plane, spanned by the unit vectors $\boldsymbol{e}_l = \boldsymbol{q}/|\boldsymbol{q}|$ and $\boldsymbol{e}_t = \boldsymbol{e}_z \times \boldsymbol{e}_l$, respectively parallel and perpendicular to the wave vector $\boldsymbol{q}$. This basis is rotated by the angle $\phi = \arctan(q_y/q_x)$ with respect to the laboratory frame.

After the pressure has been eliminated from the Fourier transformed momentum equations, the following set of ordinary differential equations is obtained

$$q^2\tilde{v}_t - \tilde{v}_{t,zz} = \frac{\tilde{F}_t}{\eta}\delta(z-z_0)\,, \tag{A.1a}$$

$$\tilde{v}_{z,zzzz} - 2q^2\tilde{v}_{z,zz} + q^4\tilde{v}_z = \frac{q^2\tilde{F}_z}{\eta}\delta(z-z_0) + \frac{iq\tilde{F}_l}{\eta}\delta'(z-z_0)\,, \tag{A.1b}$$

$$\tilde{v}_l = \frac{i\tilde{v}_{z,z}}{q}\,, \tag{A.1c}$$

where δ' is the derivative of the Dirac delta function. After some algebra, it can be shown that the traction jump due to shearing as stated in Eq. (3.6) imposes at $z = 0$ the following discontinuities

$$[\tilde{v}_{t,z}] = -iB\alpha q^2\tilde{v}_t\big|_{z=0}\,, \quad [\tilde{v}_{z,zz}] = -4i\alpha q^2\tilde{v}_{z,z}\big|_{z=0}\,, \tag{A.2}$$

where $\alpha := \kappa_\mathrm{S}/3B\eta\omega$ is a characteristic length for shear and area dilatation with $B := 2/(1+C)$. The normal traction jump as given by Eq. (3.7) leads to

$$[\tilde{v}_{z,zzz}] = 4i\alpha_\mathrm{B}^3 q^6\tilde{v}_z\big|_{z=0}\,, \tag{A.3}$$

where $\alpha_\mathrm{B}^3 := \kappa_\mathrm{B}/4\eta\omega$, with α_B being a characteristic length for bending. The dimensionless numbers β and β_B stated in Eq. (3.9) are defined as $\beta := 2z_0/\alpha$ and $\beta_\mathrm{B} := 2z_0/\alpha_\mathrm{B}$.

The Green's tensor in this basis $\{\boldsymbol{e}_l, \boldsymbol{e}_t, \boldsymbol{e}_z\}$ has the form

$$\tilde{\boldsymbol{\mathcal{G}}}(q,z,\omega) = \begin{pmatrix} \tilde{\mathcal{G}}_{ll} & 0 & \tilde{\mathcal{G}}_{lz} \\ 0 & \tilde{\mathcal{G}}_{tt} & 0 \\ \tilde{\mathcal{G}}_{zl} & 0 & \tilde{\mathcal{G}}_{zz} \end{pmatrix}. \tag{A.4}$$

The components of the Green's functions for $z \geq 0$ are expressed by

$$\tilde{\mathcal{G}}_{zz} = \frac{1}{4\eta q}\left((1+q|z-z_0|)\,e^{-q|z-z_0|} + \left(\frac{i\alpha z z_0 q^3}{1-i\alpha q} + \frac{i\alpha_\mathrm{B}^3 q^3(1+qz)(1+qz_0)}{1-i\alpha_\mathrm{B}^3 q^3}\right)e^{-q(z+z_0)}\right),$$

$$\tilde{\mathcal{G}}_{ll} = \frac{1}{4\eta q}\left((1-q|z-z_0|)e^{-q|z-z_0|} + \left(\frac{i\alpha q(1-qz_0)(1-qz)}{1-i\alpha q} + \frac{izz_0\alpha_\mathrm{B}^3 q^5}{1-i\alpha_\mathrm{B}^3 q^3}\right)e^{-q(z+z_0)}\right),$$

$$\tilde{\mathcal{G}}_{tt} = \frac{1}{2\eta q}\left(e^{-q|z-z_0|} + \frac{iB\alpha q}{2-iB\alpha q}e^{-q(z+z_0)}\right),$$

with the off-diagonal components

$$\tilde{\mathcal{G}}_{lz} = \frac{i}{4\eta q}\left(-q(z-z_0)e^{-q|z-z_0|} + \left(\frac{i\alpha z_0 q^2(1-qz)}{1-i\alpha q} - \frac{i\alpha_\mathrm{B}^3 z q^4(1+qz_0)}{1-i\alpha_\mathrm{B}^3 q^3}\right)e^{-q(z+z_0)}\right),$$

$$\tilde{\mathcal{G}}_{zl} = \frac{i}{4\eta q}\left(-q(z-z_0)e^{-q|z-z_0|} + \left(-\frac{i\alpha z q^2(1-qz_0)}{1-i\alpha q} + \frac{i\alpha_\mathrm{B}^3 q^4 z_0(1+qz)}{1-i\alpha_\mathrm{B}^3 q^3}\right)e^{-q(z+z_0)}\right).$$

The terms which contain $e^{-q|z-z_0|}$ are the Fourier-transformed elements of the Oseen tensor and do not depend on the elastic properties of the membrane. The remaining part comes from interactions

with the interface. We now back-transform (A.4) to the laboratory frame. Defining

$$\tilde{\mathcal{G}}_{\pm}(q,z,\omega) := \tilde{\mathcal{G}}_{tt}(q,z,\omega) \pm \tilde{\mathcal{G}}_{ll}(q,z,\omega)\,,$$

and performing the inverse spatial Fourier transform [89], we find that the Green's functions for a point force acting at $\boldsymbol{r}_0 = (0,0,z_0)$ can be presented in terms of the following convergent infinite integrals

$$\begin{aligned}
\mathcal{G}_{zz}(\boldsymbol{r},\omega) &= \frac{1}{2\pi}\int_0^\infty \tilde{\mathcal{G}}_{zz}(q,z,z_0,\omega)J_0(\rho q)q\mathrm{d}q\,,\\
\mathcal{G}_{xx}(\boldsymbol{r},\omega) &= \frac{1}{4\pi}\int_0^\infty \left(\tilde{\mathcal{G}}_{+}(q,z,z_0,\omega)J_0(\rho q) + \tilde{\mathcal{G}}_{-}(q,z,z_0,\omega)J_2(\rho q)\cos 2\Theta\right)q\mathrm{d}q\,,\\
\mathcal{G}_{yy}(\boldsymbol{r},\omega) &= \frac{1}{4\pi}\int_0^\infty \left(\tilde{\mathcal{G}}_{+}(q,z,z_0,\omega)J_0(\rho q) - \tilde{\mathcal{G}}_{-}(q,z,z_0,\omega)J_2(\rho q)\cos 2\Theta\right)q\mathrm{d}q\,,\\
\mathcal{G}_{xy}(\boldsymbol{r},\omega) &= \frac{\sin 2\Theta}{4\pi}\int_0^\infty \tilde{\mathcal{G}}_{-}(q,z,z_0,\omega)J_2(\rho q)q\mathrm{d}q\,,\\
\mathcal{G}_{rz}(\boldsymbol{r},\omega) &= \frac{i}{2\pi}\int_0^\infty \tilde{\mathcal{G}}_{lz}(q,z,z_0,\omega)J_1(\rho q)q\mathrm{d}q\,,\\
\mathcal{G}_{zr}(\boldsymbol{r},\omega) &= \frac{i}{2\pi}\int_0^\infty \tilde{\mathcal{G}}_{zl}(q,z,z_0,\omega)J_1(\rho q)q\mathrm{d}q\,,
\end{aligned}$$

where $\rho := \sqrt{x^2+y^2}$ is the radial distance from the origin, and $\Theta := \arctan(y/x)$ is the angle formed by the radial and x axis. Furthermore, $\mathcal{G}_{xz} = \mathcal{G}_{rz}\cos\Theta$, $\mathcal{G}_{yz} = \mathcal{G}_{rz}\sin\Theta$, $\mathcal{G}_{zx} = \mathcal{G}_{zr}\cos\Theta$, $\mathcal{G}_{zy} = \mathcal{G}_{zr}\sin\Theta$ and $\mathcal{G}_{yx} = \mathcal{G}_{xy}$. Here J_n denotes the Bessel function [90] of the first kind of order n.

In the vanishing frequency limit, or equivalently for infinite membrane shearing and bending rigidities, the well-known Blake tensor [81] is recovered for all the components of the Green's functions.

B Derivation of general mobility relations

Here we sketch the manipulations that lead from the corrected friction tensor, given by Eqs. (4.2) through (4.5), to the mobility correction in Eqs. (4.7) through (4.10). We shall focus on the tt part only, since the others follow analogously. Relation (3.5), rewritten as $\boldsymbol{\mu\zeta} = \mathbf{1}$, defines the relations between elements of the friction and mobility tensors of a particle close to a membrane. The membrane-corrected tt friction tensor and the membrane-corrected tt mobility are thus related by

$$\boldsymbol{\mu}^{tt}\boldsymbol{\zeta}^{tt} + \boldsymbol{\mu}^{tr}\boldsymbol{\zeta}^{rt} = \mathbf{1}\,, \tag{B.1}$$
$$\boldsymbol{\mu}^{tt}\boldsymbol{\zeta}^{tr} + \boldsymbol{\mu}^{tr}\boldsymbol{\zeta}^{rr} = \mathbf{0}\,, \tag{B.2}$$

from which we have

$$\boldsymbol{\mu}^{tt} = [\boldsymbol{\zeta}^{tt} - \boldsymbol{\zeta}^{tr}(\boldsymbol{\zeta}^{rr})^{-1}\boldsymbol{\zeta}^{rt}]^{-1}. \tag{B.3}$$

We know from Eqs. (4.2)-(4.5) that the corrected friction has the following structure

$$\boldsymbol{\zeta}^{tt} = \boldsymbol{\zeta}_0^{tt} + \boldsymbol{\Delta\zeta}^{tt}\,, \tag{B.4}$$
$$\boldsymbol{\zeta}^{rr} = \boldsymbol{\zeta}_0^{rr} + \boldsymbol{\Delta\zeta}^{rr}\,, \tag{B.5}$$
$$\boldsymbol{\zeta}^{tr} = \boldsymbol{\Delta\zeta}^{tr}\,, \tag{B.6}$$
$$\boldsymbol{\zeta}^{rt} = \boldsymbol{\Delta\zeta}^{rt}\,, \tag{B.7}$$

with the known distance-dependence of these elements. Moreover, for an axially symmetric particle, we have

$$\boldsymbol{\zeta}_0^{tt} = (\boldsymbol{\mu}_0^{tt})^{-1}, \qquad \boldsymbol{\zeta}_0^{rr} = (\boldsymbol{\mu}_0^{rr})^{-1}, \tag{B.8}$$

since the bulk friction and mobility tensors are diagonal. We now rewrite Eq. (B.3) as

$$\boldsymbol{\mu}^{tt} = \boldsymbol{\mu}_0^{tt} \left[\mathbf{1} + \boldsymbol{\Delta\zeta}^{tt}\boldsymbol{\mu}_0^{tt} - \boldsymbol{\Delta\zeta}^{tr} \left(\boldsymbol{\zeta}_0^{rr} + \boldsymbol{\Delta\zeta}^{rr}\right)^{-1} \boldsymbol{\Delta\zeta}^{rt}\boldsymbol{\mu}_0^{tt} \right]^{-1} \tag{B.9}$$

and expand the expression $1/(1+\delta) = 1 - \delta + \delta^2 - \dots$ around the bulk quantities. Restricting to quantities decaying slower than z_0^{-3}, we immediately find Eq. (4.7). An analogous procedure leads to the tr, rt and rr mobilities, where the elements of the bulk friction and mobility tensors combine to contribute only in the form of $\boldsymbol{\mu}_0^{dr} = \boldsymbol{\mu}_0^{rr}\boldsymbol{\zeta}_0^{rd}$ and $\boldsymbol{\mu}_0^{rd} = -\boldsymbol{\zeta}_0^{dr}\boldsymbol{\mu}_0^{rr}$. The latter relations follow from the definitions (3.3) and (3.4).

C Expressions required for the spheroid mobilities

The results for the correction are given in terms of the wall-particle distance z_0, its inclination angle θ and functions denoted by capital letters in Eqs. (6.13) through (6.23) of the dimensionless shearing and bending parameters, β and β_B. Below, we provide explicit expressions for these functions. They can conveniently be expressed in terms of higher order exponential integrals [90]. The contributions from the membrane shearing (index S) and bending (index B) are given separately. By summing up both, we arrive at the final expressions. Notably, in the limit of vanishing frequency, our results are in complete agreement with those given by Refs. [59, 91].

C.1 Translational mobility

For the functions P and Q, we find the shearing contribution as

$$\begin{aligned} P_\mathrm{S}(\beta) &= -\frac{5}{4} + \frac{\beta^2}{8} - \frac{3i\beta}{8} + \frac{2i\beta}{B}\Gamma_2 + \left(-\frac{\beta^2}{2} + \frac{i\beta}{2}\left(1 - \frac{\beta^2}{4}\right)\right) e^{i\beta}\,\mathrm{E}_1(i\beta)\,, \\ Q_\mathrm{S}(\beta) &= -\frac{3}{2} e^{i\beta}\,\mathrm{E}_4(i\beta)\,, \end{aligned}$$

and the bending part

$$\begin{aligned} P_\mathrm{B}(\beta_\mathrm{B}) &= -\frac{1}{4} + \frac{i\beta_\mathrm{B}^3}{24}\left(\phi_+ + \Gamma_\mathrm{B}\right)\,, \\ Q_\mathrm{B}(\beta_\mathrm{B}) &= -\frac{5}{2} + i\beta_\mathrm{B}\left(\left(\frac{\beta_\mathrm{B}^2}{12} + \frac{i\beta_\mathrm{B}}{6} + \frac{1}{6}\right)\phi_+ + \left(\frac{\beta_\mathrm{B}^2}{12} - \frac{i\beta_\mathrm{B}}{3} - \frac{1}{3}\right) e^{-i\beta_\mathrm{B}}\,\mathrm{E}_1(-i\beta_\mathrm{B}) + \frac{\sqrt{3}}{6}(\beta_\mathrm{B} + i)\phi_- \right), \end{aligned}$$

with

$$\begin{aligned} \phi_\pm &= e^{-i\overline{z_\mathrm{B}}}\,\mathrm{E}_1(-i\overline{z_\mathrm{B}}) \pm e^{-iz_\mathrm{B}}\,\mathrm{E}_1(-iz_\mathrm{B})\,, \\ \Gamma_2 &= e^{\frac{2i\beta}{B}}\,\mathrm{E}_1\left(\frac{2i\beta}{B}\right)\,, \\ \Gamma_\mathrm{B} &= e^{-i\beta_\mathrm{B}}\,\mathrm{E}_1(-i\beta_\mathrm{B})\,, \end{aligned}$$

where $z_\mathrm{B} := \beta_\mathrm{B} e^{2i\pi/3}$ and the bar denotes the complex conjugate. The function E_n is the generalised exponential integral, $\mathrm{E}_n(x) = \int_1^\infty t^{-n}e^{-xt}\mathrm{d}t$.

C.2 Translation-rotation coupling

The translation-rotation coupling is determined by the functions M and N, which we similarly decompose into two parts. Recalling that $B = 2/(1+C)$, the shearing part reads

$$M_{\mathrm{S}}(\beta) = \frac{3}{4} - i\beta\left(\frac{1}{4}+\frac{1}{B}\right) + \frac{3\beta^2}{8} + \frac{i\beta^3}{8} - \frac{\beta^2}{2}\left(1 + i\beta - \frac{\beta^2}{4}\right)\Gamma_1 - \frac{2\beta^2}{B^2}\Gamma_2\,,$$
$$N_{\mathrm{S}}(\beta) = -\frac{3}{4} + i\beta\left(\frac{1}{2}+\frac{2}{B}\right) - \frac{3\beta^2}{8} + \frac{i\beta^3}{8} + \beta^2\left(1 + \frac{i\beta}{4} + \frac{\beta^2}{8}\right)\Gamma_1 + \frac{4\beta^2}{B^2}\Gamma_2\,,$$

while the bending part is

$$M_{\mathrm{B}}(\beta_{\mathrm{B}}) = \frac{3}{4} - \frac{i\beta_{\mathrm{B}}^3}{8} + \frac{\beta_{\mathrm{B}}^4}{24}\Gamma_{\mathrm{B}} + \frac{\beta_{\mathrm{B}}^3}{24}\psi\,,$$
$$N_{\mathrm{B}}(\beta_{\mathrm{B}}) = \frac{9}{4} - \frac{i\beta_{\mathrm{B}}^3}{8} - \frac{\beta_{\mathrm{B}}^3}{4}\left(i - \frac{\beta_{\mathrm{B}}}{6}\right)\Gamma_{\mathrm{B}} + \frac{\beta_{\mathrm{B}}^3}{24}\psi - \frac{i\beta_{\mathrm{B}}^3}{4}\phi_+\,,$$

where we defined

$$\Gamma_1 = e^{i\beta}\,\mathrm{E}_1(i\beta)\,,$$
$$\psi = \overline{z_{\mathrm{B}}}e^{-i\overline{z_{\mathrm{B}}}}\,\mathrm{E}_1(-i\overline{z_{\mathrm{B}}}) + z_{\mathrm{B}}e^{-iz_{\mathrm{B}}}\,\mathrm{E}_1(-iz_{\mathrm{B}})\,.$$

C.3 Rotational mobility

The rotational mobility is described by a set of functions. The functions A_0 and A_2 defined for the component $\Delta\mu_{11}^{rr}$ in Eq. (6.20) are given by

$$A_{0,\mathrm{S}}(\beta) = -\frac{3}{2} + \frac{i\beta}{2}\left(1+\frac{1}{B}\right) + \beta^2\left(\frac{1}{2}+\frac{1}{B^2}\right) - \frac{i\beta^3}{2}\Gamma_1 - \frac{2i\beta^3}{B^3}\Gamma_2\,,$$
$$A_{2,\mathrm{S}}(\beta) = \frac{1}{2} + \frac{i\beta}{2}\left(\frac{1}{B}-1\right) + \beta^2\left(\frac{1}{B^2}-\frac{1}{2}\right) + \frac{i\beta^3}{2}\Gamma_1 - \frac{2i\beta^3}{B^3}\Gamma_2\,,$$
$$A_{0,\mathrm{B}}(\beta_{\mathrm{B}}) = -A_{2,\mathrm{B}}(\beta_{\mathrm{B}}) = -1 + \frac{i\beta_{\mathrm{B}}^3}{6}\left(\phi_+ + \Gamma_{\mathrm{B}}\right)\,.$$

For the component $\Delta\mu_{13}^{rr}$, the function D defined in Eq. (6.21) is given by

$$D_{\mathrm{S}}(\beta) = -\frac{1}{2} + \frac{i\beta}{2}\left(1 - \frac{1-\lambda}{B}\right) + \beta^2\left(\frac{1}{2}+\frac{\lambda}{4}-\frac{1-\lambda}{B^2}\right) + i\beta^3\Bigg(\frac{2(1-\lambda)}{B^3}\Gamma_2 - \frac{\lambda+1}{2}\Gamma_1 + \frac{\lambda}{4}\Bigg) + \frac{\lambda\beta^4}{4}\Gamma_1\,,$$
$$D_{\mathrm{B}}(\beta_{\mathrm{B}}) = -1 + \frac{3\lambda}{2} + \frac{\beta_{\mathrm{B}}^3}{4}\left(-i\lambda + \frac{2i}{3}\Gamma_{\mathrm{B}} + \frac{2i\phi_+ + \lambda\psi}{3}\right) + \frac{\lambda\beta_{\mathrm{B}}^4}{12}\Gamma_{\mathrm{B}}\,.$$

Further, the shearing related parts of C_0, C_2 and C_4 as defined for the correction $\Delta\mu_{22}^{rr}$ in Eq. (6.22)

read

$$
\begin{aligned}
C_{0,\mathrm{S}}(\beta) &= -\frac{3}{2}\left(1+\lambda^2\right) + \left(\frac{i\lambda^2\beta^2}{8} - \frac{\lambda(1-\lambda)\beta}{2} - \frac{i(1-\lambda)^2}{2}\right)\beta^3\Gamma_1 - \frac{2i}{B^3}(1-\lambda)^2\beta^3\Gamma_2 \\
&\quad + \frac{i\beta}{4}\left(\lambda^2+2+\frac{2(1-\lambda)^2}{B}\right) + \frac{\beta^2}{4}\left(\lambda^2-2\lambda+2+\frac{4(1-\lambda)^2}{B^2}\right) \\
&\quad - i\lambda\beta^3\left(\frac{1}{2}-\frac{3\lambda}{8}\right) - \frac{\lambda^2\beta^4}{8}\,, \\
C_{2,\mathrm{S}}(\beta) &= \frac{3\lambda}{4} - \beta^3(2+i\beta)\left(i - \frac{3}{32}\lambda(\beta-2i)\right)\Gamma_1 - \frac{2i}{B^3}(4-3\lambda)\beta^3\Gamma_2 + \frac{i\beta}{2}\left(\frac{3\lambda}{8}+\frac{4-3\lambda}{B}\right) \\
&\quad + \beta^2\left(\frac{3\lambda}{16}+1+\frac{4-3\lambda}{B^2}\right) + i\beta^3\left(\frac{9\lambda}{32}+1\right) - \frac{3\lambda}{32}\beta^4\,, \\
C_{4,\mathrm{S}}(\beta) &= -\frac{3}{4} + 3i\beta\left(-\frac{1}{16}+\frac{1}{2B}\right) + 3\beta^2\left(-\frac{1}{16}+\frac{1}{B^2}\right) + i\beta^3\left(-\frac{9}{32}-\frac{6}{B^3}\Gamma_2\right) \\
&\quad + \frac{3}{8}\beta^3\left(i-\beta-\frac{i}{4}\beta^2\right)\Gamma_1 + \frac{3}{32}\beta^4\,,
\end{aligned}
$$

and the bending-related parts read

$$
\begin{aligned}
C_{0,\mathrm{B}}(\beta_\mathrm{B}) &= -1 - 3\lambda(1+\lambda) + \frac{i\beta_\mathrm{B}^3}{8}\lambda(\lambda+4) - \frac{\beta_\mathrm{B}^3}{24}(i\lambda^2\beta_\mathrm{B}^2 + 4\lambda\beta_\mathrm{B} - 4i)\Gamma_\mathrm{B} \\
&\quad + \frac{\beta_\mathrm{B}^3}{6}\left(i\phi_+ - \lambda\psi + \frac{i\lambda^2}{4}\beta_\mathrm{B}(\psi+\beta_\mathrm{B}\phi_+)\right), \\
C_{2,\mathrm{B}}(\beta_\mathrm{B}) &= 6 - \frac{9}{4}\lambda - i\beta_\mathrm{B}^3\left(1-\frac{3\lambda}{32}\right) + \left(\frac{1}{3} - \frac{i\lambda\beta_\mathrm{B}}{32}\right)\beta_\mathrm{B}^4\Gamma_\mathrm{B} + \frac{\beta_\mathrm{B}^3}{3}\psi + \frac{i\lambda\beta_\mathrm{B}^4}{32}(\psi+\beta_\mathrm{B}\phi_+)\,, \\
C_{4,\mathrm{B}}(\beta_\mathrm{B}) &= \frac{9}{4} - \frac{3i\beta_\mathrm{B}^3}{32} + \frac{i\beta_\mathrm{B}^5}{32}\Gamma_\mathrm{B} - \frac{i\beta_\mathrm{B}^4}{32}(\psi+\beta_\mathrm{B}\phi_+)\,,
\end{aligned}
$$

Finally, the functions H_0 and H_2 defined for the component $\Delta\mu_{33}^{rr}$ in Eq. (6.23) read

$$
\begin{aligned}
H_{0,\mathrm{S}}(\beta) &= -1 - \frac{3}{4}\lambda^2 + i\beta\left(\frac{\lambda^2+2}{2B}+\frac{\lambda^2}{16}\right) + \beta^2\left(\frac{2+\lambda^2}{B^2}+\frac{\lambda^2}{16}\right) + \frac{\lambda^2\beta^3}{32}(i\beta^2-4i+4\beta)\Gamma_1 \\
&\quad + \beta^3\left(\frac{3i\lambda^2}{32} - \frac{2i}{B^3}(\lambda^2+2)\Gamma_2\right) - \frac{\lambda^2\beta^4}{32}\,, \\
H_{2,\mathrm{S}}(\beta) &= -\frac{1}{2} - \frac{3}{4}\lambda^2 + \beta\left(\frac{3i}{16}\lambda^2 + \frac{i\lambda}{B} + \frac{i}{2} - \frac{i}{2B}\right) + \beta^2\left(\frac{3}{16}\lambda^2 + \frac{\lambda+1}{2} + \frac{2\lambda}{B^2} - \frac{1}{B^2}\right) \\
&\quad + \frac{\beta^3}{32}\left(9i\lambda^2 + 16i\lambda + \frac{64i(1-2\lambda)\Gamma_2}{B^3} + (4+6\lambda+3i\lambda\beta)(\lambda\beta-2i\lambda-4i)\Gamma_1\right) - \frac{3\lambda^2\beta^4}{32}\,,
\end{aligned}
$$

and

$$
\begin{aligned}
H_{0,\mathrm{B}}(\beta_\mathrm{B}) &= \lambda^2\left(-\frac{3}{4} + \frac{i\beta_\mathrm{B}^3}{32} - \frac{i\beta_\mathrm{B}^5}{96}\Gamma_\mathrm{B} + \frac{i\beta_\mathrm{B}^4}{96}(\psi+\beta_\mathrm{B}\phi_+)\right), \\
H_{2,\mathrm{B}}(\beta_\mathrm{B}) &= -1 + 3\lambda - \frac{9}{4}\lambda^2 + \beta_\mathrm{B}^3\left(i\lambda\left(\frac{3}{32}\lambda-\frac{1}{2}\right) + \frac{1}{6}\left(i+\lambda\beta_\mathrm{B} - \frac{3i\lambda^2\beta_\mathrm{B}^2}{16}\right)\Gamma_\mathrm{B}\right) \\
&\quad + \frac{i\lambda^2\beta_\mathrm{B}^4}{32}(\psi+\beta_\mathrm{B}\phi_+) + \frac{\beta_\mathrm{B}^3}{6}(\lambda\psi + i\phi_+)\,.
\end{aligned}
$$

Bibliography

[1] S. Naahidi, M. Jafari, F. Edalat, K. Raymond, A. Khademhosseini, and P. Chen, J. Control. Release **166**, 182 (2013).

[2] H. Al-Obaidi and A. T. Florence, J. Drug Deliv. Sci. Technol. **30**, 266 (2015).

[3] J. Liu, T. Wei, J. Zhao, Y. Huang, H. Deng, A. Kumar, C. Wang, Z. Liang, X. Ma, and X.-J. Liang, Biomaterials **91**, 44 (2016).

[4] G. J. Doherty and H. T. McMahon, Annu. Rev. Biochem. **78**, 857 (2009).

[5] A. Meinel, B. Tränkle, W. Römer, and A. Rohrbach, Soft Matter **10**, 3667 (2014).

[6] J. Agudo-Canalejo and R. Lipowsky, ACS Nano **9**, 3704 (2015).

[7] H. A. Lorentz, Abh. Theor. Phys. **1**, 23 (1907).

[8] H. Brenner, Chem. Eng. Sci. **16**, 242 (1961).

[9] A. J. Goldman, R. G. Cox, and H. Brenner, Chem. Eng. Sci. **22**, 637 (1967).

[10] A. J. Goldman, R. G. Cox, and H. Brenner, Chem. Eng. Sci. **22**, 653 (1967).

[11] B. Cichocki and R. B. Jones, Physica A **258**, 273 (1998).

[12] J. W. Swan and J. F. Brady, Phys. Fluids **19**, 113306 (2007).

[13] T. Franosch and S. Jeney, Phys. Rev. E **79**, 031402 (2009).

[14] J. Happel and H. Brenner, *Low Reynolds number hydrodynamics: with special applications to particulate media*, Vol. 1 (Springer Science & Business Media, 2012).

[15] S. H. Lee, R. S. Chadwick, and L. G. Leal, J. Fluid Mech. **93**, 705 (1979).

[16] T. Bickel, Eur. Phys. J. E **20**, 379 (2006).

[17] T. Bickel, Phys. Rev. E **75**, 041403 (2007).

[18] G. M. Wang, R. Prabhakar, and E. M. Sevick, Phys. Rev. Lett. **103**, 248303 (2009).

[19] J. Bławzdziewicz, M. Ekiel-Jeżewska, and E. Wajnryb, J. Chem. Phys. **133**, 114702 (2010).

[20] T. Bickel, EPL (Europhys. Lett.) **106**, 16004 (2014).

[21] E. Lauga and T. M. Squires, Phys. Fluids **17**, 103102 (2005).

[22] B. U. Felderhof, Phys. Rev. E **85**, 046303 (2012).

[23] B. U. Felderhof, J. Chem. Phys. **125**, 124904 (2006).

[24] B. U. Felderhof, J. Chem. Phys. **125**, 144718 (2006).

[25] R. Shlomovitz, A. Evans, T. Boatwright, M. Dennin, and A. Levine, Phys. Rev. Lett. **110**, 137802 (2013).

[26] R. Shlomovitz, A. A. Evans, T. Boatwright, M. Dennin, and A. J. Levine, Phys. Fluids **26** (2014).

[27] T. Salez and L. Mahadevan, J. Fluid Mech. **779**, 181 (2015).

[28] A. Daddi-Moussa-Ider, A. Guckenberger, and S. Gekle, Phys. Rev. E **93**, 012612 (2016).

[29] A. Daddi-Moussa-Ider, A. Guckenberger, and S. Gekle, Phys. Fluids **28**, 071903 (2016).

[30] A. Daddi-Moussa-Ider and S. Gekle, J. Chem. Phys. **145**, 014905 (2016).

[31] B. Saintyves, T. Jules, T. Salez, and L. Mahadevan, Proc. Nat. Acad. Sci. **113**, 5847 (2016).

[32] L. P. Faucheux and A. J. Libchaber, Phys. Rev. E **49**, 5158 (1994).

[33] B. Lin, J. Yu, and S. A. Rice, Phys. Rev. E **62**, 3909 (2000).

[34] E. R. Dufresne, D. Altman, and D. G. Grier, EPL (Europhys. Lett.) **53**, 264 (2001).

[35] E. Schäffer, S. F. Nørrelykke, and J. Howard, Langmuir **23**, 3654 (2007).

[36] H. B. Eral, J. M. Oh, D. van den Ende, F. Mugele, and M. H. G. Duits, Langmuir **26**, 16722 (2010).

[37] A. E. Cervantes-Martínez, A. Ramírez-Saito, R. Armenta-Calderón, M. A. Ojeda-López, and J. L. Arauz-Lara, Phys. Rev. E **83**, 030402 (2011).

[38] S. L. Dettmer, S. Pagliara, K. Misiunas, and U. F. Keyser, Phys. Rev. E **89**, 062305 (2014).

[39] B. Tränkle, D. Ruh, and A. Rohrbach, Soft Matter **12**, 2729 (2016).

[40] P. Holmqvist, J. K. G. Dhont, and P. R. Lang, J. Chem. Phys. **126**, 044707 (2007).

[41] V. N. Michailidou, G. Petekidis, J. W. Swan, and J. F. Brady, Phys. Rev. Lett. **102**, 068302 (2009).

[42] M. Lisicki, B. Cichocki, J. K. G. Dhont, and P. R. Lang, J. Chem. Phys. **136**, 204704 (2012).

[43] S. A. Rogers, M. Lisicki, B. Cichocki, J. K. G. Dhont, and P. R. Lang, Phys. Rev. Lett. **109**, 098305 (2012).

[44] V. N. Michailidou, J. W. Swan, J. F. Brady, and G. Petekidis, J. Chem. Phys. **139**, 164905 (2013).

[45] W. Wang and P. Huang, Phys. Fluids **26**, 092003 (2014).

[46] M. Lisicki, B. Cichocki, S. A. Rogers, J. K. G. Dhont, and P. R. Lang, Soft Matter **10**, 4312 (2014).

[47] H. Kress, E. H. K. Stelzer, G. Griffiths, and A. Rohrbach, Phys. Rev. E **71**, 061927 (2005).

[48] T. Boatwright, M. Dennin, R. Shlomovitz, A. A. Evans, and A. J. Levine, Phys. Fluids **26**, 071904 (2014).

[49] F. Jünger, F. Kohler, A. Meinel, T. Meyer, R. Nitschke, B. Erhard, and A. Rohrbach, Biophys. J. **109**, 869 (2015).

[50] M. Irmscher, A. M. de Jong, H. Kress, and M. W. J. Prins, Biophys. J. **102**, 698 (2012).

[51] F. Perrin, J. Phys. Radium **5**, 497 (1934).

[52] F. Perrin, J. Phys. Radium **7**, 1 (1936).

[53] G. K. Batchelor, J. Fluid Mech. **44**, 419 (1970).

[54] A. T. Chwang and T. Y.-T. Wu, J. Fluid Mech. **67**, 787 (1975).

[55] N. J. De Mestre and W. B. Russel, J. Eng. Math. **9**, 81 (1975).

[56] D. Schiby and I. Gallily, J. Colloid Interface Sci. **77**, 328 (1980).

[57] W. H. Mitchell and S. E. Spagnolie, J. Fluid Mech. **772**, 600 (2015).

[58] J. R. Blake and G. R. Fulford, Bull. Aust. Math. Soc. **24**, 27 (1981).

[59] M. Lisicki, B. Cichocki, and E. Wajnryb, J. Chem. Phys. **145**, 034904 (2016).

[60] R. Hsu and P. Ganatos, J. Fluid Mech. **207**, 29 (1989).

[61] J. T. Padding and W. J. Briels, J. Chem. Phys. **132**, 054511 (2010).

[62] A. Neild, J. T. Padding, L. Yu, B. Bhaduri, W. J. Briels, and T. W. Ng, Phys. Rev. E **82**, 041126 (2010).

[63] M. De Corato, F. Greco, G. Davino, and P. L. Maffettone, J. Chem. Phys. **142**, 194901 (2015).

[64] Y. Han, A. M. Alsayed, M. Nobili, J. Zhang, T. C. Lubensky, and A. G. Yodh, Science **314**, 626 (2006).

[65] Y. Han, A. Alsayed, M. Nobili, and A. G. Yodh, Phys. Rev. E **80**, 011403 (2009).

[66] Z. Zheng and Y. Han, J. Chem. Phys. **133**, 124509 (2010).

[67] G. Li and J. X. Tang, Phys. Rev. E **69**, 061921 (2004).

[68] R. Duggal and M. Pasquali, Phys. Rev. Lett. **96**, 246104 (2006).

[69] B. Bhaduri, A. Neild, and T. W. Ng, Appl. Phys. Lett. **92**, 084105 (2008).

[70] F. C. Cheong and D. G. Grier, Optics express **18**, 6555 (2010).

[71] R. Colin, M. Yan, L. Chevry, J.-F. Berret, and B. Abou, EPL (Europhys. Lett.) **97**, 30008 (2012).

[72] D. Mukhija and M. J. Solomon, J. Colloid Interface Sci. **314**, 98 (2007).

[73] T. A. Waigh, Rep. Prog. Phys. **79**, 074601 (2016).

[74] B. U. Felderhof, Phys. Fluids **25**, 013101 (2013).

[75] S. Kim and S. J. Karrila, *Microhydrodynamics: principles and selected applications* (Courier Corporation, 2013).

[76] R. Skalak, A. Tozeren, R. P. Zarda, and S. Chien, Biophys. J. **13(3)**, 245 (1973).

[77] T. Krüger, F. Varnik, and D. Raabe, Comp. Math. Appl. **61**, 3485 (2011).

[78] J. B. Freund, Annu. Rev. Fluid Mech. **46**, 67 (2014).

[79] W. Helfrich, Z. Naturf. C. **28**, 693 (1973).

[80] B. Cichocki, R. B. Jones, R. Kutteh, and E. Wajnryb, J. Chem. Phys. **112**, 2548 (2000).

[81] J. R. Blake, Math. Proc. Camb. Phil. Soc. **70**, 303 (1971).

[82] C. Pozrikidis, J. Comput. Phys. **169**, 250 (2001).

[83] H. Zhao and E. S. G. Shaqfeh, Phys. Rev. E **83**, 061924 (2011).

[84] L. Zhu, *Simulation of individual cells in flow*, Ph.D. thesis (2014).

[85] H. Power and G. Miranda, SIAM J. on App. Math. **47**, pp. 689 (1987).

[86] H. Zhao, E. S. G. Shaqfeh, and V. Narsimhan, Phys. Fluids **24**, 011902 (2012).

[87] A. Guckenberger, M. P. Schraml, P. G. Chen, M. Leonetti, and S. Gekle, Comp. Phys. Comm. **207**, 1 (2016).

[88] A. R. Conn, N. I. M. Gould, and P. L. Toint, *Trust region methods*, Vol. 1 (Siam, 2000).

[89] R. Bracewell, *The Fourier Transform and Its Applications* (McGraw-Hill, 1999).

[90] M. Abramowitz, I. A. Stegun, *et al.*, *Handbook of mathematical functions*, Vol. 1 (Dover New York, 1972).

[91] M. Lisicki, *Evanescent wave dynamic light scattering by optically anisotropic Brownian particles*, Ph.D. thesis, University of Warsaw (2015).

Publication 6

Hydrodynamic mobility of a sphere moving on the centerline of an elastic tube

A. Daddi-Moussa-Ider, M. Lisicki and S. Gekle

Under review (2017)

Abstract

Elastic channels are an important component of many soft matter systems, in which hydrodynamic interactions with confining membranes determine the behavior of particles in flow. In this work, we derive analytical expressions for the Green's functions associated to a point-force (Stokeslet) directed parallel or perpendicular to the axis of an elastic cylindrical channel exhibiting resistance against shearing and bending. We then compute the leading order self- and pair-mobility functions of particles on the cylinder axis, finding that the mobilities are primarily determined by membrane shearing and that bending does not play a significant role. In the vanishing-frequency limit, the particle self- and pair-mobilities near a no-slip hard cylinder are recovered only if the membrane possess a non-vanishing shearing rigidity. We further compute the membrane deformation, finding that deformation is generally more pronounced in the axial and radial directions, for the motion along and perpendicular to the cylinder centerline, respectively. Our analytical predictions are verified and compared to fully resolved boundary integral simulations where a very good agreement is obtained.

1 Introduction

Many biological and industrial microscale processes occur in geometric confinement, which is known to strongly affect the diffusional dynamics in a viscous fluid [1, 2]. Hydrodynamic interactions with boundaries play a key role in such systems by determining their transport properties [3–7]. Tubular confinement is of particular interest, since flow in living organisms often involves channel-like structures, such as arteries in the cardiovascular system [8]. A common feature of these complex networks of channels is the elasticity of their building material. Arteries and capillaries of the blood system involve a large number of collagen and elastin filaments, which gives them the ability to stretch in response to changing pressure [9, 10]. Elastic deformation has been further utilized to control and direct fluid flow within flexible microfluidic devices [11–13].

The motion of a small sphere in a viscous fluid filling a rigid cylinder is a well studied problem. A review of most analytical developments can be found in the classic book of Happel and Brenner [14]. In particular, axial motion has been studied using the method of reflections by Faxén [15, 16], Wakiya [17], Bohlin [18] and Zimmerman [19], to name a few, expressing the mobility in power series of the ratio of particle to cylinder diameter. These works have been extended to finite-sized spheres [20, 21], pair interactions [22, 23] and recently to non-spherical particles [25]. For an arbitrarily positioned particle, and in the presence of an external Poiseuille flow, the procedure has been generalized to yield expressions in terms of the particle and channel radius, and the eccentricity of the position of the particle, as derived e.g. in the works of Happel and collaborators [26–29] and Liron and Shahar [30]. The slow motion of two spherical particles symmetrically placed about the axis of a cylinder in a direction perpendicular to their line of centers has later been studied by Greenstein and Happel [31]. Experimental verification of these results has been performed e.g. by the use of laser interferometry by Lecoq *et al.*[32] or using digital video microscopy measurements by Cui *et al.* [22]. Theoretical developments have been supplemented by numerical computations of the resistance functions for spheres, bubbles and drops in cylindrical tubes [33–38]. Other works include motion perpendicular to the axis [39], finite length of the tube [40] and the flow around a line of equispaced spheres moving at a prescribed velocity along the axis of a circular tube [41]. Transient effects have also been taken into account in the works of Felderhof, both in the case of an incompressible [42] and compressible fluid [43–45].

For elastic cylinders, most previous work has focused on the flow itself which is driven through a deformable elastic channel [46, 47] where various physiological phenomena related to the cardiovascular and respiratory systems have been observed, including the generation of instabilities [48], small-amplitude wave propagation [49, 50], hysteresis behavior of arterial walls [51] and anomalous

bubble propagation [52, 53]. Further work has been devoted to investigate the influence of elastic tube deformation on flow behavior of a shear-thinning fluid [54–56], the steady flow in thick-walled flexible elastic tubes [57, 58] or the tensile instability under an axial load [59, 60]. More recently, the lateral mobility of membrane inclusions in a cylindrical biological membrane has been studied theoretically [61, 62].

The mobility of a particle inside an elastic cylinder, despite its importance for blood flow, has not been studied so far. Motivated by this knowledge gap, we turn our attention to the problem of hydrodynamic mobility of a small spherical particle slowly moving in a viscous fluid filling a circular cylindrical elastic tube. In blood flow through small capillaries, the Reynolds number is typically very small allowing us to adopt the framework of creeping (Stokes) flow [63]. It is known from previous works on systems bounded by elastic surfaces [64] that their deformations introduce memory into the system, which may lead to transient anomalous diffusion [65, 66] or a change of sign of pair hydrodynamic interactions [67]. We determine the frequency-dependent mobility of a small particle confined in a cylindrical membrane of given elastic shearing modulus and bending rigidity in an incompressible Newtonian fluid filling the whole space. The solution is obtained by directly solving the Stokes equations in cylindrical geometry by the use of Fourier-Bessel expansion to represent the fluid velocity and pressure.

The remainder of the paper is organised as follows. In section 2, we formulate the problem of axial and radial motions of a small colloid inside an elastic tube in terms of the Stokes equations supplemented by appropriate boundary conditions. We then present the method of solving these equations and use the obtained results in section 3 to derive explicit expressions for the frequency-dependent self- and pair mobility functions for colloids moving along or perpendicular to the centreline of the tube. Further, we calculate the reaction tensor which allows to find the deformation of the membrane for a given actuation. In section 4, we compare our theoretical developments to boundary integral numerical simulations for a chosen set of parameters for particles moving under a harmonic or a steady constant external force. We conclude the paper in section 5 and relegate technical details to the appendices. In appendix A, we derive in cylindrical coordinates the traction jumps across a membrane endowed with shear and bending resistances, which serve as boundary conditions for the calculation of the relevant Stokes flow. Appendices B and C provide explicit analytical solutions for axial and radial motions, respectively, for the two limiting cases of a membrane resisting either only to shear or only to bending. The solution combining the two can be derived in the same way.

2 Theoretical description

We consider a small spherical particle of radius a fully immersed in a Newtonian fluid and moving on the axis of a cylindrical elastic tube of initial (undeformed) radius $R \gg a$. The tube membrane exhibits resistance against shear and bending. We choose the cylindrical coordinate system (r, ϕ, z) where the z coordinate is directed along the cylinder axis with the origin located at the centre of the particle (see figure 1 for an illustration of the system setup). The regions inside and outside the cylinder are labeled 1 and 2, respectively.

We proceed by computing the Green's functions which are solutions of the Stokes equations

$$\eta \boldsymbol{\nabla}^2 \boldsymbol{v}_1 - \boldsymbol{\nabla} p_1 + \boldsymbol{F}(t)\, \delta(\boldsymbol{r}) = 0\,, \tag{2.1a}$$

$$\boldsymbol{\nabla} \cdot \boldsymbol{v}_1 = 0\,, \tag{2.1b}$$

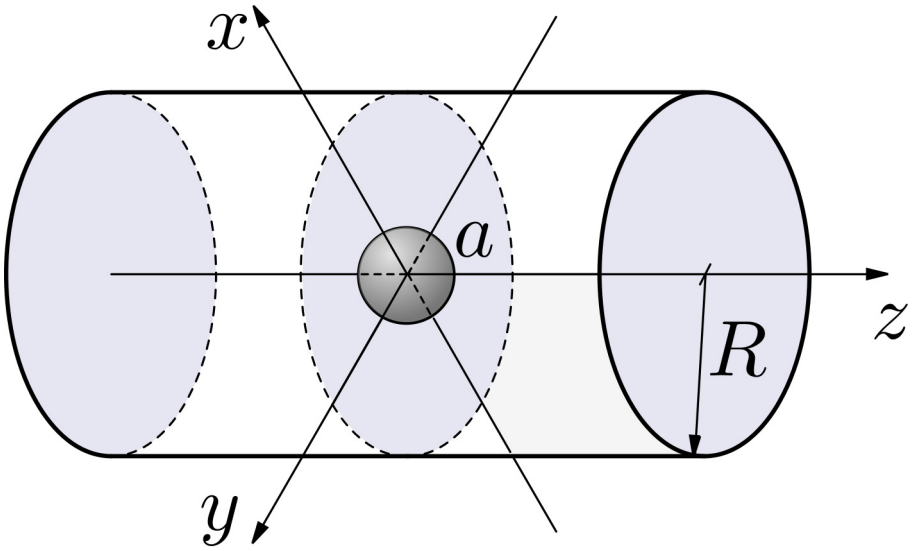

Figure 1: Illustration of the system setup. A small spherical solid particle of radius a located at the origin moving on the centreline of a deformable elastic tube of radius R.

inside the tube (for $r < R$) and

$$\eta \boldsymbol{\nabla}^2 \boldsymbol{v}_2 - \boldsymbol{\nabla} p_2 = 0\,, \tag{2.2a}$$
$$\boldsymbol{\nabla} \cdot \boldsymbol{v}_2 = 0\,, \tag{2.2b}$$

outside (for $r > R$). Here η denotes the fluid shear viscosity, assumed to be the same everywhere. $\boldsymbol{F}(t)$ is an arbitrary time-dependent point-force acting at the particle position. We therefore need to solve Eqs. (2.1) and (2.2) subject to the regularity conditions

$$|\boldsymbol{v}_1| < \infty \ \text{ for } |\boldsymbol{r}| = 0\,, \tag{2.3}$$
$$\boldsymbol{v}_1 \to \boldsymbol{0} \ \text{ for } z \to \infty\,, \tag{2.4}$$
$$\boldsymbol{v}_2 \to \boldsymbol{0} \ \text{ for } |\boldsymbol{r}| \to \infty\,, \tag{2.5}$$

together with the boundary conditions imposed at the surface $r = R$, assuming small deformations, namely the natural continuity of fluid velocity

$$[v_r] = 0\,, \tag{2.6}$$
$$[v_\phi] = 0\,, \tag{2.7}$$
$$[v_z] = 0\,, \tag{2.8}$$

and the traction jumps stemming from membrane elastic deformation

$$[\sigma_{zr}] = \Delta f_z^{\mathrm{S}}\,, \tag{2.9}$$
$$[\sigma_{\phi r}] = \Delta f_\phi^{\mathrm{S}}\,, \tag{2.10}$$
$$[\sigma_{rr}] = \Delta f_r^{\mathrm{S}} + \Delta f_r^{\mathrm{B}}\,, \tag{2.11}$$

where the notation $[w] := w(r = R^+) - w(r = R^-)$ stands for the jump of a given quantity w across the cylindrical elastic membrane. These linearised traction jumps can be decomposed into two

contributions due to shear (superscript S) and bending (superscript B). The membrane is modeled by combining the neo-Hookean model for shear [68–71], and the Helfrich model [72, 73] for bending of its surface. As derived in appendix A, the linearised traction jumps due to shear are written as

$$\Delta f_\phi^{\mathrm{S}} = -\frac{\kappa_{\mathrm{S}}}{3}\left(u_{\phi,zz} + \frac{3u_{z,\phi z}}{R} + \frac{4(u_{r,\phi}+u_{\phi,\phi\phi})}{R^2}\right), \tag{2.12a}$$

$$\Delta f_z^{\mathrm{S}} = -\frac{\kappa_{\mathrm{S}}}{3}\left(4u_{z,zz} + \frac{2u_{r,z}+3u_{\phi,z\phi}}{R} + \frac{u_{z,\phi\phi}}{R^2}\right), \tag{2.12b}$$

$$\Delta f_r^{\mathrm{S}} = \frac{2\kappa_{\mathrm{S}}}{3}\left(\frac{2(u_r+u_{\phi,\phi})}{R^2} + \frac{u_{z,z}}{R}\right), \tag{2.12c}$$

where κ_{S} is the surface shear modulus (expressed in N/m). Here $\boldsymbol{u}(\phi,z) = u_r(\phi,z)\boldsymbol{e}_r + u_\phi(\phi,z)\boldsymbol{e}_\phi + u_z(\phi,z)\boldsymbol{e}_z$ is the membrane deformation field. The comma in indices denotes a partial spatial derivative.

For bending, only a normal traction jump appears

$$\Delta f_r^{\mathrm{B}} = \kappa_{\mathrm{B}}\Big(R^3 u_{r,zzzz} + 2R(u_{r,zz}+u_{r,zz\phi\phi}) + \frac{u_r + 2u_{r,\phi\phi} + u_{r,\phi\phi\phi\phi}}{R}\Big), \tag{2.13}$$

where κ_{B} is the bending modulus (expressed in Nm). Note that Helfrich bending does not introduce a discontinuity in the tangential traction jumps [73].

The effect of these two elastic modes, given the characteristic frequency of actuation ω, is determined by two dimensionless quantities, the shear coefficient α and the bending coefficient α_{B}, defined as

$$\alpha := \frac{2\kappa_{\mathrm{S}}}{3\eta R\omega}, \qquad \alpha_{\mathrm{B}} := \frac{1}{R}\left(\frac{\kappa_{\mathrm{B}}}{\eta\omega}\right)^{1/3}. \tag{2.14}$$

Note that this definition is slightly different than in our earlier works [65]. The actuation frequency ω is assumed to be small enough so that the flow Strouhal number $\mathrm{St} = \omega R/V$ remains small, with V being the amplitude of the particle velocity.

In cylindrical coordinates, the components of the fluid stress tensor are expressed in the usual way as [74]

$$\begin{aligned}
\sigma_{\phi r} &= \eta\left(v_{\phi,r} - \frac{v_\phi + v_{r,\phi}}{r}\right),\\
\sigma_{zr} &= \eta(v_{z,r} + v_{r,z}),\\
\sigma_{rr} &= -p + 2\eta v_{r,r}.
\end{aligned}$$

A direct relationship between velocity and displacement at the undisplaced membrane $r = R$ can be obtained from the no-slip boundary condition, $\boldsymbol{v} = \partial_t \boldsymbol{u}$. Transforming to the temporal Fourier space, we have [75]

$$u_\alpha(\phi,z) = \left.\frac{v_\alpha(r,\phi,z)}{i\omega}\right|_{r=R}, \qquad \alpha \in \{r,\phi,z\}. \tag{2.15}$$

We then solve the equations of motion by expanding them in the form of Fourier integrals in two distinct regions (inside and outside the cylindrical membrane). The solution can be written in terms of integrals of harmonic functions with unknown coefficients, which we then determine from the boundary conditions of (a) continuity of radial, azimuthal and axial velocities, and (b) surface traction jumps deriving from the elastic properties of the membrane. We present the full analytic solutions for two limiting models of the membrane susceptible only to shear or bending deformations.

We begin by expressing the solution of Eqs. (2.1) inside the cylinder as a sum of a point-force

flow field and the flow reflected from the interface [76, 77]

$$\boldsymbol{v}_1 = \boldsymbol{v}^{\mathrm{S}} + \boldsymbol{v}^* \,,$$
$$p_1 = p^{\mathrm{S}} + p^* \,,$$

where $\boldsymbol{v}^{\mathrm{S}}$ and p^{S} are the Stokeslet solution in an infinite (unbounded) medium and $\boldsymbol{v}^*$ and p^* are the solutions of the homogenous (force-free) Stokes equations

$$\eta \boldsymbol{\nabla}^2 \boldsymbol{v}^* - \boldsymbol{\nabla} p^* = 0 \,, \tag{2.16a}$$
$$\boldsymbol{\nabla} \cdot \boldsymbol{v}^* = 0 \,, \tag{2.16b}$$

required such that the full flow field satisfies the regularity and boundary conditions. In the following, we shall consider the cases of particle motion parallel or perpendicular to the cylinder centreline separately.

2.1 Axial motion

The Stokeslet solution for a point-force located at the origin and directed along the cylinder axis reads [78]

$$v_r^{\mathrm{S}} = \frac{F_z}{8\pi\eta} \frac{zr}{d^3} \,, \quad v_z^{\mathrm{S}} = \frac{F_z}{8\pi\eta} \left(\frac{1}{d} + \frac{z^2}{d^3} \right) \,, \quad p^{\mathrm{S}} = \frac{F_z}{4\pi} \frac{z}{d^3} \,,$$

where $d := \sqrt{r^2 + z^2}$ is the distance from the singularity position. We now rewrite the Stokeslet solution in the form of a Fourier integral expansion noting that

$$\frac{rz}{d^3} = -\frac{\partial}{\partial r} \frac{z}{d} \,, \qquad \frac{1}{d} + \frac{z^2}{d^3} = \frac{2}{d} - \frac{\partial}{\partial z} \frac{z}{d} \,, \tag{2.17}$$

and making use of the integral relations [27, 79]

$$\frac{1}{d} = \frac{2}{\pi} \int_0^\infty K_0(qr) \cos qz \, \mathrm{d}q \,, \tag{2.18a}$$
$$\frac{z}{d} = \frac{2}{\pi} r \int_0^\infty K_1(qr) \sin qz \, \mathrm{d}q \,, \tag{2.18b}$$

wherein K_α is the αth order modified Bessel function of the second kind [80]. We thus express the axisymmetric Stokeslet solution in the integral form with the wavenumber q as

$$v_r^{\mathrm{S}}(r,z) = \frac{F_z}{4\pi^2\eta} \int_0^\infty rq K_0(qr) \sin qz \, \mathrm{d}q \,, \tag{2.19a}$$
$$v_z^{\mathrm{S}}(r,z) = \frac{F_z}{4\pi^2\eta} \int_0^\infty \Big(2K_0(qr) - qr K_1(qr) \Big) \cos qz \, \mathrm{d}q \,, \tag{2.19b}$$
$$p^{\mathrm{S}}(r,z) = \frac{F_z}{2\pi^2} \int_0^\infty q K_0(qr) \sin qz \, \mathrm{d}q \,, \tag{2.19c}$$

using the relation $\partial K_1(qr)/\partial r = -qK_0(qr) - K_1(qr)/r$.

The reflected flow can also be represented in a similar way by noting that the homogenous Stokes equations (2.16) for axisymmetric motion have a general solution expressed in terms of two harmonic

functions $\Psi_\parallel$ and $\Phi_\parallel$ as [14, p. 77]

$$v_r^* = \Psi_{\parallel,r} + r\,\Phi_{\parallel,rr}\,, \tag{2.20a}$$
$$v_z^* = \Psi_{\parallel,z} + r\,\Phi_{\parallel,rz} + \Phi_{\parallel,z}\,, \tag{2.20b}$$
$$p^* = -2\eta\,\Phi_{\parallel,zz}\,. \tag{2.20c}$$

The two functions $\Psi_\parallel$ and $\Phi_\parallel$ are solutions to the axisymmetric Laplace equation which can be written in an integral form as

$$\Phi_\parallel = \frac{F_z}{4\pi^2\eta}\int_0^\infty \phi_\parallel(q) f_\parallel(qr)\sin(qz)\,\mathrm{d}q\,, \tag{2.21a}$$
$$\Psi_\parallel = \frac{F_z}{4\pi^2\eta}\int_0^\infty \psi_\parallel(q) f_\parallel(qr)\sin(qz)\,\mathrm{d}q\,, \tag{2.21b}$$

where $\phi_\parallel$ and $\psi_\parallel$ are to be determined from the boundary conditions. At this point, the arbitrary prefactor outside the integral is chosen such that the resulting velocity and pressure fields will in the end have a similar representation as the Stokeslet solution given by Eq. (2.19). For $\Psi_\parallel$ and $\Phi_\parallel$ to be solutions to the axisymmetric Laplace equation, the function $f_\parallel$ has to satisfy the zeroth order modified Bessel equation [80]. Since the image solution inside the cylinder has to be regular at the origin owing to Eq. (2.3), we take $f_\parallel \equiv I_0$ in the inner solution. Combining Eqs. (2.20) and (2.21) together, the solution of Eq. (2.16) reads

$$v_r^*(r,z) = \frac{F_z}{4\pi^2\eta}\int_0^\infty q\Big(\big(rqI_0(qr) - I_1(qr)\big)\phi_\parallel^*(q) + I_1(qr)\psi_\parallel^*(q)\Big)\sin qz\,\mathrm{d}q\,, \tag{2.22a}$$
$$v_z^*(r,z) = \frac{F_z}{4\pi^2\eta}\int_0^\infty q\Big(\big(rqI_1(qr) + I_0(qr)\big)\phi_\parallel^*(q) + I_0(qr)\psi_\parallel^*(q)\Big)\cos qz\,\mathrm{d}q\,, \tag{2.22b}$$
$$p^*(r,z) = \frac{F_z}{2\pi^2}\int_0^\infty q^2\phi_\parallel^*(q) I_0(qr)\sin qz\,\mathrm{d}q\,. \tag{2.22c}$$

Thus the Green's function inside the elastic cylindrical channel for the axial point-force is given explicitly by summing up the Stokeslet contribution (2.19) and the reflected flow (2.22).

The outer solution for the force-free Stokes equations (2.2) has an analogous structure with the only difference that the flow has to decay at infinity by virtue of Eq. (2.5) and we therefore take $f_\parallel \equiv K_0$ leading to

$$v_{2r}(r,z) = \frac{F_z}{4\pi^2\eta}\int_0^\infty q\Big(\big(rqK_0(qr) + K_1(qr)\big)\phi_{2\parallel}(q) - K_1(qr)\psi_{2\parallel}(q)\Big)\sin qz\,\mathrm{d}q\,, \tag{2.23a}$$
$$v_{2z}(r,z) = \frac{F_z}{4\pi^2\eta}\int_0^\infty q\Big(\big(K_0(qr) - rqK_1(qr)\big)\phi_{2\parallel}(q) + K_0(qr)\psi_{2\parallel}(q)\Big)\cos qz\,\mathrm{d}q\,, \tag{2.23b}$$
$$p_2(r,z) = \frac{F_z}{2\pi^2}\int_0^\infty q^2\phi_{2\parallel}(q) K_0(qr)\sin qz\,\mathrm{d}q\,, \tag{2.23c}$$

after making use of the relations $\partial I_0(qr)/\partial r = qI_1(qr)$, $\partial I_1(qr)/\partial r = qI_0(qr) - I_1(qr)/r$ and $\partial K_0(qr)/\partial r = -qK_1(qr)$. The unknown functions $\psi_\parallel^*$, $\phi_\parallel^*$, $\psi_{2\parallel}$ and $\phi_{2\parallel}$ remain to be determined from the boundary conditions of continuous velocity and prescribed traction jumps at the membrane.

The continuity of radial and axial velocity components across the membrane expressed by Eqs. (2.6)

and (2.8) leads to the expression of the functions $\psi_{2\parallel}$ and $\phi_{2\parallel}$ in terms of $\psi_\parallel^*$ and $\phi_\parallel^*$ as

$$\psi_{2\parallel} = \frac{G_\parallel \psi_\parallel^* + (1+s^2) S_\parallel \phi_\parallel^*}{D_\parallel} + \frac{R}{s}\,, \tag{2.24a}$$

$$\phi_{2\parallel} = \frac{S_\parallel \psi_\parallel^* + G_\parallel \phi_\parallel^*}{D_\parallel} + \frac{R}{s}\,, \tag{2.24b}$$

where $s := qR$ is a dimensionless wavenumber and

$$\begin{aligned} S_\parallel &= K_1 I_0 + K_0 I_1\,, \\ G_\parallel &= \big(sK_1 - K_0\big) I_1 + \big(sK_0 + K_1\big) I_0\,, \\ D_\parallel &= sK_0^2 - sK_1^2 + 2K_0 K_1\,. \end{aligned}$$

The modified Bessel functions have the argument s which is dropped for brevity.

The form of $\psi_\parallel^*$ and $\phi_\parallel^*$ may be determined given the constitutive model of the membrane. In appendix B, we provide explicit analytical expressions for $\psi_\parallel^*$ and $\phi_\parallel^*$ by considering independently a shear-only or a bending-only membrane. An analogous resolution procedure can be employed by considering simultaneously shear and bending resistances.

For future reference, we shall express the solution near a membrane with both shear and bending rigidities as

$$\psi_\parallel^* = R\,\frac{M_\parallel}{N_\parallel}\,, \quad \phi_\parallel^* = R\,\frac{L_\parallel}{N_\parallel}\,. \tag{2.25}$$

We note that the steady solution near a hard cylinder as first computed by [30] stated by Eq. (B.4) is recovered in the vanishing frequency limit. In the following, the solution for a point-force acting perpendicular to the cylinder axis will be derived.

2.2 Radial motion

Without loss of generality, we shall consider for the radial motion that the point force is located at the origin and directed along the x direction in Cartesian coordinates. The induced velocity field reads [78]

$$v_x^{\mathrm{S}} = \frac{F_x}{8\pi\eta}\left(\frac{1}{d} + \frac{x^2}{d^3}\right)\,, \quad v_y^{\mathrm{S}} = \frac{F_x}{8\pi\eta}\frac{xy}{d^3}\,, \quad v_z^{\mathrm{S}} = \frac{F_x}{8\pi\eta}\frac{xz}{d^3}\,,$$

and the pressure

$$p^{\mathrm{S}} = \frac{F_x}{4\pi}\frac{x}{d^3}\,.$$

Setting $x = r\cos\phi$ and $y = r\sin\phi$, the radial and tangential velocities read

$$v_r^{\mathrm{S}} = \frac{F_x}{8\pi\eta}\left(\frac{1}{d} + \frac{r^2}{d^3}\right)\cos\phi\,, \qquad v_\phi^{\mathrm{S}} = -\frac{F_x}{8\pi\eta}\frac{\sin\phi}{d}\,.$$

By making use of Eqs. (2.17) and (2.18), the Stokeslet solution can thus be written in the form

of a Fourier-Bessel integral expansion as

$$v_r^{\mathrm{S}}(r,\phi,z) = \frac{F_x}{4\pi^2\eta}\cos\phi\int_0^\infty (K_0(qr)+qrK_1(qr))\cos qz\,\mathrm{d}q\,, \tag{2.26a}$$

$$v_\phi^{\mathrm{S}}(r,\phi,z) = -\frac{F_x}{4\pi^2\eta}\sin\phi\int_0^\infty K_0(qr)\cos qz\,\mathrm{d}q\,, \tag{2.26b}$$

$$v_z^{\mathrm{S}}(r,\phi,z) = \frac{F_x}{4\pi^2\eta}\cos\phi\int_0^\infty qrK_0(qr)\sin qz\,\mathrm{d}q\,, \tag{2.26c}$$

$$p^{\mathrm{S}}(r,\phi,z) = \frac{F_x}{2\pi^2}\cos\phi\int_0^\infty qK_1(qr)\cos qz\,\mathrm{d}q\,. \tag{2.26d}$$

Similar, the reflected flow can also be represented by noting that the force-free Stokes equations (2.16) have a general solution expressed in terms of three harmonic functions $\Psi_\perp$, $\Phi_\perp$ and $\Gamma_\perp$ as [14, p. 77]

$$v_r^* = \Psi_{\perp,r} + \frac{\Gamma_{\perp,\phi}}{r} + r\,\Phi_{\perp,rr}\,, \tag{2.27a}$$

$$v_\phi^* = \frac{\Psi_{\perp,\phi}}{r} - \Gamma_{\perp,r} - \frac{\Phi_{\perp,\phi}}{r} + \Phi_{\perp,\phi r}\,, \tag{2.27b}$$

$$v_z^* = \Psi_{\perp,z} + r\,\Phi_{\perp,rz} + \Phi_{\perp,z}\,, \tag{2.27c}$$

$$p^* = -2\eta\,\Phi_{\perp,zz}\,. \tag{2.27d}$$

The functions $\Psi_\perp$, $\Phi_\perp$ and $\Gamma_\perp$ are solutions to the asymmetric Laplace equation which can be written in an integral form as

$$\Phi_\perp = \frac{F_x}{4\pi^2\eta}\cos\phi\int_0^\infty \phi_\perp(q)f_\perp(qr)\cos(qz)\,\mathrm{d}q\,, \tag{2.28a}$$

$$\Psi_\perp = \frac{F_x}{4\pi^2\eta}\cos\phi\int_0^\infty \psi_\perp(q)f_\perp(qr)\cos(qz)\,\mathrm{d}q\,, \tag{2.28b}$$

$$\Gamma_\perp = \frac{F_x}{4\pi^2\eta}\sin\phi\int_0^\infty \gamma_\perp(q)f_\perp(qr)\cos(qz)\,\mathrm{d}q\,, \tag{2.28c}$$

where $\phi_\perp$, $\psi_\perp$ and $\gamma_\perp$ are wavenumber-dependent quantities to be determined from the prescribed boundary conditions at the membrane.

For $\Psi_\perp$, $\Phi_\perp$ and $\Gamma_\perp$ to be solutions to Laplace equation, the function $f_\perp$ should be solution to the first order modified Bessel equation [80]. In order to satisfy the regularity of the image solution inside the elastic cylinder as stated by Eq. (2.3), we take $f_\perp \equiv I_1$ in the inner solution. Upon combination of Eqs. (2.27) and (2.28) together, the solution of Eq. (2.16) for a radial Stokeslet reads

$$\begin{aligned} v_r^*(r,\phi,z) = \frac{F_x}{4\pi^2\eta}\frac{\cos\phi}{r}\int_0^\infty \big(\big((2+q^2r^2)I_1(qr) - qrI_0(qr)\big)\,\phi_\perp^*(q) \\ + (qrI_0(qr) - I_1(qr))\,\psi_\perp^*(q) + I_1(qr)\,\gamma_\perp^*(q)\big)\cos qz\,\mathrm{d}q\,, \end{aligned} \tag{2.29a}$$

$$\begin{aligned} v_\phi^*(r,\phi,z) = -\frac{F_x}{4\pi^2\eta}\frac{\sin\phi}{r}\int_0^\infty \big((qrI_0(qr) - 2I_1(qr))\,\phi_\perp^*(q) \\ + I_1(qr)\psi_\perp^*(q) + (qrI_0(qr) - I_1(qr))\,\gamma_\perp^*(q)\big)\cos qz\,\mathrm{d}q\,, \end{aligned} \tag{2.29b}$$

$$v_z^*(r,\phi,z) = -\frac{F_x\cos\phi}{4\pi^2\eta}\int_0^\infty q\big(qrI_0(qr)\phi_\perp^*(q) + I_1(qr)\psi_\perp^*(q)\big)\sin qz\,\mathrm{d}q\,, \tag{2.29c}$$

$$p^*(r,\phi,z) = \frac{F_x\cos\phi}{2\pi^2}\int_0^\infty q^2I_1(qr)\phi_\perp^*(q)\cos qz\,\mathrm{d}q\,. \tag{2.29d}$$

The outer solution for the force-free Stokes equations (2.2) has to decay at infinity owing to Eq. (2.5), suggesting to take $f_\perp \equiv K_1$ leading to

$$v_{2r}(r,\phi,z) = \frac{F_x}{4\pi^2\eta}\frac{\cos\phi}{r}\int_0^\infty \Big(\big((2+q^2r^2)K_1(qr) + qrK_0(qr)\big)\,\phi_{2\perp}(q) - \big(qrK_0(qr) + K_1(qr)\big)\,\psi_{2\perp}(q) + K_1(qr)\,\gamma_{2\perp}(q)\Big)\cos qz\,\mathrm{d}q\,, \tag{2.30a}$$

$$v_{2\phi}(r,\phi,z) = \frac{F_x}{4\pi^2\eta}\frac{\sin\phi}{r}\int_0^\infty \Big(\big(qrK_0(qr) + 2K_1(qr)\big)\,\phi_{2\perp}(q) - K_1(qr)\psi_{2\perp}(q) + \big(qrK_0(qr) + K_1(qr)\big)\,\gamma_{2\perp}(q)\Big)\cos qz\,\mathrm{d}q\,, \tag{2.30b}$$

$$v_{2z}(r,\phi,z) = \frac{F_x\cos\phi}{4\pi^2\eta}\int_0^\infty q\,\big(qrK_0(qr)\phi_{2\perp}(q) - K_1(qr)\psi_{2\perp}(q)\big)\sin qz\,\mathrm{d}q\,, \tag{2.30c}$$

$$p_2(r,\phi,z) = \frac{F_x\cos\phi}{2\pi^2}\int_0^\infty q^2K_1(qr)\phi_{2\perp}(q)\cos qz\,\mathrm{d}q\,. \tag{2.30d}$$

The six unknown functions can thus be determined from the imposed boundary conditions, namely the continuity of fluid velocity and the traction jumps across the membrane.

The continuity of the velocity field expressed by Eqs. (2.6) through (2.8) leads to the expression of the unknown functions $\phi_{2\perp}$, $\psi_{2\perp}$ and $\gamma_{2\perp}$ outside the cylinder in terms of $\phi^*_\perp$, $\psi^*_\perp$ and $\gamma^*_\perp$ on the inside as

$$\phi_{2\perp} = \frac{S_\perp\phi^*_\perp + (K_1+sK_0)G_\perp\psi^*_\perp + K_1G_\perp\gamma^*_\perp}{D_\perp} + \frac{R}{s}\,, \tag{2.31}$$

$$\psi_{2\perp} = \frac{s\left((2+s^2)K_0 + sK_1\right)G_\perp\phi^*_\perp + S_\perp\psi^*_\perp + sK_0G_\perp\gamma^*_\perp}{D_\perp}\,, \tag{2.32}$$

$$\gamma_{2\perp} = \frac{\left(S_\perp - G_\perp\left(sK_0 + (2+s^2)K_1\right)\right)\gamma^*_\perp}{D_\perp} - \frac{2sK_0G_\perp\phi^*_\perp - 2K_1G_\perp\psi^*_\perp}{D_\perp} - \frac{2R}{s}\,, \tag{2.33}$$

where we have defined

$$\begin{aligned} S_\perp &= -sK_0K_1\left(sI_0 + (2+s^2)I_1\right) - s^2\left(sI_0K_0^2 + I_1K_1^2\right)\,,\\ G_\perp &= -s\left(I_0K_1 + I_1K_0\right)\,,\\ D_\perp &= s\big(s^2K_0^3 + sK_0^2K_1 - sK_1^3 - (2+s^2)K_0K_1^2\big)\,. \end{aligned}$$

In appendix C, we provide explicitly the expressions of $\psi^*_\perp$, $\phi^*_\perp$ and $\gamma^*_\perp$ by considering independently membranes with pure shear or pure bending.

For future reference, we shall express the solution for a membrane endowed with both shear and bending as

$$\psi^*_\perp = R\,\frac{M_\perp}{N_\perp}\,,\quad \phi^*_\perp = R\,\frac{L_\perp}{N_\perp}\,,\quad \gamma^*_\perp = R\,\frac{K_\perp}{N_\perp}\,. \tag{2.34}$$

We note here that for cylindrical membranes, shear and bending contributions do not add up linearly in the solution of the flow field, i.e. in a similar way as previously observed between two parallel planar elastic membranes [66] or a spherical membrane [81, 82] and in contrast to the case of a single planar membrane [65].

3 Particle mobility and membrane deformation

The exact results obtained in the previous section allow for the analysis of the effect of the membrane on the axial and radial motion of a colloidal particle, particularly for the calculation of leading-order

self- and pair mobility functions [83] relevant to transport of suspensions in a cylindrical channel. A more accurate description would be achievable by considering a distribution of point forces over the particle surface. Our simpler approximation nevertheless leads to a good agreement with numerical simulations performed with truly extended particles as will be shown below.

3.1 Axial mobility

We first compute the particle self-mobility correction due to the presence of the membrane for the axisymmetric motion parallel to the cylinder axis. At leading order, the self-mobility correction is calculated by evaluating the axial velocity component of the *reflected* flow field at the Stokeslet position such that

$$\Delta\mu_{\parallel}^{\mathrm{S}} = F_z^{-1} \lim_{\boldsymbol{r}\to 0} v_z^* \,, \tag{3.1}$$

where S appearing as superscript refers to "self". By making use of Eq. (2.22b), the latter equation can be written as

$$\Delta\mu_{\parallel}^{\mathrm{S}} = \frac{1}{4\pi^2\eta} \int_0^\infty q\big(\psi_{\parallel}^* + \phi_{\parallel}^*\big)\, \mathrm{d}q \,. \tag{3.2}$$

Inserting $\psi_{\parallel}^*$ and $\phi_{\parallel}^*$ from (2.25), the scaled self-mobility correction reads

$$\frac{\Delta\mu_{\parallel}^{\mathrm{S}}}{\mu_0} = \frac{3}{2\pi}\frac{a}{R} \int_0^\infty \frac{M_{\parallel} + L_{\parallel}}{N_{\parallel}}\, s\mathrm{d}s \,, \tag{3.3}$$

where $\mu_0 = 1/(6\pi\eta a)$ is the usual bulk mobility given by the Stokes law. Notably, the correction vanishes for a very wide channel, as $R \to \infty$.

Considering a membrane with both shear and bending resistances, and by taking α to infinity, we recover the mobility correction near a hard cylinder with stick boundary conditions, namely

$$\lim_{\alpha\to\infty} \frac{\Delta\mu_{\parallel}^{\mathrm{S}}}{\mu_0} = -\frac{3}{2\pi}\frac{a}{R} \int_0^\infty \frac{w_{\parallel}}{W_{\parallel}}\, \mathrm{d}s \approx -2.10444\, \frac{a}{R} \,, \tag{3.4}$$

where numerical integration has been performed to obtain the latter estimate, which is in agreement with results known in the literature [14, 16–18]. Moreover,

$$\begin{aligned} w_{\parallel} &= (I_0K_1 + I_1K_0)s^2 - 2(I_0K_0 + I_1K_1)s + 4I_1K_0 \,, \\ W_{\parallel} &= s(I_1^2 - I_0^2) + 2I_0I_1 \,. \end{aligned}$$

The same result is obtained when considering a membrane with only shear rigidity.

It is worth noting that a bending-only membrane produces a different correction to particle self-mobility when α_{B} is taken to infinity, namely

$$\lim_{\alpha_{\mathrm{B}}\to\infty} \frac{\Delta\mu_{\parallel,\mathrm{B}}^{\mathrm{S}}}{\mu_0} = -\frac{3}{2\pi}\frac{a}{R} \int_0^\infty \frac{w_{\parallel_{\mathrm{B}}}}{W_{\parallel_{\mathrm{B}}}}\, \mathrm{d}s \approx -1.80414\, \frac{a}{R} \,, \tag{3.5}$$

where

$$\begin{aligned} w_{\parallel_{\mathrm{B}}} &= sK_0^2 \,, \\ W_{\parallel_{\mathrm{B}}} &= s(I_1K_0 - I_0K_1) + 2I_1K_1 \,. \end{aligned}$$

Clearly, Eq. (3.5) does not coincide with the hard cylinder limit predicted by Eq. (3.4). The reason is the same as discussed in the appendix below Eq. (C.6c), namely that bending only restricts normal

but not tangential motion.

We now turn our attention to hydrodynamic interactions between two particles positioned on the centreline of an elastic cylinder, with the second particle of the same radius a placed along the cylinder axis at $z = h$. For future reference, we shall denote by γ the particle located at the origin and by λ the particle at $z = h$. The leading order particle pair mobility parallel to the line of centres is readily obtained from the *total* flow field evaluated at the position of the second particle,

$$\mu_{\parallel}^{\mathrm{P}} = F_z^{-1} \lim_{\boldsymbol{r}\to\boldsymbol{r}_\lambda} v_{1z}\,, \tag{3.6}$$

where P appearing as superscript stands for "pair". The latter equation can be written in a scaled form as

$$\frac{\mu_{\parallel}^{\mathrm{P}}}{\mu_0} = \frac{3}{2}\frac{a}{h} + \frac{3}{2\pi}\frac{a}{R}\int_0^\infty \frac{M_{\parallel}+L_{\parallel}}{N_{\parallel}}\cos(\sigma s)\, s\,\mathrm{d}s\,, \tag{3.7}$$

where $\sigma := h/R$. Note that $h > 2a$ as overlap between the two particles should be avoided. The first term in Eq. (3.7) is the leading-order bulk contribution to the pair mobility obtained from the Stokeslet solution [84–86], whereas the second term is the frequency-dependent correction to the particle pair mobility due to the presence of the elastic membrane.

Similarly, for an infinite membrane shear modulus, the pair mobility near a hard cylinder limit is obtained,

$$\lim_{\alpha\to\infty}\frac{\mu_{\parallel}^{\mathrm{P}}}{\mu_0} = \frac{3}{2}\frac{a}{h} - \frac{3}{2\pi}\frac{a}{R}\int_0^\infty \frac{w_{\parallel}}{W_{\parallel}}\cos(\sigma s)\,\mathrm{d}s\,. \tag{3.8}$$

Interestingly, the latter result can also be expressed in terms of convergent infinite series as [22, 87]

$$\lim_{\alpha\to\infty}\frac{\mu_{\parallel}^{\mathrm{P}}}{\mu_0} = \frac{3}{4}\sum_{n=1}^{\infty}\big(a_n\cos(\beta_n\sigma) + b_n\sin(\beta_n\sigma)\big)e^{-\alpha_n\sigma}\,, \tag{3.9}$$

where $u_n = \alpha_n + i\beta_n$ are the complex roots of the equation $u(J_0^2(u_n) + J_1^2(u_n)) = 2J_0(u_n)J_1(u_n)$. Moreover, $a_n + ib_n = 2\Big(\pi\big(2J_1(u_n)Y_0(u_n) - u_n(J_0(u_n)Y_0(u_n) + J_1(u_n)Y_1(u_n))\big) - u_n\Big)/J_1^2(u_n)$, where J_α and Y_α are the αth order Bessel functions of the first and second kind, respectively. Although being different in form, our expressions (3.8) and (3.9) give identical numerical values. The pair mobility therefore has a sharp exponential decay as the interparticle distance becomes larger. For $\sigma \gg 1$, the series in Eq. (3.9) can conveniently be truncated at the first term to give the estimate

$$\lim_{\alpha\to\infty}\frac{\mu_{\parallel}^{\mathrm{P}}}{\mu_0} \simeq \frac{3}{4}\big(a_1\cos(\beta_1\sigma) + b_1\sin(\beta_1\sigma)\big)e^{-\alpha_1\sigma}\,, \tag{3.10}$$

where $\alpha_1 \simeq 4.46630$, $\beta_1 \simeq 1.46747$, $a_1 \simeq -0.03698$ and $b_1 \simeq 13.80821$. We further mention that the pair mobility function inside a hard cylinder undergoes a sign reversal for $\sigma \gtrsim 2.14206$ before it vanishes as σ goes to infinity [22].

3.2 Radial mobility

We now compute the particle self-mobility correction caused by the presence of the membrane for the asymmetric motion perpendicular to the cylinder axis. At leading order in the ratio a/R, the mobility corrections are calculated by evaluating the reflected fluid velocity at the point-force position. Since the particle is located on the cylinder axis, the mobility tensor possesses only two unique components:

$\Delta\mu_{\parallel}$ for axial motion and $\Delta\mu_{\perp}$ for motion perpendicular to the axis. Accordingly,

$$\Delta\mu_{\perp}^{\mathrm{S}} = F_r^{-1} \lim_{\boldsymbol{r}\to 0} v_r^* \equiv F_{\phi}^{-1} \lim_{\boldsymbol{r}\to 0} v_{\phi}^* , \tag{3.11}$$

where $F_r = F_x \cos\phi$ and $F_{\phi} = -F_x \sin\phi$. Upon using Eq. (2.29a), we readily obtain

$$\Delta\mu_{\perp}^{\mathrm{S}} = \frac{1}{8\pi^2\eta} \int_0^{\infty} q\big(\psi_{\perp}^* + \gamma_{\perp}^*\big)\, \mathrm{d}q \,. \tag{3.12}$$

Inserting $\psi_{\perp}^*$ and $\gamma_{\perp}^*$ from the general form given by (2.34), and scaling by the bulk mobility μ_0, we get

$$\frac{\Delta\mu_{\perp}^{\mathrm{S}}}{\mu_0} = \frac{3}{4\pi}\frac{a}{R} \int_0^{\infty} \frac{M_{\perp} + K_{\perp}}{N_{\perp}}\, s\mathrm{d}s \,. \tag{3.13}$$

Similar, by taking α to infinity, we recover the mobility correction near a no-slip cylinder, namely

$$\lim_{\alpha\to\infty} \frac{\Delta\mu_{\perp}^{\mathrm{S}}}{\mu_0} = -\frac{3}{4\pi}\frac{a}{R} \int_0^{\infty} \frac{w_{\perp}}{W_{\perp}}\, \mathrm{d}s \approx -1.80436\, \frac{a}{R} \,, \tag{3.14}$$

in full agreement with previous studies [39, 44], where we have defined

$$\begin{aligned} w_{\perp} &= I_0(I_0K_1 + I_1K_0)s^3 + \big((2I_0^2 - 3I_1^2)K_0 - I_0I_1K_1\big)\, s^2 - 2I_1(I_0K_0 + I_1K_1)s - 4K_0I_1^2 \,, \\ W_{\perp} &= I_0(I_0^2 - I_1^2)s^2 + I_1(I_1^2 - I_0^2)s - 2I_0I_1^2 \,. \end{aligned}$$

The same steady mobility is obtained when the membrane is endowed with pure shear.

It is worth to note that for a bending-only membrane, however, the particle self-mobility in the limit when α_{B} is taken to infinity reads

$$\lim_{\alpha_{\mathrm{B}}\to\infty} \frac{\Delta\mu_{\perp,\mathrm{B}}^{\mathrm{S}}}{\mu_0} = -\frac{3}{4\pi}\frac{a}{R} \int_0^{\infty} \frac{w_{\perp\mathrm{B}}}{W_{\perp\mathrm{B}}}\, \mathrm{d}s \approx -1.55060\, \frac{a}{R} \,, \tag{3.15}$$

where we defined

$$\begin{aligned} w_{\perp\mathrm{B}} &= s^2(sK_1 + K_0)^2 \,, \\ W_{\perp\mathrm{B}} &= s\big((s^2+3)K_1 + 2sK_0\big)\, I_0 - (s^2+3)(sK_0 + 2K_1)I_1 \,. \end{aligned}$$

Continuing, the particle pair mobility function is determined by evaluating the total velocity field at the nearby particle position leading to

$$\mu_{\perp}^{\mathrm{P}} = F_r^{-1} \lim_{\boldsymbol{r}\to\boldsymbol{r}_{\lambda}} v_{1r} \equiv F_{\phi}^{-1} \lim_{\boldsymbol{r}\to\boldsymbol{r}_{\lambda}} v_{1\phi} \,. \tag{3.16}$$

Eq. (3.16) can be written in a scaled form as

$$\frac{\mu_{\perp}^{\mathrm{P}}}{\mu_0} = \frac{3}{4}\frac{a}{h} + \frac{3}{4\pi}\frac{a}{R} \int_0^{\infty} \frac{M_{\perp} + K_{\perp}}{N_{\perp}}\, \cos(\sigma s)\; s\, \mathrm{d}s \,. \tag{3.17}$$

Similar, for an infinite membrane shear modulus, we recover the pair mobility near a hard cylinder,

$$\lim_{\alpha\to\infty} \frac{\mu_{\perp}^{\mathrm{P}}}{\mu_0} = \frac{3}{4}\frac{a}{h} - \frac{3}{4\pi}\frac{a}{R} \int_0^{\infty} \frac{w_{\perp}}{W_{\perp}}\, \cos(\sigma s)\; \mathrm{d}s \,. \tag{3.18}$$

3.3 Startup motion

Here we will derive the mobility coefficients for a particle starting from rest and then moving under a constant external force (e.g. gravity) exerted along or perpendicular to the cylinder axis. Mathematically, such force can be described by a Heaviside step function force $\boldsymbol{F}(t) = \boldsymbol{A}\,\theta(t)$ whose Fourier transform in the frequency domain reads [88]

$$\boldsymbol{F}(\omega) = \left(\pi\delta(\omega) - \frac{i}{\omega}\right)\boldsymbol{A}\,. \tag{3.19}$$

Applying back Fourier transform, the time-dependent correction to the particle mobility for a startup motion reads

$$\Delta\mu(t) = \frac{\Delta\mu(0)}{2} + \frac{1}{2i\pi}\int_{-\infty}^{+\infty}\frac{\Delta\mu(\omega)}{\omega}\,e^{i\omega t}\,\mathrm{d}\omega\,. \tag{3.20}$$

The second term in Eq. (3.20) is a real valued quantity which takes values between $-\Delta\mu(0)/2$ when $t \to 0$ and $+\Delta\mu(0)/2$ as $t \to \infty$. Since the frequency-dependent mobility corrections are expressed as a Fourier-Bessel integral over the scaled wavenumber s, the computation of the time-dependent mobility requires a double integration procedure. For this purpose, we use the Cuba Divonne algorithm [89, 90] for an accurate and fast numerical computation.

3.4 Membrane deformation

Finally, our results can be used to compute the membrane deformation resulting from an arbitrary time-dependent point-force acting along or perpendicular to the cylinder axis. The membrane displacement field is readily obtained from the velocity at $r = R$ via the no-slip boundary condition stated by Eq. (2.15). We define the membrane frequency-dependent reaction tensor as [91]

$$u_\alpha(\phi, z, \omega) = R_{\alpha\beta}(\phi, z, \omega)F_\beta(\omega)\,, \tag{3.21}$$

bridging between the membrane displacement field and the force acting on the nearby particle. Restricting to a harmonic driving force $F_\alpha(t) = A_\alpha e^{i\omega_0 t}$, the membrane deformation in the temporal domain is calculated as

$$u_\alpha(\phi, z, t) = R_{\alpha\beta}(\phi, z, \omega_0)A_\beta e^{i\omega_0 t}\,. \tag{3.22}$$

Further, the physical displacement is obtained by taking the real part of the latter equation. The radial-axial and axial-axial components of the reaction tensor are then computed from Eq. (2.23) as

$$R_{rz} = \Lambda\int_0^\infty s\Big(\big(sK_0 + K_1\big)\phi_{2\parallel} - K_1\psi_{2\parallel}\Big)\sin\left(\frac{sz}{R}\right)\mathrm{d}s\,,$$
$$R_{zz} = \Lambda\int_0^\infty s\Big(\big(K_0 - sK_1\big)\phi_{2\parallel} + K_0\psi_{2\parallel}\Big)\cos\left(\frac{sz}{R}\right)\mathrm{d}s\,,$$

with $\Lambda := 1/(4i\pi^2\eta\omega R^2)$, which give access to the radial and axial displacements after making use of Eq. (3.21). Moreover, $R_{\phi z} = 0$ due to axial symmetry.

For a point force directed perpendicular to the cylinder axis, the components of the reaction

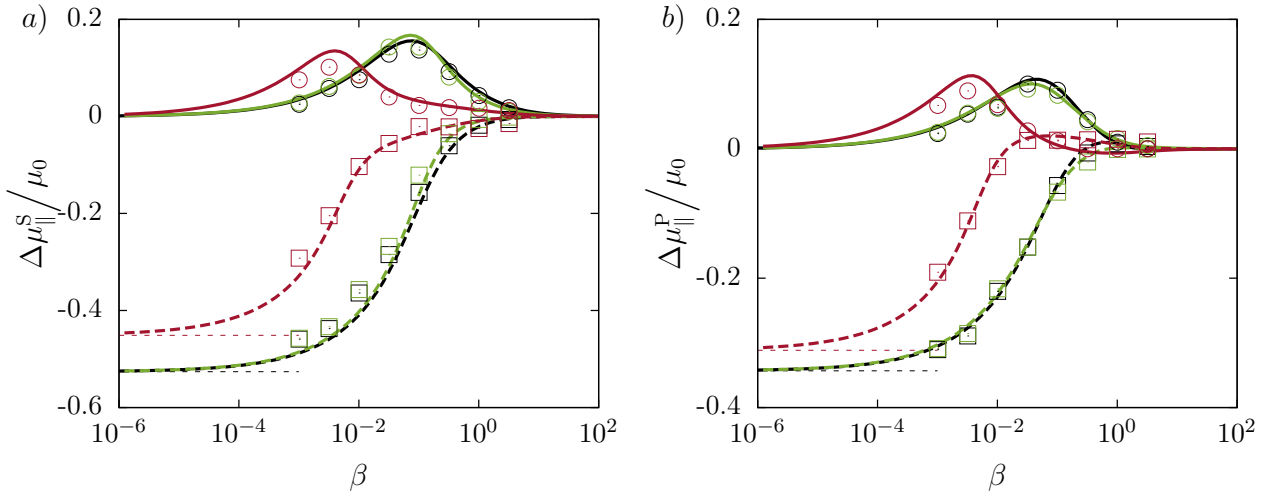

Figure 2: (Color online) *a*) The parallel component of the scaled frequency-dependent self-mobility correction versus the scaled frequency $\beta = 1/\alpha$ nearby a cylindrical membrane endowed with only-shear (green or bright gray in a black and white printout), only-bending (red or dark gray in a black and white printout) and both rigidities (black). The particle is set on the centreline of an elastic cylinder of radius $R = 4a$. Here we take a reduced bending modulus $E_{\mathrm{B}} = 1/6$. The theoretical predictions are presented as dashed and solid lines for the real and imaginary parts, respectively. Boundary integral simulations results are shown as squares for the real part and circles for the imaginary part. The horizontal dashed lines are the vanishing frequency limits given by Eqs. (3.4) and (3.5). *b*) The parallel component of the scaled frequency-dependent pair mobility correction versus the scaled frequency β. The two particles are set a distance $h = R$ apart on the centreline of an elastic cylinder of radius $R = 4a$.

tensor can readily be computed from Eqs. (2.30) to obtain

$$R_{rr} = \Lambda \int_0^\infty \left(\left((2+s^2)K_1 + sK_0\right)\phi_{2\perp} - \left(sK_0 + K_1\right)\psi_{2\perp} + K_1\gamma_{2\perp}\right) \cos\left(\frac{sz}{R}\right) \mathrm{d}s\,,$$
$$R_{\phi\phi} = -\Lambda \int_0^\infty \left(\left(sK_0 + 2K_1\right)\phi_{2\perp} - K_1\psi_{2\perp} + \left(sK_0 + K_1\right)\gamma_{2\perp}\right) \cos\left(\frac{sz}{R}\right) \mathrm{d}s\,,$$
$$R_{zr} = \Lambda \int_0^\infty s\left(sK_0\phi_{2\perp} - K_1\psi_{2\perp}\right) \sin\left(\frac{sz}{R}\right) \mathrm{d}s\,.$$

Additionally, we have $R_{r\phi} = R_{\phi r} = R_{z\phi} = 0$.

4 Comparison with Boundary Integral simulations

The accuracy of the point-particle approximation employed throughout this work can be assessed by direct comparison with fully resolved numerical simulations. To this end, we employ a completed double layer boundary integral method [92–95] which has proven to be perfectly suited for simulating solid particles in the presence of deforming boundaries. Technical details concerning the algorithm and its numerical implementation have been reported by some of us elsewhere, e.g. [66] and [96]. The cylindrical membrane has a length of $200a$, meshed uniformly with 6550 triangles, and the spherical particle is meshed with 320 triangles obtained by consecutively refining an icosahedron [97, 98].

In order to determine the particle self- and pair mobilities numerically, a harmonic force $F_{\lambda\alpha}(t) =$

$A_{\lambda\alpha}e^{i\omega_0 t}$ of amplitude $A_{\lambda\alpha}$ and frequency ω_0 is applied along the direction α at the surface of the particle labeled λ either along (z direction) or perpendicular (x direction) to the cylinder axis. After a brief transient evolution, both particles oscillate at the same frequency with different phases, i.e. $V_{\lambda\alpha} = B_{\lambda\alpha}e^{i\omega_0 t+\delta_\lambda}$ and $V_{\gamma\alpha} = B_{\gamma\alpha}e^{i\omega_0 t+\delta_\gamma}$. For the accurate determination of the velocity amplitudes and phase shifts, we use a nonlinear least-squares algorithm [99] based on the trust region method [100]. The particle self- and pair mobility functions can therefore be computed as

$$\mu^{\mathrm{S}}_{\alpha\beta} = \frac{B_{\lambda\alpha}}{A_{\lambda\beta}}\, e^{i\delta_\lambda}\,, \qquad \mu^{\mathrm{P}}_{\alpha\beta} = \frac{B_{\gamma\alpha}}{A_{\lambda\beta}}\, e^{i\delta_\gamma}\,. \tag{4.1}$$

We now define the characteristic frequency for shear, $\beta := 1/\alpha = 3\eta\omega R/(2\kappa_{\mathrm{S}})$, and for bending, $\beta_{\mathrm{B}} := 1/\alpha^3_{\mathrm{B}} = \eta\omega R^3/\kappa_{\mathrm{B}}$. We also introduce the membrane reduced bending modulus as $E_{\mathrm{B}} := \kappa_{\mathrm{B}}/(\kappa_{\mathrm{S}}R^2)$ quantifying the nonlinear coupling between shear and bending [101].

In figure 2 *a*), we show the correction to particle self-mobility versus the scaled frequency β as predicted theoretically by Eq. (3.3). The particle is set on the centreline of an elastic cylinder of radius $R = 4a$. For the simulation parameters, we take a reduced bending $E_{\mathrm{B}} = 1/6$ for which β and β_{B} have about the same order of magnitude, and thus shear and bending manifest themselves equally. We observe that the real part is a monotonically increasing function of frequency whereas the imaginary part exhibits the typical bell-shaped curve characterising dynamical systems with memory. For small forcing frequencies, the real part of the mobility correction approaches that near a no-slip hard cylinder only if the membrane possesses resistance against shear. For large forcing frequencies, both the real and imaginary parts vanish, which corresponds to the bulk behaviour. It can clearly be seen that the mobility correction is primarily determined by shear resistance and bending does not play a significant role, similarly to what has been recently observed for spherical elastic membranes [81, 82]. A good quantitative agreement is obtained between analytical predictions and numerical simulations over the whole range of applied frequencies.

Analogous predictions for the pair mobility versus the scaled frequency β are shown in figure 2 *b*). The two particles are set a distance $h = R$ apart along the axis of an elastic cylinder of radius $R = 4a$. The overall shapes resemble those observed for the self-mobility, where again the effect of shear is more pronounced. However, it can be seen that the real part for a bending-only membrane may undergo a change of sign at some intermediate frequencies in the same way as observed nearby planar membranes [67]. Interestingly, we find that the correction to the pair mobility induced by the elastic membrane is almost as large as the bulk pair mobility itself.

The frequency-dependent self- and pair mobility corrections for the motion perpendicular to the cylinder axis are shown in figure 3. We observe that the total mobility corrections are primarily determined by membrane shear resistance as it has been observed for the axial motion along the cylinder axis. Notably, the correction near a rigid cylinder is recovered only if the membrane possesses a finite resistance towards shear.

In figure 4, we show the time-dependent translational velocity of a particle starting from rest and subsequently moving under the action of a constant axial or radial force nearby a cylindrical membrane endowed with shear-only (green), bending-only (red) or both shear and bending resistances (black). The time is scaled by the characteristic time scale for shear $\tau := \beta/\omega = 3\eta R/(2\kappa_{\mathrm{S}})$. At short time scales, we observe that the mobility correction amounts to a small value since the particle does not yet feel the presence of the elastic membrane. As the time increases, the membrane effect becomes more noticeable and the mobility curves bend down substantially to asymptotically approach the correction nearby a hard cylinder if the membrane possesses a non-vanishing resistance towards shear. Moreover, we observe that the steady state is more quickly achieved for the axial (parallel) motion than for the radial motion (perpendicular), i.e. in a way similar to what has been observed nearby planar elastic membranes [65]. At the end of the simulations, the particle position changes only by

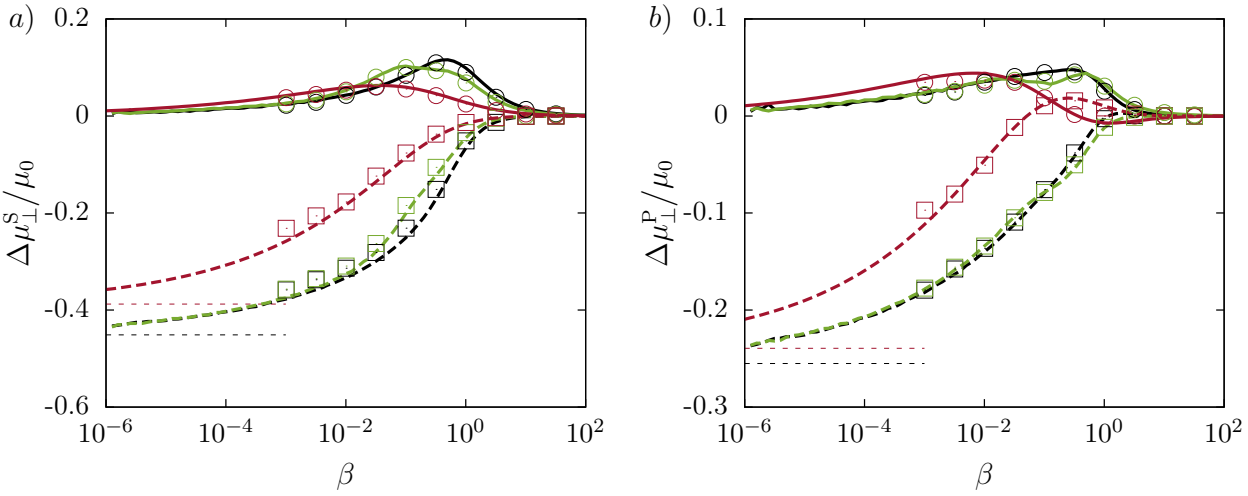

Figure 3: (Color online) The perpendicular component of the scaled frequency-dependent self a) and pair b) mobility corrections versus the scaled frequency β. The color code is the same as in figure 2.

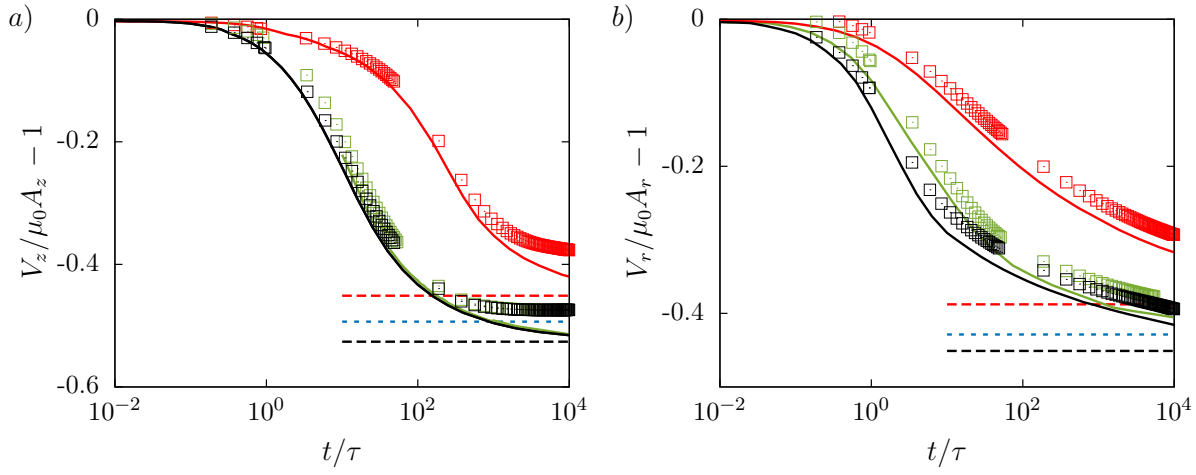

Figure 4: Translational velocity of a particle starting from rest for a) axial and b) radial motion under the action of a constant external force, obtained using the same parameters as in figure 2 for a membrane with pure shear (green or bright gray in a black and white printout), pure bending (red or dark gray in a black and white printout) and both rigidities (black). Solid lines are the analytical predictions obtained from by Eq. (3.20) and symbols are the boundary integral simulations results. Horizontal dashed lines are our theoretical predictions in the steady limit based on the point-particle approximation and the blue dotted lines are the higher order corrections given by Eqs. (4.2) and (4.3) for the axial and radial motions, respectively. Here τ is a characteristic time scale defined as $\tau := \beta/\omega$.

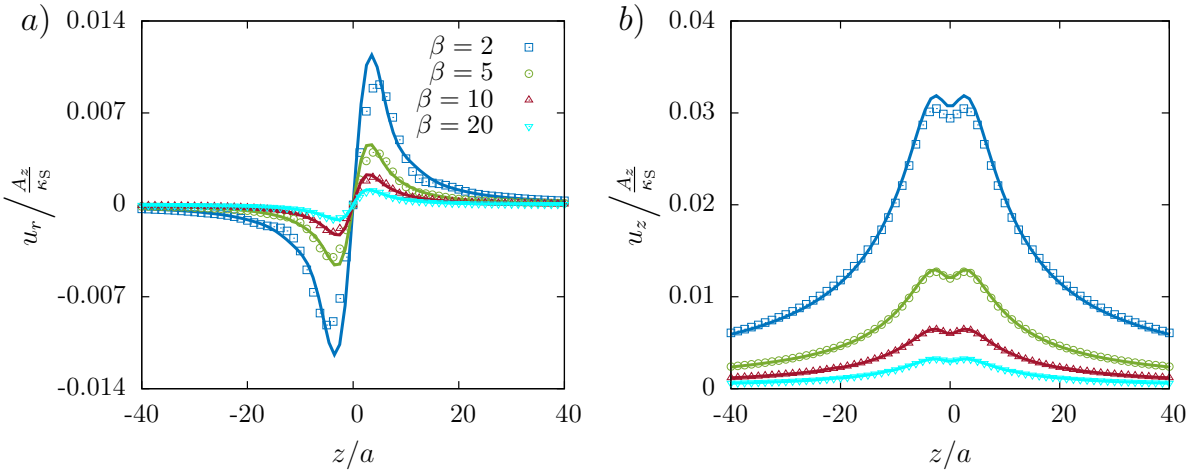

Figure 5: (Color online) The scaled radial a) and axial b) membrane displacements versus z/a at four different forcing frequencies calculated at quarter period, i.e. when $\omega_0 t = \pi/2$ and the particle reaches its maximal amplitude moving to the right along the z axis. Solid lines refer to theoretical predictions and symbols are the boundary integral simulations.

about 10 % of its radius.

Before continuing, we briefly comment on the importance of higher order terms. For this, we consider a hard cylinder for which the correction to the axial mobility can be obtained from Bohlin inverse series coefficients as [19, Tab. 2.1]

$$\lim_{\alpha\to\infty} \frac{\Delta\mu_{\parallel}^{\mathrm{S}}}{\mu_0} = -2.104443\left(\frac{a}{R}\right) + 2.086694\left(\frac{a}{R}\right)^3 + \cdots, \tag{4.2}$$

which has been truncated at the 3rd order here since higher order terms amount to an insignificant correction for $a \ll R$. For the radial motion, this reads

$$\lim_{\alpha\to\infty} \frac{\Delta\mu_{\perp}^{\mathrm{S}}}{\mu_0} = -1.804360\left(\frac{a}{R}\right) + 1.430590\left(\frac{a}{R}\right)^3 + \cdots. \tag{4.3}$$

Comparing the first and third order in the above equations for the present parameters, we find that the higher order terms lead to a correction of about 5 %.

The membrane displacements induced by axial motion of the particle are illustrated in figure 5, which includes the theoretical predictions (solid lines) and boundary integral simulations (symbols) for four different forcing frequencies. The natural scale for the displacement, A_z/κ_{S} is set by the amplitude of forcing A_z and the shear resistance κ_{S}. Here we use the same parameters as in figure 2 for a membrane with both shear and bending rigidities. We plot the axial and radial displacement of the axial section (along z) of the tube wall in the moment in which a particle moving harmonically with a very small amplitude reaches its maximal axial position. We observe that the radial displacement u_r is an odd function of z that vanishes at the origin and at infinity. The axial deformation u_z shows a fundamentally different evolution with respect to z, where the membrane is displaced along the direction of the force. Moreover, the maximum deformation reached in u_z is found to be about three times larger than that reached in u_r. Interestingly, the maximum in u_z is not attained at the particle position $z = 0$, but slightly besides. By comparing the membrane deformation at various forcing frequencies, it can rather be seen that larger frequencies induce smaller deformations as the elastic

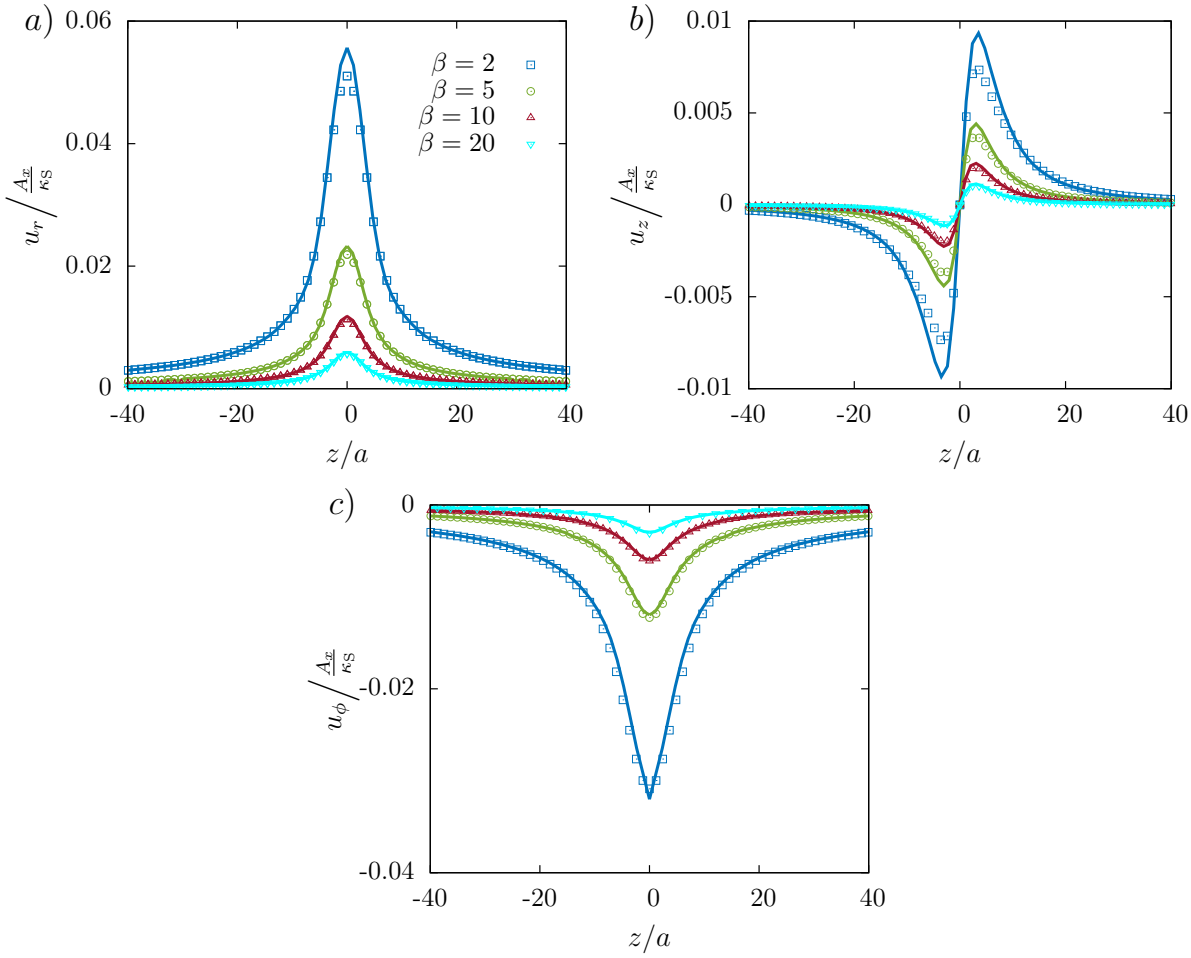

Figure 6: (Color online) The scaled radial a), azimuthal b) and axial c) membrane displacements versus z/a at four forcing frequencies calculated at quarter period for $\omega_0 t = \pi/2$ when the particle reaches its maximal radial position. Here deformations are shown in the plane of maximum deformation. Solid lines refer to theoretical predictions determined and symbols are the boundary integral simulations.

membrane does not have enough time to react to the rapidly wiggling particle.

In figure 6, we show the scaled radial, axial and azimuthal displacement fields induced by the particle radial motion upon varying the forcing frequency. Deformations are plotted when the oscillating particle reaches its maximal amplitude, in the plane of maximum deformation, i.e. $\phi = 0$ (or $y = 0$) for u_r and u_z, and $\phi = \pi/2$ (or $x = 0$) for u_ϕ for a force directed along the x direction. Not surprisingly, we observe that the membrane mainly undergoes radial deformation. The latter is found to be about twice as large as the azimuthal deformation and even six times larger that axial deformation. The numerical simulations are found to be in a very good agreement with analytical predictions, over the whole length of the deformed cylinder.

For typical situations, the order of magnitude of the forces exerted by optical tweezers on suspended particles are of the order of 1 pN [102]. For a cylinder radius of 10^{-6} m, a shear modulus of about 10^{-6} N/m and a scaled forcing frequency $\beta = 2$, the membrane undergoes a maximal deformation of about 2 % and 5 % of its undeformed radius for the axial and radial motions, respectively. As a result, deformations are small and deviations from cylindrical shape are indeed negligible.

As a final remark, we shall show that the range of frequencies employed throughout this work is

consistent with the assumption of small Reynolds and Strouhal numbers. In fact, by taking a fluid density $\rho = 10^3$ kg/m^3, a shear viscosity $\eta = 1.2 \times 10^{-3}$ Pas and a membrane bending modulus $\kappa_B = 2 \times 10^{-19}$ as typical values [70], the condition $\mathrm{Re}\,\mathrm{St} \ll 1$ leads to

$$\beta \ll \frac{3\eta^2}{2\rho R \kappa_S} \approx 2200\,, \qquad \beta_B \ll \frac{R\eta^2}{\rho \kappa_B} \approx 7200\,. \tag{4.4}$$

Clearly, both scaled frequencies satisfy these conditions in the frequency range considered in the present work.

5 Conclusions

In this paper, we derived explicit analytic expressions for the Green's functions, i.e., the flow field generated by a point particle (Stokeslet), acting either axially along or perpendicular to the centreline of an elastic cylindrical tube which exhibits resistance towards shear and bending. For this, we first derived the appropriate boundary conditions determining the surface traction jump across the membrane and then used a Fourier integral expansion to solve the Stokes equations. By examining the influence of shear and bending motion, we determined the full form of the solutions and discussed their behaviour for the whole range of actuation frequencies for arbitrary elastic parameters of the membrane – the bending rigidity κ_B and elastic modulus κ_S.

The solution was then used to compute the leading order correction to the self- and pair mobility of particles moving axially or radially in the elastic tube, which are in good agreement with fully resolved boundary integral simulations performed for the particle radius being a quarter of the channel size. We have also computed the deformation field of the membrane for an arbitrary time-dependent forcing and compared it with fully resolved numerical simulations.

The theoretical results prove that in this case the coupling between the effects of bending and shear of the membrane has a nonlinear nature, and the limit of a rigid tube is recovered only for non-zero shear resistance. We have also shown that the effects of shear are far more important for both axial and radial motions than bending and therefore determine the qualitative behaviour of the elastically confined particle. For two hydrodynamically interacting particles, the correction to pair mobility is found to be of the same order as the bulk pair mobility itself thus hinting at a possibly significant influence on particle agglomeration processes near elastic interfaces.

Acknowledgments

ADMI and SG thank the Volkswagen Foundation for financial support and acknowledge the Gauss Center for Supercomputing e.V. for providing computing time on the GCS Supercomputer SuperMUC at Leibniz Supercomputing Center. This work has been supported by the Ministry of Science and Higher Education of Poland via the Mobility Plus Fellowship awarded to ML. This article is based upon work from COST Action MP1305, supported by COST (European Cooperation in Science and Technology).

Appendix

A Membrane mechanics

In this appendix, we derive equations in cylindrical coordinates for the traction jump across a membrane endowed with shear and bending rigidities. We denote by $\boldsymbol{a} = R\boldsymbol{e}_r + z\boldsymbol{e}_z$ the position

vector of the points located at the undisplaced membrane, with R being the undeformed membrane radius. Here r, ϕ and z are used to refer to the radial, azimuthal and axial coordinates, respectively. After deformation, the vector position reads

$$\boldsymbol{r} = (R + u_r)\boldsymbol{e}_r + u_\phi \boldsymbol{e}_\phi + (z + u_z)\boldsymbol{e}_z \,, \tag{A.1}$$

where $\boldsymbol{u}$ denotes the displacement vector field. Hereafter, we shall use capital roman letters for the undeformed state and small roman letters for the deformed. The cylindrical membrane can be defined by the covariant base vectors $\boldsymbol{g}_1 := \boldsymbol{r}_{,\phi}$ and $\boldsymbol{g}_2 := \boldsymbol{r}_{,z}$. The unit normal vector $\boldsymbol{n}$ is defined as

$$\boldsymbol{n} = \frac{\boldsymbol{g}_1 \times \boldsymbol{g}_2}{|\boldsymbol{g}_1 \times \boldsymbol{g}_2|} \,. \tag{A.2}$$

Hence, the covariant base vectors read

$$\boldsymbol{g}_1 = (u_{r,\phi} - u_\phi)\boldsymbol{e}_r + (R + u_r + u_{\phi,\phi})\boldsymbol{e}_\phi + u_{z,\phi}\boldsymbol{e}_z \,, \tag{A.3}$$

$$\boldsymbol{g}_2 = u_{r,z}\boldsymbol{e}_r + u_{\phi,z}\boldsymbol{e}_\phi + (1 + u_{z,z})\boldsymbol{e}_z \,, \tag{A.4}$$

and the unit normal vector at leading order in deformation reads

$$\boldsymbol{n} = \boldsymbol{e}_r + \frac{u_\phi - u_{r,\phi}}{R}\,\boldsymbol{e}_\phi - u_{r,z}\boldsymbol{e}_z \,. \tag{A.5}$$

Note that $\boldsymbol{g}_1$ has length dimension while $\boldsymbol{g}_2$ and $\boldsymbol{n}$ are dimensionless. The covariant components of the metric tensor are defined by the scalar product $g_{\alpha\beta} = \boldsymbol{g}_\alpha \cdot \boldsymbol{g}_\beta$. The contravariant tensor $g^{\alpha\beta}$ is the inverse of the metric tensor. In a linearised form, we obtain

$$g_{\alpha\beta} = \begin{pmatrix} R^2 + 2R(u_r + u_{\phi,\phi}) & u_{z,\phi} + Ru_{\phi,z} \\ u_{z,\phi} + Ru_{\phi,z} & 1 + 2u_{z,z} \end{pmatrix} , \tag{A.6}$$

$$g^{\alpha\beta} = \begin{pmatrix} \frac{1}{R^2} - 2\frac{u_r + u_{\phi,\phi}}{R^3} & -\frac{u_{z,\phi} + Ru_{\phi,z}}{R^2} \\ -\frac{u_{z,\phi} + Ru_{\phi,z}}{R^2} & 1 - 2u_{z,z} \end{pmatrix} . \tag{A.7}$$

The covariant and contravariant tensors in the undeformed state $G_{\alpha\beta}$ and $G^{\alpha\beta}$ can immediately be obtained by considering a vanishing displacement field in Eq. (A.7).

A.1 Shear

In the following, we shall derive the traction jump equations across a cylindrical membrane endowed by an in-plane shear resistance. The two transformation invariants are given by Green and Adkins as [103, 104]

$$I_1 = G^{\alpha\beta} g_{\alpha\beta} - 2 \,, \tag{A.8a}$$

$$I_2 = \det G^{\alpha\beta} \det g_{\alpha\beta} - 1 \,. \tag{A.8b}$$

From the membrane constitutive relation, the contravariant components of the stress tensor $\tau^{\alpha\beta}$ can readily be obtained such that [69, 105]

$$\tau^{\alpha\beta} = \frac{2}{J_\mathrm{S}} \frac{\partial W}{\partial I_1} G^{\alpha\beta} + 2J_\mathrm{S} \frac{\partial W}{\partial I_2} g^{\alpha\beta} \,, \tag{A.9}$$

wherein W is the areal strain energy functional and $J_\mathrm{S} := \sqrt{1 + I_2}$ is the Jacobian determinant. In the linear theory of elasticity, $J_\mathrm{S} \simeq 1 + e$, where $e := (u_r + u_{\phi,\phi})/R + u_{z,z}$ being the dilatation

function [106]. In the present paper, we use the neo-Hookean model to describe the elastic properties of the membrane, whose areal strain energy reads [107, 108]

$$W(I_1, I_2) = \frac{\kappa_S}{6}\left(I_1 - 1 + \frac{1}{1+I_2}\right). \tag{A.10}$$

By plugging Eq. (A.10) into Eq. (A.9), the linearised in-plane stress tensor reads

$$\tau^{\alpha\beta} = \frac{2\kappa_S}{3}\begin{pmatrix} \frac{u_r+u_{\phi,\phi}}{R^3} + \frac{e}{R^2} & \frac{1}{2R}\left(u_{\phi,z} + \frac{u_{z,\phi}}{R}\right) \\ \frac{1}{2R}\left(u_{\phi,z} + \frac{u_{z,\phi}}{R}\right) & u_{z,z} + e \end{pmatrix}. \tag{A.11}$$

The equilibrium equations balancing the membrane elastic and external forces read

$$\nabla_\alpha \tau^{\alpha\beta} + \Delta f^\beta = 0\,, \tag{A.12a}$$
$$\tau^{\alpha\beta} b_{\alpha\beta} + \Delta f^n = 0\,, \tag{A.12b}$$

where $\Delta \boldsymbol{f} = \Delta f^\beta \boldsymbol{g}_\beta + \Delta f^n \boldsymbol{n}$ is the traction jump vector across the membrane. Here ∇_α stands for the covariant derivative, which for a second-rank tensor is defined as [109]

$$\nabla_\alpha \tau^{\alpha\beta} = \tau^{\alpha\beta}_{,\alpha} + \Gamma^\alpha_{\alpha\eta}\tau^{\eta\beta} + \Gamma^\beta_{\alpha\eta}\tau^{\alpha\eta}\,, \tag{A.13}$$

with $\Gamma^\lambda_{\alpha\beta}$ being the Christoffel symbols of the second kind which read [110]

$$\Gamma^\lambda_{\alpha\beta} = \frac{1}{2} g^{\lambda\eta}\left(g_{\alpha\eta,\beta} + g_{\eta\beta,\alpha} - g_{\alpha\beta,\eta}\right). \tag{A.14}$$

Moreover, $b_{\alpha\beta}$ is the curvature tensor defined by the dot product $b_{\alpha\beta} = \boldsymbol{g}_{\alpha,\beta} \cdot \boldsymbol{n}$. We obtain

$$b_{\alpha\beta} = \begin{pmatrix} u_{r,\phi\phi} - (R + u_r + 2u_{\phi,\phi}) & u_{r,\phi z} - u_{\phi,z} \\ u_{r,\theta z} - u_{\phi,z} & u_{r,zz} \end{pmatrix}. \tag{A.15}$$

At leading order in deformation, only the partial derivative remains in Eq. (A.13). After some algebra, we find that the traction jumps across the membrane given by Eqs. (A.12) are written in the cylindrical coordinate basis as

$$\frac{\kappa_S}{3}\left(u_{\phi,zz} + \frac{3u_{z,\phi z}}{R} + \frac{4(u_{r,\phi} + u_{\phi,\phi\phi})}{R^2}\right) + \Delta f_\phi = 0\,, \tag{A.16a}$$
$$\frac{\kappa_S}{3}\left(4u_{z,zz} + \frac{2u_{r,z} + 3u_{\phi,z\phi}}{R} + \frac{u_{z,\phi\phi}}{R^2}\right) + \Delta f_z = 0\,, \tag{A.16b}$$
$$-\frac{2\kappa_S}{3}\left(\frac{2(u_r + u_{\phi,\phi})}{R^2} + \frac{u_{z,z}}{R}\right) + \Delta f_r = 0\,. \tag{A.16c}$$

Note that for curved membranes, the normal traction jump does not vanish in the plane stress formulation employed throughout this work as the zeroth order in the curvature tensor is not identically null. For a planar elastic membrane however, the resistance to shear introduces a jump only in the tangential traction jumps [65–67].

Continuing, the jump in the fluid stress tensor across the membrane reads

$$[\sigma_{\beta r}] = \Delta f_\beta\,, \quad \beta \in \{z, r\}\,. \tag{A.17}$$

Therefore, From Eqs. (A.16), (A.17) and (2.15), it follows that

$$[v_{\phi,r}] = \frac{i\alpha}{2}\left(Rv_{\phi,zz} + 3v_{z,\phi z} + \frac{4(v_{r,\phi} + v_{\phi,\phi\phi})}{R}\right)\Big|_{r=R}, \tag{A.18a}$$

$$[v_{z,r}] = \frac{i\alpha}{2}\left(4Rv_{z,zz} + 2v_{r,z} + 3v_{\phi,z\phi} + \frac{v_{z,\phi\phi}}{R}\right)\Big|_{r=R}, \tag{A.18b}$$

$$\left[-\frac{p}{\eta}\right] = -i\alpha\left(\frac{2(v_r + v_{\phi,\phi})}{R} + v_{z,z}\right)\Big|_{r=R}, \tag{A.18c}$$

where $\alpha := 2\kappa_S/(3\eta R\omega)$ is a dimensionless number characteristic for shear. Note that it follows from the incompressibility equation

$$\frac{v_r + v_{\phi,\phi}}{r} + v_{r,r} + v_{z,z} = 0\,, \tag{A.19}$$

that $[v_{r,r}] = 0$. Hereafter, we shall derive the traction jump equations across a membrane possessing a bending rigidity.

A.2 Bending

Here we use the full Helfrich model for the bending energy. For small deformations and planar membranes, this is equivalent to the "linear bending model" used in our earlier works [65–67, 111], see ref. [73] for details. For a curved surface that we consider here, however, the latter leads to unphysical tangential components. The traction jump equations across the membranes are given by [73, 112]

$$\Delta \boldsymbol{f} = -2\kappa_B\left(2(H^2 - K + H_0H) + \Delta_\parallel\right)(H - H_0)\,\boldsymbol{n}\,, \tag{A.20}$$

where κ_B is the bending modulus, H and K are the mean and Gaussian curvatures, respectively given by

$$H = \frac{1}{2}\,b^\alpha_\alpha\,, \qquad K = \det\, b^\beta_\alpha\,, \tag{A.21}$$

with b^β_α being the mixed version of the curvature tensor related to the covariant representation of the curvature tensor by $b^\beta_\alpha = b_{\alpha\delta}g^{\delta\beta}$. Continuing, $\Delta_\parallel$ is the horizontal Laplace operator and H_0 is the spontaneous curvature for which we take the initial undisturbed shape here. The linearised traction jumps are therefore given by

$$-\kappa_B\Big(R^3u_{r,zzzz} + 2R(u_{r,zz} + u_{r,zz\phi\phi}) + \frac{u_r + 2u_{r,\phi\phi} + u_{r,\phi\phi\phi\phi}}{R}\Big) + \Delta f_r = 0\,. \tag{A.22}$$

and $\Delta f_\phi = \Delta f_z = 0$.

Interestingly, bending does not introduce at leading order a jump in the tangential traction [96]. The traction jump equations take the following final from

$$[v_{\phi,r}] = 0\,, \tag{A.23a}$$

$$[v_{z,r}] = 0\,, \tag{A.23b}$$

$$\left[-\frac{p}{\eta}\right] = -i\alpha_B^3\Big(R^3v_{r,zzzz} + 2R(v_{r,zz} + v_{r,zz\phi\phi}) + \frac{v_r + 2v_{r,\phi\phi} + v_{r,\phi\phi\phi\phi}}{R}\Big)\Big|_{r=R}, \tag{A.23c}$$

where $\alpha_B = (\kappa_B/(\eta\omega))^{1/3}/R$ is the dimensionless number characteristic for bending.

B Determination of the unknown functions for axial motion

In this appendix, we derive the expressions of the two functions $\psi_\parallel^*$ and $\phi_\parallel^*$ associated to the solution of the Stokes equations due to a point force directed along a cylindrical membrane possessing pure shear or pure bending rigidities.

B.1 Pure shear

As a first model, we consider an idealised membrane with a finite shear resistance and no bending resistance, such as an artificial capsule [113–117]. The tangential traction jump given by Eq. (2.9) is in leading order independent of bending resistance and readily leads to

$$\begin{aligned} &- s^2 I_1 \psi_\parallel^* - s^2\big(I_1 + sI_0\big)\phi_\parallel^* + s^2\big((i\alpha - 1)K_1 + 2i\alpha s K_0\big)\psi_{2\parallel} \\ &\quad - \big((1 + i\alpha + 2i\alpha s^2)K_1 - (1 + i\alpha)sK_0\big)s^2\phi_{2\parallel} = Rs\big(sK_0 - 2K_1\big)\,, \end{aligned} \tag{B.1}$$

where $\alpha = 2\kappa_\mathrm{S}/(3\eta R\omega)$ is the shear parameter. Neglecting the bending contribution Δf_r^B in the radial traction jump in Eq. (2.11) yields

$$2s^2 I_0 \phi_\parallel^* - i\alpha s\big(sK_0 + 2K_1\big)\psi_{2\parallel} + s\big(i\alpha(2 + s^2)K_1 + s(i\alpha - 2)K_0\big)\phi_{2\parallel} = -2RsK_0\,. \tag{B.2}$$

Eqs. (2.24) together with (B.1) and (B.2) form a linear system of equations for the four unknown functions, amenable to immediate resolution via the standard substitution method. We obtain

$$\psi_\parallel^* = R\,\frac{M_{\parallel\mathrm{S}}}{N_{\parallel\mathrm{S}}}\,, \quad \phi_\parallel^* = R\,\frac{L_{\parallel\mathrm{S}}}{N_{\parallel\mathrm{S}}}\,, \tag{B.3}$$

where the numerators read

$$\begin{aligned} M_{\parallel\mathrm{S}} &= \alpha\Big((I_0K_1 + I_1K_0)\big(3i\alpha K_0^2 - (4 + 3i\alpha)K_1^2\big)s^3 + \big(-3i\alpha I_0K_0^3 + (8 + 3i\alpha)I_1K_0^2K_1 \\ &\quad + (8 + 9i\alpha)I_0K_0K_1^2 + 3i\alpha I_1K_1^3\big)s^2 + \big(6(i\alpha - 1)I_1K_0^3 - 6(i\alpha + 1)I_0K_0^2K_1 \\ &\quad - 2(1 + 6i\alpha)I_1K_0K_1^2 - 2I_0K_1^3\big)s + 12i\alpha K_0^2K_1I_1\Big)\,, \\ L_{\parallel\mathrm{S}} &= \Big(\big(-3i\alpha I_0K_0^3 + (4 - 3i\alpha)I_1K_0^2K_1 + (4 + 3i\alpha)I_0K_0K_1^2 + 3i\alpha I_1K_1^3\big)s^2 \\ &\quad + \big(6(i\alpha - 1)I_1K_0^3 - 6(1 + i\alpha)I_0K_0^2K_1 + 2(1 - 6i\alpha)I_1K_0K_1^2 + 2I_0K_1^3\big)s \\ &\quad + 12i\alpha I_1K_0^2K_1\Big)\alpha\,, \end{aligned}$$

and the denominator

$$\begin{aligned} N_{\parallel\mathrm{S}} &= \big(3i(K_0^2 - K_1^2)(I_0^2 - I_1^2)\alpha + 4(I_1^2K_0^2 - I_0^2K_1^2)\big)\alpha s^3 + 2\alpha s^2(I_0K_0 + I_1K_1) \\ &\quad \times \big(3i\alpha(I_0K_1 - I_1K_0) + 2(I_0K_1 + I_1K_0)\big) + 4\big(-3iI_0I_1K_0K_1\alpha^2 + \alpha(I_1^2K_0^2 - I_0^2K_1^2) \\ &\quad + i(I_0K_1 + I_1K_0)^2\big)s + 8\alpha I_1K_1(I_0K_1 + I_1K_0)\,. \end{aligned}$$

Taking $\alpha \to \infty$, which is achieved either by considering an infinite shear modulus κ_S or a vanishing actuation frequency, we recover the known solution for a hard cylinder with stick boundary conditions,

namely

$$\lim_{\alpha\to\infty}\frac{\psi_\parallel^*}{R} = \frac{(I_0K_1+I_1K_0)s^2-(I_0K_0+I_1K_1)s+2I_1K_0}{s\big(sI_0^2-sI_1^2-2I_0I_1\big)}\,, \tag{B.4a}$$

$$\lim_{\alpha\to\infty}\frac{\phi_\parallel^*}{R} = \frac{2I_1K_0-(I_0K_0+I_1K_1)s}{s\big(sI_0^2-sI_1^2-2I_0I_1\big)}\,, \tag{B.4b}$$

in agreement with the results of Liron & Shahar [30]. Note that both $\psi_{2\parallel}$ and $\phi_{2\parallel}$ vanish in this limit, meaning that the fluid outside the cylinder is stagnant.

B.2 Pure bending

A complimentary model membrane involves only a finite bending resistance, as considered previously to model a typical fluid vesicle [118–121]. The effects of bending are determined by the dimensionless number $\alpha_\mathrm{B}=(\kappa_\mathrm{B}/(\eta\omega))^{1/3}/R$. We now set $\Delta f_z^\mathrm{S}=\Delta f_r^\mathrm{S}=0$ in Eqs. (2.9) and (2.11). The tangential-normal stress component is therefore continuous, leading to

$$-s^2I_1\psi_\parallel^*-s^2\big(I_1+sI_0\big)\phi_\parallel^*-s^2K_1\psi_{2\parallel}-\big(K_1-sK_0\big)s^2\phi_{2\parallel}=Rs\big(sK_0-2K_1\big)\,,$$

while the discontinuity in the normal traction jump leads to

$$\begin{aligned}s\left(2sI_0+i\alpha_\mathrm{B}^3(sI_0-I_1)(s^2-1)^2\right)\phi_\parallel^*+i\alpha_\mathrm{B}^3s(s^2-1)^2I_1\psi_\parallel^*\\ -2s^2K_0\phi_{2\parallel}=Rs\left(2+i\alpha_\mathrm{B}^3(s^2-1)^2\right)K_0\,.\end{aligned}$$

The functions $\psi_\parallel^*$ and $\phi_\parallel^*$ can be cast in a form similar to Eq. (B.3) as

$$\psi_\parallel^*=R\,\frac{M_{\parallel_\mathrm{B}}}{N_{\parallel_\mathrm{B}}}\,,\quad \phi_\parallel^*=R\,\frac{L_{\parallel_\mathrm{B}}}{N_{\parallel_\mathrm{B}}}\,, \tag{B.5}$$

with the numerators

$$\begin{aligned}M_{\parallel_\mathrm{B}}&=\alpha_\mathrm{B}^3(s^2-1)^2K_0(K_1+sK_0)\,,\\ L_{\parallel_\mathrm{B}}&=-\alpha_\mathrm{B}^3(s^2-1)^2K_0K_1\,,\end{aligned}$$

and the denominator

$$N_{\parallel_\mathrm{B}}=(s^2-1)^2\left(s(I_0K_1-I_1K_0)-2I_1K_1\right)\alpha_\mathrm{B}^3-2is(I_0K_1+I_1K_0)\,.$$

Importantly, by considering the limit $\alpha_\mathrm{B}\to\infty$ (corresponding to an infinite bending modulus of a vanishing actuation frequency) we obtain

$$\begin{aligned}\lim_{\alpha_\mathrm{B}\to\infty}\frac{\psi_\parallel^*}{R}&=\frac{K_0\big(sK_0+K_1\big)}{\big(sI_0-2I_1\big)K_1-sK_0I_1}\,,\\ \lim_{\alpha_\mathrm{B}\to\infty}\frac{\phi_\parallel^*}{R}&=-\frac{K_0K_1}{\big(sI_0-2I_1\big)K_1-sK_0I_1}\,,\end{aligned}$$

which is found to be different from the solution for a hard cylinder given by Eqs. (B.4). This difference will be explained later on, as it is characteristic for many elastohydrodynamic systems.

C Determination of the unknown functions for radial motion

In this appendix, we provide analytical expressions of the three functions $\phi_\perp^*$, $\psi_\perp^*$ and $\gamma_\perp^*$ associated to a point force acting perpendicular to a cylindrical membrane with either shear or bending rigidities.

C.1 Pure shear

We first consider an idealised membrane with a finite shear resistance and no bending resistance. The tangential traction jump along the z direction given by Eq. (2.9) is independent of bending leading to

$$s^2(I_0+sI_1)\phi_\perp^* + s(sI_0-I_1)\psi_\perp^* + s\left(s\left(1+i\alpha(3+2s^2)\right)K_0 + \left(i\alpha(5+s^2)-s^2\right)K_1\right)\phi_{2\perp} + \frac{i\alpha s}{2}\left(3sK_0+5K_1\right)\gamma_{2\perp} + s\left(s(1-i\alpha)K_0 + \left(1-i\alpha(3+2s^2)\right)K_1\right)\psi_{2\perp} = Rs(K_0-sK_1)\,, \quad \text{(C.1)}$$

and the tangential traction jump along the ϕ direction given by Eq. (2.10) leads to

$$\left((4+s^2)I_1-2sI_0\right)\phi_\perp^* + (sI_0-2I_1)\psi_\perp^* + \left((2+s^2)I_1-sI_0\right)\gamma_\perp^* + \tfrac{1}{2}\Big(\left(i\alpha\left(8+s^2\right)-(4+2s^2)\right)K_1 + s\left(i\alpha\left(4+s^2\right)-2\right)K_0\Big)\gamma_{2\perp} + \left(\left(i\alpha(8+3s^2)-(4+s^2)\right)K_1 + 2s\left(i\alpha(2+s^2)-1\right)K_0\right)\phi_{2\perp} + \left(2\left(1-i\alpha(2+s^2)\right)K_1 + s(1-2i\alpha)K_0\right)\psi_{2\perp} = RsK_1\,. \quad \text{(C.2)}$$

Continuing, te shear related part in the normal traction jump given by Eq. (2.11) yields

$$2s^2I_1\phi_\perp^* + \left(i\alpha s(4+s^2)K_0 + 2\left(i\alpha(4+s^2)-s^2\right)K_1\right)\phi_{2\perp} - i\alpha\left(2sK_0+(4+s^2)K_1\right)\psi_{2\perp} + 2i\alpha(sK_0+2K_1)\gamma_{2\perp} = -2RsK_1\,.$$

Inserting the expressions of $\phi_{2\perp}$, $\psi_{2\perp}$ and $\gamma_{2\perp}$ given by Eqs. (2.31) through (2.33) into Eqs. (C.1) through (C.3a), we obtain the unknown functions $\phi_\perp^*$, $\psi_\perp^*$ and $\gamma_\perp^*$ inside the channel. Explicit analytical expressions are not listed here due to their complexity and lengthiness. Particularly, by taking $\alpha\to\infty$, we recover the solution for a no-slip cylinder, namely

$$\lim_{\alpha\to\infty}\frac{\phi_\perp^*}{R} = \frac{s(sI_0-I_1)(I_0K_0+I_1K_1)-2I_1^2K_0}{s\left(s(sI_0-I_1)(I_0^2-I_1^2)-2I_0I_1^2\right)}\,, \quad \text{(C.3a)}$$

$$\lim_{\alpha\to\infty}\frac{\psi_\perp^*}{R} = \frac{s(I_1-sI_0)(I_0K_1+I_1K_0)}{s(sI_0-I_1)(I_0^2-I_1^2)-2I_0I_1^2}\,, \quad \text{(C.3b)}$$

$$\lim_{\alpha\to\infty}\frac{\gamma_\perp^*}{R} = 2\,\frac{sI_1(I_0K_0+I_1K_1)+2I_1^2K_0-s^2K_0(I_0^2-I_1^2)}{s\left(s(sI_0-I_1)(I_0^2-I_1^2)-2I_0I_1^2\right)}\,, \quad \text{(C.3c)}$$

and $\phi_{2\perp}=\psi_{2\perp}=\gamma_{2\perp}=0$, in complete agreement with the results by Liron & Shahar [30].

C.2 Pure bending

Neglecting the shear contribution in the tangential traction jump along the z direction given by Eq. (2.9), we obtain

$$s^2(I_0+sI_1)\phi_\perp^* + s(sI_0-I_1)\psi_\perp^* + s^2(K_0-sK_1)\phi_{2\perp} + s(K_1+sK_0)\psi_{2\perp} = Rs(K_0-sK_1)\,. \quad \text{(C.4)}$$

The traction jump along the ϕ direction stated by Eq. (2.10) is continuous, leading to

$$\begin{aligned}\left((4+s^2)I_1-2sI_0\right)\phi_\perp^*+(sI_0-2I_1)\psi_\perp^*+\left((2+s^2)I_1-sI_0\right)\gamma_\perp^*+(sK_0+2K_1)\psi_{2\perp}\\-\left(2sK_0+(4+s^2)K_1\right)\phi_{2\perp}-\left(sK_0+\left(s^2+2\right)K_1\right)\gamma_{2\perp}=RsK_1\,.\end{aligned}$$

while the discontinuity of the normal traction jump due to pure bending leads to

$$\begin{aligned}2sI_1\psi_\perp^*+\left(i\alpha_{\mathrm{B}}^3s^3\left((s^2+2)K_1+sK_0\right)-2sK_1\right)\phi_{2\perp}\\-i\alpha_{\mathrm{B}}^3s^3(sK_0+K1)\psi_{2\perp}+i\alpha_{\mathrm{B}}^3s^3K_1\gamma_{2\perp}=-2RK_1\,.\end{aligned}\tag{C.5}$$

The unknown functions $\phi_\perp^*$, $\psi_\perp^*$ and $\gamma_\perp^*$ are readily obtained after plugging the expressions of $\phi_{2\perp}$, $\psi_{2\perp}$ and $\gamma_{2\perp}$ given by Eqs. (2.31) through (2.33) into Eqs. (C.4) through (C.5). Further, by taking $\alpha_{\mathrm{B}}\to\infty$, we obtain

$$\lim_{\alpha_{\mathrm{B}}\to\infty}\frac{\phi_\perp^*}{R}=\frac{(K_0+sK_1)(sK_0+K_1)}{sK_0\left((3+s^2)I_1-2sI_0\right)-(3+s^2)(2I_1-sI_0)K_1}\,,\tag{C.6a}$$

$$\lim_{\alpha_{\mathrm{B}}\to\infty}\frac{\psi_\perp^*}{R}=\frac{(K_0+sK_1)\left(sK_0+(2+s^2)K_1\right)}{sK_0\left((3+s^2)I_1-2sI_0\right)-(3+s^2)(2I_1-sI_0)K_1}\,,\tag{C.6b}$$

$$\lim_{\alpha_{\mathrm{B}}\to\infty}\frac{\gamma_\perp^*}{R}=\frac{2K_1(K_0+sK_1)}{sK_0\left((3+s^2)I_1-2sI_0\right)-(3+s^2)(2I_1-sI_0)K_1}\,,\tag{C.6c}$$

which is not identical to the solution for a no-slip cylinder given by Eqs. (C.3), i.e. in the same way as observed for the axial motion. This feature is justified by the fact that bending does not introduce a discontinuity in the tangential traction jumps and that the normal traction jumps due to bending resistance as prescribed by Helfrich law in Eq. (2.13) depends only on the normal displacement u_r. Therefore, even when considering an infinite bending modulus, the tangential components of the membrane displacement u_ϕ and u_z are still completely free. As a result, this behaviour cannot represent the hard cylinder where all membrane displacements should be restricted. A similar feature has been found for spherical membranes [81, 82].

Bibliography

[1] J. F. Brady and G. Bossis, Ann. Rev. Fluid Mech. **20**, 111 (1988).

[2] J. Bleibel, A. Domínguez, F. Günther, J. Harting, and M. Oettel, Soft Matter **10**, 2945 (2014).

[3] Q.-H. Wei, C. Bechinger, and P. Leiderer, Science **287**, 625 (2000).

[4] C. Lutz, M. Kollmann, and C. Bechinger, Phys. Rev. Lett. **93**, 026001 (2004).

[5] P. J. A. Janssen, M. D. Baron, P. D. Anderson, J. Blawzdziewicz, M. Loewenberg, and E. Wajnryb, Soft Matter **8**, 7495 (2012).

[6] P. P. Lele, J. W. Swan, J. F. Brady, N. J. Wagner, and E. M. Furst, Soft Matter **7**, 6844 (2011).

[7] M. Gross, T. Krüger, and F. Varnik, Soft Matter **10**, 4360 (2014).

[8] A. Frey-Wyssling, ed., *Deformation and flow in biological systems* (North-Holland Publishing Co., Amsterdam, 1952).

[9] R. Shadwick, J. Exp. Biol. **202**, 3305 (1999).

[10] C. G. Caro, T. J. Pedley, R. C. Schroter, and W. A. Seed, *The Mechanics of the Circulation*, 2nd ed. (Cambridge University Press, 2011).

[11] H. A. Stone, A. D. Stroock, and A. Ajdari, Annu. Rev. Fluid Mech. **36**, 381 (2004).

[12] D. P. Holmes, B. Tavakol, G. Froehlicher, and H. A. Stone, Soft Matter **9**, 7049 (2013).

[13] B. Tavakol, M. Bozlar, C. Punckt, G. Froehlicher, H. A. Stone, I. A. Aksay, and D. P. Holmes, Soft Matter **10**, 4789 (2014).

[14] J. Happel and H. Brenner, *Low Reynolds number hydrodynamics: with special applications to particulate media*, Vol. 1 (Springer Science & Business Media, 2012).

[15] H. Faxén, Colloid. Polym. Sci. **167**, 146 (1959).

[16] H. Faxén, Ann. Phys. **373**, 89 (1922).

[17] S. Wakiya, J. Phys. Soc. Japan **8**, 254 (1953).

[18] T. Bohlin, Trans. Roy. Inst. Technol. Stockholm **155**, 64 (1960).

[19] W. B. Zimmerman, Int. J. Eng. Sci. **42**, 1753 (2004).

[20] S. Leichtberg, R. Pfeffer, and S. Weinbaum, Int. J. Multiph. Flow **3**, 147 (1976).

[21] M. Kedzierski and E. Wajnryb, J. Chem. Phys. **133**, 154105 (2010).

[22] B. Cui, H. Diamant, and B. Lin, Phys. Rev. Lett. **89**, 188302 (2002).

[23] B. Cui, B. Lin, S. Sharma, and S. A. Rice, J. Chem. Phys. **116**, 3119 (2002).

[24] K. Misiunas, S. Pagliara, E. Lauga, J. R. Lister, and U. F. Keyser, Phys. Rev. Lett. **115**, 038301 (2015).

[25] H. Y. Yeh and H. J. Keh, Eur. J. Mech. B Fluid **39**, 52 (2013).

[26] J. Happel and B. J. Bryne, Ind. Eng. Chem. **46**, 1181 (1954).

[27] H. Brenner and J. Happel, J. Fluid Mech. **4**, 195 (1958).

[28] T. Greenstein and J. Happel, J. Fluid Mech. **34**, 705 (1968).

[29] P. M. Bungay and H. Brenner, Int. J. Multiph. Flow **1**, 25 (1973).

[30] N. Liron and R. Shahar, J. Fluid Mech. **86**, 727 (1978).

[31] T. Greenstein and J. Happel, Appl. Sci. Res. **22**, 345 (1970).

[32] N. Lecoq, F. Feuillebois, N. Anthore, R. Anthore, F. Bostel, and C. Petipas, Phys. Fluids A **5**, 3 (1993).

[33] J. J. L. Higdon and G. P. Muldowney, J. Fluid Mech. **298**, 193 (1995).

[34] C. Pozrikidis, J. Eng. Math. **53**, 1 (2005).

[35] H. J. Keh and Y. C. Chang, Int. J. Multiph. Flow **33**, 726 (2007).

[36] S. Bhattacharya, C. Mishra, and S. Bhattacharya, J. Fluid Mech. **642**, 295 (2010).

[37] A. Imperio, J. T. Padding, and W. J. Briels, J. Chem. Phys. **134**, 154904 (2011).

[38] S. Navardi, S. Bhattacharya, and H. Wu, Comput. Fluids **121**, 145 (2015).

[39] H. Hasimoto, J. Phys. Soc. Japan **41**, 2143 (1976).

[40] O. Sano, J. Phys. Soc. Japan **56**, 2713 (1987).

[41] G. J. Sheard and K. Ryan, J. Fluid Mech. **592**, 233 (2007).

[42] B. U. Felderhof, J. Fluid Mech. **637**, 285 (2009).

[43] B. U. Felderhof, J. Fluid Mech. **644**, 97 (2010).

[44] B. U. Felderhof, J. Fluid Mech. **649**, 329 (2010).

[45] B. U. Felderhof and G. Ooms, J. Fluid Mech. **668**, 100 (2011).

[46] S. Rubinow and J. B. Keller, J. Theo. Biol. **35**, 299 (1972).

[47] Y.-C. Fung, *Biomechanics: circulation* (Springer Science & Business Media, 2013).

[48] C. D. Bertram, C. J. Raymond, and K. S. A. Butcher, J. Biomech. Eng. **111**, 185 (1989).

[49] J. B. Grotberg, Annu. Rev. Biomed. Eng. **3**, 421 (2001).

[50] J. B. Grotberg and O. E. Jensen, Ann. Rev. Fluid Mech. **36**, 121 (2004).

[51] S. Canic, J. Tambaca, G. Guidoboni, A. Mikelic, C. J. Hartley, and D. Rosenstrauch, SIAM J. Appl. Math. **67**, 164 (2006).

[52] A. Heap and A. Juel, Phys. Fluids **20**, 081702 (2008).

[53] A. Heap and A. Juel, J. Fluid Mech. **633**, 485 (2009).

[54] R. Zheng, N. Phan-Thien, and R. I. Tanner, Rheol. Acta **30**, 499 (1991).

[55] S. Nahar, S. A. K. Jeelani, and E. J. Windhab, Chem. Eng. Sci. **75**, 445 (2012).

[56] S. Nahar, S. A. K. Jeelani, and E. J. Windhab, Chem. Eng. Comm. **200**, 820 (2013).

[57] A. Mikelic, G. Guidoboni, and S. Canic, Netw. Heterog. Media **2**, 397 (2007).

[58] A. Marzo, X. Y. Luo, and C. D. Bertram, J. Fluid Struct. **20**, 817 (2005).

[59] H. Alexander, Int. J. Mech. Sci. **13**, 87 (1971).

[60] Y. Shan, M. P. Philen, C. E. Bakis, K.-W. Wang, and C. D. Rahn, Compos. Sci. Tech. **66**, 3053 (2006).

[61] M. Rahimi, A. DeSimone, and M. Arroyo, Soft Matter **9**, 11033 (2013).

[62] M. Rahimi, *Shape dynamics and lipid hydrodynamics of bilayer membranes: modeling, simulation and experiments*, Ph.D. thesis (2013).

[63] L. G. Leal, Ann. Rev. Fluid Mech. **12**, 435 (1980).

[64] J. Tan, A. Thomas, and Y. Liu, Soft Matter **8**, 1934 (2012).

[65] A. Daddi-Moussa-Ider, A. Guckenberger, and S. Gekle, Phys. Rev. E **93**, 012612 (2016).

[66] A. Daddi-Moussa-Ider, A. Guckenberger, and S. Gekle, Phys. Fluids **28**, 071903 (2016).

[67] A. Daddi-Moussa-Ider and S. Gekle, J. Chem. Phys. **145**, 014905 (2016).

[68] S. Ramanujan and C. Pozrikidis, J. Fluid Mech. **361**, 117 (1998).

[69] E. Lac, D. Barthès-Biesel, N. A. Pelekasis, and J. Tsamopoulos, J. Fluid Mech. **516**, 303 (2004).

[70] J. B. Freund, Annu. Rev. Fluid Mech. **46**, 67 (2014).

[71] D. Barthès-Biesel, Annu. Rev. Fluid Mech. **48**, 25 (2016).

[72] W. Helfrich, Z. Naturf. C. **28**, 693 (1973).

[73] A. Guckenberger and S. Gekle, J. Phys. Condens. Matter **29**, 203001 (2017).

[74] S. Kim and S. J. Karrila, *Microhydrodynamics: principles and selected applications* (Courier Corporation, 2013).

[75] T. Bickel, Eur. Phys. J. E **20**, 379 (2006).

[76] Y. O. Fuentes, S. Kim, and D. J. Jeffrey, Phys. Fluids **31**, 2445 (1988).

[77] Y. O. Fuentes, S. Kim, and D. J. Jeffrey, Phys. Fluids A **1**, 61 (1989).

[78] J. R. Blake, Math. Proc. Camb. Phil. Soc. **70**, 303 (1971).

[79] G. N. Watson, *A treatise on the theory of Bessel functions* (Cambridge university press, 1995).

[80] M. Abramowitz, I. A. Stegun, *et al.*, *Handbook of mathematical functions*, Vol. 1 (Dover New York, 1972).

[81] A. Daddi-Moussa-Ider and S. Gekle, Phys. Rev. E **95**, 013108 (2017).

[82] A. Daddi-Moussa-Ider, M. Lisicki, and S. Gekle, Phys. Rev. E **95**, 053117 (2017).

[83] S. Kim and R. T. Mifflin, *The Resistance and Mobility Functions of Two Equal Spheres in Low Reynolds Number Flow.*, Tech. Rep. (1984).

[84] E. R. Dufresne, T. M. Squires, M. P. Brenner, and D. G. Grier, Phys. Rev. Lett. **85**, 3317 (2000).

[85] J. W. Swan and J. F. Brady, Phys. Fluids **19**, 113306 (2007).

[86] B. Tränkle, D. Ruh, and A. Rohrbach, Soft Matter **12**, 2729 (2016).

[87] J. R. Blake, J. Fluid Mech. **95**, 209 (1979).

[88] R. Bracewell, *The Fourier Transform and Its Applications* (McGraw-Hill, 1999).

[89] T. Hahn, Comp. Phys. Comm. **168**, 78 (2005).

[90] T. Hahn, Comp. Phys. Comm. **207**, 341 (2016).

[91] T. Bickel, Phys. Rev. E **75**, 041403 (2007).

[92] N. Phan-Thien and D. Tullock, J. Mech. Phys. Solids **41**, 1067 (1993).

[93] M. Kohr and I. I. Pop, *Viscous incompressible flow for low Reynolds numbers*, Vol. 16 (Wit Pr/Comp. Mech., 2004).

[94] H. Zhao and E. S. G. Shaqfeh, Phys. Rev. E **83**, 061924 (2011).

[95] H. Zhao, E. S. G. Shaqfeh, and V. Narsimhan, Phys. Fluids **24**, 011902 (2012).

[96] A. Guckenberger, M. P. Schraml, P. G. Chen, M. Leonetti, and S. Gekle, Comp. Phys. Comm. **207**, 1 (2016).

[97] T. Krüger, F. Varnik, and D. Raabe, Comp. Math. Appl. **61**, 3485 (2011).

[98] T. Krüger, H. Kusumaatmaja, A. Kuzmin, O. Shardt, G. Silva, and E. M. Viggen, *The Lattice Boltzmann Method: Principles and Practice* (Springer, 2016).

[99] D. W. Marquardt, SIAM J. Appl. Math. **11**, 431 (1963).

[100] A. R. Conn, N. I. M. Gould, and P. L. Toint, *Trust region methods*, Vol. 1 (Siam, 2000).

[101] C. Pozrikidis, J. Fluid Mech. **440**, 269 (2001).

[102] G. Cipparrone, I. Ricardez-Vargas, P. Pagliusi, and C. Provenzano, Optics express **18**, 6008 (2010).

[103] A. E. Green and J. C. Adkins, *Large Elastic Deformations and Non-linear Continuum Mechanics* (Oxford University Press, 1960).

[104] L. Zhu, *Simulation of individual cells in flow*, Ph.D. thesis, KTH Royal Institute of Technology (2014).

[105] L. Zhu and L. Brandt, J. Fluid Mech. **770**, 374 (2015).

[106] M. H. Sadd, *Elasticity: theory, applications, and numerics* (Academic Press, 2009).

[107] T. Krüger, *Computer simulation study of collective phenomena in dense suspensions of red blood cells under shear* (Springer Science & Business Media, 2012).

[108] E. Lac and D. Barthès-Biesel, Phys. Fluids **17**, 072105 (2005).

[109] M. Deserno, Chem. Phys. Lipids **185**, 11 (2015).

[110] J. L. Synge and A. Schild, *Tensor calculus*, Vol. 5 (Courier Corporation, 1969).

[111] A. Daddi-Moussa-Ider, M. Lisicki, and S. Gekle, J. Fluid Mech. **811**, 210 (2017).

[112] O.-Y. Zhong-Can and W. Helfrich, Phys. Rev. Lett. **59**, 2486 (1987).

[113] P. R. Rao, G. I. Zahalak, and S. P. Sutera, J. Fluid Mech. **270**, 73 (1994).

[114] C. D. Eggleton and A. S. Popel, Phys. Fluids **10**, 1834 (1998).

[115] Y. Navot, Phys. Fluids **10**, 1819 (1998).

[116] Y. Sui, Y. T. Chew, P. Roy, Y. P. Cheng, and H. T. Low, Phys. Fluids **20** (2008).

[117] J. R. Clausen and C. K. Aidun, Phys. Fluids **22**, 123302 (2010).

[118] D. J. Bukman, J. H. Yao, and M. Wortis, Phys. Rev. E **54**, 5463 (1996).

[119] Z. Y. Luo, S. Q. Wang, L. He, F. Xu, and B. F. Bai, Soft Matter **9**, 9651 (2013).

[120] C. Dupont, A.-V. Salsac, D. Barthès-Biesel, M. Vidrascu, and P. Le Tallec, Phys. Fluids **27**, 051902 (2015).

[121] O. Aouane, A. Farutin, M. Thiébaud, A. Benyoussef, C. Wagner, and C. Misbah, Phys. Rev. Fluids **2**, 063102 (2017).

Publication 7

Slow rotation of a spherical particle inside an elastic tube

A. Daddi-Moussa-Ider, M. Lisicki and S. Gekle

Under review (2017)

1 Abstract

In this paper, we present an analytical calculation of the rotational mobility functions of a particle rotating on the centerline of an elastic cylindrical tube whose membrane exhibits resistance towards shearing and bending. We find that the correction to the particle rotational mobility about the cylinder axis depends solely on membrane shearing properties while both shearing and bending manifest themselves for the rotational mobility about an axis perpendicular to the cylinder axis. In the quasi-steady limit of vanishing frequency, the particle rotational mobility nearby a no-slip rigid cylinder is recovered only if the membrane possesses a non-vanishing resistance towards shearing. We further show that for the asymmetric rotation along the cylinder radial axis, a coupling between shearing and bending exists. Our analytical predictions are compared and validated with corresponding boundary integral simulations where a very good agreement is obtained.

2 Introduction

The assessment of effects of geometric confinement on the motion of microparticles in a viscous fluid is of great importance, since such conditions are found in numerous biological or industrial processes [1, 2]. In such systems, the long-range hydrodynamic interactions which determine macroscopic transport coefficients, are significantly modified due to the flows reflected from the confining boundaries [3–6]. Many of the works have been devoted to motion in tubular channels for their relevance to transport of fluids in microfluidic systems [7, 8] or in human arteries [9]. Notably, an important property of these networks of channels is the elasticity of their building material. Blood flow in capillaries relies on the collagen and elastin filaments within their wall, which enable them to deform in response to changing pressure [10, 11].

Theoretical modeling of slow viscous dynamics and hydrodynamics of particles in narrow channels has been mostly focused on flows within hard cylindrical tubes. The monograph of Happel and Brenner [3] encompasses most theoretical results available. Axial motion of a point particle has been studied extensively due to relevance to rheology measurements [12–19], with later extensions to account for the finite size [20] or non-spherical shape [21]. The motion perpendicular to the axis has been further studied by Hasimoto [22].

The first attempt to address the slow symmetric rotation of a sphere in an infinitely long hard cylinder dates back to Haberman [23] and later by Brenner and Sonshine [24] who gave the torque acting on the rotating sphere as power series of the ratio of particle to cylinder diameter. The rotation of an axisymmetric body within a circular cylinder of finite length has been investigated by Brenner [25] using the point couple approximation technique. The frictional force [26] and torque [27] exerted on a slowly rotating eccentrically positioned sphere within an infinitely long circular cylinder has been studied by Greenstein and coworkers. The latter further investigated the slow rotation of two spheres placed about the cylinder axis in a direction perpendicular to their line of centers [28]. Complementary theoretical works have been conducted by Hirschfeld and coworkers [29, 30] to determine the cylindrical wall effects on the translating-rotating particle of arbitrary shape. Additionally, perturbative solutions for the rotation of eccentric spheres flowing in a cylindrical tube have been derived by Tözeren [31–33], finding a good agreement with the previous solutions. Modeling of hydrodynamic interactions involving a torus or a circular orifice [34] has been further presented [35].

Despite an abundance of results available for hard confining boundaries, not many studies focus on the role of elasticity on the motion of microparticles in confinement. Observations of flow through a deformable elastic channel [36, 37] demonstrate phenomena that can be related to the cardiovascular and respiratory systems, including the generation of instabilities [38–40], propagation of small-amplitude waves [41, 42], and hysteretic shearing of arterial walls [43]. The flexibility in microfluidic devices has also been indicated as a potential way of controlling flow [44, 45]. More

recent works have been devoted to the influence of elastic tube deformation on flow behavior of a shear-thinning fluid [46, 47] or the steady flow in thick-walled flexible elastic tubes [48, 49]. No theoretical studies, however, explore the role of elastic confinement on the hydrodynamic mobility of particles.

This motivates us to compute the flow field generated by a particle rotating inside a realistically modeled elastic channel. We have modeled the membrane using the neo-Hookean model for shearing [50–53], and the Helfrich model [54–56] for bending of its surface. An analogous approach has been successfully applied to the motion of small particles in the presence of planar membranes [57–61], between two elastic sheets [62] and in the vicinity of a spherical elastic capsule [63, 64]. The theoretical results presented in some of these works have been favorably compared with fully resolved boundary integral method (BIM) simulations, and thus constitute a practical approximate tool for analysis of confined motion in elastically bounded systems. The present study computes the frequency-dependent rotational mobility corrections due to the elastic confinement which has not been previously analyzed.

The remainder of the paper is organized as follows. In Sec. 3, we derive analytical expressions for the flow field induced by a point-torque oriented either parallel or perpendicular to the cylinder axis, by expressing the solutions of the Stokes equations in terms of Fourier-Bessel integrals. We then compute in Sec. 4 the leading order self- and pair-mobility functions for the rotation along or perpendicular to the cylinder axis. Moreover, the membrane displacement field induced by the particle for a given actuation is presented. For a given set of parameters, we compare in Sec. 5 our analytical predictions with fully resolved boundary integral simulations, where a good agreement is obtained. Concluding remarks are offered in Sec. 6. The appendix outlines the main derivation steps for the determination of the linearized traction jumps stemming from membrane shearing and bending rigidities.

3 Theoretical description

We consider a small solid spherical particle of radius a, placed on the axis of a cylindrical elastic tube of undisturbed radius $R \gg a$. The fluid inside and outside the tube is assumed to be incompressible of the same shear viscosity η. An oscillatory torque acts on the particle inducing periodic rotational motion whose amplitude is linearly related to the amplitude of the acting torque. Our final goal is to compute the rotational mobility representing the coefficient of proportionality between torque and motion. We employ the cylindrical coordinate system (r, ϕ, z) where r is the radius, ϕ is the azimuthal angle and z is the axial direction along the cylinder axis with the origin located at the center of the particle (see Fig. 1 for an illustration of the system setup). The flow fields inside and outside the cylindrical channel are labeled 1 and 2, respectively.

We proceed by computing the rotlet solution which follows from the solution of the forced Stokes equations

$$\eta \boldsymbol{\nabla}^2 \boldsymbol{v}_1 - \boldsymbol{\nabla} p_1 + \boldsymbol{F}(\boldsymbol{r}) = 0\,, \tag{3.1a}$$

$$\boldsymbol{\nabla} \cdot \boldsymbol{v}_1 = 0\,, \tag{3.1b}$$

inside the tube (for $r < R$) and

$$\eta \boldsymbol{\nabla}^2 \boldsymbol{v}_2 - \boldsymbol{\nabla} p_2 = 0\,, \tag{3.2a}$$

$$\boldsymbol{\nabla} \cdot \boldsymbol{v}_2 = 0\,, \tag{3.2b}$$

outside (for $r > R$). Here $\boldsymbol{F}(\boldsymbol{r})$ represents an arbitrary time-dependent force density acting on the

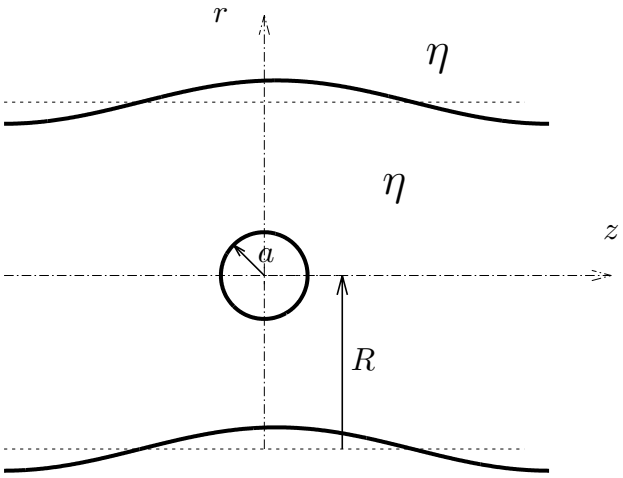

Figure 1: Illustration of the system setup. A small spherical particle of radius a placed at the origin rotating nearby an elastic tube of undisturbed radius R.

fluid. We specifically consider a distribution that has only the asymmetric dipolar term

$$\oint_S \boldsymbol{r} \times \boldsymbol{F}\, \mathrm{d}S = \boldsymbol{L}\,, \tag{3.3}$$

where the integral is taken over the surface S of the spherical particle. Since the particle is small, we shall consider its point-like limit. Then the antisymmetric dipolar term in the force multipole expansion yields the flow field induced by a rotlet of strength $\boldsymbol{L}$. The flow field around a rotlet in an infinite fluid is given by [65]

$$\boldsymbol{v}(\boldsymbol{r}) = \frac{1}{8\pi\eta}\frac{\boldsymbol{L}\times\boldsymbol{r}}{r^3}\,. \tag{3.4}$$

Our aim is to find the corresponding solution in the space confined by an elastic cylindrical tube.

For realistic parameters, we have shown in earlier work [59] that the term with a time derivative in the unsteady Stokes equations leads to a negligible contribution to the total mobility corrections and thus is not considered in the present work.

Eqs. (3.1) and (3.2) are subject to the regularity conditions

$$|\boldsymbol{v}_1| < \infty \ \text{ for } |\boldsymbol{r}| = 0\,, \tag{3.5}$$
$$\boldsymbol{v}_1 \to \boldsymbol{0} \ \text{ for } z \to \infty\,, \tag{3.6}$$
$$\boldsymbol{v}_2 \to \boldsymbol{0} \ \text{ for } |\boldsymbol{r}| \to \infty\,, \tag{3.7}$$

together with the boundary conditions imposed at the undisplaced membrane $r = R$. This commonly used simplification is justified since we are dealing with small deformations only. In other situations, when the finite amplitude of deformation is important, it becomes necessary to apply the boundary conditions at the displaced membrane, see for instance Refs. [66–70]. The velocity field across the membrane is continuous, leading to

$$[v_r] = 0\,, \tag{3.8}$$
$$[v_\phi] = 0\,, \tag{3.9}$$
$$[v_z] = 0\,, \tag{3.10}$$

while the elastic membrane introduces a discontinuity in the fluid stress tensor

$$[\sigma_{\phi r}] = \Delta f_\phi^{\mathrm{S}}\,, \tag{3.11}$$
$$[\sigma_{zr}] = \Delta f_z^{\mathrm{S}}\,, \tag{3.12}$$
$$[\sigma_{rr}] = \Delta f_r^{\mathrm{S}} + \Delta f_r^{\mathrm{B}}\,, \tag{3.13}$$

with the notation $[w] := w(r = R^+) - w(r = R^-)$ refering to the jump of a given quantity w across the membrane. The fluid stress tensor is expressed in cylindrical coordinates as [71]

$$\sigma_{\phi r} = \eta\left(v_{\phi,r} - \frac{v_\phi + v_{r,\phi}}{r}\right),$$
$$\sigma_{zr} = \eta(v_{z,r} + v_{r,z})\,,$$
$$\sigma_{rr} = -p + 2\eta v_{r,r}\,.$$

The traction jumps can be decomposed into a contribution due to the in-plane shearing elasticity (superscript S) and a contribution stemming from membrane bending rigidity (superscript B). Shearing is accounted for using the neo-Hookean model [50]. As derived in the Appendix, the linearized traction jumps due to shearing elasticity are written as

$$\Delta f_\phi^{\mathrm{S}} = -\frac{\kappa_{\mathrm{S}}}{3}\left(u_{\phi,zz} + \frac{3u_{z,\phi z}}{R} + \frac{4(u_{r,\phi} + u_{\phi,\phi\phi})}{R^2}\right), \tag{3.14a}$$
$$\Delta f_z^{\mathrm{S}} = -\frac{\kappa_{\mathrm{S}}}{3}\left(4u_{z,zz} + \frac{2u_{r,z} + 3u_{\phi,z\phi}}{R} + \frac{u_{z,\phi\phi}}{R^2}\right), \tag{3.14b}$$
$$\Delta f_r^{\mathrm{S}} = \frac{2\kappa_{\mathrm{S}}}{3}\left(\frac{2(u_r + u_{\phi,\phi})}{R^2} + \frac{u_{z,z}}{R}\right), \tag{3.14c}$$

where κ_{S} is the elastic shear modulus. The comma in indices denotes a partial spatial derivative.

Bending of the membrane is described following the Helfrich model [54, 56] as

$$\Delta f_r^{\mathrm{B}} = \kappa_{\mathrm{B}}\Big(R^3 u_{r,zzzz} + 2R(u_{r,zz} + u_{r,zz\phi\phi}) + \frac{u_r + 2u_{r,\phi\phi} + u_{r,\phi\phi\phi\phi}}{R}\Big)\,, \tag{3.15}$$

where κ_{B} is the bending modulus. Moreover, $\Delta f_\phi^{\mathrm{B}} = \Delta f_z^{\mathrm{B}} = 0$ since bending does not introduce a discontinuity in the tangential traction jumps [56].

Similar as above, we apply the no-slip boundary condition at the undisplaced membrane surface [72]

$$\frac{\partial \boldsymbol{u}(\phi, z)}{\partial t} = \boldsymbol{v}(r, \phi, z)|_{r=R}\,, \tag{3.16}$$

which in Fourier space is written as

$$\boldsymbol{u}(\phi, z) = \left.\frac{\boldsymbol{v}(r, \phi, z)}{i\omega}\right|_{r=R}. \tag{3.17}$$

Having introduced the regularity and boundary conditions, we then solve the equations of fluid motion by expanding them in the form of Fourier-Bessel integrals. For this aim, solutions will be searched for in the two distinct regions i.e. inside and outside the cylindrical membrane separately. We write the solution in terms of integrals of harmonic functions with unknown coefficients, which we then determine from the boundary conditions.

We begin by expressing the solution of Eqs. (3.1) inside the cylinder as a sum of a point-torque

(point-couple) flow field and the flow field reflected from the membrane, as

$$\boldsymbol{v}_1 = \boldsymbol{v}^{\mathrm{R}} + \boldsymbol{v}^* \,,$$
$$p_1 = p^{\mathrm{R}} + p^* \,,$$

where $\boldsymbol{v}^{\mathrm{R}}$ and p^{R} are the rotlet solution in an unbounded medium and $\boldsymbol{v}^*$ and p^* are the solutions of the homogenous Stokes equations

$$\eta \boldsymbol{\nabla}^2 \boldsymbol{v}^* - \boldsymbol{\nabla} p^* = 0 \,, \tag{3.18a}$$
$$\boldsymbol{\nabla} \cdot \boldsymbol{v}^* = 0 \,, \tag{3.18b}$$

required to satisfy the regularity and boundary conditions. In the next section, we shall first consider the axisymmetric rotational motion about the cylinder axis.

3.1 Axial rotlet

The solution for a point-torque of strength $\boldsymbol{L} = L_z \boldsymbol{e}_z$, located at the origin and directed along the z direction reads [65]

$$v_x^{\mathrm{R}} = -\frac{L_z}{8\pi\eta}\frac{y}{d^3} \,, \qquad v_y^{\mathrm{R}} = \frac{L_z}{8\pi\eta}\frac{x}{d^3} \,, \qquad v_z^{\mathrm{R}} = 0 \,,$$

and $p^{\mathrm{R}} = 0$. Here $d := \sqrt{r^2 + z^2}$ is the distance from the rotlet position. Therefore, the velocity field is purely directed along the azimuthal direction such that

$$v_r^{\mathrm{R}} = 0 \,, \qquad v_\phi^{\mathrm{R}} = \frac{L_z}{8\pi\eta}\frac{r}{d^3} = -\frac{L_z}{8\pi\eta}\frac{\partial}{\partial r}\frac{1}{d} \,. \tag{3.19}$$

By making use of the integral relation [73, 74]

$$\frac{1}{d} = \frac{2}{\pi}\int_0^\infty K_0(qr)\cos qz \,\mathrm{d}q \,, \tag{3.20}$$

wherein K_0 is the zeroth order modified Bessel function of the second kind [75], the integral representation of the azimuthal fluid velocity field due to a point-torque reads

$$v_\phi^{\mathrm{R}} = \frac{L_z}{4\pi^2\eta}\int_0^\infty q K_1(qr)\cos qz \,\mathrm{d}q \,. \tag{3.21}$$

For symmetric rotation about the cylinder axis, the homogenous Stokes equations Eqs. (3.2) and (3.18) reduce to,

$$v^*_{\phi,rr} + \frac{v^*_{\phi,r}}{r} - \frac{v^*_\phi}{r^2} + v^*_{\phi,zz} = 0 \,, \tag{3.22}$$

and analogously for v_{ϕ_2}. Using the method of separation of variables [76], and by making use of the regularity equations stated by Eqs. (3.5) through (3.7), the image solution and external fluid velocity can therefore be presented in integral form as [24]

$$v^*_\phi = \frac{L_z}{4\pi^2\eta}\int_0^\infty A^*(q) I_1(qr)\cos qz \,\mathrm{d}q \,, \tag{3.23a}$$
$$v_{\phi_2} = \frac{L_z}{4\pi^2\eta}\int_0^\infty A_2(q) K_1(qr)\cos qz \,\mathrm{d}q \,. \tag{3.23b}$$

The azimuthal velocity component across the membrane is continuous in virtue of Eq. (3.9)

leading to

$$K_1 A_2 - I_1 A^* = \frac{sK_1}{R}\,, \tag{3.24}$$

where $s := qR$. The modified Bessel functions have the argument s which is dropped here for brevity. The unknown functions A^* and A_2 are to be determined from the imposed traction jumps at the membrane.

The discontinuity of the azimuthal-normal component of the fluid stress jump stated by Eq. (3.11) leads to

$$(sI_0 - I_1)A^* + \left(\left(1 - \frac{i\alpha s^2}{2}\right)K_1 + sK_0\right)A_2 = \frac{s(sK_0 + K_1)}{R}\,, \tag{3.25}$$

where we have defined the shearing coefficient as

$$\alpha := \frac{2\kappa_{\mathrm{S}}}{3\eta R\omega}\,, \tag{3.26}$$

which quantifies the effect of shearing for a given actuation frequency ω.

Solving Eqs. (3.24) and (3.25) for the unknown coefficients A^* and A_2 we obtain

$$A^* = \frac{1}{R}\frac{i\alpha s^2 K_1^2}{(2I_0 - i\alpha s I_1)K_1 + 2K_0 I_1}\,, \tag{3.27}$$

$$A_2 = \frac{1}{R}\frac{2s(I_0 K_1 + I_1 K_0)}{(2K_0 - i\alpha s K_1)I_1 + 2I_0 K_1}\,. \tag{3.28}$$

Interestingly, the coefficients A^* and A_2 and thus the inner and outer flow fields depend solely on shear and do not depend on bending. In particular, for $\alpha = 0$, the image solution Eq. (3.23a) vanishes and the solution outside the cylinder (3.23b) is identical to the rotlet solution given by Eq. (3.21).

In the limit $\alpha \to \infty$ corresponding to the quasi-steady limit of vanishing actuation frequency, or equivalently to an infinite membrane shearing modulus, we recover the result obtained earlier by Brenner [25], namely

$$\lim_{\alpha\to\infty} A^* = -\frac{sK_1}{RI_1}\,,$$

and $A_2 = 0$ for which the outer fluid is stagnant. In the following, the solution for a radial rotlet will be derived.

3.2 Radial rotlet

Without loss of generality, we shall assume that the rotlet is exerted along the x direction. The induced velocity field reads [65]

$$v_x^{\mathrm{R}} = 0\,, \qquad v_y^{\mathrm{R}} = -\frac{L_x}{8\pi\eta}\frac{z}{d^3}\,, \qquad v_z^{\mathrm{R}} = \frac{L_x}{8\pi\eta}\frac{y}{d^3}\,,$$

and $p^{\mathrm{R}} = 0$. Transforming to cylindrical coordinates, we obtain

$$v_r^{\mathrm{R}} = -\frac{L_x}{8\pi\eta}\frac{z\sin\phi}{d^3}\,, \quad v_\phi^{\mathrm{R}} = -\frac{L_x}{8\pi\eta}\frac{z\cos\phi}{d^3}\,, \quad v_z^{\mathrm{R}} = \frac{L_x}{8\pi\eta}\frac{r\sin\phi}{d^3}\,.$$

After making use of Eq. (3.20) together with [73, 74]

$$\frac{z}{d} = \frac{2}{\pi}\,r\int_0^\infty K_1(qr)\sin qz\,\mathrm{d}q\,, \tag{3.29}$$

and by noting that

$$\frac{z}{d^3} = -\frac{1}{r}\frac{\partial}{\partial r}\frac{z}{d}, \qquad \frac{r}{d^3} = -\frac{\partial}{\partial r}\frac{1}{d}, \tag{3.30}$$

the rotlet solution can therefore be expressed in an integral form as

$$v_r^{\mathrm{R}} = -\frac{L_x}{4\pi^2\eta}\,\sin\phi \int_0^\infty qK_0(qr)\sin qz\,\mathrm{d}q\,, \tag{3.31a}$$

$$v_\phi^{\mathrm{R}} = -\frac{L_x}{4\pi^2\eta}\,\cos\phi \int_0^\infty qK_0(qr)\sin qz\,\mathrm{d}q\,, \tag{3.31b}$$

$$v_z^{\mathrm{R}} = \frac{L_x}{4\pi^2\eta}\,\sin\phi \int_0^\infty qK_1(qr)\cos qz\,\mathrm{d}q\,. \tag{3.31c}$$

The reflected flow can be represented by using the fact that the homogenous Stokes equations (3.18) have a general solution expressed in terms of three harmonic functions Φ, Ψ and Γ as [3, p. 77]

$$v_r^* = \Psi_{,r} + \frac{\Gamma_{,\phi}}{r} + r\,\Phi_{,rr}\,, \tag{3.32a}$$

$$v_\phi^* = \frac{\Psi_{,\phi}}{r} - \Gamma_{,r} - \frac{\Phi_{,\phi}}{r} + \Phi_{,\phi r}\,, \tag{3.32b}$$

$$v_z^* = \Psi_{,z} + r\,\Phi_{,rz} + \Phi_{,z}\,, \tag{3.32c}$$

$$p^* = -2\eta\,\Phi_{,zz}\,. \tag{3.32d}$$

The functions Ψ, Φ and Γ are solutions to the Laplace equation which can be written in an integral form as

$$\Phi = \frac{L_x}{4\pi^2\eta}\,\sin\phi \int_0^\infty \varphi(q)g(qr)\sin qz\,\mathrm{d}q\,, \tag{3.33a}$$

$$\Psi = \frac{L_x}{4\pi^2\eta}\,\sin\phi \int_0^\infty \psi(q)g(qr)\sin qz\,\mathrm{d}q\,, \tag{3.33b}$$

$$\Gamma = \frac{L_x}{4\pi^2\eta}\,\cos\phi \int_0^\infty \gamma(q)g(qr)\sin qz\,\mathrm{d}q\,, \tag{3.33c}$$

where φ, ψ and γ are wavenumber-dependent unknown functions to be determined from the underlying boundary conditions. Moreover, g is a solution of the first order modified Bessel equation [75]. Since the solution needs to be regular at the origin owing to Eq. (3.5), we take $g \equiv I_1$ for the image solution, directly leading to

$$v_r^* = \frac{L_x}{4\pi^2\eta}\frac{\sin\phi}{r}\int_0^\infty \Big(\big((2+q^2r^2)I_1(qr) - qrI_0(qr)\big)\,\varphi^*(q) + (qrI_0(qr) - I_1(qr))\,\psi^*(q) \\ - I_1(qr)\,\gamma^*(q)\Big)\sin qz\,\mathrm{d}q\,, \tag{3.34a}$$

$$v_\phi^* = \frac{L_x}{4\pi^2\eta}\frac{\cos\phi}{r}\int_0^\infty \Big((qrI_0(qr) - 2I_1(qr))\,\varphi^*(q) + I_1(qr)\psi^*(q) \\ + (I_1(qr) - qrI_0(qr))\,\gamma^*(q)\Big)\sin qz\,\mathrm{d}q\,, \tag{3.34b}$$

$$v_z^* = \frac{L_x}{4\pi^2\eta}\sin\phi \int_0^\infty q\,(qrI_0(qr)\varphi^*(q) + I_1(qr)\psi^*(q))\cos qz\,\mathrm{d}q\,. \tag{3.34c}$$

$$p^* = \frac{L_x}{2\pi^2}\sin\phi \int_0^\infty q^2 I_1(qr)\varphi^*(q)\sin qz\,\mathrm{d}q\,. \tag{3.34d}$$

Since the solution has to decay at infinity in virtue of Eq. (3.7), we thus take $g \equiv K_1$ for the fluid outside, leading to

$$v_{r2} = \frac{L_x}{4\pi^2\eta}\frac{\sin\phi}{r}\int_0^\infty \Big(\big((2+q^2r^2)K_1(qr) + qrK_0(qr)\big)\,\varphi_2(q) - (qrK_0(qr) + K_1(qr))\,\psi^*(q) - K_1(qr)\,\gamma^*(q)\Big)\sin qz\,\mathrm{d}q\,, \tag{3.35a}$$

$$v_{\phi 2} = \frac{L_x}{4\pi^2\eta}\frac{\cos\phi}{r}\int_0^\infty \Big(-(qrK_0(qr) + 2K_1(qr))\,\varphi_2(q) + K_1(qr)\psi^*(q) + (K_1(qr) + qrK_0(qr))\,\gamma^*(q)\Big)\sin qz\,\mathrm{d}q\,, \tag{3.35b}$$

$$v_{z2} = \frac{L_x\sin\phi}{4\pi^2\eta}\int_0^\infty q\,(-qrK_0(qr)\varphi_2(q) + K_1(qr)\psi^*(q))\cos qz\,\mathrm{d}q\,, \tag{3.35c}$$

$$p_2 = \frac{L_x\sin\phi}{2\pi^2}\int_0^\infty q^2K_1(qr)\varphi_2(q)\sin qz\,\mathrm{d}q\,. \tag{3.35d}$$

The continuity of the fluid velocity field across the membrane as stated by Eqs. (3.8) through (3.10) leads to

$$\big(sI_0 - (2+s^2)I_1\big)\,\varphi^* + (I_1 - sI_0)\psi^* + I_1\gamma^* - (K_1 + sK_0)\psi_2 + \big(sK_0 + (2+s^2)K_1\big)\,\varphi_2 - K_1\gamma_2 = -sK_0\,, \tag{3.36}$$

$$(2I_1 - sI_0)\varphi^* - I_1\psi^* + (sI_0 - I_1)\gamma^* - (sK_0 + 2K_1)\varphi_2 + K_1\psi_2 + (K_1 + sK_0)\,\gamma_2 = -sK_0\,, \tag{3.37}$$

$$-s^2I_0\varphi^* - sI_1\psi^* - s^2K_0\varphi_2 + sK_1\psi_2 = sK_1\,. \tag{3.38}$$

The unknown functions φ_2, ψ_2 and γ_2 associated to the external flow field can readily be expressed in terms of φ^*, ψ^* and γ^* by solving Eqs. (3.36) through (3.38) to obtain

$$\varphi_2 = \frac{S\varphi^* + (K_1 + sK_0)G\psi^* - K_1G\gamma^*}{D}\,, \tag{3.39}$$

$$\psi_2 = \frac{s\,\big((2+s^2)K_0 + sK_1\big)\,G\varphi^* + S\psi^* - sK_0G\gamma^*}{D} + 1\,, \tag{3.40}$$

$$\gamma_2 = \frac{2sK_0G\varphi^* + 2K_1G\psi^*}{D} + \frac{\big(S - G\,\big(sK_0 + (2+s^2)K_1\big)\big)\,\gamma^*}{D} - 1\,, \tag{3.41}$$

where we have defined

$$\begin{aligned} S &= -sK_0K_1\,\big(sI_0 + (2+s^2)I_1\big) - s^2\,\big(sI_0K_0^2 + I_1K_1^2\big)\,,\\ G &= -s\,(I_0K_1 + I_1K_0)\,,\\ D &= s\big(s^2K_0^3 + sK_0^2K_1 - sK_1^3 - (2+s^2)K_0K_1^2\big)\,. \end{aligned}$$

The expressions of φ^*, ψ^* and γ^* may be determined given the membrane constitutive model. In the following, explicit analytical expressions will be derived by considering independently an idealized membrane with pure shearing or pure bending.

Pure shearing

As a first model, we consider an idealized elastic membrane with pure shearing resistance, such as an artificial capsule [77, 78]. The traction jump along the azimuthal direction given by Eq. (3.11) depends only on membrane shearing resistance. We obtain

$$\begin{aligned}\left((4+s^2)I_1-2sI_0\right)\varphi^*+(sI_0-2I_1)\psi^*+\left(sI_0-(2+s^2)I_1\right)\gamma^*+\Big(\left(i\alpha(8+3s^2)-(4+s^2)\right)K_1\\ +2s\left(i\alpha(2+s^2)-1\right)K_0\Big)\varphi_2+\frac{1}{2}\left(\left(4+2s^2-i\alpha\left(8+s^2\right)\right)K_1+s\left(2-i\alpha\left(4+s^2\right)\right)K_0\right)\gamma_2\\ +\left(2\left(1-i\alpha(2+s^2)\right)K_1+s(1-2i\alpha)K_0\right)\psi_2=-s^2K_1\,.\end{aligned} \tag{3.42}$$

The traction jump along the axial direction stated by Eq. (3.12) is also independent of bending leading to

$$\begin{aligned}s^2(I_0+sI_1)\varphi^*+s(sI_0-I_1)\psi^*+s\left(s\left(1+i\alpha(3+2s^2)\right)K_0+\left(i\alpha(5+s^2)-s^2\right)K_1\right)\varphi_2\\ +s\left(\left(1-i\alpha(3+2s^2)\right)K_1+s(1-i\alpha)K_0\right)\psi_2-\frac{i\alpha s}{2}\left(3sK_0+5K_1\right)\gamma_2=-s(sK_0+K_1)\,.\end{aligned} \tag{3.43}$$

By considering only the shearing contribution in the normal traction jump in Eq. (3.13) we get

$$\begin{aligned}2s^2I_1\varphi^*+\left(i\alpha s(4+s^2)K_0+2\left(i\alpha(4+s^2)-s^2\right)K_1\right)\varphi_2-i\alpha\left(2sK_0+(4+s^2)K_1\right)\psi_2\\ -2i\alpha(sK_0+2K_1)\gamma_2=0\,.\end{aligned} \tag{3.44}$$

Eqs. (3.39) through (3.44) form a closed system of equations for the unknown functions. Due to their complexity, analytical expressions are not listed here. In particular, in the limit $\alpha\to\infty$ we obtain

$$\lim_{\alpha\to\infty}\varphi^*=\frac{(I_0K_1+I_1K_0)(2I_1-sI_0)}{s(sI_0-I_1)(I_0^2-I_1^2)-2I_0I_1^2}\,, \tag{3.45}$$

$$\lim_{\alpha\to\infty}\psi^*=\frac{sI_0^2(sK_0-K_1)+I_0I_1(s^2K_1-2sK_0+2K_1)-sI_1^2K_1}{s(sI_0-I_1)(I_0^2-I_1^2)-2I_0I_1^2}\,, \tag{3.46}$$

$$\lim_{\alpha\to\infty}\gamma^*=\frac{(s^2K_0+sK_1+4K_0)I_1^2+2I_0I_1K_1-sI_0^2(sK_0+K_1)}{s(sI_0-I_1)(I_0^2-I_1^2)-2I_0I_1^2}\,, \tag{3.47}$$

where the functions φ_2, ψ_2 and γ_2 vanish in this limit.

Pure bending

Another membrane model involves only a bending resistance, as commonly considered for fluid vesicles [79, 80]. Neglecting the shearing contribution in the traction jump along the ϕ direction, Eq. (3.11) reads

$$\begin{aligned}\left((4+s^2)I_1-2sI_0\right)\varphi^*+(sI_0-2I_1)\psi^*+\left(sI_0-(2+s^2)I_1\right)\gamma^*-\left((4+s^2)K_1+2sK_0\right)\varphi_2\\ +(2K_1+sK_0)\psi_2+\left(\left(2+s^2\right)K_1+sK_0\right)\gamma_2=-s^2K_1\,.\end{aligned} \tag{3.48}$$

The traction jump across the z direction in the absence of shearing is continuous leading to

$$s(I_0+sI_1)\varphi^*+(sI_0-I_1)\psi^*+s\left(K_0-sK_1\right)\varphi_2+\left(K_1+sK_0\right)\psi_2=-(sK_0+K_1)\,. \tag{3.49}$$

while the normal traction jump is discontinuous leading to

$$2I_1\varphi^* + \left(i\alpha_{\mathrm{B}}^3 s^2\left(sK_0 + (2+s^2)K_1\right) - 2K_1\right)\varphi_2 - i\alpha_{\mathrm{B}}^3 s^2(sK_0+K_1)\psi_2 - i\alpha_{\mathrm{B}}^3 s^2 K_1\gamma_2 = 0\,, \quad (3.50)$$

where we have defined the bending coefficient α_{B} as

$$\alpha_{\mathrm{B}} := \frac{1}{R}\left(\frac{\kappa_{\mathrm{B}}}{\eta\omega}\right)^{1/3}, \quad (3.51)$$

quantifying the effect of bending.

By plugging the expressions of φ_2, ψ_2 and γ_2 as given by Eqs. (3.39) through (3.41) into Eqs. (3.48) through (3.50), expressions for φ^*, ψ^* and γ^* can be obtained. In particular, by taking the limit $\alpha_{\mathrm{B}} \to \infty$ the coefficients read

$$\lim_{\alpha_{\mathrm{B}}\to\infty}\varphi^* = \frac{-sK_0(sK_0+K_1)}{sK_0\left(2sI_0-(3+s^2)I_1\right)+(3+s^2)(sI_0-2I_1)K_1}\,,$$
$$\lim_{\alpha_{\mathrm{B}}\to\infty}\psi^* = \frac{sK_0\left(sK_0+(2+s^2)K_1\right)}{sK_0\left(2sI_0-(3+s^2)I_1\right)+(3+s^2)(sI_0-2I_1)K_1}\,,$$
$$\lim_{\alpha_{\mathrm{B}}\to\infty}\gamma^* = \frac{2sK_0K_1}{sK_0\left(2sI_0-(3+s^2)I_1\right)+(3+s^2)(sI_0-2I_1)K_1}\,,$$

which are in contrast to the solution for a hard-cylinder with stick boundary conditions given by Eqs. (3.45) through (3.47). This difference is explained by the fact that bending following the Helfrich model does not lead to a discontinuity in the tangential traction jumps [56]. Moreover, the normal traction jump as stated by Eq. (3.15) depends uniquely on the radial (normal) displacement and does not involve the tangential displacements u_ϕ and u_z. As a result, even by taking an infinite membrane bending modulus, the tangential displacements are still completely free. This behavior therefore cannot represent the rigid cylinder limit where membrane deformation in all directions must be restricted. Such behavior has previously been observed near spherical membranes as well [63, 64].

Shearing and bending

For a membrane endowed simultaneously with shearing and bending rigidities, a similar resolution procedure can be employed. Explicit analytical expressions can be obtained via computer algebra systems, but they are rather complicated and are therefore not listed here. We further mention that a coupling between shearing and bending exists, meaning that the solutions derived above for pure shearing and bending cannot be added up linearly. This coupling behavior has previously been observed for two parallel planar [62] or spherical membranes [63, 64], in contrast to the single membrane case where adding up linearly the shearing and bending related solutions holds [59, 61].

In order to clarify the mentioned coupling between shear and bending, consider two different idealized membranes, one with pure bending resistance ($\alpha = 0$) and another one with pure shear resistance ($\alpha_{\mathrm{B}} = 0$). For a membrane endowed simultaneously with both shear and bending rigidities, we have shown in Eqs. (3.39)–(3.41) that the unknown functions outside the tube X_2 are related to the functions inside X^* in the following way

$$X_2 = AX^* + b\,, \quad (3.52)$$

where $X_2 = (\varphi_2, \psi_2, \gamma_2)^{\mathrm{T}}$, $X^* = (\varphi^*, \psi^*, \gamma^*)^{\mathrm{T}}$, A is a 3×3 known matrix and $b = (0, 1, -1)^{\mathrm{T}}$.

We now denote by $X_{2\mathrm{S}}$, $X_{2\mathrm{B}}$ the solutions outside the tube for a membrane with pure shear and

pure bending, respectively, and by X_{S}^*, X_{B}^* the corresponding image system solutions. Accordingly,

$$X_{2\mathrm{S}} = AX_{\mathrm{S}}^* + b\,, \qquad X_{2\mathrm{B}} = AX_{\mathrm{B}}^* + b\,, \tag{3.53}$$

leading after taking the sum member by member to

$$\hat{X}_2 = A\hat{X}^* + 2b\,, \tag{3.54}$$

where $\hat{X}_2 = X_{2\mathrm{S}} + X_{2\mathrm{B}}$ and $\hat{X}^* = X_{\mathrm{S}}^* + X_{\mathrm{B}}^*$ are the superposition solutions. Clearly, this relation is different from the original equation (3.52) since $b \neq 0$, and therefore the true solutions X_2 and X^* cannot both be identical to the superposed functions $\hat{X}_2$ and $\hat{X}^*$. As a consequence, they cannot satisfy the correct boundary conditions showing that shear and bending are coupled and cannot be added up linearly.

4 Particle rotational mobility and membrane deformation

The rotlet solution obtained in the previous section serves as a basis for the determination of the particle rotational mobilities along and perpendicular to the cylinder axis. We restrict our present consideration to the point-particle approximation, and thus the particle size is much smaller than the cylinder radius. We shall show that this approximation, despite its simplicity, can lead to a surprisingly good agreement with boundary integral simulations of truly extended particles.

4.1 Axial rotational mobility

Beginning with the rotational motion symmetrically around the cylinder axis, the leading-order correction to the rotational mobility of a point-particle is

$$\Delta\mu_{\parallel}^{\mathrm{S}} = L_z^{-1} \lim_{\boldsymbol{r}\to 0} \Omega_z^*\,, \tag{4.1}$$

with

$$\Omega_z^* = \frac{1}{2}\left(v_{\phi,r}^* + \frac{v_\phi^*}{r}\right)\,,$$

being the z component of the correction to the fluid angular velocity $\boldsymbol{\Omega}^* := \frac{1}{2}\boldsymbol{\nabla}\times\boldsymbol{v}^*$. Making use of Eq. (3.23a), we obtain

$$\Delta\mu_{\parallel}^{\mathrm{S}} = \frac{1}{8\pi^2\eta}\int_0^\infty qA^*\,\mathrm{d}q\,.$$

Scaling by the bulk rotational mobility $\mu_0^{rr} = 1/(8\pi\eta a^3)$, the scaled frequency-dependent correction to the rotational mobility takes the form

$$\frac{\Delta\mu_{\parallel}^{\mathrm{S}}}{\mu_0^{rr}} = \frac{1}{\pi}\left(\frac{a}{R}\right)^3\int_0^\infty \frac{i\alpha s^3K_1^2}{(2I_0 - i\alpha sI_1)K_1 + 2K_0I_1}\,\mathrm{d}s\,. \tag{4.2}$$

Notably, the correction at lowest order follows a cubic dependence in the ratio of particle to cylinder radius. Particularly, in the hard cylinder limit we get

$$\lim_{\alpha\to\infty}\frac{\Delta\mu_{\parallel}^{\mathrm{S}}}{\mu_0^{rr}} = -\frac{1}{\pi}\left(\frac{a}{R}\right)^3\int_0^\infty \frac{s^2K_1}{I_1}\,\mathrm{d}s \approx -0.79682\left(\frac{a}{R}\right)^3\,. \tag{4.3}$$

in agreement with the result know in the literature [24, 81–83]. We further emphasize that in the absence of shearing, the correction to the particle rotational mobility vanishes.

We now turn our attention to hydrodynamic interactions between two spherical particles of equal radius [84, 85] positioned on the centerline of an elastic cylinder. For the rest of our discussion, we shall denote by γ the particle located at $z = 0$ and by λ the particle at $z = h$. The particle rotational pair-mobility function about the line connecting the two centers is computed at leading order as

$$\mu_{\parallel}^{\mathrm{P}} = L_z^{-1} \lim_{\boldsymbol{r}\to\boldsymbol{r}_\lambda} \Omega_{1z} \,. \tag{4.4}$$

Using Eqs. (3.19) and (3.23a), we get

$$\mu_{\parallel}^{\mathrm{P}} = \frac{1}{8\pi\eta h^3} + \frac{1}{8\pi^2\eta} \int_0^\infty qA^* \cos(\sigma s)\, \mathrm{d}q \,.$$

wherein $\sigma := h/R$. The first term in the equation above is the leading-order rotational pair-mobility for two isolated spheres, i.e. in an unbounded medium [86]. Scaling by the bulk rotational mobility, we obtain

$$\frac{\mu_{\parallel}^{\mathrm{P}}}{\mu_0^{rr}} = \left(\frac{a}{h}\right)^3 + \frac{1}{\pi}\left(\frac{a}{R}\right)^3 \int_0^\infty \frac{i\alpha s^3 K_1^2 \cos(\sigma s)}{(2I_0 - i\alpha s I_1)K_1 + 2K_0 I_1}\, \mathrm{d}s \,,$$

which is dependent on membrane shearing properties only. The hard-cylinder limit is recovered by taking $\alpha \to \infty$ to obtain

$$\lim_{\alpha\to\infty} \frac{\mu_{\parallel}^{\mathrm{P}}}{\mu_0^{rr}} = \left(\frac{a}{h}\right)^3 - \frac{1}{\pi}\left(\frac{a}{R}\right)^3 \int_0^\infty \frac{s^2 K_1}{I_1} \cos(\sigma s)\, \mathrm{d}s \,, \tag{4.5}$$

that is positively defined for all values of σ. Therefore, the two particle have always the same sense of rotation around the cylinder axis, in the same way as in an unbounded flow.

4.2 Radial rotational mobility

We compute the particle self-mobility correction for the asymmetric rotation around an axis perpendicular to the cylinder axis which for a point particle situated on the cylinder axis is

$$\Delta\mu_{\perp}^{\mathrm{S}} = L_r^{-1} \lim_{\boldsymbol{r}\to 0} \Omega_r^* = L_\phi^{-1} \lim_{\boldsymbol{r}\to 0} \Omega_\phi^* \,, \tag{4.6a}$$

where $L_r = L_x \cos\phi$ and $L_\phi = -L_x \sin\phi$ and

$$\Omega_r^* = \frac{1}{2}\left(\frac{v_{z,\phi}^*}{r} - v_{\phi,z}^*\right), \qquad \Omega_\phi^* = \frac{1}{2}(v_{r,z}^* - v_{z,r}^*) \,,$$

are the corrections to the radial and azimuthal fluid angular velocity, respectively. By making use of Eqs. (3.34b) and (3.34c) we get

$$\frac{\Delta\mu_{\perp}^{\mathrm{S}}}{\mu_0^{rr}} = \frac{1}{2\pi}\left(\frac{a}{R}\right)^3 \int_0^\infty (\gamma^* + 2\varphi^*)\, s^2\, \mathrm{d}s \,.$$

Considering a membrane with both shearing and bending, and by taking the vanishing frequency limit we obtain

$$\lim_{\alpha\to\infty} \frac{\Delta\mu_{\perp}^{\mathrm{S}}}{\mu_0^{rr}} = -\frac{1}{2\pi}\left(\frac{a}{R}\right)^3 \int_0^\infty \frac{w}{W}\, \mathrm{d}s \approx -0.73555 \left(\frac{a}{R}\right)^3 , \tag{4.7}$$

in agreement with the literature [24, 81]. Moreover,

$$w = s^2\big(2I_0I_1(sK_0 - 3K_1) + sI_0^2(sK_0 + 3K_1) - I_1^2\left((s^2+8)K_0 + sK_1\right)\big)\,, \tag{4.8a}$$
$$W = sI_1^3 - (s^2+2)I_0I_1^2 - sI_0^2I_1 + s^2I_0^3\,. \tag{4.8b}$$

The same limit is obtained when considering a membrane with pure shearing. Another limit is recovered if the membrane possesses only a resistance towards bending such that

$$\lim_{\alpha\to\infty}\frac{\Delta\mu^{\mathrm{S}}_{\perp,\mathrm{B}}}{\mu_0^{rr}} = -\frac{1}{\pi}\left(\frac{a}{R}\right)^3\int_0^\infty \frac{w_{\mathrm{B}}}{W_{\mathrm{B}}}\,\mathrm{d}s \approx -0.24688\left(\frac{a}{R}\right)^3\,, \tag{4.9}$$

where we have defined

$$w_{\mathrm{B}} = s^4K_0^2\,,$$
$$W_{\mathrm{B}} = sI_0\left((3+s^2)K_1 + 2sK_0\right) - (3+s^2)(sK_0 + 2K_1)I_1\,.$$

Next, we turn our attention to the rotational pair-mobility perpendicular to the line of centers. At leading order we have

$$\mu_\perp^{\mathrm{P}} = L_r^{-1}\lim_{\boldsymbol{r}\to\boldsymbol{r}_\lambda}\Omega_{1r} = L_\phi^{-1}\lim_{\boldsymbol{r}\to\boldsymbol{r}_\lambda}\Omega_{1\phi}\,. \tag{4.10}$$

In a scaled form we obtain

$$\frac{\mu_\perp^{\mathrm{P}}}{\mu_0^{rr}} = -\frac{1}{2}\left(\frac{a}{h}\right)^3 + \frac{1}{2\pi}\left(\frac{a}{R}\right)^3\int_0^\infty(\gamma^* + 2\varphi^*)\,s^2\cos(\sigma s)\,\mathrm{d}s\,, \tag{4.11}$$

which in the vanishing frequency limit reduces to

$$\lim_{\alpha\to\infty}\frac{\mu_\perp^{\mathrm{P}}}{\mu_0^{rr}} = -\frac{1}{2}\left(\frac{a}{h}\right)^3 - \frac{1}{2\pi}\left(\frac{a}{R}\right)^3\int_0^\infty\frac{w}{W}\cos(\sigma s)\,\mathrm{d}s\,, \tag{4.12}$$

with w and W given above by Eqs (4.8). It can be shown that upon integration, the second term in the latter equation is negatively valued for all value of σ. Therefore, the two particles undergo rotation in opposite directions for all values of σ, i.e. in the same way as in a bulk fluid.

4.3 Startup rotational motion

We now compute the mobility coefficients for a particle starting from rest and then rotating under a constant external torque (e.g. a magnetic or optical torque) exerted either in the direction parallel or perpendicular to the cylinder axis. The steady torque is mathematically modeled by a Heaviside step function $\boldsymbol{L}(t) = \boldsymbol{A}\,\theta(t)$ whose Fourier transform in the frequency domain reads [87]

$$\boldsymbol{L}(\omega) = \left(\pi\delta(\omega) - \frac{i}{\omega}\right)\boldsymbol{A}\,. \tag{4.13}$$

The components of the time-dependent angular velocity can readily be obtained upon inverse Fourier transformation to obtain

$$\frac{\omega_k(t)}{\mu_0^{rr}A_k} = 1 + \frac{\Delta\mu^{\mathrm{S}}_{kk}(0)}{2} + \frac{1}{2i\pi}\int_{-\infty}^{+\infty}\frac{\Delta\mu^{\mathrm{S}}_{kk}(\omega)}{\omega}\,e^{i\omega t}\,\mathrm{d}\omega\,, \qquad k\in\{r,\phi,z\}\,. \tag{4.14}$$

We note that the third term in Eq. (4.14) is a real quantity which takes values between $-\Delta\mu^{\mathrm{S}}_{kk}(0)/2$ when $t\to 0$ and $+\Delta\mu^{\mathrm{S}}_{kk}(0)/2$ as $t\to\infty$, corresponding to the bulk and hard-wall behaviors, respec-

tively. As the frequency-dependent mobilities are expressed as integrals over the scaled wavenumber s, the computation of the time-dependent angular velocities requires a double integration procedure. For this aim, we use the Cuba Divonne algorithm [88, 89] which is found to be suitable for the numerical computation of the present double integrals.

4.4 Membrane deformation

Finally, our results can be employed to compute the membrane deformation resulting from an arbitrary time-dependent point-torque acting parallel or perpendicular to the cylinder axis. The membrane displacement field can readily be computed from the fluid velocity at $r = R$ via the non-slip relation stated by Eq. (3.17). We define the membrane frequency-dependent reaction tensor in the same way as previously defined for a point-force as [62, 90]

$$u_i(z, \phi, \omega) = Q_{ij}(z, \phi, \omega) L_j(\omega)\,, \tag{4.15}$$

relating between the membrane displacement field $\boldsymbol{u}$ and the torque $\boldsymbol{L}$ acting on the nearby particle. Considering a harmonic-type driving torque $L_i(t) = A_i e^{i\omega_0 t}$, the membrane deformation in the time domain is calculated as

$$u_i(z, \phi, t) = Q_{ij}(z, \phi, \omega_0) A_j e^{i\omega_0 t}\,. \tag{4.16}$$

The physical displacement is then obtained by taking the real part of the latter equation. From Eqs. (3.23b) and (3.28), we obtain

$$Q_{\phi z} = \Lambda \int_0^\infty \frac{2sK_1(I_0K_1 + I_1K_0)}{(2K_0 - i\alpha s K_1)I_1 + 2I_0K_1} \cos\left(\frac{sz}{R}\right) \mathrm{d}s\,,$$

wherein $\Lambda := 1/(4i\pi^2\eta\omega R^2)$, giving access to the membrane azimuthal deformation when an axial torque is exerted on the particle. We further have $Q_{rz} = Q_{zz} = 0$ due to symmetry.

Next, considering a torque acing along an axis perpendicular to the cylinder axis, we obtain

$$\begin{aligned}
Q_{r\phi} &= -\Lambda \int_0^\infty \Big(\left((2+s^2)K_1 + sK_0\right)\varphi_2 - \left(sK_0 + K_1\right)\psi^* - K_1\,\gamma^* \Big) \sin\left(\frac{sz}{R}\right) \mathrm{d}s\,,\\
Q_{\phi r} &= \Lambda \int_0^\infty \Big(-\left(sK_0 + 2K_1\right)\varphi_2 + K_1\psi^* + \left(K_1 + sK_0\right)\gamma^* \Big) \sin\left(\frac{sz}{R}\right) \mathrm{d}s\,,\\
Q_{z\phi} &= -\Lambda \int_0^\infty s\left(-sK_0\varphi_2 + K_1\psi^*\right) \cos\left(\frac{sz}{R}\right) \mathrm{d}s\,,
\end{aligned}$$

and $Q_{rr} = Q_{\phi\phi} = Q_{zr} = 0$.

5 Comparison with numerical simulations

In order to assess the validity and appropriateness of the point particle approximation employed throughout this work, we compare our analytical predictions with computer simulations performed using a completed double layer boundary integral equation method [91–95]. The method is known to be ideally suited for simulation of fluid flows in the Stokes regime [96] where both solid objects and deformed boundaries are present. Technical details regarding the method and its numerical implementation have been reported by some of us elsewhere, see e.g. Refs. [62, 97].

In the simulations, the cylindrical membrane is of length $200a$ uniformly meshed with 6550 triangles. The spherical particle is discretized by 320 triangular elements obtained by refining an icosahedron consecutively [98, 99].

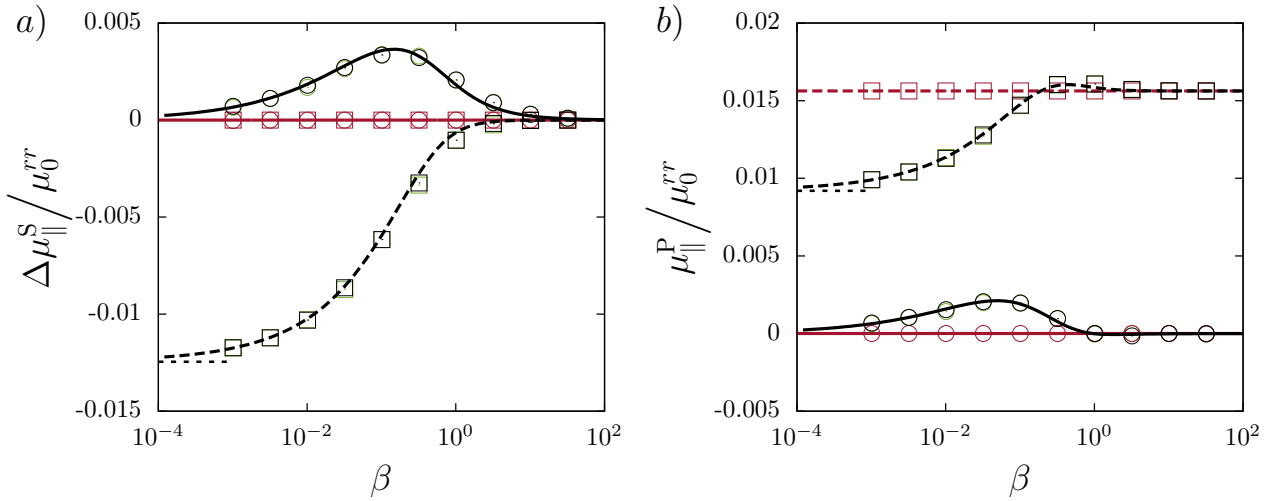

Figure 2: (Color online) The scaled frequency dependent self- (a) and pair- (b) mobilities versus the scaled frequency β for the rotational motion around the cylinder axis. The membrane is endowed with only-shearing (green), only-bending (red) or both shearing and bending rigidities (black). Green lines/symbols are hardly visible as they overlap with the black lines/symbols. Here the particle is set on the centerline of an elastic cylindrical membrane of radius $R = 4a$. For the pair-mobility, the interparticle distance is set $h = R$. The analytical predictions are shown as dashed and solid lines for the real and imaginary parts, respectively. BIM simulations are presented as squares and circles for the real and imaginary parts, respectively. The horizontal dashed lines represent the hard-cylinder limits predicted by Eq. (4.3) and (4.5) for the self- and pair-mobilities respectively. For other parameters, see main text.

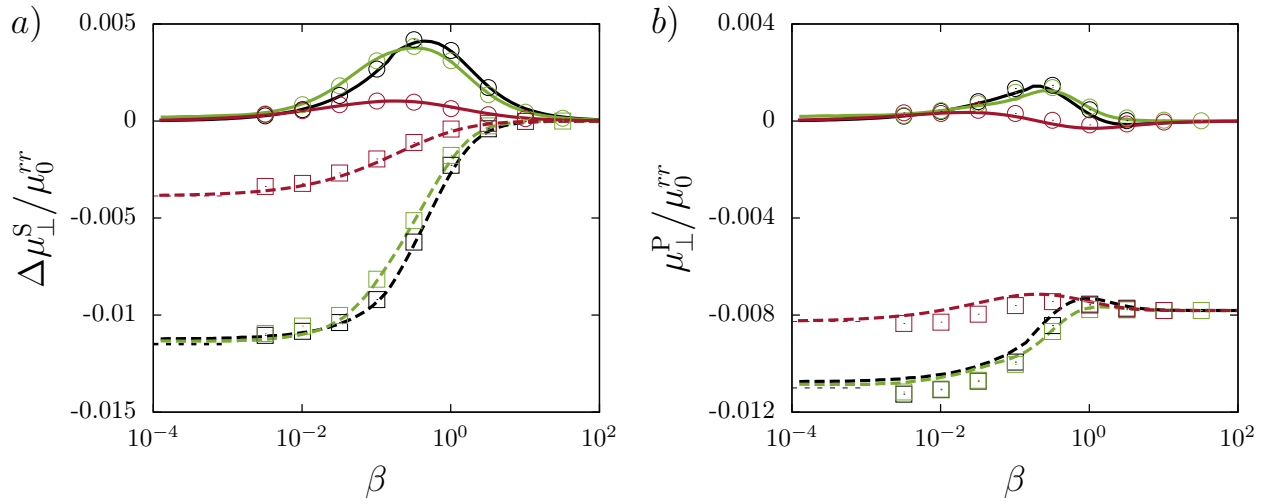

Figure 3: (Color online) The scaled frequency dependent self- (a) and pair- (b) mobilities versus the scaled frequency β for the rotational motion around an axis perpendicular to the cylinder axis. The color code is the same as in Fig. 2.

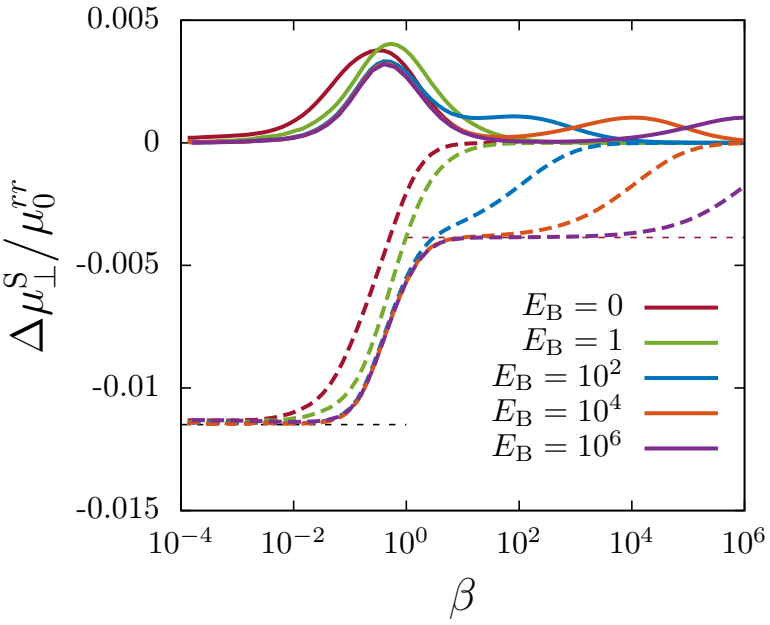

Figure 4: (Color online) Scaled particle self-mobility corrections versus β for various values of the reduced bending modulus E_B for the rotational motion around an axis perpendicular to the cylinder axis. Here we take $R = 4a$ and $C = 1$.

In order to compute numerically the particle rotational self- and pair-mobility functions, a time dependent harmonic torque $L_{\lambda i}(t) = A_{\lambda i} e^{i\omega_0 t}$ of amplitude $A_{\lambda i}$ and frequency ω_0 is exerted along the direction i at the particle labeled λ either parallel (z direction) or perpendicular (x direction) to the cylinder axis. After a short transient evolution, both particles undergo oscillatory rotation with the same frequency ω_0 but with different phases, such that $\Omega_{\lambda i} = B_{\lambda i} e^{i\omega_0 t + \delta_\lambda}$ and $\Omega_{\gamma i} = B_{\gamma i} e^{i\omega_0 t + \delta_\gamma}$. For an accurate determination of the angular velocity amplitudes and phase shifts, we use a nonlinear least-squares solver based on the trust region method [100]. The particle rotational self- and pair-mobilities are then computed as

$$\mu^{S}_{ij} = \frac{B_{\lambda i}}{A_{\lambda j}} e^{i\delta_\lambda}, \qquad \mu^{P}_{ij} = \frac{B_{\gamma i}}{A_{\lambda j}} e^{i\delta_\gamma}. \tag{5.1}$$

We then define the characteristic frequency associated to shearing as $\beta := 1/\alpha = 3\eta\omega R/(2\kappa_S)$, and for bending as $\beta_B := 1/\alpha_B^3 = \eta\omega R^3/\kappa_B$. Additionally, we define the reduced bending modulus $E_B := \kappa_B/(\kappa_S R^2)$ a parameter quantifying the relative effect between membrane shearing and bending.

As an example setup, we place a spherical particle on the centerline of an elastic cylinder of initial (undeformed) radius $R = 4a$. We mostly take a reduced bending modulus $E_B = 1/6$ for which the characteristic frequencies associated to shearing and bending have about the same order of magnitude, and thus both effects manifest themselves equally.

Fig. 2 *a*) shows the parallel component of the correction to the rotational self-mobility function upon variation of the forcing frequency β. For a membrane with bending-only resistance (shown in red), both the real and imaginary parts of the mobility correction vanish, in agreement with our theoretical prediction stated by Eq. (4.2). Not surprisingly, the torque exerted on the particle along the cylinder axis induces only membrane torsion and therefore the resulting stresses do not cause any out-of-plane deformation or bending. For a membrane with a non-vanishing shearing resistance,

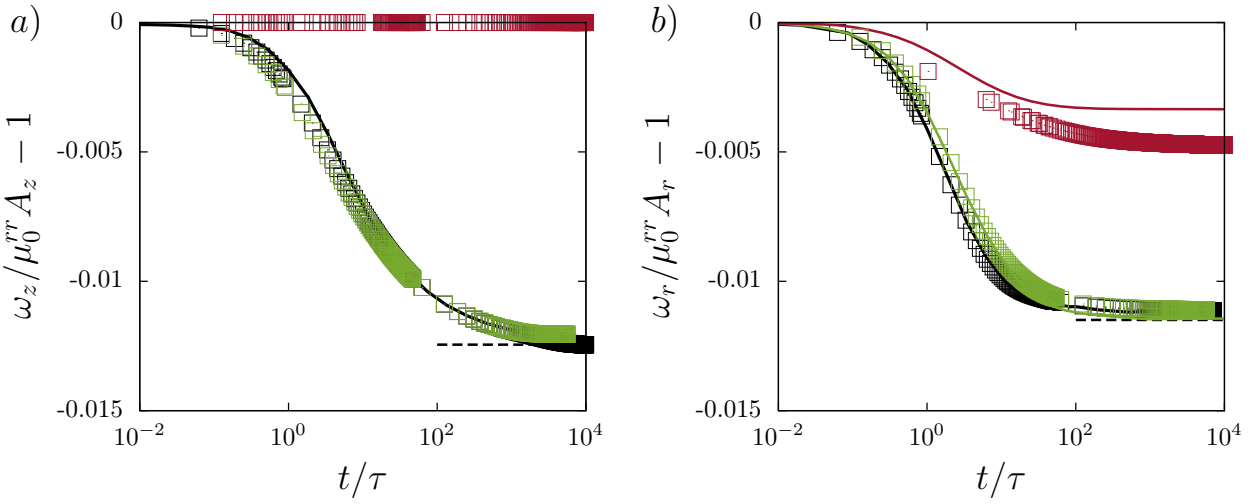

Figure 5: (Color online) Time-dependent angular velocity of a particle starting from rest for *a*) axial and *b*) radial rotational motion under the action of a constant external torque. Here we use the same parameters as in Fig. 2 with a membrane with both shearing and bending rigidities. Solid lines are the analytical predictions obtained from Eq. (4.14) whereas symbols are the boundary integral simulations results. Black dashed lines are our theoretical predictions based on the point particle approximation. Here τ is a characteristic time scale defined as $\tau := \beta/\omega$.

however, we observe that the mobility correction exhibits a monotonically increasing real part and the typical peak structure for the imaginary part. In the vanishing frequency limit, the correction to rotational mobility is identical to that predicted nearby a hard-cylinder with stick boundary conditions, given by Eq. (4.3). Moreover, the bulk behavior is recovered for large forcing frequencies where both the real and imaginary parts vanish.

In Fig. 2 *b*) we present the rotational pair-mobility function for two particles located on the cylinder centerline a distance $h = R$ apart. Similarly, a membrane with pure bending resistance does not introduce a correction to the particle pair-mobility. Yet, the latter is markedly affected by the membrane shearing resistance where the correction approaches that near a hard-cylinder in the low frequency regime. For high forcing frequencies, the pair mobility equals that of two equal-sized spheres in an unbounded medium, given at leading order by $(a/h)^3$. A good agreement is obtained between theoretical predictions and the numerical simulations we performed using a completed double layer boundary integral method.

We now carry out for the rotation about an axis perpendicular to the cylinder axis. In Fig. 3, we show the perpendicular component of the particle rotational self- and pair-mobilities nearby a membrane endowed with shearing-only (green), bending-only (red) or both shearing and bending rigidities (black). The mobility functions show basically a similar evolution as in the previous case of axisymmetric rotation around the cylinder axis. As explained before, we observe that the mobility near a no-slip cylinder is recovered only if the membrane possesses a non-vanishing shearing resistance. The pair-mobility in the high frequency regime can appropriately be estimated from the leading order bulk pair-mobility $-(1/2)(a/h)^3$.

In order to probe the effect of the aforementioned coupling between shear and bending, we show in Fig. 4 the particle self-mobility function versus β for the rotational motion perpendicular to the cylinder axis upon variation of the reduced bending modulus E_B while keeping $R = 4a$. We observe that as E_B increases, a second peak of lower amplitude emerges for higher forcing frequencies in the imaginary part. Additionally, a dispersion step in the real part occurs that bridges between the

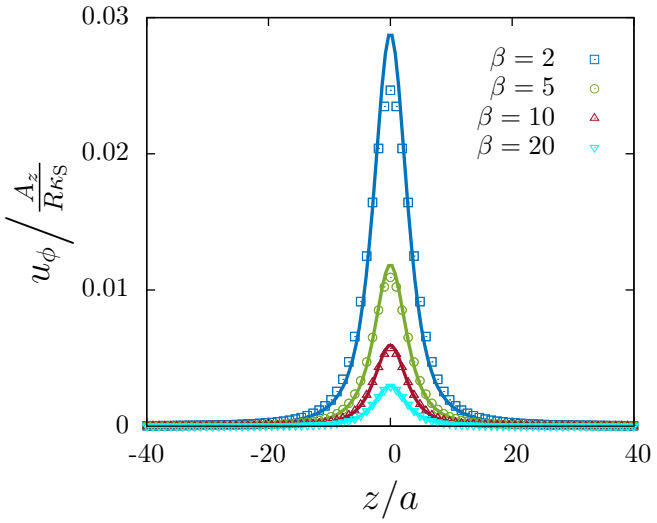

Figure 6: (Color online) The scaled azimuthal membrane displacements versus z/a at four forcing frequencies computed at quarter oscillation period for $t\omega_0 = \pi/2$. Solid lines are the analytical predictions and symbols refer to boundary integral simulations.

hard-cylinder limit Eq. (4.7) and the bending limit predicted by Eq. (4.9). In fact, the peak observed at $\beta \sim 1$ is attributed to the membrane resistance towards shear and can conveniently be estimated by a simple balance between fluid viscosity and membrane elasticity as $\omega \sim \kappa_S/(\eta R)$. The high-frequency peak is however attributed to the membrane resistance towards bending and its position can properly be estimated by a balance between fluid viscosity and bending such that $\omega \sim \kappa_B/(\eta R^3)$ corresponding to $\beta_B \sim 1$. Since $\beta_B = 2\beta/(3E_B)$, the second peak occurs at $\beta \sim E_B$. Particularly, for $E_B = 1$, the shear and bending related peaks coincide for which both effects manifest themselves equally. Analogous predictions can be made for the pair-mobility where similar conclusions can be drawn.

In Fig. 5, we show the time-dependent angular velocity of a particle initially at rest, rotating under the action of a constant external torque. We scale the time by the characteristic time scale for shearing defined as $\tau := \beta/\omega = 3\eta R/(2\kappa_S)$. At short time scales for which $t \ll \tau$, the membrane introduces a small correction to the particle mobility since it does not have enough time to react on these short time scales. As the time increases, the membrane effect becomes more important and the mobility curves bend down substantially to asymptotically approach the correction predicted nearby a hard cylinder. The steady rotational mobilities undergo small corrections relative to the bulk values, making them more difficult to obtain precisely from the simulations. This explains the small discrepancy between theory and simulations, notably for a membrane with pure bending resistance.

The membrane displacement induced by the symmetric rotation of the particle around the cylinder axis is shown in Fig. 6 where both analytical predictions (solid lines) and numerical simulations (symbols) are presented. Here we use the same parameters as in Fig. 2 and four different actuation frequencies. Displacement fields are plotted when the oscillating particle reaches its maximal angular position. We observe that the membrane azimuthal deformation exhibits a bell-shaped behavior that peaks at the origin where deformation is more pronounced. By comparing the membrane displacement field at various forcing frequencies, we observe that as the forcing frequency gets larger, the membrane undergoes remarkably smaller deformation since the membrane does not have sufficient time to respond to the fast rotating particle.

Analogous predictions for asymmetric deformation induced by the particle radial rotation are

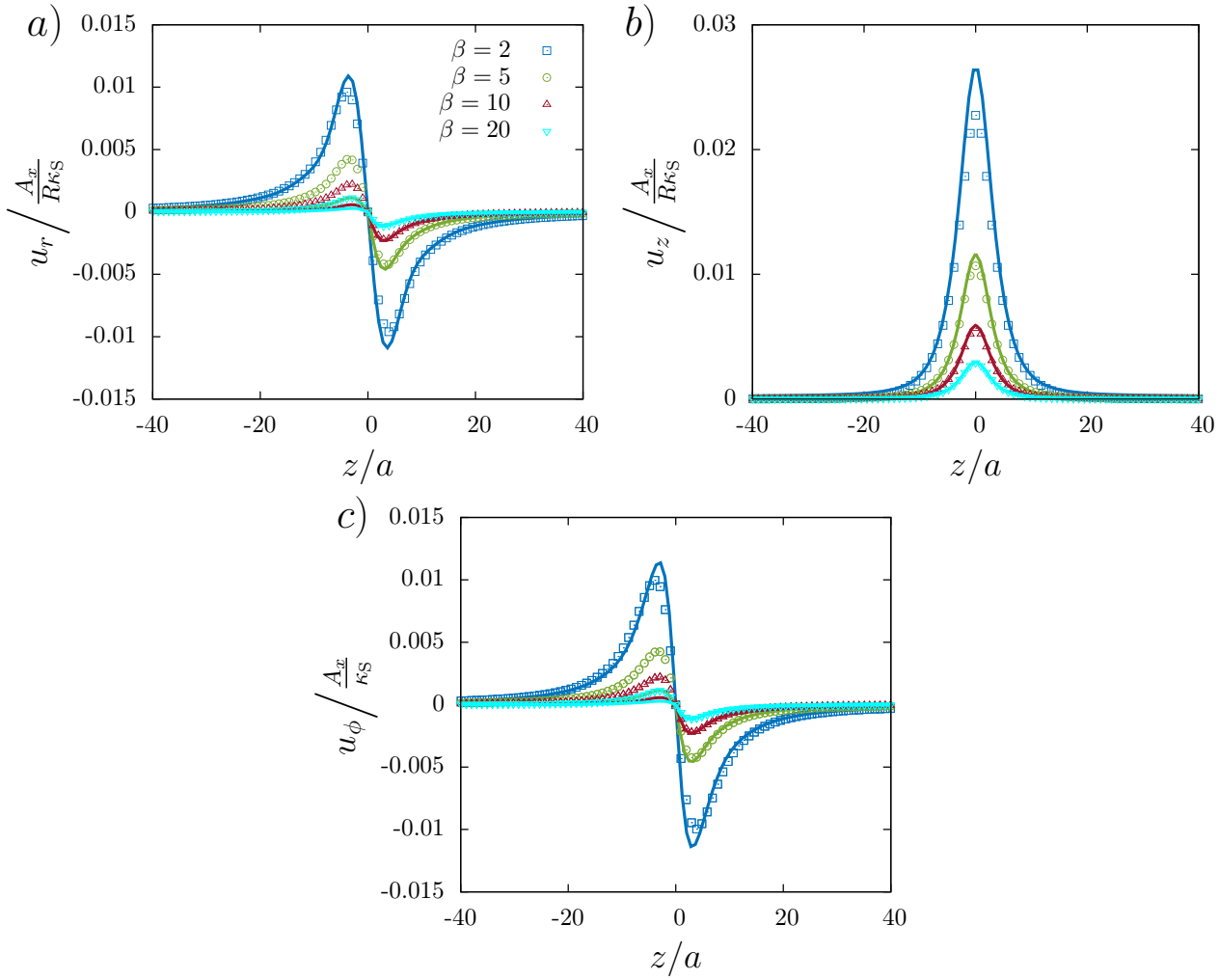

Figure 7: (Color online) The scaled radial a), axial b) and azimuthal c) membrane displacement field versus scaled distance along the axis z/a for four forcing frequencies calculated at quarter period for $\omega_0 t = \pi/2$ when the particle reaches its maximal radial position. Here deformations are shown in the plane of maximum deformation. Solid lines are the theoretical predictions and symbols refer to the boundary integral simulation results.

shown in Fig. 7. Here deformations are shown in the plan of maximum deformation, i.e. $\phi = 0$ for u_ϕ, and $\phi = \pi/2$ for u_r and u_z. The radial and azimuthal deformations have fundamentally the same evolution where both have symmetry with respect to the origin at which the deformation vanishes. On the other hand, axial deformation reaches its maximal value at the origin and decays far away as the ratio z/a gets larger. It can clearly be seen that upon particle radial rotation, the membrane undergoes primarily axial deformation with a maximum that is about three times larger than that reached in the radial or azimuthal deformations.

For typical flow parameters, the torques exerted by optical tweezers on suspended nanoparticles are of the order of 1 pN μm [101]. Assuming a cylinder radius of 10^{-6} m, a membrane shearing modulus of about 10^{-6} N/m and an actuation frequency $\beta = 2$, the membrane undergoes a maximal deformation of about 3 % of its undeformed radius. Therefore, deformations upon particle rotational motion are small and deviations from cylindrical shape are negligible.

6 Conclusions

In this contribution we have presented analytical calculations of the Stokes flow induced by a point-torque exerted parallel or perpendicular to the axis of an elastic circular tube. The membrane is modeled by a combination of the neo-Hookean model for shearing and Helfrich model for bending. The solution of the fluid flow is expressed in terms of Fourier-Bessel integrals with unknown coefficients which are determined from the boundary conditions imposed at the membrane.

The result is the Green's function for two orientations of the rotlet singularity. In the limit when shearing and bending coefficients are large, corresponding to a stiff membrane, our results converge to the expressions previously derived in literature for a hard cylindrical no-slip tube.

Our results are directly applicable to the determination of the leading-order correction to the self- and pair-mobility functions of particles rotating parallel or perpendicular to the cylinder axis. Notably, the correction to self mobility follows a cubic dependence on the ratio of particle to cylinder radius. We also find that the rotational mobilities along the axis depend solely on membrane shearing resistance and that bending does not play any role. Both shearing and bending however manifest themselves for the rotational motion along an axis perpendicular to the cylinder axis. More importantly, the steady particle mobility nearby a hard-cylinder with stick boundary conditions is recovered only if the membrane possesses a non-vanishing resistance towards shearing. As an example, we have calculated the effects of startup motion, i.e. particle initially at rest starting to rotate under a steady torque. The Green's function can also be applied to the calculation of the resulting membrane deformation. For realistic values of parameters, however, this turns out to be negligible.

Our analytical predictions are verified and supplemented by corresponding boundary integral simulations where a good agreement is obtained.

acknowledgements

ADMI and SG thank the Volkswagen Foundation for financial support and acknowledge the Gauss Center for Supercomputing e.V. for providing computing time on the GCS Supercomputer SuperMUC at Leibniz Supercomputing Center. Additionally, they thank Achim Guckenberger for fruitful discussions. This work has been supported by the Ministry of Science and Higher Education of Poland via the Mobility Plus Fellowship awarded to ML. This article is based upon work from COST Action MP1305, supported by COST (European Cooperation in Science and Technology).

Appendix

A Membrane mechanics

In this Appendix, the traction jump across a membrane endowed with shearing and bending rigidities will be derived in the cylindrical coordinates system. We denote by $\boldsymbol{a} = R\boldsymbol{e}_r + z\boldsymbol{e}_z$ the position vector of the points located at the undeformed membrane. Here R is the membrane (undeformed) radius and z is the axial distance along the cylinder axis. Here r, ϕ and z refer to the radial, azimuthal and vertical coordinates, respectively. After deformation, the vector position reads

$$\boldsymbol{r} = (R + u_r)\boldsymbol{e}_r + u_\phi \boldsymbol{e}_\phi + (z + u_z)\boldsymbol{e}_z \,, \tag{A.1}$$

where $\boldsymbol{u}$ denotes the displacement vector field, which depends on the in-plane variables ϕ and z. In the following, we shall use capital Roman letters for the undeformed state and small roman letters for the deformed. The cylindrical membrane is defined by the covariant base vectors $\boldsymbol{g}_1 := \boldsymbol{r}_{,\phi}$ and

$\boldsymbol{g}_2 := \boldsymbol{r}_{,z}$, which read

$$\boldsymbol{g}_1 = (u_{r,\phi} - u_\phi)\boldsymbol{e}_r + (R + u_r + u_{\phi,\phi})\boldsymbol{e}_\phi + u_{z,\phi}\boldsymbol{e}_z \,, \tag{A.2}$$
$$\boldsymbol{g}_2 = u_{r,z}\boldsymbol{e}_r + u_{\phi,z}\boldsymbol{e}_\phi + (1 + u_{z,z})\boldsymbol{e}_z \,. \tag{A.3}$$

The unit normal vector $\boldsymbol{n}$ is defined as

$$\boldsymbol{n} = \frac{\boldsymbol{g}_1 \times \boldsymbol{g}_2}{|\boldsymbol{g}_1 \times \boldsymbol{g}_2|} \,, \tag{A.4}$$

which, at leading order in deformation reads

$$\boldsymbol{n} = \boldsymbol{e}_r + \frac{u_\phi - u_{r,\phi}}{R}\boldsymbol{e}_\phi - u_{r,z}\boldsymbol{e}_z \,. \tag{A.5}$$

The covariant components of the first fundamental form (metric tensor) are defined by the scalar product $g_{ij} = \boldsymbol{g}_i \cdot \boldsymbol{g}_j$. Upon linearization, we obtain

$$g_{ij} = \begin{pmatrix} R^2 + 2R(u_r + u_{\phi,\phi}) & u_{z,\phi} + Ru_{\phi,z} \\ u_{z,\phi} + Ru_{\phi,z} & 1 + 2u_{z,z} \end{pmatrix} . \tag{A.6}$$

The contravariant tensor g^{ij} is the inverse of the metric tensor [102], and at leading order reads

$$g^{ij} = \begin{pmatrix} \frac{1}{R^2} - 2\frac{u_r + u_{\phi,\phi}}{R^3} & -\frac{u_{z,\phi} + Ru_{\phi,z}}{R^2} \\ -\frac{u_{z,\phi} + Ru_{\phi,z}}{R^2} & 1 - 2u_{z,z} \end{pmatrix} . \tag{A.7}$$

The covariant and contravariant tensors in the undeformed state G_{ij} and G^{ij} can immediately be obtained by considering a vanishing displacement in Eqs. (A.6) and (A.7), respectively. In the following, the traction jump equations across a cylindrical membrane endowed by an in-plane shearing resistance shall be derived.

A.1 Shearing

The two transformation invariants are given by Green and Adkins as [103, 104]

$$I_1 = G^{ij}g_{ij} - 2 \,, \tag{A.8a}$$
$$I_2 = \det G^{ij} \det g_{ij} - 1 \,. \tag{A.8b}$$

The contravariant components of the stress tensor τ^{ij} can readily be obtained from the membrane constitutive relation such that [52]

$$\tau^{ij} = \frac{2}{J_\mathrm{S}}\frac{\partial W}{\partial I_1}G^{ij} + 2J_\mathrm{S}\frac{\partial W}{\partial I_2}g^{ij} \,, \tag{A.9}$$

where $W(I_1, I_2)$ is the areal strain energy density and $J_\mathrm{S} := \sqrt{1 + I_2}$ is the Jacobian determinant, representing the ratio between the deformed and undeformed local surface area. In the linear theory of elasticity, $J_\mathrm{S} \simeq 1 + e$, where $e := (u_r + u_{\phi,\phi})/R + u_{z,z}$ is the dilatation function. In the present work, we use the neo-Hookean model to describe the elastic properties of the membrane, whose areal strain energy reads [105, 106]

$$W(I_1, I_2) = \frac{\kappa_\mathrm{S}}{6}\left(I_1 - 1 + \frac{1}{1 + I_2}\right) . \tag{A.10}$$

Plugging Eq. (A.10) into Eq. (A.9), the linearized in-plane stress tensor reads

$$\tau^{ij} = \frac{2\kappa_S}{3}\begin{pmatrix} \frac{u_r+u_{\phi,\phi}}{R^3}+\frac{e}{R^2} & \frac{1}{2R}\left(u_{\phi,z}+\frac{u_{z,\phi}}{R}\right) \\ \frac{1}{2R}\left(u_{\phi,z}+\frac{u_{z,\phi}}{R}\right) & u_{z,z}+e \end{pmatrix}. \tag{A.11}$$

The membrane elastic forces are balanced by the external forces via the equilibrium equations

$$\nabla_i \tau^{ij} + \Delta f^j = 0\,, \tag{A.12a}$$
$$\tau^{ij} b_{ij} + \Delta f^n = 0\,, \tag{A.12b}$$

where $\Delta \boldsymbol{f} = \Delta f^j \boldsymbol{g}_j + \Delta f^n \boldsymbol{n}$ is the traction jump vector across the membrane. Here ∇_i stands for the covariant derivative [107] and b_{ij} is the second fundamental form (curvature tensor) defined by the dot product $b_{ij} = \boldsymbol{g}_{i,j} \cdot \boldsymbol{n}$. At leading order we obtain

$$b_{ij} = \begin{pmatrix} u_{r,\phi\phi} - (R + u_r + 2u_{\phi,\phi}) & u_{r,\phi z} - u_{\phi,z} \\ u_{r,\theta z} - u_{\phi,z} & u_{r,zz} \end{pmatrix}. \tag{A.13}$$

After some algebra, the traction jump equations across the membrane given by Eqs. (A.12) read

$$\frac{\kappa_S}{3}\left(u_{\phi,zz} + \frac{3u_{z,\phi z}}{R} + \frac{4(u_{r,\phi}+u_{\phi,\phi\phi})}{R^2}\right) + \Delta f_\phi = 0\,, \tag{A.14a}$$
$$\frac{\kappa_S}{3}\left(4u_{z,zz} + \frac{2u_{r,z}+3u_{\phi,z\phi}}{R} + \frac{u_{z,\phi\phi}}{R^2}\right) + \Delta f_z = 0\,, \tag{A.14b}$$
$$-\frac{2\kappa_S}{3}\left(\frac{2(u_r+u_{\phi,\phi})}{R^2} + \frac{u_{z,z}}{R}\right) + \Delta f_r = 0\,. \tag{A.14c}$$

Continuing, the jump in the fluid stress tensor across the membrane reads

$$[\sigma_{jr}] = \Delta f_j\,, \quad j \in \{z, r\}\,. \tag{A.15}$$

Therefore, From Eqs. (A.14), (A.15) and (3.17), it follows that

$$[v_{\phi,r}] = \frac{i\alpha}{2}\left(Rv_{\phi,zz} + 3v_{z,\phi z} + \frac{4(v_{r,\phi}+v_{\phi,\phi\phi})}{R}\right)\bigg|_{r=R}, \tag{A.16a}$$
$$[v_{z,r}] = \frac{i\alpha}{2}\left(4Rv_{z,zz} + 2v_{r,z} + 3v_{\phi,z\phi} + \frac{v_{z,\phi\phi}}{R}\right)\bigg|_{r=R}, \tag{A.16b}$$
$$\left[-\frac{p}{\eta}\right] = -i\alpha\left(\frac{2(v_r+v_{\phi,\phi})}{R} + v_{z,z}\right)\bigg|_{r=R}, \tag{A.16c}$$

where $\alpha := 2\kappa_S/(3\eta R\omega)$ is the shearing coefficient. Note that it follows from the incompressibility equation

$$\frac{v_r + v_{\phi,\phi}}{r} + v_{r,r} + v_{z,z} = 0\,, \tag{A.17}$$

that $[v_{r,r}] = 0$. In the following, we shall derive the traction jump equations across a membrane with pure bending rigidity.

A.2 Bending

We use the Helfrich model, in which the traction jump equations across the membranes are given by [56, 59]

$$\Delta \boldsymbol{f} = -2\kappa_{\mathrm{B}} \left(2(H^2 - K + H_0 H) + \Delta_{\parallel}\right)(H - H_0)\,\boldsymbol{n}\,, \tag{A.18}$$

where κ_{B} is the bending modulus, H and K are respectively the mean and Gaussian curvatures, given by

$$H = \frac{1}{2}\, b^i_i\,, \qquad K = \det\, b^j_i\,, \tag{A.19}$$

with b^j_i being the mixed version of the curvature tensor related to the covariant representation of the curvature tensor by $b^j_i = b_{ik} g^{kj}$. Continuing, $\Delta_{\parallel}$ is the Laplace-Beltrami operator and H_0 is the spontaneous curvature, for which we take the initial undisturbed shape here. The linearized traction jump due to bending are therefore given by

$$-\kappa_{\mathrm{B}}\Big(R^3 u_{r,zzzz} + 2R(u_{r,zz} + u_{r,zz\phi\phi}) + \frac{u_r + 2u_{r,\phi\phi} + u_{r,\phi\phi\phi\phi}}{R}\Big) + \Delta f_r = 0\,. \tag{A.20}$$

and $\Delta f_\phi = \Delta f_z = 0$.

Note that bending does not introduce at leading order a jump in the tangential traction [56]. The traction jump equations take the following final from

$$[v_{\phi,r}] = 0\,, \tag{A.21a}$$

$$[v_{z,r}] = 0\,, \tag{A.21b}$$

$$\left[-\frac{p}{\eta}\right] = -i\alpha_{\mathrm{B}}^3\Big(R^3 v_{r,zzzz} + 2R(v_{r,zz} + v_{r,zz\phi\phi}) + \frac{v_r + 2v_{r,\phi\phi} + v_{r,\phi\phi\phi\phi}}{R}\Big)\Big|_{r=R}\,, \tag{A.21c}$$

where $\alpha_{\mathrm{B}} = (\kappa_{\mathrm{B}}/(\eta\omega))^{1/3}/R$ is the bending coefficient.

Bibliography

[1] K. Sharp, R. Fine, K. Schulten, and B. Honig, J. Phys. Chem **91**, 3624 (1987).

[2] J. P. Hernandez-Ortiz, C. G. Stoltz, and M. D. Graham, Phys. Rev. Lett. **95**, 204501 (2005).

[3] J. Happel and H. Brenner, *Low Reynolds number hydrodynamics: with special applications to particulate media*, Vol. 1 (Springer Science & Business Media, 2012).

[4] B. Cichocki and B. U. Felderhof, J. Chem. Phys. **89**, 1049 (1988).

[5] B. Cichocki, M. L. Ekiel-Jeżewska, and E. Wajnryb, J. Chem. Phys. **111**, 3265 (1999).

[6] M. Długosz and J. M. Antosiewicz, J. Phys. Chem. B **119**, 8425 (2015).

[7] T. M. Squires and S. R. Quake, Rev. Mod. Phys. **77**, 977 (2005).

[8] C. Wang, B. Rallabandi, and S. Hilgenfeldt, Phys. Fluids **25**, 022002 (2013).

[9] A. Frey-Wyssling, ed., *Deformation and flow in biological systems* (North-Holland Publishing Co., Amsterdam, 1952).

[10] R. E. Shadwick, J. Exp. Biol. **202**, 3305 (1999).

[11] C. G. Caro, T. J. Pedley, R. C. Schroter, and W. A. Seed, *The Mechanics of the Circulation*, 2nd ed. (Cambridge University Press, 2011).

[12] H. Faxén, Ann. Phys. **373**, 89 (1922).

[13] S. Wakiya, J. Phys. Soc. Japan **8**, 254 (1953).

[14] H. Faxén, Colloid Polym. Sci. **167**, 146 (1959).

[15] T. Bohlin, Trans. Roy. Inst. Technol. Stockholm **155**, 64 (1960).

[16] T. Greenstein, *Theoretical study of the motion of one or more spheres and a fluid in an infinitely long circular cylinder*, Ph.D. thesis (1967).

[17] T. Greenstein and J. Happel, J. Fluid Mech. **34**, 705 (1968).

[18] O. Sano, J. Phys. Soc. Japan **56**, 2713 (1987).

[19] W. B. Zimmerman, Int. J. Eng. Sci. **42**, 1753 (2004).

[20] S. Leichtberg, R. Pfeffer, and S. Weinbaum, Int. J. Multiph. Flow **3**, 147 (1976).

[21] H. Y. Yeh and H. J. Keh, Eur. J. Mech. B Fluid **39**, 52 (2013).

[22] H. Hasimoto, J. Phys. Soc. Japan **41**, 2143 (1976).

[23] W. L. Haberman, *Flow about a sphere rotating in a viscous liquid inside a coaxially rotating cylinder*, David Taylor model basin report No. 1578. (US Navy Dept., Washington DC, 1961).

[24] H. Brenner and R. M. Sonshine, Quart. J. Mech. Appl. Math. **17**, 55 (1964).

[25] H. Brenner, Appl. Sci. Res., Section A **13**, 81 (1964).

[26] T. Greenstein and T. J. Som, Phys. Fluids **19**, 161 (1976).

[27] T. Greenstein and G. L. Schiavina, Int. J. Multiph. Flow **2**, 353 (1975).

[28] T. Greenstein and J. Happel, Appl. Sci. Res. **22**, 345 (1970).

[29] B. R. Hirschfeld, *A Theoretical Study of the slow asymmetric settling of an arbitrarily-positioned particle in a circular cylinder*, Ph.D. thesis (1972).

[30] B. R. Hirschfeld, H. Brenner, and A. Falade, Physicochem. Hydrodyn. **5**, 99 (1984).

[31] H. Tözeren, J. Appl. Mech. **49**, 279 (1982).

[32] H. Tözeren, Int. J. Num. Meth. Fluids **4**, 159 (1984).

[33] H. Tözeren, J. Fluid Mech. **129**, 77 (1983).

[34] S. B. Chen, Phys. Fluids (1994-present) **25**, 043106 (2013).

[35] M. E. O'Neill, Chem. Eng. Comm. **148**, 161 (1996).

[36] S. I. Rubinow and J. B. Keller, J. Theo. Biol. **35**, 299 (1972).

[37] Y.-C. Fung, *Biomechanics: circulation* (Springer Science & Business Media, 2013).

[38] C. D. Bertram, C. J. Raymond, and K. S. A. Butcher, J. Biomech. Eng. **111**, 185 (1989).

[39] V. Shankar, J. Fluid Mech. **627**, 291 (2009).

[40] V. Shankar, J. Fluid Mech. **659**, 318 (2010).

[41] J. B. Grotberg, Annu. Rev. Biomed. Eng. **3**, 421 (2001).

[42] J. B. Grotberg and O. E. Jensen, Ann. Rev. Fluid Mech. **36**, 121 (2004).

[43] S. Canic, J. Tambaca, G. Guidoboni, A. Mikelic, C. J. Hartley, and D. Rosenstrauch, SIAM J. Appl. Math. **67**, 164 (2006).

[44] H. A. Stone, A. D. Stroock, and A. Ajdari, Annu. Rev. Fluid Mech. **36**, 381 (2004).

[45] D. P. Holmes, B. Tavakol, G. Froehlicher, and H. A. Stone, Soft Matter **9**, 7049 (2013).

[46] S. Nahar, S. A. K. Jeelani, and E. J. Windhab, Chem. Eng. Sci. **75**, 445 (2012).

[47] S. Nahar, S. A. K. Jeelani, and E. J. Windhab, Chem. Eng. Comm. **200**, 820 (2013).

[48] A. Mikelic, G. Guidoboni, and S. Canic, Netw. Heterog. Media **2**, 397 (2007).

[49] A. Marzo, X. Y. Luo, and C. D. Bertram, J. Fluid Struct. **20**, 817 (2005).

[50] S. Ramanujan and C. Pozrikidis, J. Fluid Mech. **361**, 117 (1998).

[51] D. Barthès-Biesel, Curr. Opin. Colloid Interface Sci. **16**, 3 (2011).

[52] E. Lac, D. Barthès-Biesel, N. A. Pelekasis, and J. Tsamopoulos, J. Fluid Mech. **516**, 303 (2004).

[53] D. Barthès-Biesel, Ann. Rev. Fluid Mech. **48**, 25 (2016).

[54] W. Helfrich, Z. Naturf. C. **28**, 693 (1973).

[55] O.-Y. Zhong-Can and W. Helfrich, Phys. Rev. A **39**, 5280 (1989).

[56] A. Guckenberger and S. Gekle, J. Phys. Cond. Mat. **29**, 203001 (2017).

[57] B. U. Felderhof, J. Chem. Phys. **125**, 144718 (2006).

[58] B. U. Felderhof, J. Chem. Phys. **125**, 124904 (2006).

[59] A. Daddi-Moussa-Ider, A. Guckenberger, and S. Gekle, Phys. Rev. E **93**, 012612 (2016).

[60] A. Daddi-Moussa-Ider and S. Gekle, J. Chem. Phys. **145**, 014905 (2016).

[61] A. Daddi-Moussa-Ider, M. Lisicki, and S. Gekle, J. Fluid Mech. **811**, 210 (2017).

[62] A. Daddi-Moussa-Ider, A. Guckenberger, and S. Gekle, Phys. Fluids **28**, 071903 (2016).

[63] A. Daddi-Moussa-Ider and S. Gekle, Phys. Rev. E **95**, 013108 (2017).

[64] A. Daddi-Moussa-Ider, M. Lisicki, and S. Gekle, Phys. Rev. E **95**, 053117 (2017).

[65] J. R. Blake, Math. Proc. Camb. Phil. Soc. **70**, 303 (1971).

[66] K. Sekimoto and L. Leibler, EPL **23**, 113 (1993).

[67] S. J. Weekley, S. L. Waters, and O. E. Jensen, Q. J. Mech. Appl. Math. **59**, 277 (2006).

[68] T. Salez and L. Mahadevan, J. Fluid Mech. **779**, 181 (2015).

[69] B. Saintyves, T. Jules, T. Salez, and L. Mahadevan, Proc. Nat. Acad. Sci. **113**, 5847 (2016).

[70] B. Rallabandi, B. Saintyves, T. Jules, T. Salez, C. Schönecker, L. Mahadevan, and H. A. Stone, arXiv preprint arXiv:1611.03552 (2016).

[71] S. Kim and S. J. Karrila, *Microhydrodynamics: principles and selected applications* (Courier Corporation, 2013).

[72] T. Bickel, Eur. Phys. J. E **20**, 379 (2006).

[73] G. N. Watson, *A treatise on the theory of Bessel functions* (Cambridge university press, 1995).

[74] H. Brenner and J. Happel, J. Fluid Mech. **4**, 195 (1958).

[75] M. Abramowitz and I. A. Stegun, *Handbook of mathematical functions*, Vol. 1 (Dover New York, 1972).

[76] R. Haberman, *Elementary applied partial differential equations*, Vol. 987 (Prentice Hall Englewood Cliffs, NJ, 1983).

[77] P. R. Rao, G. I. Zahalak, and S. P. Sutera, J. Fluid Mech. **270**, 73 (1994).

[78] C. Bächer, L. Schrack, and S. Gekle, Phys. Rev. Fluids **2**, 013102 (2017).

[79] D. J. Bukman, J. H. Yao, and M. Wortis, Phys. Rev. E **54**, 5463 (1996).

[80] Z. Y. Luo, S. Q. Wang, L. He, F. Xu, and B. F. Bai, Soft Matter **9**, 9651 (2013).

[81] G. H. Zheng, R. L. Powell, and P. Stroeve, Ind. Eng. Chem. Res. **31**, 1190 (1992).

[82] W. Wang and K. H. Parker, J. Fluid Mech. **283**, 287 (1995).

[83] C. M. Linton, IMA J. Appl. Math. **55**, 187 (1995).

[84] J. C. Crocker, J. Chem. Phys. **106**, 2837 (1997).

[85] E. R. Dufresne, T. M. Squires, M. P. Brenner, and D. G. Grier, Phys. Rev. Lett. **85**, 3317 (2000).

[86] B. U. Felderhof, Physica A **89**, 373 (1977).

[87] R. Bracewell, *The Fourier Transform and Its Applications* (McGraw-Hill, 1999).

[88] T. Hahn, Comp. Phys. Comm. **168**, 78 (2005).

[89] T. Hahn, Comp. Phys. Comm. **207**, 341 (2016).

[90] T. Bickel, Phys. Rev. E **75**, 041403 (2007).

[91] N. Phan-Thien and D. Tullock, J. Mech. Phys. Solids **41**, 1067 (1993).

[92] N. Phan-Thien and D. Tullock, Compt. Mech. **14**, 370 (1994).

[93] M. Kohr and I. I. Pop, *Viscous incompressible flow for low Reynolds numbers*, Vol. 16 (Wit Pr/Comp. Mech., 2004).

[94] H. Zhao and E. S. G. Shaqfeh, Phys. Rev. E **83**, 061924 (2011).

[95] H. Zhao, E. S. G. Shaqfeh, and V. Narsimhan, Phys. Fluids **24**, 011902 (2012).

[96] C. Pozrikidis, J. Comput. Phys. **169**, 250 (2001).

[97] A. Guckenberger, M. P. Schraml, P. G. Chen, M. Leonetti, and S. Gekle, Comp. Phys. Comm. **207**, 1 (2016).

[98] T. Krüger, F. Varnik, and D. Raabe, Comp. Math. Appl. **61**, 3485 (2011).

[99] T. Krüger, H. Kusumaatmaja, A. Kuzmin, O. Shardt, G. Silva, and E. M. Viggen, *The Lattice Boltzmann Method: Principles and Practice* (Springer, 2016).

[100] A. R. Conn, N. I. M. Gould, and P. L. Toint, *Trust region methods*, Vol. 1 (Siam, 2000).

[101] M. E. J. Friese, H. Rubinsztein-Dunlop, J. Gold, P. Hagberg, and D. Hanstorp, Appl. Phys. Lett. **78**, 547 (2001).

[102] M. Deserno, Chem. Phys. Lipids **185**, 11 (2015).

[103] A. E. Green and J. C. Adkins, *Large Elastic Deformations and Non-linear Continuum Mechanics* (Oxford University Press, 1960).

[104] L. Zhu, *Simulation of individual cells in flow*, Ph.D. thesis (2014).

[105] T. Krüger, *Computer simulation study of collective phenomena in dense suspensions of red blood cells under shear* (Springer Science & Business Media, 2012).

[106] L. Zhu and L. Brandt, J. Fluid Mech. **770**, 374 (2015).

[107] J. L. Synge and A. Schild, *Tensor calculus*, Vol. 5 (Courier Corporation, 1969).

Publication 8

Hydrodynamic mobility of a solid particle nearby a spherical elastic membrane: Axisymmetric motion

A. Daddi-Moussa-Ider and S. Gekle

Phys. Rev. E **95**, 013108 (2017)

DOI: 10.1103/PhysRevE.95.013108

Abstract

We use the image solution technique to compute the leading order frequency-dependent self-mobility function of a small solid particle moving perpendicular to the surface of a spherical capsule whose membrane possesses shearing and bending rigidities. Comparing our results with those obtained earlier for an infinitely extended planar elastic membrane, we find that membrane curvature leads to the appearance of a prominent additional peak in the mobility. This peak is attributed to the fact that the shear resistance of the curved membrane involves a contribution from surface-normal displacements which is not the case for planar membranes. In the vanishing frequency limit, the particle self-mobility near a no-slip hard sphere is recovered only when the membrane possesses a non-vanishing resistance towards shearing. We further investigate capsule motion, finding that the pair-mobility function is solely determined by membrane shearing properties. Our analytical predictions are validated by fully resolved boundary integral simulations where a very good agreement is obtained.

1 Introduction

Nanoparticles nowadays are widely used in medicine as therapeutic drug delivery agents because of their ability to target specific areas including tumors and inflammation sites [1, 2]. Once they are injected into the blood circulation, nanoparticles interact hydrodynamically with neighboring cell membranes in a complex fashion.

In these situations, the Reynolds number is typically very low and a complete description of particle motion is possible via the mobility tensor which gives a linear relation between the particle velocity and the force applied on it. In the presence of a boundary (interface) the mobility is anisotropic and depends on the distance between the particle and the interface. For fluid-solid and fluid-fluid interfaces these mobility tensors have been studied intensively both theoretically [3–18] and experimentally [19–35] since quite some time ago. Due to their relevance as model systems for cell membranes, also elastic interfaces have started to attract some attention recently. Here, any motion of the particle causes membrane deformation and a flow is created when the membrane relaxes back to its undeformed state, acting back on the particle motion at a later time. Accordingly the system possesses a memory and the mobility depends not only on the distance, but also on time or, after temporal Fourier-transformation, on frequency. Particle motion nearby elastic membranes has been investigated experimentally using optical traps [36–38], magnetic particle actuation [39] and quasi-elastic light scattering [40, 41], where a significant decrease in mobility normal to the cell membrane has been observed similar to that observed near a hard wall. Particle mobility inside a spherical cell has further been measured by optical microscopy [42]. Setting a particle nearby a cell membrane has been used in interfacial microrheological experiments as an efficient way to extract membrane's unknown moduli [37, 43]. Theoretical investigations near elastic interfaces have been carried out using lubrication theory [44–46], the point-particle approximation [47–54] and have recently been extended by including higher-order singularities and the hydrodynamic interaction between two particles [55]. All these works considered an infinitely large planar interface which might not always be an appropriate model for a curved cell membrane. Since their solution technique is based on 2D spatial Fourier transforms [13, 56], their approach cannot be extended to non-planar interfaces.

In this paper, we therefore employ a different approach based on the image solution technique to compute the frequency dependent mobility of a small particle moving perpendicular to an initially spherical elastic object (which can be a cell, a capsule or a vesicle) whose membrane exhibits resistance towards shearing and bending. The method has originally been introduced by Fuentes and coworkers [57, 58] who investigated the hydrodynamic interactions between two unequal viscous drops when the interparticle gap is of the order of the diameter of the smaller one.

The remainder of the paper is organized as follows. In Sec. 2, we compute the flow field by expressing the solution of the fluid motion as a multipole expansion. In Sec. 3, we give analytical expressions of the particle frequency-dependent self-mobility in terms of infinite series, nearby idealized membranes with shearing-only or bending-only rigidities. The motion of the capsule is studied in Sec. 4, finding that the pair-mobility function depends only on membrane shearing properties. A comparison between theoretical predictions and numerical simulations is provided in Sec. 5 where a very good agreement is obtained. A conclusion summarizing our results is offered in Sec. 6. The technical details are relegated to the appendices.

2 Singularity solution

In this section, we derive the image solution for a point-force acting nearby a spherical capsule of radius a. We will use the term "capsule" to denote a general soft object including cells or vesicles. The origin of spherical coordinates is located at $\boldsymbol{x}_1$, the center of the capsule. An arbitrary time-dependent point-force $\boldsymbol{F}$ is acting at $\boldsymbol{x}_2 = R\boldsymbol{e}_z$ (see Fig. 1 for an illustration of the system setup.) The problem is thus equivalent to solving the forced Stokes equations

$$\eta\boldsymbol{\nabla}^2\boldsymbol{v} - \boldsymbol{\nabla}p + \boldsymbol{F}\delta(\boldsymbol{x}-\boldsymbol{x}_2) = 0\,, \tag{2.1}$$

$$\boldsymbol{\nabla}\cdot\boldsymbol{v} = 0\,, \tag{2.2}$$

for the fluid outside the capsule and

$$\eta\boldsymbol{\nabla}^2\boldsymbol{v}^{(i)} - \boldsymbol{\nabla}p^{(i)} = 0\,, \tag{2.3}$$

$$\boldsymbol{\nabla}\cdot\boldsymbol{v}^{(i)} = 0\,, \tag{2.4}$$

inside. Here $\boldsymbol{v}$ and p denote the flow velocity and the pressure outside the capsule, and the superscript (i) denote the corresponding interior fields. For simplicity, the fluid is assumed to have the same dynamic viscosity η everywhere.

We therefore need to solve Eqs. (2.1) through (2.4) for the boundary conditions imposed at the membrane equilibrium position $r = a$,

$$[v_\theta] = 0\,, \tag{2.5}$$

$$[v_r] = 0\,, \tag{2.6}$$

$$[\sigma_{\theta r}] = \Delta f_\theta^{\mathrm{S}} + \Delta f_\theta^{\mathrm{B}}\,, \tag{2.7}$$

$$[\sigma_{rr}] = \Delta f_r^{\mathrm{S}} + \Delta f_r^{\mathrm{B}}\,, \tag{2.8}$$

where the notation $[w] := w(r=a^+) - w(r=a^-)$ represents the jump of a given quantity w across the membrane. Here we assume axisymmetry such that all azimuthal components vanish. Throughout the remainder of this paper, all the lengths will be scaled by the capsule radius a unless otherwise stated. For convenience, the transition rules to physical quantities are summarized in appendix B. The non-vanishing components of the fluid stress tensor are expressed in spherical coordinates as [59]

$$\sigma_{\theta r} = \eta\left(v_{\theta,r} - \frac{v_\theta}{r} + \frac{v_{r,\theta}}{r}\right)\,, \tag{2.9a}$$

$$\sigma_{rr} = -p + 2\eta v_{r,r}\,, \tag{2.9b}$$

where comma in indices denotes a spatial partial derivative. Note that Eqs. (2.5) and (2.6) represent the natural continuity of the flow field across the membrane, whereas Eqs. (2.7) and (2.8) are the

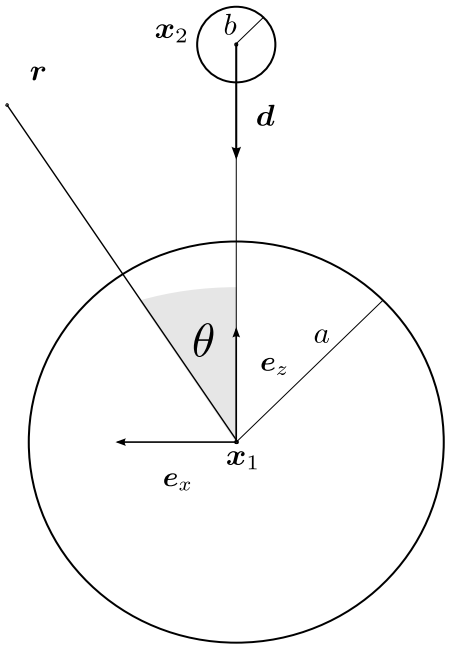

Figure 1: Illustration of the system setup. A small solid spherical particle of radius b positioned at $\boldsymbol{x}_2 = R\boldsymbol{e}_z$ nearby a large spherical capsule of radius a. In an axisymmetric configuration, the force is directed along the unit vector $\boldsymbol{d} \equiv -\boldsymbol{e}_z$.

discontinuity of the normal-tangential and normal-normal components of the fluid stress tensor at the membrane. Here Δf_θ and Δf_r are the meridional and radial traction where the superscripts S and B stand for the shearing and bending related parts, respectively. As derived in Appendix A, according to the Skalak model [60] the linearized traction due to shearing elasticity reads

$$\Delta f_\theta^{\mathrm{S}} = -\frac{2\kappa_{\mathrm{S}}}{3}\Big((1+2C)u_{r,\theta} + (1+C)u_{\theta,\theta\theta} + (1+C)u_{\theta,\theta}\cot\theta - \big((1+C)\cot^2\theta + C\big)\,u_\theta\Big)\,, \tag{2.10a}$$

$$\Delta f_r^{\mathrm{S}} = \frac{2\kappa_{\mathrm{S}}}{3}(1+2C)\left(2u_r + u_{\theta,\theta} + u_\theta\cot\theta\right)\,. \tag{2.10b}$$

The traction jump due to bending resistance can be derived from the Helfrich model [61] or by assuming a linear constitutive relation for the bending moments [62]. For small deformations, both formulations are equivalent [63] leading to the traction (cf. appendix A)

$$\Delta f_\theta^{\mathrm{B}} = \kappa_{\mathrm{B}}\left(\left(1-\cot^2\theta\right)u_{r,\theta} + u_{r,\theta\theta}\cot\theta + u_{r,\theta\theta\theta}\right)\,, \tag{2.11a}$$

$$\Delta f_r^{\mathrm{B}} = \kappa_{\mathrm{B}}\Big(\left(3\cot\theta + \cot^3\theta\right)u_{r,\theta} - u_{r,\theta\theta}\cot^2\theta + 2u_{r,\theta\theta\theta}\cot\theta + u_{r,\theta\theta\theta\theta}\Big)\,. \tag{2.11b}$$

Here $\boldsymbol{u}(\theta) = u_r(\theta)\boldsymbol{e}_r + u_\theta(\theta)\boldsymbol{e}_\theta$ denotes the membrane displacement vector, related to the fluid velocity by the no-slip relation at $r = 1$ by

$$\boldsymbol{v}|_{r=1} = \frac{\mathrm{d}\boldsymbol{u}}{\mathrm{d}t}\,, \tag{2.12}$$

which can thus be written in temporal Fourier space as $\boldsymbol{v} = i\omega\,\boldsymbol{u}$ evaluated at $r = 1$. The membrane parameters κ_{S} and κ_{B} are the shearing and bending moduli, respectively, and C is the Skalak parameter defined as the ratio between area expansion modulus κ_{A} and shear modulus κ_{S}. An

unscaled version of the above equations in physical units can be obtained by applying the rules given in appendix B.

Our resolution approach is based on the image solution method proposed by Fuentes *et al.* [57] who computed the axisymmetric motion of two viscous drops in Stokes flow. Accordingly, the exterior fluid velocity can be written as a sum of two contributions,

$$v_i = v_i^{\mathrm{S}} + v_i^* \,, \tag{2.13}$$

where $v_i^{\mathrm{S}} := \mathcal{G}_{ij}(\boldsymbol{x}-\boldsymbol{x}_2)F_j$ is the velocity field induced by a point-force acting at $\boldsymbol{x}_2$ (cf. equation (2.14)) in an infinite medium, i.e. in the absence of the capsule and v_i^* is the image system required to satisfy the boundary conditions at the capsule membrane.

Now we briefly sketch the main resolution steps. First, the velocity $\boldsymbol{v}^{\mathrm{S}}$ due to the Stokeslet acting at $\boldsymbol{x}_2$ is written in terms of spherical harmonics which are transformed afterward into harmonics based at $\boldsymbol{x}_1$ via the Legendre expansion. Second, the image system solution $\boldsymbol{v}^*$ is expressed as multipole series at $\boldsymbol{x}_1$ which subsequently is rewritten in terms of spherical harmonics centered at $\boldsymbol{x}_1$. Third, the solution inside the capsule $\boldsymbol{v}^{(i)}$ is expressed using Lamb's solution [64] also written in terms of spherical harmonics at $\boldsymbol{x}_1$. The last step consists of determining the series expansion coefficients by satisfying the boundary conditions at the membrane surface stated by Eqs. (2.5) through (2.8).

2.1 Stokeslet representation

We begin with writing the Stokeslet acting at $\boldsymbol{x}_2$,

$$v_i^{\mathrm{S}} = \mathcal{G}_{ij}F_j = \frac{1}{8\pi\eta}\left(F_i\frac{1}{s} + F_j(\boldsymbol{x}-\boldsymbol{x}_2)_i\nabla_{2j}\frac{1}{s}\right) , \tag{2.14}$$

where $s := |\boldsymbol{x}-\boldsymbol{x}_2|$. Here $\nabla_{2j} := \partial/\partial x_{2j}$ denotes the nabla operator taken with respect to the singularity position $\boldsymbol{x}_2$. Using Legendre expansion, the harmonics based at $\boldsymbol{x}_2$ can be expanded as

$$\frac{1}{s} = \sum_{n=0}^{\infty}\frac{r^{2n+1}}{R^{n+1}}\frac{(\boldsymbol{d}\cdot\boldsymbol{\nabla})^n}{n!}\frac{1}{r} \,, \tag{2.15}$$

where the unit vector $\boldsymbol{d} := (\boldsymbol{x}_1-\boldsymbol{x}_2)/R = -\boldsymbol{e}_z$, $\boldsymbol{r} = \boldsymbol{x}-\boldsymbol{x}_1$ and $r := |\boldsymbol{r}|$. Moreover, we denote by φ_n the harmonic of degree n, related to the Legendre polynomials of degree n by [65]

$$\varphi_n(r,\theta) := \frac{(\boldsymbol{d}\cdot\boldsymbol{\nabla})^n}{n!}\frac{1}{r} = \frac{1}{r^{n+1}}P_n(\cos\theta) \,. \tag{2.16}$$

For the axisymmetric case, the force is exerted along the unit vector $\boldsymbol{d}$ and can be written as $\boldsymbol{F} = F\boldsymbol{d}$. By making use of the identities

$$\boldsymbol{\nabla}_2\frac{1}{R^{n+1}} = \frac{n+1}{R^{n+2}}\,\boldsymbol{d} \,, \quad (\boldsymbol{d}\cdot\boldsymbol{\nabla}_2)\,\boldsymbol{d} = 0 \,, \tag{2.17}$$

Eq. (2.14) can therefore be written as

$$\boldsymbol{v}^{\mathrm{S}} = \frac{F}{8\pi\eta}\left[\sum_{n=0}^{\infty}(n+2)\frac{r^{2n+1}}{R^{n+1}}\,\boldsymbol{d}\,\varphi_n + \sum_{n=0}^{\infty}(n+1)\frac{r^{2n+1}}{R^{n+2}}\,\boldsymbol{r}\varphi_n\right] . \tag{2.18}$$

Hence, the Stokeslet is written in terms of harmonics based at $\boldsymbol{x}_1$. Note that the terms with $\boldsymbol{d}\,\varphi_n$ in Eq. (2.18) are not independent harmonics. For their elimination, we shall use the following

recurrence property [57]

$$\boldsymbol{d}\,\varphi_n = \frac{1}{2n+1}\Big(\boldsymbol{\nabla}\varphi_{n-1} - r^2\boldsymbol{\nabla}\varphi_{n+1} - (2n+3)\boldsymbol{r}\,\varphi_{n+1}\Big)\,, \tag{2.19}$$

leading after substitution into Eq. (2.18) to

$$\begin{aligned}\boldsymbol{v}^{\mathrm{S}} = \frac{F}{8\pi\eta}\sum_{n=1}^{\infty}\Bigg[&\left(\frac{n+3}{2n+3}\frac{r^{2n+3}}{R^{n+2}} - \frac{n+1}{2n-1}\frac{r^{2n+1}}{R^n}\right)\boldsymbol{\nabla}\varphi_n \\ &+ \left((n+1)\frac{r^{2n+1}}{R^{n+2}} - \frac{(n+1)(2n+1)}{2n-1}\frac{r^{2n-1}}{R^n}\right)\boldsymbol{r}\varphi_n\Bigg]\,.\end{aligned} \tag{2.20}$$

Note that the terms with $n = 0$ cancel so that the summation starts from $n = 1$.

2.2 Image system representation

Next, we write the image system solution following a multipole expansion approach as

$$v_i^* = \frac{F\,d_j}{8\pi\eta}\sum_{n=0}^{\infty}\left[A_n\frac{(\boldsymbol{d}\cdot\boldsymbol{\nabla})^n}{n!}\mathcal{G}_{ij}(\boldsymbol{r}) + B_n\frac{(\boldsymbol{d}\cdot\boldsymbol{\nabla})^n}{n!}\boldsymbol{\nabla}^2\mathcal{G}_{ij}(\boldsymbol{r})\right], \tag{2.21}$$

where the solution form is assumed as a result of the system axisymmetry [57] with the constants A_n and B_n to be determined by the boundary conditions. By making use of the identity

$$\frac{(\boldsymbol{d}\cdot\boldsymbol{\nabla})^n}{n!}\mathcal{G}_{ij}(\boldsymbol{r}) = \delta_{ij}\varphi_n - r_i\frac{\partial\varphi_n}{\partial x_j} - d_i\frac{\partial\varphi_{n-1}}{\partial x_j}\,.$$

together with

$$\boldsymbol{\nabla}^2\mathcal{G}_{ij}(\boldsymbol{r}) = -\frac{\partial^2}{\partial x_i\partial x_j}\frac{2}{r}\,,$$

the image solution can be written as

$$\boldsymbol{v}^* = -\frac{F}{8\pi\eta}\sum_{n=0}^{\infty}\left[A_n\Big((n-1)\boldsymbol{d}\,\varphi_n + (n+1)\boldsymbol{r}\varphi_{n+1}\Big) + 2(n+1)B_n\boldsymbol{\nabla}\varphi_{n+1}\right]. \tag{2.22}$$

Further, the elimination of the dependent harmonics $\boldsymbol{d}\,\varphi_n$ is readily achieved using Eq. (2.19). Shifting the index to start the sum from $n = 1$, we finally obtain

$$\boldsymbol{v}^* = \frac{F}{8\pi\eta}\sum_{n=1}^{\infty}\left[\left(\frac{n-2}{2n-1}r^2A_{n-1} - \frac{n}{2n+3}A_{n+1} - 2nB_{n-1}\right)\boldsymbol{\nabla}\varphi_n - \frac{2(n+1)}{2n-1}A_{n-1}\boldsymbol{r}\varphi_n\right]. \tag{2.23}$$

2.3 Solution inside the capsule

For the flow field inside the capsule, we use Lamb's general solution [66, 67], which can be expressed in terms of interior harmonics based at $\boldsymbol{x}_1$ as [57]

$$\begin{aligned}\boldsymbol{v}^{(i)} = \frac{F}{8\pi\eta}\sum_{n=1}^{\infty}\Bigg[a_n\bigg(\frac{n+3}{2}r^{2n+3}\boldsymbol{\nabla}\varphi_n + \frac{(n+1)(2n+3)}{2}r^{2n+1}\boldsymbol{r}\varphi_n\bigg)\\ + b_n\left(r^{2n+1}\boldsymbol{\nabla}\varphi_n + (2n+1)r^{2n-1}\boldsymbol{r}\varphi_n\right)\Bigg].\end{aligned} \tag{2.24}$$

The determination of the series coefficients outside the capsule A_n and B_n and inside the capsule a_n and b_n is achieved by applying the boundary conditions at the capsule membrane. This will be subject of the next subsections.

2.4 Determination of the series coefficients

Hereafter, for the sake of completeness, we shall state explicitly the expressions of the projected velocity components onto the radial and tangential directions. For this aim, we make use of the following identities for the projection onto the radial direction,

$$\boldsymbol{e}_r\cdot\boldsymbol{\nabla}\varphi_n = -\frac{n+1}{r}\varphi_n\,, \tag{2.25a}$$

$$\boldsymbol{e}_r\cdot\boldsymbol{r}\varphi_n = r\varphi_n\,. \tag{2.25b}$$

For the projection onto the tangential direction, we make use of

$$\boldsymbol{e}_\theta\cdot\boldsymbol{r}\varphi_n = 0\,. \tag{2.26}$$

We further define

$$\psi_n := \boldsymbol{e}_\theta\cdot\boldsymbol{\nabla}\varphi_n = \frac{1}{r}\frac{\partial\varphi_n}{\partial\theta}\,. \tag{2.27}$$

From Eq. (2.20), the radial and tangential components of the Stokeslet solution follow forthwith. We obtain

$$v_r^{\mathrm{S}} = \frac{F}{8\pi\eta}\sum_{n=1}^{\infty}\left[\frac{n(n+1)}{2n+3}\frac{r^{2n+2}}{R^{n+2}} - \frac{n(n+1)}{2n-1}\frac{r^{2n}}{R^n}\right]\varphi_n\,, \tag{2.28}$$

$$v_\theta^{\mathrm{S}} = \frac{F}{8\pi\eta}\sum_{n=1}^{\infty}\left[\frac{n+3}{2n+3}\frac{r^{2n+3}}{R^{n+2}} - \frac{n+1}{2n-1}\frac{r^{2n+1}}{R^n}\right]\psi_n\,. \tag{2.29}$$

Similar, from Eq. (2.23) we obtain the components of the image solutions as

$$v_r^{*} = \frac{F}{8\pi\eta}\sum_{n=1}^{\infty}\left[-\frac{n(n+1)}{2n-1}rA_{n-1} + \frac{n(n+1)}{2n+3}\frac{A_{n+1}}{r} + 2n(n+1)\frac{B_{n-1}}{r}\right]\varphi_n\,, \tag{2.30}$$

$$v_\theta^{*} = \frac{F}{8\pi\eta}\sum_{n=1}^{\infty}\left[\frac{n-2}{2n-1}r^2A_{n-1} - \frac{nA_{n+1}}{2n+3} - 2nB_{n-1}\right]\psi_n\,. \tag{2.31}$$

From Eq. (2.24), the components of the flow field inside the capsule read

$$v_r^{(i)} = \frac{F}{8\pi\eta}\sum_{n=1}^{\infty}\left[\frac{n(n+1)}{2}r^{2n+2}a_n + nr^{2n}b_n\right]\varphi_n\,, \tag{2.32}$$

$$v_\theta^{(i)} = \frac{F}{8\pi\eta}\sum_{n=1}^{\infty}\left[\frac{n+3}{2}r^{2n+3}a_n + r^{2n+1}b_n\right]\psi_n\,. \tag{2.33}$$

Pressure field

In order to proceed later, we need to express the pressure field in terms of a multipole expansion. The form of the pressure p in the exterior fluid follows from the general solution of the axisymmetric Laplace equation in spherical coordinates as

$$p = \frac{F}{8\pi}\sum_{n=1}^{\infty}(S_n + Q_n r^{2n+1})\varphi_n\,.$$

Since the form of the velocity field is known from Eqs. (2.28)–(2.31), the coefficients S_n and Q_n can be related to the coefficients of the velocity field by using Eq. (2.1) leading to

$$S_n = -2nA_{n-1}\,, \quad Q_n = \frac{2(n+1)}{R^{n+2}}\,. \tag{2.34}$$

Inside the capsule, all harmonics of negative order which lead to a singularity at $r = 0$ need to be discarded reducing the form of the pressure to

$$p^{(i)} = \frac{F}{8\pi}\sum_{n=1}^{\infty}p_n r^{2n+1}\varphi_n\,.$$

Using Eqs. (2.3), (2.32) and (2.33) we find

$$p_n = (n+1)(2n+3)a_n\,. \tag{2.35}$$

Continuity of velocity

After substituting Eqs. (2.28) through (2.33) into Eqs. (2.5) and (2.6), the continuity of the tangential and radial fluid velocity components across the membrane leads to the two following equations

$$\begin{aligned}\frac{n(n+1)}{2}a_n + nb_n &= -\frac{n(n+1)}{2n-1}A_{n-1} + \frac{n(n+1)}{2n+3}A_{n+1} + 2n(n+1)B_{n-1} + \frac{n(n+1)}{2n+3}\frac{1}{R^{n+2}}\\ &\quad - \frac{n(n+1)}{2n-1}\frac{1}{R^n}\,,\\ \frac{n+3}{2}a_n + b_n &= \frac{n-2}{2n-1}A_{n-1} - \frac{n\,A_{n+1}}{2n+3} - 2nB_{n-1} + \frac{n+3}{2n+3}\frac{1}{R^{n+2}} - \frac{n+1}{2n-1}\frac{1}{R^n}\,,\end{aligned}$$

which can be solved for the coefficients a_n and b_n to obtain

$$a_n = A_{n-1} - \frac{2n+1}{2n+3}A_{n+1} - 2(2n+1)B_{n-1} + \frac{2}{2n+3}\frac{1}{R^{n+2}}\,, \tag{2.37}$$

$$b_n = -\frac{(n+1)(2n+1)}{2(2n-1)}A_{n-1} + \frac{n+1}{2}A_{n+1} + (n+1)(2n+3)B_{n-1} - \frac{n+1}{2n-1}\frac{1}{R^n}\,. \tag{2.38}$$

Discontinuity of stress tensor

Expressions for A_n and B_n can be determined from the discontinuity of the traction across the membrane. In order to assess the effect of shearing and bending on particle self-mobility, we shall consider in the following shearing and bending effects separately.

Shearing contribution Here we consider an idealized membrane with a shearing-only resistance, such as a typical artificial capsule [68]. After setting $\Delta f_r^{\mathrm{B}} = \Delta f_\theta^{\mathrm{B}} = 0$ in the traction jump equations given by Eqs. (2.7) and (2.8), we readily obtain

$$[v_{\theta,r}] = -\alpha\Big((1+2C)v_{r,\theta} + (1+C)\left(v_{\theta,\theta\theta} + v_{\theta,\theta}\cot\theta\right) - \left((1+C)\cot^2\theta + C\right)v_\theta\Big)\Big|_{r=1}\,, \tag{2.39a}$$

$$\left[\frac{p}{\eta}\right] = \alpha(1+2C)v_{r,r}|_{r=1}\,, \tag{2.39b}$$

where $i\alpha := 2\kappa_{\mathrm{S}}/(3\eta\omega)$ upon using the incompressibility equation

$$\frac{2v_r}{r} + v_{r,r} + \frac{v_{\theta,\theta} + v_\theta\cot\theta}{r} = 0\,.$$

It follows immediately that $[v_{r,r}] = 0$. Furthermore, note that $[v_{r,\theta}] = 0$.

Continuing, we proceed first by substituting the expressions of the velocity components given by Eqs. (2.28)–(2.33) into the tangential traction jump Eq. (2.39a) and replacing a_n and b_n with their expressions given by Eqs. (2.37) and (2.38), respectively. For the determination of the unknown coefficients, we multiply both equation members by $\psi_m \sin\theta$ and integrate over the polar angle θ between 0 and π. By making use of the following orthogonality properties

$$\int_0^\pi \psi_m\psi_n \sin\theta \mathrm{d}\theta = \frac{2n(n+1)}{2n+1}\frac{\delta_{mn}}{r^{2n+4}}\,, \tag{2.40}$$

and

$$\int_0^\pi \psi_m\left(\psi_{n,\theta\theta} + \psi_{n,\theta}\cot\theta - \psi_n\cot^2\theta\right)\sin\theta\mathrm{d}\theta = -\frac{2n(n+1)(n^2+n-1)}{2n+1}\frac{\delta_{mn}}{r^{2n+4}}\,. \tag{2.41}$$

the resulting equation reads

$$\begin{aligned}(2n+1)\Big(2(2n+3)B_{n-1} - A_{n-1} + A_{n+1}\Big) = \\ -\alpha\Bigg((1+2C)n(n+1)\left(\frac{A_{n+1}}{2n+3} - \frac{A_{n-1}}{2n-1} + 2B_{n-1} - \frac{1}{2n-1}\frac{1}{R^n} + \frac{1}{2n+3}\frac{1}{R^{n+2}}\right) \\ + \left(\frac{n-2}{2n-1}A_{n-1} - \frac{n}{2n+3}A_{n+1} - 2nB_{n-1} - \frac{n+1}{2n-1}\frac{1}{R^n} + \frac{n+3}{2n+3}\frac{1}{R^{n+2}}\right) \\ \times\left(1 - (1+C)n(n+1)\right)\Bigg)\,,\end{aligned} \tag{2.42}$$

for $n \geq 1$. Next, we write a similar equation for the normal traction jump Eq. (2.39b). After substituting the velocity and the pressure into Eq. (2.39b), multiplying both members by $\varphi_m \sin\theta$ and employing the orthogonality properties

$$\int_0^\pi \varphi_n\varphi_m \sin\theta\mathrm{d}\theta = \frac{2}{2n+1}\frac{\delta_{mn}}{r^{2n+2}}\,. \tag{2.43}$$

and

$$\int_0^\pi \varphi_m \left(\varphi_{n,\theta\theta} + \varphi_{n,\theta} \cot\theta\right) \sin\theta \mathrm{d}\theta = -\frac{2n(n+1)}{2n+1} \frac{\delta_{mn}}{r^{2n+2}} \,. \tag{2.44}$$

we get after replacing a_n and b_n with their corresponding expressions

$$\begin{aligned} &-2(2n+3)(2n+1)(n+1)B_{n-1} + (2n^2+7n+3)A_{n-1} - (2n^2+3n+1)A_{n+1} \\ &= \left(-\frac{n}{2n-1}A_{n-1} + \frac{n+2}{2n+3}A_{n+1} + 2(n+2)B_{n-1} + \frac{n-1}{2n-1}\frac{1}{R^n} - \frac{n+1}{2n+3}\frac{1}{R^{n+2}} \right) \\ &\qquad \times \alpha(1+2C)n(n+1) \,, \end{aligned} \tag{2.45}$$

for $n \geq 1$.

The equations (2.42) and (2.45) form a closed linear system of equations, amenable to immediate resolution using the standard substitution method. From Eq. (2.42), B_{n-1} can be expressed in terms of A_{n-1} and A_{n+1}. We obtain

$$B_n = -\frac{A_{n+2}}{4n+10} + \frac{1}{2G}\left(\frac{G' A_n}{2n+1} + \frac{\alpha G_3}{2n+5}\frac{1}{R^{n+3}} - \frac{\alpha G_1}{2n+1}\frac{1}{R^{n+1}} \right), \tag{2.46}$$

for $n \geq 0$, where we defined

$$\begin{aligned} G &:= (C+1)\alpha n^3 + [(6C+5)\alpha + 4]n^2 + [(11C+7)\alpha + 16]n + (6C+3)\alpha + 15 \,, \\ G' &:= \alpha(1+C)n^3 + [(4C+3)\alpha + 4]n^2 + [(5C+1)\alpha + 8]n + (1+2C)\alpha + 3 \,, \\ G_1 &:= (C+1)n^3 + (3C+4)n^2 + 2(C+2)n \,, \\ G_3 &:= (1+C)n^3 + (5C+6)n^2 + (8C+10)n + (4C+2) \,. \end{aligned}$$

Next, by substituting the expression of B_{n-1} into Eq. (2.45), we obtain the general term for A_n as

$$A_n = \frac{\alpha n(n+2)}{K}\left(\frac{K_3}{R^{n+3}} - \frac{K_1}{R^{n+1}} \right), \tag{2.48}$$

for $n \geq 0$ where

$$\begin{aligned} K &:= 8(C+1)\alpha n^5 + [(4C+2)\alpha^2 + 60(C+1)\alpha + 32]n^4 + (36C+18)\alpha + 90 \\ &\quad + [(24C+12)\alpha^2 + 172(C+1)\alpha + 192]n^3 + [(44C+22)\alpha^2 + 234(C+1)\alpha + 400]n^2 \\ &\quad + [(24C+12)\alpha^2 + (150C+138)\alpha + 336]n \,, \\ K_1 &:= 4(C+1)n^4 + [(4C+2)\alpha + 20C + 28]n^3 + [(22C+11)\alpha + 31C + 75]n^2 \\ &\quad + [(36C+18)\alpha + 15C + 93]n + (18C+9)\alpha + 45 \,, \\ K_3 &:= 4(C+1)n^4 + [(4C+2)\alpha + 20C + 28]n^3 + [(18C+9)\alpha + 35C + 71]n^2 \\ &\quad + [(20C+10)\alpha + 25C + 71]n + (6C+3)\alpha + 6C + 21 \,. \end{aligned}$$

The general term for B_n can then be obtained by substituting the expressions of A_n and A_{n+2} determined from Eq. (2.48) into Eq. (2.46).

In particular, for $\alpha \to \infty$ (achieved either by taking an infinite membrane elastic modulus or by

considering a vanishing frequency) we recover the hard-sphere limit, namely

$$\lim_{\alpha\to\infty} A_n = -\left(n+\frac{3}{2}\right)\frac{1}{R^{n+1}} + \left(n+\frac{1}{2}\right)\frac{1}{R^{n+3}}\,, \tag{2.50a}$$

$$\lim_{\alpha\to\infty} B_n = -\frac{1}{4}(1-R^2)^2\frac{1}{R^{n+5}}\,, \tag{2.50b}$$

in agreement with the results by Kim and Karrila [59, p. 243] .

Bending contribution In the following, we consider an idealized membrane with a bending-only resistance such as an artificial vesicle. By setting $\Delta f_r^{\mathrm{S}} = \Delta f_\theta^{\mathrm{S}} = 0$ in the traction jump equations given by Eqs. (2.7) and (2.8), we get

$$[v_{\theta,r}] = \alpha_{\mathrm{B}}\left(\left(1-\cot^2\theta\right)v_{r,\theta} + v_{r,\theta\theta}\cot\theta + v_{r,\theta\theta\theta}\right)\big|_{r=1}\,, \tag{2.51a}$$

$$\left[-\frac{p}{\eta}\right] = \alpha_{\mathrm{B}}\left(\left(3\cot\theta+\cot^3\theta\right)v_{r,\theta} - v_{r,\theta\theta}\cot^2\theta + 2v_{r,\theta\theta\theta}\cot\theta + v_{r,\theta\theta\theta\theta}\right)\Big|_{r=1}\,, \tag{2.51b}$$

where $i\alpha_{\mathrm{B}} := \kappa_{\mathrm{B}}/(\eta\omega)$. Note that the right hand side of Eq. (2.51b) stands for the tangential biharmonic operator [69] applied to the velocity radial component v_r.

We then substitute the expressions of the velocity components given by Eqs. (2.28)–(2.33) into the tangential traction jump Eq. (2.51a) and replace a_n and b_n with their expressions given respectively by Eqs. (2.37) and (2.38). After multiplying both members by $\psi_m \sin\theta$, preforming the integration between 0 and π, and making use of the orthogonality identities (2.40) and (2.41) together with Eq. (2.27), we obtain

$$\begin{aligned}&(2n+1)\Big(2(2n+3)B_{n-1} - A_{n-1} + A_{n+1}\Big) = \\ &\alpha_{\mathrm{B}}\left(\frac{A_{n+1}}{2n+3} - \frac{A_{n-1}}{2n-1} + 2B_{n-1} - \frac{1}{2n-1}\frac{1}{R^n} + \frac{1}{2n+3}\frac{1}{R^{n+2}}\right)n(n+1)(-n^2-n+2)\,,\end{aligned} \tag{2.52}$$

for $n \geq 1$.

Next, after substitution in the normal traction jump Eq. (2.51b), multiplying both members by $\varphi_m \sin\theta$ and using Eq. (2.43) together with the orthogonality identity

$$\begin{aligned}&\int_0^\pi \varphi_m\left(\left(3\cot\theta+\cot^3\theta\right)\varphi_{n,\theta} - \varphi_{n,\theta\theta}\cot^2\theta + 2\varphi_{n,\theta\theta\theta}\cot\theta + \varphi_{n,\theta\theta\theta\theta}\right)\sin\theta\mathrm{d}\theta \\ &= \frac{2n(n-1)(n+1)(n+2)}{2n+1}\frac{\delta_{mn}}{r^{2n+2}}\,,\end{aligned}$$

we get after replacing a_n and b_n with their corresponding expressions

$$\begin{aligned}&-2(2n+3)(2n+1)(n+1)B_{n-1} + (2n^2+7n+3)A_{n-1} - (2n^2+3n+1)A_{n+1} \\ &= \alpha_{\mathrm{B}}\left(\frac{A_{n+1}}{2n+3} - \frac{A_{n-1}}{2n-1} + 2B_{n-1} - \frac{1}{2n-1}\frac{1}{R^n} + \frac{1}{2n+3}\frac{1}{R^{n+2}}\right)(n-1)n^2(n+1)^2(n+2)\,,\end{aligned} \tag{2.53}$$

for $n \geq 1$.

From Eq. (2.52), B_{n-1} can straightforwardly be expressed in terms of A_{n-1} and A_{n+1}. We obtain

$$B_n = -\frac{A_{n+2}}{4n+10} + \frac{1}{S}\left(\frac{S'A_n}{2n+1} + \alpha_{\mathrm{B}}n(n+1)(n+2)(n+3)\left(\frac{1}{2n+1}\frac{1}{R^{n+1}} - \frac{1}{2n+5}\frac{1}{R^{n+3}}\right)\right)\,, \tag{2.54}$$

for $n \geq 0$, where we defined

$$S := 2\Big(\alpha_{\mathrm{B}} n^4 + 6\alpha_{\mathrm{B}} n^3 + (11\alpha_{\mathrm{B}} + 4)n^2 + (6\alpha_{\mathrm{B}} + 16)n + 15\Big)\,,$$
$$S' := S/2 - 8n - 12\,.$$

After plugging the expression of B_{n-1} into Eq. (2.53), we get the general term of A_n as

$$A_n = \frac{\alpha_{\mathrm{B}} n^2 (n+1)(n+3)(n+2)^2}{W}\left(\frac{2n+1}{R^{n+3}} - \frac{2n+5}{R^{n+1}}\right)\,, \tag{2.56}$$

for $n \geq 0$, where

$$W := 4\alpha_{\mathrm{B}} n^6 + 36\alpha_{\mathrm{B}} n^5 + 118\alpha_{\mathrm{B}} n^4 + (168\alpha_{\mathrm{B}} + 16)n^3 + (94\alpha_{\mathrm{B}} + 72)n^2 + (12\alpha_{\mathrm{B}} + 92)n + 30\,.$$

The general term for B_n can be obtained by substituting A_n and A_{n+2} as computed from Eq. (2.56) into Eq. (2.54). Interestingly, by taking α_{B} to infinity, A_n and B_n do not tend to the hard-sphere limits as it has been shown to be the case for a shearing-only membrane. In this case we rather obtain

$$\lim_{\alpha_{\mathrm{B}}\to\infty} A_n = \frac{n(n+2)}{2(2n^2+6n+1)}\left(\frac{2n+1}{R^{n+3}} - \frac{2n+5}{R^{n+1}}\right)\,,$$
$$\lim_{\alpha_{\mathrm{B}}\to\infty} B_n = \frac{1}{4}\left(-\frac{n^2+2n-2}{2n^2+6n+1} - \frac{(n+2)(n+4)}{2n^2+14n+21}\frac{1}{R^4} + \frac{2n^4+18n^3+49n^2+42n+3}{(2n^2+6n+1)(2n^2+14n+21)}\frac{2}{R^2}\right)\frac{1}{R^{n+1}}\,.$$

A similar resolution approach can be adopted for the determination of the series coefficients when the membrane is simultaneously endowed with both shearing and bending rigidities. Analytical expression can be obtained by computer algebra software, but they are not included here due to their complexity and lengthiness. We note that the shearing and bending contributions to the particle mobility do not superpose linearly which is in contrast to a planar membrane [52] but similar to what has been observed between two planar membranes [53].

3 Particle self-mobility

In this section, we compute the correction to the particle self-mobility in the point-particle framework. Here we assume no net force on the capsule and an external force $\boldsymbol{F}_2$ on the solid particle. As shown in Appendix C, for finite membrane shearing modulus, the capsule is in fact force free.

The zeroth-order solution for the particle velocity is given by the Stokes law as $\boldsymbol{V}_2^{(0)} = \mu_0 \boldsymbol{F}_2$, where $\mu_0 := 1/(6\pi\eta b)$ is the usual bulk mobility. The first-order correction to the particle self-mobility $\Delta\mu$ is obtained by evaluating the reflected flow field at the particle position such that

$$\boldsymbol{v}^*|_{\boldsymbol{x}=\boldsymbol{x}_2} = \Delta\mu \boldsymbol{F}_2\,. \tag{3.1}$$

Since the force points along the axis of symmetry of the system, the mobility correction is a simple scalar and not a tensor as it would be for an arbitrary direction of the force. In the following, we

shall make use of the following identities

$$\frac{(\boldsymbol{d}\cdot\boldsymbol{\nabla})^n}{n!}\boldsymbol{\mathcal{G}}(\boldsymbol{r})\bigg|_{\boldsymbol{x}=\boldsymbol{x}_2}\boldsymbol{F}_2=\frac{2}{R^{n+1}}\boldsymbol{F}_2\,,$$
$$\frac{(\boldsymbol{d}\cdot\boldsymbol{\nabla})^n}{n!}\boldsymbol{\nabla}^2\boldsymbol{\mathcal{G}}(\boldsymbol{r})\bigg|_{\boldsymbol{x}=\boldsymbol{x}_2}\boldsymbol{F}_2=-\frac{2(n+1)(n+2)}{R^{n+3}}\boldsymbol{F}_2\,.$$

to finally obtain

$$\frac{\Delta\mu}{\mu_0}=\frac{3b}{4}\sum_{n=0}^{\infty}2\left(A_n-(n+1)(n+2)\xi^2B_n\right)\xi^{n+1}\,, \tag{3.3}$$

wherein $\xi:=1/R\in[0,1)$. This is the central result of our work. We recall that the unscaled form for an arbitrary capsule radius a can be obtained from Eq. (3.3) by the replacement rules in Appendix B. The number of terms to be included before the series is truncated can be estimated for a desired precision as detailed in appendix D. Due to the point-particle approximation, the particle radius only enters upon rescaling the particle self-mobility correction by the bulk mobility μ_0.

3.1 Shearing contribution

For a membrane exhibiting a shearing-only resistance, the particle self-mobility correction can be computed by plugging the expressions of B_n and A_n as stated respectively by Eqs. (2.46) and (2.48) into Eq. (3.3). By taking the limit when $\alpha\to\infty$ we recover the rigid sphere limit,

$$\frac{\Delta\mu_{\mathrm{S},\infty}}{\mu_0}:=\lim_{\alpha\to\infty}\frac{\Delta\mu_{\mathrm{S}}}{\mu_0}=-\frac{\xi^3(15-7\xi^2+\xi^4)}{4(1-\xi^2)}\frac{b}{R}\,, \tag{3.4}$$

in agreement with the result by Ekiel-Jeżewska and Felderhof [70, Eq. (2.26)]. For an infinite membrane radius, we obtain

$$\frac{\Delta\mu_{\mathrm{S},\infty}}{\mu_0}=-\frac{9}{8}\frac{b}{h}\,, \tag{3.5}$$

where $h:=R-1$ being the distance from the center of the solid particle to the closest point on the capsule surface. We thus recover the well-known result for a planar rigid wall as first calculated by Lorentz about one century ago [3].

We define the characteristic frequency for shearing as $\beta:=6B\eta\omega h/\kappa_{\mathrm{S}}$ with $B:=2/(1+C)$. In Fig. 2 we plot the variations of the scaled self-mobility correction for a shearing-only membrane versus β upon varying the particle radius b while keeping the distance from the membrane $h=2b$ and setting the Skalak parameter $C=1$. We observe that the real part of the mobility correction is a monotonically increasing function of frequency and the imaginary part exhibits the typical peak structure which is a signature of the memory effect induced by the elastic nature of the membrane. In the vanishing frequency limit, the correction is identical to that near a hard-sphere with stick boundary conditions, given by Eq. (3.4).

For sufficiently small values of b (or equivalently for larger capsule radii), we observe that in the high frequency regime for which $\beta\geq1$, both the real and imaginary parts of the mobility correction follow faithfully the evolution of those predicted for a planar membrane which is [52]

$$\frac{\Delta\mu_{\mathrm{S}}(\beta)}{\mu_0}=-\frac{9}{16}\frac{b}{h}e^{i\beta}\,\mathrm{E}_4(i\beta)\,. \tag{3.6}$$

The peak position around $\beta\sim1$ can be estimated by a simple balance between membrane elasticity and fluid viscosity as $\omega\sim\kappa_{\mathrm{S}}/(\eta h)$. A strong departure is however observed in the low frequency

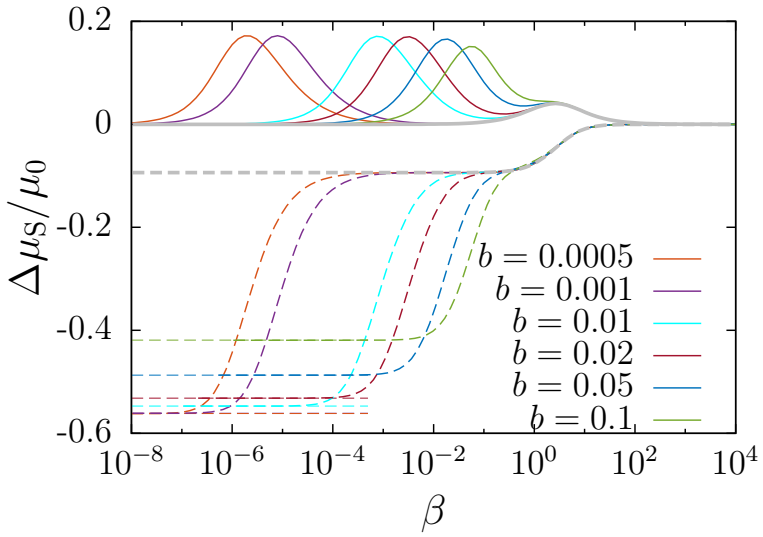

Figure 2: (Color online) Scaled particle self-mobility correction versus β for various values of b for a shearing-only membrane. The real and imaginary parts are shown as dashed and solid lines respectively. Horizontal dashed lines represent the hard-sphere limit as given by Eq. (3.4). The curve in gray corresponds to the self-mobility correction for a planar membrane as given by Eq. (3.6). Here we set the solid particle at $h = 2b$.

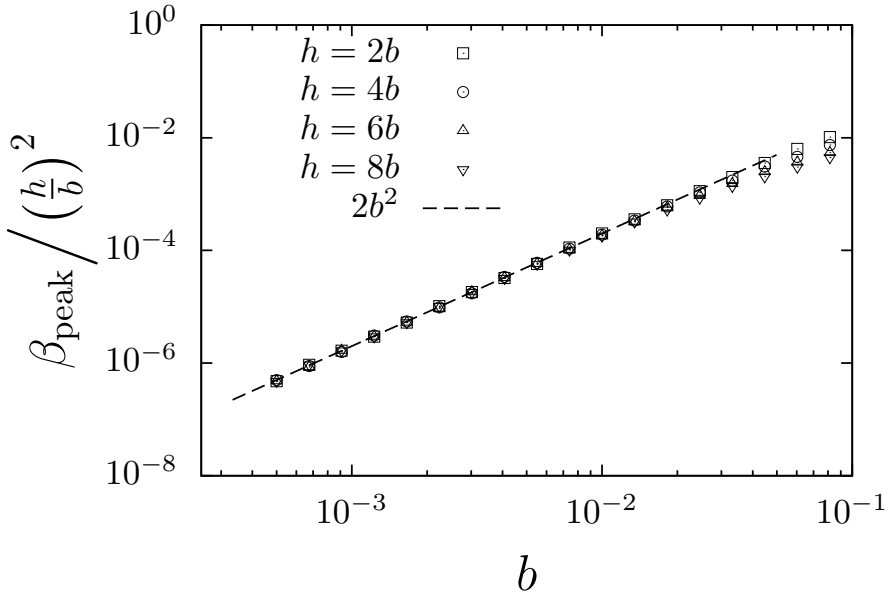

Figure 3: Log-log plot of the rescaled peak-frequency versus particle radius for different particle-to-membrane distance h.

regime where a second peak of more pronounced amplitude occurs in the imaginary part. This second peak is the most prominent signature which distinguishes the spherical membrane from the planar case. The peak height remains typically constant for a large range of values of b because the mobility correction has been rescaled by the bulk mobility.

We attribute the two peaks in Fig. 2 to in-plane deformations (u_θ) and surface-normal deformations (u_r), respectively. The radius-independent peak around $\beta \sim 1$ corresponds to in-plane deformations u_θ which are present in a similar way for the planar membrane thus explaining the agreement with Eq. (3.6). The larger and radius-dependent peak corresponds to surface-normal deformations which contribute to the traction jump even for a shear-only membrane as can be seen in Eq. (2.10). This contribution is due to the membrane curvature: in the planar case, surface-normal deformations do not contribute to the traction jump associated with shear at first order (cf. equation (A20) of Ref. [52]) and therefore this peak is not observed for the planar membrane. Indeed, upon increasing the capsule radius (decreasing b), the second peak gradually shifts towards lower frequencies and eventually disappears for $b \to 0$.

In Fig. 3, we plot the variations of the rescaled peak frequency occurring in the imaginary part of the particle self-mobility versus particle radius b at different values of h. For sufficiently small particles ($b < 0.05$), the peak frequency shows a quadratic increase with particle radius b. By rescaling the peak frequencies by $(h/b)^2$, a master curve is obtained and the peak frequency position can accurately be computed from the relation $\beta_{\text{peak}} = 2h^2$.

3.2 Bending contribution

For a bending-only membrane, the mobility correction is readily obtained after plugging the series coefficients B_n and A_n respectively given by Eqs. (2.54) and (2.56) into Eq. (3.3). In particular, by taking $\alpha_{\text{B}} \to \infty$, the leading order self-mobility correction can conveniently be approximated by

$$\frac{\Delta\mu_{\text{B},\infty}}{\mu_0} := \lim_{\alpha_{\text{B}}\to\infty} \frac{\Delta\mu_{\text{B}}}{\mu_0} \simeq -\frac{7\xi^3}{4(1-\xi^2)}\left[1+\frac{\xi^2}{5}-\frac{9\xi^4}{70}\right]\frac{b}{R}\,, \tag{3.7}$$

which, for an infinite radius reads

$$\frac{\Delta\mu_{\text{B},\infty}}{\mu_0} = -\frac{15}{16}\frac{b}{h}\,, \tag{3.8}$$

corresponding to the vanishing frequency limit for a planar membrane with bending-only as calculated in earlier work [52]. Note that this limit is the same as that for a flat fluid-fluid interface separating two immiscible liquids having the same dynamic viscosity [7].

We define the characteristic frequency for bending as $\beta_{\text{B}} := 2h(4\eta\omega/\kappa_{\text{B}})^{1/3}$. In Fig. 4, we present the particle self-mobility correction nearby a membrane exhibiting a bending-only resistance versus β_{B}. Unlike a membrane with shearing resistance only, the particle mobility correction nearby a bending-only membrane does not exhibit a second peak of pronounced amplitude. The single peak observed is the characteristic peak for bending which occurs at $\beta_{\text{B}}^3 \sim 1$ and is largely independent of the radius. In fact, this peak position can be estimated by a balance between fluid viscosity and membrane bending such that $\omega \sim \kappa_{\text{B}}/(\eta h^3)$. As can be seen from equations (2.11), the traction jump for a bending-only membrane involves only the radial deformation which explain the absence of a second peak in contrast to the two-peak structure seen in the shearing-only case.

As already pointed out in Sec. 2, the hard-sphere solution is not recovered for a bending-only membrane in the vanishing frequency limit. A similar trend has been observed in earlier work for planar membranes where bending alone is not sufficient to recover the hard-wall limit [52]. This feature is again justified by the fact that the traction jumps due to bending in Eq. (2.11) do not depend on the tangential displacement u_θ. Even when considering an infinite bending modulus κ_{B}, the tangential component of the membrane displacement is thus still completely free. This behavior

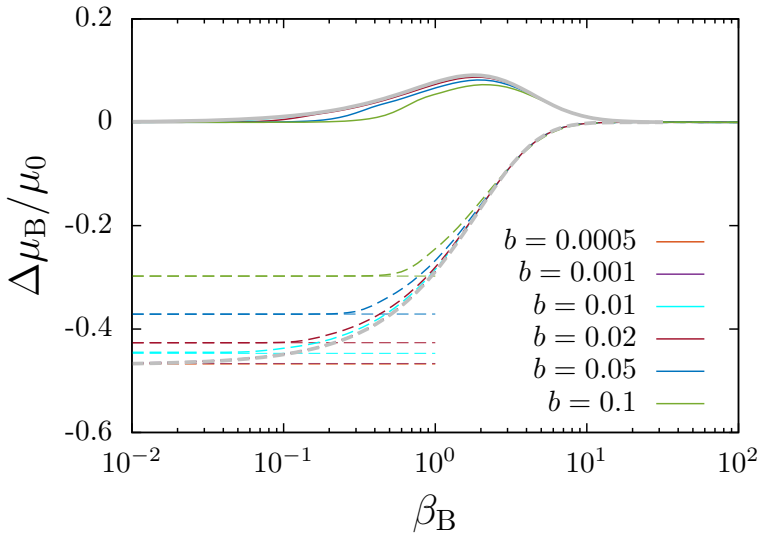

Figure 4: (Color online) Scaled self-mobility correction versus β_B for various values of the capsule radius, for a bending-only membrane. The dashed and continuous lines represent the real and imaginary parts respectively. The horizontal dashed lines are the vanishing frequency limits as approximated be Eq. (3.7). The curve in gray is the solution for a planar membrane given by Eq. (3.9). Here we take $h = 2b$.

cannot represent the hard sphere where both radial and tangential displacements are restricted.

We further remark that for smaller values of b, the evolution of both the real and imaginary part is found to be in excellent agreement with the solution for a planar membrane [52] in the whole range of frequencies:

$$\frac{\Delta\mu_B(\beta_B)}{\mu_0} = \frac{3i\beta_B}{8}\frac{b}{h}\left(\left(\frac{\beta_B^2}{12}+\frac{i\beta_B}{6}+\frac{1}{6}\right)\phi_+ + \frac{\sqrt{3}}{6}(\beta_B+i)\phi_- + \frac{5i}{2\beta_B} + \left(\frac{\beta_B^2}{12}-\frac{i\beta_B}{3}-\frac{1}{3}\right)e^{-i\beta_B}\,\mathrm{E}_1(-i\beta_B)\right), \tag{3.9}$$

with

$$\phi_\pm = e^{-i\overline{z_B}}\,\mathrm{E}_1(-i\overline{z_B}) \pm e^{-iz_B}\,\mathrm{E}_1(-iz_B)\,, \tag{3.10}$$

where $z_B := \beta_B e^{2i\pi/3}$.

We therefore conclude that for large capsules, the mobility correction for a bending-only membrane can be appropriately estimated from the planar membrane limit. For moderate capsule radii, the planar membrane prediction gives a reasonable agreement only in the high frequency regime for which $\beta_B \gg 1$.

3.3 Shearing-bending coupling

Unlike for a single planar membrane, shearing and bending are intrinsically coupled for a spherical membrane and the particle mobility near a membrane exhibiting shearing and bending resistance cannot be obtained by linear superposition as for a planar membrane [52]. A similar coupling is also observed for the mobility of a particle between two parallel planar membranes [53] as well as for thermal fluctuations of two closely-coupled [71] or "warped" [72] membranes. Therefore, the solution requires to simultaneously consider shearing and bending in the traction jump equations. In order to investigate this coupling effect, we define the reduced bending modulus as $E_B := \kappa_B/(\kappa_S h^2)$, a

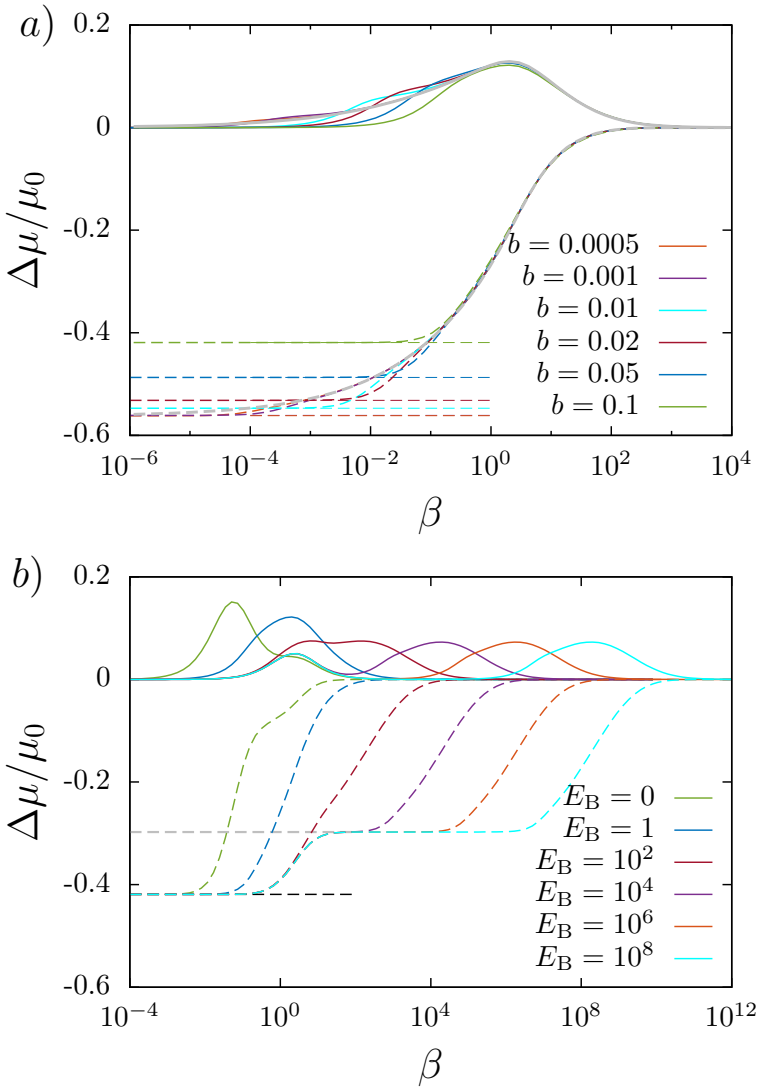

Figure 5: (Color online) *a*) Scaled particle self-mobility correction versus β for various values of the particle radius b for a membrane endowed with both shearing and bending rigidities. The real and imaginary parts are shown as dashed and solid lines respectively. Horizontal dashed lines represent the hard-sphere limit as given by Eq. (3.4). The curve in gray corresponds to the self-mobility correction for a planar membrane as obtained by linear superposition of Eqs. (3.6) and (3.9). Here we set the solid particle at $h = 2b$ and we take a reduced bending modulus $E_B = 1$. *b*) Scaled self-mobility correction versus β for various values of the reduced bending modulus. The horizontal black dashed line is the hard-sphere limit given by Eq. (3.4) whereas the gray dashed line is the infinite bending rigidity limit for a bending-only membrane as given by Eq. (3.7). Here we take $b = 1/10$ and $h = 2b$.

parameter that quantifies the relative contributions of shearing and bending.

In Fig. 5 *a*) we show the scaled self-mobility correction versus β nearby a membrane with both shearing and bending resistances upon varying b. We observe that in the high frequency regime, i.e. for $\beta > 1$, the mobility correction follows faithfully the evolution predicted for a planar membrane. For lower values of b, the planar membrane solution provides a very good estimation even deeper into the low frequency regime. Here, we take $h = 2b$ and a reduced bending modulus $E_B = 1$, for which shearing and bending manifest themselves equally.

In Fig. 5 *b*), we show the mobility correction versus β for a membrane with both rigidities

upon varying the reduced bending modulus E_B while keeping $b = 1/10$ and $h = 2b$. For $E_\mathrm{B} = 0$ corresponding to a shearing-only membrane, a low frequency peak as in Fig. 2 is observed. For $E_\mathrm{B} \approx 1$ and above, this peak quickly disappears which confirms our hypothesis that it is due to radial deformations as reasoned above: In the case of large bending resistance these deformations are suppressed and therefore the peak height diminishes and eventually disappears.

The imaginary part exhibits an additional peak of typically constant height that is shifted progressively toward the higher frequency domain for increasing E_B. From the definitions of β and β_B, it can be seen that

$$\beta_\mathrm{B}^3 = \frac{16}{3BE_\mathrm{B}}\,\beta\,. \tag{3.11}$$

Therefore, the peak observed at $\beta \sim 1$ is attributed to shearing whereas the high frequency peak is attributed to bending because $\beta \sim E_\mathrm{B}$ when $\beta_\mathrm{B}^3 \sim 1$. Particularly, for $E_\mathrm{B} = 1$, the position of the two peaks coincides as $\beta \sim \beta_\mathrm{B}^3$ for which shearing and bending have equal contribution.

4 Capsule motion and deformation

Next, we examine the capsule motion induced by the nearby moving solid particle. For this aim, we define the pair-mobility function μ^P as the ratio between the centroid velocity of the capsule V_1 and the force F_2 applied on the solid particle, i.e. $V_1 = \mu^\mathrm{P} F_2$. The net translational velocity of the capsule can readily be computed by volume integration of the z component of the fluid velocity inside the capsule [73],

$$V_1(\omega) = \frac{2\pi}{\Omega}\int_0^\pi\int_0^1 v_z^{(i)}(r,\theta,\omega)\,r^2\sin\theta\,\mathrm{d}r\mathrm{d}\theta\,, \tag{4.1}$$

where $\Omega := 4\pi/3$ being the volume of the undeformed capsule and $v_z^{(i)} = v_r^{(i)}\cos\theta - v_\theta^{(i)}\sin\theta$. Analytical expressions for $v_r^{(i)}$ and $v_\theta^{(i)}$ are given by Eqs. (2.32) and (2.33) respectively. After computation, only the terms with $n = 1$ of the series remain. The frequency-dependent pair-mobility reads

$$\mu^\mathrm{P} = -\frac{1}{8\pi\eta}(a_1 + b_1)\,, \tag{4.2}$$

which can be simplified to obtain

$$6\pi\eta\mu^\mathrm{P} = \frac{3}{2}\xi - \frac{\xi^3}{2}\frac{3 + (1+2C)\alpha}{5 + (1+2C)\alpha}\,. \tag{4.3}$$

The leading order pair-mobility correction is therefore expressed as a Debye-type model with a relaxation time given by

$$\tau = \frac{15}{2(1+2C)}\frac{\eta}{\kappa_\mathrm{S}}\,. \tag{4.4}$$

Interestingly, the pair-mobility μ^P depends only on the shear resistance of the membrane, but not on membrane bending properties. In the limiting cases, we recover two known results. First, for an infinite membrane shearing modulus, we get the leading-order pair-mobility between two unequal hard-spheres

$$\lim_{\alpha\to\infty} 6\pi\eta\mu^\mathrm{P} = \frac{3}{2}\xi - \frac{\xi^3}{2}\,. \tag{4.5}$$

Second, for a vanishing membrane shearing modulus, we obtain the leading-order pair-mobility

between a solid particle and a viscous drop

$$\lim_{\alpha\to 0} 6\pi\eta\mu^{\mathrm{P}} = \frac{3}{2}\xi - \frac{3}{10}\xi^3\,, \tag{4.6}$$

both of which are in agreement with those reported by Fuentes *et al.* [57, Eq. (12)].

Membrane deformation

In this subsection, we compute the capsule deformation resulting from an arbitrary time-dependent point-force F acting nearby the spherical capsule. The membrane displacement field is related to the fluid velocity at $r = 1$ via the no-slip equation given by Eq. (2.12). In order to proceed, we define the frequency-dependent reaction tensor ψ_{ij} as

$$u_i(\theta,\omega) = \psi_{ij}(\theta,\omega)F_j(\omega)\,. \tag{4.7}$$

By setting a harmonic driving force $F_i(t) = K_i e^{i\omega_0 t}$, which in the frequency domain reads $F_i(\omega) = 2\pi K_i\delta(\omega-\omega_0)$, the membrane time-dependent displacement can readily be evaluated by inverse Fourier transform of Eq. (4.7) to obtain

$$u_i(\theta,t) = \psi_{ij}(\theta,\omega_0)K_j e^{i\omega_0 t}\,. \tag{4.8}$$

In an axisymmetric situation, we are interested in the components ψ_{rz} and $\psi_{\theta z}$ of the reaction tensor, giving access to the displacements u_r and u_θ under the action of a point force directed along the z direction. By making use of Eqs. (2.32) and (2.33), we immediately obtain

$$\psi_{rz} = -\frac{1}{8\pi\eta i\omega}\sum_{n=1}^{\infty}\left[\frac{n(n+1)}{2}a_n + nb_n\right]P_n(\cos\theta)\,, \tag{4.9a}$$

$$\psi_{\theta z} = -\frac{1}{8\pi\eta i\omega}\sum_{n=1}^{\infty}\left[\frac{n+3}{2}a_n + b_n\right]\frac{\mathrm{d}P_n(\cos\theta)}{\mathrm{d}\theta}\,. \tag{4.9b}$$

The first derivative of Legendre polynomial can be computed using the recurrence formula [65]

$$\frac{\mathrm{d}P_n(\cos\theta)}{\mathrm{d}\theta} = -\frac{n}{\sin\theta}\Big[P_{n-1}(\cos\theta) - \cos\theta P_n(\cos\theta)\Big]\,.$$

5 Comparison with boundary integral simulations

In order to assess the appropriateness of the point particle approximation employed throughout this work, we shall compare our analytical predictions with fully resolved boundary integral simulations of truly extended particles. The simulations are based on the completed double-layer boundary integral equation method (CDLBIEM) [74–76] which allows for the efficient simulation of deformable as well as truly solid objects. Details on the algorithm and its implementation have been reported elsewhere, see for instance Refs. [53, 77, 78].

For the determination of the solid particle self-mobility, a harmonic oscillating force $Ke^{i\omega_0 t}$ is applied at the surface of the particle along the z direction. After a transient evolution, the particle begins to oscillate with the same frequency ω_0 as $V_2 e^{i(\omega_0 t+\delta_2)}$. The velocity amplitude V_2 and phase shift δ_2 are accurately determined by fitting the numerically recorded velocity using the trust region method [79]. The frequency-dependent self-mobility of the solid particle is then computed as $\mu = (V_2/K)e^{i\delta_2}$. Under the effect of the oscillating force, the volume centroid of the capsule undergoes

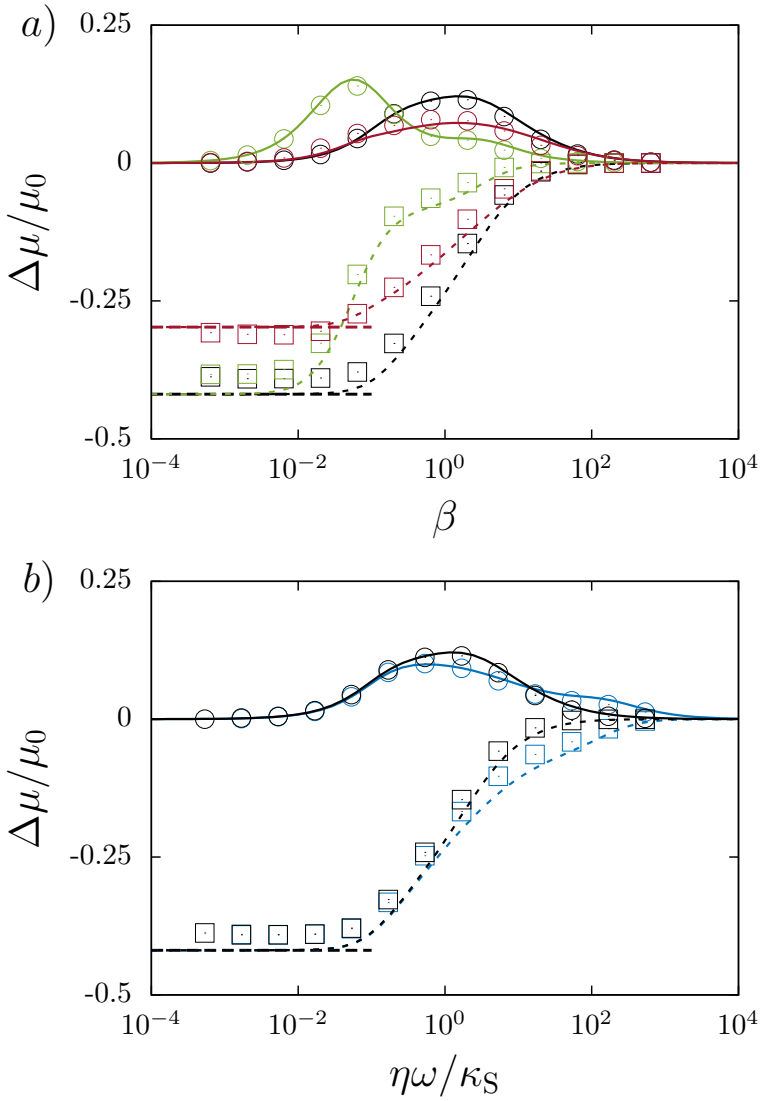

Figure 6: (Color online) *a*) Scaled frequency-dependent particle mobility correction versus the scaled frequency β nearby a membrane endowed with only shearing (green / light gray), only bending (red / dark gray) and both rigidities (black). The small particle has a radius $b = 1/10$ set a distance $h = 2b$. Here we take $C = 1$ and a reduced bending modulus $E_B = 2/3$. The theoretical predictions are shown as dashed lines for the real parts and as solid lines for the imaginary parts. Symbols refer to boundary integral simulations where the real and imaginary parts are shown as squares and circles respectively. The horizontal dashed lines are the vanishing frequency limits given by Eqs. (3.4) and (3.7). *b*) shows the scaled frequency-dependent mobility correction versus $\eta\omega/\kappa_S$ nearby a membrane endowed with both shearing and bending rigidities for $C = 1$ (black) and $C = 100$ (blue / dark gray) for the same set of parameters in *a*).

an oscillatory motion along the z direction as $X_1 e^{i(\omega_0 t+\delta_1)}$. The capsule pair-mobility is therefore computed as $\mu^P = (i\omega_0 X_1/K)e^{i\delta_1}$.

In Fig. 6 *a*), we present the scaled self-mobility correction versus the scaled frequency β as given theoretically by Eq. (3.3). The solid particle has a radius $b = 1/10$ positioned at $h = 2b$ nearby a large capsule. For the simulations parameters, we take $C = 1$ and $E_B = 2/3$. Results for shearing-only and bending-only membrane are also shown in green and red respectively. We observe that in the

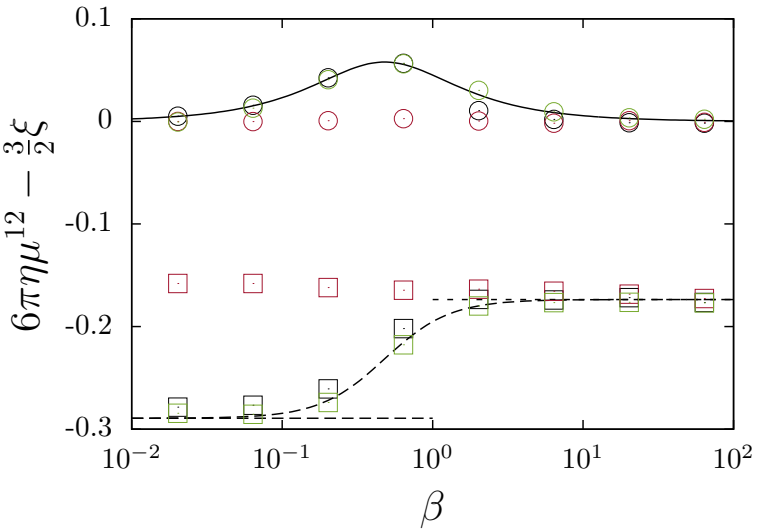

Figure 7: (Color online) Scaled Pair-mobility correction versus the scaled frequency nearby a membrane possessing only shearing (green / light gray), only bending (red / dark gray) and both rigidities (black). The analytical prediction given by Eq. (4.3) is shown as dashed line for the real part and as solid line for the imaginary part. Simulation results are shown as squares and circles for the real and imaginary parts, respectively. The horizontal dashed lines are the vanishing frequency limit predicted by Eq. (4.5) where the dotted lines are the limit corresponding to vanishing membrane moduli as given by Eq. (4.6).

low-frequency regime, the near hard-sphere mobility correction is approached only if the membrane exhibits a resistance towards shearing, in agreement with theoretical calculations.

In Fig. 6 *b*), we show the scaled self-mobility correction for $C = 1$ and $C = 100$. A very large C is typical for vesicles or red blood cells [80–82] where the surface area remains almost unchanged during deformation. We observe that the effect of area expansion is more pronounced in the high frequency regime. A very good agreement is obtained between analytical predictions and boundary integral simulations over the whole range of applied frequencies.

We now turn to the motion of the capsule. In Fig. 7, we show the correction to the scaled pair-mobility versus the scaled frequency β. The correction for a shearing-only membrane is almost indistinguishable from that of a membrane with both shearing and bending rigidities. In the low-frequency regime for which $\beta \ll 1$, the pair-mobility correction approaches that near a hard-sphere given by Eq. (4.5). On the other hand, in the high-frequency regime for which $\beta \gg 1$, the correction approaches that near a viscous drop as given by Eq. (4.6). Moreover, the correction nearby a bending-only membrane remains typically unchanged over the whole range of frequencies, and equals that for a viscous drop. Indeed, these observations are in complete agreement with the analytical prediction stated by Eq. (4.3).

In Fig. 8, we show the membrane scaled radial and meridional displacements versus the polar angle θ at quarter period for $t\omega_0 = \pi/2$. The natural scale for membrane deformation is K_z/κ_S the ratio between the forcing amplitude K_z and the shearing resistance κ_S. We observe that the radial displacement u_r is a monotonically decreasing function of θ and eventually changes sign at some intermediate angle. On the other hand, the meridional displacement u_θ is negatively valued and vanishes at $\theta = 0$ and $\theta = \pi$ due to the system axial symmetry, suggesting the existence of an extremum in between. Moreover, the maximum displacement reached in u_r is found to be about 3 times larger in comparison to that reached in u_θ.

By examining the displacement at various forcing frequencies, we observe that larger frequencies

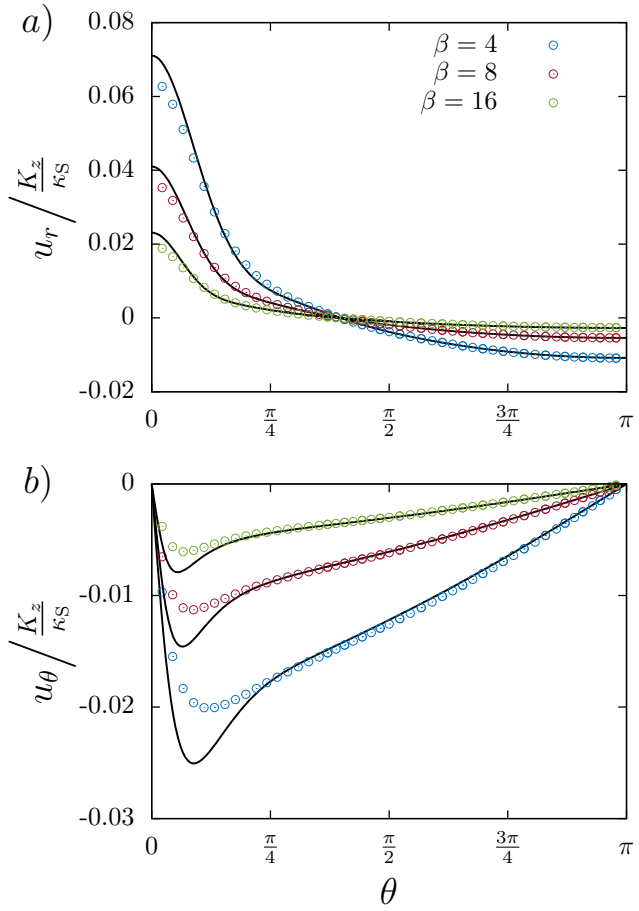

Figure 8: (Color online) Scaled radial a) and meridional b) membrane displacement versus the polar angle θ for three scaled forcing frequencies β at quarter period for $t\omega_0 = \pi/2$. Solid lines are the theoretical predictions obtained from Eqs. (4.9a) and (4.9b) and symbols are boundary integral simulations.

induce remarkably smaller deformation since the capsule membrane does not have enough time to respond to the fast oscillating particle. In typical situations, the forces acting by optical tweezers on suspended particles are of the order of 1 pN [83] and the capsule has a radius 10^{-6} m and a shearing modulus 5×10^{-6} N/m [84]. For a forcing frequency $\beta = 4$, the membrane undergoes a maximal deformation of about 1 % of its undeformed radius. Therefore, deformations are significantly small and deviations from sphericity are negligible. The analytical predictions based on the linear theory of small deformation are found to be in a good agreement with simulations. A small deviation is observed notably for u_θ at small angles which is possibly due to a finite size effect since the analytical predictions are based on the point-particle approximation whereas simulations treat truly extended particle of finite size.

6 Conclusion

Using the image solution technique, we have computed the leading-order hydrodynamic self-mobility of a solid spherical particle axisymmetrically moving nearby a large deformable capsule whose membrane exhibits resistance towards shearing and bending. The mobility corrections are expressed in terms of infinite but convergent series whose coefficients are frequency-dependent complex quantities. We have

shown that in the vanishing frequency limit, the particle self-mobility near a hard sphere is recovered only when the membrane possesses a resistance towards shearing. For a large membrane radius, our results perfectly overlap with those obtained earlier for a planar membrane in the high frequency regime. The major qualitative difference between the planar and the spherical membrane is the existence of a second, low-frequency peak in the imaginary part (and a corresponding dispersion step in the real part) caused by shear resistance. The appearance of two peaks can be understood by the simple fact that the membrane traction jump stemming from shear resistance contains contributions from normal (radial) as well as in-plane (tangential) displacements. For a planar membrane, only in-plane displacements contribute to shear resistance which explains why the observed peak disappears at large radii. For a bending-only membrane, curvature effects are much less pronounced and the planar membrane gives a fairly good approximation even deep in the low frequency regime.

Considering the capsule motion, we have found that the pair-mobility function depends solely on the membrane shearing properties and it can be well described by a Debye-like model with a single relaxation time. The pair-mobility function for a bending-only membrane is therefore frequency-independent and it is identical to that for a viscous drop. We have further found that the point particle approximation despite its simplicity leads to a very good agreement with the numerical simulations preformed for a truly extended particle using a completed double layer boundary integral method.

7 Acknowledgments

The authors thank the Volkswagen Foundation for financial support and acknowledge the Gauss Center for Supercomputing e.V. for providing computing time on the GCS Supercomputer SuperMUC at Leibniz Supercomputing Center. We thank Achim Guckenberger and Maciej Lisicki for useful discussions and technical support.

Appendices

A Membrane mechanics

In this appendix, we shall derive equations in spherical coordinates for the traction jump across a membrane endowed with shearing and bending rigidities. Here we follow the convention in which the symbols for the radial, azimuthal and polar angle coordinates are taken as r, ϕ and θ respectively, with the corresponding orthonormal basis vectors $\boldsymbol{e}_r$, $\boldsymbol{e}_\phi$ and $\boldsymbol{e}_\theta$. Similar, all the lengths will be scaled by capsule radius a. We denote by $\boldsymbol{a} = \boldsymbol{e}_r$ the position vector of the points located at the undisplaced membrane. After axisymmetric deformation, the vector position reads

$$\boldsymbol{r} = (1 + u_r)\boldsymbol{e}_r + u_\theta \boldsymbol{e}_\theta \,, \tag{A.1}$$

where u_r and u_θ denote the radial and meridional displacements. In the following, capital Roman letters shall be reserved for the undeformed state while small letters for the deformed. The spherical membrane can be defined by the covariant base vectors $\boldsymbol{g}_1 := \boldsymbol{r}_{,\theta}$ and $\boldsymbol{g}_2 := \boldsymbol{r}_{,\phi}$. The unit normal vector $\boldsymbol{n}$ is defined in such a way to form a direct trihedron with $\boldsymbol{g}_1$ and $\boldsymbol{g}_2$. The covariant base vectors are

$$\boldsymbol{g}_1 = (u_{r,\theta} - u_\theta)\boldsymbol{e}_r + (1 + u_r + u_{\theta,\theta})\boldsymbol{e}_\theta \,, \tag{A.2a}$$

$$\boldsymbol{g}_2 = \big((1 + u_r)\sin\theta + u_\theta \cos\theta\big)\boldsymbol{e}_\phi \,, \tag{A.2b}$$

and the unit normal vector at leading order in deformation reads

$$\boldsymbol{n} = \boldsymbol{e}_r - (u_{r,\theta} - u_\theta)\,\boldsymbol{e}_\theta\,. \tag{A.3}$$

Note that $\boldsymbol{g}_1$ and $\boldsymbol{g}_2$ have (scaled) length dimension while $\boldsymbol{n}$ is dimensionless. In the deformed state, the components of the metric tensor are defined by the scalar product $g_{\alpha\beta} = \boldsymbol{g}_\alpha \cdot \boldsymbol{g}_\beta$. The contravariant tensor $g^{\alpha\beta}$, defined as the inverse of the metric tensor, is linearized as

$$g^{\alpha\beta} = \begin{pmatrix} 1 - 2\epsilon_{\theta\theta} & 0 \\ 0 & \frac{1-2\epsilon_{\phi\phi}}{\sin^2\theta} \end{pmatrix}, \tag{A.4}$$

where $\epsilon_{\alpha\beta}$ represents the components of the in-plane strain tensor written in spherical coordinates as [85]

$$\epsilon_{\theta\theta} = u_r + u_{\theta,\theta}\,, \tag{A.5a}$$
$$\epsilon_{\phi\phi} = u_r + u_\theta \cot\theta\,. \tag{A.5b}$$

The contravariant tensor in the undeformed state $G^{\alpha\beta}$ can immediately be obtained by considering a vanishing strain tensor in Eq. (A.4).

A.1 Shearing contribution

In this subsection, we shall derive the traction jump equations across a membrane endowed with an in-plane shearing resistance. The two invariants of the strain tensor are given by Green and Adkins as [86, 87]

$$I_1 = G^{\alpha\beta} g_{\alpha\beta} - 2\,, \tag{A.6a}$$
$$I_2 = \det G^{\alpha\beta} \det g_{\alpha\beta} - 1\,. \tag{A.6b}$$

The contravariant components of the stress tensor $\tau^{\alpha\beta}$ can then be obtained provided knowledge of the membrane constitutive elastic law, whose areal strain energy functional is $W(I_1, I_2)$, such that [88]

$$\tau^{\alpha\beta} = \frac{2}{J_\mathrm{S}} \frac{\partial W}{\partial I_1} G^{\alpha\beta} + 2J_\mathrm{S} \frac{\partial W}{\partial I_2} g^{\alpha\beta}\,, \tag{A.7}$$

where $J_\mathrm{S} := \sqrt{1 + I_2}$ is the Jacobian determinant, prescribing the ratio between deformed and undeformed local areas. In the linear theory of elasticity, $J_\mathrm{S} \simeq 1 + e$, where $e := \epsilon_{\theta\theta} + \epsilon_{\phi\phi}$ being the trace of the in-plane strain tensor, commonly know as the dilatation. In this work, we use the Skalak model to describe the elastic properties of the capsule membrane, whose areal strain energy reads [84, 89]

$$W(I_1, I_2) = \frac{\kappa_\mathrm{S}}{12}\left(I_1^2 + 2I_1 - 2I_2 + CI_2^2\right), \tag{A.8}$$

where $C := \kappa_\mathrm{A}/\kappa_\mathrm{S}$. Note that for $C = 1$, the Skalak model is equivalent to the Neo-Hookean model for small deformations [88]. After plugging Eq. (A.8) into Eq. (A.7), the linearized in-plane stress tensor reads

$$\tau^{\alpha\beta} = \frac{2\kappa_\mathrm{S}}{3} \begin{pmatrix} \epsilon_{\theta\theta} + Ce & 0 \\ 0 & \frac{\epsilon_{\phi\phi}+Ce}{\sin^2\theta} \end{pmatrix}. \tag{A.9}$$

The membrane equilibrium equations balancing the elastic and external forces read

$$\nabla_\alpha \tau^{\alpha\beta} + \Delta f^\beta = 0\,, \tag{A.10a}$$
$$\tau^{\alpha\beta} b_{\alpha\beta} + \Delta f^n = 0\,, \tag{A.10b}$$

where $\Delta \boldsymbol{f} = \Delta f^\beta \boldsymbol{g}_\beta + \Delta f^n \boldsymbol{n}$ is the traction jump across the membrane and ∇_α denotes the covariant derivative defined for a second-rank tensor as

$$\nabla_\alpha \tau^{\alpha\beta} = \tau^{\alpha\beta}_{,\alpha} + \Gamma^\alpha_{\alpha\eta}\tau^{\eta\beta} + \Gamma^\beta_{\alpha\eta}\tau^{\alpha\eta}\,, \tag{A.11}$$

and $\Gamma^\lambda_{\alpha\beta}$ are the Christoffel symbols of the second kind defined as [90] [ch. 2]

$$\Gamma^\lambda_{\alpha\beta} = \frac{1}{2} g^{\lambda\eta}\left(g_{\alpha\eta,\beta} + g_{\eta\beta,\alpha} - g_{\alpha\beta,\eta}\right)\,. \tag{A.12}$$

Continuing, $b_{\alpha\beta}$ is the second fundamental form (curvature tensor) defined as

$$b_{\alpha\beta} = \boldsymbol{g}_{\alpha,\beta} \cdot \boldsymbol{n}\,. \tag{A.13}$$

Note that at zeroth order, the non-vanishing components of the Christoffel symbols are $\Gamma^\phi_{\phi\theta} = \Gamma^\phi_{\theta\phi} = \cot\theta$ and $\Gamma^\theta_{\phi\phi} = -\sin\theta\cos\theta$. After some algebra, we find that the meridional tangential traction jump across the membrane given by Eq. (A.10a) reads

$$\tau^{\theta\theta}_{,\theta} + \Gamma^\phi_{\phi\theta}\tau^{\theta\theta} + \Gamma^\theta_{\phi\phi}\tau^{\phi\phi} + \Delta f^\theta = 0\,. \tag{A.14}$$

At zeroth order, the non-vanishing components of the curvature tensor are $b_{\theta\theta} = -1$ and $b_{\phi\phi} = -\sin^2\theta$. For the normal traction jump Eq. (A.10b) we therefore get

$$-\tau^{\theta\theta} - \sin^2\theta\,\tau^{\phi\phi} + \Delta f^n = 0\,. \tag{A.15}$$

After substitution and writing the projected equations in the spherical coordinates basis vectors, we immediately get the following set of equations,

$$\frac{2\kappa_\mathrm{S}}{3}\Big((1+C)\epsilon_{\theta\theta,\theta} + C\epsilon_{\phi\phi,\theta} + (\epsilon_{\theta\theta} - \epsilon_{\phi\phi})\cot\theta\Big) + \Delta f_\theta = 0\,, \tag{A.16a}$$
$$-\frac{2\kappa_\mathrm{S}}{3}(1+2C)\,(\epsilon_{\theta\theta} + \epsilon_{\phi\phi}) + \Delta f_n = 0\,. \tag{A.16b}$$

We further mention that for curved membranes, the normal traction jump does not vanish in the *plane stress* formulation employed here because the zeroth order in the curvature tensor is not identically null. Indeed, this is not the case for a planar elastic membrane where the resistance to shearing only introduces a jump in the tangential traction jumps [52, 53].

By substituting $\epsilon_{\theta\theta}$ and $\epsilon_{\phi\phi}$ with their expressions, Eqs. (A.16) turn into the traction jumps equations (2.10).

A.2 Bending contribution

For the bending resistance, we use the linear model, in which the bending moment is related to the curvature tensor via [91, 92]

$$M^\beta_\alpha = -\kappa_\mathrm{B}\left(b^\beta_\alpha - B^\beta_\alpha\right)\,, \tag{A.17}$$

where κ_B is the bending modulus and the spontaneous curvature is set to $B_\alpha^\beta = \boldsymbol{G}_{\alpha,\beta}\cdot\boldsymbol{n}$ corresponding to the undeformed sphere. The mixed version of the curvature tensor b_α^β is related to the covariant representation via $b_\alpha^\beta = b_{\alpha\delta}g^{\delta\beta}$. The contravariant components of the transverse shearing vector $\boldsymbol{Q}$ is obtained from a local torque balance with the applied moment as $Q^\beta = \nabla_\alpha M^{\alpha\beta}$. Note that the raising and lowering indices operations imply that $M^{\alpha\beta} = g^{\alpha\gamma}g^{\beta\delta}M_{\gamma\delta}$ and that $M_{\alpha\beta} = M_\alpha^\delta g_{\delta\beta}$. The meridional force reads

$$Q^\theta = -\kappa_\mathrm{B}\Big(\left(1-\cot^2\theta\right)u_{r,\theta} + u_{r,\theta\theta}\cot\theta + u_{r,\theta\theta\theta}\Big)\,.$$

The membrane equilibrium equations balancing the bending forces reads

$$-b_\alpha^\beta Q^\alpha + \Delta f^\beta = 0\,, \tag{A.18a}$$
$$\nabla_\alpha Q^\alpha + \Delta f^n = 0\,, \tag{A.18b}$$

where for a first-rank tensor (vector) the covariant derivative is defined as $\nabla_\beta Q^\alpha = \partial_\beta Q^\alpha + \Gamma^\alpha_{\beta\delta}Q^\delta$. The equilibrium equations can thus be written as

$$-\kappa_\mathrm{B}\left(\left(1-\cot^2\theta\right)u_{r,\theta} + u_{r,\theta\theta}\cot\theta + u_{r,\theta\theta\theta}\right) + \Delta f_\theta = 0\,, \tag{A.19a}$$
$$-\kappa_\mathrm{B}\Big(\left(3\cot\theta+\cot^3\theta\right)u_{r,\theta} - u_{r,\theta\theta}\cot^2\theta + 2u_{r,\theta\theta\theta}\cot\theta + u_{r,\theta\theta\theta\theta}\Big) + \Delta f_n = 0 \tag{A.19b}$$

corresponding to the traction jump given in Eq. (2.11).

B Transformation equations between the scaled and physical quantities

In this appendix, we shall state the transformation relations between the scaled and physical quantities. The physical quantities are denoted by a tilde while the absence of tilde refers to the scaled ones. For the variables with the dimension of length, such as r and R, we have $\tilde{r} = ra$ and $\tilde{R} = Ra$. For the velocity we have $\tilde{v} = va$, for the force $\tilde{F} = Fa$, for the fluid viscosity $\tilde{\eta} = \eta/a$, for the pressure $\tilde{p} = p/a$ and similar for the traction jump $\tilde{\Delta f} = \Delta f/a$. For the shearing modulus $\tilde{\kappa_\mathrm{S}} = \kappa_\mathrm{S}$, for the bending modulus $\tilde{\kappa_\mathrm{B}} = \kappa_\mathrm{B}a^2$. It follows that $\tilde{\alpha} = \alpha a$ and $\tilde{\alpha_\mathrm{B}} = \alpha_\mathrm{B}a^3$.

C Force-free condition

In this appendix, we shall show that for finite shearing modulus, the force free condition assumed for the capsule is satisfied.

The induced hydrodynamic force on the capsule is computed by integrating the normal stress vector over the capsule's outside surface A^+ as [93]

$$\boldsymbol{F}_1 = \int_{A^+}\boldsymbol{\sigma}\cdot\boldsymbol{e}_r\,\mathrm{d}A = A_0\boldsymbol{F}_2\,, \tag{C.1}$$

meaning that the hydrodynamic force in the multipole expansion is given only by the coefficient of the monopole field [59]. For shearing-only and bending-only membranes, we have shown that $A_0 = 0$ as can be inferred from Eqs. (2.48) and (2.56). This is the case also for a membrane with both shearing and bending resistances. We therefore conclude that no net force is exerted on the capsule.

We note that, for infinite shearing modulus, i.e. in the hard-sphere limit, $A_0 \neq 0$ as can clearly be seen in Eq. (2.50a). Additional singularities therefore need to be added to the reflected flow field

in order to ensure the force free assumption (see Ref. [57] for further details.)

D Estimation of the number of terms required for the computation of particle self-mobility

In this appendix, we shall determine the number of terms required for the computation of particle self-mobility in order to achieve a given precision.

Let us denote by $f_n(\xi)$ the general term of the function series giving the particle mobility correction in Eq. (3.3). For a large value of n, we have the leading order asymptotic behavior

$$f_n(\xi) = \frac{3b}{8}\left(1-\xi^2\right)^2 n^2 \xi^{2n+4} + \mathcal{O}\left(n\xi^{2n}\right) , \tag{D.1}$$

which does not depend on capsule shearing and bending properties. In order to compute an infinite series numerically up to a given precision, we define the truncation error as

$$E(N) := \left| \sum_{n=N+1}^{\infty} f_n(\xi) \right| \simeq \frac{3b}{8} \frac{-N^2\xi^4 + (2N^2+2N-1)\xi^2 - (N+1)^2}{1-\xi^2} \xi^{2N+6} .$$

Given a certain precision ε, the number of terms N required to achieve the desired precision can be determined by solving the inequality $E(N) < \varepsilon$. For example, by taking $h = 2b$, $b = 1/10$ and requiring a precision $\varepsilon = 10^{-4}$, only 29 terms in the series are needed. For $b = 10^{-3}$ however, 2993 terms are needed. As a result, more terms are required for convergence when the capsule radius is taken very large, i.e. when $\xi \sim 1$. By requiring a precision $\varepsilon = 10^{-6}$, 44 and 4316 terms are necessary for $b = 1/10$ and $b = 10^{-3}$ respectively. A precision of $\varepsilon = 10^{-4}$ has been consistently adopted throughout this work.

Bibliography

[1] H. Maeda, H. Nakamura, and J. Fang, Adv. Drug Deliv. Rev. **65**, 71 (2013).

[2] D. Chu, J. Gao, and Z. Wang, ACS Nano **9**, 11800 (2015).

[3] H. A. Lorentz, Abh. Theor. Phys. **1**, 23 (1907).

[4] H. Brenner, Chem. Eng. Sci. **16**, 242 (1961).

[5] A. J. Goldman, R. G. Cox, and H. Brenner, Chem. Eng. Sci. **22**, 637 (1967).

[6] A. J. Goldman, R. G. Cox, and H. Brenner, Chem. Eng. Sci. **22**, 653 (1967).

[7] S. H. Lee, R. S. Chadwick, and L. G. Leal, J. Fluid Mech. **93**, 705 (1979).

[8] S. H. Lee and L. G. Leal, J. Fluid Mech. **98**, 193 (1980).

[9] B. Cichocki and R. B. Jones, Physica A **258**, 273 (1998).

[10] L. P. Faucheux and A. J. Libchaber, Phys. Rev. E **49**, 5158 (1994).

[11] B. U. Felderhof, J. Phys. Chem. B **109**, 21406 (2005).

[12] E. Lauga and T. M. Squires, Phys. Fluids **17**, 103102 (2005).

[13] T. Bickel, Phys. Rev. E **75**, 041403 (2007).

[14] J. W. Swan and J. F. Brady, Phys. Fluids **19**, 113306 (2007).

[15] T. Franosch and S. Jeney, Phys. Rev. E **79**, 031402 (2009).

[16] J. Bławzdziewicz, M. Ekiel-Jeżewska, and E. Wajnryb, J. Chem. Phys. **133**, 114703 (2010).

[17] J. Bławzdziewicz, M. Ekiel-Jeżewska, and E. Wajnryb, J. Chem. Phys. **133**, 114702 (2010).

[18] M. Lisicki, B. Cichocki, and E. Wajnryb, J. Chem. Phys. **145**, 034904 (2016).

[19] E. R. Dufresne, D. Altman, and D. G. Grier, Europhys. Lett. **53**, 264 (2001).

[20] M. D. Carbajal-Tinoco, R. Lopez-Fernandez, and J. L. Arauz-Lara, Phys. Rev. Lett. **99**, 138303 (2007).

[21] P. Huang and K. Breuer, Phys. Rev. E **76**, 046307 (2007).

[22] C. K. Choi, C. H. Margraves, and K. D. Kihm, Phys. Fluids **19**, 103305 (2007).

[23] E. Schäffer, S. F. Nørrelykke, and J. Howard, Langmuir **23**, 3654 (2007).

[24] G. M. Wang, R. Prabhakar, and E. M. Sevick, Phys. Rev. Lett. **103**, 248303 (2009).

[25] V. N. Michailidou, G. Petekidis, J. W. Swan, and J. F. Brady, Phys. Rev. Lett. **102**, 068302 (2009).

[26] Y. Kazoe and M. Yoda, Appl. Phys. Lett. **99**, 124104 (2011).

[27] M. Lisicki, B. Cichocki, J. K. G. Dhont, and P. R. Lang, J. Chem. Phys. **136**, 204704 (2012).

[28] S. A. Rogers, M. Lisicki, B. Cichocki, J. K. G. Dhont, and P. R. Lang, Phys. Rev. Lett. **109**, 098305 (2012).

[29] S. L. Dettmer, S. Pagliara, K. Misiunas, and U. F. Keyser, Phys. Rev. E **89**, 062305 (2014).

[30] M. Lisicki, B. Cichocki, S. A. Rogers, J. K. G. Dhont, and P. R. Lang, Soft Matter **10**, 4312 (2014).

[31] W. Wang and P. Huang, Phys. Fluids **26**, 092003 (2014).

[32] K. Misiunas, S. Pagliara, E. Lauga, J. R. Lister, and U. F. Keyser, Phys. Rev. Lett. **115**, 038301 (2015).

[33] Y. Liu, J. Bławzdziewicz, B. Cichocki, J. K. G. Dhont, M. Lisicki, E. Wajnryb, Y.-N. Young, and P. R. Lang, Soft Matter **11**, 7316 (2015).

[34] B. Tränkle, D. Ruh, and A. Rohrbach, Soft Matter **12**, 2729 (2016).

[35] J. C. Benavides-Parra, D. Jacinto-Méndez, G. Brotons, and M. D. Carbajal-Tinoco, J. Chem. Phys. **145**, 114902 (2016).

[36] R. Shlomovitz, A. Evans, T. Boatwright, M. Dennin, and A. Levine, Phys. Rev. Lett. **110**, 137802 (2013).

[37] T. Boatwright, M. Dennin, R. Shlomovitz, A. A. Evans, and A. J. Levine, Phys. Fluids **26**, 071904 (2014).

[38] F. Jünger, F. Kohler, A. Meinel, T. Meyer, R. Nitschke, B. Erhard, and A. Rohrbach, Biophys. J. **109**, 869 (2015).

[39] M. Irmscher, A. M. de Jong, H. Kress, and M. W. J. Prins, Biophys. J. **102**, 698 (2012).

[40] D. Mizuno, Y. Kimura, and R. Hayakawa, Phys. Rev. E **70**, 011509 (2004).

[41] Y. Kimura, T. Mori, A. Yamamoto, and D. Mizuno, J. Phys. Condens. Matter **17**, S2937 (2005).

[42] A. E. Cervantes-Martínez, A. Ramírez-Saito, R. Armenta-Calderón, M. A. Ojeda-López, and J. L. Arauz-Lara, Phys. Rev. E **83**, 030402 (2011).

[43] T. A. Waigh, Rep. Prog. Phys. **79**, 074601 (2016).

[44] T. Salez and L. Mahadevan, J. Fluid Mech. **779**, 181 (2015).

[45] B. Saintyves, T. Jules, T. Salez, and L. Mahadevan, Proc. Nat. Acad. Sci. **113**, 5847 (2016).

[46] B. Rallabandi, B. Saintyves, T. Jules, T. Salez, C. Schönecker, L. Mahadevan, and H. A. Stone, arXiv preprint arXiv:1611.03552 (2016).

[47] T. Bickel, Eur. Phys. J. E **20**, 379 (2006).

[48] B. U. Felderhof, J. Chem. Phys. **125**, 144718 (2006).

[49] P. Vorobev, Phys. Rev. E **77**, 046306 (2008).

[50] R. Shlomovitz, A. A. Evans, T. Boatwright, M. Dennin, and A. J. Levine, Phys. Fluids **26** (2014).

[51] T. Bickel, EPL (Europhys. Lett.) **106**, 16004 (2014).

[52] A. Daddi-Moussa-Ider, A. Guckenberger, and S. Gekle, Phys. Rev. E **93**, 012612 (2016).

[53] A. Daddi-Moussa-Ider, A. Guckenberger, and S. Gekle, Phys. Fluids **28**, 071903 (2016).

[54] A. Daddi-Moussa-Ider, M. Lisicki, and S. Gekle, J. Fluid Mech. **811**, 210 (2017).

[55] A. Daddi-Moussa-Ider and S. Gekle, J. Chem. Phys. **145**, 014905 (2016).

[56] M. Thiébaud and T. Bickel, Phys. Rev. E **81**, 031602 (2010).

[57] Y. O. Fuentes, S. Kim, and D. J. Jeffrey, Phys. Fluids **31**, 2445 (1988).

[58] Y. O. Fuentes, S. Kim, and D. J. Jeffrey, Phys. Fluids A **1**, 61 (1989).

[59] S. Kim and S. J. Karrila, *Microhydrodynamics: principles and selected applications* (Courier Corporation, 2013).

[60] R. Skalak, A. Tozeren, R. P. Zarda, and S. Chien, Biophys. J. **13(3)**, 245 (1973).

[61] W. Helfrich, Z. Naturf. C. **28:693** (1973).

[62] C. Pozrikidis, J. Fluid Mech. **440**, 269 (2001).

[63] A. Guckenberger and S. Gekle, J. Phys. Cond. Mat. (submitted).

[64] H. Lamb, *Hydrodynamics* (Cambridge university press, 1932).

[65] M. Abramowitz, I. A. Stegun, *et al.*, *Handbook of mathematical functions*, Vol. 1 (Dover New York, 1972).

[66] R. G. Cox, J. Fluid Mech. **37**, 601 (1969).

[67] C. Misbah, Phys. Rev. Lett. **96**, 028104 (2006).

[68] M. Rachik, D. Barthès-Biesel, M. Carin, and F. Edwards-Levy, J. Colloid Interface Sci. **301**, 217 (2006).

[69] M. R. Spiegel, *Mathematical handbook of formulas and tables* (McGraw-Hill, 1968).

[70] M. L. Ekiel-Jeżewska and B. U. Felderhof, J. Chem. Phys. **142**, 014904 (2015).

[71] T. Auth, S. A. Safran, and N. S. Gov, Phys. Rev. E **76**, 051910 (2007).

[72] A. Košmrlj and D. R. Nelson, Phys. Rev. E **89**, 022126 (2014).

[73] B. U. Felderhof, J. Chem. Phys. **125**, 124904 (2006).

[74] M. Kohr and I. I. Pop, *Viscous incompressible flow for low Reynolds numbers*, Vol. 16 (Wit Pr/Comp. Mech., 2004).

[75] H. Zhao and E. S. G. Shaqfeh, Phys. Rev. E **83**, 061924 (2011).

[76] H. Zhao, E. S. G. Shaqfeh, and V. Narsimhan, Phys. Fluids **24**, 011902 (2012).

[77] A. Guckenberger, M. P. Schraml, P. G. Chen, M. Leonetti, and S. Gekle, Comput. Phys. Commun. **207**, 1 (2016).

[78] A. Guckenberger and S. Gekle, arXiv preprint arXiv:1608.05196 (2016).

[79] A. R. Conn, N. I. M. Gould, and P. L. Toint, *Trust region methods*, Vol. 1 (Siam, 2000).

[80] T. Krüger, F. Varnik, and D. Raabe, Comp. Math. Appl. **61**, 3485 (2011).

[81] J. B. Freund, Phys. Fluids **25**, 110807 (2013).

[82] S. Gekle, Biophys. J. **110**, 514 (2016).

[83] G. Cipparrone, I. Ricardez-Vargas, P. Pagliusi, and C. Provenzano, Optics express **18**, 6008 (2010).

[84] J. B. Freund, Annu. Rev. Fluid Mech. **46**, 67 (2014).

[85] M. H. Sadd, *Elasticity: theory, applications, and numerics* (Academic Press, 2009).

[86] A. E. Green and J. C. Adkins, *Large Elastic Deformations and Non-linear Continuum Mechanics* (Oxford University Press, 1960).

[87] L. Zhu, *Simulation of individual cells in flow*, Ph.D. thesis (2014).

[88] E. Lac, D. Barthès-Biesel, N. A. Pelekasis, and J. Tsamopoulos, J. Fluid Mech. **516**, 303 (2004).

[89] T. Krüger, *Computer simulation study of collective phenomena in dense suspensions of red blood cells under shear* (Springer Science & Business Media, 2012).

[90] J. L. Synge and A. Schild, *Tensor calculus*, Vol. 5 (Courier Corporation, 1969).

[91] C. Pozrikidis, J. Comput. Phys. **169**, 250 (2001).

[92] L. Zhu and L. Brandt, J. Fluid Mech. **770**, 374 (2015).

[93] B. U. Felderhof, Phys. Rev. E **89**, 033001 (2014).

Publication 9

Hydrodynamic mobility of a solid particle nearby a spherical elastic membrane. II. Asymmetric motion

A. Daddi-Moussa-Ider, M. Lisicki and S. Gekle

Phys. Rev. E **95**, 053117 (2017)

DOI: 10.1103/PhysRevE.95.053117

Abstract

In this paper, we derive analytical expressions for the leading-order hydrodynamic mobility of a small solid particle undergoing motion tangential to a nearby large spherical capsule whose membrane possesses resistance towards shearing and bending. Together with the results obtained in the first part (Daddi-Moussa-Ider and Gekle, Phys. Rev. E **95**, 013108 (2017)) where the axisymmetric motion perpendicular to the capsule membrane is considered, the solution of the general mobility problem is thus determined. We find that shearing resistance induces a low-frequency peak in the particle self-mobility, resulting from the membrane normal displacement in the same way, although less pronounced, to what has been observed for the axisymmetric motion. In the zero frequency limit, the self-mobility correction near a hard sphere is recovered only if the membrane has a non-vanishing resistance towards shearing. We further compute the in-plane mean-square displacement of a nearby diffusing particle, finding that the membrane induces a long-lasting subdiffusive regime. Considering capsule motion, we find that the correction to the pair-mobility function is solely determined by membrane shearing properties. Our analytical calculations are compared and validated with fully resolved boundary integral simulations where a very good agreement is obtained.

1 Introduction

Transport processes on the microscale play a key role in many biological and industrial applications [1, 2]. Typical examples include drug delivery involving nanoparticles required to reach specific areas of patients' bodies [3, 4], problems of blood circulation [5–7], and also motion in crowded cellular environments [8–10]. A common feature of these processes is the presence of nearby interfaces, thus the motion occurs predominantly in geometric confinement. In living systems, the confining boundaries often possess a certain degree of elasticity which introduces additional memory effects to the system [11–13].

At small length scales, aqueous systems are typically characterized by a negligibly small Reynolds number, and the resulting overdamped motion can therefore be accurately described within the framework of linear Stokes equations [14, 15]. The relations between forces and velocities of particles in flow are therefore linear and quantified by the hydrodynamic mobility coefficients. They are determined by the long-range, fluid-mediated hydrodynamic interactions.

In this work, we focus on the case of a small colloidal particle translating under the action of a force in the presence of a nearby large spherical elastic capsule. This system may be looked upon as a simplistic model of transport of colloids close to cellular membranes [16–18]. Our aim is to assess the effects of elasticity on the motion of the particle itself, and also on the deformable capsule. A similar problem has been examined before by Fuentes and coworkers [19, 20], who have treated analytically the case of interactions between two unequal spherical drops at moderate separations. Being purely viscous, however, that system does not possess a memory and thus leads to hydrodynamic mobilities which are independent of frequency. Their idea of solution relied on the image singularities technique, i.e. finding an appropriate system of images for a given distribution of forces outside a spherical droplet. Inspired by this work, we aim to find the analytical expression for the Green's function for a point-force near a spherical capsule. The surface of the capsule is made of an elastic membrane [21], which resists against shearing and bending deformation, and is modeled using the combined Skalak [22] and Helfrich [23] models. This model has been successfully used in our previous works for the case of confinement by one [13, 24, 25] or two planar membranes [26]. Further theoretical investigations near elastic interfaces have been carried out via soft lubrication theory [27–29].

In the preceding paper [30] (hereafter referred to as part I), we have derived the expression for the Green's function in the case when the point-force is directed along the symmetry axis, joining the centers of the particle and the capsule. In this contribution, we extend these results by providing

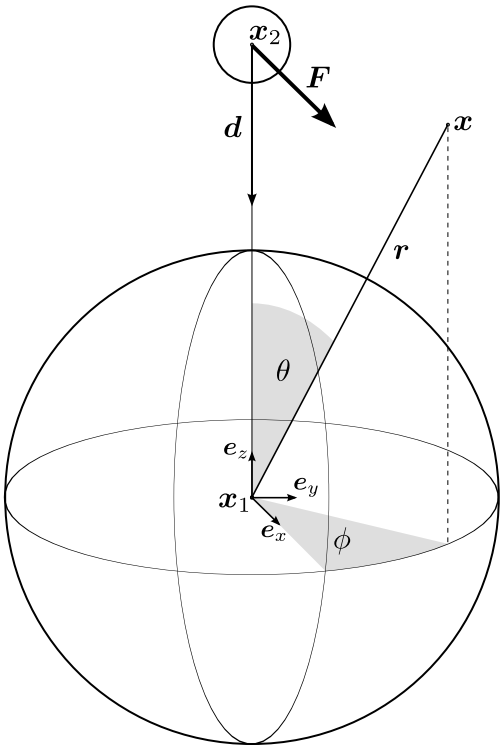

Figure 1: The configuration of the system. A small solid particle of radius b situated at $\boldsymbol{x}_2 = R\boldsymbol{e}_z$ nearby a large spherical capsule of undeformed radius a. In an asymmetric situation, the force is directed perpendicularly to $\boldsymbol{d}$ shown here along the x-direction.

a direct solution for the case when the point-force acts tangentially to the surface of the membrane, thus determining together the solution of the general mobility problem. The Green's function is then used to evaluate the frequency-dependent self-mobility of a small particle moving close to the capsule, and the pair-mobility, which quantifies the effect of the force on the motion of the capsule itself. The solution is also used to compute the resulting deformation of the spherical capsule. The theoretical predictions at zero frequency are in agreement with the hard-sphere limit provided that the membrane possesses a non-vanishing resistance towards shearing. Our analytical results comply with fully resolved boundary integral simulations which we have performed to validate the model.

The paper is organized as follows. In Sec. 2, the solution of the fluid motion inside and outside the elastic capsule is expressed in terms of multipole expansions. In Sec. 3, analytical expressions of the particle frequency-dependent self-mobility nearby a membrane with pure shearing or pure bending are obtained in the point-particle framework and expressed in terms of infinite but convergent series. We compute in Sec. 4 the particle in-plane mean-square displacement, finding that the membrane introduces a memory in the system, leading at intermediate time scales of motion to a subdiffusive behavior of the nearby particle. Capsule motion and membrane deformation are computed in Sec. 5. In Sec. 6, a comparison between analytical predictions and fully resolved boundary integral simulations is made where a very good agreement is obtained. Concluding remarks are offered in Sec. 7. Mathematical details which are not essential to understand our approach are given in the appendices.

2 Singularity solution

We are interested in the flow field due to a point-force (Stokeslet) acting close to a large spherical capsule, for which we shall find a fully analytical solution. The Stokeslet is oriented perpendicularly to the line connecting its position and the center of the capsule. We introduce a spherical coordinate system, centered at the capsule position $\boldsymbol{x}_1$, with the point-force acting at $\boldsymbol{x}_2 = R\boldsymbol{e}_z$. The whole system is sketched in Fig. 1.

Mathematically, the problem is reduced to solving the forced Stokes equations outside the capsule

$$\eta\boldsymbol{\nabla}^2\boldsymbol{v} - \boldsymbol{\nabla}p + \boldsymbol{F}\delta(\boldsymbol{x}-\boldsymbol{x}_2) = 0\,, \tag{2.1}$$
$$\boldsymbol{\nabla}\cdot\boldsymbol{v} = 0\,, \tag{2.2}$$

and homogeneous equations for the fluid inside

$$\eta\boldsymbol{\nabla}^2\boldsymbol{v}^{(i)} - \boldsymbol{\nabla}p^{(i)} = 0\,, \tag{2.3}$$
$$\boldsymbol{\nabla}\cdot\boldsymbol{v}^{(i)} = 0\,. \tag{2.4}$$

Here $\boldsymbol{v}$ and p denote the exterior velocity and pressure fields and the superscript (i) stands for the corresponding interior fields. For simplicity, we assume the fluid to have the same dynamic viscosity η everywhere. The boundary conditions are imposed at $r = a$. We require the natural continuity of the fluid velocity field

$$[v_\theta] = 0\,, \tag{2.5}$$
$$[v_\phi] = 0\,, \tag{2.6}$$
$$[v_r] = 0\,, \tag{2.7}$$

and a fluid stress jump across the membrane imposed by its elastic properties,

$$[\sigma_{\theta r}] = \Delta f_\theta^{\mathrm{S}} + \Delta f_\theta^{\mathrm{B}}\,, \tag{2.8}$$
$$[\sigma_{\phi r}] = \Delta f_\phi^{\mathrm{S}} + \Delta f_\phi^{\mathrm{B}}\,, \tag{2.9}$$
$$[\sigma_{rr}] = \Delta f_r^{\mathrm{S}} + \Delta f_r^{\mathrm{B}}\,, \tag{2.10}$$

where the notation $[w] := w(r = a^+) - w(r = a^-)$ for the jump of a quantity w across the membrane and the superscripts S and B denoting the shearing and bending related parts in the traction jump, respectively. Throughout the remaining of the paper, we scale all the lengths by the capsule radius a. The corresponding quantities in physical units can be obtained by the transformation rules given in Appendix B of part I [30]. The components of the fluid stress tensor in spherical coordinates read [15]

$$\sigma_{\theta r} = \eta\left(v_{\theta,r} - \frac{v_\theta}{r} + \frac{v_{r,\theta}}{r}\right)\,, \tag{2.11a}$$
$$\sigma_{\phi r} = \eta\left(\frac{v_{r,\phi}}{r\sin\theta} + v_{\phi,r} - \frac{v_\phi}{r}\right)\,, \tag{2.11b}$$
$$\sigma_{rr} = -p + 2\eta v_{r,r}, \tag{2.11c}$$

where the indices after commas indicate partial spatial derivatives, e.g. $v_{r,\phi} \equiv \partial v_r/\partial\phi$, etc.

We model the elastic properties of the membrane by introducing its resistance towards shearing and bending. As derived in the Appendix, the linearized traction jumps due to shearing according to the Skalak model [22, 31], characterized by a coefficient λ, in terms of the membrane deformation

$\boldsymbol{u}$ read

$$\Delta f_\theta^{\mathrm{S}} = -\kappa_{\mathrm{S}}\Big[(2\lambda-1)u_{r,\theta} + \lambda u_{\theta,\theta\theta} + \lambda u_{\theta,\theta}\cot\theta - u_\theta\left(\lambda\cot^2\theta + \lambda - 1\right) + \frac{u_{\theta,\phi\phi}}{2\sin^2\theta} \tag{2.12a}$$
$$- \left(\lambda+\frac{1}{2}\right)\frac{\cot\theta}{\sin\theta}\,u_{\phi,\phi} + \left(\lambda-\frac{1}{2}\right)\frac{u_{\phi,\phi\theta}}{\sin\theta}\Big],$$
$$\Delta f_\phi^{\mathrm{S}} = -\kappa_{\mathrm{S}}\Big[(2\lambda-1)\frac{u_{r,\phi}}{\sin\theta} + \left(\lambda+\frac{1}{2}\right)\frac{\cot\theta}{\sin\theta}\,u_{\theta,\phi} + \left(\lambda-\frac{1}{2}\right)\frac{u_{\theta,\phi\theta}}{\sin\theta} + \frac{1}{2}\left(1-\cot^2\theta\right)u_\phi \tag{2.12b}$$
$$+ \frac{u_{\phi,\theta}}{2}\cot\theta + \frac{u_{\phi,\theta\theta}}{2} + \lambda\frac{u_{\phi,\phi\phi}}{\sin^2\theta}\Big],$$
$$\Delta f_r^{\mathrm{S}} = \frac{2\kappa_{\mathrm{S}}}{3}(2\lambda-1)\left(2u_r + u_{\theta,\theta} + u_\theta\cot\theta + \frac{u_{\phi,\phi}}{\sin\theta}\right), \tag{2.12c}$$

where $\lambda := C+1$ with C being the ratio of the area expansion modulus κ_{A} and the shear modulus κ_{S} [32].

The stress jump related to bending is derived from a linear isotropic model for the bending moments which is equivalent to the well-known Helfrich model [23] for small deformations [33, 34]. The linearized traction due to bending reads (cf. Appendix)

$$\Delta f_\theta^{\mathrm{B}} = \kappa_{\mathrm{B}}\Big[\left(1-\cot^2\theta\right)u_{r,\theta} + u_{r,\theta\theta}\cot\theta + u_{r,\theta\theta\theta} + (1+\cot^2\theta)\left(u_{r,\phi\phi\theta} - 2u_{r,\phi\phi}\cot\theta\right)\Big], \tag{2.13a}$$
$$\Delta f_\phi^{\mathrm{B}} = \kappa_{\mathrm{B}}(1+\cot^2\theta)\big(u_{r,\phi\theta}\cot\theta + 2u_{r,\phi} + u_{r,\phi\theta\theta} + (1+\cot^2\theta)u_{r,\phi\phi\phi}\big)\sin\theta, \tag{2.13b}$$
$$\Delta f_r^{\mathrm{B}} = \kappa_{\mathrm{B}}\Big[\left(3\cot\theta+\cot^3\theta\right)u_{r,\theta} - u_{r,\theta\theta}\cot^2\theta + 2u_{r,\theta\theta\theta}\cot\theta + u_{r,\theta\theta\theta\theta}$$
$$+ (1+\cot^2\theta)\big(2u_{r,\phi\phi\theta\theta} - 2u_{r,\phi\phi\theta}\cot\theta + (1+\cot^2\theta)(4u_{r,\phi\phi} + u_{r,\phi\phi\phi\phi})\big)\Big], \tag{2.13c}$$

where $\boldsymbol{u}(\theta,\phi)$ is the membrane displacement field. These expressions reduce to the axisymmetric case of part I by setting $u_\phi = 0$ and dropping all ϕ-derivatives. The displacement is related to the fluid velocity at $r=1$ via the no-slip condition,

$$\boldsymbol{v}|_{r=1} = \frac{\mathrm{d}\boldsymbol{u}}{\mathrm{d}t},$$

which in the Fourier space takes the form

$$\boldsymbol{v}|_{r=1} = i\omega\,\boldsymbol{u}. \tag{2.14}$$

Our approach is inspired by the work of Fuentes *et al.* [20], who computed the solution of the Stokes equation nearby a viscous drop for the asymmetric force case. We write the exterior fluid velocity outside the capsule as

$$\boldsymbol{v} = \boldsymbol{v}^{\mathrm{S}} + \boldsymbol{v}^*,$$

where $v_i^{\mathrm{S}} := \mathcal{G}_{ij}(\boldsymbol{x}-\boldsymbol{x}_2)F_j$ is the velocity field induced by a point-force acting at $\boldsymbol{x}_2$ in an infinite fluid, and $\boldsymbol{v}^*$ is the flow due to an image system required to satisfy the boundary conditions at the capsule membrane, also called the reflected flow.

Now we sketch briefly the main steps of our solution methodology. Firstly, we express the Stokeslet velocity $\boldsymbol{v}^{\mathrm{S}}$ at $\boldsymbol{x}_2$ in terms of spherical harmonics, which are then transformed into harmonics centered at $\boldsymbol{x}_1$ via the Legendre expansion. Secondly, we write a multipole expansion for the image system $\boldsymbol{v}^*$ at $\boldsymbol{x}_1$, and afterward we rewrite it in terms of spherical harmonics based at $\boldsymbol{x}_1$. Thirdly, the solution

inside the capsule $\boldsymbol{v}^{(i)}$ is written using Lamb's general solution [35], also expressed in terms of spherical harmonics at $\boldsymbol{x}_1$. The last step consists of determining the unknown series expansion coefficients by satisfying the boundary conditions at the membrane stated by Eqs. (2.5) through (2.10).

In conjunction with the results of part I on the axisymmetric motion, the general solution of the Stokes equations for an arbitrary force direction is thus obtained.

2.1 Stokeslet representation

We begin with writing the Stokeslet positioned at $\boldsymbol{x}_2$,

$$\boldsymbol{v}^{\mathrm{S}} = \boldsymbol{\mathcal{G}} \cdot \boldsymbol{F} = \frac{1}{8\pi\eta}\left(\frac{\mathbf{1}}{s} + \boldsymbol{s}\boldsymbol{\nabla}_2\frac{1}{s}\right)\cdot\boldsymbol{F}, \tag{2.15}$$

where $\boldsymbol{s} := \boldsymbol{x} - \boldsymbol{x}_2$ and $s := |\boldsymbol{s}|$. Here $\nabla_{2j} := \partial/\partial x_{2j}$ denotes the gradient operator taken with respect to $\boldsymbol{x}_2$. Using the Legendre expansion, the harmonics based at $\boldsymbol{x}_2$ can be expressed in terms of those centered at $\boldsymbol{x}_1$ as

$$\frac{1}{s} = \sum_{n=0}^{\infty} \frac{r^{2n+1}}{R^{n+1}} \frac{(\boldsymbol{d}\cdot\boldsymbol{\nabla})^n}{n!}\frac{1}{r}\,,$$

with the unit vector $\boldsymbol{d} := (\boldsymbol{x}_1 - \boldsymbol{x}_2)/R = -\boldsymbol{e}_z$, $\boldsymbol{r} = \boldsymbol{x} - \boldsymbol{x}_1$, and $r := |\boldsymbol{r}|$. The derivatives with respect to $\boldsymbol{x}_2$ are taken care of by noting that

$$\boldsymbol{\nabla}_2\frac{1}{R^{n+1}} = \frac{n+1}{R^{n+2}}\,\boldsymbol{d}\,, \qquad (\boldsymbol{d}\cdot\boldsymbol{\nabla}_2)\,\boldsymbol{d} = 0\,.$$

Moreover, we denote by φ_n the harmonic of degree n, related to the Legendre polynomials of degree n, P_n by [36]

$$\varphi_n(r,\theta) := \frac{(\boldsymbol{d}\cdot\boldsymbol{\nabla})^n}{n!}\frac{1}{r} = \frac{1}{r^{n+1}}P_n(\cos\theta)\,.$$

In this work, we focus our attention on the asymmetric case when the force is purely tangential and therefore $\boldsymbol{F}\cdot\boldsymbol{d} = 0$. Taking this into account, the Stokeslet in Eq. (2.15) can be written as

$$8\pi\eta\boldsymbol{v}^{\mathrm{S}} = \boldsymbol{F}\sum_{n=0}^{\infty}\frac{r^{2n+1}}{R^{n+1}}\,\varphi_n - \boldsymbol{r}\sum_{n=1}^{\infty}\frac{r^{2n+1}}{R^{n+2}}\,(\boldsymbol{F}\cdot\boldsymbol{\nabla})\,\varphi_{n-1} - \boldsymbol{d}\sum_{n=1}^{\infty}\frac{r^{2n+1}}{R^{n+1}}\,(\boldsymbol{F}\cdot\boldsymbol{\nabla})\,\varphi_{n-1}\,.$$

Thus we have expressed the Stokeslet solution in terms of spherical harmonics centered at $\boldsymbol{x}_1$. By defining $\boldsymbol{t} = \boldsymbol{F}\times\boldsymbol{d}$, we have the identity

$$\boldsymbol{d}(\boldsymbol{F}\cdot\boldsymbol{\nabla})\varphi_n = (\boldsymbol{t}\times\boldsymbol{\nabla})\varphi_n + (n+1)\boldsymbol{F}\varphi_{n+1}\,. \tag{2.16}$$

Moreover, for $\boldsymbol{F}\cdot\boldsymbol{d} = 0$, we can write

$$(2n+3)\boldsymbol{r}\psi_n = -r^2\boldsymbol{\nabla}\psi_n + \boldsymbol{\nabla}\psi_{n-2} - (2n+1)(n+1)\boldsymbol{F}\varphi_n - (2n+1)\boldsymbol{\gamma}_{n-1}\,, \tag{2.17}$$

where we have defined

$$\psi_n = (\boldsymbol{F}\cdot\boldsymbol{\nabla})\varphi_n\,, \qquad \boldsymbol{\gamma}_n = (\boldsymbol{t}\times\boldsymbol{\nabla})\varphi_n\,.$$

Note that the harmonics ψ_n are defined differently than in part I and that the additional set $\boldsymbol{\gamma}_n$ is not required for the simpler axisymmetric case of part I. Finally, the Stokeslet can be written as

$$\begin{aligned} 8\pi\eta\boldsymbol{v}^{\mathrm{S}} = \sum_{n=1}^{\infty} \Bigg[\frac{n-2}{(2n-1)n} \frac{r^{2n+1}}{R^n} - \frac{n}{(n+2)(2n+3)} \frac{r^{2n+3}}{R^{n+2}} \Bigg] \boldsymbol{\nabla}\psi_{n-1} \\ - \frac{2}{n+1} \frac{r^{2n+1}}{R^{n+1}} \boldsymbol{\gamma}_{n-1} + \Bigg[\frac{(n-2)(2n+1)}{n(2n-1)} \frac{r^{2n-1}}{R^n} - \frac{r^{2n+1}}{R^{n+2}} \Bigg] \boldsymbol{r}\psi_{n-1}. \end{aligned} \tag{2.18}$$

We have chosen the vector basis functions here to be $\boldsymbol{\nabla}\psi_n$, $\boldsymbol{r}\psi_n$, and $\boldsymbol{\gamma}_n$. We now proceed to deriving analogous expansions for the reflected flow and the velocity inside the capsule, in order to finally match them using the boundary conditions given above.

2.2 Image system representation

The corresponding image system representation can be written as a multipole expansion, which involves the derivatives of the free-space Green's function $\boldsymbol{\mathcal{G}}(\boldsymbol{r})$, as [15]

$$8\pi\eta\boldsymbol{v}^* = \sum_{n=0}^{\infty} \left[A_n \frac{(\boldsymbol{d}\cdot\boldsymbol{\nabla})^n}{n!} \boldsymbol{\mathcal{G}}(\boldsymbol{r}) + B_n \frac{(\boldsymbol{d}\cdot\boldsymbol{\nabla})^n}{n!} \nabla^2 \boldsymbol{\mathcal{G}}(\boldsymbol{r}) \right] \cdot \boldsymbol{F} + \sum_{n=0}^{\infty} \left[C_n \frac{(\boldsymbol{d}\cdot\boldsymbol{\nabla})^n}{n!} (\boldsymbol{t}\times\boldsymbol{\nabla}) \frac{1}{r} \right]. \tag{2.19}$$

We convert these expressions into harmonics φ_n using the identity

$$\frac{(\boldsymbol{d}\cdot\boldsymbol{\nabla})^n}{n!} \mathcal{G}_{ij}(\boldsymbol{r}) = \delta_{ij}\varphi_n - r_i \nabla_j \varphi_n - d_i \nabla_j \varphi_{n-1},$$

and the fact that the Laplacian of the Oseen tensor is written conveniently as

$$\nabla^2 \boldsymbol{\mathcal{G}}(\boldsymbol{r}) = -2\boldsymbol{\nabla}\boldsymbol{\nabla}\frac{1}{r}.$$

Making use of Eq. (2.16), the image system solution can finally be written as

$$8\pi\eta\boldsymbol{v}^* = \sum_{n=0}^{\infty} \left[A_n \Big((1-n)\boldsymbol{F}\varphi_n - \boldsymbol{r}\psi_n \Big) - 2B_n \boldsymbol{\nabla}\psi_n \right] + \sum_{n=1}^{\infty} \left[C_n - A_{n+1} \right] \boldsymbol{\gamma}_n. \tag{2.20}$$

2.3 The interior solution

The interior solution has a generic form derived first by Lamb [15, 35]. It involves three families of unknown coefficients and can be written in the asymmetric situation as

$$\begin{aligned} 8\pi\eta\boldsymbol{v}^{(i)} = \sum_{n=1}^{\infty} c_n \Big[r^{2n-1}\boldsymbol{\gamma}_{n-1} + (2n-1) r^{2n-3} (\boldsymbol{t}\times\boldsymbol{r})\varphi_{n-1} \Big] + b_n \Bigg[\frac{r^{2n+1}}{n} \boldsymbol{\nabla}\psi_{n-1} \\ + \frac{2n+1}{n} r^{2n-1} \boldsymbol{r}\psi_{n-1} \Bigg] + a_n \Bigg[\frac{n+3}{2n} r^{2n+3} \boldsymbol{\nabla}\psi_{n-1} + \frac{(n+1)(2n+3)}{2n} r^{2n+1} \boldsymbol{r}\psi_{n-1} \Bigg]. \end{aligned} \tag{2.21}$$

We note that the interior solution here has three unknown coefficients while the axisymmetric motion in part I involves only two.

2.4 The full flow field

The velocity fields $\boldsymbol{v}^{\mathrm{S}}$, $\boldsymbol{v}^{*}$, and $\boldsymbol{v}^{(i)}$ thus suffice to describe the flow in the whole space. The matching conditions at the surface of the capsule are determined by the known stress jump due to the membrane elasticity and continuity of the velocity field, as expressed by Eqs. (2.5) through (2.10). These allow computation of the free constants (A_n, B_n, C_n for the reflected flow, and a_n, b_n, c_n for the inner flow) as detailed in Appendix B.

3 Particle self-mobility

In the preceding section, we have computed the Green's function for the problem of a point-force acting in the direction tangential to the surface of an elastic spherical capsule. The exterior velocity field due to a Stokeslet is then given by $\boldsymbol{v}^{\mathrm{S}} + \boldsymbol{v}^{*}$. In this section, we discuss the consequences of the presence of the membrane for the motion of the nearby particle. In order to assess the effects of the presence of the capsule, we now compute the leading-order correction term to the particle self-mobility. We assume an external force $\boldsymbol{F}_2$ to be acting on the solid particle and no force or torque to be exerted on the capsule.

The zeroth-order solution for the particle velocity is $\boldsymbol{V}_2^{(0)} = \mu_0 \boldsymbol{F}_2$ as given by the Stokes law with $\mu_0 := 1/(6\pi\eta b)$ being the usual bulk mobility. The leading-order correction to the particle self-mobility is computed from the image solution as

$$\boldsymbol{v}^{*}\big|_{\boldsymbol{x}=\boldsymbol{x}_2} = \Delta\mu \boldsymbol{F}_2 \,. \tag{3.1}$$

Making use of the following relations

$$\begin{aligned}
\frac{(\boldsymbol{d}\cdot\boldsymbol{\nabla})^n}{n!}\boldsymbol{\mathcal{G}}(\boldsymbol{x}-\boldsymbol{x}_1)\bigg|_{\boldsymbol{x}=\boldsymbol{x}_2}\cdot\boldsymbol{F}_2 &= \frac{1}{R^{n+1}}\boldsymbol{F}_2\,,\\
\frac{(\boldsymbol{d}\cdot\boldsymbol{\nabla})^n}{n!}\boldsymbol{\nabla}^2\boldsymbol{\mathcal{G}}(\boldsymbol{x}-\boldsymbol{x}_1)\bigg|_{\boldsymbol{x}=\boldsymbol{x}_2}\cdot\boldsymbol{F}_2 &= \frac{(n+1)(n+2)}{R^{n+3}}\boldsymbol{F}_2\,,\\
\frac{(\boldsymbol{d}\cdot\boldsymbol{\nabla})^n}{n!}(\boldsymbol{t}\times\boldsymbol{\nabla})\frac{1}{r}\bigg|_{\boldsymbol{x}=\boldsymbol{x}_2} &= -\frac{n+1}{R^{n+2}}\boldsymbol{F}_2\,,
\end{aligned}$$

together with Eq. (2.19), the scaled particle self-mobility function reads

$$\frac{\Delta\mu}{\mu_0} = \frac{3b}{4}\sum_{n=0}^{\infty}\left[A_n + (n+1)(n+2)\xi^2 B_n - (n+1)\xi C_n\right]\xi^{n+1}\,, \tag{3.2}$$

where $\xi := 1/R \in [0,1)$. We denote by $f_n(\xi)$ the general term of the function series giving the particle scaled mobility correction stated above. For large n, we obtain the leading order asymptotic behavior

$$f_n(\xi) = \frac{3b}{16}\left(1-\xi^2\right)^2 n^2 \xi^{2n+4} + \mathcal{O}\left(n\xi^{2n}\right)\,, \tag{3.3}$$

which is independent of shearing and bending properties. The number of terms required for convergence can thus be estimated for a given precision as in Appendix C of part I [30].

It is worth to mention here that for finite membrane shearing modulus (i.e. for a non hard-sphere), no net force is exerted on the spherical capsule, since $A_0 = 0$. In this case, the capsule is also torque-free, since $C_0 - A_1 = 0$. For a hard-sphere, however, additional singularities should be involved in the computation of particle mobility to ensure the force- and torque-free assumptions (see Fuentes *et al.* [20] for further details.)

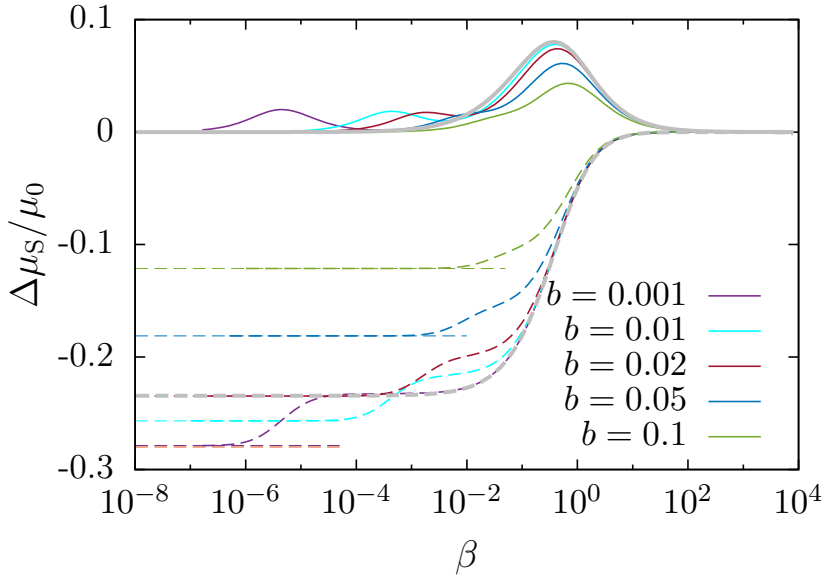

Figure 2: (Color online) Scaled particle self-mobility correction versus scaled frequency β for various values of the small particle radius b for a membrane with pure shearing. The real and imaginary parts are shown as dashed and solid lines, respectively. Dashed lines on the vertical axis at small β represent the hard-sphere limit given by Eq. (3.4). The curve in gray corresponds to the self-mobility correction for a planar membrane given by Eq. (3.6). Here the solid particle is set at $h = 2b$.

3.1 Shearing contribution

For a membrane exhibiting a shearing-only resistance, the self-mobility correction can be computed by plugging the expressions of A_n, B_n and C_n as stated respectively by Eqs. (B.26), (B.27) and (B.28) into Eq. (3.2). By taking the limit $\alpha \to \infty$ we recover the rigid sphere limit,

$$\frac{\Delta\mu_{S,\infty}}{\mu_0} := \lim_{\alpha\to\infty} \frac{\Delta\mu}{\mu_0} = -\frac{\xi^5(17+\xi^2)}{16(1-\xi^2)}\frac{b}{R}\,, \tag{3.4}$$

in agreement with the result by Ekiel-Jeżewska and Felderhof [37, Eq. (2.26)]. Taking in addition an infinite membrane radius, we obtain

$$\frac{\Delta\mu_{S,\infty}}{\mu_0} = -\frac{9}{16}\frac{b}{h}\,, \tag{3.5}$$

where $h := R - 1$ is the distance separating the center of the solid particle to the closest point on the capsule surface. We therefore recover the leading-order mobility correction for the motion parallel to a planar hard-wall as computed by Lorentz [38].

To characterize the dynamic effects at different forcing frequencies, we define the dimensionless shearing frequency as $\beta := 6B\eta\omega h/\kappa_S$ where $B := 2/\lambda$. In Fig. 2 we show the scaled self-mobility correction for a membrane with pure shearing with $C = 1$ ($\lambda = 2$) versus the scaled frequency β upon variation of the particle radius b while keeping $h = 2b$. We remark that the real part of the mobility correction (shown as dashed lines) is an increasing function of frequency while the imaginary part (shown as solid lines) has the typical peak structure attributed to the memory effect induced by membrane elasticity. In the vanishing frequency limit, the mobility correction near a hard-sphere given by Eq. (3.4) is recovered.

As the particle radius decreases, we observe that in the high frequency regime both the real and

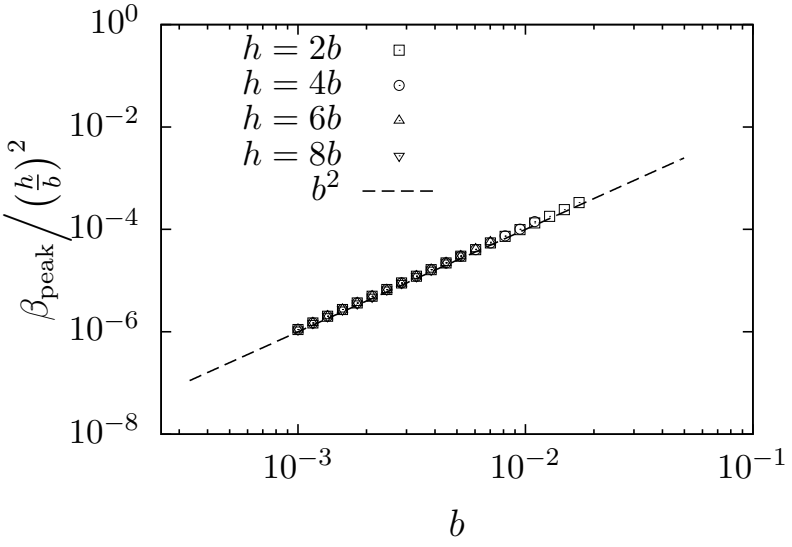

Figure 3: Log-log plot of the rescaled peak-frequency β_{peak} versus b for different particle-to-membrane distance h.

imaginary parts follow faithfully the evolution predicted for a planar membrane which reads [13]

$$\frac{\Delta\mu_{\text{S}}}{\mu_0} = \frac{3}{8}\frac{b}{h}\left[-\frac{5}{4} + \frac{\beta^2}{8} + i\lambda\beta e^{i\lambda\beta}\,\text{E}_1\left(i\lambda\beta\right) - \frac{3i\beta}{8} + \left(-\frac{\beta^2}{2} + \frac{i\beta}{2}\left(1 - \frac{\beta^2}{4}\right)\right) e^{i\beta}\,\text{E}_1(i\beta)\right]. \quad (3.6)$$

The peak occurring at $\beta \sim 1$ can be estimated by a balance between membrane elasticity and fluid viscosity as $\omega \sim \kappa_{\text{S}}/(\eta h)$. This peak is attributed to membrane in-plane displacements u_θ and u_ϕ which are observed in the same way for planar membranes. The second peak of small amplitude occurring in the low frequency regime is attributed to membrane normal displacement along u_r which is not involved in the traction jumps for planar membranes. In fact, for the axisymmetric motion examined in part I [see 30, Fig. 2], we observe that the low-frequency peak has a remarkably higher amplitude since the membrane displacement u_r manifests itself in a more pronounced way for the motion perpendicular than for the motion parallel to the membrane.

Interestingly, the frequency corresponding to the left peak of the imaginary part of the mobility correction is found to be proportional to b^2, as plotted in Fig. 3. For different radii and separations, the same master curve is recovered and the second peak frequency position can conveniently be estimated from the relation $\beta_{\text{peak}} = h^2$. It is worth noting that a scaling relation $\beta_{\text{peak}} = 2h^2$ has been obtained for the axisymmetric motion considered in part I.

3.2 Bending contribution

For a membrane possessing only bending rigidity, the self-mobility correction is determined by plugging the expressions of A_n, B_n and C_n as stated respectively by Eqs. (B.33), (B.34) and (B.35) into Eq. (3.2). By taking the limit $\alpha_{\text{B}} \to \infty$, the leading-order self-mobility can be approximated by

$$\frac{\Delta\mu_{\text{B},\infty}}{\mu_0} := \lim_{\alpha_{\text{B}}\to\infty} \frac{\Delta\mu}{\mu_0} \simeq -\frac{\xi^5}{70(1-\xi^2)}\left[-9 + 71\xi^2 - \frac{183}{2}\xi^4 + \frac{341}{8}\xi^6\right]\frac{b}{R}, \quad (3.7)$$

which for an infinite radius reads

$$\frac{\Delta\mu_{\text{B},\infty}}{\mu_0} = -\frac{3}{32}\frac{b}{h},$$

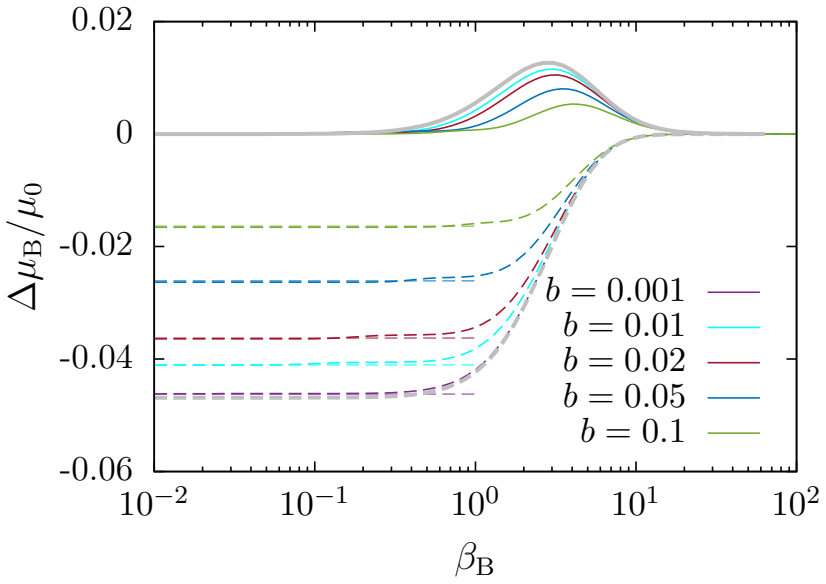

Figure 4: (Color online) Scaled self-mobility correction versus β_B for various values of the capsule radius, for a membrane with pure bending. The dashed and continuous lines represent the real and imaginary parts, respectively. The horizontal dashed lines are the vanishing frequency limits approximated by Eq. (3.7). The curve shown in gray is the solution given by Eq. (3.8) for a planar membrane. Here we take $h = 2b$.

corresponding to the vanishing frequency limit for an idealized membrane with pure bending. Note that this limit is different from the hard-sphere limit but identical to that of a planar interface separating two immiscible fluids having the same viscosity [14, 39]. A similar behavior has been observed for planar membranes with pure bending resistance. This can be justified by the fact that the bending traction jump stated by Eq. (2.13) is determined only by the radial displacement u_r and does not involve the tangential displacements u_θ and u_ϕ. As a result, even for an infinite bending modulus, the membrane tangential displacements remain completely free. This behavior is in contrast to the hard-sphere where all the displacement field components are restricted.

We define the characteristic frequency for bending as $\beta_B := 2h(4\eta\omega/\kappa_B)^{1/3}$. In Fig. 4, we show the scaled self-mobility correction versus β_B of a particle moving nearby a membrane with bending-only resistance. Unlike a membrane with pure shearing resistance, the second low frequency peak is not observed nearby a membrane with pure bending resistance. This can be understood since the traction jumps due to bending involve only the radial displacement u_r. The peak observed at $\beta_B^3 \sim 1$ is the characteristic peak for bending which can be estimated by a simple balance between membrane bending and fluid viscosity as $\omega \sim \kappa_B/(h^3\eta)$. This trend is in contrast to what has been observed for membrane with pure shearing resistance where the traction jumps involve both the radial and tangential displacements.

For sufficiently small values of b, we observe that both the real and imaginary parts of the mobility correction are in good agreement with the planar membrane solution [13]

$$\frac{\Delta\mu_B(\beta_B)}{\mu_0} = \frac{3}{64}\frac{b}{h}\left[-2 + \frac{i\beta_B^3}{3}\left(\phi_+ + e^{-i\beta_B}\,\mathrm{E}_1(-i\beta_B)\right)\right], \tag{3.8}$$

wherein

$$\phi_+ = e^{-i\overline{z_B}}\,\mathrm{E}_1(-i\overline{z_B}) + e^{-iz_B}\,\mathrm{E}_1(-iz_B)\,,$$

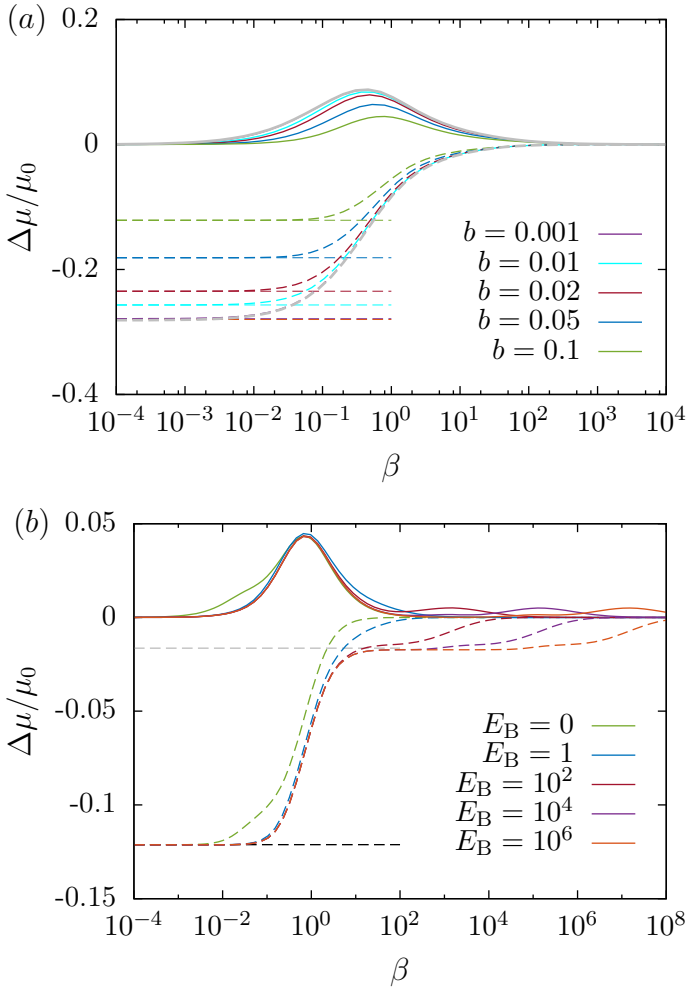

Figure 5: (Color online) *a*) Scaled particle mobility correction versus β for various values b for a membrane possessing both shearing and bending rigidities. The real and imaginary parts are shown as dashed and solid lines, respectively. Horizontal dashed lines are the hard-sphere limit given by Eq. (3.4). The curve shown in gray corresponds to the mobility correction for a planar elastic membrane [13] as obtained by linear superposition of Eqs. (3.6) and (3.8). Here the solid particle is set at $h = 2b$ and the membrane has a reduced bending modulus $E_B = 1$. *b*) Scaled mobility correction versus β for various values of E_B. The horizontal dashed line in black is the hard-sphere limit given by Eq. (3.4), whereas the gray dashed line corresponds to the infinite bending rigidity limit predicted for a bending-only membrane as given by Eq. (3.7). Here we take $b = 1/10$ and $h = 2b$.

and $z_B = \beta_B e^{2i\pi/3}$. As a result, a very good estimate of particle mobility can be made for large capsules with bending-only resistance from the planar membrane limit. For moderate and small capsule radii however, the planar membrane solution leads to a reasonable agreement only in the high frequency regime for which $\beta_B > 1$, in the same way as observed in part I for the motion perpendicular to the membrane [30].

3.3 Shearing-bending coupling

Unlike for a planar membrane, shearing and bending are intrinsically coupled for a spherical membrane. As a result, the mobility correction is not a linear superposition of independent contributions from shearing and bending. A similar coupling behavior is observed between two planar elastic interfaces [26] or thermally fluctuating membranes [40, 41]. In order to investigate this coupling, we define the reduced bending modulus as $E_{\mathrm{B}} := \kappa_{\mathrm{B}}/(\kappa_{\mathrm{S}} h^2)$, a parameter that quantifies the relative contributions of shearing and bending.

In Fig. 5 *a*) we show the scaled self-mobility correction versus β nearby a membrane with both shearing and bending resistances upon varying b. We observe that in the high frequency regime, i.e. for $\beta > 1$, the mobility correction follows the evolution predicted for a planar elastic membrane. For lower values of b, the planar membrane prediction leads to a very good estimation even deeper into the low-frequency regime. In the following, we take $h = 2b$ and a membrane reduced bending modulus $E_{\mathrm{B}} = 1$, for which shearing and bending effects manifest themselves equally.

In Fig. 5 *b*), we show the particle self-mobility correction versus the scaled frequency β for a membrane with both shearing and bending rigidities upon varying the reduced bending modulus E_{B} while keeping $b = 1/10$ and $h = 2b$. For $E_{\mathrm{B}} = 0$ (shearing-only membrane), a low frequency peak as in Fig. 2 emerges. For higher values of E_{B} this peak completely disappears confirming our hypothesis that it is due to radial deformations which are suppressed by bending resistance.

The imaginary part exhibits a high frequency peak of typically constant height for increasing E_{B}. Since β and β_{B} are related by

$$\beta_{\mathrm{B}}^3 = \frac{16}{3BE_{\mathrm{B}}}\,\beta\,,$$

the peak observed at $\beta \sim 1$ is attributed to shearing, whereas the peak occurring in the high frequency regime is attributed to bending, since $\beta \sim E_{\mathrm{B}}$ for $\beta_{\mathrm{B}}^3 \sim 1$. Particularly, for $E_{\mathrm{B}} = 1$, the position of the two peaks coincides as $\beta \sim \beta_{\mathrm{B}}^3$ for which shearing and bending effects have equal contribution.

4 Diffusion nearby cell membranes

The analytical predictions of the particle self-mobility presented in the previous section serve as a basis for the study of particle diffusional motion nearby spherical cell membranes. The determination of the mean-square displacement (MSD) requires as an intermediate step the computation of the velocity autocorrelation function which is derived from the fluctuation-dissipation theorem as [42, 43]

$$\phi_v(t) = \frac{k_{\mathrm{B}}T}{2\pi}\int_{-\infty}^{\infty}\left(\mu(\omega) + \overline{\mu(\omega)}\right)e^{i\omega t}\,\mathrm{d}\omega\,, \tag{4.1}$$

wherein k_{B} is the Boltzmann constant and T is the absolute temperature of the system. In this way, the particle MSD is computed as

$$\langle \Delta r(t)^2 \rangle = 2\int_0^t (t-s)\phi_v(s)\,\mathrm{d}s\,. \tag{4.2}$$

Further, for the sake of convenience, we define the excess MSD as the membrane induced *scaled* correction to the full MSD as [13]

$$\Delta(t) := 1 - \frac{\langle \Delta r(t)^2 \rangle}{2D_0 t}\,, \tag{4.3}$$

wherein $D_0 = \mu_0 k_{\mathrm{B}} T$ is the usual bulk diffusion coefficient predicted from Einstein theory [44, 45].

In typical physiological situations, red blood cell membranes have a shear modulus $\kappa_{\mathrm{S}} = 5 \times 10^{-6}\mathrm{N/m}$, a bending modulus $\kappa_{\mathrm{B}} = 2 \times 10^{-19}\mathrm{Nm}$ [31] and a discocyte shape of local radius $a = 10\mu\mathrm{m}$.

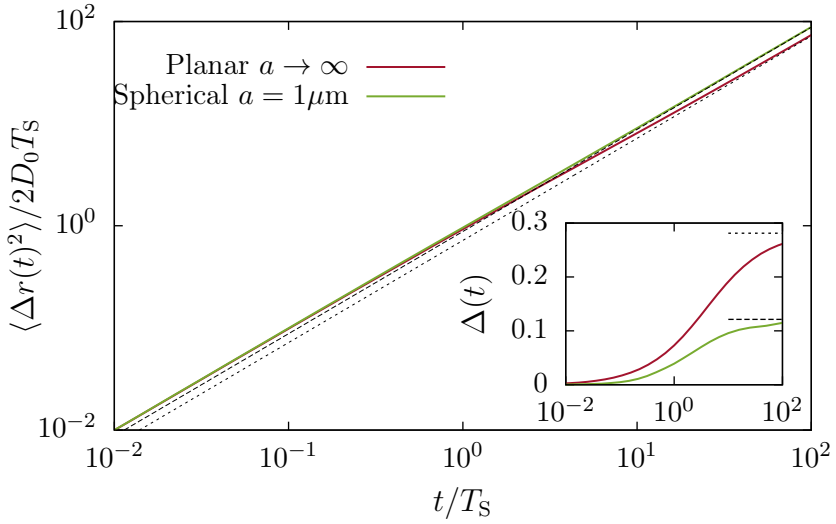

Figure 6: Mean-square displacement versus time for Brownian motion of a 100nm particle parallel to a planar and a spherical red blood cell membrane with curvature radius $a = 1\mu$m. Dotted and dashed lines represent the corresponding MSDs near a hard wall or sphere, respectively. The inset shows the variation of the excess MSD as defined by Eq. (4.3).

We then consider a solid particle of radius $b = a/10$ located a distance $h = 2b$ for which the reduced bending modulus $E_B = 1$. We scale the time by the characteristic time scale for shearing $T_S = 6h\eta/\kappa_S$ which is of about 0.3 μs considering a typical dynamic viscosity of blood plasma $\eta = 1.2$ mPas.

In Fig. 6, we show the scaled MSD versus the scaled time for a particle diffusing nearby a planar or a spherical membrane using the above mentioned parameters. We observe that at short time scales of motion, the MSD follows a linear bulk behavior and the corresponding excess MSD amounts to very small values. This behavior is justified by the fact that the particle does not yet perceive the presence of the membrane at these very short time scales. As the time increases, the effect of the membrane becomes noticeable and the particle experiences at intermediate time scales a long-lasting subdiffusive regime that can extend up to 10^2 T_S nearby a spherical membrane and even further for a planar membrane. In the steady limit in which $t \gg T_S$, the MSD progressively approaches the value predicted nearby a hard boundary. For the current set of physically realistic parameters, the steady excess MSD is found to be about twice larger for a planar membrane than that for a spherical membrane. Therefore, accounting for membrane curvature becomes crucial for an accurate and precise computation of the particle diffusional motion.

5 Capsule motion and deformation

Having analyzed the capsule-induced correction to the self-mobility, we now focus on the motion of the capsule itself. This is characterized by the pair-mobility μ^{12}, defined as the ratio between the velocity of the capsule centroid V_1 and the force F_2 applied on the nearby solid particle such that $V_1 = \mu^{12}F_2$. Without loss of generality, we assume that the force is directed along the x direction. The capsule translational velocity can be computed by volume integration of the fluid velocity inside the capsule [46],

$$V_1(\omega) = \frac{1}{\Omega}\int_0^1 \left\langle v_x^{(i)}(r,\phi,\theta,\omega)\right\rangle r^2\,\mathrm{d}r,$$

wherein $\Omega := 4\pi/3$ is the volume of the undeformed capsule, $\langle\cdot\rangle$ denotes angular averaging defined by Eq. (B.6), and $v_x^{(i)} = v_r^{(i)}\sin\theta\cos\phi + v_\theta^{(i)}\cos\theta\cos\phi - v_\phi^{(i)}\sin\phi$. After integration, only the terms with $n = 1$ of the series remain, leading to the frequency-dependent pair-mobility

$$\mu^{12} = -\frac{1}{8\pi\eta}(a_1 + b_1 - c_2)\,,$$

which after computation simplifies to

$$6\pi\eta\mu^{12} = \frac{3}{4}\,\xi + \frac{\xi^3}{4}\frac{3 + (2\lambda-1)\alpha}{5 + (2\lambda-1)\alpha}\,. \tag{5.1}$$

The correction to the pair-mobility can therefore be expressed as a Debye-type model with a relaxation time given by

$$\tau = \frac{15}{2(2\lambda-1)}\frac{\eta}{\kappa_{\mathrm{S}}}\,,$$

which is identical to that obtained for the axisymmetric motion [30].

In the limiting cases, two known results are recovered. Firstly, for $\alpha \to \infty$, we obtain the leading-order pair-mobility between two unequal hard-spheres

$$\lim_{\alpha\to\infty} 6\pi\eta\mu^{12} = \frac{3}{4}\,\xi + \frac{\xi^3}{4}\,. \tag{5.2}$$

Secondly, for $\alpha \to 0$, we get the leading-order pair-mobility between a solid particle and large spherical viscous drop

$$\lim_{\alpha\to 0} 6\pi\eta\mu^{12} = \frac{3}{4}\,\xi + \frac{3}{20}\,\xi^3\,, \tag{5.3}$$

both of which are in agreement with the results by Fuentes *et al.* [20, Eq. (16)].

Membrane deformation

The force exerted on the particle induces a fluid motion which creates imbalance in the stress tensor across the membrane. As a result, the membrane deforms elastically. We now compute the capsule deformation field resulting from a nearby point-force. To leading order in deformation, the displacement of the membrane is related to the fluid velocity via the no-slip relation given by Eq. (2.14). From Eqs. (B.5) and (B.12) we obtain

$$u_r = \frac{1}{8\pi\eta i\omega}\sum_{n=1}^{\infty}\left[\frac{n+1}{2}a_n + b_n - c_{n+1}\right]\psi_{n-1}\,, \tag{5.4}$$

$$\boldsymbol{\Pi u} = \frac{1}{8\pi\eta i\omega}\left[\sum_{n=1}^{\infty}\left(\frac{c_{n+3}}{n+2} - \frac{c_{n+1}}{n} + \frac{b_n}{n} + \frac{n+3}{2n}a_n\right)\boldsymbol{\Psi}_{n-1} - \sum_{n=0}^{\infty}\frac{n+1}{n+2}c_{n+3}\,\boldsymbol{\Gamma}_n\right], \tag{5.5}$$

where $\boldsymbol{\Pi}$ denotes the projection operator defined as

$$\boldsymbol{\Pi} := \mathbf{1} - \boldsymbol{e}_r\boldsymbol{e}_r\,,$$

and

$$\boldsymbol{\Gamma}_n := \boldsymbol{\Pi}\boldsymbol{\gamma}_n\,, \qquad \boldsymbol{\Psi}_n := \boldsymbol{\Pi}\boldsymbol{\nabla}\psi_n\,.$$

We define the frequency-dependent reaction tensor R_{ij} relating the membrane displacement to

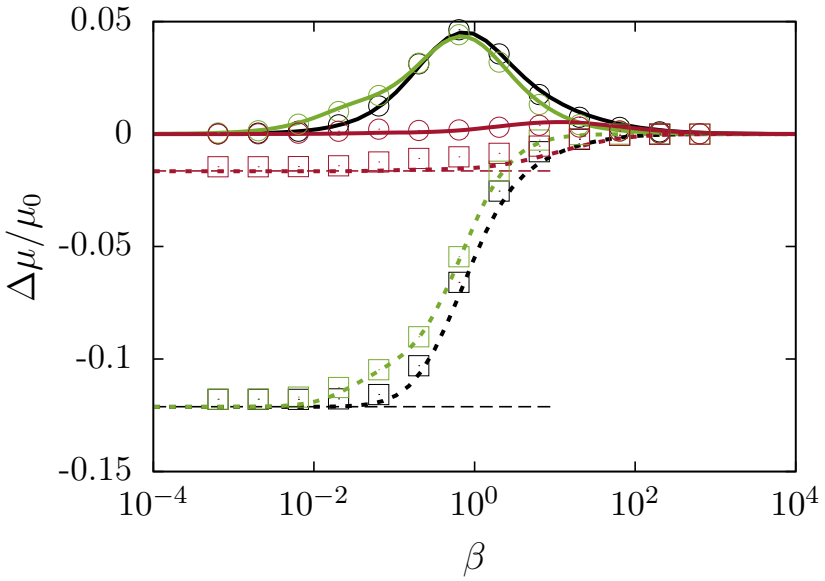

Figure 7: (Color online) Scaled frequency-dependent particle self-mobility correction versus the scaled frequency β nearby a membrane endowed with only shearing (green), only bending (red) and both rigidities (black). The small particle of radius $b = 1/10$ is at a distance $h = 2b$. Here we take a Skalak ratio $C = 1$ and a reduced bending modulus $E_B = 2/3$. The theoretical predictions are presented as dashed lines for the real parts and as solid lines for the imaginary parts. Symbols refer to boundary integral simulations where the real and imaginary parts are shown as squares and circles, respectively. The horizontal dashed lines are the vanishing frequency limits predicted by Eqs. (3.4) and (3.7).

the point-force as [47]

$$u_i(\phi,\theta,\omega) = R_{ij}(\phi,\theta,\omega)F_j(\omega)\,.$$

In particular, by considering a harmonic driving force $F_i(t) = K_i e^{i\omega_0 t}$ of frequency ω_0, which in the frequency domain has the form $F_i(\omega) = 2\pi K_i \delta(\omega - \omega_0)$, the membrane displacement in the temporal domain obtained upon inverse Fourier transform is calculated as

$$u_i(\phi,\theta,t) = R_{ij}(\phi,\theta,\omega_0)K_j e^{i\omega_0 t}\,.$$

Explicit expression for the reaction tensor can readily be obtained from Eqs. (5.4) and (5.5) upon separating out the force $\boldsymbol{F}$ in ψ_{n-1}, $\boldsymbol{\Psi}_{n-1}$ and $\boldsymbol{\Gamma}_n$.

6 Comparison with boundary integral simulations

In order to assess the validity and accuracy of the point-particle approximation used throughout this work, we compare our analytical predictions with fully resolved numerical simulations. The simulation method is based on the completed double layer boundary integral equation method (CDLBIEM) [48–51], which has been proven to be perfectly suited for simulating deformable soft objects and solid particles in the vanishing Reynolds number regime. Further technical details regarding the algorithm and its numerical implementation have been reported by some of us elsewhere, see e.g. Ref. [26] and [33].

In Fig. 7, we show the scaled particle self-mobility correction versus the scaled frequency predicted theoretically by Eq. (3.2). The solid particle of radius $b = 1/10$ is positioned at $h = 2b$ close to a large spherical capsule. Here we take the same simulation parameters as in part I for a Skalak ratio

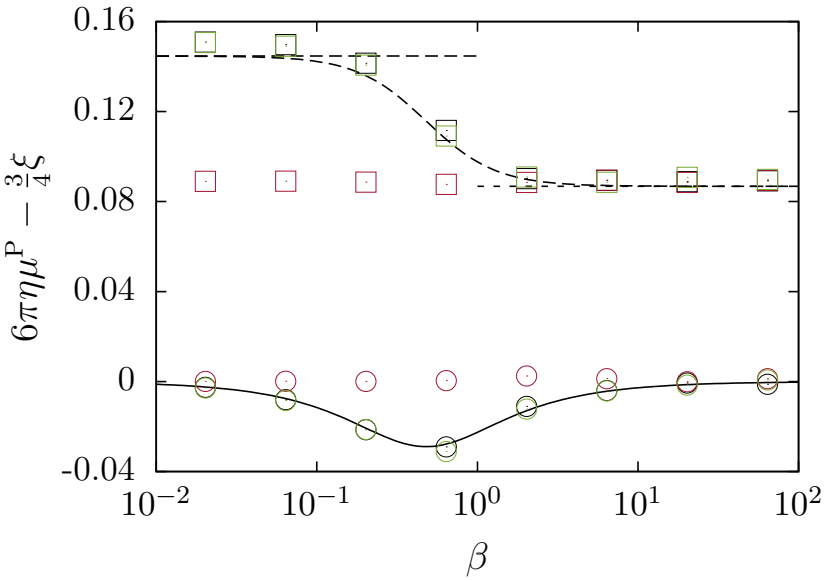

Figure 8: (Color online) The scaled pair-mobility correction versus the scaled frequency nearby a membrane possessing only shearing (green), only bending (red) and both rigidities (black). The analytical prediction given by Eq. (5.1) is shown as dashed line for the real part and as solid line for the imaginary part. Simulation results are shown as squares and circles for the real and imaginary parts, respectively. The horizontal long-dashed line is the hard-sphere limit predicted by Eq. (5.2) where the short-dashed line is the viscous drop limit given by Eq. (5.3).

$C = 1$ ($\lambda = 2$) and a reduced bending modulus $E_{\mathrm{B}} = 2/3$. We also show results for an idealized membrane with pure shearing (green) and pure bending (red).

We observe that shearing resistance manifests itself in a more pronounced way compared to bending. The mobility correction nearby a hard-sphere is recovered only if the membrane possesses a non-vanishing resistance towards shearing, in line with theoretical predictions. A very good agreement is obtained between analytical predictions and boundary integral simulations over the whole range of applied frequencies.

Next, we turn our attention to the motion of the capsule induced by the nearby solid particle. In Fig. 8 we plot the scaled pair-mobility correction versus the scaled frequency as predicted theoretically by Eq. (5.1). We observe that the correction for a membrane with pure shearing is almost identical to that of a membrane with both shearing and bending resistances, thus confirming the dominant contribution of shearing to the pair-mobility. For small forcing frequencies, the correction approaches that near a hard-sphere given by Eq. (5.2). On the other hand, the correction approaches that near a viscous drop for high frequencies as given by Eq. (5.3). The correction nearby a membrane with pure bending remains typically constant upon changing the actuation frequency, and equals to that predicted nearby a viscous drop, in agreement with theoretical predictions.

In Fig. 9, we present a comparison between analytical prediction and boundary integral simulations of the capsule deformation for a membrane possessing both shearing and bending resistances, using the same parameters as in Fig. 7. The displacement field is shown in the plane of maximal deformation (the plane $\phi = 0$ for u_r and u_θ and the plane $\phi = \pi/2$ for u_ϕ), plotted at quarter period for which $t\omega_0 = \pi/2$ i.e. when the oscillating particle reaches its maximal position. We observe that the radial displacement vanishes at the capsule poles and shows a non-monotonic dependence on the polar angle θ. On the other hand, the in-plane displacements u_θ and u_ϕ are monotonically decreasing functions of θ and reach their maximum at $\theta = 0$. We observe that the in-plane displacement along the membrane

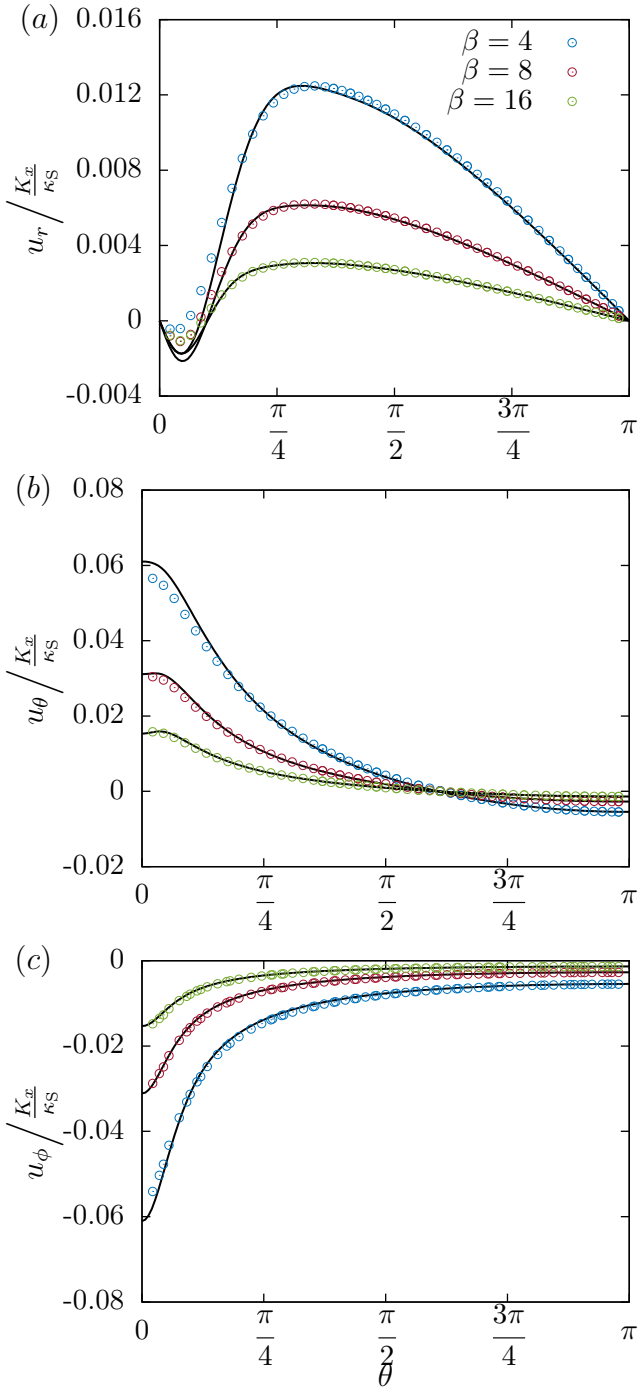

Figure 9: (Color online) The membrane displacement versus the polar angle θ in the plane of maximum displacement (the plane $\phi = 0$ for u_r and u_θ and the plane $\phi = \pi/2$ for u_ϕ) for three scaled forcing frequencies β at quarter period for $t\omega_0 = \pi/2$. Solid lines are the theoretical predictions obtained from Eqs. (5.4) and (5.5) and symbols are boundary integral simulations.

is about five times larger than the radial displacement, in contrast to the axisymmetric motion where the radial displacement is found to be about three times larger than tangential displacement. By analyzing the displacement at various actuation frequencies, we observe that larger frequencies induce smaller deformation as the capsule membrane does not have enough time to respond to the

fast wiggling particle. As shown in part I for typical situations, taking a forcing frequency $\beta = 4$ induces a maximal membrane deformation of about 1 % of its initially undeformed radius. As a result, departure from sphericity is negligible and the system can accurately be studied within the frame of the linear theory of elasticity adopted throughout this work. The analytical predictions are found to be in a very good agreement with boundary integral simulations.

7 Conclusions

This work, together with an earlier paper [30], provides a complete solution of the hydrodynamic problem of flow induced by a point-force acting close to an elastic spherical capsule. The answer is formulated in terms of the Green's function. The problem for the force acting along the symmetry axis of the system has been treated in the first part of our considerations, while here we have extended the results to account for the force being tangential to the surface of the sphere. Together with the result of part I, the fluid flow field and thus the particle mobility functions can then be obtained for an arbitrary direction of motion. The solution has been found using the image technique. Giving all the technical details, we have done our calculations for the two cases of a membrane exhibiting resistance against shearing and bending, respectively, and explicit formulas have been presented. The same technique has been used to assess the combined effect of the two deformation modes.

We have then used the solution to characterize various dynamic effects related to this motion. To explore the effect of confinement on the motion of the particle, we have calculated the leading-order frequency-dependent hydrodynamic self-mobility of a small solid sphere moving close to the capsule. We have shown that shearing resistance induces a second low-frequency peak resulting from the membrane normal displacement. Moreover, we have demonstrated, in agreement with previous studies in different complex geometries, that in the vanishing frequency limit the particle self-mobility near a hard sphere is recovered only when the membrane possesses a non-zero resistance against shearing. By applying the fluctuation-dissipation theorem, we find that the elastic nature of the membrane introduces a memory in the system resulting to a long-lived subdiffusive regime on nearby Brownian particles. The planar membrane assumption is found to be not valid for strongly curved membranes where the steady excess MSD is significantly smaller than that predicted for the planar case.

The effect of the point-force on the capsule has been quantified in two ways. Firstly, we have calculated and analyzed the pair-mobility function, which is determined solely by the shearing properties of the membrane. We have shown it to be well described by a Debye-like model with a single relaxation time. Secondly, we have computed, in leading order, the deformation of the membrane due to the action of a point-force nearby.

All the theoretical results shown in the paper have been favorably verified in representative cases by fully resolved numerical simulations for a truly extended particle using the completed double layer boundary integral method.

Acknowledgments

ADMI and SG thank the Volkswagen Foundation for financial support and acknowledge the Gauss Center for Supercomputing e.V. for providing computing time on the GCS Supercomputer SuperMUC at Leibniz Supercomputing Center. This work has been supported by the Ministry of Science and Higher Education of Poland via the Mobility Plus Fellowship awarded to ML. This article is based upon work from COST Action MP1305, supported by COST (European Cooperation in Science and Technology).

Appendices

A Membrane mechanics

In this appendix, we derive the traction jumps across a membrane endowed with shearing and bending rigidities expressed in the spherical coordinates system for an asymmetric deformation. Here we follow the convention in which the symbols for the radial, azimuthal and polar angle coordinates are taken as r, ϕ and θ respectively, with the corresponding orthonormal basis vectors $\boldsymbol{e}_r$, $\boldsymbol{e}_\phi$ and $\boldsymbol{e}_\theta$.

Similarly, all the lengths shall be scaled by the capsule radius a. We denote by $\boldsymbol{a} = \boldsymbol{e}_r$ the position vector of the points situated at the undisplaced membrane. After deformation, the vector position reads

$$\boldsymbol{r} = (1 + u_r)\boldsymbol{e}_r + u_\theta \boldsymbol{e}_\theta + u_\phi \boldsymbol{e}_\phi \,, \tag{A.1}$$

where $\boldsymbol{u}$ denotes the displacement vector field. In the following, capital roman letters will be reserved for the undeformed state while small letters for the deformed. The spherical membrane can be defined by the covariant base vectors $\boldsymbol{g}_1 := \boldsymbol{r}_{,\theta}$ and $\boldsymbol{g}_2 := \boldsymbol{r}_{,\phi}$, where commas in indices denote spatial derivatives. The unit vector $\boldsymbol{n}$ normal to the membrane is defined in such a way to form a direct trihedron with $\boldsymbol{g}_1$ and $\boldsymbol{g}_2$. The covariant base vectors are

$$\boldsymbol{g}_1 = (u_{r,\theta} - u_\theta)\boldsymbol{e}_r + (1 + u_r + u_{\theta,\theta})\boldsymbol{e}_\theta + u_{\phi,\theta}\boldsymbol{e}_\phi \,, \tag{A.2a}$$

$$\boldsymbol{g}_2 = (u_{r,\phi} - u_\phi \sin\theta)\boldsymbol{e}_r + (u_{\theta,\phi} - u_\phi \cos\theta)\boldsymbol{e}_\theta + ((1 + u_r)\sin\theta + u_\theta \cos\theta + u_{\phi,\phi})\,\boldsymbol{e}_\phi \,, \tag{A.2b}$$

and the linearized unit normal vector reads

$$\boldsymbol{n} = \boldsymbol{e}_r - (u_{r,\theta} - u_\theta)\,\boldsymbol{e}_\theta - \left(\frac{u_{r,\phi}}{\sin\theta} - u_\phi\right)\boldsymbol{e}_\phi \,. \tag{A.3}$$

Note that $\boldsymbol{g}_1$ and $\boldsymbol{g}_2$ have (scaled) length dimension while the normal vector $\boldsymbol{n}$ is dimensionless. In the deformed state, the components of the metric tensor are defined by the scalar product $g_{\alpha\beta} = \boldsymbol{g}_\alpha \cdot \boldsymbol{g}_\beta$. The contravariant tensor $g^{\alpha\beta}$, being the inverse of the metric tensor is linearized as

$$g^{\alpha\beta} = \begin{pmatrix} 1 - 2\epsilon_{\theta\theta} & -\frac{2\epsilon_{\theta\phi}}{\sin\theta} \\ -\frac{2\epsilon_{\theta\phi}}{\sin\theta} & \frac{1-2\epsilon_{\phi\phi}}{\sin^2\theta} \end{pmatrix} , \tag{A.4}$$

wherein $\epsilon_{\alpha\beta}$ are the components of the in-plane strain tensor expressed in spherical coordinates as [52]

$$\epsilon_{\theta\theta} = (u_r + u_{\theta,\theta})\,, \tag{A.5a}$$

$$\epsilon_{\theta\phi} = \frac{1}{2}\left(\frac{u_{\theta,\phi}}{\sin\theta} + u_{\phi,\theta} - u_\phi \cot\theta\right) , \tag{A.5b}$$

$$\epsilon_{\phi\phi} = \left(u_r + \frac{u_{\phi,\phi}}{\sin\theta} + u_\theta \cot\theta\right) . \tag{A.5c}$$

The contravariant tensor in the undeformed state $G^{\alpha\beta}$ is readily obtained by considering a vanishing strain tensor in Eq. (A.4).

A.1 Shearing contribution

In this subsection, we derive the traction jump equations across a membrane endowed with a pure shearing resistance. The two strain tensor invariants are given by Green and Adkins as [53–55]

$$I_1 = G^{\alpha\beta} g_{\alpha\beta} - 2\,, \tag{A.6a}$$

$$I_2 = \det G^{\alpha\beta} \det g_{\alpha\beta} - 1\,. \tag{A.6b}$$

The stress tensor contravariant components $\tau^{\alpha\beta}$ can be obtained provided knowledge of the constitutive elastic law of the membrane, whose areal strain energy functional is $W(I_1, I_2)$, such that [56]

$$\tau^{\alpha\beta} = \frac{2}{J_\mathrm{S}} \frac{\partial W}{\partial I_1} G^{\alpha\beta} + 2J_\mathrm{S} \frac{\partial W}{\partial I_2} g^{\alpha\beta}\,, \tag{A.7}$$

wherein $J_\mathrm{S} := \sqrt{1 + I_2}$ is the Jacobian determinant, quantifying the ratio between deformed and undeformed local areas. In the linear theory of elasticity, $J_\mathrm{S} \simeq 1 + e$, with $e := \epsilon_{\theta\theta} + \epsilon_{\phi\phi}$ being the trace of the in-plane strain tensor, also know as the dilatation function [57]. In this work, we use the Skalak model to describe the elastic properties of the capsule membrane such that [58–61]

$$W(I_1, I_2) = \frac{\kappa_\mathrm{S}}{12} \left(I_1^2 + 2I_1 - 2I_2 + C I_2^2 \right)\,, \tag{A.8}$$

where $C := \kappa_\mathrm{A}/\kappa_\mathrm{S}$ is a dimensionless parameter defined as the ratio between the area expansion and shear modulus. We note that for $C = 1$, the Skalak model and the Neo-Hookean model are equivalent for small deformations [56]. Upon plugging Eq. (A.8) into Eq. (A.7), the linearized in-plane stress tensor reads

$$\tau^{\alpha\beta} = \frac{2\kappa_\mathrm{S}}{3} \begin{pmatrix} \epsilon_{\theta\theta} + Ce & \frac{\epsilon_{\theta\phi}}{\sin\theta} \\ \frac{\epsilon_{\theta\phi}}{\sin\theta} & \frac{\epsilon_{\phi\phi} + Ce}{\sin^2\theta} \end{pmatrix}\,. \tag{A.9}$$

The membrane equilibrium equations which balance the elastic and external forces read

$$\nabla_\alpha \tau^{\alpha\beta} + \Delta f^\beta = 0\,, \tag{A.10a}$$

$$\tau^{\alpha\beta} b_{\alpha\beta} + \Delta f^n = 0\,, \tag{A.10b}$$

where $\Delta \boldsymbol{f} = \Delta f^\beta \boldsymbol{g}_\beta + \Delta f^n \boldsymbol{n}$ is the traction jump and ∇_α stands for the covariant derivative defined for a second-rank tensor as [62]

$$\nabla_\alpha \tau^{\alpha\beta} = \tau^{\alpha\beta}_{,\alpha} + \Gamma^\alpha_{\alpha\eta} \tau^{\eta\beta} + \Gamma^\beta_{\alpha\eta} \tau^{\alpha\eta}\,, \tag{A.11}$$

and $\Gamma^\lambda_{\alpha\beta}$ are the Christoffel symbols of the second kind defined as [63]

$$\Gamma^\lambda_{\alpha\beta} = \frac{1}{2} g^{\lambda\eta} \left(g_{\alpha\eta,\beta} + g_{\eta\beta,\alpha} - g_{\alpha\beta,\eta} \right)\,. \tag{A.12}$$

Further, $b_{\alpha\beta}$ is the second fundamental form (curvature tensor) defined as

$$b_{\alpha\beta} = \boldsymbol{g}_{\alpha,\beta} \cdot \boldsymbol{n}\,. \tag{A.13}$$

In spherical coordinates, the non-vanishing components of the Christoffel symbols at zeroth order are $\Gamma^\phi_{\phi\theta} = \Gamma^\phi_{\theta\phi} = \cot\theta$ and $\Gamma^\theta_{\phi\phi} = -\sin\theta\cos\theta$. We find after some algebra that the tangential traction

jumps across the membrane as given by Eq. (A.10a) read

$$\tau^{\theta\theta}_{,\theta} + \tau^{\theta\phi}_{,\phi} + \Gamma^{\phi}_{\phi\theta}\tau^{\theta\theta} + \Gamma^{\theta}_{\phi\phi}\tau^{\phi\phi} + \Delta f^{\theta} = 0\,, \tag{A.14a}$$

$$\tau^{\theta\phi}_{,\theta} + \tau^{\phi\phi}_{,\phi} + \left(2\Gamma^{\phi}_{\phi\theta} + \Gamma^{\phi}_{\theta\phi}\right)\tau^{\theta\phi} + \Delta f^{\phi} = 0\,. \tag{A.14b}$$

At zeroth order, the non-vanishing components of the curvature tensor are $b_{\theta\theta} = -1$ and $b_{\phi\phi} = -\sin^2\theta$. For the normal traction jump Eq. (A.10b) we obtain

$$-\tau^{\theta\theta} - \sin^2\theta\tau^{\phi\phi} + \Delta f^{n} = 0\,. \tag{A.15}$$

After substitution and writing the projected equations in the spherical coordinates basis, we immediately get the following set of equations for the traction jump,

$$\Delta f_\theta = -\frac{2\kappa_\mathrm{S}}{3}\left((1+C)\epsilon_{\theta\theta,\theta} + C\epsilon_{\phi\phi,\theta} + \frac{\epsilon_{\theta\phi,\phi}}{\sin\theta} + (\epsilon_{\theta\theta} - \epsilon_{\phi\phi})\cot\theta\right), \tag{A.16a}$$

$$\Delta f_\phi = -\frac{2\kappa_\mathrm{S}}{3}\left(\epsilon_{\theta\phi,\theta} + \frac{1}{\sin\theta}\left(C\epsilon_{\theta\theta,\phi} + (1+C)\epsilon_{\phi\phi,\phi}\right) + 2\epsilon_{\theta\phi}\cot\theta\right), \tag{A.16b}$$

$$\Delta f_n = \frac{2\kappa_\mathrm{S}}{3}(1+2C)\left(\epsilon_{\theta\theta} + \epsilon_{\phi\phi}\right)\,. \tag{A.16c}$$

It is worth to mention here that for curved membranes, the normal traction jump does not vanish in the *plane stress* formulation employed throughout this work as the zeroth order in the curvature tensor is not identically null. In fact, this is not the case for a planar elastic membrane where the resistance to shearing introduces a jump in the tangential traction jumps only [13, 24, 26]. By substituting $\epsilon_{\theta\theta}$, $\epsilon_{\phi\phi}$ and $\epsilon_{\theta\phi}$ with their expressions, Eqs. (A.16) turn into the traction equations given by Eq. (2.12) of the main text. In the following, the traction jump equations across a membrane with a bending rigidity shall be derived.

A.2 Bending contribution

For the membrane resistance towards bending, we use the linear isotropic model, in which the bending moment is related to the curvature tensor via [64]

$$M^{\beta}_{\alpha} = -\kappa_\mathrm{B}\left(b^{\beta}_{\alpha} - B^{\beta}_{\alpha}\right)\,, \tag{A.17}$$

where κ_B is the membrane bending modulus. This model is equivalent to the Helfrich model for small deformations [34]. The mixed version of the curvature tensor b^{β}_{α} is related to its covariant representation by $b^{\beta}_{\alpha} = b_{\alpha\delta}g^{\delta\beta}$. The contravariant components of the transverse shearing vector $\boldsymbol{Q}$ can be obtained from a local torque balance with the applied moment as $Q^{\beta} = \nabla_\alpha M^{\alpha\beta}$. We note that the raising and lowering indices operations implies that $M^{\alpha\beta} = M^{\alpha}_{\delta}g^{\delta\beta}$. Therefore, the components of the shearing force read

$$Q^{\theta} = -\kappa_\mathrm{B}\Big[\left(1-\cot^2\theta\right)u_{r,\theta} + u_{r,\theta\theta}\cot\theta + u_{r,\theta\theta\theta} + (1+\cot^2\theta)\left(u_{r,\phi\phi\theta} - 2u_{r,\phi\phi}\cot\theta\right)\Big]\,, \tag{A.18a}$$

$$Q^{\phi} = -\kappa_\mathrm{B}(1+\cot^2\theta)\Big(u_{r,\phi\theta}\cot\theta + 2u_{r,\phi} + u_{r,\phi\theta\theta} + (1+\cot^2\theta)u_{r,\phi\phi\phi}\Big)\,. \tag{A.18b}$$

The equilibrium equations read

$$-b_\alpha^\beta Q^\alpha + \Delta f^\beta = 0\,, \tag{A.19a}$$
$$\nabla_\alpha Q^\alpha + \Delta f^n = 0\,, \tag{A.19b}$$

where for a first-rank tensor the covariant derivative is defined as $\nabla_\beta Q^\alpha = \partial_\beta Q^\alpha + \Gamma^\alpha_{\beta\delta} Q^\delta$. By substituting Q^θ and Q^ϕ with their expressions, we thus obtain the traction jumps given by Eqs. (2.13) of the main text.

B Determination of the unknown coefficients

In this appendix, we present technical details regarding the determination of the unknown coefficients (A_n, B_n, C_n for the reflected flow, and a_n, b_n, c_n for the inner flow). For that purpose, we first project the velocities on the surface of the membrane onto the radial and tangential directions following the approach of Fuentes *et al* [19, 20].

B.1 Velocity projections

For the radial projection, we use the following identities

$$\boldsymbol{e}_r \cdot \boldsymbol{\nabla}\psi_{n-1} = -\frac{n+1}{r}\,\psi_{n-1}\,, \tag{B.1a}$$
$$\boldsymbol{e}_r \cdot \boldsymbol{r}\psi_{n-1} = r\psi_{n-1}\,, \tag{B.1b}$$
$$\boldsymbol{e}_r \cdot \boldsymbol{\gamma}_{n-1} = -\frac{1}{r}\,\psi_{n-2}\,, \tag{B.1c}$$
$$\boldsymbol{e}_r \cdot (\boldsymbol{t}\times\boldsymbol{r})\,\varphi_{n-1} = 0\,. \tag{B.1d}$$

Moreover, the projection of Eq. (2.17) onto the radial direction leads to

$$\boldsymbol{e}_r \cdot \boldsymbol{F}\varphi_n = \frac{1}{2n+1}\left(\frac{\psi_{n-2}}{r} - r\psi_n\right)\,. \tag{B.2}$$

Therefore, the radial components can all be expressed in terms of a single harmonic ψ_n. Using these identities in Eqs. (2.18), (2.20) and (2.21), we obtain

$$8\pi\eta v_r^{\mathrm{S}} = \sum_{n=1}^{\infty}\left[\frac{n-2}{2n-1}\frac{r^{2n}}{R^n} - \frac{n}{2n+3}\frac{r^{2n+2}}{R^{n+2}}\right]\psi_{n-1}\,, \tag{B.3}$$
$$8\pi\eta v_r^{*} = \sum_{n=1}^{\infty}\left[-\frac{n+1}{2n-1}rA_{n-1} + \frac{n+3}{2n+3}\frac{A_{n+1}}{r} + 2(n+1)\frac{B_{n-1}}{r} - \frac{C_n}{r}\right]\psi_{n-1}\,, \tag{B.4}$$
$$8\pi\eta v_r^{(i)} = \sum_{n=1}^{\infty}\left[\frac{n+1}{2}a_n r^{2n+2} + b_n r^{2n} - c_{n+1}r^{2n}\right]\psi_{n-1}\,. \tag{B.5}$$

For the projection onto the tangential direction, we need to use the orthogonality properties of spherical harmonics on a spherical surface. To this end, we introduce the following notation for the average of a given scalar quantity M over a sphere,

$$\langle M\rangle := \frac{1}{2\pi}\int_0^{2\pi}\int_0^{\pi} M\sin\theta\,\mathrm{d}\theta\,\mathrm{d}\phi\,, \tag{B.6}$$

which we will use extensively for writing the orthogonality properties of the considered functions. In particular, we have

$$\langle \varphi_{m-1}\varphi_{n-1}\rangle = \frac{2}{2n+1}\frac{\delta_{mn}}{r^{2n+2}}\,,$$
$$\langle \psi_{m-1}\psi_{n-1}\rangle = \frac{n(n+1)}{2n+1}\frac{\delta_{mn}}{r^{2n+2}}\,.$$

We also define the operator

$$\boldsymbol{\Pi} := \mathbf{1} - \boldsymbol{e}_r\boldsymbol{e}_r\,,$$

which projects vectors on a plane tangent to the spherical membrane surface. By applying the projection operator to Eq. (2.17), we obtain

$$(n+1)(\boldsymbol{\Pi}\boldsymbol{F})\varphi_n = \frac{1}{2n+1}\left(\boldsymbol{\Psi}_{n-2} - r^2\boldsymbol{\Psi}_n\right) - \boldsymbol{\Gamma}_{n-1}, \tag{B.7}$$

where we have defined

$$\boldsymbol{\Gamma}_n := \boldsymbol{\Pi}\boldsymbol{\gamma}_n\,, \qquad \boldsymbol{\Psi}_n := \boldsymbol{\Pi}\boldsymbol{\nabla}\psi_n\,.$$

We also note the relation

$$(2n-1)\boldsymbol{\Pi}(\boldsymbol{t}\times\boldsymbol{r})\varphi_{n-1} = \boldsymbol{\Gamma}_{n-3} - r^2\boldsymbol{\Gamma}_{n-1} + (2n-3)(\boldsymbol{\Pi}\boldsymbol{F})\varphi_{n-2}\,, \tag{B.8}$$

which upon using Eq. (B.7) gives

$$(2n-1)\boldsymbol{\Pi}(\boldsymbol{t}\times\boldsymbol{r})\varphi_{n-1} = \frac{1}{n-1}\left(\boldsymbol{\Psi}_{n-4} - r^2\boldsymbol{\Psi}_{n-2}\right) - \frac{n-2}{n-1}\boldsymbol{\Gamma}_{n-3} - r^2\,\boldsymbol{\Gamma}_{n-1}\,. \tag{B.9}$$

Applying the projection relations Eq. (B.7) and (B.9) to Eqs. (2.18), (2.20) and (2.21), we finally obtain

$$8\pi\eta\,\boldsymbol{\Pi}\boldsymbol{v}^{\mathrm{S}} = \sum_{n=1}^{\infty}\left[\frac{n-2}{(2n-1)n}\frac{r^{2n+1}}{R^n} - \frac{n}{(n+2)(2n+3)}\frac{r^{2n+3}}{R^{n+2}}\right]\boldsymbol{\Psi}_{n-1} + \sum_{n=0}^{\infty} -\frac{2}{n+2}\frac{r^{2n+3}}{R^{n+2}}\,\boldsymbol{\Gamma}_n\,, \tag{B.10}$$

$$\begin{aligned}8\pi\eta\,\boldsymbol{\Pi}\boldsymbol{v}^{*} = &\sum_{n=1}^{\infty}\left[-\frac{n}{(n+2)(2n+3)}A_{n+1} + \frac{n-2}{n(2n-1)}\,r^2A_{n-1} - 2B_{n-1}\right]\boldsymbol{\Psi}_{n-1}\\ &+\sum_{n=0}^{\infty}\left[C_n - \frac{2}{n+2}A_{n+1}\right]\boldsymbol{\Gamma}_n\,,\end{aligned} \tag{B.11}$$

$$\begin{aligned}8\pi\eta\,\boldsymbol{\Pi}\boldsymbol{v}^{(i)} = &\sum_{n=1}^{\infty}\left[\frac{r^{2n+3}}{n+2}c_{n+3} - \frac{r^{2n+1}}{n}c_{n+1} + b_n\frac{r^{2n+1}}{n} + a_n\frac{n+3}{2n}r^{2n+3}\right]\boldsymbol{\Psi}_{n-1}\\ &+\sum_{n=0}^{\infty} -\frac{n+1}{n+2}\,r^{2n+3}c_{n+3}\,\boldsymbol{\Gamma}_n\,.\end{aligned} \tag{B.12}$$

The functions $\boldsymbol{\Psi}_{n-1}$ and $\boldsymbol{\Gamma}_n$ satisfy the following orthogonality relations

$$\langle \boldsymbol{\Psi}_{m-1}\cdot\boldsymbol{\Psi}_{n-1}\rangle = \frac{n^2(n+1)^2}{2n+1}\frac{\delta_{mn}}{r^{2n+4}}\,, \tag{B.13}$$

$$\langle \boldsymbol{\Gamma}_{m}\cdot\boldsymbol{\Gamma}_{n}\rangle = \frac{4(n+1)^3}{(2n+1)(2n+3)}\frac{\delta_{mn}}{r^{2n+4}}\,, \tag{B.14}$$

and also for cross terms

$$\langle \mathbf{\Psi}_{m-1} \cdot \mathbf{\Gamma}_n \rangle = \frac{n^2(n+1)}{2n+1} \frac{\delta_{mn}}{r^{2n+4}} \,. \tag{B.15}$$

We note that their derivatives with respect to r needed for the computation of stresses can be obtained from

$$\mathbf{\Psi}_{n-1,r} = -\frac{n+2}{r} \mathbf{\Psi}_{n-1} \,,$$
$$\mathbf{\Gamma}_{n,r} = -\frac{n+2}{r} \mathbf{\Gamma}_n \,.$$

Having introduced these tools, we now proceed to the calculation of the fluid velocity coefficients.

B.2 Pressure field

The pressure field can be found by multipole expansion. The general form of the pressure p in the exterior fluid is written as a sum of exterior and interior harmonics as

$$8\pi p = \sum_{n=1}^{\infty} \left(S_n + Q_n r^{2n+1} \right) \psi_{n-1} \,.$$

The coefficients S_n and Q_n can be related to the coefficients of the velocity thanks to the Stokes equation (2.1), leading to

$$S_n = -2A_{n-1} \,, \qquad Q_n = -\frac{2}{R^{n+2}} \,.$$

For the fluid inside the capsule, all harmonics of negative order that lead to a singularity at the origin should be discarded, thus reducing the form of the pressure to

$$8\pi p^{(i)} = \sum_{n=1}^{\infty} p_n r^{2n+1} \psi_{n-1} \,,$$

leading upon using Eq. (2.3) to

$$p_n = \frac{(n+1)(2n+3)}{n} a_n \,.$$

B.3 Continuity of velocity

After substituting the radially projected velocities given by Eqs. (B.3) through (B.5) into Eq. (2.7), the continuity of the radial component at the membrane leads to

$$\begin{aligned} &\frac{n+3}{2n+3} A_{n+1} - \frac{n+1}{2n-1} A_{n-1} + 2(n+1) B_{n-1} - C_n + \frac{n-2}{2n-1} \frac{1}{R^n} - \frac{n}{2n+3} \frac{1}{R^{n+2}} \\ =&\frac{n+1}{2} a_n + b_n - c_{n+1}, \end{aligned} \tag{B.16}$$

in direct analogy with Fuentes *et al*[20].

Substituting Eqs. (B.10) through (B.12) into Eq. (2.5) and (2.6), the continuity of the tangential

velocity across the membrane leads to the two following equations

$$-\frac{n}{(n+2)(2n+3)}A_{n+1}+\frac{n-2}{n(2n-1)}A_{n-1}-2B_{n-1}+\frac{n-2}{n(2n-1)}\frac{1}{R^n} \tag{B.17}$$
$$-\frac{n}{(n+2)(2n+3)}\frac{1}{R^{n+2}}=\frac{c_{n+3}}{n+2}-\frac{c_{n+1}}{n}+\frac{b_n}{n}+\frac{n+3}{2n}a_n\,,$$
$$\frac{2}{n+2}A_{n+1}-C_n+\frac{2}{n+2}\frac{1}{R^{n+2}}=\frac{n+1}{n+2}c_{n+3}\,. \tag{B.18}$$

We note that Fuentes *et al.* [20, p. 64] reported $-2B_{n-1}$ with an erroneous plus sign, which we correct here.

Solving Eqs. (B.16), (B.17) and (B.18) for the unknown coefficients inside the capsule a_n, b_n and c_n leads to

$$a_n=A_{n-1}-\frac{2n^2+7n+3}{2n^2+5n+3}A_{n+1}-2(2n+1)B_{n-1}+\frac{2n+1}{n+1}C_n-\frac{2n}{2n^2+5n+3}\frac{1}{R^{n+2}}\,, \tag{B.19}$$
$$b_n=-\frac{2n^3+n^2-10n+3}{2(n-1)(2n-1)}A_{n-1}+\frac{n+3}{2}A_{n+1}+(2n^2+5n+3)B_{n-1}-\frac{n}{n-1}C_{n-2} \tag{B.20}$$
$$-\frac{2n+3}{2}C_n+\frac{n(n+1)}{(2n-1)(n-1)}\frac{1}{R^n}\,,$$
$$c_n=\frac{2}{n-2}A_{n-2}-\frac{n-1}{n-2}C_{n-3}+\frac{2}{n-2}\frac{1}{R^{n-1}}\,. \tag{B.21}$$

B.4 Discontinuity of stress tensor

Expressions for A_n, B_n and C_n can be determined from the discontinuity of the fluid stress tensor across the membrane. In order to gauge the effect of membrane shearing and bending on the particle mobility, we hereafter consider shearing and bending effects separately.

Pure shearing

For the sake of clarity, we write the radial and tangential velocities respectively stated by Eqs. (B.3)-(B.5) and (B.10)-(B.12) as

$$v_r=\sum_{n=1}^{\infty}\rho_n\psi_{n-1}\,,\qquad \boldsymbol{\Pi v}=\sum_{n=1}^{\infty}\alpha_n\boldsymbol{\Psi}_{n-1}+\sum_{n=0}^{\infty}\beta_n\boldsymbol{\Gamma}_n\,,$$

for the fluid velocity outside the capsule wherein ρ_n, α_n and β_n are functions of r only. Analogous expressions can be written for the radial and tangential velocities inside with the corresponding coefficients $\rho_n^{(i)}$, $\alpha_n^{(i)}$ and $\beta_n^{(i)}$.

Eqs. (2.8) and (2.9) with the shearing part only, as given by Eqs. (2.12a) and (2.12b), can be cast in the following form

$$\sum_{n=1}^{\infty}\tilde{\alpha}_n\boldsymbol{\Psi}_{n-1}+\sum_{n=0}^{\infty}\tilde{\beta}_n\boldsymbol{\Gamma}_n=\sum_{n=1}^{\infty}\alpha_n\boldsymbol{F}_n+\sum_{n=0}^{\infty}\beta_n\boldsymbol{G}_n+\sum_{n=1}^{\infty}\rho_n\boldsymbol{f}_n\,, \tag{B.22}$$

where

$$\tilde{\alpha}_n=\alpha_{n,r}-\alpha_{n,r}^{(i)}-(n+2)\left(\alpha_n-\alpha_n^{(i)}\right)\,,$$

and analogously for $\tilde{\beta}_n$. Expressions for $\boldsymbol{F}_n$, $\boldsymbol{G}_n$ and $\boldsymbol{f}_n$ can readily be obtained by identification.

Multiplying both members of Eq. (B.22) by $\boldsymbol{\Psi}_{m-1}$ and by $\boldsymbol{\Gamma}_m$, and averaging over the surface of the sphere allows us to use the following orthogonality relations

$$\begin{aligned}
\langle \boldsymbol{F}_n \cdot \boldsymbol{\Psi}_{m-1} \rangle &= \frac{\alpha n^2 (n+1)^2}{2n+1} \left(n(n+1)\lambda - 1 \right) , \\
\langle \boldsymbol{G}_n \cdot \boldsymbol{\Psi}_{m-1} \rangle &= \frac{\alpha n^2 (n+1)}{2n+1} \left(n(n+1)\lambda - 1 \right) , \\
\langle \boldsymbol{f}_n \cdot \boldsymbol{\Psi}_{m-1} \rangle &= -\frac{\alpha n^2 (n+1)^2}{2n+1} \left(2\lambda - 1 \right) , \\
\langle \boldsymbol{F}_n \cdot \boldsymbol{\Gamma}_m \rangle &= \frac{\alpha n^2 (n+1)}{2n+1} \left(n(n+1)\lambda - 1 \right) , \\
\langle \boldsymbol{G}_n \cdot \boldsymbol{\Gamma}_m \rangle &= \frac{\alpha n (n+1)}{2(2n+1)(2n+3)} \big(12 + 22n + 13n^2 + 2n^3 + 2n^2(2n+3)\lambda \big) , \\
\langle \boldsymbol{f}_n \cdot \boldsymbol{\Gamma}_m \rangle &= -\frac{\alpha n^2 (n+1)}{2n+1} \left(2\lambda - 1 \right) ,
\end{aligned}$$

where $i\alpha = 2\kappa_{\mathrm{S}}/(3\eta\omega)$. Combining these with Eqs. (B.13) through (B.15), we get

$$(n+1)\tilde{\alpha}_n + \tilde{\beta}_n = \alpha \Big[\left[(n+1)\alpha_n + \beta_n \right] \left[n(n+1)\lambda - 1 \right] - (n+1)(2\lambda - 1)\rho_n \Big] , \tag{B.23}$$

$$\begin{aligned}
\tilde{\alpha}_n + \frac{4(n+1)^2}{(2n+3)n^2} \tilde{\beta}_n = \alpha \Big[& \left(n(n+1)\lambda - 1 \right) \alpha_n \\
& + \frac{12 + 22n + 13n^2 + 2n^3 + 2n^2(2n+3)\lambda}{2n(2n+3)} \beta_n - (2\lambda - 1)\rho_n \Big] .
\end{aligned} \tag{B.24}$$

Further, the normal traction jump, given by Eqs. (2.10) and (2.12c), can be written as

$$\sum_{n=1}^{\infty} \left(p_n - p_n^{(i)} \right) \psi_{n-1} = \alpha(2\lambda - 1) \sum_{n=1}^{\infty} \left[\rho_{n,r} - (n+1)\rho_n \right] \psi_{n-1} ,$$

leading directly to

$$p_n - p_n^{(i)} = \alpha(2\lambda - 1) \left[\rho_{n,r} - (n+1)\rho_n \right] . \tag{B.25}$$

Eqs. (B.23), (B.24) and (B.25) together with (B.19) through (B.21) form a closed system of equations amenable to immediate resolution by the standard substitution method. Finally, we obtain

$$A_n = \frac{\alpha n}{K} \left(\frac{K_1}{R^{n+1}} - \frac{K_3}{R^{n+3}} \right) , \tag{B.26}$$

with the auxiliary functions

$$\begin{aligned}
K_1 &= (2n+3)(n-1) \big[(4-\alpha)(n^2 + 4n + 3) + 3 + \big(2n^2 + (2\alpha + 5)n + 6\alpha \big) (n+1)\lambda \big] , \\
K_3 &= (2n+1)(n+1) \big[(4-\alpha)(n^2 + 4n + 3) + 3 + \big(2n^2 + (2\alpha + 7)n + 6\alpha + 6 \big) (n+1)\lambda \big] , \\
K &= 8\lambda\alpha n^5 + 2 \left[(2\lambda - 1)\alpha^2 + 30\lambda\alpha + 16 \right] n^4 + 4 \left[3(2\lambda - 1)\alpha^2 + 43\lambda\alpha + 48 \right] n^3 \\
&\quad + 2 \left[11(2\lambda - 1)\alpha^2 + 117\lambda\alpha + 200 \right] n^2 + 6 \left[2(2\lambda - 1)\alpha^2 + (25\lambda - 2)\alpha + 56 \right] n \\
&\quad + 18(2\lambda - 1)\alpha + 90 .
\end{aligned}$$

Further, we express B_n in terms of A_n and A_{n+2} as

$$B_n = -\frac{n+1}{2(n+3)(2n+5)}A_{n+2} + \frac{1}{2G}\left[\frac{1}{2n+1}\left(G'A_n + \frac{\alpha n G_1}{R^{n+1}}\right)\right. \\ \left. - \frac{\alpha(n+1)G_3}{(n+3)(2n+5)\left(\alpha n^2 + (5\alpha+4)n + 4\alpha + 10\right)}\frac{1}{R^{n+3}}\right], \tag{B.27}$$

with

$$\begin{aligned} G &= \lambda\alpha n^3 + ((6\lambda-1)\alpha+4)\,n^2 + [(11\lambda-4)\alpha+16]\,n + 3(2\lambda-1)\alpha + 15\,,\\ G' &= \lambda\alpha n^3 + [(4\lambda-1)\alpha+4]\,n^2 + [(5\lambda-4)\alpha+8]\,n + (2\lambda-1)\alpha + 3\,,\\ G_1 &= \lambda n^2 + n - (\lambda+1)\,,\\ G_3 &= \lambda\alpha n^5 + [(7\lambda+1)\alpha+4\lambda]\,n^4 + [3(\lambda+4)\alpha + 2(17\lambda-6)]\,n^3\\ &\quad + [2(52\lambda-47) - (71\lambda-51)\alpha]\,n^2 + 2\,[67\lambda - 171 - 2(41\lambda-22)\alpha]\,n\\ &\quad - 48(2\lambda-1)\alpha + 30(2\lambda-11)\,. \end{aligned}$$

The last coefficient, C_n, is found as

$$C_n = \frac{2}{n+2}A_{n+1} + \frac{2n(n+3)\alpha}{(n+2)\left(\alpha n^2 + (3\alpha+4)n + 6\right)}\frac{1}{R^{n+2}}\,. \tag{B.28}$$

In particular, for $\alpha \to \infty$ (obtained either by considering an infinite shearing modulus or a vanishing forcing frequency), we recover the coefficients near a hard-sphere with stick boundary conditions, namely

$$\begin{aligned} \lim_{\alpha\to\infty} A_n &= \frac{1}{2(n+2)}\left(\frac{(2n+3)(n-1)}{R^{n+1}} - \frac{(2n+1)(n+1)}{R^{n+3}}\right),\\ \lim_{\alpha\to\infty} B_n &= \frac{n-1}{4(n+2)}\frac{1}{R^{n+1}} + \frac{n+1}{4(n+4)}\frac{1}{R^{n+5}} - \frac{n^2+3n-1}{2(n+2)(n+4)}\frac{1}{R^{n+3}}\,,\\ \lim_{\alpha\to\infty} C_n &= \frac{2n+3}{n+3}\left(\frac{1}{R^{n+2}} - \frac{1}{R^{n+4}}\right), \end{aligned}$$

all in agreement with the results of Fuentes *et al.* [20], and as given in Kim and Karrila [15, p. 246].

Pure bending

In complete analogy with the previous section, Eqs. (2.8) and (2.9) with the right-hand side given by (2.13b) and (2.13a), respectively, can be written as

$$\sum_{n=1}^{\infty}\tilde{\alpha}_n\boldsymbol{\Psi}_{n-1} + \sum_{n=0}^{\infty}\tilde{\beta}_n\boldsymbol{\Gamma}_n = \sum_{n=1}^{\infty}\rho_n\boldsymbol{g}_n\,, \tag{B.29}$$

where $\boldsymbol{g}$ can directly be determined by identification. Multiplying both members of Eq. (B.29) by $\boldsymbol{\Psi}_{m-1}$ and by $\boldsymbol{\Gamma}_m$, averaging over the surface of the sphere upon making use of the following

orthogonality relations

$$\langle \boldsymbol{g}_n \cdot \boldsymbol{\Psi}_{m-1} \rangle = -\alpha_{\mathrm{B}} \frac{(n^2-1)n^2(n+1)(n+2)}{2n+1} \delta_{mn} \,,$$
$$\langle \boldsymbol{g}_n \cdot \boldsymbol{\Gamma}_m \rangle = -\alpha_{\mathrm{B}} \frac{(n^2-1)n^2(n+2)}{2n+1} \delta_{mn} \,,$$

together with Eqs. (B.13) through (B.15), we get

$$\tilde{\alpha}_n + \frac{1}{n+1}\tilde{\beta}_n = -\alpha_{\mathrm{B}}(n-1)(n+2)\rho_n \,, \tag{B.30}$$
$$\tilde{\alpha}_n + \frac{4(n+1)^2}{n^2(2n+3)}\tilde{\beta}_n = -\alpha_{\mathrm{B}}(n-1)(n+2)\rho_n \,, \tag{B.31}$$

where $i\alpha_{\mathrm{B}} = \kappa_{\mathrm{B}}/(\eta\omega)$.

For the normal traction jump, Eq. (2.10) with (2.13c) can be written as

$$-\sum_{n=1}^{\infty} \left(p_n - p_n^{(i)} \right) \psi_{n-1} = \sum_{n=1}^{\infty} \rho_n H_n \,.$$

After making use of the orthogonality property

$$\langle H_n \psi_{m-1} \rangle = -\alpha_{\mathrm{B}} \frac{(n^2-1)n^2(n+1)(n+2)}{2n+1} \delta_{mn} \,,$$

we obtain

$$p_n - p_n^{(i)} = -\alpha_{\mathrm{B}}(n^2-1)n(n+2)\rho_n \,. \tag{B.32}$$

Solving the system of equations formed of Eqs. (B.30), (B.31) and (B.32) together with (B.19) through (B.21), we obtain the first set of coefficients as

$$A_n = \frac{\alpha_{\mathrm{B}} w}{W} \left[\frac{(2n+5)(n-1)}{R^{n+1}} - \frac{(2n+1)(n+1)}{R^{n+3}} \right], \tag{B.33}$$

where

$$w = n^2(n+1)(n+2)(n+3),$$
$$W = 30 + (12\alpha_{\mathrm{B}} + 92)n + (94\alpha_{\mathrm{B}} + 72)n^2 + (168\alpha_{\mathrm{B}} + 16)n^3 + 118\alpha_{\mathrm{B}} n^4 + 36\alpha_{\mathrm{B}} n^5 + 4\alpha_{\mathrm{B}} n^6.$$

For the set B_n, we find

$$B_n = -\frac{(n+1)A_{n+2}}{2(n+3)(2n+5)} + \frac{1}{S}\left[\frac{S' A_n}{2n+1} + \alpha_{\mathrm{B}} n(n+3) \left(\frac{(n+1)^2}{2n+5} \frac{1}{R^{n+3}} - \frac{n^2-1}{2n+1} \frac{1}{R^{n+1}} \right) \right], \tag{B.34}$$

where we defined

$$S = 2\big[\alpha_{\mathrm{B}} n^4 + 6\alpha_{\mathrm{B}} n^3 + (11\alpha_{\mathrm{B}} + 4)n^2 + 2(3\alpha_{\mathrm{B}} + 8)n + 15\big] \,,$$
$$S' = \frac{S}{2} - 8n - 12 \,.$$

Finally, the last set is simply given by

$$C_n = \frac{2A_{n+1}}{n+2} \,. \tag{B.35}$$

The same resolution procedure can be applied to the evaluation of the series coefficients when the membrane is endowed simultaneously with both shearing and bending resistances. Analytical expressions can be derived by computer algebra software but they are not listed here due to their complexity and lengthiness. It is worth to mention that a coupling between shearing and bending exists, i.e. in the same way as observed in part I [30] and for two parallel planar membranes [26] but in contrast to what has been observed for a single membrane [13, 25].

Bibliography

[1] J. Wang and W. Gao, ACS Nano **6**, 5745 (2012).

[2] W. Gao, D. Kagan, O. S. Pak, C. Clawson, S. Campuzano, E. Chuluun-Erdene, E. Shipton, E. E. Fullerton, L. Zhang, E. Lauga, and J. Wang, Small **8**, 460 (2012).

[3] R. Singh and J. W. Lillard, Exp. Mol. Pathol. **86**, 215 (2009).

[4] S. Naahidi, M. Jafari, F. Edalat, K. Raymond, A. Khademhosseini, and P. Chen, J. Control. Release **166**, 182 (2013).

[5] J. Tan, A. Thomas, and Y. Liu, Soft Matter **8**, 1934 (2012).

[6] W. Gao and J. Wang, Nanoscale **6**, 10486 (2014).

[7] M. Hofmann-Amtenbrink, D. W. Grainger, and H. Hofmann, Nanomed. Nanotech. Biol. Med. **11**, 1689 (2015).

[8] Z. Zhou, J.-B. Fan, H.-L. Zhu, F. Shewmaker, X. Yan, X. Chen, J. Chen, G.-F. Xiao, L. Guo, and Y. Liang, J. Biol. Chem. **284**, 30148 (2009).

[9] C. Chen, F. Loe, A. Blocki, Y. Peng, and M. Raghunath, Adv. Drug Deliv. Rev. **63**, 277 (2011).

[10] F. Höfling and T. Franosch, Rep. Prog. Phys. **76**, 046602:1 (2013).

[11] T. Bickel, Eur. Phys. J. E **20**, 379 (2006).

[12] T. Bickel, Europhys. Lett. **106**, 16004 (2014).

[13] A. Daddi-Moussa-Ider, A. Guckenberger, and S. Gekle, Phys. Rev. E **93**, 012612 (2016).

[14] J. Happel and H. Brenner, *Low Reynolds number hydrodynamics: with special applications to particulate media*, Vol. 1 (Springer Science & Business Media, 2012).

[15] S. Kim and S. J. Karrila, *Microhydrodynamics: principles and selected applications* (Courier Corporation, 2013).

[16] H. Kress, E. H. K. Stelzer, G. Griffiths, and A. Rohrbach, Phys. Rev. E **71**, 061927 (2005).

[17] S. B. Chen, Phys. Fluids **25**, 043106 (2013).

[18] F. Jünger, F. Kohler, A. Meinel, T. Meyer, R. Nitschke, B. Erhard, and A. Rohrbach, Biophys. J. **109**, 869 (2015).

[19] Y. O. Fuentes, S. Kim, and D. J. Jeffrey, Phys. Fluids **31**, 2445 (1988).

[20] Y. O. Fuentes, S. Kim, and D. J. Jeffrey, Phys. Fluids A **1**, 61 (1989).

[21] D. Barthès-Biesel, Ann. Rev. Fluid Mech. **48**, 25 (2016).

[22] R. Skalak, A. Tozeren, R. P. Zarda, and S. Chien, Biophys. J. **13(3)**, 245 (1973).

[23] W. Helfrich, Z. Naturf. C. **28**, 693 (1973).

[24] A. Daddi-Moussa-Ider and S. Gekle, J. Chem. Phys. **145**, 014905 (2016).

[25] A. Daddi-Moussa-Ider, M. Lisicki, and S. Gekle, J. Fluid Mech. **811**, 210 (2017).

[26] A. Daddi-Moussa-Ider, A. Guckenberger, and S. Gekle, Phys. Fluids **28**, 071903 (2016).

[27] T. Salez and L. Mahadevan, J. Fluid Mech. **779**, 181 (2015).

[28] B. Saintyves, T. Jules, T. Salez, and L. Mahadevan, Proc. Nat. Acad. Sci. **113**, 5847 (2016).

[29] B. Rallabandi, B. Saintyves, T. Jules, T. Salez, C. Schönecker, L. Mahadevan, and H. A. Stone, arXiv preprint arXiv:1611.03552 (2016).

[30] A. Daddi-Moussa-Ider and S. Gekle, Phys. Rev. E **95**, 013108 (2017).

[31] J. B. Freund, Annu. Rev. Fluid Mech. **46**, 67 (2014).

[32] T. Krüger, F. Varnik, and D. Raabe, Comp. Math. Appl. **61**, 3485 (2011).

[33] A. Guckenberger, M. P. Schraml, P. G. Chen, M. Leonetti, and S. Gekle, Comp. Phys. Comm. **207**, 1 (2016).

[34] A. Guckenberger and S. Gekle, J. Phys. Cond. Mat. (submitted) (2017).

[35] H. Lamb, *Hydrodynamics* (Cambridge university press, 1932).

[36] M. Abramowitz, I. A. Stegun, *et al.*, *Handbook of mathematical functions*, Vol. 1 (Dover New York, 1972).

[37] M. L. Ekiel-Jeżewska and B. U. Felderhof, J. Chem. Phys. **142**, 014904 (2015).

[38] H. A. Lorentz, Abh. Theor. Phys. **1**, 23 (1907).

[39] S. H. Lee, R. S. Chadwick, and L. G. Leal, J. Fluid Mech. **93**, 705 (1979).

[40] T. Auth, S. A. Safran, and N. S. Gov, Phys. Rev. E **76**, 051910 (2007).

[41] A. Košmrlj and D. R. Nelson, Phys. Rev. E **89**, 022126 (2014).

[42] R. Kubo, Rep. Prog. Phys. **29**, 255 (1966).

[43] R. Kubo, M. Toda, and N. Hashitsume, "Statistical physics II" (1985).

[44] A. Einstein, Ann. Phys. **17**, 549 (1905).

[45] A. Einstein, Ann. Phys. **19**, 289 (1906).

[46] B. U. Felderhof, Phys. Rev. E **89**, 033001 (2014).

[47] T. Bickel, Phys. Rev. E **75**, 041403 (2007).

[48] N. Phan-Thien, D. Tullock, V. Ilic, and S. Kim, Computational Mechanics **10**, 381 (1992).

[49] M. Kohr and I. I. Pop, *Viscous incompressible flow for low Reynolds numbers*, Vol. 16 (Wit Pr/Comp. Mech., 2004).

[50] H. Zhao and E. S. G. Shaqfeh, Phys. Rev. E **83**, 061924 (2011).

[51] H. Zhao, E. S. G. Shaqfeh, and V. Narsimhan, Phys. Fluids **24**, 011902 (2012).

[52] M. H. Sadd, *Elasticity: theory, applications, and numerics* (Academic Press, 2009).

[53] A. E. Green and J. C. Adkins, *Large Elastic Deformations and Non-linear Continuum Mechanics* (Oxford University Press, 1960).

[54] L. Zhu, *Simulation of individual cells in flow*, Ph.D. thesis (2014).

[55] L. Zhu and L. Brandt, J. Fluid Mech. **770**, 374 (2015).

[56] E. Lac, D. Barthès-Biesel, N. A. Pelekasis, and J. Tsamopoulos, J. Fluid Mech. **516**, 303 (2004).

[57] A. E. H. Love, *A treatise on the mathematical theory of elasticity*, Vol. 1 (Cambridge University Press, 2013).

[58] Y. Sui, H. T. Low, Y. T. Chew, and P. Roy, Phys. Rev. E **77**, 016310 (2008).

[59] T. Krüger, *Computer simulation study of collective phenomena in dense suspensions of red blood cells under shear* (Springer Science & Business Media, 2012).

[60] S. Gekle, Biophys. J. **110**, 514 (2016).

[61] C. Bächer, L. Schrack, and S. Gekle, Phys. Rev. Fluids **2**, 013102 (2017).

[62] M. Deserno, Chem. Phys. Lipids **185**, 11 (2015).

[63] J. L. Synge and A. Schild, *Tensor calculus*, Vol. 5 (Courier Corporation, 1969).

[64] C. Pozrikidis, J. Comput. Phys. **169**, 250 (2001).

Publication 10

Creeping motion of a solid particle inside a spherical elastic cavity

A. Daddi-Moussa-Ider and S. Gekle

In preparation (2017)

Abstract

On the basis of the linear hydrodynamic equations, we present a fully analytical theory of the creeping motion of a solid particle moving inside a spherical elastic cavity which can be seen as a model system for a living cell. In the particular situation where the particle is concentric with the cavity, we use the stream function technique to find exact analytical solutions of the fluid motion equations on both sides of the elastic cavity. In this particular situation, we find that the solution of the hydrodynamic equations is solely determined by membrane shearing properties and that bending does not play a role. For an arbitrary position within the spherical cavity, we employ the image solution technique to compute the axisymmetric flow field induced by a point-force (Stokeslet). We then obtain analytical expressions of the leading order mobility functions describing the fluid mediated hydrodynamic interactions between the particle and confining elastic cavity. In the vanishing frequency limit, we find that the particle self-mobility is lower than that predicted inside a rigid cavity. Considering the cavity motion, we find that the pair-mobility function is determined only by membrane shearing properties. Our analytical predictions are supplemented and validated by fully resolved boundary integral simulations where a very good agreement is obtained over the whole range of applied forcing frequencies.

1 Introduction

Transport phenomena are ubiquitous in nature and are essential for the understanding of a variety of processes in biological physics, chemistry and bioengineering [1–3]. Prime examples include the paracellular transport of drugs and macromolecules across an epithelium in organs and target-tissues [4, 5], and the active locomotion of swimming microorganisms inside living cells [6, 7].

In the microscopic world, the fluid motion is well described by the linear Stokes equations where the viscous forces play a dominant role compared to the inertial forces. In these situations, a full representation of the motion of suspended particles is achieved by the mobility tensor [8] which bridges between the velocity moments of the particle and the moments of the force density on its surface. In biological media, the motion of suspended tracer particles is sensitive to the mechanical state of living cells and the experimentally recorded trajectories can provide useful information about the membrane structure [9] or the nature of active processes driving particle motion inside living cells [10]. Over the last few decades, intracellular particle tracking experiments have widely been used as a powerful and often accurate tool for the characterization and diagnostic of individual living cells [11–14] or the determination of the cell mechanical properties [15–17].

From a theoretical point of view, particle motion inside a rigid spherical cavity with a fluid velocity satisfying the no-slip boundary condition at the inner cavity is well understood and has been solved since some time ago. The exact solution of fluid flow takes a particularly simple form when the particle is located at the center of the cavity and can be determined using the stream function technique as derived e.g. by Happel and Brenner [18]. The first attempt to obtain the fundamental solution to the Stokes equations due to a point force acting in a Newtonian fluid bounded by a rigid spherical contained dates back to Oseen [19] who used the image solution technique. Complementary works which represent extensions of Oseen's solution, commonly known under the name of sphere theorem, have been later presented by Butler [20], Collins [21, 22], Hasimoto [23–25], Shail [26, 27] and Sellier [28], to name a few. A more transparent form of the solution has been presented by Maul and Kim [29, 30] where both the axisymmetric and asymmetric Stokeslets have been considered independently. Their results are more useful for computational purposes using boundary integral methods [31] and their resolution approach is based on the method presented by Fuentes *et al.* [32, 33]. The latter computed the flow field due to a Stokeslet acting outside a viscous drop using the image solution technique. The coupling and rotational mobilities have been later reconsidered by Felderhof

and Sellier [34] who employed the point-particle approximation which is valid when particle radius is very small compared to that of the cavity. More recently, a combination of multipole expansion and Faxén's theorem has been used by Aponte-Rivera and Zia [35], providing the elements of the grand mobility tensor of finite-sized particles moving inside a rigid spherical cavity.

Despite enormous studies on particle motion inside a rigid cavity, to the best of our knowledge, no works have been conducted yet to investigate particle motion inside an elastic cavity. Indeed, elastic interfaces stand apart from rigid boundaries as they endow the system with memory, leading to a long-lived transient anomalous subdiffusive behavior of nearby particles [36, 37]. Accordingly, particle mobility does not depend only on geometry but also on the actuation frequency of the system. The goal of this work is to compute analytically and numerically the frequency-dependent mobility function of a solid particle moving inside a spherical elastic cavity. The membrane cavity is modeled as a thin two-dimensional surface made of an hyperelastic material endowed with a shearing elasticity and a bending rigidity. Membrane resistance towards shearing stresses is modeled by the well-established Skalak model [38] which is used as a practical model for capsules and red blood cells [39]. For calculating the membrane bending forces, we compare two models. The first model is based on the Helfrich free energy functional [40] which is often used for lipid bilayers and biological membranes. The second model is the linear isotropic model which is derived from the linear elastic theory of plates and shells.

When the particle is concentric with the cavity, we use the stream function technique to find exact solutions of the equations of fluid motion. For an arbitrary position within the cavity, we use the image solution technique to find analytical expressions of the axisymmetric flow field due to a Stokeslet and the leading order correction to the particle mobility. Moreover, we investigate the cavity motion, finding that the correction to the pair-mobility function for an arbitrary eccentricity within the cavity is solely determined by membrane shearing properties and that bending does not a play a role. In order to assess the validity and appropriateness of our analytical predictions, we compare our results with fully resolved boundary integral simulations where a very good agreement is obtained.

The remainder of the paper is organized as follows. In Sec. 2, we present the stream function technique and determine exact expressions of the flow field and the hydrodynamic mobility functions. We then present in Sec. 3 the image solution technique and compute the particle mobilities in the point-particle framework. Concluding remarks summarizing our findings and results are offered in Sec. 4.

2 Stream functions

We consider the steady translational motion of a spherical solid particle of radius b inside a spherical elastic cavity of initial (undeformed) radius a. The origin of coordinates is located at $\boldsymbol{x}_1$ the center of the cavity and the solid particle is located at $\boldsymbol{x}_2 = R\boldsymbol{e}_z$, with $R < a - b$, as schematically illustrated in Fig. 1.

For small amplitude and frequency of motion, the fluid dynamics inside and outside the cavity is governed by the steady Stokes equations

$$\eta \boldsymbol{\nabla}^2 \boldsymbol{v}_\alpha - \boldsymbol{\nabla} p_\alpha = 0\,, \tag{2.1}$$

$$\boldsymbol{\nabla} \cdot \boldsymbol{v}_\alpha = 0\,, \tag{2.2}$$

where $\alpha = 1$ for the fluid inside and $\alpha = 2$ for the fluid outside. The fluid on both sides has the same dynamic viscosity η. For the sake of convenience, we shall scale from now on all the lengths by the cavity radius a.

We begin with the relatively simple situation where the two spheres are concentric corresponding

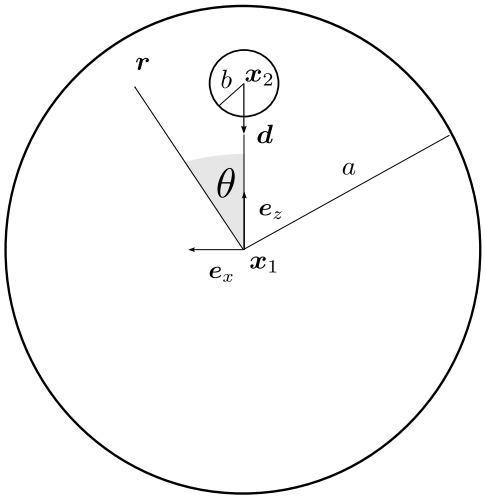

Figure 1: Illustration of the system setup. A small solid particle of radius b positioned at $\boldsymbol{x}_2 = R\boldsymbol{e}_z$ inside a large spherical elastic cavity of radius a. The Stokeslet is directed along $\boldsymbol{d}$ connecting the centers of the particle and the cavity.

to $\boldsymbol{x}_2 = \boldsymbol{x}_1$ and thus $R = 0$. Since the flow is axisymmetric, it is more convenient to express the solution of the equations of motion in term of the stream function. Accordingly, the solution is reduced to the search of a single scalar function instead of solving simultaneously for the velocity field and pressure. The stream functions inside and outside the elastic cavity satisfy [18]

$$E^4\psi_\alpha(r,\theta) = 0\,, \qquad \alpha \in \{1,2\}\,, \tag{2.3}$$

where r and θ are the radial distance and polar angle, respectively, and the operator E^2 in spherical coordinates reads

$$E^2 = \frac{\partial}{\partial r^2} + \frac{\sin\theta}{r^2}\frac{\partial}{\partial\theta}\left(\frac{1}{\sin\theta}\frac{\partial}{\partial\theta}\right)\,. \tag{2.4}$$

We now assume that the particle moves in the positive z direction with a constant velocity U. Additionally, we require the regularity conditions for the solution outside the cavity

$$\frac{\psi_2}{r^2} \to 0 \quad \text{as} \quad r \to \infty\,, \tag{2.5}$$

and no regularity conditions for the solution inside are required. The boundary conditions that must be satisfied on the particle surface read [18, p. 119]

$$\psi_1|_{r=b} = -\frac{Ub^2}{2}\sin^2\theta\,, \tag{2.6}$$

$$\psi_{1,r}\big|_{r=b} = -Ub\sin^2\theta\,. \tag{2.7}$$

The general solution for the steam function in Eq. (2.3) as suggested by the regularity and boundary conditions has been derived earlier by Happel and Brenner [18] and can be written as

$$\psi_1 = \left(Ar + Dr^2 + Er^4 + \frac{F}{r}\right)\sin^2\theta\,, \tag{2.8}$$

$$\psi_2 = \left(Gr + \frac{H}{r}\right)\sin^2\theta\,, \tag{2.9}$$

where A, D, E, F, G and H are six unknown constants to be determined from the boundary conditions imposed at the particle and cavity surfaces.

The flow radial and meridional velocity components are then computed from the stream functions as

$$v_r = -\frac{\psi_{,\theta}}{r^2 \sin\theta}\,, \qquad v_\theta = \frac{\psi_{,r}}{r \sin\theta}\,, \tag{2.10}$$

leading to

$$v_{1r} = -\left(\frac{2A}{r} + 2D + 2Er^2 + \frac{2F}{r^3}\right)\cos\theta\,, \tag{2.11}$$

$$v_{1\theta} = \left(\frac{A}{r} + 2D + 4Er^2 - \frac{F}{r^3}\right)\sin\theta\,, \tag{2.12}$$

for the fluid inside and

$$v_{2r} = -\frac{2}{r}\left(G + \frac{H}{r^2}\right)\cos\theta\,, \tag{2.13}$$

$$v_{2\theta} = \frac{1}{r}\left(G - \frac{H}{r^2}\right)\sin\theta\,, \tag{2.14}$$

for the fluid outside.

Continuing, the general expressions of the hydrodynamic pressure inside and outside the spherical cavity can readily be determined from the momentum equation (2.1) to obtain

$$\frac{p_1}{\eta} = -2\left(\frac{A}{r^2} + 10Er\right)\cos\theta\,, \tag{2.15}$$

$$\frac{p_2}{\eta} = -\frac{2G}{r^2}\cos\theta\,. \tag{2.16}$$

Having expressed the general solution of fluid motion on both sides of the cavity, we now determine the six unknown coefficients by applying the appropriate boundary conditions: (a) the non-slip conditions given by Eqs. (2.6) and (2.7) imposed at the particle surface, (b) the natural continuity of the fluid velocity between the two sides of the cavity and (c) the discontinuity of the fluid stress tensor due to the presence of the elastic membrane. Mathematically, we may formulate the problem as

$$[v_r] = 0\,, \tag{2.17}$$

$$[v_\theta] = 0\,, \tag{2.18}$$

$$[\sigma_{\theta r}] = \Delta f_\theta^{\mathrm{S}} + \Delta f_\theta^{\mathrm{B}}\,, \tag{2.19}$$

$$[\sigma_{rr}] = \Delta f_r^{\mathrm{S}} + \Delta f_r^{\mathrm{B}}\,, \tag{2.20}$$

where the notation $[w] := w_2(r=1) - w_1(r=1)$ represents the jump of a quantity w across the cavity membrane. In spherical coordinates, the non-vanishing components of the fluid stress tensor are expressed in the usual way as [8]

$$\sigma_{\theta r} = \eta\left(v_{\theta,r} - \frac{v_\theta}{r} + \frac{v_{r,\theta}}{r}\right)\,, \tag{2.21}$$

$$\sigma_{rr} = -p + 2\eta v_{r,r}\,, \tag{2.22}$$

where comma in indices denotes a spatial partial derivative. Furthermore, Δf_r and Δf_θ stand for the

radial and meridional traction jump across the cavity where the superscripts S and B respectively stand for the shearing and bending related parts. As derived in earlier work [41], the traction due to shearing elasticity according to the Skalak model reads

$$\Delta f_\theta^{\mathrm{S}} = -\frac{2\kappa_{\mathrm{S}}}{3}\bigg((1+2C)u_{r,\theta} + (1+C)u_{\theta,\theta\theta} + (1+C)u_{\theta,\theta}\cot\theta - \left((1+C)\cot^2\theta + C\right)u_\theta\bigg)\,, \quad (2.23)$$

$$\Delta f_r^{\mathrm{S}} = \frac{2\kappa_{\mathrm{S}}}{3}(1+2C)\left(2u_r + u_{\theta,\theta} + u_\theta\cot\theta\right)\,, \quad (2.24)$$

where κ_{S} is the shearing modulus (expressed in N/m) and C is a dimensionless number commonly known in the blood flow community as the Skalak parameter [42–45], defined as the ratio between area expansion modulus κ_{A} and shearing modulus κ_{S}. Moreover, u_r and u_θ are respectively the membrane radial and meridional displacements, related to the fluid velocity in Fourier space by the no-slip relation imposed at $r = 1$ by [46]

$$v_\alpha|_{r=a} = i\omega\, u_\alpha\,, \qquad \alpha \in \{r, \theta\}\,. \quad (2.25)$$

Additionally, we include a resistance towards bending which can be modeled following the celebrated Helfrich model [40, 47] or by assuming a linear isotropic model for the bending moments following a thin-shell theory approach [48]. The two formulations are equivalent for a planar membrane but not necessarily for membranes of arbitrary geometry [49]. Considering first a linear isotropic model, the traction jumps due to bending read [41]

$$\Delta f_\theta^{\mathrm{B}} = \kappa_{\mathrm{B}}\bigg(\left(1-\cot^2\theta\right)u_{r,\theta} + u_{r,\theta\theta}\cot\theta + u_{r,\theta\theta\theta}\bigg)\,, \quad (2.26)$$

$$\Delta f_r^{\mathrm{B}} = \kappa_{\mathrm{B}}\bigg(\left(3\cot\theta + \cot^3\theta\right)u_{r,\theta} - u_{r,\theta\theta}\cot^2\theta + 2\cot\theta u_{r,\theta\theta\theta} + u_{r,\theta\theta\theta\theta}\bigg)\,, \quad (2.27)$$

where κ_{B} is the membrane bending modulus (expressed in Nm). Considering next the Helfrich model, the traction jump reads [49]

$$\Delta \boldsymbol{f} = -2\kappa_{\mathrm{B}}\left(2(H^2 - K + H_0 H) + \Delta_{\parallel}\right)(H - H_0)\,\boldsymbol{n}\,, \quad (2.28)$$

where H and K are the mean and Gaussian curvatures, respectively given by

$$H = \frac{1}{2}\,b_\alpha^\alpha\,, \qquad K = \det\, b_\alpha^\beta\,, \quad (2.29)$$

with b_α^β being the mixed version of the curvature tensor. The other quantities are the spontaneous curvature H_0 which we take the initial undeformed shape here, the vector normal to the spherical cavity $\boldsymbol{n}$ and the Laplace-Beltrami operator $\Delta_{\parallel}$ [50]. Accordingly, bending introduces a discontinuity only in the normal traction such that

$$\Delta f_\theta^{\mathrm{B}} = 0\,, \quad (2.30)$$

$$\Delta f_r^{\mathrm{B}} = \kappa_{\mathrm{B}}\bigg(4u_r + (5+\cot^2\theta)\cot\theta\, u_{r,\theta} + (2-\cot^2\theta)u_{r,\theta\theta} + 2\cot\theta\, u_{r,\theta\theta\theta} + u_{r,\theta\theta\theta\theta}\bigg)\,. \quad (2.31)$$

It is worth to mention here that the traction jumps due to membrane bending depend only on the normal (radial) displacement in contrast to the traction jumps due to shearing which may depend on both the normal and tangential displacements.

Employing the no-slip conditions stated by Eqs. (2.6) and (2.7) together with the boundary

conditions imposed at the membranes stated by Eqs. (2.17) through (2.20), and solving for the unknown coefficients by considering first a linear-isotropic model for bending, we obtain

$$A = -6bU\lambda\left((1+2C)(1-b^5)\alpha+5\right)\,, \tag{2.32}$$
$$D = 5bU\lambda\alpha(1+2C)\left(1-b^2\right)\,, \tag{2.33}$$
$$E = -3bU\lambda\alpha(1+2C)(1-b^2)\,, \tag{2.34}$$
$$F = 2b^3U\lambda\left((1+2C)(1-b^3)\alpha+5\right)\,, \tag{2.35}$$
$$G = A\,, \tag{2.36}$$
$$H = 2bU\lambda\left((1+2C)\left(1-b^5\right)\alpha+5b^2\right)\,, \tag{2.37}$$

where we have defined

$$i\alpha = \frac{2\kappa_{\mathrm{S}}}{3\eta\omega}\,, \tag{2.38}$$

as a characteristic number associated to membrane resistance towards shearing and

$$\lambda^{-1} := 40 + 2\alpha(1-b)(1+2C)\left(4-b(1+b)\left(1-9b^2\right)\right)\,. \tag{2.39}$$

Interestingly, the same solution is obtained when considering the Helfrich model for the traction jumps as given by Eqs. (2.30) and (2.31). We therefore conclude that the stream functions for a particle concentric to the cavity are solely determined by membrane shearing resistance and do not depend on membrane bending.

2.1 Particle mobility

The exact analytical solution obtained for the stream functions can be used for the computation of the particle self-mobility function. The force exerted by the fluid on the sphere is calculated from the stream function using the formula [18, p. 115]

$$F_2 = \eta\pi\int_0^\pi \rho^3\frac{\partial}{\partial r}\left(\frac{E^2\psi_1}{\rho^2}\right)r\,\mathrm{d}\theta = 8\pi\eta A\,, \tag{2.40}$$

and is equivalent to the expression given by Stimson and Jeffery [51]. Here $\rho = r\sin\theta$ is the polar distance. We define the membrane correction factor K as the ratio between the drag in the presence of the outer spherical membrane and the drag in a bulk fluid such that $F_2 = -6\pi\eta bUK$, leading to

$$K = \frac{4\left((1+2C)(1-b^5)\alpha+5\right)}{20+\alpha(1-b)(1+2C)\left(4-b(1+b)\left(1-9b^2\right)\right)}\,. \tag{2.41}$$

Equivalently, the fluid mediated hydrodynamic interactions can also be assessed by determining the correction to the particle self-mobility function defined in a scaled form as

$$\frac{\Delta\mu}{\mu_0} := \frac{1}{K} - 1 = -\frac{5}{4}\frac{b\alpha(1+2C)\left(1-b^2\right)^2}{5+\alpha(1+2C)(1-b^5)}\,, \tag{2.42}$$

where $\mu_0 = 1/(6\pi\eta b)$ is the usual bulk mobility. Not surprisingly, the frequency-dependent particle mobility is solely determined by membrane shearing properties. At leading order in b, Eq. (2.42) can be expanded as

$$\frac{\Delta\mu}{\mu_0} = -\frac{5}{4}\frac{\alpha(1+2C)}{5+\alpha(1+2C)}\,b + \mathcal{O}(b^3)\,, \tag{2.43}$$

and is commonly denominated the mobility correction in the point-particle approximation. Taking

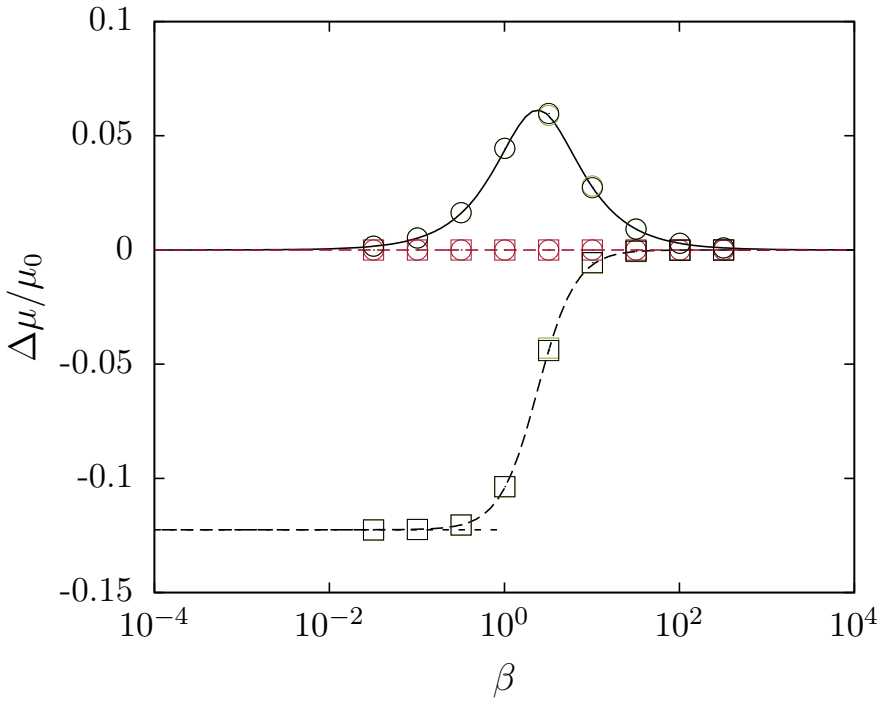

Figure 2: (Color online) The scaled self-mobility correction versus the scaled frequency β inside a spherical elastic cavity whose membrane is endowed with pure shearing (green), pure bending (red) of both shearing and bending rigidities (black). The small solid particle has a radius $b = 1/10$ concentric to a large spherical cavity of unit radius. For the membrane parameters, we take $C = 1$ and a reduced bending modulus $E_{\mathrm{B}} = 8/3$. The analytical predictions are shown as solid lines for the imaginary parts and as dashed lines for the real parts. Symbols refer to the boundary integral simulations where squares are for the real part and circles are for the imaginary part. The horizontal dashed line represent the vanishing frequency limit predicted by Eq. (2.44).

$\alpha \to \infty$, corresponding to an infinite shearing modulus or equivalently to a vanishing actuation frequency, we obtain

$$\lim_{\alpha\to\infty} \frac{\Delta\mu}{\mu_0} = -\frac{5}{4}\frac{b\left(1-b^2\right)^2}{1-b^5} = -\frac{5}{4}\,b + \mathcal{O}(b^3)\,. \tag{2.44}$$

For a rigid spherical cavity with stick boundary conditions at the inner surface, the cavity does not move and thus creating an additional resistance to the motion of the particle. Accordingly, the particle mobility is obtained as

$$\mu_{\mathrm{R}} = \lim_{\alpha\to\infty} \mu - \frac{1}{6\pi\eta}\,, \tag{2.45}$$

where the subscript R stands for rigid and the second term on the right hand side is the bulk mobility of the cavity. Scaling by the particle bulk mobility, the correction for a hard cavity reads

$$\frac{\Delta\mu_{\mathrm{R}}}{\mu_0} = -b\left(1 + \frac{5}{4}\frac{\left(1-b^2\right)^2}{1-b^5}\right) = -\frac{9}{4}\,b + \mathcal{O}(b^3)\,, \tag{2.46}$$

in full agreement with the solution by Happel and Brenner [18] and with the solution by Aponte-Rivera and Zia [35], who accounted for the particle finite-size up to the 5th order in b. Therefore, apart from a term b, the mobility in the vanishing frequency limit for an elastic cavity as given by Eq. (2.44)

is identical to that obtained inside a rigid cavity given by Eq. (2.46). Indeed, the additional term is due to the fact that the rigid cavity remains at rest while the elastic cavity necessarily undergoes translational motion.

In a way analogous to a planar elastic membrane [36], we define the characteristic frequency for shearing as $\beta := 6B\eta h\omega/\kappa_S$ where $B := 2/(1+C)$, where $h = 1-R$ is the distance from the particle center to the closest point on the cavity surface, such that $h = 1$ for concentric spheres. In Fig. 2, we show the scaled correction to the frequency-dependent self-mobility versus the scaled frequency β. Here the particle has a radius $b = 1/10$ concentric to a spherical elastic cavity of unit radius. We consider the situations where the membrane is endowed with pure shearing (green), pure bending (red) or both rigidities (black). We take a Skalak parameter $C = 1$ and a reduced bending modulus $E_B := \kappa_B/(h^2\kappa_S) = 8/3$. We observe that the correction to the particle mobility depends uniquely on membrane shearing resistance, and thus in full agreement with our theoretical calculations. We find that the real part (shown as dashed line) is a logistic-like function whereas the imaginary part exhibits at intermediate frequencies around $\beta \sim 1$ the typical peak structure. The latter is a clear signature of the memory effect induced by the elastic nature of the membrane on the system. In the high frequency limit, the correction to the mobility vanish and thus we recover the behavior in a bulk fluid. In the low frequency limit, the correction approaches that predicted theoretically by Eq. (2.44) which is the same apart from a term b as the hard cavity limit given by Eq. (2.46). A prefect agreement is obtained between the exact analytical calculations and the numerical simulations we have performed using a completed double layer boundary integral method.

2.2 Cavity motion

In the following, we examine the motion of the cavity induced by a concentric solid particle translating along the z direction. For that purpose, we define the pair-mobility function μ^{12} as the ratio between the capsule velocity V_1 and the force exerted by the solid particle on the fluid. The net translational velocity of the cavity can be computed by volume integration of the z component of the fluid velocity inside the cavity [52],

$$V_1(\omega) = \frac{2\pi}{\Omega}\int_0^\pi\int_b^1 v_{1z}(r,\theta,\omega)\, r^2 \sin\theta \,\mathrm{d}r\,\mathrm{d}\theta\,, \tag{2.47}$$

where $\Omega := 4\pi/3$ is the volume of the undeformed cavity and $v_{1z} = v_{1r}\cos\theta - v_{1\theta}\sin\theta$ is the fluid velocity along the z direction, where the radial and meridional velocities can be obtained from Eqs. (2.11) and (2.12), respectively. This leads to the pair-mobility written in a scaled form as

$$6\pi\eta\mu^{12} = \frac{3}{2}\left(1-b^2\right) - \frac{\alpha}{4}\frac{(1+2C)(1-b)^3(1+b)\left(3b^2(2+b)+2(1+2b)\right)}{5+\alpha(1+2C)\left(1-b^5\right)}\,. \tag{2.48}$$

The first term on the right-hand side in the above equation represents the bulk contribution coming from the Stokeslet in an unbounded medium whereas the second term is the frequency-dependent correction due to the presence of the elastic cavity. The correction can therefore be expressed as a Debye-like model with a single relaxation time given by

$$\tau = \frac{15}{2(1+2C)\left(1-b^5\right)}\frac{\eta}{\kappa_S}\,. \tag{2.49}$$

At leading order in b, the scaled pair-mobility given by Eq. (2.48) reads

$$6\pi\eta\mu^{12} = \frac{3}{2} - \frac{\alpha}{2}\frac{1+2C}{5+\alpha(1+2C)} + \mathcal{O}(b^2)\,. \tag{2.50}$$

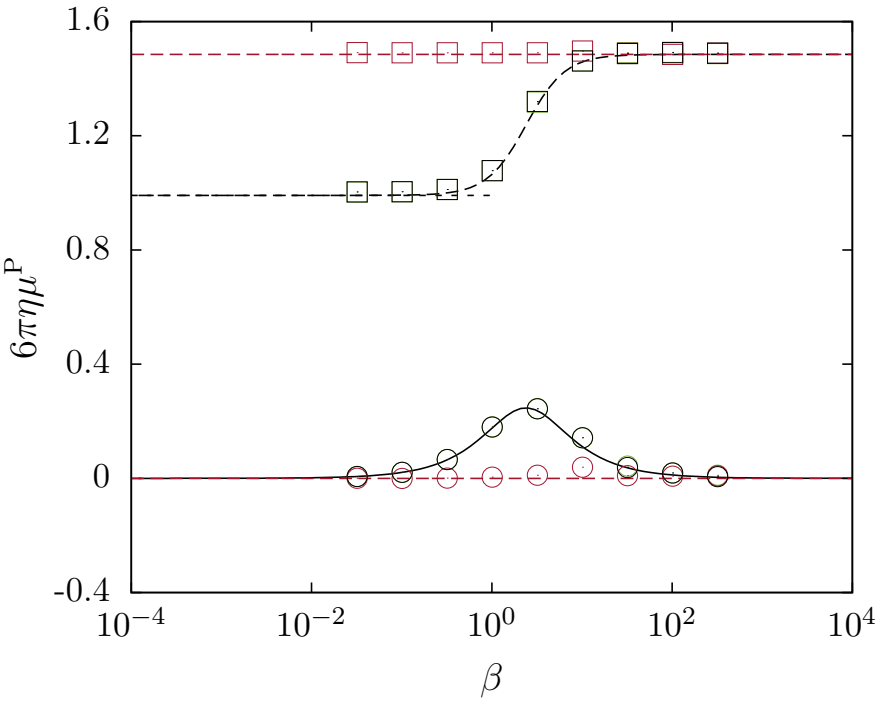

Figure 3: (Color online) The scaled pair-mobility versus the scaled frequency for a membrane cavity endowed with pure shearing (green), pure bending (red) or both rigidities (black). The analytical prediction given by Eq. (2.48) is shown as dashed and solid lines for the real and imaginary parts, respectively. Symbols refer to the corresponding BIM simulations. Horizontal dashed in the low frequency regime corresponds to the limit predicted theoretically by Eq. (2.51). Here we use the same particle/membrane parameters as in Fig. 2.

Taking $\alpha \to \infty$, Eq. (2.48) yields the following

$$\lim_{\alpha\to\infty} 6\pi\eta\mu^{12} = \frac{(1-b^2)\left(4+b^3\left(5-9b^2\right)\right)}{4\left(1-b^5\right)} = 1+\mathcal{O}\left(b^2\right)\,, \tag{2.51}$$

We further mention that the hydrodynamic force acting by the fluid on the cavity internal surface S_1 is readily determined by integrating the normal stress vector over the surface to obtain

$$\boldsymbol{F}_1 = -\int_{S_1} \boldsymbol{\sigma}\cdot\boldsymbol{e}_r\,\mathrm{d}S = -8\pi\eta A\,\boldsymbol{e}_z\,, \tag{2.52}$$

which is found to be the same in magnitude but opposite in sign as the force $\boldsymbol{F}_2$ acting by the fluid on the solid particle.

In Fig. 3 we show the scaled pair-mobility function versus the scaled frequency β using the same parameters as in Fig. 2. For a membrane with pure bending, the real part of the pair-mobility amounts to $(3/2)(1-b^2)$ and the imaginary part vanishes and thus recovering the behavior observed in a bulk fluid. On the other hand, a membrane endowed with shearing resistance shows a more richer dynamics where the pair-mobility depends strongly on the actuation frequency. Indeed, the pair-mobility for a cavity membrane possessing both shearing and bending rigidities is undistinguished from that of a membrane with a pure shearing. A very good agreement is obtained between theory and simulations.

Analogous exact analytical predictions using the stream function technique can be carried out for an arbitrary position within the spherical cavity where the general solution may conveniently be

expressed in term of an infinite series involving Legendre functions. Nevertheless, due the complex nature of the underlying boundary conditions, the resolution is laborious and non-trivial. In order to overcome this difficulty, we shall employ as an alternative way, a fundamentally different approach based on the image solution technique to compute the flow field induced by a Stokeslet acting inside a spherical elastic cavity. This will result to the computation of the hydrodynamic mobility functions in the point-particle approximation, valid when $b \ll 1$ as it is detailed in the next section.

3 Singularity solution

The following image solution technique has originally been proposed by Fuentes *et al.* [32, 33] who computed the flow field induced by a point-force acting outside a spherical drop. The same approach has been employed by us in earlier works [41, 53] to address the fluid motion induced by a point-force acting nearby a spherical elastic membrane with shearing and bending rigidities. Accordingly, the fluid flow inside the cavity can be written as a sum of two distinct contributions

$$\boldsymbol{v} = \boldsymbol{v}^{\mathrm{S}} + \boldsymbol{v}^{*}\,, \tag{3.1}$$

where $\boldsymbol{v}^{\mathrm{S}}$ is the velocity field induced by a point-force acting at the particle position $\boldsymbol{x}_2$, and $\boldsymbol{v}^{*}$ is the image solution required to satisfy the regularity and boundary conditions.

Now we briefly sketch the main resolution steps. First, the velocity $\boldsymbol{v}^{\mathrm{S}}$ due to the Stokeslet is written in terms of spherical harmonics which are then transformed into harmonics based at $\boldsymbol{x}_1$ via the Legendre expansion. Second, the image system solution $\boldsymbol{v}^{*}$ and the solution outside the capsule $\boldsymbol{v}^{(o)}$ are respectively expressed as interior and exterior harmonics based at $\boldsymbol{x}_1$ using Lamb's general solution [54, 55]. The last step consists of determining the series unknown expansion coefficients by satisfying the boundary conditions at the membrane surface stated by Eqs. (2.17) through (2.20).

3.1 Stokeslet solution

We begin with writing the Stokeslet acting at $\boldsymbol{x}_2$,

$$v_i^{\mathrm{S}} = \mathcal{G}_{ij} F_j = \frac{1}{8\pi\eta}\left(F_i \frac{1}{s} + F_j(\boldsymbol{x}-\boldsymbol{x}_2)_i \nabla_{2j}\frac{1}{s}\right)\,, \tag{3.2}$$

where $s := |\boldsymbol{x}-\boldsymbol{x}_2|$. Here $\nabla_{2j} := \partial/\partial x_{2j}$ stands for the nabla operator taken with respect to the singularity position $\boldsymbol{x}_2$. Using Legendre expansion, the harmonics based at $\boldsymbol{x}_2$ can be expanded as

$$\frac{1}{s} = \sum_{n=0}^{\infty} R^n\, \varphi_n(r,\theta)\,, \tag{3.3}$$

where the unit vector $\boldsymbol{d} := (\boldsymbol{x}_1 - \boldsymbol{x}_2)/R = -\boldsymbol{e}_z$, the position vector $\boldsymbol{r} = \boldsymbol{x} - \boldsymbol{x}_1$ and $r := |\boldsymbol{r}|$. Furthermore, φ_n are the harmonics of degree n, related to the Legendre polynomials of degree n by [56]

$$\varphi_n(r,\theta) := \frac{(\boldsymbol{d}\cdot\boldsymbol{\nabla})^n}{n!}\frac{1}{r} = \frac{1}{r^{n+1}}\,P_n(\cos\theta)\,. \tag{3.4}$$

For the axisymmetric case, the force is exerted along the unit vector $\boldsymbol{d}$ and can thus be written as $\boldsymbol{F} = F\boldsymbol{d}$. By making use of the identities

$$\boldsymbol{\nabla}_2 R^n = -nR^{n-1}\,\boldsymbol{d}\,, \quad (\boldsymbol{d}\cdot\boldsymbol{\nabla}_2)\,\boldsymbol{d} = 0\,, \tag{3.5}$$

Eq. (3.2) can therefore be written as

$$\boldsymbol{v}^{\mathrm{S}} = -\frac{F}{8\pi\eta}\sum_{n=0}^{\infty} R^{n-1}\big[(n-1)R\,\boldsymbol{d} + n\,\boldsymbol{r}\big]\varphi_n\,. \tag{3.6}$$

Hence, the Stokeslet at $\boldsymbol{x}_2$ is written in terms of harmonics based at $\boldsymbol{x}_1$. Note that the terms with $\boldsymbol{d}\,\varphi_n$ in Eq. (3.6) are not independent harmonics. For their elimination, we shall use [41]

$$\boldsymbol{d}\,\varphi_n = \frac{1}{2n+1}\left[\boldsymbol{\nabla}\varphi_{n-1} - r^2\boldsymbol{\nabla}\varphi_{n+1} - (2n+3)\boldsymbol{r}\,\varphi_{n+1}\right],$$

leading after substitution into Eq. (3.6) to

$$\boldsymbol{v}^{\mathrm{S}} = \frac{F}{8\pi\eta}\sum_{n=1}^{\infty}\left[\left(\frac{n-2}{2n-1}\,r^2R^{n-1} - \frac{n}{2n+3}\,R^{n+1}\right)\boldsymbol{\nabla}\varphi_n - \frac{2(n+1)}{2n-1}\,R^{n-1}\boldsymbol{r}\varphi_n\right]. \tag{3.7}$$

For future reference, we shall state explicitly the projected velocity components onto the radial (normal) and meridional (tangential) directions. For that purpose, we shall make use of the following identities

$$\boldsymbol{e}_r\cdot\boldsymbol{\nabla}\varphi_n = -\frac{n+1}{r}\,\varphi_n\,, \tag{3.8a}$$

$$\boldsymbol{e}_r\cdot\boldsymbol{r}\varphi_n = r\varphi_n\,, \tag{3.8b}$$

$$\boldsymbol{e}_\theta\cdot\boldsymbol{r}\varphi_n = 0\,, \tag{3.8c}$$

leading to the Stokeslet solution

$$v_r^{\mathrm{S}} = \frac{F}{8\pi\eta}\sum_{n=1}^{\infty}\left[-\frac{n(n+1)}{2n-1}\,rR^{n-1} + \frac{n(n+1)}{2n+3}\frac{R^{n+1}}{r}\right]\varphi_n\,, \tag{3.9}$$

$$v_\theta^{\mathrm{S}} = \frac{F}{8\pi\eta}\sum_{n=1}^{\infty}\left[\frac{n-2}{2n-1}\,r^2R^{n-1} - \frac{n}{2n+3}\,R^{n+1}\right]\psi_n\,, \tag{3.10}$$

where we have defined

$$\psi_n := \boldsymbol{e}_\theta\cdot\boldsymbol{\nabla}\varphi_n = \frac{1}{r}\frac{\partial\varphi_n}{\partial\theta}\,. \tag{3.11}$$

The pressure can directly be determined by integration of Eq. (2.1) to obtain

$$p^{\mathrm{S}} = \frac{F}{8\pi}\sum_{n=1}^{\infty} -2nR^{n-1}\varphi_n\,. \tag{3.12}$$

We further note that φ_n and ψ_n constitute sets of independent harmonics satisfying the properties

$$\int_0^\pi \varphi_n\varphi_m\sin\theta\,\mathrm{d}\theta = \frac{2}{2n+1}\frac{\delta_{mn}}{r^{2n+2}}\,. \tag{3.13}$$

$$\int_0^\pi \psi_m\psi_n\sin\theta\,\mathrm{d}\theta = \frac{2n(n+1)}{2n+1}\frac{\delta_{mn}}{r^{2n+4}}\,. \tag{3.14}$$

In the following, the image system solution and the the solution inside the cavity shall be derived.

3.2 Image system solution

For the image system solution inside the cavity, we use Lamb's general solution [55, 57], which can be written in terms of *interior* harmonics based at $\boldsymbol{x}_1$ as

$$\begin{aligned}\boldsymbol{v}^* = \frac{F}{8\pi\eta}\sum_{n=1}^{\infty}\Bigg[A_n\bigg(\frac{n+3}{2}r^{2n+3}\,\boldsymbol{\nabla}\varphi_n + \frac{(n+1)(2n+3)}{2}\,r^{2n+1}\boldsymbol{r}\varphi_n\bigg)\\ + B_n\left(r^{2n+1}\boldsymbol{\nabla}\varphi_n + (2n+1)r^{2n-1}\boldsymbol{r}\varphi_n\right)\Bigg].\end{aligned} \tag{3.15}$$

After making use of Eqs. (3.8a) through (3.8c), the projected components of the image system solution read

$$v_r^* = \frac{F}{8\pi\eta}\sum_{n=1}^{\infty}\left[\frac{n(n+1)}{2}\,r^{2n+2}A_n + nr^{2n}B_n\right]\varphi_n\,, \tag{3.16}$$

$$v_\theta^* = \frac{F}{8\pi\eta}\sum_{n=1}^{\infty}\left[\frac{n+3}{2}\,r^{2n+3}A_n + r^{2n+1}B_n\right]\psi_n\,, \tag{3.17}$$

and the solution for the pressure field inside the cavity is obtained as

$$p^* = \frac{F}{8\pi}\sum_{n=1}^{\infty}(n+1)(2n+3)A_n r^{2n+1}\varphi_n\,. \tag{3.18}$$

3.3 Solution outside the cavity

We use Lamb's general solution which can be written in terms of *exterior* harmonics based at $\boldsymbol{x}_1$ as

$$\boldsymbol{v}^{(o)} = \frac{F}{8\pi\eta}\sum_{n=1}^{\infty}\left[a_n\bigg(-\frac{n-2}{2}\,r^2\,\boldsymbol{\nabla}\varphi_n + (n+1)\,\boldsymbol{r}\varphi_n\bigg) + b_n\boldsymbol{\nabla}\varphi_n\,,\right]. \tag{3.19}$$

which can be projected onto normal and tangential components to obtain

$$v_r^{(o)} = \frac{F}{8\pi\eta}\sum_{n=1}^{\infty}\left[\frac{n(n+1)}{2}\,ra_n - \frac{n+1}{r}\,b_n\right]\varphi_n\,, \tag{3.20}$$

$$v_\theta^{(o)} = \frac{F}{8\pi\eta}\sum_{n=1}^{\infty}\left[-\frac{n-2}{2}\,r^2a_n + b_n\right]\psi_n\,. \tag{3.21}$$

The pressure field outside the cavity can then be presented as

$$p^{(o)} = \frac{F}{8\pi}\sum_{n=1}^{\infty}n(2n-1)a_n\varphi_n\,. \tag{3.22}$$

Having expressed the general solution for the velocity and pressure fields, we now proceed for the determination of the unknown coefficients inside the cavity A_n and B_n, and outside the cavity a_n and b_n.

3.4 Determination of the series coefficients

Continuity of velocity

The continuity of the radial and meridional velocities as stated by Eqs. (2.17) and (2.18) leads to

$$\begin{aligned}\frac{a_n}{2}-\frac{b_n}{n}&=\frac{A_n}{2}+\frac{B_n}{n+1}-\frac{R^{n-1}}{2n-1}+\frac{R^{n+1}}{2n+3}\,,\\ -\frac{n-2}{2}\,a_n+b_n&=\frac{n+3}{2}\,A_n+B_n+\frac{n-2}{2n-1}\,R^{n-1}-\frac{nR^{n+1}}{2n+3}\,.\end{aligned}$$

Solving these two equations for a_n and b_n, the coefficients outside the cavity can be expressed in terms of those inside as

$$a_n=\frac{2n+3}{2}\,A_n+\frac{2n+1}{n+1}\,B_n-\frac{2}{2n-1}\,R^{n-1}\,, \tag{3.23}$$

$$b_n=\frac{n(2n+1)}{4}\,A_n+\frac{n(2n-1)}{2(n+1)}\,B_n-\frac{n}{2n+3}\,R^{n+1}\,. \tag{3.24}$$

The coefficients A_n and B_n can be determined from the traction jump equations stemming from membrane shearing and bending resistances. In order to probe the effect of these two elasticity modes in more depth, we shall consider in the following idealized membranes with pure shearing or pure bending resistances.

Discontinuity of stress tensor

Shearing contribution We first consider a membrane with only-shearing resistance such as that of a typical artificial capsule designed for drag delivery [44]. It follows from Eqs. (2.19) and (2.20) representing the tangential and normal traction jumps that

$$[v_{\theta,r}]=-\alpha\Big((1+2C)v_{r,\theta}+(1+C)\left(v_{\theta,\theta\theta}+v_{\theta,\theta}\cot\theta\right)-\left((1+C)\cot^2\theta+C\right)v_\theta\Big)\Big|_{r=1}\,, \tag{3.25}$$

$$\left[-\frac{p}{\eta}\right]=-\alpha(1+2C)v_{r,r}|_{r=1}\,, \tag{3.26}$$

where again $i\alpha:=2\kappa_{\mathrm{S}}/(3\eta\omega)$ is a shearing parameter. In order to handle the derivatives with respect to r, we shall make use of the identities

$$\varphi_{n,r}=-\frac{n+1}{r}\,\varphi_n\,,\qquad \psi_{n,r}=-\frac{n+2}{r}\,\psi_n\,, \tag{3.27}$$

By making use of the orthogonality property given by Eq. (3.14) together with

$$\int_0^\pi \psi_m\left(\psi_{n,\theta\theta}+\psi_{n,\theta}\cot\theta-\psi_n\cot^2\theta\right)\sin\theta\,\mathrm{d}\theta=-\frac{2n(n+1)(n^2+n-1)}{2n+1}\frac{\delta_{mn}}{r^{2n+4}}\,, \tag{3.28}$$

the tangential traction jump equation given by Eq. (3.25) leads to

$$\begin{aligned}(2n+1)(2n+3)A_n+\frac{2(4n^2-1)}{n+1}\,B_n=\alpha\Big((1+2C)(n+1)\left(na_n-2b_n\right)\\ +\left(1-(1+C)n(n+1)\right)\left(-(n-2)a_n+2b_n\right)\Big)\,.\end{aligned} \tag{3.29}$$

Further, the contribution due to shearing to the normal traction equation given by Eq. (3.26) results to

$$(n-2)(2n+1)(2n+3)A_n + \frac{2n(4n^2-1)}{n+1}\,B_n = \alpha(1+2C)(n+1)\left(-n^2 a_n + 2(n+2)b_n\right)\,. \quad (3.30)$$

Eqs. (3.29) and (3.30) together with Eqs. (3.23) and (3.24) form a closed system of linear equations amenable to direct resolution via the standard substitution technique. We obtain

$$A_n = \frac{\alpha n(n+2)}{K}\left(\frac{2n+1}{2n+3}\,R^{n+1}\,K_+ - R^{n-1}\,K_-\right)\,, \quad (3.31)$$

$$B_n = \frac{\alpha(n+1)}{2M}\left(\frac{2n+1}{2n-1}\,R^{n-1}\,M_- - n(n+2)R^{n+1}\,M_+\right)\,, \quad (3.32)$$

where the coefficients K, $K_\pm$, M and $M_\pm$ have rather complex and lengthy expressions and are therefore provided in the appendix. Particularly, by taking $\alpha \to \infty$, corresponding to taking an infinite shearing modulus or a vanishing frequency limit, we obtain

$$\lim_{\alpha\to\infty} A_n = \frac{2n+1}{2n+3}\,R^{n+1} - R^{n-1}\,, \quad (3.33)$$

$$\lim_{\alpha\to\infty} B_n = \frac{(n+1)(2n+1)}{2(2n-1)}\,R^{n-1} - \frac{n+1}{2}\,R^{n+1}\,. \quad (3.34)$$

The latter limit is identical to the solution obtained for a point-force acting inside a rigid spherical cavity with stick boundary conditions. Moreover, both a_n and b_n vanish in this limit in which the fluid outside the cavity is at rest.

Bending contribution Next, we consider a membrane endowed with pure bending resistance such as that of a fluid vesicle [58, 59]. As already pointed out, two models are commonly used to describe membrane resistance towards bending. We shall first provide explicit analytical expressions by assuming a linear isotropic model for the bending moments. The corresponding traction jump equations given by Eqs. (2.19) and (2.20) read

$$[v_{\theta,r}] = \alpha_{\mathrm{B}}\Big(\left(1-\cot^2\theta\right)v_{r,\theta} + v_{r,\theta\theta}\cot\theta + v_{r,\theta\theta\theta}\Big)\Big|_{r=1}\,, \quad (3.35)$$

$$\left[-\frac{p}{\eta}\right] = \alpha_{\mathrm{B}}\Big(\left(3\cot\theta+\cot^3\theta\right)v_{r,\theta} - \cot^2\theta\,v_{r,\theta\theta} + 2\cot\theta\,v_{r,\theta\theta\theta} + v_{r,\theta\theta\theta\theta}\Big)\Big|_{r=1}\,, \quad (3.36)$$

where $i\alpha_{\mathrm{B}} := \kappa_{\mathrm{B}}/(\eta\omega)$ is a bending parameter. By making use of Eqs. (3.14) and (3.28), the tangential traction jump reads

$$(2n+1)(2n+3)A_n + \frac{2(4n^2-1)}{n+1}\,B_n = \alpha_{\mathrm{B}}(n^2+n-2)(n+1)\left(na_n - 2b_n\right)\,, \quad (3.37)$$

Continuing, using Eq. (3.13) together with the orthogonality relation

$$\int_0^\pi \varphi_m\Big(\left(3\cot\theta+\cot^3\theta\right)\varphi_{n,\theta} - \varphi_{n,\theta\theta}\cot^2\theta + 2\varphi_{n,\theta\theta\theta}\cot\theta + \varphi_{n,\theta\theta\theta\theta}\Big)\sin\theta\mathrm{d}\theta$$
$$= \frac{2n(n-1)(n+1)(n+2)}{2n+1}\frac{\delta_{mn}}{r^{2n+2}}\,,$$

the normal traction jump reads

$$(n-2)(2n+1)(2n+3)A_n + \frac{2n(4n^2-1)}{n+1}\,B_n = -\alpha_{\mathrm{B}} n(n-1)(n+1)^2(n+2)\,(na_n - 2b_n)\,. \quad (3.38)$$

Solving the system of linear equations arising from Eqs. (3.23) and (3.24) together with (3.37) and (3.38) leads to the determination of the unknown coefficients. We obtain

$$A_n = \frac{\alpha_{\mathrm{B}} n^2(n+2)^2(n^2-1)}{K_{\mathrm{B}}}\left(\frac{2n-1}{2n+3}\,R^{n+1} - R^{n-1}\right), \quad (3.39)$$

$$B_n = \frac{\alpha_{\mathrm{B}} n(n+2)(n-1)(n+1)^2(n^2+2n-2)}{2K_{\mathrm{B}}}\left(\frac{2n+3}{2n-1}\,R^{n-1} - R^{n+1}\right), \quad (3.40)$$

where

$$K_{\mathrm{B}} = 2\alpha_{\mathrm{B}} n^6 + 6\alpha_{\mathrm{B}} n^5 - \alpha_{\mathrm{B}} n^4 + 4(2-3\alpha_{\mathrm{B}})n^3 + (12-\alpha_{\mathrm{B}})n^2 + 2(3\alpha_{\mathrm{B}}-1)n - 3\,. \quad (3.41)$$

Taking the limit $\alpha_{\mathrm{B}} \to \infty$, which corresponds to taking an infinite membrane bending modulus or a vanishing forcing frequency, the two coefficients read

$$\lim_{\alpha_{\mathrm{B}}\to\infty} A_n = \frac{n(n+2)}{2n^2+2n-3}\left(\frac{2n+3}{2n-1}\,R^{n-1} - R^{n+1}\right),$$

$$\lim_{\alpha_{\mathrm{B}}\to\infty} B_n = \frac{(n+1)(n^2+2n-2)}{2(2n^2+2n-3)}\left(\frac{2n+3}{2n-1}\,R^{n-1} - R^{n+1}\right),$$

which are found to be different from the solution previously obtained when taking $\alpha \to \infty$ in a shearing-only membrane, as can clearly be seen from Eqs. (3.33) and (3.34).

Continuing, we next consider the Helfrich model for membrane bending, leading to the traction jumps equations

$$[v_{\theta,r}] = 0\,, \quad (3.42)$$

$$\left[-\frac{p}{\eta}\right] = \alpha_{\mathrm{B}}\Big(4v_r + (5+\cot^2\theta)\cot\theta\, v_{r,\theta} + (2-\cot^2\theta)v_{r,\theta\theta} + 2\cot\theta\, v_{r,\theta\theta\theta} + v_{r,\theta\theta\theta\theta}\Big)\Big|_{r=1}\,. \quad (3.43)$$

After making use of the orthogonality property (3.13) together with

$$\int_0^\pi \varphi_m\big(4\varphi_n + (5+\cot^2\theta)\cot\theta\,\varphi_{n,\theta} + (2-\cot^2\theta)\varphi_{n,\theta\theta} + 2\cot\theta\,\varphi_{n,\theta\theta\theta} + \varphi_{n,\theta\theta\theta\theta}\big)\sin\theta\,\mathrm{d}\theta = \frac{2(n+2)^2(n-1)^2}{2n+1}\,\frac{\delta_{mn}}{r^{2n+2}}\,, \quad (3.44)$$

we obtain the two following equations

$$(2n+1)(2n+3)A_n + \frac{2(4n^2-1)}{n+1}\,B_n = 0\,, \quad (3.45)$$

$$(n-2)(2n+1)(2n+3)A_n + \frac{2n(4n^2-1)}{n+1}\,B_n = -\alpha_{\mathrm{B}}(n+2)^2(n-1)^2(n+1)(na_n - 2b_n)\,. \quad (3.46)$$

which upon making use of Eqs. (3.23) and (3.24) and solving for A_n and B_n yields

$$A_n = \frac{\alpha_{\mathrm{B}}(n-1)^2 n(n+1)(n+2)^2}{K_{\mathrm{H}}} \left(\frac{2n-1}{2n+3} R^{n+1} - R^{n-1} \right) , \tag{3.47}$$

$$B_n = \frac{\alpha_{\mathrm{B}}(n-1)^2 n(n+1)^2(n+2)^2}{2K_{\mathrm{H}}} \left(\frac{2n+3}{2n-1} R^{n-1} - R^{n+1} \right) , \tag{3.48}$$

with

$$K_{\mathrm{H}} = 2\alpha_{\mathrm{B}} n^6 + 6\alpha_{\mathrm{B}} n^5 - 2\alpha_{\mathrm{B}} n^4 + 2(4 - 7\alpha_{\mathrm{B}}) n^3 + 12n^2 + 2(4\alpha - 1)n - 3 . \tag{3.49}$$

Similar, by taking the limit $\alpha_{\mathrm{B}} \to \infty$, Eqs. (3.42) and (3.43) lead to

$$\lim_{\alpha_{\mathrm{B}} \to \infty} A_n = \frac{1}{2} \left(\frac{2n-1}{2n+3} R^{n+1} - R^{n-1} \right) , \tag{3.50}$$

$$\lim_{\alpha_{\mathrm{B}} \to \infty} B_n = \frac{n+1}{4} \left(\frac{2n+3}{2n-1} R^{n-1} - R^{n+1} \right) . \tag{3.51}$$

Clearly, the coefficients also differ from those obtained previously for a shearing-only membrane given by Eqs. (3.33) and (3.34).

3.5 Particle mobility

The leading-order particle mobility is obtained by evaluating the image system solution given by Eq. (3.15) at the particle position as

$$\boldsymbol{v}^*|_{\boldsymbol{x}=\boldsymbol{x}_2} = \Delta\mu \, \boldsymbol{F} , \tag{3.52}$$

leading to the particle mobility correction, which can conveniently be written in a scaled form as an infinite series

$$\frac{\Delta\mu}{\mu_0} = -\frac{3b}{8} \sum_{n=1}^{\infty} \left[n(n+1) R^{n+1} A_n + 2n R^{n-1} B_n \right] . \tag{3.53}$$

In the particular case when $R = 0$ corresponding to the concentric case earlier treated in Sec. 2, only the term with $n = 1$ remains and we recover the leading-order self-mobility

$$\left. \frac{\Delta\mu}{\mu_0} \right|_{R=0} = -\frac{3b}{4} B_1 = -\frac{5}{4} \frac{\alpha(1+2C)}{5 + \alpha(1+2C)} \, b , \tag{3.54}$$

in full agreement with Eq. (2.43) obtained using the stream function technique. Clearly, the mobility correction depends only on membrane resistance towards shearing since $B_1 = 0$ for bending-only membranes (see Eqs. (3.40) and (3.48) for the general expressions of B_n using the two bending models.)

Now, by taking the limit $\alpha \to \infty$ in Eq. (3.53), the correction to the particle self-mobility reads

$$\lim_{\alpha \to \infty} \frac{\Delta\mu}{\mu_0} = b \left(1 - \frac{9}{4} \frac{1}{1 - R^2} \right) . \tag{3.55}$$

The same limit is obtained when considering a membrane with pure shearing. For a large cavity radius, Eq. (3.55) reduces to the leading-order mobility correction nearby a no-slip planar wall as

first obtained using the method of reflection by Lorentz [60], mainly

$$\lim_{\alpha\to\infty}\frac{\Delta\mu}{\mu_0}=-\frac{9}{8}\frac{b}{h}+\mathcal{O}\left(\frac{1}{a}\right). \tag{3.56}$$

By considering the coefficients (3.33) and (3.34) associated to a hard cavity, the scaled correction to the particle mobility reads [28, 34]

$$\frac{\Delta\mu_{\mathrm{R}}}{\mu_0}=-\frac{9}{4}\frac{b}{1-R^2}, \tag{3.57}$$

being identical to the leading-order correction given by Eq. (2.46) for $R=0$. Again, the mobility inside a hard cavity is recovered in the vanishing frequency limit apart from a term b as explained in Eq. (2.45).

In fact, the sum over n in Eq. (3.53) and the limit when $\alpha\to\infty$ cannot be swapped. In other words, taking the limit when $\alpha\to\infty$ before evaluating the sum as it is the case for a hard cavity does not lead to the same result as evaluating the sum first and then taking the limit as it is done for an elastic cavity. This is justified by the fact that the dominated convergence theorem does not hold here for the infinite series given by Eq. (3.53).

Now by considering a membrane with pure bending resistance modeled by the Helfrich model, the mobility correction in the vanishing frequency limit reads

$$\lim_{\alpha_{\mathrm{B}}\to\infty}\frac{\Delta\mu}{\mu_0}=b\left(1-\frac{15}{8}\frac{1}{1-R^2}\right). \tag{3.58}$$

We further recover for large cavity radius the well know mobility correction nearby a planar interface separating two fluids having the same viscosity, namely [61, 62]

$$\lim_{\alpha_{\mathrm{B}}\to\infty}\frac{\Delta\mu}{\mu_0}=-\frac{15}{16}\frac{b}{h}+\mathcal{O}\left(\frac{1}{a}\right). \tag{3.59}$$

In Fig. 4 we show the scaled frequency-dependent self-mobility correction versus the scaled frequency β for a particle of radius $b=1/10$ located at $R=4/5$ inside a spherical cavity. Unlike the situation where the particle is concentric to the cavity, a contribution from bending resistance arises. We observe that the Helfrich model (thick red lines) leads to a better agreement with the BIM simulations than the linear isotropic model (thin red lines). Considering the shearing-only membrane, we observe that a second peak of more pronounced amplitude arises in the low frequency regime. This peak does not occur in planar membranes but has been observed previously for a particle moving outside a large spherical capsule [41, 53]. In fact, the peak is attributed to the fact that the traction jumps due to shearing involve a contribution from the normal displacement in contrast to planar membranes where these traction jumps depend solely on the in-plane tangential displacements. Only one single peak however occurs for a bending-only membrane for both models since the traction jumps due to bending involve only the normal deformations and thus explaining the absence of the second peak.

3.6 Cavity motion

Finally, the cavity translational velocity is computed by integrating the fluid velocity as stated by Eq. (2.47) with the exception that the radial variable r is integrated between 0 and 1. We find that

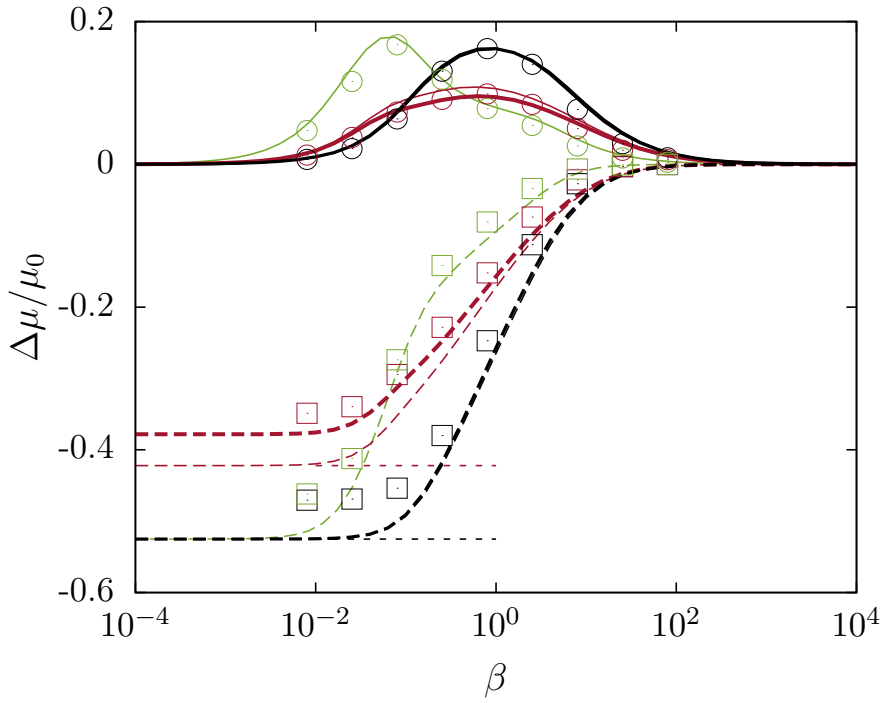

Figure 4: (Color online) The scaled frequency-dependent mobility correction versus the scale frequency inside a spherical elastic cavity with pure shearing (green), pure bending (red) and both shearing and bending (black). The thin and thick red lines correspond to the linear isotropic model and Helfrich model respectively. The particle has a radius $b = 1/10$ and is positioned at $R = 4/5$. Horizontal dashes lines shown in black and red correspond to the vanishing-frequency limits predicted by Eqs. (3.55) and (3.58), respectively. Here we use the same membrane parameters as in Fig. 2.

only the term with $n = 1$ of the series remains leading to

$$\mu^{12} = -\frac{1}{8\pi\eta}\left(A_1 + B_1 - 2 + \frac{2}{5}R^2\right), \tag{3.60}$$

which, upon substitution of the coefficients with their expressions yields

$$6\pi\eta\mu^{12} = \frac{3}{2} - \frac{3}{10}R^2 - \frac{5-3R^2}{10}\frac{\alpha(1+2C)}{5+\alpha(1+2C)}. \tag{3.61}$$

Interestingly, even for $R \neq 0$, the pair-mobility depends solely on membrane shearing and bending does not play a role, i.e. in the same way as observed for a concentric sphere. As $\alpha \to \infty$, the pair-mobility tends to unity independently of the value of R. In particular, for $R = 0$ we recover the leading-order solution given by Eq. (2.50) obtained for two concentric spheres. The correction to the pair-mobility follows a Debye-like model with a relaxation time given by the leading-order term in Eq. (2.49).

Similar, it can be shown that the force exerted by the fluid on the internal surface of the cavity is equal in magnitude but opposite in sign to the friction force $\boldsymbol{F}_2$ acting on the particle.

In Fig. 5 we show the scaled pair-mobility function versus the scaled frequency using the same parameters as in Fig. 4. The pair-mobility for a bending-only membrane remains unchanged and amounts to $3/2 - 3R^2/10$ in the whole range of forcing frequencies. For a cavity with a finite shearing resistance, the real part is a monotonically increasing function of frequency that varies between 1

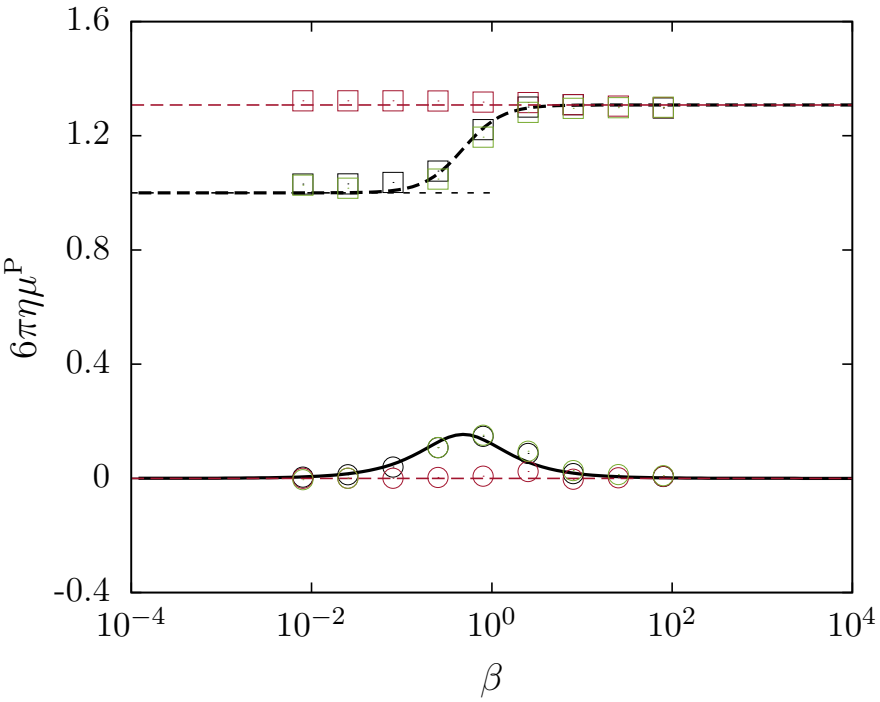

Figure 5: (Color online) The scaled pair-mobility versus the scaled frequency for cavity with only-shearing (green), only-bending (red) or both shearing and bending (black). The particle has a radius $b = 1/10$ and is positioned at $R = 4/5$. The analytical prediction stated by Eq. (3.61) is shown as dashed and solid lines for the real and imaginary parts, respectively, while symbols are the BIM simulations. Horizontal dashed in the low frequency regime corresponds to one. For the membrane parameters, see Fig. 2.

and $3/2 - 3R^2/10$ while the imaginary parts exhibits the usual bell-shaped behavior with the typical peak at $\beta \sim 1$. Our analytical predictions are favorably compared with BIM simulations.

4 Conclusions

In this paper, we have presented an analytical theory of the creeping motion of small particle slowly moving inside a large spherical elastic cavity. We have modeled the membrane resistance towards shearing forces by the Skalak model which incorporates into a single strain energy functional both the resistance towards shearing and area conservation. We have assessed two different models for bending namely the Helfrich model and the linear isotropic model.

We have first solved the underlying equations of fluid motion in the relatively simple situation where the particle is concentric to the cavity, where exact analytical solutions are obtained and expressed in a closed mathematical form using the stream function technique. In this case, we have found that the fluid flow is solely determined by membrane shearing and that bending does not play any role. Moreover, we have shown that in the vanishing frequency limit, the particle hydrodynamic mobility is larger than that obtained inside a rigid cavity with stick boundary conditions at its inner surface. This behavior has been justified by the fact that a steady rigid cavity exerts an additional hindrance in particle motion and thus reducing particle hydrodynamic mobility significantly.

For an arbitrary position of the particle inside the spherical cavity, we have used the image solution technique to find analytical expression of the axisymmetric flow field induced by a point

force acting on the fluid. This leads to expressions of the mobility functions in the point-particle framework, valid when the particle size is smaller than that of the spherical elastic cavity. Considering the motion of the cavity, we find that the pair-mobility function depends uniquely on membrane shearing properties and that for an arbitrary value of the particle eccentricity. As an example setup, we have favorable compared our analytical predictions with fully resolved numerical simulations that we have performed using a completed double layer boundary integral method.

Acknowledgments

The authors thank the Volkswagen Foundation for financial support and acknowledge the Gauss Center for Supercomputing e.V. for providing computing time on the GCS Supercomputer SuperMUC at Leibniz Supercomputing Center.

Appendices

A Mathematical expression

The analytical expressions of the functions appearing in Eqs. (3.31) and (3.32) are given for the series coefficient A_n by

$$
\begin{aligned}
K_+ &= 2(1+C)n^3 + ((2\alpha+5)C+\alpha+1)\,n^2 + (1+C)n - (1+2C)(1+\alpha)\,,\\
K_- &= 2(1+C)n^3 + ((2\alpha+3)C+\alpha-1)\,n^2 + (1+C)n - (1+2C)\alpha + 1\,,\\
K &= 4(1+C)\alpha n^5 + \big(16 + (1+2C)\alpha^2 + 10(1+C)\alpha\big)\,n^4 + 2\,\big(16 + (1+2C)\alpha^2 + 3(1+C)\alpha\big)\,n^3\\
&\quad + \big(8 - (1+2C)\alpha^2 - (1+C)\alpha\big)\,n^2 - \big(8 + 2(1+2C)\alpha^2 + (7+C)\alpha\big)\,n - 3(1+\alpha)\,,
\end{aligned}
$$

and for B_n by

$$
\begin{aligned}
M_- &= -12 + 2(1+C)n^5 + ((2\alpha+5)C+\alpha+1)\,n^4 + ((4\alpha+3)C+2\alpha-5)\,n^3 + (9-(1+2C)\alpha)\,n^2\\
&\quad - 2\,((1+2C)\alpha-5)\,n\,,\\
M_+ &= 2(1+C)n^3 + ((2\alpha+3)C+\alpha-1)\,n^2 + (1+C)n - \alpha(1+2C) + 1\,,\\
M &= 4(1+C)\alpha n^5 + \big(16 + (1+2C)\alpha^2 + 10(1+C)\alpha\big)\,n^4 + 2\,\big(16 + (1+2C)\alpha^2 + 3(1+C)\alpha\big)\,n^3\\
&\quad + \big(8 - (1+2C)\alpha^2 - (1+C)\alpha\big)\,n^2 - \big(8 + 2(1+2C)\alpha^2 + (C+7)\alpha\big)\,n - 3(1+\alpha)\,,
\end{aligned}
$$

Bibliography

[1] R. B. Bird, W. E. Stewart, and E. N. Lightfoot, *Transport phenomena* (John Wiley & Sons, 2007).

[2] R. B. Schoch, J. Han, and P. Renaud, Rev. Mod. Phys. **80**, 839 (2008).

[3] D. Chowdhury, A. Schadschneider, and K. Nishinari, Phys. Life Rev. **2**, 318 (2005).

[4] J. Panyam and V. Labhasetwar, Adv. Drug Deliv. Rev. **55**, 329 (2003).

[5] L. M. Bareford and P. W. Swaan, Adv. Drug Deliv. Rev. **59**, 748 (2007).

[6] J. Bereiter-Hahn and M. Vöth, Microsc. Res. Tech. **27**, 198 (1994).

[7] W. Wang, S. Li, L. Mair, S. Ahmed, T. J. Huang, and T. E. Mallouk, Angew. Chem. Int. Ed. **53**, 3201 (2014).

[8] S. Kim and S. J. Karrila, *Microhydrodynamics: principles and selected applications* (Courier Corporation, 2013).

[9] I. F. Sbalzarini and P. Koumoutsakos, J. Struct. Biol. **151**, 182 (2005).

[10] N. Gal, D. Lechtman-Goldstein, and D. Weihs, Rheol. Acta **52**, 425 (2013).

[11] Y. Li, J. Schnekenburger, and M. H. G. Duits, J. Biomed. Opt. **14**, 064005 (2009).

[12] D. Ott, P. M. Bendix, and L. B. Oddershede, ACS Nano **7**, 8333 (2013).

[13] É. Fodor, M. Guo, N. S. Gov, P. Visco, D. A. Weitz, and F. van Wijland, EPL (Europhysics Letters) **110**, 48005 (2015).

[14] T. J. Lampo, S. Stylianidou, M. P. Backlund, P. A. Wiggins, and A. J. Spakowitz, Biophys. J. (2017).

[15] S. Yamada, D. Wirtz, and S. C. Kuo, Biophys. J. **78**, 1736 (2000).

[16] D. T. Chen, E. R. Weeks, J. C. Crocker, M. F. Islam, R. Verma, J. Gruber, A. J. Levine, T. C. Lubensky, and A. G. Yodh, Phys. Rev. Lett. **90**, 108301 (2003).

[17] A. El Kaffas, D. Bekah, M. Rui, J. C. Kumaradas, and M. C. Kolios, Phys. Med. Biol. **58**, 923 (2013).

[18] J. Happel and H. Brenner, *Low Reynolds number hydrodynamics: with special applications to particulate media*, Vol. 1 (Springer Science & Business Media, 2012).

[19] C. W. Oseen, "Hydrodynamik," (1927).

[20] S. F. J. Butler, in *Math. Proc. Cambridge Philos. Soc.*, Vol. 49 (Cambridge Univ Press, 1953) pp. 169–174.

[21] W. D. Collins, Mathematika **1**, 125 (1954).

[22] W. D. Collins, Mathematika **5**, 118 (1958).

[23] H. Hasimoto, J. Phys. Soc. Japan **11**, 793 (1956).

[24] H. Hasimoto, J. Phys. Soc. Japan **61**, 3027 (1992).

[25] H. Hasimoto, Phys. Fluids **9**, 1838 (1997).

[26] R. Shail, Quart. J. Mech. App. Math. **40**, 223 (1987).

[27] R. Shail and S. Onslow, Mathematika **35**, 233 (1988).

[28] A. Sellier, Comput. Model. Eng. Sci. **25**, 165 (2008).

[29] C. Maul and S. Kim, Phys. Fluids **6**, 2221 (1994).

[30] C. Maul and S. Kim, in *The Centenary of a Paper on Slow Viscous Flow by the Physicist HA Lorentz* (Springer, 1996) pp. 119–130.

[31] C. Pozrikidis, J. Comput. Phys. **169**, 250 (2001).

[32] Y. O. Fuentes, S. Kim, and D. J. Jeffrey, Phys. Fluids **31**, 2445 (1988).

[33] Y. O. Fuentes, S. Kim, and D. J. Jeffrey, Phys. Fluids **1**, 61 (1989).

[34] B. U. Felderhof and A. Sellier, J. Chem. Phys. **136**, 054703 (2012).

[35] C. Aponte-Rivera and R. N. Zia, Phys. Rev. Fluids **1**, 023301 (2016).

[36] A. Daddi-Moussa-Ider, A. Guckenberger, and S. Gekle, Phys. Rev. E **93**, 012612 (2016).

[37] A. Daddi-Moussa-Ider, A. Guckenberger, and S. Gekle, Phys. Fluids **28**, 071903 (2016).

[38] R. Skalak, A. Tozeren, R. P. Zarda, and S. Chien, Biophys. J. **13(3)**, 245 (1973).

[39] T. W. Secomb, Ann. Rev. Fluid Mech. **49**, 443 (2017).

[40] W. Helfrich, Z. Naturf. C. **28**, 693 (1973).

[41] A. Daddi-Moussa-Ider and S. Gekle, Phys. Rev. E **95**, 013108 (2017).

[42] T. Krüger, F. Varnik, and D. Raabe, Comp. Math. Appl. **61**, 3485 (2011).

[43] T. Krüger, *Computer simulation study of collective phenomena in dense suspensions of red blood cells under shear* (Springer Science & Business Media, 2012).

[44] D. Barthès-Biesel, Ann. Rev. Fluid Mech. **48**, 25 (2016).

[45] S. Gekle, Biophys. J. **110**, 514 (2016).

[46] T. Bickel, Eur. Phys. J. E **20**, 379 (2006).

[47] A. Guckenberger, M. P. Schraml, P. G. Chen, M. Leonetti, and S. Gekle, Comp. Phys. Comm. **207**, 1 (2016).

[48] C. Pozrikidis, J. Fluid Mech. **440**, 269 (2001).

[49] A. Guckenberger and S. Gekle, J. Phys. Cond. Mat. (accepted) .

[50] M. Deserno, Chem. Phys. Lipids **185**, 11 (2015).

[51] M. Stimson and G. B. Jeffery, Proc. Roy. Soc. London. Series A **111**, 110 (1926).

[52] B. U. Felderhof, J. Chem. Phys. **125**, 124904 (2006).

[53] A. Daddi-Moussa-Ider, M. Lisicki, and S. Gekle, Phys. Rev. E (accepted) (2017).

[54] H. Lamb, *Hydrodynamics* (Cambridge university press, 1932).

[55] R. G. Cox, J. Fluid Mech. **37**, 601 (1969).

[56] M. Abramowitz, I. A. Stegun, *et al.*, *Handbook of mathematical functions*, Vol. 1 (Dover New York, 1972).

[57] C. Misbah, Phys. Rev. Lett. **96**, 028104 (2006).

[58] B. Kaoui, T. Krüger, and J. Harting, Soft Matter **8**, 9246 (2012).

[59] B. Kaoui and J. Harting, Rheol. Acta , 1 (2016).

[60] H. A. Lorentz, Abh. Theor. Phys. **1**, 23 (1907).

[61] S. H. Lee, R. S. Chadwick, and L. G. Leal, J. Fluid Mech. **93**, 705 (1979).

[62] T. Bickel, Phys. Rev. E **75**, 041403 (2007).

Acknowledgments

> Knowledge is in the end based on acknowledgement.
>
> Ludwig Wittgenstein

This work would not have been possible without the support of many people. Foremost, I would like to thank my family for their love and wonderful trust. I owe a special thanks to my parents for believing in me and for their continuous encouragements and inspiration throughout my life. Moreover, I thank my brother Nadir for his unconditional support and precious help.

I would like to thank my mentor and advisor Prof. Dr. Stephan Gekle for welcoming me in his group and offering me the opportunity to conduct my doctoral studies in a so kind and so exciting environment. That was a real fun three years in Bayreuth. I thank Stephan for suggesting such a challenging and interesting research topic, for his powerful supervision, enthusiasm, precious advices, tremendous guidance I receive and for the confidence he had in me. Many thanks for him for giving me the opportunity to conduct research visits at the University of Cambridge to work with Dr. Maciej Lisicki on fascinating and timely research questions. I am grateful to Maciej for his fruitful collaboration and for walking me around the city and colleges. I would like to thank Prof. Dr. Eric Lauga for his kind hospitality and for making the visit possible. My profound thanks go to Prof. Dr. Howard A. Stone and his formidable postdoc Dr. Bhargav Rallabandi for their warm welcome and generous assistance during my visit to Princeton.

I also thank my colleague Achim Guckenberger for providing the core of the boundary integral code which served as a basis for the implementation of the completed double layer extension. I thank him for his expertise and inputs which have helped me throughout this work. I also thank all the administration staff at the Physics Department in particular Mr. Markus Hilt for keeping the computers running and Mrs. Claudia Brandt for taking care of paperwork. Furthermore, I thank all the current and former members of our group especially Ali Ghaemi, Sebastian Müller, Aflah Elouneg, Christian Schaaf and Miriam Jahn. Thanks to Christian Bächer for reviewing the German version of the thesis abstract.

Also, I thank all my friends and all my schoolmate who encouraged me with their faith in me particularly Dr. Mustafa Hadj-Nacer, Ismail Oukid, Ghalib Fissah, Hocine Bouchenak, Ali Kerroum, Ahmed Benaddoun, Mohammed Seddik Benyahia, Mohammed Abderrahmane and Bachir Fartas. Many thanks to all the researchers and all the teachers who participated in our training and education throughout our studies.

Thanks to the members of the jury for taking the time and care to read this thesis.

Finally, I would like to thank the Volkswagen foundation for financial support and the Gauss Center for Supercomputing e.V. for providing computing time on the GCS Supercomputer SuperMUC at Leibniz Supercomputing Center.

Erklärung

Hiermit versichere ich an Eides statt, dass ich die vorliegende Arbeit selbständig verfasst und keine anderen als die angegebenen Quellen und Hilfsmittel verwendet habe.

Weiterhin erkläre ich hiermit, dass ich bisher keinen anderweitigen Promotionsversuch unternommen habe und Hilfe von gewerblichen Promotionsberatern bzw. -vermittlern weder bisher in Anspruch genommen habe noch künftig in Anspruch nehmen werde.

Bayreuth, den 26 Juli 2017

Abdallah Daddi-Moussa-Ider